

## FIRST LASING OF THE THIRD STAGE OF NOVOSIBIRSK FEL\*

O.A.Shevchenko<sup>#</sup>, V.S.Arbutov, K.N.Chernov, I.V. Davidyuk, E.N.Dementyev, B.A.Dovzhenko, Ya.V.Getmanov, B.A.Knyazev, E.I.Kolobanov, A.A.Kondakov, V.R.Kozak, E.V.Kozyrev, V.V.Kubarev, G.N.Kulipanov, E.A.Kuper, I.V.Kuptsov, G.Ya.Kurkin, S.V.Motygin, V.N.Osipov, V.M.Petrov, L.E.Medvedev, V.K.Ovchar, A.M.Pilan, V.M.Popik, V.V.Repkov, T.V.Salikova, M.A.Scheglov, I.K.Sedlyarov, G.V.Serdobintsev, S.S.Serednyakov, A.N.Skrinsky, S.V.Tararyshkin, V.G.Tcheskidov, A.G. Tribendis, N.A.Vinokurov, P.D.Vobly  
BINP, Novosibirsk, Russia

### Abstract

Novosibirsk FEL facility is based on the first in the world multi-turn energy recovery linac (ERL). It comprises three FELs (stages). FELs on the first and the second tracks were commissioned in 2004 and 2009 respectively and operate for users now. The third stage FEL is installed on the fourth track of the ERL. It includes three undulator sections and 40-meters-long optical cavity. The design tuning range of this FEL is from 5 to 20 microns and the design average power at bunch repetition rate 3.74 MHz is about 1 kW. Recent results of the third stage FEL commissioning are reported.

### OVERVIEW OF THE NOVOSIBIRSK FEL FACILITY

#### Accelerator Design and Basic Parameters

The Novosibirsk FEL facility is based on the multiturn energy recovery linac (ERL) which scheme is shown in Fig. 1. The advantage of this scheme is that high energy electrons can be obtained with shorter linac as the beam goes through the linac several times before it enters undulator.

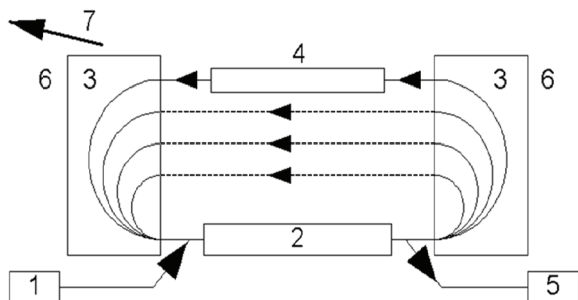


Figure 1: Simplest multiturn ERL scheme: 1 – injector, 2 – linac, 3 – bending magnets, 4 – undulator, 5 – dump.

Multiturn ERLs look very promising for making ERLs less expensive and more flexible, but they have some serious intrinsic problems. Particularly in the simplest scheme shown in Fig. 1 one has to use the same tracks for accelerating and decelerating beams which essentially complicates adjustment of the magnetic system.

At present the Novosibirsk ERL is the only one multiturn ERL in the world. It has rather complicated lattice as it can be seen from Fig. 2. The ERL can operate in three modes providing electron beam for three different FELs. The whole facility can be treated as three different ERLs (one-turn, two-turn and four-turn) which use the same injector and the same linac. The one-turn ERL is placed in vertical plane. It works for the THz FEL which undulators are installed at the floor. This part of the facility is called the first stage. It was commissioned in 2003 [1].

The other two ERL beamlines are placed in horizontal plane at the ceiling. At the common track there are two round magnets. By switching these magnets on and off one can direct the beam either to horizontal or to vertical beamlines. The 180-degree bending arcs also include small bending magnets with parallel edges and quadrupoles. To reduce sensitivity to the power supply ripples, all magnets on each side are connected in series. The quadrupole gradients are chosen so that all bends are achromatic. The vacuum chambers are made from aluminium. They have water-cooling channels inside.

The second horizontal track has bypass with the second FEL undulator. The bypass provides about 0.7 m lengthening of the second orbit. Therefore when the beam goes through the bypass it returns back to the linac in decelerating phase and after two decelerations it finally comes to the dump. This part (the second stage) was commissioned in 2009. The final third stage will include full-scale four-turn ERL and FEL installed on the last track.

The basic beam and linac parameters common for all three ERLs are listed in Table 1.

Table 1: Basic ERL Parameters

Injection energy, MeV	2
Main linac energy gain, MeV	11
Charge per bunch, nC	1.5
Normalized emittance, mm-mrad	30
RF frequency, MHz	180.4
Maximum repetition rate, MHz	90.2

\*Work supported by by Russian Science Foundation (project 14-12-00480)

<sup>#</sup>O.A.Shevchenko@inp.nsk.su

# THREE PLUS DECADES OF TAPERED UNDULATOR FEL PHYSICS\*

William M. Fawley, Sincrotrone Trieste S.C.p.A., Trieste, Italy, and  
SLAC National Accelerator Laboratory, Menlo Park, California, 94025 USA<sup>†</sup>

## Abstract

Beginning with the classic 1981 work of Kroll-Morton-Rosenbluth [1], multiple generations of FEL scientists have studied and used experimentally undulator tapering to improve and optimize the radiation output of both amplifier and oscillator FELs. Tapering has undergone a renaissance of interest, in part to make possible TW instantaneous power levels from x-ray FELs. In this talk, I will give a highly personalized (and undoubtedly strongly biased) historical survey of tapering studies beginning with the ELF 35-GHz experiments at Livermore in the mid-1980's and continuing up to quite recent studies at the LCLS at both soft and hard x-ray wavelengths.

## SOME GENERAL COMMENTS

Not wanting to put together pages and pages of dusty, historical material covering my tapering experiences since the early 1980's, I will instead limit myself to a few suggestions to my younger, brighter, and far more energetic FEL colleagues concerning subject areas of our current millenium where it is \*possible\* (but not certain!) that additional work on tapering theory could be useful and productive.

Regarding optimizing "KMR-style" tapers, I think it is quite evident at this FEL 2015 conference that numerous groups (*e.g.*, UCLA/SLAC, Lund, DESY, Diamond/Daresbury) realize that allowing a variable ponderomotive phase  $\psi_R(z)$  can lead to much greater power output over a fixed undulator length than would be keeping  $\psi_R$  rigidly fixed. (Moreover, as I tried to stress in my talk, KMR themselves knew this and T. Scharlemann and I from the mid-1980's had a ramping option for  $\psi_R$  in the FRED&GINGER self-design algorithm). However, it is not clear to me personally that there is a unique (or even semi-unique) strategy that can maximize the trapping fraction in the undulator region just downstream of the nominal saturation point  $z_{SAT}$  that will work over a broad range of FEL parameters such as  $Z_R/L_G$ , Twiss- $\beta/L_G$ ,  $4\pi\epsilon_N/\lambda_s$ ,  $\sigma_E/\rho$ , *etc.* (here all the standard abbreviations hold...). My guess is that when emittance and incoherent energy spread are non-trivial relative to the size of the FEL parameter  $\rho$ , one may need to be very

careful in increasing  $\psi_R$  too rapidly in  $z$ . Effects such as these mean that if the bucket area does not increase sufficiently quickly with  $z$  due to an increasing radiation power, then there will likely be a lot of detrapping in the first couple gain lengths beyond the nominal saturation point from particles near the outer edges of bucket. There is also the issue for high electron beam energy FELs such as LCLS or XFEL that depend upon quadrupole-based strong focusing that the variation of wiggle-period-averaged  $p_{||}$  over a betatron period can be another source of detrapping lightly-bound electrons.

Regarding sidebands, during the olden days of the LLNL high gain amplifier work, I started a paper (never finished after my departure from the shortly-to-collapse LLNL FEL program) on SASE-stimulated sideband limits to stable tapering. This was stimulated by the desire to see if one could get a solid criterion for the necessary seed power (presumably higher due to the detrapping effects of sidebands than would be necessary from just final spectral bandwidth considerations). This subject is now (refreshingly???) current again with the interest in reaching TW power levels from x-ray FELs. My feeling is that there has been no truly definitive work on to what degree will tapering control sideband growth in situations where one wants reasonably stable trapping over as many as 10 gain lengths beyond  $z_{SAT}$ . I also suspect that whatever work was done in the 1990's concerning detrapping due to sidebands should likely be redone and extended by considering 2015-style high brightness e-beams in which the particles might be more deeply trapped initially in the saturation region. Moreover, with 3 (or is it 4) orders of additional computational power now available, it is useful for someone to look at the various characteristics of sideband growth (*e.g.*, radiation mode size and shape, sensitivity to different focusing schemes and different ratios of the betatron to the synchrotron wavelength). If in fact SASE-initiated sidebands are a true issue in terms of detrapping, perhaps there are clever schemes in terms of detuning *a' la* I-SASE that can reduce the effective sideband growth rate.

Regarding tapering SASE-mode amplifiers, I do not believe we in the community know at all what the best strategy is in terms of a variable  $\psi_R(z)$  that will work over a broad range of parameters. The statistical irregularities of the depths of the ponderomotive wells from one SASE-spike to another suggests there may \*not\* be one taper that works best for all. Sam Krinsky and Robert Gluckstern) did some very nice work [2] in the early-2000's on the general statistical properties of SASE spikes in the exponential gain region leading up to  $z_{SAT}$ . Perhaps some clever soul can do similar analysis that could extend this analysis to a few gain lengths beyond  $z_{SAT}$ . Then ideally, this soul could *also* use the resultant properties to find an indication as to how best

\* My FEL work over these last 3+ decades has been funded by numerous entities including the taxpayers of the European Union via the FERMI project of Elettra-Sincrotrone Trieste and the taxpayers of the USA via the Office of Science in the Dept. of Energy through grants to SLAC, Argonne, and Lawrence Berkeley National Labs, and also via DARPA and the Strategic Defense Initiative Organization (the "Star Wars" people) within the Dept. of Defense through grants to Lawrence Livermore National Laboratory. DISCLAIMER: the views and opinions expressed herein are those solely of the author, completely privately funded, and hopefully unpolluted by any publicly-supported political correctness or toadiness. Few neurons were harmed in the writing of this paper.

<sup>†</sup> william.fawley@elettra.eu

# X-RAY FEL R&D: BRIGHTER, BETTER, CHEAPER

Zhirong Huang

SLAC National Accelerator Laboratory, Menlo Park, CA, USA

## Abstract

The X-ray free-electron lasers (FELs), with nine to ten orders of magnitude improvement in peak brightness over the third-generation light sources, have demonstrated remarkable scientific capabilities. Despite the early success, X-ray FELs can still undergo dramatic transformations with accelerator and FEL R&D. In this paper, I will show examples of recent R&D efforts to increase X-ray coherence and brightness, to obtain better control of X-ray temporal and spectral properties, and to develop concepts for compact coherent sources.

## INTRODUCTION

X-ray FEL or XFEL is a breakthrough in light source development and enables atomic-scale imaging at femtosecond (fs) time resolution [1–3]. Despite the early success, it is widely recognized that XFELs continue to have significant potential for improvement. New methods have been rapidly developing to provide FEL seeding, extremely short x-ray pulses, variable double pulses, two-color FEL generation, and polarization control. Many of the proposals were implemented in the LCLS since 2011 through the so-called FEL R&D program that I have the privilege to contribute. Here I present a personal (incomplete) overview. I also like to discuss dreams/progress towards compact XFELs and conclude with some final remarks.

## IMPROVING TEMPORAL COHERENCE (BRIGHTER)

Typical XFEL pulses are made of a few tens to hundreds of coherent spikes of fs duration, each with no fixed phase relation to the others due to the self-amplified spontaneous emission process. Longitudinal coherence can be imposed by a post-SASE monochromator, but typically with reduced intensity and increased intensity fluctuations. External seeding at radiation wavelengths down to a few nanometers was demonstrated at the FERMI FEL at Synchrotron Trieste with high-gain harmonics generation from an UV laser [4]. At shorter radiation wavelengths around 1 nm or below, external laser seeding becomes increasingly difficult, while self-seeding can be a viable alternative.

Following a proposal from DESY [5], a collaboration between SLAC, Argonne and the Technical Institute for Superhard and Novel Carbon Materials in Russia successfully implemented hard X-ray self-seeding at LCLS in 2012. One out of 33 undulator sections (U16) was removed in order to install a chicane and an in-line single diamond crystal. The thin crystal transmits most of the SASE pulse but also generates a trailing monochromatic seed pulse. The chicane can delay the electron bunch to temporally overlap with the seed

and to amplify the seed in the second part of the undulator array (U17-U33). Self-seeding at the angstrom wavelength scale, with a factor of about 40 bandwidth reduction, was demonstrated [6]. Hard X-ray self-seeding is in operation since 2013 and provides seeded beams from 5 keV to 9.5 keV with two to four times more photons per pulse than SASE using a post-monochromator. In a recent warm dense matter dynamic compression experiment, the unique properties of the seeded X-rays provide plasmon spectra of this complex state that yield the temperature and density with unprecedented precision at micrometer-scale resolution [7].

After the success of hard X-ray self-seeding, a compact soft X-ray self-seeding system was designed and implemented upstream of the hard X-ray self-seeding section in 2013 [8]. This system covers the photon energy range from 0.5 keV to 1 keV with a fwhm bandwidth of  $2 \times 10^{-4}$ . The SXRSS system relies on a grating monochromator consisting of a variable line spacing toroidal grating followed by a plane mirror, slit and two mirrors. The four-dipole chicane is similar to the hard X-ray one and displaces, de-bunches and delays the electron beam. Although still being optimized, the soft X-ray self-seeding system has demonstrated a bandwidth of  $3\text{--}5 \times 10^{-4}$ , wavelength stability of  $1 \times 10^{-4}$ , and an increase in peak brightness by a factor of up to 5 across the photon energy range [9].

One of the main challenges for seeded FELs is the electron energy stability. Since the radiation wavelength is fixed by seeding, the relative electron energy jitter should be less than the fractional FEL bandwidth divided by 2. Intense efforts have been launched to reduce the LCLS energy jitter. These includes injector RF tune-up and compression scheme optimization [10]. Underlying hardware instability has also been carefully scrutinized and improved over recent years [11]. High-power RF terminating loads and higher-rated deuterium thyratrons are forthcoming. Since 2012, both hard and soft X-ray energy jitters have been reduced by a factor of 2, and the hard X-ray self-seeding pulse intensity has increased by about a factor of 3 [12].

The measured spectrum of the soft X-ray self-seeding at LCLS has a pedestal-like distribution around the seeded frequency [9], which limits the spectral purity and seeding applications without a post-undulator monochromator. In a separate contribution to these proceedings [13], we study the origins of the pedestals and focus on the contributions of microbunching instability prior to the FEL undulator. We show that both energy and density modulations can induce sidebands in a seeded FEL. Theory and simulations are used to analyze the sideband content relative to the seeding signal. The results place a tight constraint on the longitudinal phase space uniformity for a seeded FEL.

ISBN 978-3-95450-134-2

# TRANSFORMING THE FEL: COHERENCE, COMPLEX STRUCTURES, AND EXOTIC BEAMS

E. Hemsing\*

SLAC National Accelerator Laboratory, Menlo Park, California 94025, USA

## Abstract

Modern high brightness electron beams used in FELs are extremely versatile and highly malleable. This flexibility can be used to precisely tailor the properties of the FEL light for improved temporal coherence (as in external or self-seeding), but can also be exploited in new ways to generate exotic FEL modes of twisted light that carry orbital angular momentum (OAM) for new science. In this paper I briefly review the history of the work on OAM light production in FELs, and describe how lasers and undulator harmonics can be combined to produce both simple and complex e-beam distributions that emit intense, coherent, and highly tunable OAM light in future FELs.

## INTRODUCTION: FEL TAILORING

Free-electron lasers (FELs) are composite systems of accelerators, electron beam (e-beam) optics, and undulators that produce widely tunable light with exceptional brightness at wavelengths down to hard x-rays for a broad range of studies. The versatility of FELs is derived from the fact that the e-beams that form the lasing medium can be precisely manipulated to tailor the properties of the radiated light. These ‘beam shaping’ manipulations, which range from coarse shaping of the e-beam current profile to precision shaping of the distribution at optical or shorter wavelengths, are used primarily to tailor the temporal shape of the FEL pulse. Because the typical SASE FEL pulse is composed of many temporal spikes, the aim of these schemes is to improve the longitudinal coherence and produce Fourier Transform-limited pulses. To this end, such techniques can also be combined with ‘radiation shaping’ techniques that exploit characteristic features of the undulator radiation to further broaden the landscape of designer FEL photon beams.

The past decade has shown tremendous progress in the development of such ‘beam by design’ concepts [1], in some cases turning proposed techniques into experimental realities over the course of just a few years. This is due in part to the confluence of rapidly advancing technologies that yield higher brightness e-beams, highly stable sub-ps lasers, and tunable undulator systems. The diagram in Figure 1 shows a sample of a number of different schemes designed to tailor the FEL output through either direct shaping of the electron beam (beam shaping) or through shaping using intrinsic features of the undulator radiation (radiation shaping). The slotted foil technique [2], for example, is a method of selecting only a short portion (or portions) of the electron beam to lase by spoiling the emittance of or removing the rest of the beam. Laser-based e-beam shaping techniques (shown

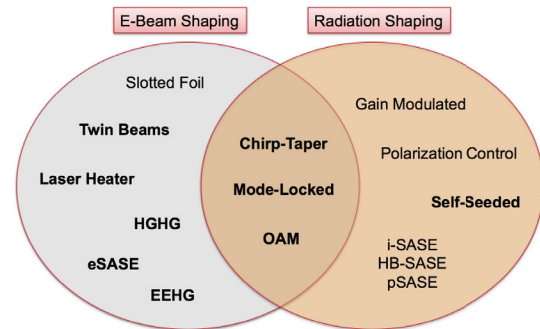


Figure 1: Diagram of example FEL pulse shaping schemes. In bold are those that are based on lasers.

in bold) such as HGHG and EEHG rely on external lasers to precisely rearrange the e-beam phase space to produce coherent density bunching at high harmonics. Such microbunched beams then radiate coherent pulses with bandwidths much narrower than the intrinsic FEL bandwidth. Radiation shaping with the i-SASE, HB-SASE, or pSASE techniques, on the other hand, seeks to take control over the natural slippage between the e-beam and the co-propagating radiation to communicate phase information over different portions of the beam to improve the temporal coherence. In another example, the polarization of the FEL pulse can be controlled using different combinations of linear or circularly polarized undulators, delays, and undulator tapering. Several schemes rely on specific combinations of both types of shaping. In the laser-based ‘chirp-taper’ technique designed to produce ultrashort pulses, for example, the resonant frequency of the undulators is tapered along the length to exactly match the energy chirp of a short portion of an e-beam that has been modulated by a few-cycle laser pulse.

The concentration on tailoring the temporal profile stems from the fact that the high-gain FEL is nearly diffraction limited and thus already has a high degree of transverse coherence, even for SASE. The lowest order transverse mode also has the highest gain, so the radiation at the fundamental frequency is gaussian-like and is peaked on axis. While it is fortunate that such ubiquitous modes are generated as a matter of course, there are numerous emerging applications and research opportunities where higher order transverse modes, specifically modes that carry orbital angular momentum (OAM), provide additional degrees of freedom that may be specifically exploited to probe the deep structure and behavior of matter.

\* ehemsing@slac.stanford.edu

# OPTIMIZATION OF A HIGH EFFICIENCY FREE ELECTRON LASER AMPLIFIER

E.A. Schneidmiller, M.V. Yurkov, DESY, Hamburg, Germany

## Abstract

Technique of undulator tapering in the post-saturation regime is used at the existing X-ray FELs for increasing the radiation power. We present comprehensive analysis of the problem in the framework of one-dimensional and three-dimensional theory. We find that diffraction effects essentially influence on the choice of the tapering strategy. Our studies resulted in a general law of the undulator tapering for a seeded FEL amplifier as well as for SASE FEL.

## INTRODUCTION

Effective energy exchange between the electron beam moving in an undulator and electromagnetic wave happens when resonance condition takes place. In this case electromagnetic wave advances electron beam by one radiation wavelength while electron beam passes one undulator period. When amplification process enters nonlinear stage, the energy losses by electrons become to be pronouncing which leads to the violation of the resonance condition and to the saturation of the amplification process. Application of the undulator tapering [1] allows to a further increase of the conversion efficiency. An idea is to adjust undulator parameters (field or period) according to the electron energy loss such that the resonance condition is preserved.

It is generally accepted that in the framework of the one-dimensional theory an optimum law of the undulator tapering should be quadratic [2–9]. Similar physical situation occurs in the FEL amplifier with a waveguide [2]. In this case radiation is confined within the waveguide. Parameters of FEL amplifiers operating in the infrared, visible, and x-ray wavelength ranges are such that these devices are described in the framework of three dimensional theory with an “open” electron beam, i.e. physical case of diffraction in a free space. In this case the diffraction of radiation is an essential physical effect influencing optimization of the tapering process. Discussions and studies on the optimum law of the undulator tapering in the three-dimensional case are in the progress for more than 20 years. Our previous studies were mainly driven by occasional calculations of perspective FEL systems for high power scientific (for instance, FEL based  $\gamma\gamma$  - collider ) and industrial applications (for instance, for isotope separation, and lithography [10–12]). Their parameter range corresponded to the limit of thin electron beam (small value of the diffraction parameter). In this case linear undulator tapering works well from almost the very beginning [6]. Comprehensive study devoted to the global optimization of tapered FEL amplifier with “open” electron beam has been presented in [4]. It has been shown that: i) tapering law should be linear for the case of thin electron beam, ii) optimum tapering at the initial stage should

follow quadratic dependence, iii) tapering should start approximately two field gain length before saturation. New wave of interest to the undulator tapering came with the development of x-ray free electron lasers [13–20]. Undulator tapering has been successfully demonstrated at long wavelength FEL amplifiers [2, 21], and is routinely used at x-ray FEL facilities LCLS and SACLA [16, 17]. Practical calculations of specific systems yielded in several empirical laws using different polynomial dependencies (see [22, 23] and references therein).

Comprehensive analysis of the problem of the undulator tapering in the presence of diffraction effects has been performed in [24, 25]. It has been shown that the key element for understanding the physics of the undulator tapering is given by the model of the modulated electron beam which provides relevant interdependence of the problem parameters. Finally, application of similarity techniques to the results of numerical simulations led to the universal law of the undulator tapering. In this paper we extend studies [24, 25] to the case of SASE FEL.

## BASIC RELATIONS

We consider axisymmetric model of the electron beam. It is assumed that transverse distribution function of the electron beam is Gaussian, so rms transverse size of matched beam is  $\sigma = \sqrt{\epsilon\beta}$ , where  $\epsilon$  is rms beam emittance and  $\beta$  is focusing beta-function. An important feature of the parameter space of short wavelength FELs is that the space charge field does not influence significantly the amplification process, and in the framework of the three-dimensional theory the operation of the FEL amplifier is described by the following parameters: the diffraction parameter  $B$ , the energy spread parameter  $\hat{\Lambda}_T^2$ , the betatron motion parameter  $\hat{k}_\beta$  and detuning parameter  $\hat{C}$  [9, 26]:

$$B = 2\Gamma\sigma^2\omega/c, \quad \hat{C} = C/\Gamma, \\ \hat{k}_\beta = 1/(\beta\Gamma), \quad \hat{\Lambda}_T^2 = (\sigma_E/\mathcal{E})^2/\rho^2, \quad (1)$$

where  $\Gamma = [I\omega^2\theta_s^2 A_{JJ}^2/(I_A c^2 \gamma_z^2 \gamma)]^{1/2}$  is the gain parameter,  $\rho = c\gamma_z^2 \Gamma/\omega$  is the efficiency parameter, and  $C = 2\pi/\lambda_w - \omega/(2c\gamma_z^2)$  is the detuning of the electron with the nominal energy  $\mathcal{E}_0$ . Note that the efficiency parameter  $\rho$  entering equations of three dimensional theory relates to the one-dimensional parameter  $\rho_{1D}$  as  $\rho_{1D} = \rho/B^{1/3}$  [9, 27]. The following notations are used here:  $I$  is the beam current,  $\omega = 2\pi c/\lambda$  is the frequency of the electromagnetic wave,  $\theta_s = K/\gamma$ ,  $K$  is the rms undulator parameter,  $\gamma_z^2 = \gamma^{-2} + \theta_s^2$ ,  $k_w = 2\pi/\lambda_w$  is the undulator wavenumber,  $I_A = 17$  kA is the Alfvén current,  $A_{JJ} = 1$  for helical undulator and  $A_{JJ} = J_0(K^2/2(1 + K^2)) - J_1(K^2/2(1 + K^2))$  for planar undulator.  $J_0$  and  $J_1$  are the Bessel functions of the first

# ESTIMATE OF FREE ELECTRON LASER GAIN LENGTH IN THE PRESENCE OF ELECTRON BEAM COLLECTIVE EFFECTS\*

S. Di Mitri<sup>#</sup>

Elettra Sincrotrone Trieste, 34149 Basovizza, Trieste, Italy

S. Spampinati

Department of Physics, University of Liverpool, Liverpool L69 7ZX, United Kingdom

Cockcroft Institute, Sci-Tech Daresbury, Warrington WA4 4AD, United Kingdom

## Abstract

A novel definition for the three-dimensional free electron laser gain length is proposed [1], which takes into account the increase of electron beam projected emittance as due, for example, to geometric transverse wakefield and coherent synchrotron radiation developing in linear accelerators. The analysis shows that the gain length is affected by an increase of the electron beam projected emittance, even though the slice (local) emittance is preserved, and found to be in agreement with Genesis code simulation results. It is then shown that the minimum gain length and the maximum of output power may notably differ from the ones derived when collective effects are neglected. The proposed model turns out to be handy for a parametric study of electron beam six-dimensional brightness and FEL performance as function, e.g., of bunch length compression factor, accelerator alignment tolerances and optics design.

## WORK PLAN

Following our work in [1], which relies in turn on the formalism developed in [2,3,4]:

- We analytically evaluate the electron beam 6-D energy-normalized brightness,  $B_{n,6D}$ , in the presence of short-range geometric transverse wakefield (GTW) in accelerating structures and coherent synchrotron radiation (CSR) emitted in magnetic compressors. We extend our previous study [5] to include the analytical estimate of the final slice energy spread when microbunching instability (MBI) is suppressed with a laser heater [6]. This estimate makes use of the analytical model for the MBI given in [7,8].

- We show that the physical picture proposed in [4] for the beam motion in an undulator also applies to angular perturbations caused by GTW and CSR in the accelerator. Consequently, we establish an explicit connection between the FEL performance, so far only predicted on the basis of the electron bunch's slice parameters, and a more complete set of sources of  $B_{n,6D}$  degradation that is including projected beam parameters.

- An analytical formula is given for estimating the self-amplified spontaneous emission (SASE) FEL [9,10] 3-D power gain length's [11] increase due to collective effects, the power saturation length and the peak power at saturation. We extend the discussion beyond SASE to the

case of externally seeded FELs.

## THEORETICAL MODEL

GTW and CSR offset individual “macro-slices” both in configuration and velocity spaces. The macro-slices are modelled to be as long as several cooperation lengths, since GTW and CSR-induced transverse kicks are typically correlated with  $z$ , the longitudinal coordinate internal to the bunch, on the length scale of few to hundreds microns. Neglecting for the moment any slice emittance growth from the injector to the undulator, the projected emittance growth is entirely due to mismatch of the bunch macro-slices in the transverse phase space. We take this growth into account through the mechanism described by Tanaka *et al.* [4]. In that work, the authors identify two distinct processes that increase  $L_{g,1D}$ . One is a lack of overlapping between the spontaneous undulator radiation, whose wavefront follows the electrons' local direction of motion, and the FEL radiation, whose wavefront is preserved when the electrons are transversally kicked by lattice errors. The other process is electrons' bunching smearing due to longitudinal dispersion of electrons transversally kicked by lattice errors.

We recognize that the electrons' angular divergence has two contributions: one is incoherent and due to the finite beam emittance as depicted in Xie's [11] and Saldin's [12] models; the other is coherent, being the tilt of the macro-slice centroids with respect to the reference trajectory. The coherent divergence adds to (and in some cases, surpasses) the incoherent one and may amplify the effect of bunching smearing. In order to take into account the coherent motion of electrons, we apply the physical picture depicted in [4] to individual macro-slices. Each macro-slice is transversally kicked by collective effects in the linac and thus moves along the undulator on a different trajectory than other macro-slices, as shown in Fig. 1.

We call  $\sqrt{\langle \theta_{coll}^2 \rangle}$  the rms angular divergence of the macro-slice centroids at the undulator. Being a quantity averaged over the bunch duration,  $\sqrt{\langle \theta_{coll}^2 \rangle}$  is an indicator of the mismatch of the macro-slices in the transverse phase space, projected onto the  $z$ -coordinate. We assume that the charge transverse distribution at the undulator is matched to some design Twiss parameters, and that a smooth optics is implemented along the

\*Work supported by the FERMI project of Elettra Sincrotrone Trieste.

<sup>#</sup>simone.dimitri@elettra.eu

# OPERATING OF SXFEL IN A SINGLE STAGE HIGH GAIN HARMONIC GENERATION SCHEME

Guanglei Wang, Weiqing Zhang, Guorong Wu, Dongxu Dai, Xueming Yang<sup>#</sup>  
State Key Laboratory of Molecular Reaction Dynamics, Dalian Institute of Chemical Physics,  
Chinese Academy of Sciences, Dalian 116023, P. R. China

## Abstract

The beam energy spread at the entrance of undulator system is of paramount importance for efficient density modulation in high-gain seeded free-electron lasers (FELs). In this paper, the dependencies of high harmonic bunching efficiency in the high-gain harmonic generation (HG) schemes on the electron energy spread distribution are studied. Theoretical investigations and multi-dimensional numerical simulations are applied to the cases of uniform and saddle beam energy distributions and compared to a traditional Gaussian distribution. It shows that the uniform and saddle electron energy distributions significantly enhance the performance of HG-FELs. A numerical example demonstrates that, with the saddle distribution of sliced beam energy spread controlled by a laser heater, the 30th harmonic radiation can be directly generated by a single-stage seeding scheme for a soft x-ray FEL facility.

## INTRODUCTION

In recent years, enormous progresses have been achieved in the seeded free-electron lasers (FELs), which hold great potential to deliver high brilliance radiation pulses with excellent longitudinal coherence in the extreme ultraviolet and even x-ray regions. The first seeding scheme, i.e., high-gain harmonic generation (HG) has been fully demonstrated at BNL [1-4] and is currently used to deliver coherent extreme ultraviolet FEL pulses to users at FERMI [5]. For a long time, it is thought that the frequency multiplication factor of a single-stage HG is usually limited within  $\sim 10$  [1,6], due to the tradeoff between the energy modulation and the energy spread requirement for exponential amplification process of FEL. Therefore, a complicated multi-stage HG scheme [7-9] has been theoretically proposed and experimentally demonstrated for short wavelength production from a commercially available seed laser.

Up to now, the bunching performance assessment for seeded FELs is on the basis of assumption that the electron beam at the entrance of undulator has an energy spread of Gaussian distribution, which however is not true, e. g., in the specific case with a laser heater in the LINAC [10-11]. Laser heater is widely utilized in high-gain FEL facilities to suppress the gain of the micro-bunching instability via Landau damping by controllable increasing the beam energy spread. It is found that a non-Gaussian energy distribution can be induced by a laser heater and inherited in the main LINAC section,

depending upon details of the transverse overlap between the laser beam and the electron beam in the laser heater system. A recent experiment at FERMI [5,12] demonstrates that the non-Gaussian beam energy spread induced by the laser heater may expand the harmonic number of a single-stage HG to several tens [13-14]. Meanwhile, one cannot exclude other unknown schemes lie beyond the horizon for controlling beam energy spread distribution in future.

Considering that the initial energy distribution of electron beam is one of the most critical elements in the bunching process of seeded FELs, in this paper, the possible beam energy distribution influences on density modulation efficiency in various seeded FEL schemes have been studied. In Section II, by using a set of nominal parameters of Shanghai soft x-ray free-electron laser facility (SXFEL) [15], the bunching efficiencies in HG schemes with different electron beam energy spread distribution are theoretically derived and numerically simulated, which shows that the uniform and saddle cases may significantly enhance the bunching performance of HG. It indicates that the beam energy distribution is of great importance for HG scheme, the frequency up-conversion number of a single-stage HG can be improved to 30 or even higher with a uniform or saddle electron energy distribution. A followed start-to-end example in Section III demonstrated that the saddle distribution of sliced beam energy spread controlled by a laser-heater can be maintained in the following accelerations of LINAC, and the saddle beam energy distribution is capable of driving a 30<sup>th</sup> harmonic up-conversion in a single-stage HG operation of SXFEL, even though it has a larger sliced beam energy spread than a Gaussian case. Finally, we present our conclusions in Section IV.

## ENERGY SPREAD DISTRIBUTION EFFECTS ON SEEDING SCHEME

In order to obtain a comprehensible idea of the energy spread distribution effects on different seeded configurations, by using the nominal parameters of SXFEL, uniform and saddle energy spread distributions are investigated for the density modulation process and compared to the previous Gaussian distribution case in this section, under the same RMS deviation, i.e., beam energy spread. SXFEL aims at generating coherent 8.8 nm FEL pulses from 264 nm seed laser through a two-stage HG. In the nominal design of SXFEL, an 840 MeV electron beam with sliced energy spread of 84 keV, i.e., a relative energy spread of  $1 \times 10^{-4}$ ,

<sup>#</sup>xmyang@dicp.ac.cn

# INFLUENCE OF HORIZONTAL CONSTANT MAGNETIC FIELD ON HARMONIC UNDULATOR RADIATIONS AND GAIN

H. Jeevakhan, P. K. Purohit, Applied Science Department, NITTTTR, Bhopal, India  
G Mishra, SOP, DAVV, Indore, India

## Abstract

Harmonic undulators has been analyzed in the presence of constant magnetic field along the direction perpendicular to the main undulator field. Effect of constant magnetic field magnitude on trajectory of electron beam, intensity of radiation and FEL gain at fundamental and third harmonics has been evaluated. Performance of harmonic undulator in the presence horizontal component of earth's magnetic field is the practical realization of the suggested scheme

## INTRODUCTION

Current researches in science calls for an ultrafast, high brightness and X –ray light source . Fourth generation FEL systems are use to lase at X ray wavelength region [1, 2]. FEL is produced by interaction of relativistic electron beam, an electromagnetic wave travelling in the same direction and undulator. FEL differs from other conventional lasing systems in terms of operation mechanism and assembly as well [3, 4]. Novel design and error analysis of undulator are among the major and important part in FEL research. Concept of Harmonic undulator is given to use undulator assembly with slight modification and radiating lower wavelength with modest electron beam. Structure of undulator is optimized to enhance the output radiation and gain in FEL systems [5-9].

In this paper we have modeled an harmonic undulator with additional horizontal magnetic field. In real applications this component can be realized with earth's horizontal magnetic field component. In the related work, K Zhukovsky has given an analytical model and discuss the effect of horizontal field constituent of undulator radiation and compare it with other factor such as energy spread in beam, emittance and focusing components [10]. N. O. Strelnikov et al presents experimental and modeling results concerning the effects of the interaction of Earth's magnetic field with different types of Insertion devices [11]. In the previous paper [9], we have presented semi analytical results for the effect of constant magnetic field along the direction parallel to undulator field. In this paper we have added a constant field perpendicular to undulator field. The effect of additional field in horizontal direction on harmonic undulator radiations and gain has been analyzed.

## UNDULATOR FIELD

We have considered a constant magnetic field in the direction perpendicular to planar undulator magnetic field encompass with harmonic field

$$B = [B_0\kappa, a_0B_0\sin k_u z + a_1B_0\sinh k_u z, 0] \quad (1)$$

where,  $k_u = \frac{2\pi}{\lambda_u}$  undulator wave number,  $\lambda_u$  is undulator wave length,  $h$  is harmonic integer,  $B_0$  is peak magnetic field,  $a_0$  and  $a_1$  controls the ratio of main undulator field to additional harmonic field  $\kappa$  is the magnitude of constant magnetic field. For practical purpose it is replica of horizontal component of earth magnetic field.

The velocity can be evaluated by using Lorentz force equation:

$$\frac{dv}{dt} = -\frac{e}{\gamma mc} (\vec{v} \times \vec{B}) \quad (2)$$

This gives

$$\beta_x = -\frac{K}{\gamma} \left[ \cos(\Omega_u t) + \Delta \frac{\cos(h\Omega_u t)}{h} \right]$$

$$\beta_y = -\frac{K}{\gamma} [\kappa \Omega_u t] \quad (3)$$

$$\beta_z = \beta^* - \frac{K^2}{2\gamma^2} \left[ \frac{1}{2} \cos(2\Omega_u t) + \frac{1}{2} \left( \frac{\Delta}{h} \right)^2 \cos(2h\Omega_u t) + \left( \frac{\Delta}{h} \right) \cos(1+h)\Omega_u t + \left( \frac{\Delta}{h} \right) \cos(1-h)\Omega_u t + (\kappa \Omega_u t)^2 \right] \quad (4)$$

where  $K = \frac{a_0 e B_0}{\Omega_u m_0 c}$  is the undulator parameter and  $\Delta = \frac{a_1}{a_0}$ , and  $\beta^* = 1 - \frac{1}{2\gamma^2} \left[ 1 + \frac{K^2 + K_1^2}{2} \right]$  with  $K_1 = \frac{\Delta K}{h}$ .

The electron trajectory along z direction is given by

$$\frac{z}{c} = \beta^* t - \frac{K^2}{8\gamma^2 \Omega_u} \sin(2\Omega_u t) - \frac{K_1^2}{8\gamma^2 h \Omega_u} \sin(2h\Omega_u t) - \frac{K K_1}{2\gamma^2 (1-h)\Omega_u} \sin(1-h)\Omega_u t - \frac{K K_1}{2\gamma^2 (1+h)\Omega_u} \sin(1+h)\Omega_u t - \frac{K^2 \kappa^2 \Omega_u^2 t^3}{6\gamma^2} \quad (5)$$

The spectral properties of radiation can be evaluated from Lienard-Wiechart integral [12],

$$\frac{d^2 I}{d\omega d\Omega} = \frac{e^2 \omega^2}{4\pi^2 c} \left| \int_{-\infty}^{\infty} \{ \hat{n} \times (\hat{n} \times \hat{\beta}) \} \exp \left[ i\omega \left( t - \frac{z}{c} \right) \right] dt \right| \quad (6)$$

where the integration is carried over undulator length,  $T = \frac{2N\pi}{\Omega_u}$  and  $\omega$  is the emission frequency. Introducing the variables

$$z_1 = -\frac{\omega K^2}{8\gamma^2 \Omega_u}, \quad z_2 = -\frac{\omega K_1^2}{8\gamma^2 h \Omega_u}, \\ z_3 = -\frac{\omega K K_1}{2\gamma^2 (1-h)\Omega_u} \quad \text{and} \quad z_4 = -\frac{\omega K K_1 \kappa}{2\gamma^2 (1+h)\Omega_u}.$$

The brightness expression is reduced to

# THEORETICAL COMPUTATION OF THE POLARIZATION CHARACTERISTICS OF AN X-RAY FREE-ELECTRON LASER WITH PLANAR UNDULATOR

Gianluca Geloni, European XFEL GmbH, Hamburg, Germany

Vitali Kocharyan, Evgeni Saldin, Deutsches Elektronen-Synchrotron (DESY), Hamburg, Germany

## Abstract

We show that radiation pulses from an X-ray Free-Electron Laser (XFEL) with a planar undulator, which are mainly polarized in the horizontal direction, exhibit a suppression of the vertical polarization component of the power at least by a factor  $\lambda_w^2/(4\pi L_g)^2$ , where  $\lambda_w$  is the length of the undulator period and  $L_g$  is the FEL field gain length. We illustrate this fact by examining the XFEL operation under the steady state assumption. In our calculations we considered only resonance terms: in fact, non resonance terms are suppressed by a factor  $\lambda_w^3/(4\pi L_g)^3$  and can be neglected. While finding a situation for making quantitative comparison between analytical and experimental results may not be straightforward, the qualitative aspects of the suppression of the vertical polarization rate at XFELs should be easy to observe. We remark that our exact results can potentially be useful to developers of new generation FEL codes for cross-checking their results.

## INTRODUCTION

In this paper we quantify the small component of the electric field in the vertical direction in radiation pulses produced by an XFEL with horizontal planar undulator. In particular, we show that for a typical XFEL setup the horizontally polarized component of radiation is greatly dominant, and that only less than one part in a million of the total intensity is polarized in the vertical plane.

The study of XFEL polarization characteristics is obviously deeply related to the problem of electromagnetic wave amplification in XFEL, which refers to a particular class of self-consistent problems. It can be separated into two parts: the solution of the dynamical problem, i.e. finding the motion of the electrons in the beam under the action of given electromagnetic fields, and the solution of the electrodynamic problem, i.e. finding the electromagnetic fields generated by a given contribution of charge and currents. The problem is closed by simultaneous solution of the field equations and of the equations of motion.

Let us consider the electrodynamic problem more in detail. The equation for the electric field  $\vec{E}$  follows the inhomogeneous wave equation

$$c^2 \nabla^2 \vec{E} - \frac{\partial^2 \vec{E}}{\partial t^2} = 4\pi c^2 \vec{\nabla} \rho + 4\pi \frac{\partial \vec{j}}{\partial t}. \quad (1)$$

Once the charge and current densities  $\rho$  and  $\vec{j}$  are specified as a function of time and position, this equation allows one to calculate the electric field  $\vec{E}$  at each point of space and

time [1]. The current density source provides the main contribution to the radiation field in an FEL amplifier, and the contribution of the charge density source to the amplification process is negligibly small. This fact is commonly known and accepted in the FEL community.<sup>1</sup>

Due to linearity, without the gradient term the solution of Eq. (1) exhibits the property that the radiation field  $\vec{E}$  points in the same direction of the current density  $\vec{j}$ . An important limitation of such approximation arises when we need to quantify the linear vertical field generated in the case of an XFEL with planar undulator. In the case  $\vec{j}$  points in the horizontal direction (for a horizontal planar undulator), according to Eq. (1), which is exact, only the charge term is responsible for a vertically polarized component of the field: if it is neglected, one cannot quantify the linear vertical field anymore.

Similar to the process of harmonic generation, the process of generation of the vertically polarized field component can be considered as a purely electrodynamic one. In fact, the vertically polarized field component is driven by the charge source, but the bunching contribution due to the interaction of the electron beam with the radiation generated by such source can be neglected. This leads to important simplifications. In fact, in order to perform calculations of the radiation including the vertically polarization component one can proceed first by solving the self-consistent problem with the current source only. This can either be done in an approximated way using an analytical model for the FEL process or, more thoroughly, exploiting any existing FEL code. Subsequently, the solution to the self-consistent problem can be used to calculate the first harmonic contents of the electron beam density distribution. These contents enter as known sources in our electrodynamic process, that is Eq. (1). Solution of that equation accounting for these sources gives the desired polarization characteristics.

Approximations particularly advantageous for our theoretical analysis include the modeling of the electron beam density as uniform, and the introduction of a monochromatic seed signal. Realistic conditions satisfying these assumptions are the use of a sufficiently long electron bunch with a longitudinal stepped profile and the application of a scheme in the SASE mode of operation for narrowing down the radiation bandwidth. In the framework of this model it becomes possible to describe analytically all the polarization properties of the radiation from an XFEL.

<sup>1</sup> However, we have been unable to find a proof of this fact in literature, except book [2] and review [3], which are only the publications, to the authors' knowledge, dealing with this issue.

# EFFICIENT ELECTRON SOURCES OF COHERENT SPONTANEOUS RADIATION WITH COMBINED HELICAL AND UNIFORM MAGNETIC FIELDS

N. Balal<sup>1#</sup>, V. L. Bratman<sup>1,2</sup>, E. Magori<sup>1</sup>

<sup>1</sup>Ariel University, Ariel, Israel

<sup>2</sup>Institute of Applied Physics, Russian Academy of Sciences, Nizhny Novgorod, Russia

## Abstract

Two methods to mitigate repulsion of electrons in dense bunches from photo-injectors with a relatively low particle energy and to enhance the power of terahertz radiation have been studied. First method is based on using very short bunches and small undulator periods that allows a significant shortening radiation sections. According to simulations bunches with duration (50-100) fs and energy 6 MeV that presumably could be formed in the constructing Israeli THz FEL [1] would fairly effectively radiate at frequencies up to (10-20) THz. The second method is based on an idea recently proposed by A.V. Savilov for longitudinal electron bunching [2, 3]. This is possible when a bunch moves in a combined magnetic field of a solenoid and of a undulator and the electron cyclotron frequency is sufficiently large in comparison with their undulator frequency. In such situation, an increase/decrease of particle energy in the repulsed Coulomb field of space charge leads to a decrease/increase in particle longitudinal momentum. Correspondingly, Coulomb repulsion can lead to an effective attraction of the particles (this effect is analogous to the known cyclotron negative-mass instability). A large value of the uniform field that is necessary in this method can be used to easily obtain a undulator field by inserting a simple steel helix inside a pulsed solenoid. Simulations confirm that the particle attraction can provide a powerful and narrowband radiation of the bunch with electron energy (5-6) MeV and duration 0.3 ps at the frequencies up to 3 THz.

## SHORT BUNCHES IN MICROUNDULATORS

The first opportunity may be realized if bunches with duration of about of 100 fs or even shorter are formed at the entrance of a radiation section. In this case, one can use a mm-period undulator (microundulator) and produce the radiation with the frequency up to 10 THz and higher. A small undulator period provides a relatively narrowband radiation at comparably short radiation length where the longitudinal particles expansion is not too large even at very high bunch charges if the corresponding energy chirp is also used. For such situation, we propose a helical undulator in the form of a set of a helically spaced magnet block interspaced with a preliminarily non-magnetized steel helix; such a set with helically periodic elements

being inserted into a solenoid redistributes its field adding the required helical component in it (Fig. 1). The magnet block should be permanently magnetized toward the solenoid field. This method was successfully developed for a plane prototype in [4]. A strong solenoid field prevents also the transverse particles expansion. According to simulations on the basis Microwave Studio code the optimized undulator systems of such a kind with the ratio of longitudinal helix thickness to the separations 1:2 can provide a strong transverse helical field with the amplitude up to (0.7-1.0) T at an acceptable gap-period ratio 1:3 (Table 1). Such fields provide, in particular, a sufficiently large undulator parameter  $K=0.3-0.4$  at the small period of (4-5) mm. Simulations of Coherent Spontaneous Undulator Radiation of an electron bunch in a combined magnetic field of the solenoid and steel and preliminarily magnetized helical insertions was carried out on the basis of a self-consistent one-dimensional model of the bunch in the form of a charged plane layer using simple formulas for the field of an arbitrary moving charged plane [5]. Such one-dimensional simulations were used for estimations of interaction and radiation from thin disc-like electron bunches with the following parameters: charge (50-200) pC, radius 0.4 mm, duration (50-100) fs, energy 5.5 MeV and a large energy chirp (0.3-1.0) MeV moving in a waveguide mounted into the undulator with the length (5-10) cm. According to calculations one may expect to obtain in such situation narrowband picosecond pulses with the radiation frequency up to (10-20) THz and energy up to (0.1-0.4)  $\mu$ J.

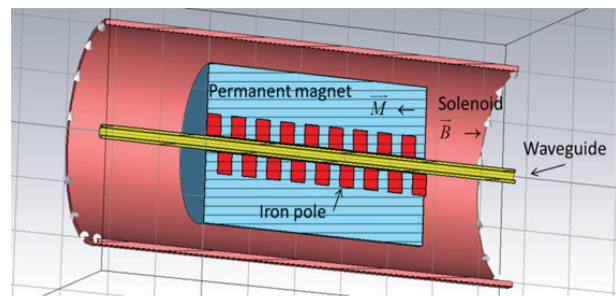


Figure 1: Microundulator for a source of Coherent Spontaneous Radiation of a dense electron bunch with the frequency up to (10-20) THz consisting of a solenoid and insertions in the form of a magnetized block and a non-magnetized steel helix.

#nezahb@ariel.ac.il

# LINAC DESIGN OF THE IR-FEL PROJECT IN CHINA\*

Zhigang He, Wei Xu, Shancai Zhang<sup>†</sup>, Lin Wang, Qika Jia  
NSRL USTC, HeFei, AnHui 230039, China

## Abstract

We are building an infrared free-electron laser (IR-FEL) facility that will operate from 5  $\mu\text{m}$  to 200  $\mu\text{m}$ . This FEL source is driven by a linac, which is composed of a triode electron gun, a subharmonic prebuncher, a buncher, two accelerators, and a beam transport line. The linac is required to operate from 15 to 60 MeV at 1 nC charge, while delivering a transverse rms emittance of smaller than 30 mm-mrad in a 5 ps rms length, smaller than 240 keV rms energy spread bunch at the Far-infrared and Mid-infrared undulators. In this article, the preliminary Linac design studies are described.

## INTRODUCTION

The basic layout of the FEL facility is shown in Fig. 1. The accelerating system consists of a 100 kV triode electron gun, a bunching system, and two accelerators. The energy range between 15 and 25 MeV will be covered with the first accelerator (A1) for the far-infrared radiation, and the range between 25 to 60 MeV with the second accelerator (A2) for the middle-infrared radiation. As to the requirement of the FEL physics [1], the electron beam characteristics are listed in Table 1.

Table 1: Electron Beam Characteristics

	Energy (E)	15-60 MeV
	Energy spread ( $\delta E$ )	< 240 keV
	Emittance ( $\varepsilon_n$ )	< 30 mm-mrad
	Charge (Q)	1 nC
micro pulse	Peak current ( $I_p$ )	> 95 A
	Pulse length ( $\sigma_t$ )	2-5 ps
	Repetition rate	$\frac{476}{n(=1,2,3,4,5)}$ MHz
	Pulse width	5-10 $\mu\text{s}$
macro pulse	Average current (I)	$\sim 300$ mA
	Repetition rate	20 Hz

## DESCRIPTION OF THE LINAC

As shown in Fig. 1, the Linac consists of a:

- 100 keV electron gun
- 476 MHz subharmonic standing wave pre-buncher
- 2856 MHz fundamental frequency traveling wave buncher
- two 2856 MHz fundamental frequency traveling wave accelerators

- set of solenoid focusing coil from the gun exit to the end of the first accelerator
- magnetic compressor (chicane)
- two beam transport systems

The triode gun can be driven by the grid for the pulsed mode. A 476 MHz signal during 10  $\mu\text{s}$  is carried to the HV deck. A frequency divider is used to control the repetition rate of the micro pulses. The electron gun pulser could offer the pulsed signal of up to 200 V/1 ns every 2, 4, 8, 16, or 32 ns. We expect to obtain micro pulses of 1-2 A/1 ns at the gun output. The operating mode of the electron gun is similar to the gun of the CLIO FEL [2, 3], while RF gated electron guns are adopted by the FELIX FEL [4, 5] and FHI FEL [6].

The pre-buncher will be a 20 cm long stainless steel re-entrant standing wave cavity operating at 476 MHz. With a gap voltage of 40 kV, the bunch length could be compressed by about 20 times in 24 cm long drift space downstream from the pre-buncher exit at the entrance of the buncher.

For further bunch length compression, a traveling wave buncher operating at 2856 MHz is used, which consists of an input coupler, 11 cells, and an output coupler. The phase velocities  $\beta_\phi$  of the first four cells are 0.63, 0.8, 0.915, and 0.958 respectively, and that of the rest of the cells is 1. With a 9 MV/m gradient (about 5 MW input power), the bunch length can be compressed to 4.5 ps (rms) and the beam energy is about 3.1 MeV at the exit of the buncher.

The two 2 meters long traveling wave accelerators are also operating at 2856 MHz, which consists of input and output couplers and 57 cells. Because of the high average current, the beam loading effect should be considered in the accelerators. As to our design structures, the acceleration gradient of the cells are shown in Fig. 2. When the beam current is 300 mA, one accelerator can offer about 30 MeV beam energy increase with 20 MW input power.

To improve the gain of the short wavelength radiation, a higher peak current bunch may be required. The chicane could be as a backup apparatus to obtain a shorter bunch. Because the peak current is above 100 A at the exit of A1, the magnetic compressor is not used normally.

The main functions of the beam transport systems are beam matching and beam energy filtering. Energy slits will be used in the dispersion section to filter out the electrons with great energy spread.

## BEAM DYNAMICS

The code PARMELA is used for beam dynamics simulation. The initial beam current and bunch length are 1.5 A and 1 ns respectively.

Figure 3 shows the simulated longitudinal distribution state and phase space of the electron bunch at the exit of the

\* Supported by National Natural Science Foundation of China (No. 21327901).

<sup>†</sup> Corresponding author, email: shancai@ustc.edu.cn

## THE STATUS OF CLARA, A NEW FEL TEST FACILITY

J. A. Clarke<sup>1</sup>, D. Angal-Kalinin<sup>1</sup>, P. A. Atkinson, N. Bliss, A. D. Brynes<sup>1</sup>, R. Buckley<sup>1</sup>, S. Buckley<sup>1</sup>, R. Cash, N. Collomb, L. Cowie<sup>1</sup>, G. Cox, G.P. Diakun<sup>1</sup>, S. Dobson, D.J. Dunning<sup>1</sup>, B.D. Fell, A. Gallagher, P. Goudket<sup>1</sup>, A.R. Goulden<sup>1</sup>, S. A. Griffiths, C. Hill, C. Hodgkinson, D.M.P. Holland<sup>1</sup>, P. C. Hornickel<sup>1</sup>, F. Jackson<sup>1</sup>, S.P. Jamison<sup>1</sup>, J.K. Jones<sup>1</sup>, T. J. Jones, K.B. Marinov<sup>1</sup>, B. Martlew, P.A. McIntosh<sup>1</sup>, J.W. McKenzie<sup>1</sup>, K.J. Middleman<sup>1</sup>, B.L. Milityn<sup>1</sup>, A.J. Moss<sup>1</sup>, B.D. Muratori<sup>1</sup>, M.D. Roper<sup>1</sup>, L.K. Rudge<sup>1</sup>, Y. Saveliev<sup>1</sup>, B. J. A. Shepherd<sup>1</sup>, E. Snedden<sup>1</sup>, R.J. Smith<sup>1</sup>, S.L. Smith<sup>1</sup>, M. Surman<sup>1</sup>, T. Thakker<sup>1</sup>, N.R. Thompson<sup>1</sup>, R. Valizadeh<sup>1</sup>, A.E. Wheelhouse<sup>1</sup>, J. Williams, P.H. Williams<sup>1</sup>, STFC Daresbury Laboratory, Sci-Tech Daresbury, Warrington, UK  
 R. Bartolini<sup>2</sup>, I. Martin, Diamond Light Source, Oxfordshire, UK  
 A. Kolano, University of Huddersfield, UK  
 G. Burt<sup>1</sup>, P. Ratoff<sup>1</sup>, University of Lancaster, UK  
 S. Spampinati<sup>1</sup>, C. Welsch<sup>1</sup>, Y. Wei<sup>1</sup>, A. Wolski<sup>1</sup>, University of Liverpool, UK  
 R.B. Appleby<sup>1</sup>, K. Hanahoe<sup>1</sup>, O. Mete<sup>1</sup>, H.L. Owen<sup>1</sup>, G. Xia<sup>1</sup>, University of Manchester, UK  
 S. Boogert, A. Lyapin, E. Yamakawa, John Adams Institute at Royal Holloway, University of London, UK  
 L. Campbell, A.J.T. Colin, J.R. Henderson, B. Hidding, B.W.J. McNeil, University of Strathclyde, UK  
 J. Smith, Tech-X UK Ltd, Daresbury Innovation Centre, Daresbury, UK  
 V.V. Paramonov, A. K. Skasyrskaya, Institute for Nuclear Research, Moscow, Russian Federation  
<sup>1</sup>Cockcroft Institute, Sci-Tech Daresbury, Warrington, UK  
<sup>2</sup>John Adams Institute, University of Oxford, UK

### Abstract

CLARA is a new FEL test facility being developed at STFC Daresbury Laboratory in the UK. The main motivation for CLARA is to test new FEL schemes that can later be implemented on existing and future short wavelength FELs. Particular focus will be on ultra-short pulse generation, pulse stability, and synchronisation with external sources. The project is now underway and the Front End section (photoinjector and first linac) installation will begin later this year. This paper will discuss the progress with the Front End assembly and also highlighting other topics which are currently receiving significant attention.

### INTRODUCTION

CLARA will be a dedicated FEL test facility in the UK, capable of testing new FEL schemes that have the capability to enhance the performance of short wavelength FELs worldwide. The primary focus of CLARA will be on ultrashort pulse generation, stability, and synchronisation. Enhancements in these three areas will have a significant impact on the experimental capabilities of FELs in the future.

The wavelength range chosen for the CLARA FEL is 400 – 100 nm, appropriate for the demonstration of advanced FEL concepts on a relatively low energy accelerator. Key drivers for this choice are the availability of suitable seed sources for interacting with the electron beam and the availability of single shot diagnostic techniques for the characterisation of the output. The

proposal is to study short pulse generation over the range 400 – 250 nm, where suitable nonlinear materials for single shot pulse profile characterisation are available. For schemes requiring only spectral characterisation (for example producing coherent higher harmonics of seed sources, or improving the spectral brightness of SASE) the operating wavelength range will be 266 – 100 nm. Generating these wavelengths will be readily achievable with the 250 MeV maximum energy of CLARA.

Since the Conceptual Design Report was published in 2013 [1] there has been significant progress in the overall design of the facility, with special attention paid to the Front End injection section (up to 50 MeV) and the FEL layout itself. The injection section is currently being procured and assembled offline and it will be installed in November 2015 with commissioning planned for April 2016. A schematic layout of the full facility is given in Fig. 1.

### FRONT END SECTION

The CLARA Front End includes the RF photoinjector, a 2 m long S-band linac, a straight ahead line into a temporary combined Faraday cup/beam dump and a dog-leg to transport the beam into the already operational VELA facility [2]. Initially the existing 2.5 cell S-band RF gun currently used at VELA will be used for the CLARA Front End [3]. This is limited to 10 Hz repetition rate, at bunch charges of up to 250 pC. The gun is fed with a 10 MW klystron with a power available for the gun of 8.5 MW. Maximum beam momentum measured at this

## PRESENT STATUS OF SOURCE DEVELOPMENT STATION AT UVSOR-III\*

Najmeh Sadat Mirian<sup>#</sup>, Jun-ichiro Yamazaki, Kenji Hayashi, Masahiro Katoh, UVSOR, Okazaki, Japan

Masahito Hosaka, Yoshifumi Takashima, Nagoya University, Nagoya, Japan

Naoto Yamamoto, Taro Konomi, KEK, Tsukuba, Japan

Heishun Zen, Kyoto University, Kyoto, Japan

### Abstract

Construction and development of a source development station are in progress at UVSOR-III, a 750 MeV electron storage ring. It is equipped with an optical klystron type undulator system, a mode lock Ti:Sa Laser system, a dedicated beam-line for visible-VUV radiation and a parasitic beam-line for THz radiation. New light port to extract edge radiation was constructed recently. An optical cavity for a resonator free electron laser is currently being reconstructed. Some experiments such as coherent THz radiation, coherent harmonic radiation, laser Compton Scattering gamma-rays and optical vortices are in progress.

### INTRODUCTION

UVSOR is a synchrotron light source, which was constructed in 1980's. Using a part of the ring, various light source technologies, such as resonator free electron laser [1] and its applications [2], coherent harmonic generation [3] and coherent synchrotron radiation via laser modulation [4], laser Compton scattering [5] have been developed. These research works had been carried out by parasitically using an undulator and a beam-line for photo-electron spectroscopy [6]. Under Quantum Beam Technology Program of MEXT in Japan, we started constructing a new experiment station dedicated for light source developments. FY2010, we created a new straight section by moving the injection line. FY2011, a new optical klystron was constructed and installed. FY2009-2010, the seed laser system was upgraded and moved to the new station. FY2011, two beam-lines dedicated for coherent light source development were constructed. In FY2012, another upgrade program for the storage ring was funded, in which all the bending magnets were replaced [7]. After this major upgrade, we started to call the machine UVSOR-III. Because we had to pay a lot of efforts for the machine conditioning, we have to slow-down the construction of the source development station for a few years. In FY2014, the mirror chambers of the optical cavity were installed. The experiments have started on coherent THz edge radiation, optical vortex beam, and laser Compton scattering gamma-rays. In this paper, we will report the most recent status of the source development station at UVSOR-III.

\*Some parts of this work were supported by JSPS KAKENHI Grant Number 26286081, 26390111 and MEXT Quantum Beam Technology Program.

<sup>#</sup>nsmirian@ims.ac.jp

### FACILITY STATUS

#### Accelerators

The recent view of UVSOR-III storage ring is shown in Fig. 1. The main parameters of the ring are listed in Table 1. The ring is normally operated at 750 MeV for synchrotron radiation users in multi-bunch mode. On the other hand, in many of the source development studies, the ring is operated at lower energy (600~500MeV) and in single bunch mode. The studies are carried out in dedicated beam times for machine studies. Usually every weekend and Monday can be used for machine studies. In addition, a few weeks a year are usually reserved for machine studies.

The electron beam is supplied by an injector which consists of a 15 MeV linear accelerator and a full energy booster synchrotron. Top-up operation is possible, even for the low energy single bunch operation.

Since the major upgrade in 2012, we have observed that the threshold current of the transverse single bunch instability was lowered. Currently we can accumulate around 50 mA in a single bunch, however, it is difficult to accumulate more. This problem is currently under investigation.

The source development station was constructed by utilizing one of 4m straight section in the ring. It is comprised of an optical klystron, an optical cavity, a seed laser system and beam-lines. The layout of the accelerator part is shown in Fig. 2.



Figure 1: Recent View of UVSOR-III Storage Ring and Synchrotron Radiation beam-lines.

## THE FERMI SEEDED FEL FACILITY: OPERATIONAL EXPERIENCE AND FUTURE PERSPECTIVES

Luca Giannessi\*, Enrico Allaria, Laura Badano, Filippo Bencivenga, Carlo Callegari, Flavio Capotondi, Davide Castronovo, Paolo Cinquegrana, Marcello Coreno, Riccardo Cucini, Ivan Cudin, Miltcho B. Danailov, Gerardo D'Auria, Raffaele De Monte, Giovanni De Ninno, Paolo Delgiusto, Alexander Demidovich, Simone Di Mitri, Bruno Diviacco, Alessandro Fabris, Riccardo Fabris, William M. Fawley, Mario Ferianis, Eugenio Ferrari, Paola Finetti, Paolo Furlan Radivo, Giulio Gaio, David Gauthier, Federico Gelmetti, Fatma Iazzourene, Maya Kiskinova, Stefano Krecic, Marco Lonza, Nicola Mahne, Michele Manfreda, Claudio Masciovecchio, Massimo Milloch, Fulvio Parmigiani, Giuseppe Penco, Lorenzo Pivetta, Oksana Plekan, Mauro Predonzani, Kevin Prince, Emiliano Principi, Emanuele Pedersoli, Lorenzo Raimondi, Primoz Rebernik Ribic, Fabio Rossi, Eléonore Roussel, Luca Rumiz, Claudio Scafuri, Claudio Serpico, Paolo Sigalotti, Michele Svandrlík, Cristian Svetina, Mauro Trovò, Alessandro Vascotto, Marco Veronese, Roberto Visintini, Dino Zangrando, Marco Zangrando Elettra, Trieste, Italy

### Abstract

FERMI is the seeded FEL user facility in Trieste, Italy, producing photons from the VUV to the soft X-rays with a high degree of coherence and spectral stability. Both FEL lines, FEL-1 and FEL-2, are available for users, down to the shortest wavelength of 4 nm. We report on the completion of the commissioning of the high energy FEL line, FEL-2, on the most recent progress obtained on FEL-1 and on the operational experience for users, in particular those requiring specific FEL configurations, such as two-colour experiments. We will also give a perspective on the improvements and upgrades which have been triggered based on our experience, aiming to maintain as well as to constantly improve the performance of the facility for our user community.

### INTRODUCTION

The distinguishing features that make the FERMI FEL facility [1-3] attractive for the scientific community are the wavelength tunability, the spectral stability, the high degree of longitudinal and transverse coherence with pulses close to the Fourier limit. The capability of providing pulses with different polarizations in various controllable configurations [4,5] and the availability of a synchronized user laser (IR &UV) with very low time jitter with respect to the FEL pulses [6], are other important and unique characteristics of FERMI.

FERMI FEL-1, the VUV to EUV line covering photon energies between 12 eV and 62 eV [2], has been operating for external users since December 2012. FEL-2, covering the EUV to soft X-rays photon energy range (62 eV to 310 eV) [3], reached in September 2014 the nominal energy per pulse of 10  $\mu$ J at the short-wavelength end of the spectral range (4 nm) [7] and is now also available for user experiments. In optimized conditions the spectral

quality and operating characteristics of FEL-1 and FEL-2 are similar, with the latter more critical in terms of tuneup and stability requirements. An upgrade program has been started to guarantee for FEL-2 the same robustness, reliability and flexibility of FEL-1.

Three beamlines, each one with its own experimental station, are open for users: Diffraction and Projection Imaging (DiProI) [8], Elastic and Inelastic Scattering TIMEX (EIS-TIMEX) [9], Low Density Matter (LDM) [10]. Three more will be available for users in 2016.

### FEL-2 COMMISSIONING RESULTS

In order to efficiently seed the electron beam at low wavelengths, FEL-2 is based on a double stage cascaded HGHG scheme. The external laser seeds the 1<sup>st</sup> stage that consists of a modulator and a radiator with two sections; the photon pulse generated in the 1<sup>st</sup> stage seeds the 2<sup>nd</sup> one, consisting of a second modulator and a radiator with six sections. The magnetic chicane after the 1<sup>st</sup> stage delays the electron beam with respect to the photon pulse, so that the latter overlaps with fresh electrons.

First lasing of FEL-2 was successfully demonstrated in October 2012 at 14.4 nm and 10.8 nm [3]. The performance of FEL-2 was extended to progressively shorter wavelengths and optimized during the following commissioning periods. In September 2014 specified operating conditions were attained at the lower end of the nominal wavelength interval of FEL-2, namely 4.0 nm [7]. These performances were confirmed in March 2015. These results were achieved after an accurate machine optimization, by setting the peak bunch current to 700 A and the beam energy at 1.5 GeV, by keeping the emittance around 1.5 mm mrad for a properly matched beam at the undulator entrance and by an accurate control of the beam transport along the undulators. The main parameters of FEL-2 are listed in Table 1.

\*luca.giannessi@elettra.eu

# STATUS OF THE SOFT X-RAY USER FACILITY FLASH

K. Honkavaara\*, B. Faatz, J. Feldhaus, S. Schreiber, R. Treusch, M. Vogt  
DESY, Hamburg, Germany<sup>†</sup>

## Abstract

Since 10 years FLASH at DESY (Hamburg, Germany) has provided high brilliance FEL radiation at XUV and soft x-ray wavelengths for user experiments. Recently FLASH has been upgraded with a second undulator beamline, FLASH2, whose commissioning takes place parallel to user operation at FLASH1. This paper summarizes the performance of the FLASH facility during the last user period from January 2014 to April 2015.

## INTRODUCTION

Since summer 2005, FLASH [1–4], the free-electron laser (FEL) user facility at DESY (Hamburg), has delivered high brilliance XUV and soft X-ray FEL radiation for photon experiments. In order to fulfill the continuously increasing demands on the beam time and on the photon beam properties, FLASH is now upgraded with a second undulator beamline (FLASH2), being the first FEL facility worldwide operating simultaneously two undulator lines. The first lasing of FLASH2 was achieved in August 2014 [5]. A brief history of FLASH from a superconducting accelerator technology test facility [6] to a soft x-ray FEL user facility can be found in [3] and references therein.

Figure 1 shows an aerial view of the north side of the DESY area in summer 2014. The FLASH facility with its two experimental halls is in the middle: the FLASH1 hall (recently named as "Albert Einstein") is on the right, the new FLASH2 hall ("Kai Siegbahn") on the left. Next to FLASH are the experimental hall of the PETRA III synchrotron light source (left) and the construction site of PETRA III extension (right).



Figure 1: Aerial view of the FLASH facility. The FLASH1 experimental hall is on the right, the new FLASH2 hall on the left.

\* katja.honkavaara@desy.de

<sup>†</sup> for the FLASH team

This paper reports the status of the FLASH facility and its performance during the 5<sup>th</sup> user period in 2014/15. Part of this material has presented also in previous conferences, most recently in [4].

## FLASH FACILITY

Up to 800  $\mu$ s long trains of high quality electron bunches are generated by an RF-gun based photoinjector. An exchangeable Cs<sub>2</sub>Te photocathode [7] is installed on the backplane of the normal conducting RF-gun. The photocathode laser system has two independent lasers, a third one is in the commissioning phase [8]. The bunch train repetition rate is 10 Hz, and different discrete bunch spacings between 1  $\mu$ s (1 MHz) and 25  $\mu$ s (40 kHz) are possible.

A linac consisting of seven superconducting TESLA type 1.3 GHz accelerating modules accelerates the electron beam up to 1.25 GeV. The linearization of the energy chirp in the longitudinal phase space is realized by a module with four 3.9 GHz (third harmonic of 1.3 GHz) superconducting cavities downstream the first accelerating module. The RF-gun and the accelerator modules are regulated by a sophisticated MTCA.4 based low level RF (LLRF) system [9, 10]. The electron beam peak current of the order of a few kAs is achieved by compressing the electron bunches by two magnetic chicane bunch compressors at beam energies of 150 MeV and 450 MeV, respectively.

The use of superconducting technology allows operation with long RF-pulses, i.e. with long electron bunch trains. The bunch train can be shared between the two undulator lines, allowing to serve simultaneously two photon experiments, one at FLASH1 and the other at FLASH2, both at 10 Hz pulse train repetition rate. The separation of the two bunch trains is realized by using a kicker-septum system downstream the last accelerating module.

The production of FEL radiation, both at FLASH1 and FLASH2, is based on the SASE (Self Amplified Spontaneous Emission) process. FLASH1 has six 4.5 m long fixed gap (12 mm) undulator modules, FLASH2 twelve 2.5 m long variable gap undulators. Later, FLASH2 can be upgraded with hardware allowing a seeded operation. A planar electromagnetic undulator, installed downstream of the FLASH1 SASE undulators, provides, on request, THz radiation for user experiments. A place for a THz undulator is available also at FLASH2.

A schematic layout of the FLASH facility is shown in Fig. 2. More details of the FLASH facility and its subsystems can be found, for example, in [3, 4], and references therein. Photon beamlines and photon diagnostics are described in [2, 11, 12].

# STATUS OF THE FABRICATION OF PAL-XFEL MAGNET POWER SUPPLIES\*

Seong Hun Jeong<sup>#</sup>, Ki-Hyeon Park, Hyung Suck Suh, Sang-Bong Lee, Bongi Oh, Young-Gyu Jung, Hong-Gi Lee, Dong Eon Kim, Heung-Sik Kang, In Soo Ko  
PAL, Pohang, Republic of Korea

## Abstract

The PAL-XFEL has been constructing including a 10 GeV linac, hard X-ray and soft X-ray beam lines. The PAL-XFEL required for about six hundreds of magnet power supply (MPS). The nine different prototypes of MPS are developing to confirm the performance, functions, size, heat load and so on. This paper describes the test results of the prototype MPS in major specifications. All MPSs have to be installed until the end of September in 2015. The installation progress of the MPS was also described.

## INTRODUCTION

The PAL-XFEL accelerator needs many kinds of power supplies for different magnet types. Table 1 shows the specifications of the power supplies needed for the PAL-XFEL.

The MPS for corrector magnets are divided into 4 families based on the current rating and stability, 10 A 10 ppm, 10 A 50 ppm, 12 A 10 ppm and 12A 50 ppm.

The MPSs for the dipole and quadrupole were categorized into two types, unipolar and bipolar. And it was grouped to five types according to its current ratings.

Table 1: MPS Specifications

Magnet	MPS type	Qty	Stability (ppm)
Corrector	Digital	395	10 & 50
Quadrupole	Unipolar	122	100
	Bipolar	86	
Dipole	Unipolar	20	20
	Bipolar	2	
Solenoid	Bipolar	3	20

## BASIC STRUCTURE

The configuration of the designed MPS was similar with others [1]. The input stage consisted of transformer, full rectifier and a damped low pass filter. The commercial switching mode power supply (SMPS) was often adopted for low power less than 400 W instead. Transformer connection was one of delta or wye windings or sometimes both of them where high stability was required. The low pass filter at the input stage should be needed. Figure 1 shows the general hardware configuration of the MPS.

The topology of the power convertor was either buck

for unipolar or H- or half-bridge for bipolar. The output stage was composed of a low pass filter to reduce the switching noise. The output filter composed of two stage LC filters where the pole of the first stage was about ~KHz and second one was between higher than one-half and full of the switching frequency.

The DSP TMS320F28335 from TI Co was used to control the duty of the PWM and to interface surrounding peripherals. It has six enhanced PWM modules with 150 ps micro edge positioning (MEP) technology [2]. Thus effective PWM resolutions can be increased up to about 18-bit in case of switching frequency of 25 KHz. Without MEP, the normal PWM resolution is about 12-bit, which can't offer the sufficient resolution for the high stability.

The power supply performs the Ethernet communication by the single chip WEB server. The WEB server exchanges all power supply data via RS232 connection with the FPGA.

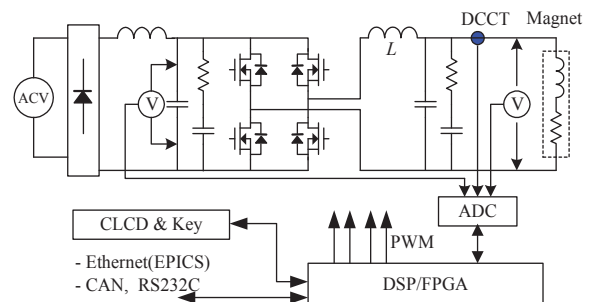


Figure 1: Block diagram of the buck type magnet power supply.

## CONTROL SCHEME

The control loops for the developed MPS are given in Fig. 2. A cascaded current and voltage feedback loop was applied to the MPS compensator [3]. The inner voltage loop worked to reject the voltage fluctuation of the output stage. The voltage loop has a small time constant comparing to outer current loop. Thus it can be shown as constant by the outer loop.

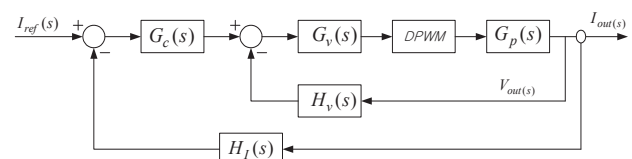


Figure 2: Block diagram of complete current loop system.

The current and voltage compensators were applied a proportional-integral (PI) type which was very common

# BEAM COMMISSIONING PLAN FOR THE SwissFEL HARD-X-RAY FACILITY

T. Schietinger on behalf of the SwissFEL team,  
Paul Scherrer Institut, CH-5232 Villigen PSI, Switzerland

## Abstract

The SwissFEL facility currently being assembled at the Paul Scherrer Institute is designed to provide FEL radiation in the photon wavelength range between 0.1 and 7 nm. The commissioning of the first phase, comprising the electron injector, the main electron linear accelerator and the first undulator line, named Aramis and dedicated to the production of hard X-rays, is planned for the years 2016 and 2017. We present an overview of the beam commissioning plan elaborated in accordance with the installation schedule to bring into operation the various subsystems and establish beam parameters compatible with first pilot user experiments in late 2017.

## INTRODUCTION

SwissFEL is an X-ray Free-Electron-Laser facility under construction at the Paul Scherrer Institute (PSI) in Switzerland [1]. Its two undulator lines, named Aramis and Athos, are designed to deliver hard X-rays in the wavelength range between 0.1 and 0.7 nm and soft X-rays between 1 and 7 nm, respectively. Figure 1 shows a schematic overview of the facility, annotated with relevant machine and beam parameters. In a first phase, only the Aramis beamline will be realized, with Athos to be completed in a second phase, currently foreseen for the period 2018–20. After an extensive design and development phase, including beam development work [2] and component tests [3] at a dedicated injector test facility [4], the SwissFEL-Aramis facility is currently in the installation phase, with first beam commissioning scheduled for early 2016. The commissioning phase is foreseen to extend over two years, with installation activities continuing in parallel or in between. First pilot user experiments are expected for late 2017.

We give an overview of the various commissioning steps. While the sequence of commissioning tasks will remain the same apart from further refinements or small rearrangements due to possible changes, the dates are subject to change depending on the overall progress of component delivery and installation. The SwissFEL commissioning plan is part of a global project plan (dubbed Planning-Installation-Commissioning, or PIC, plan), which ensures the overall consistency of the project schedule taking into account all dependencies. It is updated on a regular basis reflecting progress achieved on building construction, component delivery and installation. The dates presented here have been derived from the latest PIC plan update (July 2015).

## COMMISSIONING OVERVIEW

The SwissFEL commissioning, up to the end of the first project phase, can be split into three phases: the injector phase (first acceleration stage, up to a beam energy of 320 MeV), the linac phase (transmission through the full accelerator and undulator line, but no intentional generation of X-rays yet) and the FEL phase (final phase with X-rays from the undulators). The SwissFEL commissioning objectives have been formulated in terms of a set of milestones, specifying electron beam energy and bunch charge, repetition rate, and photon wavelength and pulse energy to be achieved for three specific dates, see Table 1.

The start of beam development activities is usually dictated by the installation and start-up schedule of the necessary infrastructure. In particular in the later stages of commissioning, progress towards reaching the final beam energy, and thus the final photon wavelength, will be driven entirely by the deployment schedule of the RF stations powering the main linac.

The special location of SwissFEL in a freely accessible forest outside the PSI site requires particular consideration to radiation issues. As a consequence, every commissioning step involving a significant change in beam parameters is followed by extensive radiation mappings of the building and the surrounding areas.

The commissioning work will be performed in eight-hour shifts, following the existing PSI shift schedule for simplicity. Due to the limited manpower available, only two shifts per work day will be staffed, with the third shift (during the night) being used for long-term stability tests and the like. On weekends it is foreseen to staff one shift per day on average. Shift crews will consist of a shift leader (typically a beam dynamics expert) a shift expert (from a PSI expert group, such as diagnostics, RF, controls etc., but also beam dynamics, depending on the specific commissioning task or issue), and, as far as available, a member of the PSI operation section. For all the critical hardware systems, on-call services will be maintained by the expert groups. The absence of scheduled, dedicated night shifts considerably simplifies both the organizational aspects of shift work and the associated formal approval procedure.

The numbers of shifts needed during each commissioning phase to reach the milestones have been estimated as 155 for injector commissioning, 135 for linac commissioning and 204 for FEL commissioning. In addition, some 28 weeks are needed for the commissioning of the photonics infrastructure in the optical and experimental hutches.

ISBN 978-3-95450-134-2

# COMPARISON OF ASTRA SIMULATIONS WITH BEAM PARAMETER MEASUREMENTS AT THE KAERI ULTRASHORT PULSE FACILITY

H. W. Kim<sup>#,1,2</sup>, K. H. Jang<sup>1,2</sup>, Y. U. Jeong<sup>1,2</sup>, Y. Kim<sup>1,2</sup>, K. Lee<sup>1,2</sup>, S. H. Park<sup>1,2</sup>,  
N. Vinokurov<sup>1,2,3</sup>, S. V. Miginsky<sup>1,2,3</sup>,

I. Baek<sup>1</sup>, M. Chae<sup>1</sup>, B. Gudkov<sup>1</sup>, B. Han<sup>1</sup>, S. Park<sup>1</sup>, S. Setiniyaz<sup>1</sup>

<sup>1</sup>KAERI, Daejeon, Republic of Korea

<sup>2</sup>UST Accelerator and Nuclear fusion physics engineering, Daejeon, Republic of Korea

<sup>3</sup>Budker INP SB RAS, Novosibirsk, Russia

## Abstract

An RF-photogun-based Linear accelerator for ultrashort electron beam generation is under construction at Korea Atomic Energy Research Institute (KAERI) [1]. This facility are mainly composed of an 1.5 cell S-band (2.856 GHz) RF gun, a travelling wave type linac 3m long and 90-degree achromatic bends.

We have performed computer simulation using ASTRA code to investigate the electron beam dynamics in the system with the input data of bead tested gun electric field distribution and the magnetic fields of the magnets [2]. We will present the simulated and experimental electron beam parameters.

## INTRODUCTION

Ultrafast electron diffraction (UED) [3-7] are powerful tools for the study of the time-resolved molecular structure and material science. The UED can reveal inter-nuclear coordinates with high temporal and spatial resolution, therefore observing a change of structure on ultrafast time scale with milliangstrom accuracy.

Figure 1 shows the schematics of experimental setup for relativistic UED at KAERI. The UED beamline is designed to provide electron beams with low emittance and ultrashort pulses. The emitted electron beams are accelerated in high RF field to  $\sim 3$  MeV. The electron beams can be deflected by a first bending magnet installed right after the RF gun. Each beamline has second bending magnet similar to the first one and three quadrupole magnets between the bending magnets. Two bending and three quadrupole magnets compose the 90-degree achromatic bend. The deflected electron beams will be used for UED experiments.

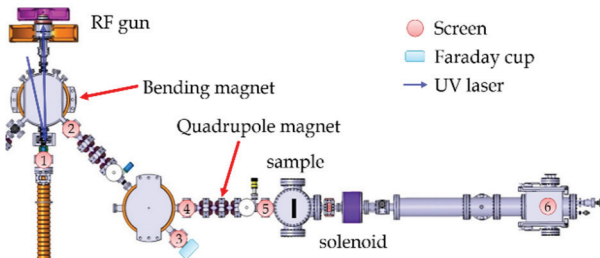


Figure 1: Schematic diagram of UED beamline at the KAERI and experimental setup.

We measured field distributions of all components and we simulated beam dynamics using measured field distributions.

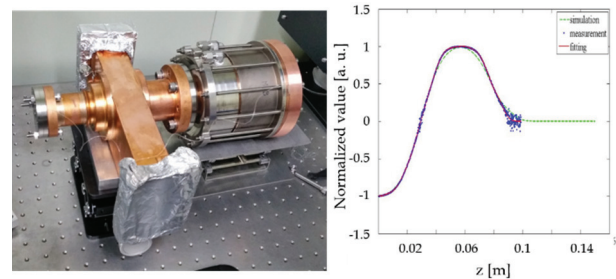


Figure 2: Photo of experimental setup for bead test and measured field distribution.

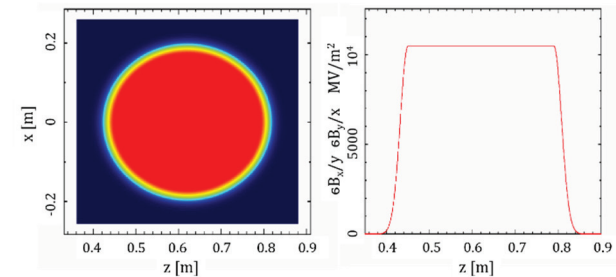


Figure 3: Magnetic field distribution of the 45-degree bending magnet.

Figure 2 shows experimental setup for bead test (left) and measurement data. The RF photogun has a coaxial coupler, which provide axisymmetric accelerating field.

Figure 3 shows magnetic field distribution of a 45-degree bending magnet. The shape of bending magnet is round which has horizontal focusing properties and simplifies alignment because of input and output directions cross in the centroid of the magnet. To achromaticity and isochronism UED beamline contains a second 45-degree bending magnet and three quadrupole lenses. The quadrupole lenses have square yoke (see Fig. 4). The manufacturing and assembly have been simplified.

We have performed computer simulation using ASTRA code to investigate the electron beam dynamics in the system with the measured field data.

# LCLS-II INJECTOR BEAMLINE DESIGN AND RF COUPLER CORRECTION\*

F. Zhou<sup>#</sup>, D. H. Dowell, R.K. Li, T. O. Raubenheimer, J. F. Schmerge, SLAC, Stanford, CA 94309, USA

C. Mitchell, C. Papadopoulos, F. Sannibale, LBNL, Berkeley, CA 94720, USA  
 A. Vivoli, FNAL, Batavia, IL 60510, USA

## Abstract

LCLS-II CW injector beamline consists of a 186 MHz normal conducting (NC) RF gun for beam generation and acceleration to 750 keV, two solenoids for the beam focusing, two BPMs, 1.3 GHz NC RF buncher for bunch compression down to 3-4 ps rms, 1.3 GHz superconducting standard 8-cavity cryomodule to boost beam energy to about 98 MeV. The beamline is being optimized to accommodate all essential components and maximize beam quality. The beamline layouts and beam dynamics are presented and compared. The 3D RF field perturbation due to cavity couplers where the beam energy is very low (<1 MeV) causes significant emittance growth especially for a large-size beam. A theory of rotated fields predicted and simulations verified using a weak skew quadrupole located even a significant distance from the perturbation can completely eliminate the emittance growth. A layout for future upgrade is developed. The results are presented and analysed.

## INTRODUCTION

LCLS-II [1] currently under construction at SLAC National Accelerator Laboratory is a continuous wave (CW) x-ray free electron laser (FEL) user facility driven by a 4 GeV superconducting linac. To meet with the x-ray FEL requirements, the LCLS-II injector must simultaneously deliver high repetition rate up to 1 MHz and high brightness electron beam with normalized emittance of <0.4  $\mu\text{m}$  at nominal 100 pC/bunch and peak current 12 A [2-3]. The major beam requirements for LCLS-II injector are summarized, as presented in Table 1.

Table 1: Major LCLS-II Injector Beam Requirements

Parameters	Nominal
RF gun energy (keV)	750
Electron energy (MeV)	98
Bunch repetition rate (MHz)	0.62 (0.93 max)
Nominal/max bunch charge (pC)	100/300
Peak current for 100/300 pC (A)	12/30
Nominal average current (mA)	0.062
Slice emittance for 100/300 pC ( $\mu\text{m}$ )	0.4/0.6
Bunch length for 100/300 pC (mm)	1/1.4
Slice energy spread 100/300 pC (keV)	1/5
Cathode QE lifetime	0.5%
Dark current (nA)	<400

\*The work is supported by DOE under grant No. DE-AC02-76SF00515.  
<sup>#</sup> zhoufeng@slac.stanford.edu

The proposed full LCLS-II CW injector consists of a CW RF gun operating at 186 MHz (7<sup>th</sup> sub-harmonic of 1.3 GHz for superconducting linac) for beam generation and acceleration, two solenoids for the beam focusing and emittance compensation, two BPMs for measurements of beam positions and bunch charge, 1.3 GHz 2-cell RF buncher for the bunch compression down to 3-4 ps rms from 10-15 ps rms, beam current diagnostic ICT, a standard 1.3 GHz superconducting 8-cavity cryomodule (CM) to boost beam energy from <1 MeV to 98 MeV, laser heater for suppression of micro-bunching instability, beam collimation systems and a dedicated diagnostic section. Figure 1 shows the schematic layout of the full LCLS-II injector. As the electron beam emittance and bunch length have been frozen at the CM end, the interest of this paper only focuses on the front part of the injector from the cathode to the CM end. This paper only discusses the beam dynamics issues. Technical details of the CW RF gun and cathode/laser performance are described elsewhere [4-5].

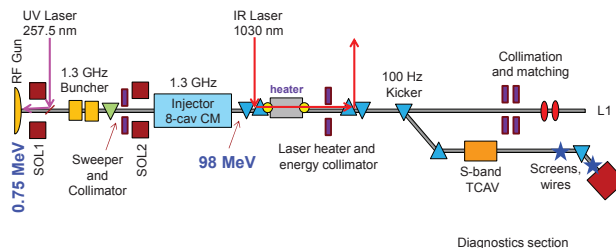


Figure 1: Schematic of the full LCLS-II injector. The front part of the injector discussed in this paper starts from the cathode to the CM end; downstream of the CM includes laser heater system, collimation systems and a dedicated beam diagnostics beamline.

## INJECTOR BEAMLINE DEVELOPMENTS

The injector front beamline (called injector for simplification) is being optimized since the conceptual design report (CDR) of the LCLS-II project launched in summer 2013. The LCLS-II injector beamline is required:

- To accommodate essential beam components and diagnostics, and adapt to the standard 8-cavity CM.
- To maximize electron beam performance in 6-d phase spaces.
- To make large half physical aperture for beam pipe, >4 times rms beam size to avoid the CW electron beam loss.

For the CDR, the distance from the 2<sup>nd</sup> solenoid (SOL2) to the 1<sup>st</sup> cavity (CAV1) of the 8-cavity CM was about 1

## STATUS, PLANS AND RECENT RESULTS FROM THE APEX PROJECT AT LBNL\*

F. Sannibale, K.M. Baptiste, C.W. Cork, S. De Santis, M. Dickinson, L. Doolittle, J. Doyle, J. Feng, D. Filippetto, G. Harris, G. Huang, M. J. Johnson, M. Jones, T. D. Kramasz, S. Kwiatowski, D. Leitner, R. Lellinger, C.E. Mitchell, V. Moroz, E. Norum, H.A. Padmore, G.J. Portmann, H. Qian, J.W. Staples, D.L. Syversrud, M. Vinco, S. Virostek, R. Wells, M. Zolotorev, Lawrence Berkeley National Laboratory, Berkeley, CA 94720, USA  
R. Huang, NSRL, University of Science and Technology of China, Hefei, Anhui, 230029, China

### Abstract

The Advanced Photo-injector EXperiment (APEX) at the Lawrence Berkeley National Laboratory (LBNL) is dedicated to the demonstration of the capability of an electron injector based on the VHF-gun, the new concept RF gun developed at LBNL, of delivering the beam quality required by MHz-class repetition rate X-Ray free electron lasers. Project status, plans, and recent results are presented.

### INTRODUCTION

APEX, the Advanced Photo-injector EXperiment at the Lawrence Berkeley National Laboratory (LBNL) is dedicated to the development and test of an injector based on the VHF-Gun [1-3], a new concept high repetition rate high-brightness electron gun. The successful development of such an injector will critically impact the performance of future 4th generation light sources when MHz-class repetition rates are required. In particular, the baseline of the SLAC LCLS-II project [4] includes an injector based on such a gun.

The VHF-Gun is a normal-conducting continuous wave (CW) RF gun where electrons are generated by laser-induced photo-emission on high quantum efficiency (QE) cathodes and accelerated up to the nominal energy of 750 keV. The gun cavity resonates at 186 MHz, the 7<sup>th</sup> sub-harmonic of 1.3 GHz or the 8<sup>th</sup> sub-harmonic of 1.5 GHz, the two dominant superconducting linac technologies. The low frequency makes the resonator size large enough to lower the power density on the cavity walls at a level that conventional cooling techniques can be used to run in CW mode, while maintaining the high accelerating fields required for the high brightness performance. A second advantage of the low frequency is the long wavelength that allows for large apertures on the cavity walls with negligible field distortion. Such apertures provide the vacuum conductance necessary to achieve the low pressures required to operate the sensitive QE cathodes with acceptable lifetime. A last advantage of such a scheme is that it is based on mature and reliable RF and mechanical technology, an important characteristic to achieve the reliability required to operate in a user facility.

The APEX project was initiated at the end of 2009 and

\* Work supported by the Director of the Office of Science of the US Department of Energy under Contract no. DEAC02-05CH11231

was organized in 3 stages (Phase 0, I and II), with the first two (now completed) dedicated to the development and testing of the gun, cathode testing and electron beam characterization at the gun energy. In Phase II, presently in its very final installation phase, a buncher and a linac are added to the VHF-Gun to compress and accelerate the beam up to 20-30 MeV reducing space charge forces in order to perform a reliable characterization of the gun/injector brightness and compression performance.

The commissioning of the VHF-Gun and the demonstration of all its major design goals are reported elsewhere [5], here we concentrate on the status of the installation of Phase-II of APEX and on the more recent commissioning results.

### PHASE-II DESCRIPTION

Figure 1 shows the CAD layout of APEX Phase-II. The vacuum loadlock that allows replacing the reactive high quantum efficiency (QE) without breaking vacuum, and the VHF-Gun are visible in the left-bottom corner of the figure.

In Phase-II a 1.3 GHz CW buncher is inserted downstream the gun followed by a linac composed by three 1.3 GHz pulsed accelerating section. A suite of beam diagnostics systems capable of 6D beam phase-space characterization completes the accelerator layout.

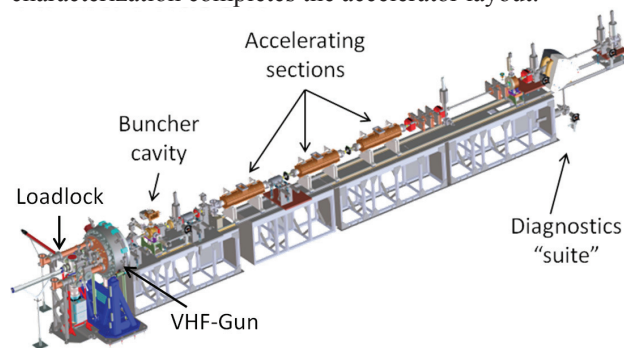


Figure 1: APEX Phase-II Layout.

The buncher, shown in Fig. 2, uses a two-cell design optimized for high shunt impedance and for being multipacting free over the whole range of power [6]. The main parameters for the buncher are shown in Table 1. The RF power is fed in each cell by two coaxial couplers terminated with a loop that couples the magnetic field in the cell. Two additional flanges in each of the cells are

# ELECTRON BEAM PROPERTIES FROM A COMPACT SEEDED TERAHERTZ FEL AMPLIFIER AT KYOTO UNIVERSITY

K. Damminsek<sup>#</sup>, S. Rimjaem, C. Thongbai

Plasma and Beam Physics (PBP) Research Facility, Department of Physics and Materials Science,  
Faculty of Science, Chiang Mai University, Chiang Mai 50200 Thailand

S. Suphakul, H. Ohgaki, H. Zen

Institute of Advanced Energy, Kyoto University, Gokasho, Uji, Kyoto 611-0011 Japan

## Abstract

A compact seeded Terahertz FEL amplifier is started construction at the Institute of Advanced Energy, Kyoto University, Japan. The system consists of a 1.6 cell BNL type S-Band photocathode RF-gun, a magnetic bunch compressor in form of a chicane, triplet quadrupole magnets and a short planar undulator. Electron beams from the photocathode

RF-gun were measured and compared with the RARMELA simulation results. Numerical and experimental studies on the contribution of the space charge effect were carried out. By using the RF power of 9 MW, the RF phase of 40 degree, the laser pulse energy of 20  $\mu$ J and the solenoid magnet current of 135 A, the electron beam with a bunch charge of 50 pC, a beam energy of around 5 MeV and an RMS emittance of 6-8 mm-mrad was achieved.

## INTRODUCTION

The Institute of Advanced Energy has developed the compact seeded THz-FEL (IR-FEL) amplifier [1]. The system was designed to be simple, compact and economical aimed to use in scientific researches. The system consists of a 1.6 cell BNL type S-Band photocathode RF-gun, a magnetic bunch compressor in form of a chicane, triplet quadrupole magnets and a short planar undulator. The photocathode RF gun succeeded to generate the first beam in May, 2015. The electron beam properties, i.e. a bunch charge, a beam energy and a transverse beam emittance from the photocathode RF gun were measured. These electron beam properties are compared with the simulation results using the program PARMELA [2] to check the system. Since the energy of the electron beam would be low, around 5 MeV, the space charge effect should affect the beam properties strongly and it might be difficult to obtain a short bunch beam to generate intense THz radiation. Therefore, the study on the beam properties from the RF gun is crucial both by experiment and by simulation.

The 1.6 cell BNL type S-Band photocathode RF-gun has been developed at KEK [3]. The gun has two cavities, the first cavity is a half-cell type and the second cavity is a full-cell type. The photocathode of the RF-gun is the copper one during this study. A high power microwave transported from a 10 MW klystron, travels through a

waveguide, which is connected at the upper wall of the second cavity. The microwave is fed into the first cavity via the central iris between two cavities. The effective length of half-cell and full-cell are 3.4135 cm and 9.0405 cm, respectively. The microwave has a pulse duration of 2  $\mu$ s with a maximum macro-pulse repetition rate of 10 Hz. The photocathode drive laser consists of a mode-locked Nd:YVO<sub>4</sub> laser (GE-100-VAN-89.25 MHz-CLX-Flexible AOM, Time-Bandwidth), two amplifiers, beam position stabilizers and SHG-FHG [4]. The laser wavelength is 266 nm with a pulse duration of 8 ps at FWHM. The repetition rate of the injected laser is one thirty second of the RF frequency (89.25 MHz), which is defined by mode-lock frequency and designed to synchronize the cavity frequency of the MIR-FEL system. This is because the laser system is also used for the photocathode mode operation of the existing S-band linac [4]. A solenoid magnetic field is used to compensate a very strong space-charge effect on the electron beam. The limitation of the power supply used for the solenoid magnet is 200 A with a solenoid field around 300 mT. Beside the experiments, numerical simulations using the program PARMELA were performed to study the electron motion in the RF gun as well as to investigate accelerated electron beam properties which are charge, energy, energy spread, emittance and pulse width.

## METHODOLOGY

To investigate a transverse profile, dark current and bunch charge of the electron beam produced from the photocathode RF-gun of a compact seeded terahertz FEL amplifier, we used a fluorescence screen, a CCD camera, an electron exaction window and a Faraday cup as shown in Fig. 1(left). The typical Faraday cup signal of the electron charge measurement is shown in Fig. 1(right). Unfortunately, we did not have enough time to prepare in vacuum measurement. Thus, the charge measurement was performed in air. The photoelectron beams hit the exaction window inside a vacuum chamber. The window made of copper with a thickness of 0.2 mm. The energy loss of electron at the copper window is calculated to be 230 keV at the kinetic energy of the beam of 4.5 MeV [5]. An emitted electron beam from the copper window traveled in the air, then, it is observed by using the Faraday cup. The cup itself is made of graphite for absorbing the electron beam by using the in air measurement technique. The electron bunch charge is obtained by using an Eq. 1:

<sup>#</sup> kantaphon.damminsek@gmail.com

# PAL XFEL PULSE MODULATOR SYSTEM TEST RESULTS USING A HIGH PRECISION CCPS\*

S.H. Kim<sup>#1</sup>, S.S. Park<sup>1</sup>, S.J. Kwon<sup>1</sup>, Y.J. Park<sup>1</sup>, G.H. Kim<sup>1</sup>, H.S. Lee<sup>1</sup>, H.S. Kang<sup>1</sup>, I.S. Ko<sup>1</sup>,  
M.H. Cho<sup>1</sup>, D.S. Kim<sup>2</sup>, S.Y. Lee<sup>2</sup>, M.H. Seo<sup>2</sup>, H.S. Shin<sup>3</sup>, K.Y. Jang<sup>3</sup>

<sup>1</sup>Pohang Accelerator Laboratory, Pohang City, Kyungbuk 790-784, Korea

<sup>2</sup>Dawonsy cop., Siheung City, Kyunki 429-850, Korea

<sup>3</sup>POSCO ICT, Seongnam City, Kyunki 463-400, Korea

## Abstract

PAL XFEL is supposed to install 51 units of the pulse modulator power supplies for a 10-GeV linear accelerator using S-band (2856 MHz) cavities. The requirements of the modulator stability really become very tight. The stability on beam voltage is required to be less than 50 ppm. In order to obtain the high precision stability from the modulator system, we have newly produced a capacitor charging power supply (CCPS) and obtained the target stability with 10 ppm (STD) accuracy from measuring PFN (Pulse Forming Network). The CCPS generates a maximum output voltage of 50 kV at average current of 2.4 A with 4 units of the CCPS. The modulator peak output capacity is 400 kV, 500 A and 7.5  $\mu$ s at a pulse repetition rate of 60 pps using CCPS, a modified type-E PFN, and a pulse transformer. In this paper, the test results of the modulator system will be described.

## INTRODUCTION

In order to obtain the energy of 10 GeV from PAL XFEL, We are expecting to employ 51 units of pulse modulators with matching klystrons. Among the 51 units, s-band types are fifty units, and x-band type is one. The requirements of a beam voltage stability and RF phase stability are 0.005% (std) and 0.1 degree (std), respectively. The high precision CCPS has been employed to meet the requirement for the modulator stability. We are supposed to use three types of klystrons: an equal number of modulators with 48 of the s-band 80 MW klystrons, two of the s-band 25 MW klystrons, and one of the x-band klystron.

## MODULATOR SYSTEM

51 units of the pulse modulator power supplies will be installed for a 10-GeV linear accelerator until the end of September this year. There are three types of klystrons: the s-band 80 MW, 25 MW klystrons, and the x-band 50 MW klystron.

### Klystron Tube

The performance parameters of the s-band Toshiba E37320 klystrons and XL4 klystron are shown in the tables below. The XL4, x-band klystron, is used to power x-band structures of PAL XFEL for beam phase space linearization.

\*Work supported by the Korean Ministry of Education  
#ksangh@postech.ac.kr

Table 1: S-band Klystron Specifications

Description	Unit	Value
Frequency	MHz	2,856
Peak output RF power	MW	80
RF pulse	$\mu$ s	4
Cathode voltage (Vk)	kV	400
Beam current (Ik)	A	500
$\mu$ -perveance		1.85~2.0
Repetition rate (Max)	Hz	60

Table 2: X-band Klystron Specifications

Description	Unit	Value
Frequency	GHz	11,424
Peak output RF power	MW	50
RF pulse	$\mu$ s	2
Cathode voltage (Vk)	kV	450
Beam current (Ik)	A	360
$\mu$ -perveance		1.2
Repetition rate (Max)	Hz	120

### Modulator

The specifications of the PAL XFEL modulator are output power of 200 MW, beam voltage of 400 kV, beam current of 500 A, pulse width of 7.5  $\mu$ s and repetition rate of 60 Hz. Table 3 summarizes the specifications of the modulator.

Table 3: Modulator Specifications

Description	Unit	Value
Peak power	MW	200
Average charging power	kW	120
Repetition rate (normal)	Hz	60
Pulse peak output voltage	kV	400
Pulse peak output current	A	500
PFN voltage stability (rms)	ppm	< 10
Flat-top width	$\mu$ s	4.0

Figure 1 shows the simplified circuit diagram of the PAL XFEL modulator. In order to charge to PFN capacitor, CCPS are used, which are newly produced by

# STUDY OF SMITH-PURCELL FREE ELECTRON LASER USING ELECTRON BUNCH PRODUCED BY MICRO-PULSE ELECTRON GUN

Jifei Zhao\*, Deyu Yang, Ziqin Yang, Weiwei Tan, Yujia Yang, Xiangyang Lu†  
 Institute of Heavy Ion Physics, Peking University, Beijing100871, China

## Abstract

A Micro-Pulse electron Gun (MPG) with the frequency of 2856 MHz has been designed, constructed and tested. Some primary experimental studies have been carried out and electron beam with the average current of 18 mA has been detected which holds promise to use as an electron source of Smith-Purcell Free Electron Laser (SP-FEL) to produced Coherent Radiation. It is well known that Smith-Purcell radiation is one of the achievable ways to produce FEL. After many years study in theory and experiment, lots of new mechanisms and appearances have been discovered. Coherent Smith-Purcell Radiation was discovered in 1990s as well. Obviously, MPG is one of ideal electron sources of CSPR for that S-band electron source can increase energy density and produce frequency-locked SP radiation at these frequencies. And this will be displayed in the simulation of this article.

## INTRODUCTION

Since the multipacting effect was firstly discovered by Farnsworth in 1934[1], it has been deeply investigated in many areas, such as RF structure related accelerator [2-5], high power microwave generators [6, 7]. Some applications of the multipacting effect require suppressing the secondary-electron emission electron while the others, crossed-field devices for instance, need to enhance the emission [8]. Micro-Pulse electron Gun (MPG) which has been proposed by Mako for more than two decades [9] needs to select the materials judiciously. Due to its self-bunching property and choosing suitable secondary-electron-emission material, MPG is capable of providing high Pulse Repetitions Frequency (PRF) which means high current and short pulse electron beams [10]. The features of high PRF and short pulse make MPG one of the most appropriate electron sources to do some research of frequency locked Coherent Smith-Purcell Radiation (CSPR) which was discovered in 1990s.

This paper presents studies on the steady state multipacting in a MPG and the simulation of Smith-Purcell FEL using electron bunch produced by MPG. In the first section, the requirements for the steady multipacting are proposed by analyzing the self-bunching effects and conditions of secondary electron emission. In the second section, the primary experimental results are obtained through the experiments carried out on a 2.856 GHz MPG cavity. Finally, the further experimental arrangements are given. And Smith-Purcell FEL is investigated by using Particle In Cell (PIC) simulation method.

\* Email: zjif@pku.edu.cn

† Corresponding author, email: xylyu@pku.edu.cn

## REQUIREMENTS FOR STEADY STATE MULTIPACTING

### The MPG Model

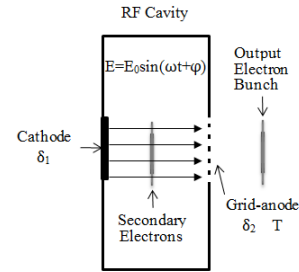


Figure 1: The schematic diagram of MPG model.

The MPG model is shown in Fig. 1. It consists three parts: an pill-box RF cavity working  $TM_{010}$  mode, a secondary emission surface with Secondary Emission Yield (SEY)  $\delta_1$ , a grid-anode, SEY  $\delta_2$  and transmission coefficient  $T$ , which is opaque to the microwave field but let the electrons partially go out the RF cavity. When MPG working, the microwave electric field -anode changes as sine wave with time. And the secondary electrons move between cathode and grid under the action of electric field.

### The Self-bunching Effects

The self-bunching effects have been reported in many articles [11, 12]. They can be explained by the following ways.

Firstly, we divide the cavity length into  $N$  parts and every part is  $dz$ . The electric field acting on every electron in  $n$ th can be expressed

$$E_n = E_0 \times \sin(\omega \sum_{i=1}^{n-1} t_i + \varphi) \quad (1)$$

where  $t_i$  is the travelling time of electron in  $i$ th part. And the acceleration can be written (non-relativistic electrons)

$$a_n = \frac{E_n e}{m} \quad (2)$$

Then the travelling time is

$$t_n = \frac{(v_{n-1}^2 + 2a_n dz)^{\frac{1}{2}} - v_{n-1}}{a_n} \quad (3)$$

where  $v_{n-1}$  is the velocity of electron in  $(n-1)$ th part.

# NUMERICAL SIMULATIONS OF A SUB-THz COHERENT TRANSITION RADIATION SOURCE AT PITZ

P. Boonpornprasert\*, M. Krasilnikov, F. Stephan, DESY, Zeuthen, Germany  
B. Marchetti, DESY, Hamburg, Germany

## Abstract

The Photo Injector Test facility at DESY, Zeuthen site (PITZ), develops high brightness electron sources for modern linac-based Free Electron Lasers (FELs). The PITZ accelerator can be considered as a proper machine for the development of an IR/THz source prototype for pump and probe experiments at the European XFEL. For this reason, the radiation generated by high-gain FEL and Coherent Transition Radiation (CTR) produced by the PITZ electron beam has been studied. In this paper, numerical simulations on the generation of CTR based on the PITZ accelerator are presented. The beam dynamics simulations of electron bunches compressed by velocity bunching are performed by using the ASTRA code. The characteristics of CTR are calculated numerically by using the generalized Ginzburg-Frank formula. The details and results of the simulations are described and discussed.

## INTRODUCTION

The Photo Injector Test facility at DESY, Zeuthen site (PITZ), has been established to develop, study and optimize high brightness electron sources for modern linac-based short-wavelength Free-Electron Lasers (FELs) like FLASH and the European XFEL. The concept of generating IR/THz radiation by electron bunches from a "PITZ-like" linear accelerator for pump and probe experiments at the European XFEL was presented in Ref. [1]. In order to study and demonstrate the capabilities of IR/THz generation from such an accelerator, PITZ has continued the case study for such a prototype IR/THz source. The main goal of the development is to generate radiation that covers wavelengths from IR ( $\mu\text{m}$ ) to THz (cm) with a variety of field patterns (from single-cycle to narrow-band), and with a high level of peak and average radiation power from the PITZ accelerator. In addition, developments and studies on radiation based electron bunch diagnostics and photon diagnostics can be done at the same time. The radiation generations using high-gain FELs and Coherent Transition Radiation (CTR) have been studied and preliminary results have been obtained.

The layout for the simulations of radiation generation as shown in Fig. 1 is similar to the current PITZ beamline with some additional radiators. The layout consists of a 1.6-cell L-band photocathode RF gun surrounded by main and bucking solenoids, a cut disk structure (CDS) booster, screen stations, quadrupole magnets and dipole magnets. The CTR station is placed at 16.30 m downstream from the cathode. An APPLE-II type undulator is placed at the end of beamline for the high-gain FEL radiation using Self-Amplification of

Spontaneous Emission (SASE) process. Preliminary start-to-end simulations for the SASE FEL using the PITZ accelerator and covering radiation wavelength from 20  $\mu\text{m}$  to 100  $\mu\text{m}$  were studied and presented in Ref. [2].

In principle, the radiation wavelength of the CTR emitted from a relativistic electron bunch is longer than or comparable to the bunch length. Therefore, in order to cover radiation frequencies in the THz region, the electron bunch length must be in the sub-ps scale. The nominal FWHM bunch length of the electron beam at PITZ is about 2 ps to 20 ps, it is obvious then that the beam needs to be compressed in order to fulfill our request.

In this paper, we present methods and results of numerical simulations of the CTR source based on the PITZ accelerator. The paper is organized as follows: the details and results of the bunch compression simulations using the velocity bunching are described in the next section. Then, the characteristics of the CTR obtainable from the compressed bunches are calculated numerically and discussed. Finally, our conclusion and outlook are presented.

## SIMULATIONS OF VELOCITY BUNCHING

We would like to maximize the electron bunch charge in order to increase the CTR intensity and to minimize the bunch length in order to broaden the spectral bandwidth. The photocathode laser system at PITZ is able to produce pulses having gaussian temporal pulse shape with minimum FWHM length of 2.43 ps. The electron bunch charge can be varied by adjusting the laser pulse energy. With this laser temporal length and large laser spot size on the cathode (rms size of 1 mm), it is possible to reach about 1 nC bunch charge.

When accelerating on-crest from the gun and the booster with their possible maximum peak electric fields, the beam can be accelerated up to about 22 MeV/c mean momentum. Since the peak electric field at the cathode has to be high enough for extracting the expected bunch charge from the cathode, the RF phase in the gun was fixed to its Maximum Mean Momentum Gain (MMM) phase and we use only the booster for the velocity bunching. However, the minimum beam momentum is limited to about 15 MeV/c in order to prevent from too strong space-charge domination problems during the beam transport and a too big emission angle from the CTR which is directly proportional to  $1/\gamma$  where  $\gamma$  is the Lorentz factor of the electron beam.

The ASTRA code [3] was used for tracking the electron beams from the cathode to the CTR station which is placed 16.30 m downstream from the cathode as shown in

\* prach.boonpornprasert@desy.de

# BEAM OPTICS MEASUREMENTS AT FERMI BY USING WIRE-SCANNER

G. Penco<sup>#1</sup>, A. Abrami<sup>1</sup>, I. Cudin<sup>1</sup>, S. Di Mitri<sup>1</sup>, M. Ferianis<sup>1</sup>, E. Ferrari<sup>1</sup>, G. Gaio<sup>1</sup>, L. Giannessi<sup>1,2</sup>, S. Grulja<sup>1</sup>, G.L. Orlandi<sup>3</sup>, C. Ozkan Loch<sup>3</sup>, R. Sauro<sup>1</sup>, L. Sturari<sup>1</sup>

<sup>1</sup>Elettra-Sincrotrone Trieste S.C.p.A., Basovizza, Italy

<sup>2</sup>ENEA C.R. Frascati, Roma, Italy

<sup>3</sup>Paul Scherrer Institut, 5232 Villigen PSI, Switzerland

## Abstract

Measuring and controlling the electron beam optics is an important ingredient to guarantee high performance of a free-electron laser. In the FERMI linac, the Courant-Snyder parameters and the transverse emittances are routinely measured by detecting the beam spot size as a function of a scanning quadrupole placed upstream (i.e. quadrupole scan method). The beam spot size is usually measured with an OTR screen that unfortunately suffers from coherent optical transition radiation (C-OTR) that introduces spurious light and corrupts the image. Moreover, the beam size at the end of the FERMI linac is focused to a few tens of microns and this makes it difficult to precisely measure it with the OTR system, which has an estimated resolution of 20  $\mu\text{m}$ . For this reason, a wire-scanner system has been installed at the end of the linac just in the waist of the optics channel. The wire-scanner is a SwissFEL prototype (Paul Scherrer Institut, Villigen CH) installed in FERMI in order to study the hardware and beam loss monitor performances at the GeV energy scale. The beam optics measurements performed with the wire-scanner is here presented, and the obtained results are more in agreement with the theoretical expectations. A more reliable beam optics estimation at the end of the linac has allowed better matching it to the nominal lattice and transporting it up to the undulator chain, providing important benefits to the FEL performance.

## INTRODUCTION

FERMI is a single-pass seeded free-electron laser (FEL) based upon the High Gain Harmonic Generation (HG) principle [1]. It is composed by two FEL lines that are now completely commissioned and in operation for providing intense photons ( $\sim 100\text{s uJ/pulse}$ ) for Users experiments: FEL-1 covers the range from 100nm to 10nm and FEL-2 from 20nm to 4nm [2,3].

The FERMI FEL high performance strongly relies on the capability of producing very high quality and bright electron beams.

The electron beam is generated in a RF photoinjector [4], and accelerated to 1.2-1.5 GeV by an S-band linac [5]. Two magnetic bunch compressors are placed respectively at 300MeV and at 650MeV and are utilized to shorten the electron bunch from few ps to hundreds of fs, increasing the peak current to 500-800A according to the desired operation parameters. One of the main goals in the beam transport and optimization from the injector to the undulators consists in preserving the

transverse emittance and limiting the undesirable effects inducing emittance growth. At this purpose, the electron beam Courant-Snyder parameters, i.e.  $\beta$  and  $\alpha$  functions, and the transverse emittance are routinely measured in strategic regions along the linac and the undulators lines, and an optimization procedure is implemented to match the optics to the lattice design. These diagnostic stations are placed after the injector ( $\sim 100$  MeV), after the first bunch compressor, at the end of the linac, and in front of the modulator. In this paper we focus on the 15-meter long optics diagnostic station located at the end of the linac, whose schematic layout is shown in Fig. 1.

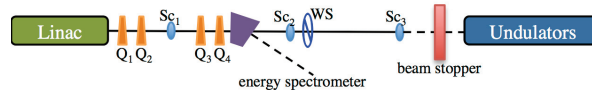


Figure 1: Diagnostic station layout at the end of the FERMI linac, including quadrupoles (Q), YAG-OTR multi-screens system (Sc) and the wire-scanner that has been installed 64 cm downstream the screen Sc<sub>2</sub>.

## THE WIRE-SCANNER PROTOTYPE AT FERMI

The nominal optics design at the end of the linac is reported in Fig. 2.

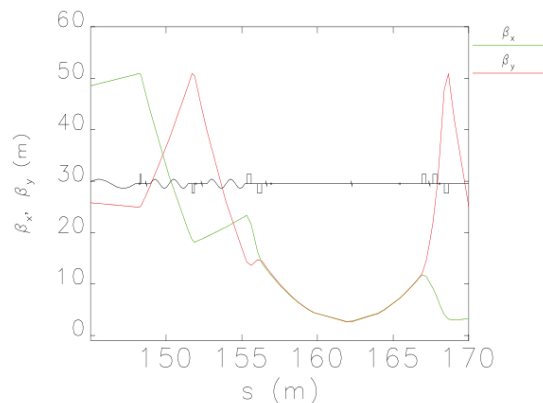


Figure 2: The horizontal and vertical  $\beta$ -function along the straight path at the end of the linac. The origin ( $s=0\text{m}$ ) of the horizontal axis corresponds to the electron source, i.e. the photo-cathode plate.

The quadrupoles Q<sub>3</sub> and Q<sub>4</sub>, see Fig. 1, are usually used only when the beam is sent into the spectrometer beam-line, to increase the measurement resolution of the longitudinal phase space [6], and are completely switched

# FEMTOSECOND SYNCHRONIZATION OF 80-MHz TI:SAPPHIRE PHOTOCATHODE LASER OSCILLATOR WITH S-BAND RF OSCILLATOR\*

Heewon Yang<sup>#</sup>, Chan-Gi Jeon, Kwangyun Jung, Jungwon Kim, KAIST, Daejeon, South Korea  
 Byunghoon Han, Young Uk Jeong, KAERI, Daejeon, South Korea  
 Hayun Chung, Korea University Sejong Campus, Sejong, South Korea

## Abstract

We present the femtosecond synchronization between an 800-nm photocathode laser and an S-band RF oscillator using an optical-RF phase detection system at KAERI-WCI Accelerator. A 79.33-MHz commercial Ti:sapphire photocathode laser oscillator is locked to a 2.856-GHz RF master oscillator (RMO) using a fiber-loop-based optical-microwave phase detector (FLOM-PD), which results in 13 fs (rms) out-of-loop residual timing jitter integrated from 1 Hz to 10 MHz offset frequency. We also measured the long-term out-of-loop timing drift between the 800-nm optical pulse train and the RF signal, which results in 28 fs (rms) integrated over 1 hour.

## INTRODUCTION

Investigation on atomic and molecular scale dynamics has recently become an active field of research. The time-resolved pump-probe experiment using ultrafast electron beams or X-rays can observe the atomic scale phenomena with femtosecond time resolution. In doing so, femtosecond-precision synchronization between lasers and RF sources is crucial to achieve femtosecond-resolution measurements. As a result femtosecond-precision laser-RF synchronization has been actively studied in the last decade [1-5]. For large-scale FELs, RF-modulated cw lasers or low-jitter mode-locked lasers at telecommunication wavelength have been used as the optical master oscillator (OMO) and the timing signals generated from the OMO are distributed via stabilized fiber links. However, for smaller-scale FELs and UED, this approach may be a complex and high cost method. In this paper, as an alternative, we studied the possibility of using the commercial Ti:sapphire photocathode laser as the OMO as well. We show 13 fs (rms) synchronization between a Ti:sapphire photocathode laser and an RF oscillator. We also measured the long-term out-of-loop timing drift of 27.8 fs (rms) integrated over an hour. To achieve this <30 fs stability long-term synchronization, we used a fiber-loop optical-microwave phase detector (FLOM-PD) to measure and lock the phase difference between optical and RF signals [6].

## SYNCHRONIZATION OF PHOTOCATHODE LASER TO RMO

A 79.33 MHz repetition rate Ti:sapphire laser (Coherent

Vitara-T) and a 2.856-GHz RF oscillator (Keysight N5181B) are used in this work. Figure 1 shows the structure of the FLOM-PD. The FLOM-PD is based on the fiber Sagnac-loop interferometer, and it detects phase difference between optical pulse train and RF signal using phase error-dependent intensity imbalance between two detector outputs [6]. The FLOM-PD can reduce the excess phase noise and drift added in the optical-to-electronic conversion process compared to direct photodetection method.

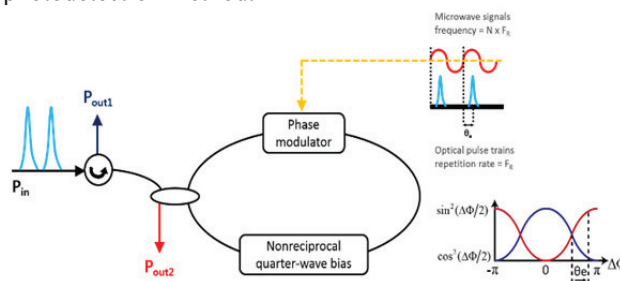


Figure 1: Schematic fiber-loop-based optical-microwave phase detector [6].

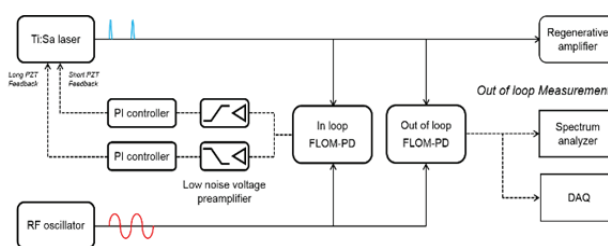


Figure 2: Schematic of the synchronization system.

Figure 2 shows the schematic of the synchronization between a photocathode laser and an RF oscillator. The synchronization setup is composed of three parts, a photocathode laser, an RF oscillator and a FLOM-PD. A Ti:sapphire laser generates 480 mW average output power with 79.33 MHz repetition rate. The laser is locked to a 2.856-GHz RF oscillator, which is used as an RF master oscillator (RMO). One FLOM-PD is used to lock the laser with the RMO and the other FLOM-PD is used to measure the residual phase noise and drift in an out-of-loop way. To operate a FLOM-PD, we used 12 mW average optical power and +19 dBm average RF power. The in-loop FLOM-PD measures phase difference between optical and RF signals and generates an error signal. Two piezoelectric transducers (PZT) inside the Ti:sapphire laser are controlled by using the error signal from FLOM-PD. The high and low offset frequency noise

\*Work supported by the KAERI Project, South Korea.  
 #hwyang@kaist.ac.kr

# STABILIZATION OF MAGNETRON FREQUENCY FOR A MICROTRON-DRIVEN FEL\*

B. A. Gudkov<sup>#</sup>, S. Bae, K. H. Jang, Y. U. Jeong, H. W. Kim, K. Lee, J. Mun, S. H. Park, G. I. Shim, KAERI, Daejeon, Korea

S. V. Miginsky, N. A. Vinokurov, KAERI, Daejeon, Korea, and Budker INP, Novosibirsk, Russia

## Abstract

Under KAERI WCI program we develop a compact pulsed microtron-driven FEL. Electron bunches are accelerated in the microtron and transported by the beamline to the undulator. The RF cavity in the microtron is fed by the magnetron. Any accelerator driver for a FEL should provide an electron beam having very stable parameters such as electron energy, beam current and especially repetition rate in a train. All mentioned parameters depend on magnetron current. It means that special attention should be paid for the shape of a current pulse, supplied to the magnetron from the modulator. We developed the modulator project with a computer control that will provide an arbitrary shape of the magnetron current. A simplified prototype was fabricated and tested. The methods of controlling of the pulse shape are considered. Simulation and experimental results are presented.

## INTRODUCTION

If one wants to obtain the maximum monochromatic FEL emission, the repetition rate of microbunches should be equal within a train and in all the trains. If maximum power is necessary, while monochromaticity is not so important, frequency ramp within a train can be used, as described in [1]. In this case, initially the detuning is significant, optimal for amplification. It increases the rise time, thus lengthen the emission pulse. Then the detuning comes to zero, and a FEL transits to so called spiking mode, and the spectrum broadens. Thus, in different cases, one can need absolutely stable or increasing in a certain way through a train repetition rate.

A magnetron, unlike a klystron, is an oscillator, but not an amplifier, so one cannot obtain stable frequency using a high-stable low-power master oscillator. The magnetron frequency depends on many factors: the mechanical tuning, the magnetic field, the anode current, the load impedance, and the temperature.

The magnetron is coupled to RF cavity of the microtron via a waveguide and an isolator. Isolator usually is tuned to allow some portion of reflected power to come back to the magnetron. Quality factor of the RF cavity is approximately of order higher than of magnetron.

In case of narrow band resonant load, the frequency pulling effect may take place. The presence or absence of

the effect depends on waveguide length, reflected power level and on cavity and magnetron detuning.

Thus, one should provide stable flat top current pulse through a magnetron or some specific current pulse shape for a frequency ramp within a train.

Ability to form an arbitrary shape of a current pulse is a universal solution.

## EQUIVALENT CIRQUIT

Volt-Ampere characteristic of a magnetron one can see in Fig. 1. Typical threshold voltage is 45-50kV depending on the magnetic field in a magnetron. There is no current for low voltage across the magnetron due to so-called magnetic isolation. Differential resistance  $dU/dI$  in the conducting area is 50-70 Ohm.

First approach for equivalent circuit of the magnetron may be series connected resistor, an ideal diode and Zener diode with a threshold voltage  $V_{th}$ . Another possibility is to use an ideal voltage source instead of Zener diode.

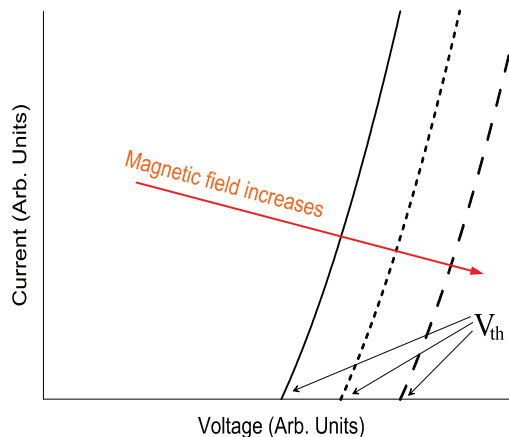


Figure 1: Volt –Ampere characteristic of a magnetron.

Simplified equivalent circuit of the modulator and the magnetron is shown in Fig. 2, where:

$L_s$  is a leakage inductance of the HV transformer, referenced to the secondary side of the transformer,

$C_s$  - the sum of the stray capacitances of the W2 and of a high voltage cable,

$R_d$  - differential resistance of the magnetron,

$D$  - ideal diode (magnetron conducts current only one direction)

$V_{th}$  -Zener diode with threshold voltage  $V_{th}$ .

Capacitor  $C_1$  is charged from power supply (not shown) before the pulse is triggered.

\*Work was supported by the World Class Institute (WCI) program of the National Research Foundation of Korea (NRF) funded by the Ministry of Education, Science and Technology of Korea (MEST) (NRF Grant Number: WCI 2011-001).

# e-mail: b\_a\_gudkov@mail.ru

# FIRST RESULTS OF COMMISSIONING OF THE PITZ TRANSVERSE DEFLECTING STRUCTURE

H. Huck\*, G. Asova<sup>†</sup>, M. Bakr<sup>‡</sup>, P. Boonpornprasert, A. Donat, J. Good, M. Gross, C. Hernandez-Garcia<sup>§</sup>, I. Isaev, L. Jachmann, D. Kalantaryan, M. Khojayan, W. Koehler, G. Kourkafas, M. Krasilnikov, D. Malyutin<sup>¶</sup>, D. Melkumyan, A. Oppelt, M. Otevrel, M. Pohl, Y. Renier, T. Rublack, J. Schultze, F. Stephan, G. Trowitzsch, G. Vashchenko, R. Wenndorff, Q. Zhao, DESY, Zeuthen, Germany  
D. Churanov, L. Kravchuk, V. Paramonov, I. Rybakov, A. Zavadtsev, D. Zavadtsev, INR of the RAS, Moscow, Russia  
M. Lalayan, A. Smirnov, N. Sobenin, MEPHI, Moscow, Russia  
C. Gerth, M. Hoffmann, M. Hüning, DESY, Hamburg, Germany  
O. Lishilin, G. Pathak, Hamburg University, Hamburg, Germany

## Abstract

For successful operation of X-ray Free Electron Lasers, one crucial parameter is the ultrashort electron bunch length yielding a high peak current and a short saturation length. In order to effectively compress the bunches during the acceleration process, a detailed understanding of the full longitudinal phase space distribution already in the injector is required. Transverse deflecting RF structures (TDS) can shear the bunch transversely, mapping the longitudinal coordinate to a transverse axis on an observation screen downstream. In addition to the bunch length, the slice emittance along the bunch as well as the full longitudinal phase space can be obtained. At the Photo Injector Test Facility at DESY, Zeuthen site (PITZ), an S-band traveling wave TDS is under commissioning since 2015. This cavity is a prototype for the TDS in the injector part of the European XFEL and has been designed and manufactured by the Institute for Nuclear Research (INR RAS, Moscow, Russia). In this paper, first commissioning results of the system at PITZ are presented and discussed.

## INTRODUCTION

Multi-GeV electron beams with high peak currents, required for the operation of X-ray Free Electron Lasers (XFELs), are generated as initially long bunches to reduce space charge effects, and are later compressed at moderate to high energies. Bunch compressors, typically realized as magnetic chicanes following off-crest acceleration, shape the longitudinal phase space for subsequent acceleration and, eventually, for the lasing process in the FEL undulators. To prevent degradation of the overall beam quality, bunch compression in the European XFEL is split into three stages at increasing beam energies. Three transverse deflecting structures are foreseen as diagnostic tools after the second and third bunch compressor and in the injector part of

the European XFEL [1, 2]. A prototype of the latter, designed [3] and manufactured by the Institute for Nuclear Research of the Russian Academy of Sciences, is under commissioning at the Photo Injector Test Facility at DESY, Zeuthen site (PITZ).

## TDS Working Principle

Quickly changing transverse RF fields deflect electrons depending on their arrival time with respect to the RF phase (Fig. 1). In the linear region around the zero-crossing phase, the longitudinal axis is projected linearly onto the vertical axis of a downstream screen, while the horizontal screen coordinate shows the horizontal beam size of the slices. By scanning the focusing strength of a quadrupole magnet, the slice emittance along the bunch can be obtained. Furthermore, live images of the full longitudinal phase space can be observed when combining the vertical TDS deflection with a horizontally dispersive dipole.

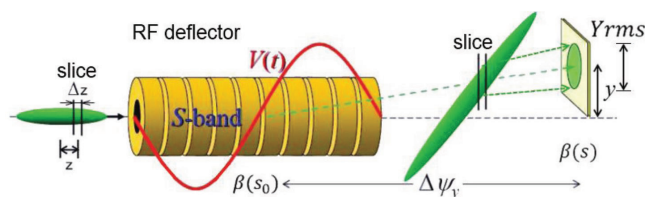


Figure 1: TDS principle: Depending on their longitudinal position, electrons are deflected by transverse RF fields and observed on a screen several meters downstream [4].

Assuming a pure drift space of length  $L$  between TDS and screen, a slice of momentum  $p$  at the relative longitudinal position  $z$  in the bunch hits the screen at vertical position [5]

$$y = S \cdot z = \frac{eV_0 k}{pc} \cdot L \cdot z, \quad (1)$$

where the  $S$ -parameter depends on the deflecting voltage  $V_0$  and wave number  $k$ . In the general case, the longitudinal

\* holger.huck@desy.de

<sup>†</sup> on leave from INRNE, Sofia, Bulgaria

<sup>‡</sup> on leave from Assiut University, Assiut, Egypt

<sup>§</sup> on leave from Jlab, Newport News, USA

<sup>¶</sup> now at HZB, Berlin, Germany

# IMPLEMENTATION OF MTCA.4-BASED CONTROLS FOR THE PULSED OPTICAL SYNCHRONIZATION SYSTEMS AT DESY\*

M. Felber<sup>#</sup>, L. Butkowski, M. K. Czwalińska, M. Fenner, C. Gerth, M. Heuer, M. Killenberg, T. Lamb, U. Mavrič, J. Mueller, P. Peier, K. Przygoda, S. Ruzin, H. Schlarb, C. Sydlo, M. Titberidze, F. Zummack, DESY, Hamburg, Germany  
T. Kozak, P. Prędko, TUL-DMCS, Łódź, Poland  
E. Janas, ISE-WUT, Warsaw, Poland

## Abstract

With the current state of the synchronization system at FLASH (Free-electron Laser in Hamburg) the arrival time between electron bunches and optical laser pulses can be synchronized to a level of 30 fs rms, e.g. for pump-probe experiments. In the course of the development of an up-scaled system for the European XFEL and the migration of control hardware to the modern MTCA.4 (Micro Telecommunications Computing Architecture) platform, all involved components of the system will be replaced with new developments. The front-end devices are upgraded. FPGAs (Field Programmable Gate Arrays) are performing the data processing and feedback calculations. In order to facilitate the firmware development, a toolset (Rapid-X) was established which allows application engineers to develop, simulate, and generate their code without help from FPGA experts in a simple and efficient way. A software tool kit (MTCA4U) provides drivers and tools for direct register access e.g. via Matlab or Python and a control system adapter, which allows the server applications to be written control system independent. In this paper, an overview on the synchronization setups and their upgrades as well as an introduction to the new hardware is given. The Rapid-X and MTCA4U tool kits are presented followed by a status report on the implementation of the new developments.

## INTRODUCTION

Like most other accelerator sub-systems the various setups of which the optical synchronization systems at FLASH and the European XFEL are constructed can be divided in four layers:

- 1) The front-end device, usually an electro-optic and/or an opto-mechanic setup connecting another component of the accelerator with the signals from the synchronization system.
- 2) The electronic hardware which is the platform for readout and processing of signals generated by the front-end device and actuating on it. It also connects to a CPU providing a physical interface to the external world. For the computation usually FPGAs are used.
- 3) The firmware running on an FPGA which can be divided in two layers. The base is the hardware specific

part which provides access to the peripherals like ADCs (Analog to Digital Converters), DACs (Digital to Analog Converters), and memory. The second part is application specific and can incorporate algorithms for the computation of physically meaningful numbers from the front-end signals and - in many cases - a feedback control loop.

4) The software layer which can also be separated in at least two parts. One is that it provides a framework for connecting to the firmware registers via specific drivers, e.g. to set and read parameters. The other is to process this data e.g. for displaying or performing supervision in an application code. The latter can also calculate algorithms and perform feedback control but opposed to the firmware the higher latency only allows for slower (low bandwidth) control loops. Usually the application software is integrated in the accelerator control system, in this case it is called server but it can also be an independent program or script.

Growing demands for the synchronization of FELs in number of setups and their performance triggers continuous upgrades on all four of the mentioned aspects which will be described in the following chapters.

## FRONT-END DEVICES

The optical synchronization system has been operated at FLASH since 2009 [1]. It is based on the distribution of 200 fs long laser pulses at 1550 nm with a repetition rate of 216.7 MHz, 1/6 of the main 1.3 GHz RF. This reference signal can be used at remote locations in the accelerator for bunch arrival time monitors (BAMs) [2], RF reference stabilization (REFM-opt) [3] or laser synchronization (L2L) [4]. In a recent publication, a synchronization of 30 fs rms between the FEL and the Pump-Probe was experimentally shown [5]. In order to achieve this level of performance an active beam-based feedback (BBFB) stabilization [6] of the electron bunch arrival time with help of the fs-precise BAM measurements has to be applied as well as optical lock of the pump-probe laser to the reference with the scheme of two-color balanced optical cross-correlation. For attaining even better stability in future and to cope with the growing number of clients, all sub-systems of the optical synchronization are being improved. The European XFEL is being equipped with the improved designs from the start while FLASH is being upgraded and extended step by step.

\*This work has partly been funded by the Helmholtz Validation Fund Project MTCA.4 for Industry (HVF-0016)  
#matthias.felber@desy.de

# TURBO-ICT PICO-COULOMB CALIBRATION TO PERCENT-LEVEL ACCURACY

F. Stulle\*, J. Bergoz, Bergoz Instrumentation, Saint-Genis-Pouilly, France

## Abstract

We report on the calibration methods implemented for the Turbo-ICT and the BCM-RF. They allow to achieve percent-level accuracy for charge and current measurements. Starting from the Turbo-ICT and BCM-RF working principle, we discuss the scientific fundamentals of their calibration and the practical implementation in a test bench. Limits, both principle and practical, are reviewed. Achievable accuracy is estimated.

## INTRODUCTION

The Turbo-ICT sensor and its corresponding BCM-RF electronics can accurately measure charges of ultra-short particle bunches as well as average currents of CW beams of such bunches [1,2].

When excited by a single bunch, the Turbo-ICT output signal is a short resonance at a fixed frequency  $f_{res}$  but charge-proportional amplitude. The BCM-RF works in sample-and-hold mode and measures the apex of this resonance. The maximum possible bunch repetition rate is approximately 2 MHz. For calibration the relation between Turbo-ICT input charge  $Q_{in}$  and BCM-RF output voltage  $U_{BCMRF}$  is determined.

When excited by a CW beam, the Turbo-ICT output signal is a sine wave of frequency  $f_{res}$  and current-proportional amplitude. The BCM-RF works in track-continuous mode and measures the apex of this sine wave. The Turbo-ICT resonance frequency  $f_{res}$  must match the bunch repetition rate  $f_{rep}$  or a harmonic. For calibration the relation between average input current  $\langle I_{cw,in} \rangle$  and BCM-RF output voltage  $U_{BCMRF}$  is determined.

In the following, we discuss the Turbo-ICT and BCM-RF working principle. The calibration methods for both modes of operation are described and the achievable accuracies are estimated.

## TURBO-ICT / BCM-RF PRINCIPLE

To determine charge or current the BCM-RF measures on a logarithmic scale the apex of the Turbo-ICT output signal. Hence, the apex should depend only on input charge or current. Most notably, any current transformer's output pulse shape is usually dependent on input pulse shape, which could induce a variation of the apex even for constant charge or current. Only for "sufficiently short" input pulses this dependence is negligible.

It is required that an input pulse must be considerably shorter than the Turbo-ICT resonance wave length, which is fulfilled, e.g., in laser-plasma accelerators or X-ray free-electron lasers. Details are given in Appendix A.

## Turbo-ICT Pulse Response

The spectral response  $Q_{out}(f)$  of a Turbo-ICT to an incoming current pulse  $I_{in}(t)$  is the product of the incoming pulse's spectrum  $Q_{in}(f)$  and the Turbo-ICT's transmission coefficient  $S_{21}(f)$ , e.g. as obtained from S-parameter measurements using a vector network analyser (VNA):

$$Q_{out}(f) = Q_{in}(f) S_{21}(f).$$

Using the inverse Fourier transform the time-domain output current pulse  $I_{out}(t)$  can be determined:

$$I_{out}(t) = \int_{-\infty}^{+\infty} Q_{in}(f) S_{21}(f) e^{i2\pi ft} df.$$

For "sufficiently short" input pulses,  $I_{out}(t)$  can be approximated:

$$I_{out}(t) \approx Q_{in} \int_{-\infty}^{+\infty} S_{21}(f) e^{i2\pi ft} df = Q_{in} M(t). \quad (1)$$

That means, for "sufficiently short" input pulses the Turbo-ICT output pulse has always the same shape  $M(t)$  scaled by the input pulse charge  $Q_{in}$ .

$M(t) = \int_{-\infty}^{+\infty} S_{21}(f) e^{i2\pi ft} df$  is the Turbo-ICT's response to a Dirac pulse, i.e. to an infinitely short current pulse, normalized by the pulse's charge; its units are Ampère per Coulomb. Figure 1 shows a typical  $S_{21}(f)$  of a Turbo-ICT and the corresponding Dirac response.

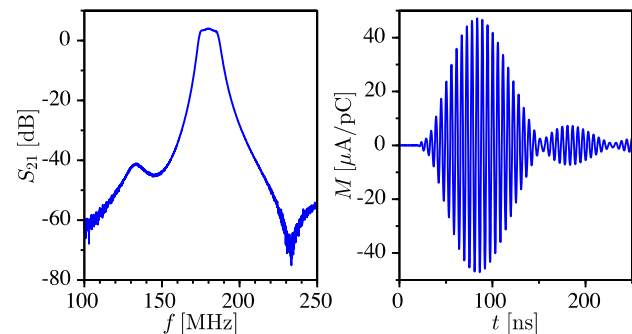


Figure 1: Typical Turbo-ICT response in frequency-domain (left) and in time-domain (right).

## Turbo-ICT Dirac Response Correction

As mentioned above, the Turbo-ICT Dirac response can be reconstructed from the Turbo-ICT's  $S_{21}$ :

$$M(t) = \int_{-\infty}^{+\infty} S_{21}(f) e^{i2\pi ft} df.$$

While this equation is in theory correct, it is in practice not sufficient. Around the Turbo-ICT, the measurement setup is not perfectly matched to 50  $\Omega$  wave impedance. Reflections occur during the VNA measurements, lowering power and current passing the Turbo-ICT. Such effects will not be present in the accelerator. Consequently, the measured transmission coefficient  $S_{21,VNA}$  is not exactly representative of the real  $S_{21,ACC}$  in the accelerator.

\*stulle@bergoz.com

# ALL-FIBER APPROACH TO LONG-TERM STABLE TIMING DISTRIBUTION SYSTEM

M. Xin\*, K. Şafak, F. X. Kärtner, CFEL, DESY, Hamburg, Germany  
P. T. Callahan, M. Y. Peng, F. X. Kärtner, MIT, Cambridge, Massachusetts, USA

## Abstract

A complete fiber-optic, high-precision, long-term stable timing distribution system is demonstrated over a 3.5-km polarization-maintaining fiber link for synchronization of next generation X-ray free-electron lasers. The residual timing jitter at [1 Hz, 1 MHz] is below 0.7 fs, and the RMS drift (<1 Hz) is 3.3 fs over 200 hours of continuous operation. This all-fiber-optic implementation will greatly reduce the complexity of optical alignment in timing distribution and improve the overall mechanical and timing stability of the system.

## INTRODUCTION

Next generation FELs, such as the European XFEL [1] in Hamburg and Linac Coherent Light Source II [2] in Stanford, are predicted to deliver X-ray pulses shorter than 10 fs. Unlocking the high temporal-resolution capabilities of these facilities will require extremely stable timing distribution systems [3, 4] delivering better than 10-fs precision between optical and radio frequency (RF) sources located over kilometer distances. Over the past decade, we have been advancing a pulsed-optical timing distribution system [5-7] that uses the ultralow-noise pulse train from a mode-locked (master) laser as its timing signal. The timing signal is transferred through timing-stabilized fiber links from a central location to multiple end stations, where efficient and robust synchronization is realized using balanced optical cross-correlators (BOC) [8] for optical sources and balanced optical-microwave phase detectors [7] for RF sub-systems. Real facilities such as FLASH and the European XFEL need fiber networks consisting of 20 or more timing links, which require tremendous attention to the alignment and stability of the free-space optics to minimize timing-drifts induced by beam pointing instabilities. This situation also necessitates preamplification of the master laser's output to overcome excessive free-space to fiber coupling losses to provide adequate power for all timing links. To eliminate free-space optics and its disadvantages from the timing distribution system, we have developed integrated, fiber-coupled balanced optical cross-correlators (FC-BOC) using periodically-poled  $\text{KTiOPO}_4$  (PPKTP) waveguides [9, 10]. These waveguides exhibit second harmonic (SH) conversion efficiencies up to 1.02 % / [ $\text{W}\cdot\text{cm}^2$ ] (20 times higher than the bulk optical devices), which will decrease the power demand from the master laser and consequently support more timing links. Furthermore, the robustness and ease of implementation of these fiber-coupled devices will eliminate alignment-related problems observed in

free-space optics. In this paper, we present an all-fiber implementation of the pulsed-optical timing distribution system using FC-BOCs.

## EXPERIMENTAL SETUP

A diagram of the experimental setup is shown in Fig. 1(a). The master laser operates at 1554-nm center wavelength with +22.4-dBm average output power, 150 fs pulse width and 216.66-MHz repetition rate. Its repetition rate is locked to a RF synthesizer (RF-S) to reduce the timing drift below 10 Hz. The only free-space part built in this experiment is the initial power separation elements comprised of one polarization beam splitter (PBS) and 3 half-wave plates. Furthermore, polarization-maintaining (PM) fiber components are chosen over standard single-mode (SM) fiber for the construction of the setup, as previous results obtained with SM fiber has showed substantial polarization-mode-dispersion effects in the out-of-loop link stabilization measurements [3]. After the PBS, the output of the master laser is coupled into two separate fiber paths: the out-of-loop reference path and the link stabilization unit. The out-of-loop reference path is a 1-m long PM fiber serving as the reference arm for the out-of-loop FC-BOC. The link stabilization unit starts with a fiber-coupled polarization beam splitter (FC-PBS1) which divides the optical power further into two segments. The first segment (traveling to the right through FC-PBS1 in Fig. 1(a)) is directed into the timing link which consists of a fiber-coupled faraday rotator (FC-FR), a fiber-coupled motorized delay line (FC-MD) with 560-ps range, a PM fiber stretcher (PM-FS), and a 3.5-km PM dispersion-compensated fiber spool (PM-DCF). The second segment is sent into a 0.5-m fiber having a fiber-coupled faraday mirror (FC-FM) at the end. The FC-FM turns the polarization of the pulses by  $\pi/2$  upon reflection and guides them into the in-loop FC-BOC to serve as the reference pulses for the timing stabilization of the 3.5-km link.

Both of the two FC-BOCs are PPKTP waveguide chips in fiber-coupled packages with internal temperature control [10]. A schematic of the module is shown in Fig. 1(b). The wavelength division multiplexer (WDM) consists of a fiber-coupled dichroic beam-splitter cube coupling the input pulses into the waveguide for cross-correlation and separates the SH return path from the fundamentals. The forward and backward SH signals are then fed to the ports of a fiber-coupled BPD (FC-BPD).

\* ming.xin@desy.de

# INFLUENCE OF ENVIRONMENT CHANGES ON LIBERA SYNC 3 LONG-TERM STABILITY

S. Zorzut, M. Cargnelutti, Instrumentation Technologies, Solkan, Slovenia  
S.G. Hunziker, Paul Scherrer Institut, Villigen, Switzerland

## Abstract

Libera Sync 3 is intended to be used as a reference clock transfer system in the latest fourth generation light sources where the required long-term stability is in the range of a few tens of femtoseconds of drift per day [1]. The system has an outstanding added jitter performance below 4 fs in the 10 Hz to 10 MHz frequency range. The system has been developed in collaboration with the Paul Scherrer Institute (PSI) and first units are already installed in the SwissFEL machine. In this article we present the influence of temperature and humidity changes on the long-term phase stability of the system.

## INTRODUCTION

Libera Sync 3 solution is based on a continuous wave (CW) modulation of an optical carrier in which phase detection and stabilization are done in the radio frequency (RF) domain [2]. The system is composed of a transmitter and a receiver units (Figure 1) connected by two optical fiber links that are laid in the installation tunnel as it is depicted in Figure 2. Additional Ethernet connection is used for data exchange between the units and for remote monitoring and control of Libera Sync 3.



Figure 1: Libera Sync 3 transmitter and receiver units.

The two optical fiber links are used in order to overcome optical limitations, mainly due to the Rayleigh backscattering effect [3, 4]. One fiber is used to transfer a low-noise signal while the second is used to transfer a low-drift reference signal.

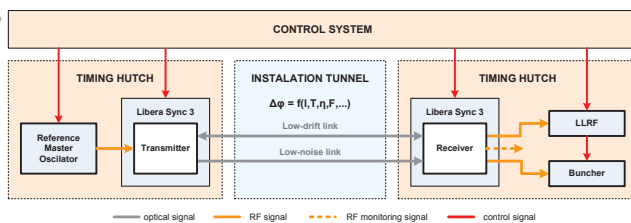


Figure 2: Installation of Libera Sync 3 system in the accelerator environment.

Libera Sync 3 compensates both the phase drifts in the electronics and in the low-drift optical link. All the components outside the phase compensation loops are sensitive to environmental changes, especially temperature and humidity changes. To reduce such influences different compensation techniques like thermal stabilization of critical components and usage of thermally compensated materials are applied, but nevertheless some residual sensitivity to environmental changes still exist.

## PERFORMANCE MEASUREMENTS

Jitter and long term stability are two key performance parameters for Libera Sync 3.

### Jitter Performance

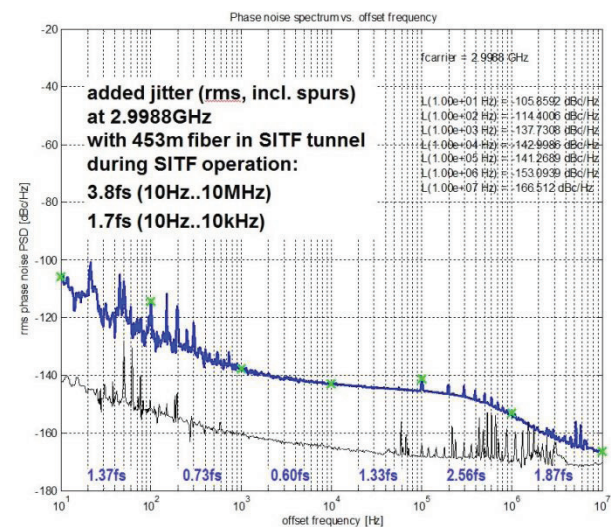


Figure 3: Libera Sync 3 added phase noise and jitter. The black curve shows the limit of the measuring setup.

Figure 3 shows Libera Sync 3 measured phase noise and jitter at 2998.8 MHz that was done at PSI. The added jitter in the frequency range from 10 Hz to 10 MHz is 3.8 fs.

### Long-term Phase Stability

The long-term phase stability of the Libera Sync 3 was measured using a standalone phase detector unit which compared the output RF signal from the Libera Sync 3 system with the reference signal. The drift of setup itself is estimated to be on the order of a few femtoseconds peak-to-peak per day. Figure 4 shows block diagram of the measurement setup.

## A LASER HEATER FOR CLARA

S. Spampinati, University of Liverpool and The Cockcroft Institute, Warrington, Cheshire, U.K.  
B.D.Muratori, N.R. Thompson, P.H.Williams, ASTeC, Daresbury Laboratory, Warrington,  
Cheshire, U.K.

### Abstract

CLARA is a new FEL test facility, being developed at STFC Daresbury Laboratory in UK, based on a high brightness electron linac. The electron beam of CLARA can potentially be affected by the longitudinal microbunching instability leading to a degradation of the beam quality. The inclusion of a laser heater in the linac design can allow control of the microbunching instability, the study of microbunching and deliberate increase of the final energy spread to study energy spread requirements of the FEL schemes tested at CLARA. We present the initial design and layout of the laser heater system for CLARA and its expected performance.

### INTRODUCTION

CLARA (Compact Linear Accelerator for Research and Applications) is a proposed 250MeV, 100-400nm FEL test facility at Daresbury Laboratory [1]. The purpose of CLARA is to test, explore and ultimately validate new schemes for FEL light generation in areas such as ultra-short pulse generation, temporal coherence and pulse-tailoring. The accelerator itself will consist of 4 S-Band normal conducting linear accelerators with a medium-energy variable bunch compression scheme, feeding into a flexible arrangement of FEL modulators and radiators. For seeding purposes the accelerator includes a pre-FEL dogleg where modulated laser light can be introduced. The accelerator will be driven by a high rep-rate RF photo-cathode S-Band electron gun, operating in single bunch mode at up-to 100Hz, and with bunch charges up to 250pC. Peak currents at the FEL are expected to be in the 500A range running the linac with the magnetic bunch compressor. An increased current in the 1-2 KA range can be obtained through the use of a velocity-bunching scheme in the first two linac structures [2]. The CLARA linac is potentially affected by the longitudinal microbunching instability (MBI) [3-5], as are other accelerators that drive high gain free electron laser (FEL) facilities [6,7], that produce short wavelength ( $\sim 1-5\mu\text{m}$ ) energy and current modulations. These can both degrade the FEL spectrum and reduce the power by increasing the slice energy spread. This instability is presumed to start at the photoinjector exit growing from a pure density modulation caused by shot noise and/or unwanted modulations in the photoinjector laser temporal profile. As the electron beam travels along the linac to reach the first bunch compressor (BC1), the density modulation leads to an energy modulation via longitudinal space charge. The resultant energy modulations are then transformed into higher density modulations by the bunch compressor. The increased current non-uniformity leads

to further energy modulations along the rest of the linac. Coherent synchrotron radiation in the bunch compressor can further enhance these energy and density modulations [8,9]. The main solution to prevent MBI, used in several FEL facilities, is the laser heater (LH) [10,11].

A laser heater consists of a short, planar undulator located in a magnetic chicane where an external infrared laser pulse is superimposed temporally and spatially over the electron beam. The electron-laser interaction within the undulator produces an energy modulation on a longitudinal scale length corresponding to the laser wavelength.

The second half of the LH chicane smears the energy modulation in time, leaving the beam with an almost pure incoherent energy spread. This controllable incoherent energy spread suppresses further MBI growth via energy Landau damping in the bunch compressor. A layout of a laser heater is shown in Fig. 1.

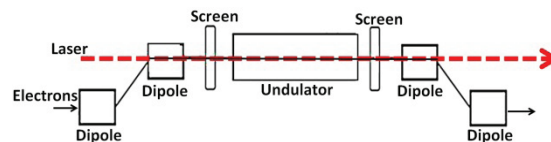


Figure 1: Laser heater layout.

The presence of the laser heater in a test facility like CLARA could be exploited to study further some less explored aspects of MBI such as the microbunching induced by the laser heater chicane and the MB competition between different sections of the accelerator [12].

The laser heater can also be used to modulate the electron beam energy spread to control the FEL temporal and spectral properties [13] or to deliberately increase of the final energy spread to study energy spread requirements of the FEL schemes tested at CLARA. The laser heater chicane could be also used to implement the diagnostics presented in [14]. These are all possible experiments of relevance to future FEL facilities. Consequently a space for a laser heater system has been left in the linac layout. Due to space constraints and to the necessity to avoid long strait sections at low energy the more convenient location for the laser heater is just before the bunch compressor at a beam energy of 125-210 MeV. In this case the beam present a significant energy chirp ( $\sim 2\%$ ) and this is a difference respect to other facility [6,7]. The effect of the chirp on the laser heater will be analysed.

After the first acceleration stage a set of 4 quadrupoles allows matching of the optical functions into the laser heater chicane and 4 additional quadrupoles follow the

# THE BINP HLS TO MEASUREMENT VERTICAL CHANGES ON PAL-XFEL BUILDINGS AND GROUND\*

Hyojin Choi<sup>†</sup>, Kwang Won Seo, Kyehwan Gil, Seung Hwan Kim, Heung-Sik Kang  
 Department of Accelerator, PAL-XFEL, Pohang, Korea

## Introduction

General matters about the hydrostatic leveling system (HLS) to be installed in PAL-XFEL were explained in Reference [1]. This paper will introduce principles of measuring water pipes that are references of HLS and Ultrasonic-type HLS of the Budker Institute of Nuclear Physics (BINP).

## WATER VOLUME CHANGING BY TIDAL EFFECTS

The strength of gravity of planets in the solar system follows Isaac Newton's law of gravity and the superposition principle. There are three elements changing the gravity of the earth: the earth's orbit, the moon's orbit and leaning of the earth's rotational axis. As shown by Figure 1, the orbit of the earth circling the sun is oval. The sun's tide generating force changes according to positions of the earth's orbit.

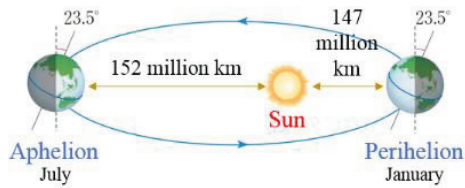


Figure 1: Earth's orbit.

As shown by Figure 2, the effects of tide generating force appear due to complex movements, such as the earth's rotation, the moon's orbit and the leaning of the moon's orbital plane. It is very difficult to gain theoretical access to them and they can be various depending on factors (such as composition of the continental ground, latitude, longitude and altitude) affecting regions whose tide generating force is to be measured, so it is difficult to analyze them. The effects of the tide generating force changing over time lead to changes in gravity and in consequence the earth's land and sea affected by gravity display tidal phenomena over time.

The tide generating force can be measured using an earth tide meter or a gravity meter. Figure 3 shows changes in the tide generating force measured in Korea using an earth tide meter. Changes in the tide generating force cause changes in the water volume and they appear as changes in the water height inside a water pipe in the process of measuring HLS. As explained in Reference [1], water produces volume changes because of various outside effects in addition to the tide generating force. In

\*Work supported by Ministry of the Science, ICT and Future Planning  
<sup>†</sup>choihyo@postech.ac.kr

the case of water in a glass, the water height changes about  $2\mu\text{m}/\text{deg}/\text{cm}$  because of temperature and the figure is about Max.  $0.6\mu\text{m}/\text{cm}$  because of tides. There should be no temperature changes in order to observe the water height changing by tidal effects.

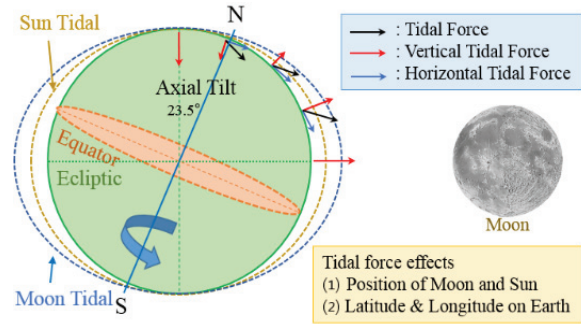


Figure 2: Distribution of the tidal force on the earth.

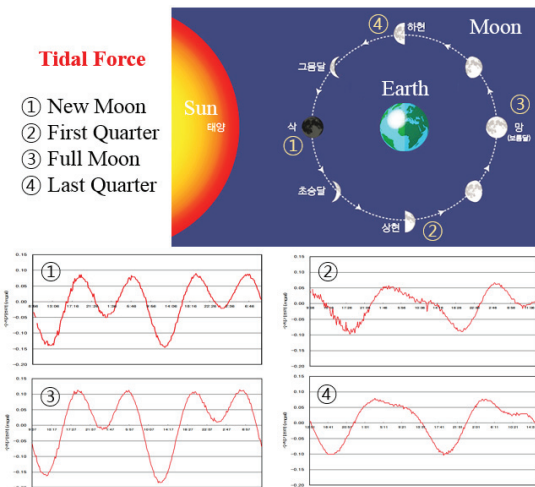


Figure 3: The tide generating force depending on positions of the sun and the moon.

Although the water volume inside a water pipe dynamically changes moment by moment due to temperature inside a tunnel and tides, the water height of the entire area of the water pipe will be maintained in the short term if the flow inside the water pipe is large enough. The space inside the water pipe is closed and hydrostatic levelling measurement is made under the condition where the amount of water is the same even if the water volume changes. As shown by Figure 4, water pipes are installed on the floor inside the tunnel. As long as an accelerator works, entries to the tunnel are prevented and there is no vibration caused by people.

# THE DESIGN OF LOW NOISE MAGNET POWER SUPPLY\*

K. H. Park<sup>#</sup>, S. H. Jeong, Y. G. Jung, D. E. Kim, H. S. Suh, H. G. Lee, S. B. Lee, B.G. Oh,  
W. S. Choi, I. S. Ko, PAL, POSTECH, Pohang, Korea

## Abstract

The accelerator facility needs a high stable magnet power supply (MPS). The stability requirements of the some MPSs in accelerator facility were in the range of the ~10 ppm. There are many noise sources which affect the stability of the MPS. Thus the design of the MPS requests much attention on the noise reduction scheme from the design stage. The noise on the MPS divided into some sources such as the ripple voltage coming from rectifier on the DC link, switching noise from the high voltage switch, and so on. This paper dealt the ripple components analysis, oversampling converter and digital voltmeter for the high precision stability measurement.

## INTRODUCTION

The stability of the magnet power supply (MPS) was related to the noise components generated by MPS itself. The sources to give the poor output stability of the MPS were divided into two types as ripple components and switching noise. The ripple components came from rectifier which inevitably generated by the harmonic components of the line frequency such as 60Hz, 120Hz and so on. And the other noises were developed at inter PCBs or cables between modules due to parasitic inductance and capacitance on fast rising and falling time of the pulse when switching state. The proper signal processing in digital and analogue to increase signal to noise ratio was needed to the high stability MPS.

This paper describes some design schemes that was implemented into the MPS were described such as ripple voltage analysis, and oversampling converter for high resolution. And this paper shows the working process of the dual slop integrator for analogue to digital converter (ADC). And the aperture time of the DVM3458A affects the measurement precision in the ~ppm range.

## REDUCTION LINK VOLTAGE RIPPLE

The full wave rectifier of three-phase AC input of wye or delta-connection or both of them was composed for the DC link voltage of the MPS. The Fourier series expansion of the link voltage in the case of full wave rectifier of three phase AC line is given as the following equation

$$V_{\text{link}} = \frac{3\sqrt{3}}{\pi} V_m \left( 1 - \sum_{k=1}^{\infty} \frac{2}{36k^2} \cos(6k\omega t) \right).$$

The spectrum of the  $V_{\text{link}}$  contains sixth multipole components of the line frequency. It is corresponded to 360 Hz in the case of the 60 Hz AC input. The switching

frequency of 25 KHz of the MPS was much higher than the multipole components of 360 Hz, thus it was acted as sampling frequency while it satisfied the Nyquist sampling theorem as the following equation [1].

$$F_s \geq 2F_c,$$

where  $F_s$  is the sampling frequency and  $F_c$  is the highest frequency in the signal.

The FETs worked as analogue switch devices in the sampling process. The cut-off frequency of the output filter of the MPS was located around ~KHz, thus the rectified ripple components passed without any attenuation. Figure 1 showed the simulation results of the PSPICE for a three phase full rectifier. The ripple components of the link voltage were appeared at the output stage with 0.5 V<sub>pp</sub>, which affected to the output stability about 10 mA<sub>pp</sub> fluctuation with same frequency.

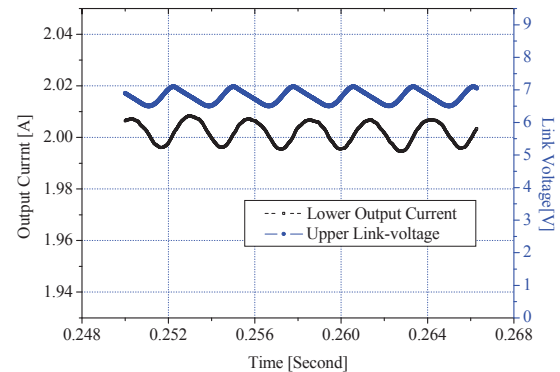


Figure 1: Ripple components on the output stage.

To reduce this effect of the ripple components, a proper low-pass filter should be configured into the input rectifier. The parallel damped filter was preferred to building the MPS as described in Ref. [2]. The cut-off frequency of the filter should be ranged ~10 Hz, that was dependent on the required stability.

## OVERSAMPLING CONVERSION

Oversampling method represents that the ADC converts analogue signal into digital with a higher sampling rate than the required bandwidth of interest. This method combined with suitable digital signal processing like average and decimation is able to improve signal-to-noise ratio (SNR). With the improved SNR the effective bit resolution of ADC will be increased [3].

The MPS is designed by the switching mode thus it cannot be avoided switching noise generated during the switch transition. Furthermore, there are many other noise

\*Work supported by Ministry of Science, ICT & Future Planning  
#pkh@postech.ac.kr

## DESIGN, DEVELOPMENT AND TEST OF THE MAGNETS FOR PAL-XFEL\*

Hyung Suck Suh, Bongi Oh, Dong Eon Kim, Heung-Sik Kang, Hong-Gi Lee, In Soo Ko,  
Ki-Hyeon Park, Moo Hyun Cho, Sang-Bong Lee, Seong Hun Jeong, Young-Gyu Jung  
PAL, Pohang, Republic of Korea

### Abstract

PAL-XFEL is now being constructed with the goal of 0.1 nm hard X-ray in Pohang, Korea. As the first phase we will construct 10 GeV linac, one hard X-ray and one soft X-ray beamlines which require 6 different families of 46 dipole magnets, 11 families of 209 quadrupole magnets, and 3 families of 48 corrector magnets. We have designed these magnets with considering the efficient production and the proper power supplies. This paper describes an outline of the design and test results of the magnets until now.

### INTRODUCTION

The PAL(Pohang Accelerator Laboratory)-XFEL is a 0.1-nm hard X-ray FEL project starting from 2011. Three hard X-ray and two soft X-ray branches are planned. As the first phase of this project, one hard X-ray (HX1) and one soft X-ray (SX1) which consist of 51 dipole and 209 quadrupole magnets will be constructed [1].

We have designed all magnets on our own by using OPERA and ANSYS codes [2, 3]. Every magnet is designed to maintain the maximum temperature rise of coils below 20 K for 120% of the nominal currents. In the process of the design, it was helpful to parameterize the main variables of the magnets in a spread sheet for easy estimation by changing some parameter. Now we are manufacturing and testing the magnets. Two Hall probe measurement benches were used to measure the magnetic field for the dipole magnets and the quadrupole magnets respectively.

### DIPOLE MAGNETS

The dipole magnets were classified into six kinds according to the pole gap, the effective magnetic length, and the maximum magnetic field. The results of the classification are listed in Table 1.

Most dipole magnets have the same pole gaps of 30 mm except D6 of 15 mm for the self-seeding. D1, D2, and D4 have H-type core shape, and D3, D6, and D7 have C-type. All dipole magnets of D1~D6 for the bunch compressor, the chicane, and the self-seeding have the trim coils with 1% of the main field.

The pole profiles of magnets are optimized by the small bumps at the tip of the pole for the field uniformity. The requirements for the field uniformity are different from each magnet.

Table 1: The Families of Dipole Magnets (D5 was replaced with D2.)

Family	Magnetic length [m]	Max. field [T]	Qty	Position
D1	0.20	0.80	6	BC1
D2	0.70	1.00	19	BC2,BC3, BAS1
D3	1.44	1.30	11	BAS2,3,4
D4	0.17	0.312	4	Laser Heater
D6	0.30	0.485	4	Self seeding
D7	0.75	1.164	2	Tune-up dump

We have tested all prototype dipole magnets. Most magnets satisfied the field requirements. But D1 and D7 didn't satisfy the field uniformity slightly. We have calculated the magnetic field by using B-H table of Chinese low carbon steel (DT4), and manufactured magnets by using the same materials. But a little difference between the calculated and measured field uniformities has arisen. So we used shims (10x10 mm<sup>2</sup> wide, 1mm thick, steel plates) to improve the field uniformity. The shims were placed on the chamfer sides of front and end sides of lower and upper poles. Figure 1 shows the field distribution of FEM model and the magnetic field measurement scene of D1.

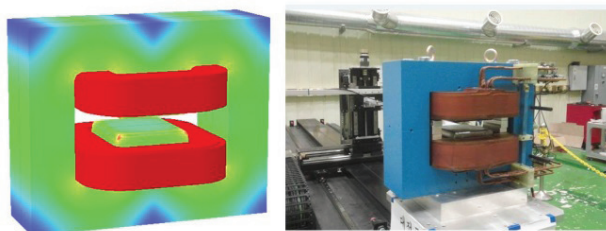


Figure 1: D1 dipole magnet (Left: magnetic field distribution of FEM model, Right: magnetic field measurement by Hall probe).

The field uniformities of D1 are shown in Figure 2, where the calculated one is drawn with a green dashed line, measured without shims with a blue dash-dot line, and measured with shims with a red line. The requirement of the 3-dimensional field uniformity is less than 1.0E-4 for  $|x| < 17$  mm, and less than 5.0E-4 for  $|x| < 41$  mm. And we confirmed that the field uniformities of field integral along straight line are very similar to that along the curved orbit.

# DEVELOPMENT OF COHERENT TERAHERTZ WAVE SOURCES USING LEBRA AND KU-FEL S-BAND LINACS\*

N. Sei, H. Ogawa, Research Institute for Measurement and Analytical Instrumentation, National Institute of Advanced Industrial Science and Technology (AIST),

1-1-1 Umezono, Tsukuba, Ibaraki 305-8568, Japan

K. Hayakawa, T. Tanaka, Y. Hayakawa, K. Nakao, T. Sakai, K. Nogami, M. Inagaki, Laboratory for Electron Beam Research and Application (LEBRA), Nihon University,

7-24-1 Narashinodai, Funabashi, 274-8501, Japan

H. Ohgaki, H. Zen, Institute for Advanced Energy, Kyoto University, Gokasho, Uji, Kyoto 611-0011, Japan

## Abstract

In an infrared free-electron laser (FEL) facility using an S-band linac, a short-bunched electron beam is required to obtain a high FEL gain. Generally, the bunch length of the electron beam is compressed to 1 ps or less before interaction with the photons accumulated in the FEL resonator. This suggests that the electron beam dedicated to the FEL lasing is suitable for generation of high-peak-power coherent radiation in terahertz (THz) wave region. With the compressed electron beams the coherent THz-wave sources have been developed at Laboratory for Electron Beam Research and Application in Nihon University and mid-infrared FEL facility in Kyoto University. The observed energy has been higher than 100  $\mu$ J per macropulse in both infrared facilities.

## INTRODUCTION

To increase a gain of a free-electron laser (FEL), high electron charge and short pulse width are required for the electron beam used in an infrared FEL facility. Although it is necessary to consider slippage of the electron beam in an insertion device, the root-mean-square (RMS) bunch length of the electron beam is often compressed to 1 ps or less before the insertion device.

Then, the electron beam in the infrared FEL facility is suitable for generating intense coherent radiation in a terahertz (TH) wave region, which lies between the microwaves and the infrared region. A lot of materials have unique absorptive and dispersive properties in the THz wave region [1]. Because the coherent radiation is broad band, it is useful for THz spectroscopy [2]. By combining the probe light of the coherent radiation with the pump light of the infrared FEL, it is expected to clarify dynamics of the molecular vibrations. Because the maximum electric field of the coherent radiation becomes more than 100 kV/cm, it can cause nonlinear optical effects in the THz region [3]. Multiphoton absorption will be also observed by using high-repetition coherent radiation.

Therefore, National Institute of Advanced Industrial Science and Technology (AIST) has developed intense THz-wave sources at infrared FEL facilities in

cooperation with Nippon University and Kyoto University. We have already observed coherent synchrotron radiation (CSR) in both infrared FEL facilities. In this article, we will report the status and the new plan of the developments of the coherent radiation THz-wave sources.

## THZ-WAVE SOURCES AT LEBRA

At the Laboratory for Electron Beam Research and Application (LEBRA) at Nihon University, an S-band linac is used to generate unique light sources. The electron-beam energy can be adjusted from 30 to 125 MeV, and the charge in a micropulse is approximately 30 pC in full-bunch mode, where the electron beam is bunched in 350-ps intervals. The LEBRA has two monochromatic light sources, which are the infrared FEL in a wavelength region of 1–6  $\mu$ m and the parametric X-ray radiation (PXR) in an energy region of 5–34 keV [4, 5]. The electron beam is transported from the S-band linac to the FEL straight section or the PXR straight section with the separate 90° arc sections, which can

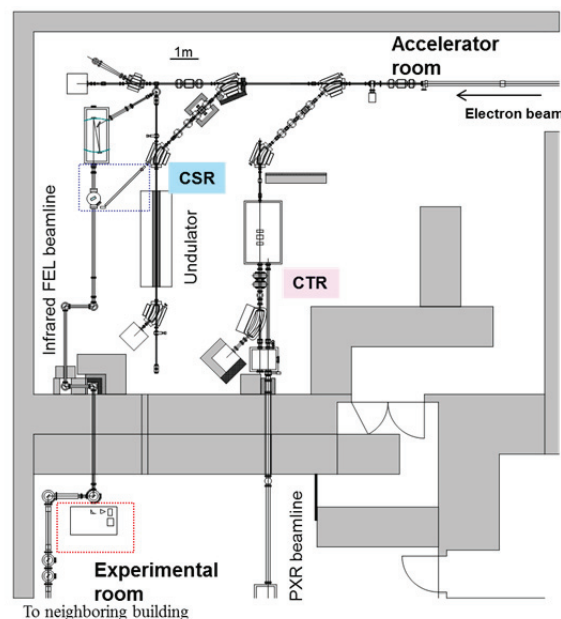


Figure 1: Layout of the experimental setup of coherent radiations at the LEBRA.

\*Work supported by sei.n@aist.go.jp

# LINEAR VLASOV SOLVER FOR MICROBUNCHING GAIN ESTIMATION WITH INCLUSION OF CSR, LSC AND LINAC GEOMETRIC IMPEDANCES

C. -Y. Tsai<sup>#</sup>, Department of Physics, Virginia Tech, Blacksburg, VA 24061, USA  
 D. Douglas, R. Li, and C. Tennant, Jefferson Lab, Newport News, VA 23606, USA

## Abstract

As is known, microbunching instability (MBI) has been one of the most challenging issues in designs of magnetic chicanes for short-wavelength free-electron lasers or linear colliders, as well as those of transport lines for recirculating or energy recovery linac machines. To more accurately quantify MBI in a single-pass system and for more complete analyses, we further extend and continue to increase the capabilities of our previously developed linear Vlasov solver [1] to incorporate more relevant impedance models into the code, including transient and steady-state free-space and/or shielding coherent synchrotron radiation (CSR) impedances, the longitudinal space charge (LSC) impedances, and the linac geometric impedances with extension of the existing formulation to include beam acceleration [2]. Then, we directly solve the linearized Vlasov equation numerically for microbunching gain amplification factor. In this study we apply this code to a beamline lattice of transport arc [3] following an upstream linac section. The resultant gain functions and spectra are presented here, and some results are compared with particle tracking simulation by ELEGANT [4]. We also discuss some underlying physics with inclusion of these collective effects and the limitation of the existing formulation. It is anticipated that this more thorough analysis can further improve the understanding of MBI mechanisms and shed light on how to suppress or compensate MBI effects in lattice designs.

## INTRODUCTION

The beam quality preservation is of a general concern in delivering a high-brightness beam through a transport line or recirculation arc in the design of modern accelerators. Microbunching instability (MBI) has been one of the most challenging issues associated with such beamline designs. Any source of beam performance limitations in such recirculation or transport arcs must be carefully examined in order to preserve the beam quality, such as the coherent synchrotron radiation (CSR), longitudinal space-charge (LSC) and/or other high-frequency impedances that can drive microbunching instabilities.

To accurately quantify the direct consequence of microbunching effect, i.e. the gain amplification factor, we further extend our previously developed semi-analytical simulation code [1] to include more relevant impedance models, including CSR, LSC and linac geometric impedances. The LSC effect stems from (upstream) ripple on top of an electron beam and can accumulate an amount of

energy modulation when the beam traverses a long section of a beamline. Such energy modulation can then convert to density modulation via momentum compaction  $R_{56}$  downstream the beamline [5, 6]. In addition, along the beamline, CSR due to electron radiation emission inside bending dipoles can have a significant effect on further amplifying such density to energy modulation [5, 6]. The accumulation and conversion between density and energy modulations can possibly cause serious microbunching gain amplification (or, MBI).

In this paper, we first introduce the methods of microbunching gain calculation: a kinetic model based on linearized Vlasov equation [7, 8], and particle tracking by ELEGANT as a benchmarking against our code. Then we briefly summarize the impedance models used in our simulations. After that, we illustrate simulation results: the gain functions and spectra for our example lattice, including a transport arc following a section of upstream linac. Finally, we discuss the underlying physics and summarize our observation from the simulation results.

## METHODS

To quantify the MBI in a transport or recirculation beamline, we estimate the microbunching amplification factor  $G$  (or, bunching factor  $g_k$ ) by two distinct methods. The first one, based on a kinetic model, is to solve a (linearized) Vlasov equation [7,8]. This method is of our primary focus in this paper. The second one, served as a benchmarking of the first method, is based on particle tracking method (here we use ELEGANT [4]). For the former, after mathematical simplification of the linearized Vlasov equation, we actually solve a general form of Volterra integral equation for the bunching factor. In our code, to facilitate us in simulating ERL-based lattices which sometimes contain vertical spreaders and/or recombiners, we extend the existing formulation to include both transverse horizontal and vertical bends. Also, we consider the presence of linac sections in a general beamline; the formulation of Volterra integral equation would be slightly modified [2] to accommodate RF acceleration or deceleration. In sum, the governing equation for bunching factor  $g_k$  is summarized below,

$$g_k(s) = g_k^{(0)}(s) + \int_0^s K(s,s')g_k(s')ds' \quad (1)$$

where the kernel function can be particularly expressed as

$$K(s,s') = \frac{ik_0 C(s) I_0 C(s')}{\gamma_0 I_A} \hat{R}_{56}(s' \rightarrow s) Z(kC(s'), s') \times [\text{Landau damping}] \quad (2)$$

for the [Landau damping] term

<sup>#</sup> jcytsai@vt.edu

# INTRABEAM SCATTERING IN HIGH BRIGHTNESS ELECTRON LINACS\*

S. Di Mitri<sup>#</sup>, Elettra Sincrotrone Trieste, 34149 Basovizza, Trieste, Italy

## Abstract

Intra-beam scattering (IBS) of a high brightness electron beam in a linac has been studied analytically, and the expectations found to be in reasonable agreement with particle tracking results from the Elegant code. It comes out that, under standard conditions for a linac driving a free electron laser, IBS plays no significant role in the development of microbunching instability. A partial damping of the instability is envisaged, however, when IBS is enhanced either with dedicated magnetic insertions, or in the presence of an electron beam charge density at least 4 times larger than that produced by present photo-injectors.

## INTRODUCTION

The question to which extent intra-beam scattering (IBS) affects the properties of high brightness electron bunches in linacs was posed in [1,2], with attention to the interplay of IBS and microbunching instability (MBI). Following our study in [3], here we aim to provide a quantitative answer and an outlook, by comparing the analysis and particle tracking runs of the ELEGANT code [4], whereas IBS was simulated following prescriptions given in [2,5].

In particular, we wonder whether IBS could play a role when the beam transverse dimension is squeezed with strong focusing (“low-beta”) FODO cells, so to increase the IBS longitudinal growth rate. At first glance, the idea of using IBS to increase the energy spread of an electron bunch traveling in a dedicated FODO channel seems to be attractive for the following reasons: i) IBS heats the beam by avoiding cost, complexities and maintenance of a laser heater (LH) system [6]; ii) the heating level is tunable with the quadrupoles’ focusing strength; iii) it provides longitudinally uncorrelated energy spread, thus avoiding any side effect associated to the energy modulation induced in a LH at the infrared laser wavelength (*e.g.*, the so-called trickle heating) [7]. We will see however that, to be as effective as a LH, the enhancement of IBS requires a long and densely packed FODO channel. An alternative compact lattice in which the beam recirculates through low-beta FODO channels is investigated. This solution, however, turns out to be not practical because of the coherent synchrotron radiation (CSR) instability that develops through the arcs.

## THEORETICAL BACKGROUND

Ultra-relativistic electron bunches in modern accelerators generally have much smaller velocity spread in the longitudinal direction of motion than in the

transverse planes owing to the relativistic contraction by the Lorentz factor  $\gamma$ :  $\sigma_\delta/\gamma \ll \sigma_{x'}, \sigma_{y'}$ , where  $\sigma_\delta$  is the beam rms fractional energy spread and  $\sigma_{x',y'}$  the rms angular divergence. If the bunch’s charge density is high enough and the bunch travels a long path, multiple Coulomb scattering tends to redistribute the beam momenta from the transverse degree of freedom to the longitudinal one. This process is called IBS and its longitudinal growth rate may be comparable to the beam damping time in low emittance electron storage rings. The instantaneous growth rate of the energy spread of a bunched beam circulating in a ring was given in [8,9]. Since there are no synchrotron oscillations in a linac, the formula for a coasting beam should be used here (which results in a growth rate a factor 2 larger than that of a bunched beam) [8]:

$$\frac{1}{\sigma_\delta} \frac{d\sigma_\delta}{dt} \approx \frac{r_e^2 c N}{8\gamma^2 \varepsilon_{n,x} \sigma_x \sigma_z \sigma_\delta^2} \ln \left( \frac{\Delta\gamma_{\max}}{\Delta\gamma_{\min}} \right) \quad (1)$$

Here  $r_e$  is the electron classical radius,  $\beta c \approx c$  the electron velocity,  $N$  the number of electrons in the bunch,  $\varepsilon_{n,x} = \varepsilon_{n,y}$  the rms normalized transverse emittance of a round beam, and  $\sigma_z$  the rms bunch length. The argument of the Coulomb logarithm is the ratio of the maximum and the minimum energy exchange due to a single scattering event,

$$\Delta\gamma_{\max} \propto \gamma^2 \sigma_{x'}, \quad \Delta\gamma_{\min} \propto r_e / (\sigma_x \sigma_{x'}) \approx \gamma r_e / \varepsilon_{n,x} \quad [1].$$

Following an argument made in [10], we consider that the IBS energy distribution has a nearly Gaussian core with a long tail. Since we are mostly interested in the energy spread of the Gaussian core, we set the maximum energy transfer to  $\Delta\gamma_{\max} = \gamma \cdot 10^{-5}$  as also done in [1], and find that the logarithm is of the order of 10 for a normalized emittance of  $\sim 1 \mu\text{m}$ . Then, Eq. 1 can be integrated and it yields to the final fractional rms energy spread in the presence of IBS cumulated over the distance  $\Delta s$  [3]:

$$\sigma_\delta \approx \sqrt{\sigma_{\delta,0}^2 + \frac{2r_e^2 N}{\gamma^2 \varepsilon_{n,x} \sigma_x \sigma_z} \Delta s} \equiv \sqrt{\sigma_{\delta,0}^2 + \sigma_{\delta,IBS}^2}, \quad (2)$$

with  $\sigma_{\delta,0}$  the initial rms fractional incoherent energy spread. Equation 2 is an approximate expression for smooth betatron oscillations, neither energy dispersion nor particle acceleration.

If we apply Eq. 2 to the low energy part of a linac, we find that an electron beam from a state-of-the-art photo-injector, *e.g.* with beam charge  $Q = 0.5 \text{ nC}$ ,  $\sigma_z = 750 \mu\text{m}$ ,  $\varepsilon_n = 0.6 \mu\text{m rad}$ ,  $\sigma_x = 150 \mu\text{m}$  and  $\gamma = 300$ , collects an absolute rms energy spread  $\sigma_{E,IBS} \approx 3 \text{ keV}$  over  $\Delta s \sim 30 \text{ m}$ . This is comparable to the typical value of  $\sigma_{E,0} \approx 2 \text{ keV}$  out of the photo-injector [11], and still far from the amount of

\*Work supported by the FERMI project of Elettra Sincrotrone Trieste.  
#simone.dimitri@elettra.eu

## WAKE FIELD POTENTIALS OF “DECHIRPERS”\*

A. Novokhatski<sup>#</sup>, SLAC National Accelerator Laboratory, Menlo Park, CA 94025, USA

### Abstract

A corrugated structure, which is used in “dechirper” devices, is usually a pipe or two plates with small corrugations (bumps) on the walls. There is a good single-mode description of the wake potentials excited by a relativistic bunch if the wave length of the mode is much longer than the distance between the bumps in the pipe. However, ultra-short bunches, which are now used in FELs, excite much higher frequency fields and the corresponding wake potentials will be very different from the single-mode description. We have made analyzes of these wake potentials based on a numerical solution of Maxwell’s equations. It was confirmed that the behavior of the wake fields of ultra-short bunches in corrugated structures is not much different from the fields excited usually in accelerating structures where the wake potentials are described by the exponential function. We also carried out calculations for a similar device, that was installed and measured at the Pohang Accelerator Laboratory, Korea. We find very good agreement with the experimental results.

### INTRODUCTION

The precise knowledge of the wake fields generated in different elements of free electron lasers (FEL) including accelerator, beam transport and undulators has become very important with increasing power and efficiency of X-ray production. Usually it is a “negative” effect. For example in Ref.[1] it is demonstrated how the wake fields generated in collimators may decrease the FEL performance. However the effect from wake fields can also be “positive” if this field is used to improve the energy spectrum. These wake fields can be generated in the accelerator (linac) or in special devices – “dechirpers”. To our knowledge this word was introduced in ref. [2] for the first time.

There are several publications which have some sort of formula for the wake fields in corrugated structures. The references to these publications can be found in Ref.[3-4]. These formulas are derived from the assumption of a single dominating mode and the Green’s function for the wake potentials is described as a damped cosine function. Although they referred to our 1997 publication [5], where we found a similarity to the wake fields in corrugated structures with the fields in a tube with a thin dielectric layer, the authors do not fully analyze the applicability of the single mode approach to describe wake fields of very short bunches. A corrugated wall structure is planned for use in the device that makes an additional energy loss along the very short bunches of the LCLS [4]. It now becomes very important to check how well a single mode approach can describe the fields, that are excited in

corrugated structures and perhaps another description must be used. For the FEL application the dechirper has a small sized corrugation structure, of order of millimeters. Electron bunches in the FEL have a length of micron. If we scale the bunch length together with the structure size up ten times or more we will get geometry environments that are very similar to the linear accelerating structures. As we know, the wake fields in the accelerating structures are not described by a single mode. There is another description, which contains all modes. Such as the Green’s function for the TESLA accelerating structure [6] or the SLAC accelerating structure [7]. We may assume that the wake potentials of a corrugated structure excited by short bunches are also described by this or a similar function. To check this assumption we calculated wake potentials of the corrugated structure using a computer code NOVO [8], which was specially designed to calculate wake fields of very short bunches. This code has been benchmarked based on a good agreement with the wake fields measured in the LCLS-LTU [9]. Recently the code was extended for the wake field calculations in rectangular beam chambers [10].

### A DECHIRPER

As mentioned above, a dechirper takes energy from the beam through the interaction of the bunch electromagnetic field with a metal corrugated structure. The practical design of the dechirper consists of two identical movable parallel plates (jaws) with corrugated walls in a form of the periodic set of planar diagrams. A schematic drawing of the dechirper is shown in Fig. 1. The dechirper, which is planned to be installed at LCLS, has the following parameters of the corrugated structure. The period is 0.5 mm, the thickness of a diaphragm is a half of a period and the transverse sizes of a diaphragm are:  $h=0.5$  mm,  $L_x=12$  mm. Definitions of the sizes are given in Fig. 1. The total length  $L$  of the corrugated structure is 2 m. The gap between two jaws is adjustable. The nominal gap is 1.4 mm.

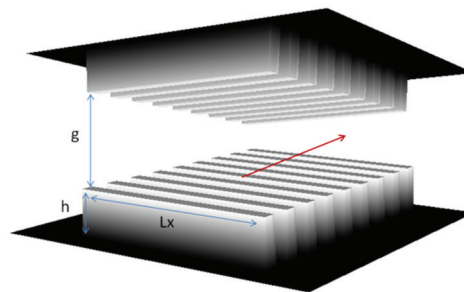


Figure 1: A schematic drawing of a dechirper. The red line shows a bunch trajectory.

\*Work supported by DoE Contract No. DOE-AC02-76SF00515  
<sup>#</sup>novov@slac.stanford.edu

# THE EFFECT OF WAKE FIELDS ON THE FEL PERFORMANCE\*

A. Novokhatski<sup>#</sup>, F.-J. Decker, Yu. Nosochkov, M. Sullivan  
 SLAC National Accelerator Laboratory, Menlo Park, California, 94025, U.S.A.

## Abstract

When a beam travels near collimator jaws, it gets an energy loss and a transverse kick due to the back reaction of the beam field diffracted on the collimator's jaws. The effect becomes very important for an intense short bunch when a tight collimation of the background beam halo is required. In the Linac Coherent Light Source (LCLS) at SLAC a collimation system is used to protect the undulators from radiation due to particles in the beam halo. The collimators in the LCLS must remove the halo particles before they affect and eventually degrade the very precise fields of the permanent magnet undulators [1]. The wake field effect from the collimators not only brings an additional energy jitter and change of the trajectory of the beam, but also rotates the beam on the phase plane that consequently leads to a degradation of the performance of the Free Electron Laser (FEL) at LCLS. In this paper, we describe a model of the wake field radiation in the SLAC linac collimators. We also present results of experimental measurements, which clearly confirm our model.

## INTRODUCTION

The effect of collimators with small apertures on the transverse beam dynamics was observed during the operation of the Stanford Linear Collider (SLC) [2]. The problem of wake fields excited by collimators becomes more important for linac operation and x-ray production at LCLS. The backward reaction of the wake field from the collimators on the beam brings an additional energy jitter and a change of the trajectory of the beam. It leads also to a degradation of the FEL performance at the LCLS. This is because of the special character of the wake fields: the response reaction depends on the longitudinal position of the particles in the bunch. The "head" of the bunch is not deflected at all, but the "tail" gets the maximum deflection force. This kind of kick leads to the bunch being geometrically tilted. Because the "tail" of the bunch may oscillate in the lattice, the orientation of the bunch in space will oscillate too. Effectively the transverse projected emittance is increased and the FEL performance is degraded.

## SLAC LINAC COLLIMATOR

Nine adjustable beam collimators are used in the LCLS operation, mainly accomplished in two main sections: at end of the SLAC linac and in the region from the linac to the undulators (LTU). Each collimator is composed of horizontal and vertical pairs of rectangular collimator jaws. The geometry of a collimator assembly is very

complicated because each jaw is independently and remotely adjustable and can completely shadow the beam path. A collimator is essentially a kind of assembly of RF cavities coupled to the beam. Bellows with a chamber form two quarter-wave coaxial cavities. There are several trapped RF modes inside the collimator volume. In a multi-bunch operation, some energy is deposited in this region. One jaw can be in a position that is too close to the beam path while the other jaw is moved out. The jaws have a titanium alloy body with a slightly curved face (10-m radius) and a titanium-nitride jaw surface for improved conductivity and survivability against beam hits [3]. Currently the gap between jaws is kept approximately  $\pm 1.6$  mm in all collimators. However, the spontaneous beam halo requires smaller gaps.

## A TRANVERSE KICK FROM A COLLIMATOR JAW

Based on the analytical estimates [4] we assume that the kick from a collimator jaw is inversely proportional to the distance to this jaw. We estimate a kick for a particle with longitudinal position  $s$  in a bunch as

$$g(s) = \frac{Z_0}{4\pi} I_b \frac{s}{\delta}, \quad (1)$$

where  $\delta$  is a transverse distance from the bunch to the collimator jaw,  $I_b$  is the bunch current, and  $Z_0$  is impedance of free space. The average bunch kick will be

$$g_{av} = \frac{1}{8\pi\epsilon_0} \frac{Q}{\delta}. \quad (2)$$

Opposite to the energy loss, which is proportional to the bunch current, the average kick is determined by a bunch charge  $Q$  and the proximity of the beam to the edge of the collimator jaw. The nonlinear behaviour of the kick leads immediately to emittance growth if a bunch travels very close to a collimator jaw edge. However, even a linear kick may increase the effective or projected emittance because a bunch "head" and a bunch "tail" will get different kicks. A "head" will receive nothing, but a "tail" will get a maximum kick.

## A DIPOLE KICK FROM A COLLIMATOR WITH TWO JAWS

If we know a kick from one jaw, we can calculate a kick from a collimator with two jaws. Each jaw attracts the beam and the total kick must be the sum of the two kicks

\*Work was supported by DOE-AC02-76SF00515.  
<sup>#</sup>novo@slac.stanford.edu

# REVERSIBLE ELECTRON BEAM HEATER WITHOUT TRANSVERSE DEFLECTING CAVITIES

G. Stupakov and P. Emma

SLAC National Accelerator Laboratory, Menlo Park, CA, USA

## Abstract

In Ref. [1] a technique to suppress the instability with the help of a reversible electron beam heater was proposed. It employs transverse deflecting cavities synchronized in a way that one of the cavities, located before a bunch compressor, generates a slice energy spread, while the other one removes it after the beam passes through the bunch compressor. In this paper we demonstrate that a reversible heater equivalent to that of [1] can be designed using much simpler elements: bend magnets and quadrupoles in combination with the energy chirp of the beam.

## INTRODUCTION

The performance of modern free electron lasers is often limited by the microbunching instability in the electron beam that develops during its acceleration and transportation to the undulator. A search of new methods for effective suppression of the instability is crucial for future FELs, especially the ones that use external seeding. One of the promising approaches to this problem is the idea of a reversible electron beam heater proposed in Ref. [1]. It employs transverse deflecting cavities (TDS) synchronized in a way that one of the cavities, located before a bunch compressor, introduces a slice energy spread, and the other one removes it after the bunch compressor. Being an attractive concept, it however imposes extremely tight tolerances on the synchronization of the cavities. It also adds a considerable cost of the RF structures and an additional RF power system to the accelerator.

An ideal reversible heater has to perform two actions. First, it should increase the slice energy spread in the beam before the bunch compressor to the level that suppresses generation of microbunching instability due to coherent synchrotron radiation in the compressor, and to remove it afterwards restoring the beam to the original energy spread (amplified by the compression factor). Second, it is also desirable that the heater destroys energy and density modulations in the beam which are accumulated before the compressor—these are usually associated with the longitudinal space charge impedance and earlier compressing stages. Of course, the heater should not noticeably increase the transverse emittance of the beam.

In this paper we show how a reversible heater can be implemented using DC magnets without TDS. We simplify our analysis by assuming thin elements and neglecting the optics associated with drifts between them.

## REVERSIBLE HEATER USING TDS

Here we give a brief description of the reversible heater based on transverse deflecting cavities and analyze, following [1], its effect on the energy spread of the beam and the beam emittance. While our analysis can be easily extended for a broader range of distribution functions, to evaluate the effect of the heater, for specificity, we consider an initial 4D Gaussian distribution function of the beam

$$f_0(x, x', z, \eta) = A \exp \left[ -\frac{1}{2} \left( \frac{x^2}{\sigma_{x0}^2} + \frac{x'^2}{\sigma_{x'0}^2} + \frac{z^2}{\sigma_{z0}^2} + \frac{\eta^2}{\sigma_{\eta0}^2} \right) \right], \quad (1)$$

where  $x$  and  $x'$  are the transverse coordinate and angle,  $z$  is the longitudinal coordinate in the beam,  $\eta = \Delta E/E$  is the relative energy deviation, and  $\sigma_{x0}$ ,  $\sigma_{x'0}$ ,  $\sigma_{z0}$  and  $\sigma_{\eta0}$  are the standard deviations for the corresponding variables. In the distribution function (1) we ignore the transverse coordinates  $y$  and  $y'$ . The normalization constant  $A$  is such that  $\int f_0 dx dx' dz d\eta = 1$ .

When the beam with the initial distribution function (1) passes through a system under consideration the distribution function is transformed,  $f_0(x, x', z, \eta) \rightarrow f_1(x, x', z, \eta)$ , where  $f_1$  is the distribution function at the exit. To find  $f_1$ , we use the formalism of linear optics with  $4 \times 4$  beam transport matrices that act on vector  $(x, x', z, \eta)$ . To take into account the acceleration before the BC that generates an energy chirp  $h$  (that is a linear correlation between the energy  $\eta$  and the longitudinal coordinate  $z$ ) we will use the matrix  $R_c(h)$ ,

$$R_c(h) = \begin{pmatrix} 1 & 0 & 0 & 0 \\ 0 & 1 & 0 & 0 \\ 0 & 0 & 1 & 0 \\ 0 & 0 & h & 1 \end{pmatrix}. \quad (2)$$

For a bunch compressor (BC) we will use the matrix

$$R_{BC} = \begin{pmatrix} 1 & 0 & 0 & 0 \\ 0 & 1 & 0 & 0 \\ 0 & 0 & 1 & r \\ 0 & 0 & 0 & 1 \end{pmatrix}, \quad (3)$$

with  $r$  being the {5, 6} element of the 6-dimensional transport matrix of the compressor.

In linear optics, the  $R$ -matrix for a short transverse deflecting cavity is given by

$$R_{TDS}(K) = \begin{pmatrix} 1 & 0 & 0 & 0 \\ 0 & 1 & K & 0 \\ 0 & 0 & 1 & 0 \\ K & 0 & 0 & 1 \end{pmatrix}, \quad (4)$$

# FRONT END SIMULATIONS AND DESIGN FOR THE CLARA FEL TEST FACILITY

J.W. McKenzie, A.D. Brynes, B.L. Milityn, STFC Daresbury Laboratory,  
Warrington, WA4 4AD, UK

## Abstract

We present the design and simulations of the Front End for CLARA (Compact Linear Accelerator for Research and Applications), the proposed UK FEL test facility at Daresbury Laboratory. This is based around an S-band RF photocathode gun. Initially this will be the 2.5 cell gun, currently used on VELA facility at Daresbury, which is limited to 10 Hz repetition rate. Later, this will be upgraded to a 1.5 cell gun, currently under development, which will allow repetition rates of up to 400 Hz to be reached. The beam will be accelerated up to 50 MeV with a booster linac which will be operated in both bunching and boosting modes for different operating regimes of CLARA. Simulations are presented for a currently achieved performance of the RF system and drive laser with optimisation of the laser pulse lengths for various operational modes of CLARA.

## INTRODUCTION

CLARA (Compact Linear Accelerator for Research and Applications) is a proposed 250 MeV FEL test facility at Daresbury Laboratory [1]. It will comprise a photoinjector, a four section S-band linac and FEL test area. The first 2 m long linac section serves as a booster or a buncher. CLARA is designed to test out various novel FEL schemes which require different beam pulses varying from ultra short very high current bunches for single-spike SASE to relatively long for seeded FEL. To cover all the range of the bunch lengths, longitudinal compression is going to be provided through both magnetic compression and velocity bunching. For many of these schemes, the required beam parameters can be met by either compression scheme. However, seeded FEL operation can only be met with the magnetic compression as a constant current profile is desired along the bunch, while single-spike SASE can only be met with velocity bunching to a very short bunch with high peak current. A comparison of the compression schemes can be found in [2].

A staged approach is taken to construction and commissioning, with stage one comprising of a photoinjector and booster linac to be installed in 2016. This links in to the existing VELA facility at Daresbury [3] and shares its RF and laser infrastructure.

The electron source for CLARA will initially be the 2.5 cell S-band RF gun currently used at VELA. This is limited to 10 Hz repetition rate, at bunch charges of up to 250 pC. The gun is fed from a 10 MW klystron with 8.5 MW of power available at the gun. The maximum beam momentum measured around 5.0 MeV/c. To reach repetition rates of up to 400 Hz, a 1.5 cell High Repetition

Rate S-band Gun (HRRG) has been designed and is currently under construction [4].

The VELA photoinjector laser will also be used to drive CLARA, with a beam split in the transport line. The laser pulse has a length of 76 fs rms that allows short low charge electron bunches to be produced. In this paper we analyse the beam parameters which can be obtained with the currently achieved performance of the RF system and laser and investigate the use of a longer pulse laser for the different modes of CLARA.

## OPERATION OF THE BASELINE INJECTOR WITH REDUCED GUN FIELD

The original design of the 2.5-cell gun assumed operation at a peak field of 100 MV/m. However, the measured beam momentum in VELA is lower than was expected based on simulations and measured quality factors [5]. To match the measured beam momentum of 5 MeV/c, simulations show the peak electric field to be 70 MV/m.

In this work, beam dynamics simulations were carried out with the ASTRA code. The photoinjector laser spot size was simulated as a 1 mm diameter flat-top with a 76 fs rms Gaussian temporal profile. An intrinsic emittance of the beam from the copper photocathodes assumed to be of 0.9 mm·mrad per mm rms as per LCLS measurements [6].

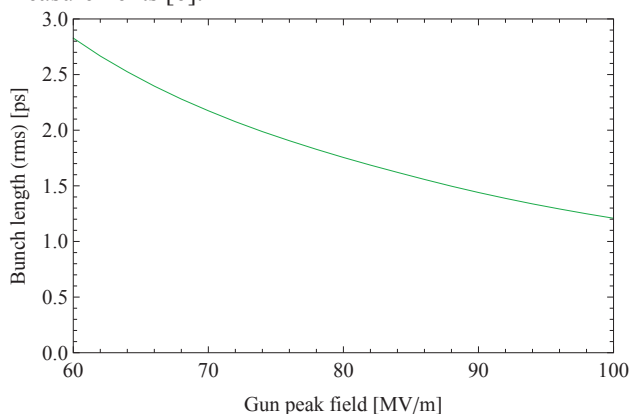


Figure 1: Simulated dependence of the length of a 250 pC bunch at the exit of the 2.5 cell gun.

Due to the short laser pulse length, the gun operates in the “blow-out” regime, where the space-charge expands emitted bunch. Thus, the electron bunch length in this case is determined by the bunch charge and the rate of acceleration. Fig. 1 shows how the rms length of a 250 pC bunch after the gun depends on the peak field (for the same operational phase). It can be seen then that reducing the gun peak field from 100 MV/m to 70 MV/m, causes

# RFTweak 5 – AN EFFICIENT LONGITUDINAL BEAM DYNAMICS CODE

Bolko Beutner\*, Martin Dohlus, Hannes Dinter  
Deutsches Elektronen-Synchrotron (DESY), Hamburg, Germany

## Abstract

The shaping of the longitudinal phase space in bunch compression systems is essential for efficient FEL operation. RF systems and self-field interactions contribute to the overall phase space structure. The design of the various facilities relies on extensive beam dynamics simulations to define the longitudinal dynamics. However, in everyday control room applications such techniques are often not fast enough for efficient operation, e.g. for SASE tuning. Therefore efficient longitudinal beam dynamics codes are required while still maintaining reasonable accuracy. Our approach is to pre-calculate most of the required data for self-field interactions and store them on disc to reduce required online calculation time to a minimum. In this paper we present the fast longitudinal tracking code RFTweak 5, which includes wakes, space charge, and CSR interactions. With this code the full European XFEL with a 1M particles bunch is calculated on the order of minutes on a standard laptop. Neglecting CSR effects this time reduces to seconds.

## INTRODUCTION

RFTweak 5 is a fast tracking code for longitudinal phase space dynamics. A strong use case is the online setup of bunch compression in the control room during e.g. SASE tuning. The concept of the code is similar to LiTrack [1], which is written in MATLAB as well. RFTweak 5 includes effects of longitudinal wakes, space charge interactions as well as coherent synchrotron radiation (CSR) emission. While the underlying code is applicable to different electron linacs, the graphical user interface (GUI) of the code is build specifically for FLASH and the European XFEL. An example is shown in Fig. 1.

## OVERVIEW OF THE TRACKING PROCEDURE

Beam-lines defined in RFTweak 5 consisting primarily of two different element types. Elements which keep the individual longitudinal particle position offset fixed while the energy is altered (Type 1) and the opposite in which the energy is constant and the position is modified (Type 2). Examples are RF structures or bunch compression chicane respectively. We assume a sufficiently high beam energy to justify the assumption of fixed longitudinal position offsets in straight sections (Type 1 elements like drifts, quadrupoles, or RF structures). Furthermore, the assumption is made that elements with longitudinal dispersion (Type 2 like chicanes or energy collimator) consist purely of magnetic fields.

\* bolko.beutner@desy.de

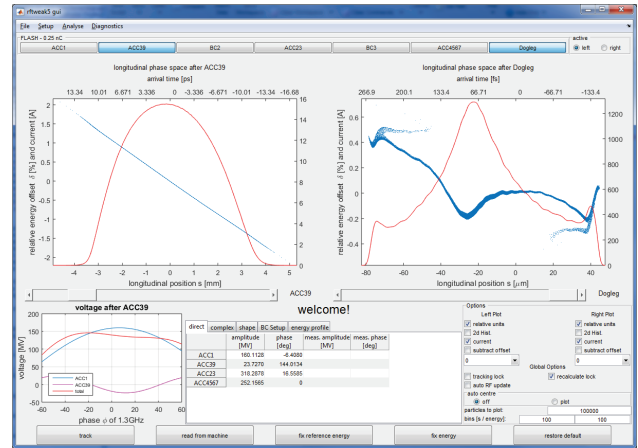


Figure 1: Layout of the main GUI for FLASH. Two phase space distributions are displayed at selected positions along the machine. Various options are available, like the display as point cloud or density histograms or the subtraction of polynomial offsets of various order. RF parameters of the linac can be entered by the user or read from the control system. Resulting voltage profiles after the lineariser cavities are directly displayed.

Self field interactions are neglected but CSR effects can be included as described later.

Both types of elements are described by the polynomial expansion

$$s_{n+1}^i = s_n^i + R_{56}\delta E_{i,n} + T_{566}\delta E_{i,n}^2 + \dots \quad (1)$$

$$\delta E_{i,n+1} = \delta E_{i,n} + A + Bs_n^i + Cs_n^{i2} + \dots, \quad (2)$$

with the normalised energy offset  $\delta E_{i,n}$  of particle  $i$  at element  $n$ , some coefficients  $A, B, C$  representing longitudinal fields, and the longitudinal dispersion parameters  $R_{56}, T_{566}, \dots$ .

In the first case the coefficients are obtained from a Taylor expansion of the longitudinal dispersion [2], in the latter the Taylor series expansion represents the longitudinal electric fields, e.g. the RF voltage.

Elements of Type 2 can include additional effects of longitudinal wakes. These wakes are either determined by geometry (e.g. cavities, changes in beam pipe diameter) or space charge. For FLASH and the European XFEL the geometric wakes are stored in a database [3]. In this database the integrated wakes per section are summarised as greens functions (wakes of an infinitesimal short bunch). Space charge wakes, which are dependent on the energy profile and the transverse beam dimensions, are summarised per section as well. These wake functions are calculated given

## TECHNOLOGY MATURATION FOR THE MaRIE 1.0 X-FEL\*

J.W. Lewellen<sup>#</sup>, K. Bishofberger, B.E. Carlsten, L. Duffy, F.L. Krawczyk, Q.R. Marksteiner, D.C. Nguyen, S.J. Russell, R. L. Sheffield, N. Yampolsky, LANL, Los Alamos, NM 87545, USA

### Abstract

Los Alamos National Laboratory is proposing a high-energy XFEL, named MaRIE, to meet its mission needs. MaRIE will be required to generate coherent 42+ keV photons, and, due to space constraints at the LANSCE accelerator complex at Los Alamos, MaRIE’s design electron beam energy is 12 GeV. This combination places significant restrictions upon the MaRIE electron beam parameters, in particular the transverse emittance and energy spread at the undulator entrance. We are developing approaches to meet these requirements, but these often require solutions extending beyond the current state-of-the-art in X-FEL design.

To reduce overall project risk, therefore, we have identified a number of key experimental and modeling / simulation efforts intended to address both the areas of greatest uncertainty in the preliminary MaRIE design, and the areas of largest known risk. This paper describes the general requirements for the MaRIE X-FEL, our current areas of greatest concern with the preliminary design concept, and our corresponding Technology Maturation Plan (TMP).

### INTRODUCTION

The Matter-Radiation Interactions in Extremes (MaRIE) facility is intended to provide unprecedented time- and space-resolved measurements on multiple scales, but with particular emphasis on mesoscale phenomena in dense materials such as metals at up to GHz measurement rates [1]. The MaRIE concept leverages the existing LANSCE 1-MW, 0.8-GeV proton accelerator [2] for multi-probe measurement capabilities.

MaRIE 1.0 is the initial implementation of the MaRIE facility, and includes at its core a 42-keV X-ray free-electron laser (X-FEL) driven by a 12-GeV superconducting linac. The X-FEL must be co-located with the existing LANSCE facility to fully realize the multi-probe promise of MaRIE; however, this imposes several constraints on the overall design of the MaRIE X-FEL linac, in particular the length available for the accelerator, over and above the stringent beam quality required by the 42-keV photon energy goal.

Electron beam radiography (eRad) is a highly desirable option for MaRIE. While most of our initial modelling and simulation work has focused upon the requirements for the X-FEL, the option to support eRad operations should not be precluded by the MaRIE linac design. Emittance and bunch length are not critical parameters for eRad bunches, but eRad requires bunch charges of 2 nC, and the MaRIE

linac must be capable of providing both eRad and XFEL bunches within the same macropulse.

While our initial design simulations indicate the MaRIE linac design is feasible, we have identified several areas of particular concern where the performance of the MaRIE driver linac must be extended beyond the current state-of-the-art. A technical maturation plan (TMP) has been developed to explore the relevant physics and ameliorate risk early in the MaRIE project.

### REQUIRED PERFORMANCE

MaRIE requires an extraordinarily bright electron beam in order to drive the SASE process to saturation within the X-FEL. (While the eRad beam should not be challenging to generate, copropagating it with an X-FEL drive beam raises additional questions and concerns. However, the MaRIE TMP is currently focused primarily on the challenges surrounding the X-FEL design.) Table 1 summarizes the parameters and performance requirements for the MaRIE linac.

Table 1: MaRIE Drive Linac Performance Requirements

Parameter	Units	Value
Beam energy	GeV	12
Linac frequency	GHz	1.3
Cavity gradient	MV/m	31.5
Max. macropulse duration	μs	100
Bunches / macropulse		10 – 100
X-FEL bunch charge	nC	0.1 nominal 0.2 max
eRad bunch charge	nC	2
Intrabunch energy spread		$\leq 1 \cdot 10^{-4}$
Slice energy spread		$\leq 1.5 \cdot 10^{-4}$
RMS slice emittance	μm	$\leq 0.2$
RMS bunch length	fs	12

### IDENTIFIED KEY RISK AREAS

The MaRIE beam requirements at the undulator drive requirements for the remainder of the linac. While based on existing technology to the extent feasible, MaRIE’s performance requirements demand beyond-state-of-the-art performance in several areas.

\*Work supported by the US DOE / NNSA under contract # jwlewellen@lanl.gov DE-AC52-06NA25396.

# TRANSVERSE EMITTANCE MEASUREMENT OF KAERI LINAC WITH THICK LENS QUADRUPOLE SCAN

Sadiq Setiniyaz\*, In-Hyung Baek, MoonSik Chae, Boris Gudkov, Byung-Heon Han, Kyu Ha Jang, Young Uk Jeong, Hyun Woo Kim, Jinhee Nam, Sunjeong Park, KAERI, Daejeon, Republic of Korea  
 Sergey Miginsky and Nikolay Vinokurov  
 Budker INP RAS, Novosibirsk, Russia and KAERI, Daejeon, Republic of Korea

## Abstract

The UED (Ultrafast Electron Diffraction) beamline of KAERI (Korea Atomic Energy Research Institute) WCI (World Class Institute) Center has been completed and successfully commissioned. Transverse emittance of the electron beam was measured at the entrance of the UED chamber with the quadrupole scan technique. In this technique, larger drift distance between the quad and screen is preferred because it gives better thin lens approximation. A space charge dominated beam however, will undergo emittance growth in the long drift caused by the space charge force. We suggest mitigating this growth by introducing quadrupole scan with short drift and without thin lens approximation. We shall discuss the measurement process and results.

## INTRODUCTION

The RF photogun of KAERI WCI Center is designed to generate sub-picosecond electron bunches with energy around 3.2 MeV. The beam can be delivered to UED experiments or can be further accelerated up to 20-30 MeV by the main accelerating cavity for X-ray/THz pump and probe experiments as shown in the Fig. 1. The UED section of beamline is designed to supply electron bunches with 0.1 ps length, 1 pC charge, and nominal energy of 3 MeV a ninety degree using an achromatic bend by velocity bunching [1]. The UED section has been successfully commissioned recently and electron beam parameters were measured.

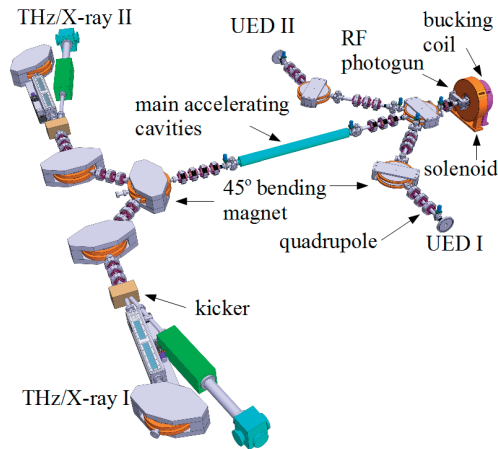


Figure 1: KAERI WCI center electron beamline layout.

Transverse emittance and Twiss parameters are important parameters of an accelerator to quantify the beam quality and match optics. Most common methods to measure emittance are quadrupole scan [2–6], the slit and collector [7, 8], the pepper-pot [9]. In the quadrupole scan, the beamsizes is measured as a function of the quadrupole magnetic field strength [2]. Imaging screens like OTR (Optical Transition Radiation), YAG (Yttrium aluminium garnet), or phosphor screens are used to observe beam profile along with a synchronized camera. Generally, thin lens approximation is applied and rms beamsizes obtained from the beam profile are used to extract the emittance and Twiss parameters by fitting a parabolic function.

The thin lens approximation is effective when  $\sqrt{k_1}L \ll 1$ , where  $k_1$  is quad strength and  $L$  is its effective length. The quad here is viewed as a thin focusing/de-focusing lens. In quadrupole scanning method, for a better thin lens approximation  $k_1$  is kept small while the drift distance between the quad and screen is set as large as possible (usually few meters). But a space charge dominated beam pass through a long drift will experience emittance growth due to the space charge force [10]. This growth can be mitigated by shortening drift length and extracting emittance without using thin lens approximation. In our case, drift length is 23 cm.

## THICK LENS QUADRUPOLE SCAN

In quadrupole scan, a quadrupole magnet and a screen are used to measure the emittance and Twiss parameters of the beam. The screen is separated from the quad by a drift distance. Transfer matrix of the scanning region  $\mathbf{M}$  is given by the matrix product of the transfer matrices of drift  $\mathbf{S}$  and quad  $\mathbf{Q}$

$$\mathbf{M} = \mathbf{S}\mathbf{Q} = \begin{pmatrix} m_{11} & m_{12} \\ m_{21} & m_{22} \end{pmatrix}. \quad (1)$$

Here  $\mathbf{S}$  and  $\mathbf{Q}$  are given by

$$\mathbf{Q} = \begin{pmatrix} \cos\sqrt{k_1}L & \frac{1}{\sqrt{k_1}}\sin\sqrt{k_1}L \\ -\sqrt{k_1}\sin\sqrt{k_1}L & \cos\sqrt{k_1}L \end{pmatrix}, \quad (2)$$

$$\mathbf{S} = \begin{pmatrix} 1 & l \\ 0 & 1 \end{pmatrix}, \quad (3)$$

where  $l$  is the drift length. The beam matrix at the screen ( $\sigma_s$ ) is related to the beam matrix of the quadrupole ( $\sigma_q$ ) using the similarity transformation [11]

$$\sigma_s = \mathbf{M}\sigma_q\mathbf{M}^T. \quad (4)$$

\* sadik82@gmail.com

## ELECTRON BUNCH LENGTH MEASUREMENT USING RF DEFLECTING CAVITY

Sunjeong Park<sup>#</sup>, Kyunpook National University, Daegu and KAERI, Daejeon, Republic of Korea  
Hyun Woo Kim, Sangyoon Bae, Junggho Mun, Kyuha Jang, Young Uk Jeong, Nikolay Vinokurov,  
KAERI, Daejeon, Republic of Korea  
Eun-San Kim, Kyunpook National University, Daegu, Republic of Korea

### Abstract

Recently, the RF photogun based-ultrafast electron diffraction (UED) system has been developed in KAERI. In the system, the emitted electron bunches are experimentally confirmed to be accelerated up to 3 MeV at 5 MW of RF power. And the time duration of the each bunch is initially designed to be less than 50 fs at the sample position. To analyse the performance of the system and to measure exactly the length of the electron bunches, we developed a rectangular type of S-band deflecting cavity working on  $TM_{120}$  mode. The principle of electron deflecting in the cavity, design & mechanical fabrication process and test results will be present in the conference.

### INTRODUCTION

To understand the ultrafast dynamics of atoms or molecules, we use the X-FEL or ultrafast electron diffraction (UED) system. Those systems can provide the pulses with high temporal and spatial resolution. UED system using electron bunches with a few MeV has compact size compared with X-FEL, while it still can make the femtosecond time resolution or over sub nanometers of atomic spatial dimension [1].

Figure 1 shows schematics of the KAERI UED system. The RF photocathode gun is equipped at the system for the electron generation. The electron beam emitted from photocathode by fs laser is accelerated to 3 MeV by input RF power to reduce the space charge effect. After the gun, the electron beam is focused by several magnets, and the electron bunch length would be less than 50 fs. To measure the longitudinal distribution of the electron bunch, we are going to use an RF deflecting cavity working on  $TM_{120}$  mode. A strong transverse magnetic field deflects the beam passing through the cavity. After that the transverse beam size at the screen located downstream at the cavity is related to the bunch length at the deflector position.

The temporal resolution of deflecting cavity can be calculated by using following equation:

$$\Delta t = \Delta x \frac{U/e}{L\pi f V_t}$$

To get the temporal resolution less than 20 fs, the RF input power at the cavity is estimated to be 2 MW. To improve the resolution of measurement, the 10  $\mu\text{m}$  slit would be used at upstream of the deflecting cavity.

### RF DESIGN

We design the RF deflecting cavity similar to a rectangular cavity which drives 2.856 GHz working on  $TM_{120}$  mode [2]. The distribution of electromagnetic field in the cavity is shown in Figure 2.

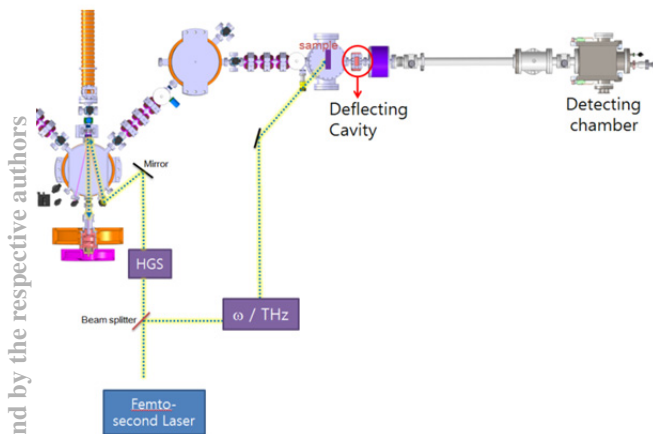


Figure 1: Schematic of the Korea Atomic Energy Research Institute (KAERI) UED system.

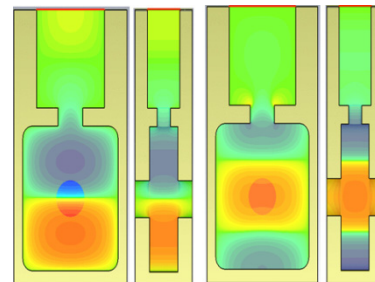


Figure 2: Electric field (left) and magnetic field (right) distribution of  $TM_{120}$  mode in the deflecting cavity.

Figure 3 shows the simulation results of the RF deflecting cavity. The resonance frequency of the results is higher than expected value because of error at the simulation.

\*Work supported by the WCI Program of NRF of Korea (NRF Grant Number: WCI 2011-001) and the RFBR Grant 11-02-91320-SIG\_a.  
#Sunjeong@kaeri.re.kr

# TRANSVERSE-EMITTANCE PRESERVING TRANSFER LINE AND ARC COMPRESSOR FOR HIGH BRIGHTNESS ELECTRON SOURCES\*

S. Di Mitri<sup>#</sup>, M. Cornacchia, Elettra Sincrotrone Trieste, 34149 Basovizza, Trieste, Italy  
 S. Spampinati, Department of Physics, University of Liverpool, Liverpool L69 7ZX, United Kingdom, and Cockcroft Institute, Sci-Tech Daresbury, Warrington WA4 4AD, United Kingdom

## Abstract

Minimizing transverse emittance is essential in single- or few-passes accelerators designed to deliver high brightness electron beams. Emission of coherent synchrotron radiation (CSR) is an important factor of emittance degradation. We have demonstrated, with analytical and experimental results, that this perturbation may be cancelled by imposing certain conditions on the electron optics when the bunch length is constant along the line. This scheme of CSR suppression is then enlarged, analytically and numerically, to cover the case of varying bunch length in a periodic arc compressor. The proposed solution holds the promise of cost-saving of compact transfer lines with large bending angles, and new schemes for beam longitudinal gymnastics both in recirculating and in single-pass accelerators driving free electron lasers.

## INTRODUCTION

The advent of sub-ps electron beams with very high brightness in free electron lasers (FELs) [1] and in linear colliders has raised the awareness of the accelerator community to the effect of the coherent synchrotron radiation (CSR) on beam transverse emittance [2–5]. The CSR field affects the electron transverse motion both with radial forces and by changing the particle energy in the dispersive line. In the latter case, the particle starts a betatron oscillation around a new reference trajectory, thus increasing its Courant-Snyder (C-S) invariant [6]. The synchrotron radiation emission is coherent for wavelengths comparable to the electron bunch length and it induces a variation of the particle energy that is correlated with the longitudinal coordinate along the bunch. The removal of that correlation may therefore suppress the CSR-driven emittance growth [7,8].

In the following, we show that linear optics formalism can be used to describe the effect of consecutive *identical* CSR energy kicks on the beam transverse emittance; CSR emission is assumed to happen in the 1-D (longitudinal) and steady-state approximation [9]. The analytical prediction for the final emittance as function of the optics setting in a substantially isochronous transfer line was validated experimentally in the FERMI FEL [10,11] high energy Spreader line [12]. We then show that the same formalism can be extended to the case of a non-isochronous beam line, made of several large-angle dipole magnets, with limited impact on the beam emittance [13].

\*Work supported by the FERMI project and the ODAC project of Elettra Sincrotrone Trieste.  
<sup>#</sup>simone.dimitri@elettra.eu

## ISOCHRONOUS LINE

The FERMI achromatic system, denoted henceforth as Spreader, is made of two identical double bend achromats (DBA), as sketched in Fig.1. Each DBA includes two FODO cells and their nominal setting ensures  $\Delta\mu = \pi$  between the dipoles, and symmetric Twiss functions  $\beta$  and  $\alpha$ , with values  $\beta_1$  ( $\alpha_1$ ) and  $\beta_4$  ( $\alpha_4$ ) in the dipoles of the first and the second achromat, respectively. The two DBAs are separated by 7 quadrupoles with a phase advance of  $\pi$  between them. In the following, the C-S formalism is applied to the particle motion in the Spreader with the aforementioned notation. Only the motion in the bending plane is considered.

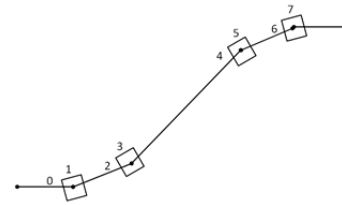


Figure 1: Sketch of the FERMI Spreader (not to scale). The design optics gives a betatron phase advance of  $\pi$  in the bending plane between two consecutive dipoles. There are quadrupoles between the dipoles (not shown here). Copyright of American Physical Society [12].

The initial particle coordinates relative to the reference trajectory are  $x_0 = 0, x'_0 = 0$  and the initial particle C-S invariant is  $2J_0 = 0$ . The variable subscript refers to the point along the lattice, as indicated in Fig.1. After the CSR kick in the first dipole, the particle transverse coordinates become:

$$\begin{cases} x_1 = \eta\delta \equiv \sqrt{2J_1\beta_1} \cos\Delta\mu|_{\Delta\mu=0} = \sqrt{2J_1\beta_1} \\ x'_1 = \eta'\delta \equiv -\frac{\sqrt{2J_1}}{\beta_1} (\alpha_1 \cos\Delta\mu + \sin\Delta\mu)|_{\Delta\mu=0} = -\alpha_1 \sqrt{\frac{2J_1}{\beta_1}} \end{cases} \quad (1)$$

Here  $\delta$  is the single particle relative energy deviation induced by CSR. After the CSR kick, the particle C-S invariant has grown to

$$2J_1 = \gamma_1 x_1^2 + 2\alpha_1 x_1 x'_1 + \beta_1 x_1'^2 = H_1 \delta^2, \quad \text{where}$$

$$H_1 = \gamma_1 \eta^2 + 2\alpha_1 \eta \eta' + \beta_1 \eta'^2 \text{ and } \gamma_1 = \left( \frac{1 + \alpha_1^2}{\beta_1} \right).$$

At the

second dipole, after  $\pi$  phase advance and in the presence of the second CSR kick, we have:

# FIRST SIMULATION RESULTS ON FREE ELECTRON LASER RADIATION IN DISPLACED PHASE-COMBINED UNDULATORS\*

N.S. Mirian,<sup>†</sup>

UVSOR Facility, Institute for Molecular Science (IMS), Okazaki, Japan and  
School of Particle and Accelerator Physics, IPM, Tehran, Iran

E. Salehi, Department of Physics, Amirkabir University of Technology, Tehran, Iran

## Abstract

This report deals with self amplified spontaneous emission free electron laser (FEL) amplifier where the FEL emission is obtained from displaced phase combined undulators. Magnetic field of this adjustment methods in three dimensions is presented. The electron dynamics is investigated. The simulation method and results are explained. The radiation properties of the fundamental resonance and third harmonic through the phase combined undulators are compared with the normal undulator with the same undulator deflection parameter.

## INTRODUCTION

In free electron laser (FEL), a relativistic and high current electron beam passes through a periodic, transverse magnetic undulator field and produces electromagnetic wave. Undulator, as a major component in the FEL, converts the energy of the electron beam to that of the radiation field [1,2].

We know that when the gap between the top and bottom magnetic arrays is relatively narrow, the magnetic arrays of undulators subject to a significant attractive force. Therefore, the undulators usually require rigid mechanical components and frames to control the magnetic gap precisely. Further, a large number of components are required to administrate the mechanical load along the undulator axis and forbear the deformation of the magnetic arrays. If we remove the attractive force between the two arrays of the undulator, the heavy and large base frame is not necessary, and the undulator will be designed to be much more compact and lightweight.

Recently, Kinjo et. al in Ref. [3] have employed phase-combined undulators (PCUs) in two new methods to make fine adjustment of the magnetic force in the insertion device. In the PCUs the phase between the lower and upper Halbach arrays is shifted such that the undulator has no magnetic force without using any cancellation system. By developing the principle of PCU, Kinjo et al. [3] divided the undulator into a number of sections such that half of them are phase-shifted in one direction and the others are shifted in opposed direction, without breaking the periodic condition in the undulator field. In their first method, they suggested an additional phase shift by a relative longitudinal displacement of  $\delta$  to each section of the PCU; this method is referred to as the displacement method. In the second method, they used the

easy axis rotation, which is hereinafter referred to as the rotation method.

In this report, we investigate the evolution of the electron beam and radiation in the FEL by employing the displaced PCU.

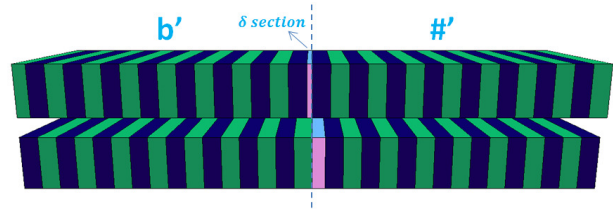


Figure 1: Conceptual diagram of the PCU.

## GENERAL DISCUSSION

According to Ref. [3], by displacing upper or lower magnet array by  $-\lambda_u/4$ , the vertical force between the two arrays can be eliminated; while the shear longitudinal force that appears in the two arrays may be positive or negative depending on whether the upper or lower magnetic array is displaced. For significant reduction of the attractive force between the two arrays and longitudinal force, the PCU is composed of two kinds of sections as shown in Fig. 1. The blue blocks show the vertical polarization and the green blocks show the horizontal polarization. In one kind of section called  $b'$ , the upper magnets array are displaced by  $-\lambda_u/4$ , while in the next kind of section called  $\#$ , the lower magnets array are displaced by  $-\lambda_u/4$ . Composition of these two sections can eliminate the shear longitudinal force. In the displacement adjusting method the relative longitudinal displacement of  $\delta$  is added to each section, as shown in Fig. 1. In this figure,  $D$  shows the number of sections and the symbol  $\#'$  ( $b'$ ) denotes the lower (upper) array of magnets that is displaced by  $-\lambda_u/4 - \delta$ . Then, the magnetic field in three dimensions takes form

$$\mathbf{B}_{\#', b'} = \begin{bmatrix} \pm \frac{B_0}{2} \sinh(\frac{k_u x}{\sqrt{2}}) [\cos(k_u z) e^{\pm \frac{k_u y}{\sqrt{2}}} - \cos(k_u z - k_u (\frac{\lambda_u}{4} + \delta)) e^{\mp \frac{k_u y}{\sqrt{2}}}] \\ \frac{B_0}{2} \cosh(\frac{k_u x}{\sqrt{2}}) [\cos(k_u z) e^{\pm \frac{k_u y}{\sqrt{2}}} + \cos(k_u z - k_u (\frac{\lambda_u}{4} + \delta)) e^{\mp \frac{k_u y}{\sqrt{2}}}] \\ \pm \frac{B_0 \sqrt{2}}{2} \cosh(\frac{k_u x}{\sqrt{2}}) [-\sin(k_u z) e^{\pm \frac{k_u y}{\sqrt{2}}} + \sin(k_u z - k_u (\frac{\lambda_u}{4} + \delta)) e^{\mp \frac{k_u y}{\sqrt{2}}}] \end{bmatrix} \quad (1)$$

The magnetic field of the displaced PCU on axis is

$$\mathbf{B}(z) = B_0 \cos(k_u(z - \Delta)) \left[ \cos(k_u \Delta) \hat{j} + (-1)^d \sin(k_u \Delta) \hat{k} \right], \quad (2)$$

\* Work supported by Institute for Research in Fundamental Sciences (IPM)

<sup>†</sup> nsmirian@ims.ac.jp

# HARMONIC GENERATION IN TWO ORTHOGONAL UNDULATORS\*

Najmeh Sadat Mirian<sup>†</sup>

UVSOR Facility, Institute for Molecular Science (IMS), Okazaki, Japan and  
School of Particle and Accelerator Physics, IPM, Tehran, Iran

## Abstract

In this report, the harmonic generation in two orthogonal undulators is under discussion. There is a possibility of generation of the even and odd harmonics as well as non-integer harmonics in two orthogonal undulators. By considering the first order of electron velocity, the total energy radiated per unit solid angle per unit frequency interval for a single electron traveling along the undulators is derived. Also a numerical simulation of one-dimensional non-averaged equations is conducted to present the self amplified spontaneous emission of harmonic generation in two orthogonal undulators.

## INTRODUCTION

Modern high intensity sources are based on the electron radiation through undulator in synchrotrons and free electron lasers (FEL). Free electron lasers that are mostly based on self amplified spontaneous emission, hold great prospects as high power, coherent, and tunable radiation in the high frequency region of the electromagnetic spectrum [1,2]. The angular distribution of the radiation in undulators is obtained by computing the amount of energy lost by the particle in a retarded time during the emission of the signal. In practice, the spectrum of the radiation depends on the detailed motion of the electron and on the direction from which the electron is observed.

In a planar undulator with an ideal sinusoidal periodic magnetic field, the electrons radiate at odd harmonics due to their non-uniform axial motion. In ideal helical undulator, because of the constant longitudinal velocity, the spectrum is centered about the resonance frequency and there is no significant harmonic growth.

The two orthogonal undulators in FEL has been proposed as away toward the product of two tunable color radiation pulses with different polarizations, while the total length of device dose not change with the respect to the usual single-color FEL [3,4]. The form of this undulator is composed of two linear undulators orthogonally polarized with different periods. The possibility of generation of two radiation waves with different frequencies and different polarizations was investigated. We showed that by changing dependently the strength of the two magnetic fields, we can control the final power and the saturation length.

This report focuses on studying the harmonic generation in the two-orthogonal undulators in two different methods.

\* Work supported by Institute for Research in Fundamental Sciences (IPM)  
<sup>†</sup> nsmirian@ims.ac.jp

## FIELD EQUATIONS

The undulator magnetic field, in the paraxial approximation, is described by the following expression

$$\mathbf{B}_w = B_{w2} \cos(k_{02}z) \hat{e}_x + B_{w1} \cos(k_{01}z) \hat{e}_y, \quad (1)$$

where  $B_{wi}$  is the untapered undulator field amplitude,  $k_{01,02} = 2\pi/\lambda_{01,02}$  are undulator wave numbers and  $K_{1,2} = |eB_{w1,2}\lambda_{01,2}/mc^2|$  are the deflecting parameters. We assume  $n\lambda_{01} = m\lambda_{02}$ , which permits us to treat the cases of a harmonic relation between  $\lambda_{01}$  and  $\lambda_{02}$  and of rational  $m/n$ . The proper resonance relation in this magnetic file has been obtained as [3,4]

$$\lambda_{1,2} = \frac{\lambda_{01,02}}{\gamma} \left( 1 + \frac{K_1^2}{2} + \frac{K_2^2}{2} \right), \quad (2)$$

where  $\lambda_1$  and  $\lambda_2$  are, respectively, fundamental resonance wavelength in the x and y direction. The one-dimensional vector potential can be assumed to be

$$\mathbf{A} = i \sum_h \left[ A_{1h} e^{i(k_{1z}z - \omega_1 t)} \hat{e}_x + A_{2h} e^{i(k_{2z}z - \omega_2 t)} \hat{e}_y \right], \quad (3)$$

where  $h$  is the harmonic number. The vector potential amplitudes  $A_{1,2h} = A_{1,2h}^{(1)} + i A_{1,2h}^{(2)}$ , are assumed to vary slowly in  $z$  and  $t$ . By using Maxwell-Poisson equation in Gaussian gauge, and the slowly varying envelope approximation (SVEA), the two polarization amplitudes take the following independent differential form:

$$\frac{\partial}{\partial z} A_{1,2h} + \frac{1}{c} \frac{\partial}{\partial t} A_{1,2h} = \frac{2\pi en}{k_{1,2}} \sum_h \beta_{x,y} \delta(z - z_j) e^{-i\alpha_{1,2h}j}, \quad (4)$$

$$\alpha_{1,2h} = h(k_{1,2}z - \omega_{1,2}t) = h\alpha_{1,2},$$

where  $\omega_{1,2} = k_{1,2}c$  is radiation frequency for fundamental resonance. Similar to the way used in Ref [4] after averaging of Maxwell's equation over time scale  $\ell/c$  (where  $\ell = n\lambda_1 = m\lambda_2$ ), we have

$$\left( \frac{\partial}{\partial z} - \frac{\partial}{\partial t} \right) \begin{pmatrix} a_{1h}^{(1)} \\ a_{1h}^{(2)} \end{pmatrix} = \frac{\omega_p^2}{2h\omega_1 c} \beta_{z,0} \begin{pmatrix} \left\langle \frac{u_x}{|u_z|} \cos(\alpha_{1h}) \right\rangle \\ - \left\langle \frac{u_x}{|u_z|} \sin(\alpha_{1h}) \right\rangle \end{pmatrix}, \quad (5)$$

$$\left( \frac{\partial}{\partial z} - \frac{\partial}{\partial t} \right) \begin{pmatrix} a_{2h}^{(1)} \\ a_{2h}^{(2)} \end{pmatrix} = \frac{\omega_p^2}{2h\omega_2 c} \beta_{z,0} \begin{pmatrix} \left\langle \frac{u_y}{|u_z|} \cos(\alpha_{2h}) \right\rangle \\ - \left\langle \frac{u_y}{|u_z|} \sin(\alpha_{2h}) \right\rangle \end{pmatrix}, \quad (6)$$

$a_h^{(1,2)} = e \frac{A_h^{(1,2)}}{mc^2}$  is the normalized amplitude,  $\omega_p^2 = 4\pi e^2 n/mc^2$  is the square of plasma frequency, and  $\mathbf{u} = \mathbf{P}/mc = \gamma\beta$  is a dimensionless variable. The averaging operator is defined as

## CARRIER-ENVELOPE-PHASE STABLE LINEARLY AND CIRCULARLY POLARIZED ATTOSECOND PULSE SOURCES

Z. Tibai<sup>#</sup>, Zs. Nagy-Csiha, G. Almási, J. Hebling, Institute of Physics, University of Pécs, Hungary  
 Gy. Tóth, J.A. Fülöp, MTA-PTE High Field Terahertz Research Group, 7624 Pécs, Hungary

### Abstract

We recently proposed a robust method for producing few-cycle attosecond pulse generation in the extreme ultraviolet spectral range. It is based on radiation of relativistic ultrathin electron layers, which are produced with inverse free electron laser process. In the present article the energy of this attosecond source is investigated numerically for the linearly and circularly polarized cases.

### INTRODUCTION

In recent years a few phenomenon depending on carrier-envelope-phase (CEP) was recognized [1]. Waveform-controlled few-cycle laser pulses enabled the generation of isolated attosecond pulses and their application to the study of electron dynamics in atoms, molecules, and solids [2].

EUV pump—EUV probe experiments can be carried out at free-electron lasers (FELs) [3,4]; however, the temporal resolution is limited to the fs regime. Various schemes, such as the longitudinal space charge amplifier [5], or two-color enhanced self-amplified spontaneous emission (SASE) [6] were proposed for attosecond pulse generation at FELs. A very recent scheme suggests possible generation of sub-attosecond pulses in the hard X-ray region [7]. But the stochastic pulse shape is disadvantageous; furthermore there are no reliable techniques available for CEP control of attosecond pulses. Recently we proposed a robust method for producing waveform- and CEP-controlled attosecond pulses in the EUV spectral range [8]. Here we investigate numerically the feasibility and stability of this technique.

### SIMPLE SETUP

Our proposed setup is shown in Fig. 1. A relativistic electron beam e.g. from a LINAC is sent through a modulator undulator (MU) where a TW-power laser beam is superimposed on it in order to generate nanobunches by the inverse free-electron laser (IFEL) action. The nanobunched electron beam then passes through a radiator undulator (RU) consisting of a single or a few periods. The radiator undulator is placed behind the modulator undulator at a position where the nanobunch length is shortest. Of course, efficient coherent radiation generation is possible only if the nanobunch length is shorter than the half period of the radiation.

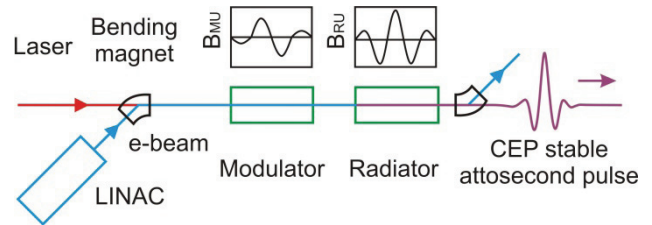


Figure 1: Layout of the setup.

### SIMULATION METHOD

The General Particle Tracer (GPT) [9] numerical code was used for simulation of nanobunching in the modulator undulator. In the simulations the parameters of the electron bunch before the nanobunching were chosen according to published parameters of the electron bunches created by the accelerator of FLASH at DESY, Germany (Table 1) [10,11]. Electron bunches with 60 μm transversal size were assumed.

Table 1: Parameters used in the Simulations

Parameter	Value
<i>E</i> -beam energy ( $\gamma$ )	2000
<i>E</i> -beam charge	250 pC
<i>E</i> -beam energy spread ( $1\sigma$ )	0.05 %
<i>E</i> -beam Normalized emittance	1.4 mm mrad

Inside the modulator undulator the interaction between the electrons, the magnetic field of the undulator, and the electromagnetic field of the modulator laser with 516 nm wavelength and 10 TW power ( $P_L$ ) introduces a periodic energy modulation of the electrons. This energy modulation leads to the formation of nanobunches in the drift space behind the MU. The charge of a single nanobunch is 1.0 pC and according to the simulations, its length can be as short as 6 nm (at 4.9 m behind the center of the modulator undulator).

The temporal shape of the ultrashort pulses emitted by these extremely short electron nanobunches in the RU, were calculated at a plane 8 m behind the middle of the RU.

The wavelength of the EUV radiation ( $\lambda_r$ ) is determined by the well-known resonance condition:

$$\lambda_r = \frac{\lambda_{RU} \left( 1 + \frac{K_{RU}^2}{2} \right)}{2\gamma^2}, \quad (1)$$

<sup>#</sup>tibai@fizika.ttk.pte.hu

# EFFICIENCY ENHANCEMENT OF A HARMONIC LASING FREE ELECTRON LASER

E. Salehi, Department of Physics, Amirkabir University of Technology, Tehran, Iran  
 N.S. Mirian\*, UVSOR Facility, Institute for Molecular Science, Okazaki, Japan and  
 School of Particle and Accelerator Physics, Institute for Research in Fundamental Sciences (IPM),  
 Tehran, Iran

B. Maraghechi, Department of Physics, Amirkabir University of Technology, Tehran, Iran

## Abstract

The harmonic lasing free-electron laser amplifier, in which two wigglers is employed in order for the fundamental resonance of the second wiggler to coincide with the third harmonic of the first wiggler to generate ultraviolet radiation, is studied. A set of coupled nonlinear first-order differential equations describing the nonlinear evolution of the system, for a long electron bunch, is solved numerically by CYRUS code. Thermal effects in the form of longitudinal velocity spread are also investigated. The second wiggler field decreases linearly and nonlinearly at the point where the radiation of the third harmonic saturates to enhance the efficiency. The optimum starting point and the slope of the tapering of the amplitude of the wiggler are found by a successive run of the code. It is found that tapering can increase the saturated power of the third harmonic considerably.

## INTRODUCTION

High-gain free-electron laser(FEL) amplifiers hold great prospects as high power, coherent, and tunable radiation in the x-ray regions of the electromagnetic spectrum. Utilizing nonlinear harmonic generation when bunching the harmonics is driven by the fundamental frequency in the vicinity of saturation is a possible way for obtaining x-ray wavelengths [1–7].

Recently, McNeil et al. [8] proposed a harmonic lasing FEL amplifier in a one-dimensional limit that can be extended to higher harmonics by suppressing the interaction at the fundamental resonance while allowing the harmonics to evolve to saturation. To suppress the interaction at the fundamental resonance without affecting the third harmonic lasing, they proposed two different settings for the undulator are considered by changing the wiggler magnetic field while keeping the wiggler period,  $\lambda_w$ , and the initial average electron beam energy,  $\gamma$ , constant.

The intrinsic efficiency of the FEL is low. By increasing the energy of the electron beam, the efficiency reduces further. Therefore, for the x-ray FEL, efficiency is very low. For this reason, much attention has been given in the literature to schemes for the FEL efficiency enhancement [9–13].

The purpose of the present study is to use the concept of the linear and nonlinear tapering of the wiggler field to increase the efficiency of the harmonic lasing FEL. To this end, by decreasing the wiggler amplitude linearly or non-

linearly at the saturation point, the resonance condition of the FEL is restored, which will result in higher intensity UV radiation. The slippage of the radiation with respect to the long electron bunch is ignored. Equations describing harmonic lasing FEL are derived. This set of equations is solved numerically using CYRUS 1D code in one-dimension [14]. CYRUS, which was developed by N. S. Mirian et al to study nonlinear harmonic generation. This code like MEDUSA employs nonaveraged equations [15, 16]. The third harmonic lasing is considered so that the operating wavelength is in the ultraviolet (UV) domain.

## BASIC EQUATIONS

The numerical simulation of the harmonic lasing is conducted using the CYRUS 1D code that is written in standard FORTRAN 90. This code like MEDUSA [15, 16] employs nonaveraged equations. The formulation treats the planar wiggler model and the radiation field is represented as a superposition of Gaussian modes [17]. The vector potential of the radiation field, in plane-polarized form, is

$$\delta\mathbf{A}(\mathbf{z}, t) = \sum_{l,n,h} [\delta A_h^{(1)} \sin(\varphi_h) + \delta A_h^{(2)} \cos(\varphi_h)] \mathbf{e}_x \quad (1)$$

where  $\delta A_h^{(i)}$  with  $i = 1, 2$  are the amplitudes that are assumed to vary slowly in  $z$  and  $t$  and  $h = 1, 3, \dots$  denotes the harmonic number,  $\alpha_h = h(k_0 z - \omega t)$  is the phase of the  $h$ th harmonic of the angular frequency  $\omega$ . Averaging Maxwell's equations over the time scale  $2\pi/\omega$ , the field equations take the form

$$\left(\frac{\partial}{\partial z}\right) \begin{pmatrix} \delta a_h^{(1)} \\ \delta a_h^{(2)} \end{pmatrix} = \frac{\omega_b^2}{2h\omega c} \begin{pmatrix} \langle \frac{u_x}{|u_z|} \cos\alpha_h \rangle \\ \langle -\frac{u_x}{|u_z|} \sin\alpha_h \rangle \end{pmatrix} \quad (2)$$

where  $\delta a_h^{(i)} = e\delta A_h^{(i)}/m_e c^2$  are the normalized amplitudes,  $\omega_b^2 = 4\pi e^2 n_b/m_e c^2$  is the square of the beam plasma frequency. The averaging operator is defined as

$$\langle (\dots) \rangle = \int_0^{2\pi} \frac{\sigma(\psi_0)}{2\pi} d\psi_0 \int_0^\infty dp G_0(p_z) (\dots) \quad (3)$$

Here,  $\sigma(\psi_0)$  is the phase distribution at entry time. Also,  $G_0(p_z)$  is the initial momentum space distribution which is

\* nsmrian@ims.ac.jp

# THREE-DIMENSIONAL SIMULATION OF A HARMONIC LASING FREE-ELECTRON LASER AMPLIFIER

E. Salehi, B. Maraghechi

Department of Physics, Amirkabir University of Technology, Tehran, Iran,  
N.S. Mirian\*

UVSOR Facility, Institute for Molecular Science, Okazaki, Japan and  
School of Particle and Accelerator Physics, IPM, Tehran, Iran

## Abstract

Three-dimensional simulation of harmonic lasing Free-electron laser is represented in the steady-state regime. Here, the third harmonic of the first wiggler is adjusted at the fundamental resonance of the second wiggler by reducing the magnetic field strength of the second wiggler. The hyperbolic wave equations can be transformed into parabolic diffusion equations by using the slowly varying envelope approximation. A set of coupled nonlinear first-order differential equations describing the nonlinear evolution of the system is solved numerically by CYRUS3D code. This set of equations describes self-consistently the longitudinal spatial dependence of the radiation waists, curvatures, and amplitudes together with the evaluation of the electron beam. Thermal effects in the form of longitudinal velocity spread are also investigated.

## INTRODUCTION

High-gain free electron laser (FEL) amplifiers hold great prospects of reaching coherent high power radiation in the x-ray region of the electromagnetic spectrum. In recent years, a great effort of researchers has been devoted to studying the process of higher harmonic generation in achieving lasing at shorter wavelengths [1–5].

Radiation of the electron beam in the planar wiggler contains odd harmonics but the output power at the  $h$ th harmonics is rather small and is of the order of  $10^{-h}$  times the power of the fundamental [1, 3–5]. Recently, McNeil et al. [6] proposed a harmonic lasing method for FEL amplifiers that can amplify the higher harmonics by suppressing the interaction at the fundamental resonance. They showed that this configuration can significantly extend the operation band of user facilities.

Reference [6] has outlined two methods for suppressing the interaction at the fundamental resonance while allowing the third harmonic to evolve to saturation. The first method is based upon shifting the phase of the fundamental between the wiggler segments, which can be controlled by various techniques [7]. For the  $h$ th harmonic, this phase shift should be  $2\pi n/h$ , where  $n = 1, 2, 3, \dots$  is an integer number and  $h = 3, 5, 7, \dots$  is the harmonic number. The second method is detuning of the fundamental by considering two different segments for the wiggler. Two segments of the wiggler have different magnetic field intensity while the wiggler period,

$\lambda_w$ , and the initial average electron beam energy,  $\gamma$ , are kept constant.

The thermal effect of the electron beam is particularly important for higher harmonics, because they are more sensitive to the energy spread than the fundamental one [8, 9]. The energy spread is considered as a Gaussian energy distribution in MEDUSA code for nonlinear harmonic generation [10]. Also, in reference [7], the energy spread effects are included that the gain length for the detuning of the fundamental is compared with the third harmonic in conventional FEL.

The aim of this paper is to present a three-dimensional simulation of the emission at the fundamental and third harmonic in the non-wiggler-averaged-orbit approximation of the harmonic lasing FEL with source-dependent expansion [11–14]. Therefore, the source function is incorporated self-consistently into the functional dependence of the radiation waist, the radiation wavefront curvature, and the radiation amplitude instead of using the usual modal expansion consisting of vacuum Laguerre-Gaussian or Hermite-Gaussian functions. It is important to emphasize that no wiggler average is imposed on the orbit equations. Therefore, it is possible to treat the injection of the beam into the wiggler, with the ease of inclusion of external focusing or dispersive magnetic components in the beam line and the facility for using an actual magnetic field in the numerical solution. The third harmonic lasing is considered so that the operating wavelength is in the EUV domain. The slippage of the radiation with respect to the long electron bunch is ignored.

The code which is written for this purpose is named CYRUS 3D, which was developed by PhD students in Amirkabir University and Institute for Research in Fundamental Sciences (IPM). This code follows MEDUSA 3D [10] formulation.

## DESCRIPTION OF THE SIMULATION CODE

The simulation code for three-dimensional non-wiggler averaged-orbit formulation is CYRUS 3D code, that was written in standard Fortran 95. This code is time independent with harmonics and thermal effects taken into account. It models planar wiggler and the electromagnetic field is represented as a superposition of Gauss-Hermit modes in the slowly varying amplitude approximation. Electron trajectories are integrated using the three-dimensional(3D) Lorentz

\* nsmirian@ims.ac.jp

# FREE-ELECTRON LASER DRIVEN BY A 500 MeV LASER PLASMA ACCELERATOR BEAM

W.Qin, S.Huang, L.Zeng, X.Yan, K.Liu, J.Chen, IHIP, Peking University, Beijing 100871, China  
Y. Ding, Z. Huang, SLAC, Menlo Park, CA 94025, USA

## Abstract

A laser plasma accelerator is under construction at Peking University and several hundred MeV electron beams are expected. In this paper we discuss applying a 500 MeV beam with 1% relative energy spread to FEL. Bunch decompression method is considered to deal with the large energy spread of the beam. Emittance growth induced by large divergence and energy spread during beam transport has been treated with the chromatic matching manipulation. Simulation shows that 100 MW level, 6.3 fs, 0.008 bandwidth output can be obtained for 30 nm FEL. TGU method with assumed matched beam is also discussed as a comparison.

## INTRODUCTION

Laser Plasma Accelerator (LPA) is considered as a promising candidate to drive compact short-wavelength Free-Electron Laser (FEL) owing to its capability to generate high energy electron beams in centimeter scale, which is of great interest for university scale labs. Undulator radiation utilizing laser plasma accelerated beam has been reached in the VUV and soft-X region [1, 2]. However, the percent level relative energy spread and chromatic induced emittance degradation during beam transport hinder the application of LPA beam to short-wavelength FEL. Controlled injection to improve beam quality and stability is being pursued by the LPA community. Even though, with presently demonstrated LPA beam, FEL may be realized when undulator adjustment and beam manipulation are performed to meet the requirement of high-gain FEL. To overcome the energy spread issue, two methods have been proposed, i.e., a proper dispersed beam coupled to a Transverse Gradient Undulator (TGU) [3] and a decompressed beam coupled to a longitudinally tapered undulator [4, 5]. However, chromatic effect induced emittance growth during beam transport can seriously affect either of the two energy spread compensation scheme. Recently, a so-called chromatic matching manipulation which synchronizes the energy slice waist slippage and the FEL slippage is proposed to address the chromatic effect for the decompression scheme [6]. For the TGU scheme, a matching beamline with sextupoles to correct the chromaticity is necessary [7].

In this paper, we discuss the application of an expected 500 MeV LPA beam at Peking University to a 30 nm FEL. Bunch decompression method with chromatic matching manipulation is considered, while TGU scheme with the LPA beam assumed to be matched at the undulator entrance is also discussed as a comparison.

## LASER PLASMA ACCELERATOR AT PKU

Peking University is developing a multi-functional laser plasma acceleration experimental platform (see Fig.1) utilizing a high contrast 5 Hz, 200 TW, 800 nm laser system. After two stage CPA compression, the laser pulse with 5J energy is compressed to 25 fs. For laser proton acceleration, the laser is transported to the plasma mirror chamber to further increase its contrast ratio, then interact with a solid target to produce 15 MeV proton beam. For laser electron acceleration, the laser pulse is directly delivered to the gas target chamber to interact with a supersonic gas jet. The 200 TW laser system is ready to deliver the pulse, while the first experiment is still under preparation. A gas jet of adjustable length and several diagnostic devices including a 2 GeV electron spectrometer are also ready. Expected electron beam parameters for the first experiment are several hundred MeV energy with several MeV energy spread, tens of pC bunch charge, 0.1 mm-mrad normalized emittance.

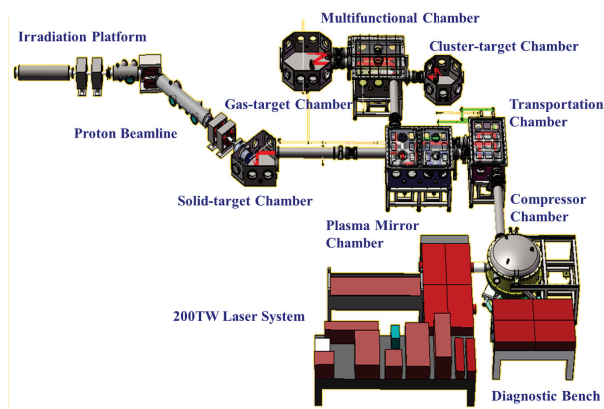


Figure 1: Laser plasma accelerator at Peking University.

## BEAM MANIPULATION

Based on the capability of laser plasma accelerator at PKU, we discuss using a 500 MeV, 10 fs (FWHM), 40 pC LPA beam with 1% rms relative energy spread and 0.1 mm-mrad rms normalized emittance to drive 30 nm FEL. The parameters are summarized in Table 1. The beam is assumed to be 6D Gaussian in phase space and no correlation in both transverse and longitudinal phase space. Due to the  $\mu\text{m}$  scale beta function in plasma accelerator, the initial rms beam divergence is at mrad level, which is orders larger than that of electron beam from conventional accelerator. Large beam divergence leads to fast beam expansion at the very beginning of the transport beamline. Along with large energy spread, beam divergence drastically increase the chromatic

# SUB-RADIANCE AND ENHANCED-RADIANCE OF UNDULATOR RADIATION FROM A CORRELATED ELECTRON BEAM\*

R. Ianconescu, University of Tel-Aviv, Tel-Aviv and Shenkar College, Ramat Gan, Israel  
 E. Hemsing, A. Marinelli, SLAC, Menlo Park, California, USA  
 A. Nause, UCLA, Los Angeles, USA  
 A. Gover, University of Tel-Aviv, Tel-Aviv, Israel

## Abstract

The radiant intensity of Synchrotron Undulator Radiation (UR) depends on the current noise spectrum of the electron beam injected into the wiggler. The current noise spectrum and intensity can be controlled (suppressed or enhanced relative to the shot-noise level) by the effect of collective longitudinal space charge interaction in drift and dispersion sections [1]. This new control lever is of significant interest for possible control of SASE in FEL, since UR is the incoherent seed of SASE. Thus, control of spontaneous UR is a way to enhance the coherence of seeded FEL [2, 3], or alternatively, obtain enhanced radiation from a cascade noise-amplified electron beam [4]. The dependence of UR emission on the current noise is primarily a result of the longitudinal correlation of the e-beam distribution due to the longitudinal space charge effect. However, at short wavelengths, 3-D effects of transverse correlation and effects of emittance disrupt the proportionality relation between the UR intensity and e-beam current noise. We present analysis and simulation of UR sub-radiance/enhanced-radiance under various ranges of beam parameters, and compare to recent experimental observations [1].

## INTRODUCTION

This study is an extension of previous work on current noise correlation effects due to longitudinal space charge (LSC) interactions effects in a drifting electron beam, such as microbunching instability [5] and e-beam noise suppression effects [6–14] which are of particular interest at the short wavelength limit [15] where it may be relevant for coherence enhancement of XUV FELs. The understanding and control of UR from a correlated electron beam is of major interest because UR is an important source of radiation for applications, and it is the start radiation field of SASE FEL. UR can be also an efficient diagnostic mean for evaluating e-beam current noise in a wide range of the spectrum, especially because it emits radiation on axis (contrary to OTR diagnostics). 3D correlation effects on UR that have been observed experimentally [1] have received little attention so far. The model presented in this paper is intended for study of such 3D effects.

## SPONTANEOUS RADIATION EMISSION FROM FREE ELECTRONS

The radiation mode expansion analysis of superradiant emission from particulate current in [16] can be extended to

\* This research was supported in part by a grant from the United States-Israel Binational Science Foundation(BSF), Jerusalem, ISRAEL

analysis of radiation into plane waves from any free electron radiation source in the far field zone. This results in a dipole antenna expression for the spectral radiant intensity

$$\frac{d^2\check{W}}{d\omega d\Omega} = \frac{\eta_0 k^2}{16\pi^3} |\check{d}|^2 \sin^2 \psi, \quad (1)$$

where

$$\check{d}(\omega, k) \equiv \sum_j \Delta \check{d}_j, \quad (2)$$

$$\Delta \check{d}_j \equiv -e \int_{-\infty}^{\infty} dt v_{-j}(t) e^{i\omega t - i\mathbf{k} \cdot \mathbf{r}_j(t)}, \quad (3)$$

and

$$\underline{k} = k(\hat{e}_x \sin \Theta_x + \hat{e}_y \sin \Theta_y + \hat{e}_z \cos \Theta) \quad (4)$$

## SPONTANEOUS EMISSION FROM A CORRELATED ELECTRON BEAM

Here we extend the radiation mode expansion formulation of [16] for superradiance and stimulated superradiance from an electron beam to the case of emission from a correlated or uncorrelated electron beam into plane waves in the far field. This includes the cases of a randomized (Poisson distribution) electron beam producing conventional incoherent spontaneous emission, a prebunched beam producing superradiant emission, a random beam of super-Poissonian distribution producing enhanced radiance spontaneous emission or a beam of sub-Poissonian distribution that produces sub-radiance (suppressed spontaneous emission). So far, the formulation is valid for general radiation schemes of free electrons. In the next section we specify to the case of undulator radiation.

For spontaneous emission, the system is stationary in the sense that it is not sensitive to the absolute time of the interaction. Defining  $t_{0j}$  the time electron  $j$  enters the interaction region,  $\Delta \check{d}_j$  in Eq. (3) is written as

$$\Delta \check{d}_j = -e \int_{t_{0j}}^{t_j(L)} dt v_j^{(0)}(t - t_{0j}) e^{i\omega t - i\mathbf{k} \cdot \mathbf{r}_j^{(0)}(t - t_{0j})}, \quad (5)$$

and we set the integration limits from the entering time  $t_{0j}$  to the exit time  $t_j(L)$ ,  $L$  being the interaction length. By changing variable  $t' = t - t_{0j}$ , we obtain

$$\Delta \check{d}_j = \Delta \check{d}_j^{(0)} e^{i\omega t_{0j}} \quad (6)$$

where

$$\Delta \check{d}_j^{(0)} = -e \int_0^{\Delta t_j(L)} dt' v_j^{(0)}(t') e^{i\omega t' - i\mathbf{k} \cdot \mathbf{r}_j^{(0)}(t')}. \quad (7)$$

# ON THE IMPORTANCE OF ELECTRON BEAM BRIGHTNESS IN HIGH GAIN FREE ELECTRON LASERS\*

S. Di Mitri<sup>#</sup>, Elettra Sincrotrone Trieste, 34149 Basovizza, Trieste, Italy

## Abstract

Linear accelerators delivering high brightness electron beams are essential for driving short wavelength, high gain free-electron lasers (FELs). The FEL radiation output efficiency is often parametrized through the power gain length that relates FEL performance to the electron beam quality at the undulator. Experimental data and simulation results of existing and planned FEL facilities, collected in [1], are used to explicit the relationship between the FEL output wavelength and the electron beam six-dimensional brightness. Following [2], practical formulas are provided that show the dependence of the exponential gain length on the beam brightness.

## 6-D ELECTRON BEAM BRIGHTNESS

In the context of an electron bunch, the 4-dimensional (4-D) brightness,  $B_{4D}$ , can be defined as the peak current divided by its 4-D transverse phase space volume that is the product of the transverse emittances [3]. Owing to the fact that linac-driven free electron lasers (FELs) are sensitive to the beam relative energy spread and local charge density, it is convenient to parameterize the linac performance in terms of the 6-D brightness,  $B_{6D}$ , which is the total bunch charge divided by its 6-D phase space volume. The 6-D volume includes, in addition to the four transverse positions and slopes, the normalized longitudinal emittance, which scales as the product of bunch length and absolute energy spread. In the following, we assume the particle beam in the ultra-relativistic approximation, so that the longitudinal charge distribution is assumed to be constant during acceleration.

In general, we may define the brightness either locally, *i.e.*, for each bunch slice (in this case, the brightness depends on the z-coordinate inside the bunch), or for the whole bunch, thus involving the bunch total charge and projected emittances. The transverse rms normalized emittances are invariant under acceleration and linear transport, presuming collective effects, such as space charge, may be neglected. The same is true for the longitudinal rms normalized emittance if the energy spread is intended as uncorrelated, *i.e.*, without any energy chirp.

The presence of nonlinear motion and collective effects along the beam delivery system may dilute the normalized emittances from their values at the injection point. Following [2], we introduce an effective degradation factor  $\zeta \geq 1$  in each plane of the particle motion so that  $\epsilon_{nx,f} = \zeta_x \gamma_0 \epsilon_{x,0}$ ,  $\epsilon_{ny,f} = \zeta_y \gamma_0 \epsilon_{y,0}$ , and

$\epsilon_{nz,f} = \sigma_{z,f} \sigma_{E,f} = \zeta_z \sigma_{z,0} \sigma_{E,0}$ , with obvious notation. We are

now able to relate the 6-D normalized brightness at the undulator,  $B_{n,f}$ , to that at the linac injection,  $B_{n,0}$ :

$$B_{n,f} \equiv \frac{Q}{\epsilon_{nx,f} \epsilon_{ny,f} \epsilon_{nz,f}} = \frac{Q}{\zeta_x \zeta_y \zeta_z \gamma_0^2 \epsilon_{x,0} \epsilon_{y,0} \epsilon_{z,0}} = \frac{B_{n,0}}{\zeta_x \zeta_y \zeta_z} \quad (1)$$

In the ideal case of vanishing nonlinear and collective effects,  $\zeta_x, \zeta_y, \zeta_z \rightarrow 0$  in Eq. 1 and thereby the 6-D normalized brightness is preserved at the injector level under acceleration and linear bunch length compression.

## IMPORTANCE OF PROJECTED BEAM PARAMETERS

In contrast to linear colliders, where particle collisions effectively integrate over the entire bunch length, the FEL process takes place over short fractions of the electron bunch length. In fact, slice emittance and slice energy spread may vary significantly along the bunch and thus give local regions where lasing may or may not occur [4]. One could therefore argue that only slice electron beam quality is of interest, each slice being at maximum as long as the slippage length of the photon beam over the electrons, cumulated along the undulator length. In the following, we make the case that other considerations related to the electron beam control and optimization of the FEL performance justify an optimization of  $B_{6D}$  defined in terms of the projected beam emittances. We will limit the discussion to the transverse emittances; correlations in the longitudinal plane are discussed in [1,2].

The need to control beam size and angular divergence along the undulator calls for measurements and manipulation of the electron beam optical (Twiss or envelope) parameters, which have to be matched to the design ones [5–8]. As a practical matter, optics matching is routinely performed by measuring the projected electron bunch transverse size [9]. From an operational point of view, it is therefore important to ensure that the projected transverse emittances and Twiss parameters be as close as possible to the slice ones, because this guarantees that most of the bunch slices are matched to the design optics and that they overlap in the transverse phase space. During beam transport and acceleration, at least two collective effects threaten locally to offset bunch slices in the transverse (and longitudinal) phase space, namely coherent synchrotron radiation (CSR) and geometric transverse wakefield (GTW). Specific optics designs can be adopted to minimize those collective effects (for a review of these topics, see for example [1]).

The projected emittance can be considered a good marker also for externally-seeded FEL performance. In

\*Work supported by the FERMI project of Elettra Sincrotrone Trieste.  
#simone.dimitri@elettra.eu

# GENERATING A SINGLE-SPIKE SASE PULSE IN THE SOFT X-RAY REGIME BY VELOCITY BUNCHING\*

Jaeyu Lee, Bonghun Oh, Moohyun Yoon<sup>#</sup>, POSTECH, Pohang, Korea

## Abstract

A bright ultrashort X-ray pulse emerges as a valuable tool for many fields of research nowadays. The single-spike operation of X-ray FEL is one way of making a bright ultrashort X-ray pulse. It requires extreme bunching and a magnetic chicane is a conventional compressor. In a low charge range, a magnetic chicane can be replaced by the velocity bunching technique. In this paper, we present the result of particle tracking simulation generating a single-spike soft X-ray SASE pulse without a magnetic chicane.

## INTRODUCTION

XFEL based on SASE principle generates a fully coherent radiation in the transverse plane because the transverse emittance of the electron beam is usually tailored to smaller than the diffraction-limited emittance. In the longitudinal plane however, the coherence is rather poor because radiation starts from the shot noise. Therefore, efforts have been made to improve the SASE FEL's longitudinal coherence. One of the methods which is rather straightforward to implement is to create a single-spike radiation pulse on the order of a few hundred attosecond, two orders of magnitude shorter than the pulse length from a typical SASE FEL so that great enhancement of the longitudinal coherence is achieved.

In this regard, there are two different schemes to obtain an attosecond XFEL. The first scheme is to manipulate an initially long electron bunch and achieve lasing only part of the bunch in the longitudinal axis which is short enough for single-spike radiation. The other scheme is to enhance the bunching process to make an ultrashort electron bunch. As mentioned above, the radiation of SASE FEL has temporal fluctuation; it is a stream of many coherent pulses which separate each other. Single coherent pulse or single spike has space of  $2\pi L_{c,1D}$  in between, which is given by

$$2\pi L_{c,1D} = \frac{\lambda_r}{2\sqrt{3}\rho}, \quad (1)$$

where  $L_{c,1D}$  is called the cooperation length and  $\lambda_r$  is the radiation wavelength, and  $\rho$  is the pierce parameter. Making ultrashort electron bunch for single-spike operation has advantages in the clearness of single spike but making ultrashort bunch is technically difficult. Low charge is preferred to shorten the electron bunch but it also increases difficulties in the beam diagnosis.

The velocity bunching (VB) [1] is a technique to achieve bunching of electrons in the longitudinal direction which is effective when the electron speed is not close to the speed

of light. Therefore, the VB process can take place between the rf gun and main accelerating cavities. VB can be an alternative of the magnetic chicane usually employed in the SASE FEL and is effective especially when the bunch charge is low. Therefore, it will be a very interesting question if one can achieve a desirable bunch length to generate a single spike radiation pulse in SASE FEL with a very small charge of a several pico-Coulombs. One may also anticipate that even VB can eliminate the need for magnetic chicane or at least minimize the use of chicane. The aim of this report is to propose the use of VB combined with a low charge of picocoulomb order for a single spike generation of SASE soft X-ray FEL.

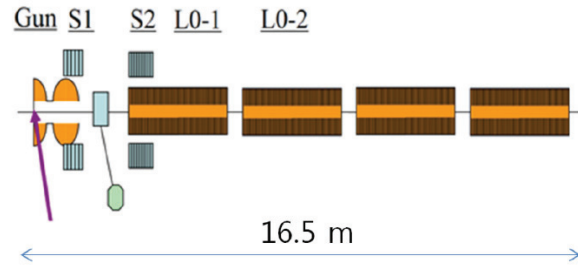


Figure 1: Layout of the injector lattice for the Soft X-ray FEL design.

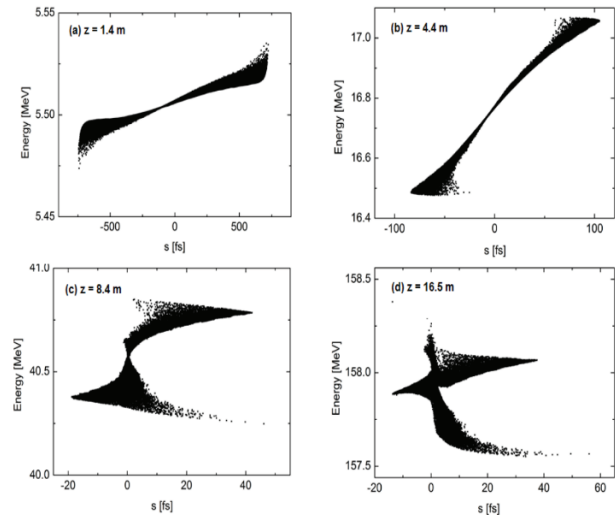


Figure 2: Longitudinal phase space distribution in the injector.

## INJECTOR AND LINAC

We designed the injector linac similar to the LCLS injector [2] which consists of a photo-cathode gun, two solenoids, and two 3-m long S-band accelerating sections L01 and L02. 200,000 particle tracking in the injector linac was performed with ASTRA [3]. Optimization for parameters was carried out through the Multi-Objective

\*Work supported by POSTECH Basic Science Research Institute Grant and Ministry of Science, ICT and future Planning (MISP) of Korean government.  
#moohyun@postech.ac.kr

# NEW SOFT X-RAY UNDULATOR LINE USING 10 GEV ELECTRON BEAM IN PAL-XFEL

C. H. Shim, I. S. Ko, Pohang University of Science and Technology, Pohang 790-784, Korea  
 Y. W. Parc<sup>#</sup>, Pohang Accelerator Laboratory, Pohang 790-784, Korea

## Abstract

PAL-XFEL is designed to have five undulator lines and only two undulator lines, the HXR undulator line with 10 GeV electron beam and the SXR undulator line with 3.15 GeV electron beam, will be installed during phase I. A photon beam energy from 0.28 to 1.24 keV will be provided at the SXR undulator line and different range from 2 to 20 keV will be supplied at the HXR undulator line. According to existing schedule, however, photon beam energy from 1.24 to 2 keV won't be provided in PAL-XFEL. In this research, new soft X-ray undulator line for PAL-XFEL using 10 GeV electron beam in main linac is proposed to cover the vacant photon energy. Four candidates are evaluated by estimating and comparing FEL performances using Ming Xie's formula.

## INTRODUCTION

Pohang Accelerator Laboratory X-ray Free Electron Laser (PAL-XFEL) is designed to have three undulator lines at the end of 10 GeV main linac and two undulator lines at the end of 3.15 GeV branch linac as shown in Fig.1 [1,2]. But only two among five undulator lines will be installed during phase I. One is the hard X-ray (HXR) undulator line with 10 GeV electron beam and the other is the soft X-ray (SXR) undulator line with 3.15 GeV electron beam. Main parameters of PAL-XFEL are listed in Table.1.

A photon beam with energy from 2 to 20 keV will be supplied at the HXR undulator line. Another photon beam with different energy from 0.28 to 1.24 keV will be provided at the SXR undulator line. According to existing schedule, photon beam with energy from 1.24 to 2 keV won't be usable in PAL-XFEL. In this vacant region, however, it is estimated that there are some demands for outstanding experiments [3] and therefore that region has to be covered in the near future. There are two main ways to cover the vacant region: One is extending photon energy supply of existing undulator lines. The other is designing new undulator line using one of three available undulator lines.

In this research, new SXR undulator line for PAL-XFEL using 10 GeV electron beam in main linac is proposed.

Table 1: Main Parameters of Current PAL-XFEL

	Hard X-Ray	Soft X-Ray
Location	Main Linac	Branch Linac
Energy	4 – 10 GeV	2.5 – 3.15 GeV
FEL Photon Energy	Und. Gap Change (Max. Energy Fix)	
	12.4 – 20.0 keV (0.1 – 0.06 nm)	0.41 – 1.24 keV (3 – 1 nm)
	Energy Change (Min. Und. Gap Fix)	
	2.0 – 12.4 keV (0.6 – 0.1 nm)	0.28 – 0.41 keV (4.5 – 3 nm)
Und. Period	26 mm	35 mm
Peak Current	3 kA	2 kA
Normalized Slice Emittance	0.4 mm-mrad	0.6 mm-mrad
Slice Energy Spread	1.5 MeV	1.5 MeV
Bunch Length	18 um (60 fs)	27 um (90 fs)

Evaluation is conducted by comparing estimated FEL performances of existing undulator lines and newly designed undulator lines in the vacant region. All estimation of FEL performances are based on Ming Xie's formula [4]. Time-dependent simulation is also performed with selected solution by GENESIS 1.3 using real beam parameter [5].

## EXISTING UNDULATOR LINE

There are two undulator lines, the HXR and SXR undulator lines, according to existing schedule in PAL-XFEL, so two specific candidates are also available. Each parameters of two lines are listed in Table 1.

### Soft X-Ray (SXR) Undulator Line

In the SXR undulator line, electron beam energy is fixed at maximum values, 3.15 GeV, as shown by blue dashed

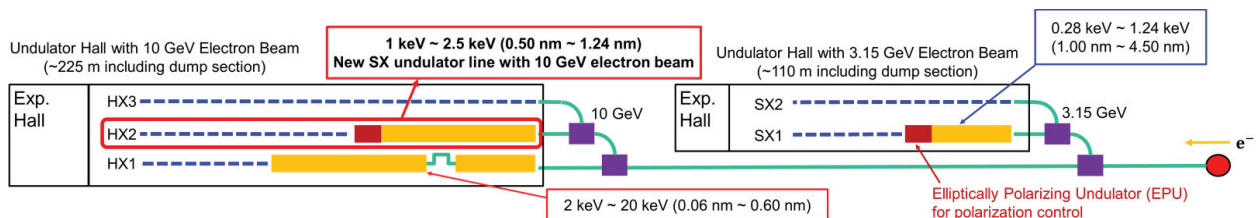


Figure 1: Schematic diagram about undulator lines of PAL-XFEL.

#young1@postech.ac.kr

# FEL OPERATION MODES OF THE MAX IV SHORT PULSE FACILITY

Alan Mak\*, Francesca Curbis, Sverker Werin, MAX IV Laboratory, Lund University, Sweden

## Abstract

The Short Pulse Facility (SPF) of the MAX IV Laboratory in Lund, Sweden features the production of ultrashort, incoherent x-ray pulses. It is driven by a 3-GeV linac and comprises two 5-metre undulator modules. While the SPF is designed for spontaneous radiation, we explore alternative operation modes in which the SPF functions as a simple free-electron laser (FEL). In this article, we characterize two of them in time-dependent numerical simulations. We perform a sensitivity study on the electron beam parameters and examine the technique of single-step tapering.

## INTRODUCTION

The MAX IV facility in Lund, Sweden includes a Short Pulse Facility (SPF) [1] in addition to two storage rings. Commissioning is in progress as of 2015.

The SPF is situated at the end of the 3-GeV injector (see Fig. 1). It consists of two variable-gap, planar undulator modules, with a length of 5 metres each. The injector provides short electron bunches, which enable the SPF to produce incoherent x-ray pulses as short as 100 fs. From the same injector, electrons are also extracted at 1.5 GeV and 3 GeV for the top-up of the two storage rings (see Fig. 1).

In addition, the MAX IV facility was designed to enable future expansion. Two x-ray FELs (shown in grey in Fig. 1) can potentially be constructed as branch lines parallel to the SPF. They are set out in the long-term strategic plan of the laboratory [2]. In one of the branch lines, an extra linac section is envisaged, so as to provide the FEL with an electron energy of 5 – 6 GeV.

While the SPF is designed for spontaneous radiation, we explore alternative operation modes which enable the observation of coherent gain as a result of self-amplified spontaneous emission (SASE). In these operation modes, the SPF functions as a simple FEL, whereby the necessary techniques for a full-fledged FEL can be developed and tested.

To lay the foundation for future experimental work, we investigate two of such operation modes with the simulation code GENESIS [3]. In the first case, we study the sensitivity of the radiation power to the electron beam parameters. In the second case, we study the technique of single-step tapering [4, 5].

## THEORETICAL BACKGROUND

### Saturation Length and Power

Many properties of a high-gain FEL are characterized by the dimensionless Pierce parameter, which is defined as [6]

$$\rho = \frac{1}{2\gamma} \left( \frac{I}{I_A} \right)^{1/3} \left( \frac{\lambda_w K f_B}{2\sqrt{2}\pi\sigma_x} \right)^{2/3}. \quad (1)$$

\* alan.mak@maxlab.lu.se

Here  $\gamma$  is the electron beam energy normalized to the electron rest energy  $m_e c^2$ .  $I$  is the peak current.  $I_A = m_e c^3 / e = 17.045$  kA is the Alfvén current.  $\sigma_x$  is the rms radius of the electron beam.  $\lambda_w$  is the undulator period.  $K$  is the undulator parameter.  $f_B = J_0(\xi) - J_1(\xi)$  is the Bessel factor for planar undulators, with  $\xi = K^2 / [2(K^2 + 2)]$ .

Using the Pierce parameter, the saturation length can be estimated by the relation

$$L_{\text{sat}} \approx \frac{\lambda_w}{\rho}, \quad (2)$$

and the saturation power by the relation

$$P_{\text{sat}} \approx \rho P_{\text{beam}}, \quad (3)$$

where  $P_{\text{beam}} = \gamma m_e c^2 I / e$  is the electron beam power [6]. According to these relations,  $L_{\text{sat}}$  decreases with  $\rho$ , while  $P_{\text{sat}}$  increases with  $\rho$ .

In the SPF, the total undulator length  $L_w$  is only 10 m. In order to observe exponential power growth, it is preferable to choose an operation mode with  $L_{\text{sat}} < L_w$ , so that the exponential growth regime will, in principle, occur completely within the undulator line.

### Single-Step Tapering

The purpose of single-step tapering is to enhance the power, and hence the energy extraction efficiency, of an FEL. It involves the use of two undulator segments with different undulator parameters. While the parameter of the first segment is  $K$ , the parameter of the second segment is decreased to  $K - \Delta K$ . A recent work by Li and Jia [5] provides a theoretical estimate of the optimal  $\Delta K$ , given by

$$\frac{\Delta K}{K} = 2\sqrt{2}\rho \left( 1 + \frac{2}{K^2} \right). \quad (4)$$

According to this relation, the optimal  $\Delta K$  depends on the Pierce parameter  $\rho$ .

## OPERATION MODES

We study two selected operation modes of the SPF using the simulation code GENESIS [3] in the time-dependent mode. The main parameters are shown in Table 1.

In Table 1, the saturation length  $L_{\text{sat}}$  and saturation power  $P_{\text{sat}}$  are estimated by Eqs. (2) and (3). For case A, the parameters are chosen so that the estimated  $L_{\text{sat}}$  is slightly shorter than the total undulator length  $L_w$ . For case B, the parameters are chosen so that the estimated  $L_{\text{sat}}$  is within the first of the two undulator modules.

In the simulations, there is a break section of 1 m between the two 5-metre-long undulator modules. As in the real facility, no focusing elements are inserted to the break section. The electron beam size in the SPF can be adjusted only by changing the twiss parameters at the entrance.

## SEEDED FEL STUDY FOR CASCADED HGHG OPTION FOR FLASH2

G. Feng<sup>#</sup>, I. Zagorodnov, M. Dohlus, T. Limberg, W. Decking, J. Boedewadt, DESY, Hamburg, Germany  
 K. Hacker, Technische Universität Dortmund, Germany  
 T. Plath, University of Hamburg, Germany

### Abstract

The free electron laser (FEL) facility at DESY in Hamburg (FLASH) is the world's first FEL user facility which can produce extreme ultraviolet (XUV) and soft X-ray photons. In order to increase beam time delivered to users, a major upgrade named FLASH II is in progress. As a possibility, a seeding undulator section can be installed between the extraction arc section and the SASE undulator of FLASH2. In this paper, a possible seeding scheme for the cascaded HGHG option for FLASH2 is presented. The SASE undulator of FLASH2 can be used as the second radiator of the cascaded HGHG section. Parameters optimization for the accelerating modules and for the bunch compressors has been done to meet the requirement for the electron bunches. In the beam dynamics simulation, collective effects were taken into account. Particle distribution generated from the beam dynamics simulation was used for the seeded FEL study. Space charge and CSR impacts on the microbunches were included during the cascaded HGHG simulation. The simulation results show that FEL radiation with the wavelength of a few nms and with high monochromaticity can be seeded at FLASH2.

### INTRODUCTION

FLASH has been an FEL user facility since 2005 which can produce FEL radiation in the wavelength range from 4.1nm to 45nm [1]. In order to increase the beam time, a major upgrade, FLASH II, is in progress. Behind the main linac, three fast vertical kickers and a DC Septum distribute the electron beam either to the dogleg section of FLASH1 or to the extraction arc of FLASH2 [2]. As the extension of FLASH, the beamline of FLASH2 has been constructed in a separate tunnel. SASE FEL radiation in the wavelength range from 4 nm to 80nm can be produced from the SASE undulator of FLASH2 [3]. Gap of the SASE undulator is variable for relaxing the dependency of the radiation wavelength on the electron beam energy and for independent operation of FLASH1 and FLASH2. As a possibility, a seeding undulator section can be installed between the extraction arc and the SASE undulator of FLASH2. Maybe it can allow for different seeding schemes, like HHG, HGHG and several combinations of them [4]. In this paper, seeded FEL study for the cascaded HGHG option for FLASH2 is presented. The SASE undulator of FLASH2 has been used as the second radiator of the cascaded HGHG in the simulation.

A single stage HGHG section which can also be used as the first stage of the cascaded HGHG consists of a dispersive chicane and two undulator sections: a modulator and a radiator. In the modulator, a seeding

laser modulates the electron energy distribution. In the dispersive chicane, the energy modulation is transformed into a density modulation: microbunching. Because the microbunching will have a significant harmonic content, the radiator can be tuned to a higher harmonic of the seed laser. When the bunched electron beam enters the it can emit coherent, intense FEL radiation.

The seed laser which will be used for FLASH2 is a Ti:Sapphire laser at a repetition rate of 100 kHz. After frequency up conversion, the laser wavelength ranges from 200 nm to 270 nm [5]. In the seeded FEL study, the electron beam with energy of 1 GeV has been used and the seeding laser has wavelength of 266 nm. In order to avoid particle loss in terms of FEL bandwidth and to reduce the beam instability due to microbunching, the amplitude of energy modulation in the modulator is limited to less than 1 MeV. Figure 1 gives the estimation of bunching factor as a function of harmonics of the seed laser for different initial uncorrelated energy spread. One can see at the 7<sup>th</sup> harmonic, the bunching factor can reach 0.2 in the case of 100 keV uncorrelated energy spread. For FLASH, it is possible to obtain electron bunches with a smaller uncorrelated energy spread, when the peak current is low enough. Therefore, in the following study, the peak current of the electron bunch is limited lower than 1.5 kA and the first radiator is tuned to the 7<sup>th</sup> harmonic of the seed laser.

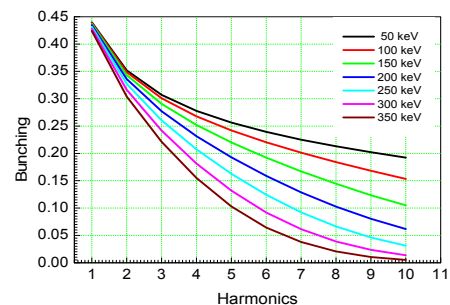


Figure 1: Bunching factor for HGHG with different initial slice energy spreads.

### BEAM DYNAMICS SIMULATION

The seed laser has the wavelength of 266nm, the pulse duration is 100 fs and the pulse energy is 6  $\mu$ J [5]. The total length of the pulse is about 90  $\mu$ m. In order to get long enough electron bunch for HGHG option, especially for cascaded HGHG, beam dynamics with 1 nC bunch charge case has been studied.

Description of the RF cavities and the magnets is from the FLASH 2 lattice definition which has been written in Elegant format [6]. There are some restrictions in the beam dynamics simulation. Same as the normal operation case, the beam energies which were used in the

# SCHEME TO INCREASE THE OUTPUT AVERAGE SPECTRAL FLUX OF THE EUROPEAN XFEL AT 14.4 keV

Gianluca Geloni, European XFEL GmbH, Hamburg, Germany

Vitali Kocharyan, Evgeni Saldin, Deutsches Elektronen-Synchrotron (DESY), Hamburg, Germany

## Abstract

Inelastic X-ray scattering and nuclear resonance scattering are limited by the photon flux available at SR sources, up to  $1e10$  ph/s/meV at 14.4 keV. A thousand-fold increase may be obtained by exploiting high repetition rate self-seeded pulses at the European XFEL. We report on a feasibility study for an optimized configuration of the SASE2 beamline combining self-seeding and undulator tapering at 14.4 keV. One should perform monochromatization at 7.2 keV by self-seeding, and amplify the seed in the first part of the output undulator. Before saturation, the electron beam is considerably bunched at the 2nd harmonic. A second part of the output undulator tuned to 14.4 keV can thus be used to obtain saturation at this energy. One can further prolong the exchange of energy between the photon and the electron beam by tapering the last part of the output undulator. Start-to-end simulations demonstrate that self-seeding, combined with undulator tapering, allows one to achieve more than a hundred-fold increase in average spectral flux compared with the nominal SASE regime at saturation, resulting in a spectral flux of order  $1e13$  ph/s/meV. A more detailed description of this study can be found in [1].

## INTRODUCTION AND METHOD

Inelastic X-ray scattering from electrons [2]- [8] (IXS) and Nuclear Resonant Scattering [9]- [13] (NRS) are important techniques for probing condensed matter by successfully exploiting the high brightness of synchrotron radiation sources. Inelastic scattering relies on the transfer of momentum and energy from the photon field to the sample. Such transfer is detected as a change of momentum and energy of the scattered photons, and allows for the study of a number of excitations with different characteristic lengths and time scales, related to the momentum and energy transfer. In particular, the highest temporal resolution is achieved for very small energy transfer, and calls for a very high average spectral density of the incident X-ray radiation.

In [14] it was studied how sub-meV inelastic X-ray scattering experiments could benefit from high-repetition rate, seeded XFELs. In that case, the method exploited Hard X-ray Self-Seeding (HXRSS) and tapering at the European XFEL around the photon energy of 9 keV in combination with a new concept for monochromatization and spectral analysis [15–17], which is expected to lead to Ultra-High Resolution IXS (UHRIX) momentum-resolved experiments with 0.1-meV spectral and  $0.02\text{-nm}^{-1}$  momentum transfer resolution. In that work we showed that the European XFEL equipped with HXRSS can lead to a photon flux of order

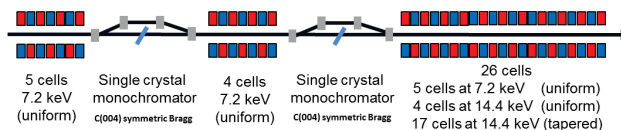


Figure 1: Layout of the SASE2 undulator at the European XFEL configured for HXRSS and tapered operation, as discussed in this work.

$10^{14}$  ph/s/meV at the sample, about four orders of magnitude larger than what is presently achievable at synchrotrons.

A continuation of that kind of studies includes the investigation of the average spectral density achievable at high-repetition self-seeded FEL at higher X-ray energies. The most natural application of these kind of X-ray sources is for NRS experiments. Similarly as for IXS applications, also NRS analyzers are limited, in resolution, by the flux available at synchrotrons. For instance, at 14.4 keV, the maximum spectral flux available at third generation synchrotron radiation sources is of order  $10^{10}$  photons per second per meV bandwidth.

Here we propose a way to increase such spectral flux up to about three orders of magnitude at the SASE2 beamline of the European XFEL. This will enable NRS experiments with very high, sub-meV resolution, and can be achieved by exploiting a combination of three different factors and techniques: first, the high-repetition rate of the European XFEL [18]; second, the HXRSS setup [19]- [37] that will be installed at SASE2 [38]; third, Coherent Harmonic Generation (CHG) [39]- [57]; and finally, fourth, post-saturation tapering [58]- [70].

X-Ray Free Electron Lasers (XFELs) are capable of producing X-ray pulses with unprecedented power spectral density. However, the average spectral flux strongly depends on the maximal repetition rate that can be achieved by the linac driver of each XFEL setup. In particular, the European XFEL [18] will be driven by a superconducting accelerator, which enables up to 27000 pulses per second, more than two orders of magnitude higher than what can be achieved with a normal-conducting linac. A straightforward analysis (see section ) for the case of the SASE2 beamline of the European XFEL at 14.4 keV shows that one can obtain up to about  $10^{11}$  ph/s/meV for the SASE case at saturation. This number is already one order of magnitude better than what can be achieved at synchrotrons that can provide about  $10^{10}$  ph/s/meV around 14.4 keV. However, the average spectral flux can be further increased of other two orders of magnitude by combining together HXRSS, CHG, and post-saturation tapering techniques.

# NOVEL OPPORTUNITIES FOR SUB-meV INELASTIC X-RAY SCATTERING AT HIGH-REPETITION RATE SELF-SEEDED X-RAY FREE-ELECTRON LASERS

Oleg Chubar, Brookhaven National Laboratory, New York, USA

Gianluca Geloni, Anders Madsen, European XFEL GmbH, Hamburg, Germany

Vitali Kocharyan, Evgeni Saldin, Svitozar Serkez, DESY, Hamburg, Germany

Yuri Shvyd'ko, Advanced Photon Source, Argonne National Laboratory, Argonne, IL 60439, USA

John Sutter, Diamond Light Source Ltd, Didcot, Oxfordshire, OX11 0DE, UK

## Abstract

Inelastic x-ray scattering (IXS) is an important tool for studies of equilibrium dynamics in condensed matter. A new spectrometer recently proposed for ultra-high-resolution IXS (UHRIX) has achieved 0.6 meV and  $0.25 \text{ nm}^{-1}$  spectral and momentum transfer resolutions, respectively [1]. However, further improvements down to 0.1 meV and  $0.02 \text{ nm}^{-1}$  are required to close the gap in energy-momentum space between high and low frequency probes. We show that this goal can be achieved by further improvements in x-ray optics and by increasing the spectral flux of the incident x-ray pulses. UHRIX performs best at energies from 5 to 10 keV, where a combination of self-seeding and undulator tapering at the SASE2 beamline of the European XFEL promises up to a hundred-fold increase in average spectral flux compared to nominal SASE pulses at saturation, or three orders of magnitude more than possible with storage-ring based radiation sources. Wave-optics propagation shows that about  $7 \times 10^{12}$  ph/s in a  $90\text{-}\mu\text{eV}$  bandwidth can be achieved on the sample. This will provide unique new possibilities for IXS. Extended information about our work can be found in [2].

## INTRODUCTION

Momentum resolved inelastic x-ray scattering (IXS) is a technique introduced [3, 4] and widely used [5–9] at synchrotron radiation facilities for studies of atomic-scale dynamics in condensed matter. A photon with energy  $E_i$  and momentum  $\mathbf{K}_i$  changes its energy and momentum to  $E_f$  and  $\mathbf{K}_f$  in a inelastic scattering process in the sample and leaves behind a collective excitation with energy  $\varepsilon = E_i - E_f$  and momentum  $\mathbf{Q} = \mathbf{K}_i - \mathbf{K}_f$ , respectively. IXS provides access to dynamics on a length scale  $\lambda = 2\pi/Q$  and a time scale  $t = 2\pi\hbar/\varepsilon$  simultaneously. Presently, together with IXS there are a few inelastic scattering techniques allowing probes of a limited region in the time-length scale: in fact, a gap remains in experimental capabilities between the low-frequency (visible and ultraviolet light) and the high-frequency (x-rays and neutrons) inelastic scattering techniques. Because of this, dynamics in the range from about 1-100 picosecond (ps) on atomic- and meso-scales is still inaccessible. However, this region is of vital importance for disordered systems and, therefore, to the study of many outstanding problems in condensed matter dynamics, such as the nature of the liquid to glass transition.

IXS could in principle penetrate this unexplored dynamic range of excitations<sup>1</sup>, but this would require solving two long-standing challenges. First, IXS spectrometers in their traditional implementation have not improved the best numbers in energy ( $\approx 1.5 \text{ meV}$ ) and momentum transfer ( $\approx 1.5 \text{ nm}^{-1}$ ) resolutions for the past 20 years [10, 11]. Second, the IXS signal is very weak. Hence, more efficient IXS spectrometers with better resolution and more powerful x-ray sources are required to advance the field. Recently, a new type of dispersive spectrometer was tested for the first time. This ultra-high-resolution IXS (UHRIX) spectrometer [1] achieved a spectral resolution of 0.6 meV at a momentum transfer down to  $0.25 \text{ nm}^{-1}$ . Additionally, the spectral contrast improved by an order of magnitude compared to the traditional IXS spectrometers [3, 10–14]. To sharpen the desired resolution to 0.1 meV and  $0.02\text{-nm}^{-1}$  and to ensure higher contrast, we propose to further develop the angular dispersive x-ray optical scheme [15, 16] and to replace scanning IXS spectrometers with broadband imaging spectrographs [17]<sup>2</sup>.

Complementarily, high-repetition rate seeded x-ray free-electron lasers (XFELs) hold the promise to overcome the problem of weak IXS signals. Low-gain x-ray free-electron laser oscillators (XFELOs) may in time produce a spectral flux of up to  $10^{14} - 10^{15}$  photons/s/meV [19, 20], but currently they are still under development [21]. High-gain XFELs under operation are limited, in average flux, by their low repetition rate [22, 23]. In contrast, at the European XFEL [24], owing to superconducting accelerator technology, Self-Amplified Spontaneous Emission (SASE) will allow for the production of average output fluxes of about  $10^{12}$  photons/s/meV at 9 keV (the optimum working energy of the UHRIX setup), which is already more than one order of magnitude greater than at synchrotron radiation facilities [9]. The spectral flux can be further substantially increased by self-seeding [25, 26], which will be first be available, at the European XFEL, at the SASE2 beamline [27]. Another order of magnitude increase in flux can be gained by tapering the magnetic field of the seeded undulator [28–35].

<sup>1</sup> INS cannot enter this region because of the kinematic limitation. The low-frequency probes cannot enter this region because their photon wavelengths are too long.

<sup>2</sup> A Fourier-transform IXS technique has been demonstrated recently [18], which could be considered as a powerful complementary approach for studies of *non-equilibrium* excitation with ultra-high spectral resolution.

# MULTISTAGE CSR MICROBUNCHING GAIN DEVELOPMENT IN TRANSPORT OR RECIRCULATION ARCS

C. -Y. Tsai<sup>#</sup>, Department of Physics, Virginia Tech, Blacksburg, VA 24061, USA  
 D. Douglas, R. Li, and C. Tennant, Jefferson Lab, Newport News, VA 23606, USA

## Abstract

Coherent synchrotron radiation (CSR) induced microbunching instability has been one of the most challenging issues in the design of modern accelerators. A linear Vlasov solver has been developed [1] and applied to investigate the physical processes of microbunching gain amplification for several example lattices [2]. In this paper, by further extending the concept of stage gain as proposed by Huang and Kim [3], we develop a method to characterize the microbunching development in terms of stage orders that allow the quantitative comparison of optics impacts on microbunching gain for different lattices. We find that the microbunching instability in our demonstrated arcs has a distinguishing feature of multistage amplification (e.g. up to 6th stage amplification for our example transport arcs, in contrast to two-stage amplification for a typical 4-dipole bunch compressor chicane). We also try to connect lattice optics pattern with the obtained stage gain functions by a physical interpretation. This Vlasov analysis is validated by ELEGANT [4] tracking results with excellent agreement.

## OVERVIEW OF CSR MICROBUNCHING INSTABILITY THEORY IN A SINGLE-PASS SYSTEM

Theoretical formulation of the CSR-induced microbunching instability in a single-pass system (e.g. a bunch compressor chicane) has been developed based on the linearized Vlasov equation [3, 5]. The formulation assumes initial modulation wavelength is small compared with the whole bunch duration (i.e. coasting-beam approximation) and treat the CSR effect as a small perturbation. By the method of characteristics, the equation that governs the evolution of the complex bunching factor can be written as [5]

$$b_k(s) = b_k^{(0)}(s) + \int_0^s K(s, s') b_k(s') ds' \quad (1)$$

where the bunching factor  $b_k(s)$  is defined as the Fourier transform of the perturbed phase space distribution and the kernel function is particularly expressed as

$$K(s, s') = \frac{ik}{\gamma} \frac{I(s)}{I_A} C(s') R_{56}(s' \rightarrow s) Z(kC(s'), s') \times [\text{Landau damping}] \quad (2)$$

for [Landau damping] term

$$[\text{Landau damping}] = \exp \left\{ \frac{-k^2}{2} \left[ \epsilon_{z,0} \left( \beta_{z,0} R_{51}^2(s, s') + \frac{R_{52}^2(s, s')}{\beta_{z,0}} \right) + \sigma_z^2 R_{56}^2(s, s') \right] \right\} \quad (3)$$

with

<sup>#</sup> jcytsai@vt.edu

$$R_{56}(s' \rightarrow s) = R_{56}(s) - R_{56}(s') + R_{51}(s') R_{52}(s) - R_{51}(s) R_{52}(s') \quad (4)$$

$$\text{and } R_{5i}(s, s') = C(s) R_{5i}(s') - C(s') R_{5i}(s).$$

Here the kernel function  $K(s, s')$  describes relevant collective effects,  $g_k(s)$  the resultant bunching factor as a function of the longitudinal position given a wavenumber  $k$ , and  $g_k^{(0)}(s)$  is the bunching factor in the absence of collective effect.  $I(s)$  is the beam current at  $s$  and  $I_A$  is the Alfven current.

In this paper, we are interested in the bunching factor evolution subject to the CSR effect. For an ultrarelativistic electron beam traversing through a bending magnet, the CSR effect, described in terms of the impedance, can be expressed as [6, 7]

$$Z_{CSR}^{ss}(k(s); s) = \frac{-ik(s)^{1/3} A}{|\rho(s)|^{2/3}}, \quad A \approx -0.94 + 1.63i \quad (5)$$

where  $k = 2\pi/\lambda$  is the modulation wave number,  $\rho$  is the bending radius.

Here we presumed the CSR interaction be in the steady state and only in the longitudinal direction with negligible shielding effect. So far we have obtained the governing equation for the bunching factor and given the 1-D steady-state ultrarelativistic CSR impedance. In the following two sections, we would introduce two methods to solve Eq. (1), i.e. the direct solution and iterative solution, and define the microbunching gain functions associated with the two kinds of solutions, respectively, for our subsequent analysis.

## DIRECT SOLUTION

Here by ‘‘direct solution’’ we mean self-consistent solution of Eq. (1), as summarized below. First, we rewrite Eq. (1) by expressing the bunching factors in vector forms and the kernel function in a matrix form, and we have after taking the inverse on both sides,

$$\mathbf{b}_k = (\mathbf{I} - \mathbf{K})^{-1} \mathbf{b}_k^{(0)} \quad (6)$$

provided the inverse matrix of  $(\mathbf{I} - \mathbf{K})$  exists.

To quantify the microbunching instability in a single-pass system, we define the microbunching gain as functions of the global longitudinal coordinate  $s$  as well as the initial modulation wavelength  $\lambda$  (or,  $k = 2\pi/\lambda$ )

$$G(s, k = 2\pi/\lambda) \equiv \frac{b_k(s)}{b_k^{(0)}(0)} \quad (7)$$

Hereafter, we simply call  $G(s)$  the gain function as a function of  $s$  given a specific modulation wavenumber, and denote  $G_f(\lambda)$  gain spectrum as a function of  $\lambda$  at a specific location (e.g. denoted with a subscript ‘‘ $f$ ’’ at the exit of a beamline). Before ending this section, it deserves to mention the physical meaning of Eq. (1 or 6) and Eq. (7) with CSR effect [3]: a density perturbation at  $s'$  induced an energy modulation through CSR impedance

# REVIEW OF EXPERIMENTAL RESULTS FROM HIGH BRIGHTNESS DC GUNS: HIGHLIGHTS IN FEL APPLICATIONS

Nobuyuki Nishimori, JAEA, Tokai, Naka, Ibaraki 319-1195, Japan

## Abstract

Future energy recovery linac light sources and high repetition rate X-ray FELs require high-brightness and high-current electron guns. A DC photoemission gun is one of the most promising candidates for such guns, because a record high current of 75 mA and generation of high brightness beam satisfying LCLS-II injector specifications were recently demonstrated at the Cornell photoinjector with a 400 kV photoemission gun. Further increases of gun high voltage and cathode gradient are desirable to reduce space charge induced emittance growth especially for higher bunch charge applications. Employment of a segmented insulator is a key to reach higher voltage. This technique led to generation of a 500 keV beam from the JAEA gun with 160 mm acceleration gap, conditioning voltage more than 500 kV at the Cornell gun with gap < 50 mm, and demonstration of 500 kV holding for 10 hours at the KEK gun with 70 mm gap. In this paper, recent experimental results of high brightness DC guns are presented.

## INTRODUCTION

High repetition rate FELs such as LCLS-II and high power FEL for EUV lithography require a high-brightness and high-current electron gun [1,2]. A normal conducting RF gun operating at 186 MHz has been developed for the next generation FELs and recent experimental results are described in the FEL2014 [3]. In this paper we focus on experimental results from high brightness DC guns as another candidates for the high repetition rate FELs. Those DC gun-based photoinjectors are designed and constructed being inspired by the great success of Jefferson laboratory energy recovery linac (ERL) FEL [4].

The recent highlight in FEL applications is the first demonstration of cathode thermal emittance dominated high bunch charge beams satisfying LCLS-II injector specifications at the Cornell photoinjector [5]. The cathode thermal emittance is given by [6]

$$\varepsilon_{n,th} = \sigma_x \sqrt{\frac{MTE}{mc^2}},$$

where  $MTE$  is cathode mean transverse energy,  $\sigma_x$  is the initial rms size of the beam and  $mc^2$  is the electron rest energy. The charge  $q$  can be generated from cathode as long as the external cathode gradient  $E$  is greater than the image charge field given by  $q/\varepsilon_0 \pi (2\sigma_x)^2$  [7]. The thermal emittance for charge  $q$  and cathode gradient  $E$  is thus given by [6]

$$\varepsilon_{n,th} \geq \frac{1}{2} \sqrt{\frac{q}{\pi \varepsilon_0 E}} \sqrt{\frac{MTE}{mc^2}}.$$

Substitution of cathode gradient  $E = 4.3$  MV/m, and  $MTE = 140$  meV of NaKSb cathode used for the Cornell experiment yields minimum thermal emittance of  $\varepsilon_{n,th} = 0.11$   $\mu\text{m}$  for 20 pC, 0.24  $\mu\text{m}$  for 100 pC, and 0.41  $\mu\text{m}$  for 300 pC. Although those emittance values are within the LCLS-II specifications summarized in Table 1, it had been considered to be difficult to preserve the thermal emittance through a DC gun-based photoinjector. Recently the Cornell photoinjector demonstrated that the emittance at the injector exit increases only by 50% or less from the cathode thermal emittance, satisfying the LCLS-II specifications [5]. The sophisticated injector design, excellent injector components including the 400 kV photoemission gun and advanced beam transport techniques relying on space charge simulation codes led to preservation of the high brightness performance from the cathode through the injector accelerator with bunch compression required for LCLS-II specifications.

Generation of a record high average current of 75 mA demonstrated at the Cornell photoinjector is also a highlight in FEL applications [8,9]. The average current is three orders of magnitudes greater than LCLS-II specification and high enough for high power EUV FEL. Generation of both cathode emittance dominated high bunch charge and high current beams was achieved with the same NaKSb cathode.

Table 1: LCLS-II Injector Specifications [5]

Bunch charge	95% $\varepsilon_n$ ( $\mu\text{m}$ )	Peak current (A)
20 pC	0.25	5
100 pC	0.40	10
300 pC	0.60	30

Further increase of the gun high voltage is desirable to reduce space charge induced emittance growth especially for FELs driven by high bunch charge. Employment of a segmented insulator is a key to reach higher voltage [10]. This technique led to the first demonstration of 500 keV beam from a photoemission DC gun with 160 mm acceleration gap at Japan Atomic Energy Agency (JAEA) [11]. The cathode gradient is 5.8 MV/m without Pierce-type focusing electrode. The gun has been used for commissioning of the compact ERL (cERL) at KEK for more than two years [12]. The gun operational voltage at the cERL is however limited to 390 kV, because the insulator is operated with eight segments due to the failures of two segments out of the full ten. Recently a new two segmented insulator was installed on the top of

# nishimori.nobuyuki@jaea.go.jp

# OVERVIEW OF ALTERNATIVE BUNCHING AND CURRENT-SHAPING TECHNIQUES FOR LOW-ENERGY ELECTRON BEAMS\*

Philippe Piot<sup>1,2</sup>

<sup>1</sup> Department of Physics and Northern Illinois Center for Accelerator & Detector Development, Northern Illinois University, DeKalb, IL 60115, USA

<sup>2</sup> Accelerator Physics Center, Fermi National Accelerator Laboratory, Batavia, IL 60510, USA

## Abstract

Techniques to bunch or shape an electron beam at low energies ( $\mathcal{E} < 15$  MeV) have important implications toward the realization of table-top radiation sources or to the design of compact multi-user free-electron lasers. This paper provides an overview of alternative methods recently developed including techniques such as wakefield-based bunching, space-charge-driven microbunching via wave-breaking, ab-initio shaping of the electron-emission process, and phase space exchangers. Practical applications of some of these methods to foreseen free-electron-laser configurations are also briefly discussed.

## INTRODUCTION

Schemes to enhance the peak current of electron bunches have a vast range of applications. In radiation processes radiating at a given wavelength  $\lambda$ , electrons within a duration  $\tau \leq \lambda/c$  radiate in phase thereby enhancing the radiation flux [1]. Likewise low-energy *short* electron bunches can be injected in short-wavelength accelerators, e.g., based on laser-plasma wakefield [2]. In addition to compression, the capability to tailor the current profile of these electron bunches can also serve further applications, e.g., to produced narrow-band radiation (using a train of short electron bunches) [1], enhance the transformer ratio for beam-driven accelerator (ramped current profiles [3]) or mitigate phase-space dilutions arising from collective effects, e.g., coherent synchrotron radiation [4].

Techniques to alter the current distribution can be casted into four categories: (i) ab-initio tailoring of the emission process, (ii) introduction of energy-position correlation within the bunch with subsequent bunching in longitudinally-dispersive beamline, (iii) the direct shaping of the beam by ab-initio shaping of the bunch at its formation stage, and (iv) phase-space manipulations between two degrees of freedoms to map a transversely tailored distribution onto the current profile.

Throughout this paper we employ the longitudinal phase space (LPS) coordinates  $(\zeta, \delta)$  associated to an electron within the bunch. Here  $\zeta$  is the axial position with respect to the bunch centre and  $\delta$  is the fractional momentum spread.

\* This work was supported by the US-DOE contract DE-SC0011831 with Northern Illinois University. Fermilab is operated by Fermi Research Alliance, LLC under Contract No. DE-AC02-07CH11359 with the US DOE.

## AB INITIO METHODS

### Photoemission from Shaped Laser Pulses

Photoemission electron source are widespread in operating and foreseen FEL facilities. The electron bunches produced in this type of sources have, at best, durations comparable to the illuminating laser pulse. However the duration is influenced by space charge and RF effects (in the case of RF guns). Figure 1 illustrates the typically achieved compression for a low (0 nC) and high (1 nC) bunch charge. Some bunch compression can be achieved by phasing the laser closer to zero crossing phase ( $\varphi = 0^\circ$  in our convention) to the detriment of the transverse emittance. On another hand employing shorter laser bunch results in operating the source in the "blow-out" regime which leads to a large space-charge-induced bunch lengthening [5–7]. The latter regime of operation leads to linearized longitudinal phase space (LPS) which can be subsequently manipulated to yield very short bunches [5].

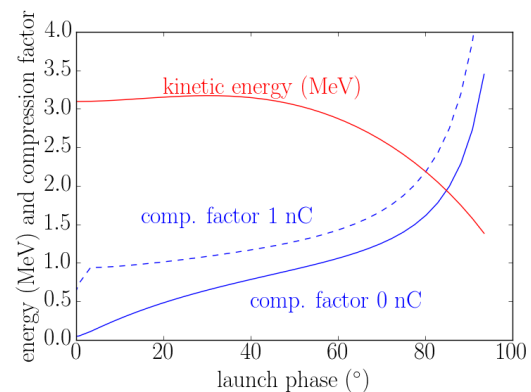


Figure 1: Compression factor (defined as the ratio of the final electron-bunch duration to laser-pulse duration) computed for an L-band RF gun with a 3-ps laser pulse with (dash line) and without (solid trace) accounting for space charge effects.

An interesting area of research is the possibility of tailoring the temporal profile of the emission process. This is particularly attractive in photoemission sources where the emitted electron-bunch distribution initially mirrors the temporal profile of the laser pulse impinging on the cathode. Consequently, laser shaping plays a central role and methods to temporally tailor the laser have been extensively investigated in combination with photo-emission electron sources.

# ALKALI CATHODE TESTING FOR LCLS-II AT APEX\*

H. Qian, D. Filippetto, J. Feng, J. Nasiatka, H. Padmore, F. Sannibale<sup>†</sup>,  
LBNL, Berkeley, CA 94720, USA  
R. Li, J. Schmerge, F. Zhou, SLAC, Menlo Park, CA 94025, USA

## Abstract

Electron sources of high brightness and high bunch charge ( $\sim 300$  pC) with MHz repetition rate are one of the key technologies for next generation X-FEL facilities such as the LCLS-II at SLAC and the Euro XFEL at DESY. The Advanced Photoinjector EXperiment (APEX) at the Lawrence Berkeley National Laboratory (LBNL) is developing such an electron source based on high quantum efficiency (QE) alkali photocathodes and the VHF-Gun, a new scheme normal conducting RF gun developed at LBNL. The VHF-Gun already demonstrated stable CW operation with high gradient (20 MV/m), high gun voltage ( $\sim 750$  kV) and low vacuum pressure ( $\sim 3 \times 10^{-10}$  torr) laying the foundation for the generation of high brightness electron beams. In this paper, we report the test and characterization of two different alkali cathodes in high average current (several hundreds of pC per bunch with MHz repetition rate) operation at APEX. Measurements include cathode life time, QE map evolution and thermal emittance characterization, to investigate the compatibility of such cathodes with APEX gun for the challenging requirements of LCLS-II.

## INTRODUCTION

Next revolutionary FEL light source facilities, such as the LCLS-II at SLAC [1], requires MHz beam repetition rate with similar peak brightness as the state of the art  $\sim 100$  Hz FEL drivers [2]. From the perspective of electron source, such a requirement translates to an electron gun of both high electric field and high duty cycle, and a photocathode of high quantum efficiency ( $\sim 1\%$ ), low thermal emittance ( $< 1$  mm.mrad/mm) and long life time ( $> 1$  week) [3].

R&D on innovative electron gun technologies addressing the need of simultaneous high peak field and high duty cycle, from DC sources to Superconducting Radiofrequency Guns has made a lot of progress [3]. Though normal conducting high frequency ( $\sim$  GHz) RF guns have provided beams of tremendous high peak brightness with 100 Hz repetition rate, they are criticized for not being able to reach higher duty cycle due to thermal load. Our group at Lawrence Berkeley National Laboratory has focused the effort on the new type of normal conducting RF gun resonating in the VHF frequency range (APEX, [4]), which has achieved reliable operation in continuous wave mode (CW) with accelerating fields (in excess of 20 MV/m) required to produce low emittance-high charge electron beams with high peak current needed to drive

the next generation of Free Electron Lasers [5]. The basic gun parameters for cathode testing are shown in Table 1.

Table 1: Nominal APEX VHF Gun Parameters

Parameter	Value	Unit
$E_{cathode}$ in CW mode	20	MV/m
$f_{rf}$	185.71	MHz
$E_k$	758	keV
Base Pres. rf off	$4 \times 10^{-11}$	Torr
Base Pres. rf on	$3 \times 10^{-10}$	Torr

High brightness, high-yield photocathode materials are essential for high repetition rate electron sources. Unfortunately, such materials are usually very reactive semiconductors and their performances tend to degrade very fast with time and extracted charge, which can be a serious limitation to the operation of a future facility like LCLS-II and has been subject of intense studies in recent years [6]. The degradation of high QE semiconductor photocathodes are mainly due to three reasons, first is reaction with residual gases in vacuum, second is back bombardment of ionized residual gases or field emitted electrons, third is laser heating. Two categories of alkali photocathodes are tested at APEX gun to characterize its feasibility to host high QE semiconductor cathodes. First is UV sensitive  $Cs_2Te$  cathode, and second is the green sensitive antimonide cathodes ( $Cs_3Sb$  and  $K_2CsSb$ ). The  $Cs_2Te$  cathode testing inside APEX gun has finished [7], and testing of antimonide cathodes just started, both are presented in this paper.

## APEX BEAMLINE AND LASER SYSTEM

Cathode testing is done using the APEX phase I beamline, as shown in Fig. 1. It starts with the core part, the VHF gun and cathode loadlock system, and a set of beam diagnostics follows, such as ICT, YAG screen, Farady cup, emittance slits, deflecting cavity and energy spectrometer magnet, which are used to characterize both cathode and beam transverse and longitudinal phase space.

The  $Cs_2Te$  cathode is tested with a home made Yb-doped fiber laser system [8]. The 37.14 MHz oscillator seed a chain of Yb-doped fiber amplifiers. The repetition rate is reduced down to 1 MHz during amplification. The total IR beam is about 1 W, and after two second harmonic generations, both green and UV laser are available for the cathode testing. Recently, a similar commercial laser with 2 W IR power is installed, and will be used for antimonide cathode testing and APEX phase II commissioning.

\* Work supported by the Director of the Office of Science of the US Department of Energy under Contract no. DEAC02-05CH11231

<sup>†</sup> fsannibale@lbl.gov

# EMITTANCE MEASUREMENTS OF THE ELECTRON BEAM AT PITZ FOR THE COMMISSIONING PHASE OF THE EUROPEAN XFEL

G. Vashchenko\*, G. Asova†, M. Bakr‡, P. Boonpornprasert, J. D. Good, M. Gross, C. Hernandez-Garcia§, H. Huck, I. Isaev, D. Kalantaryan, G. Kourkafas, M. Krasilnikov, D. Malyutin, D. Melkumyan, A. Oppelt, M. Otevrel, Y. Renier, T. Rublack, F. Stephan, Q. Zhao¶, Deutsches Elektronen-Synchrotron, Zeuthen site, Zeuthen, Germany  
O. Lishilin, G. Pathak, Hamburg University, Hamburg, Germany

## Abstract

For the operation of free electron lasers (FELs) like the European XFEL and FLASH located at DESY, Hamburg Site, high quality electron beams are required already from the source. The Photo Injector Test facility at DESY, Zeuthen Site (PITZ), was established to develop, characterize and optimize electron sources for such FELs. Last year the work at PITZ focused on the optimization of a photo injector operated very close to the startup parameters of the European XFEL. This implies photocathode laser pulses with a Gaussian temporal profile of about 11 – 12 ps FWHM to drive the photo gun operated at a gradient of about 53 MV/m. Significant effort was spent on the electron beam characterization and optimization for various bunch charges. Emittance measurements were performed as a function of major accelerator parameters such as main solenoid current, laser spot size on the cathode and the gun launching phase. The requirement on the beam emittance for a bunch charge of 500 pC for the European XFEL commissioning phase has been demonstrated. Results of these studies accompanied with the corresponding simulations are presented in this paper.

## INTRODUCTION

Free electron lasers like the European XFEL and FLASH require high quality electron beams already from the photo injector [1, 2]. The commissioning phase of the European XFEL injector section is planned to start end of 2015. For the commissioning phase there are reduced requirements on the operation conditions and electron beam quality as compared to the nominal ones in order to simplify the commissioning phase and operate the machine at most stable, reliable and robust conditions. Namely, it is planned to use a gun gradient reduced from 60 MV/m to 53 MV/m which corresponds to a reduced electron beam momentum after the gun from about 6.7 MeV/c to 6.1 MeV/c. The photocathode laser system used for the commissioning phase will produce transversally uniform pulses which correspond to the nominal operation, while the temporal profile will be Gaussian with a full width at half maximum (FWHM) of about 13 ps as compared to the nominal flat-top profile with an FWHM

of 20 ps and rise/fall times of 2 ps. Various electron beam charges (0.1 – 1 nC) with corresponding electron beam quality are planned to be used for the nominal operation of the European XFEL [3]. For SASE (Self Amplified Spontaneous Emission) commissioning it is currently planned to use a bunch charge of 500 pC, which is in the middle of the nominal charge range. For this charge the requirement on the normalized transverse slice emittance during the commissioning phase is 1 mm mrad at the undulator section.

The possibility to run the European XFEL photo injector with the aforementioned parameters was validated at the Photo Injector Test facility at DESY, Zeuthen site (PITZ), which serves as an injector test-bed for FLASH and the European XFEL. A schematic layout of PITZ is presented in Fig. 1. Conditioning and characterization of the normal conducting L-band RF gun cavities is performed at PITZ for their further usage at the European XFEL and FLASH. The photoelectrons are produced with a Cs<sub>2</sub>Te semiconductor photocathode. UV laser pulses which are transversely uniform and temporally Gaussian, with an estimated FWHM of about 11 – 12 ps, are currently used. The produced photoelectrons are accelerated in the gun cavity and are focused with the main solenoid installed at the exit of the gun. The bucking solenoid installed upstream the cavity is used to compensate the field of the main solenoid at the cathode plane in order to avoid initial angular momentum in the electron beam which spoils the electron beam quality. During the last run period the RF gun was operated at a maximum on-axis peak field of about 53 MV/m and 640  $\mu$ s RF pulse length as required for the commissioning phase of the European XFEL. Several diagnostic devices are installed downstream the gun for the electron beam characterization (see Fig. 1). Further beam acceleration is done using a normal conducting L-band Cut Disk Structure (CDS) booster cavity which can increase the momentum of the electron beam up to about 22 MeV/c. The first Emittance Measurement SYstem (EMSY1) is installed directly at the exit of the CDS booster at about 5.3 m downstream the cathode. The transverse projected normalized emittance of the electron beam is measured using the conventional slit scan method based on a direct measurement of the electron beam size and angular spread [4]. More details about the PITZ setup can be found elsewhere [4–6].

\* Grygorii.Vashchenko@desy.de

† on leave from INRNE-BAS, 1784 Sofia, Bulgaria

‡ on leave from Assiut University, 71515 Assiut, Arab Republic of Egypt

§ on leave from JLab, Newport News, VA 23606, USA

¶ on leave from IMP/CAS, 730000 Lanzhou, China

# SUPPRESSION OF FEL LASING BY A SEEDED MICROBUNCHING INSTABILITY\*

C. Lechner<sup>†</sup>, A. Azima, M. Drescher, L. L. Lazzarino, Th. Maltezopoulos, V. Miltchev, T. Plath, J. Rönsch-Schulenburg, J. Rossbach, University of Hamburg, Hamburg, Germany  
 K. E. Hacker, S. Khan, R. Molo, DELTA, TU Dortmund University, Dortmund, Germany  
 S. Ackermann, J. Bödewadt, G. Brenner, M. Dohlus, N. Ekanayake, T. Golz, T. Laarmann, T. Limberg, E. Schneidmiller, N. Stojanovic, M. Yurkov, DESY, Hamburg, Germany

## Abstract

Collective effects and instabilities due to longitudinal space charge and coherent synchrotron radiation can degrade the quality of the ultra-relativistic, high-brightness electron bunches driving free-electron lasers (FELs). In this contribution, we demonstrate suppression of FEL lasing induced by a laser-triggered microbunching instability at the free-electron laser FLASH. The interaction between the electron bunches and the 800-nm laser pulses takes place in an undulator upstream of the FEL undulators. A significant decrease of XUV photon pulse energies has been observed in coincidence with the laser-electron overlap in the modulator. We discuss the underlying mechanisms based on longitudinal space charge amplification (LSCA) [1] and present measurements.

## INTRODUCTION

The microbunching instability (MBI) due to longitudinal space-charge (LSC) forces in linear accelerators can compromise the quality of high-brightness electron bunches. This affects electron beam diagnostics as well as the FEL performance. For instance, emission of coherent optical transition radiation (COTR) was observed at several facilities [2–5] and it has to be mitigated for accurate measurements of the transverse beam profile. The longitudinal space-charge amplifier (LSCA) proposed in Ref. [1] is a concept to exploit these instabilities for the production of short-wavelength radiation. As illustrated in Fig. 1, an LSCA comprises multiple amplification stages, each one consisting of an electron beamline followed by a dedicated dispersive element. In the

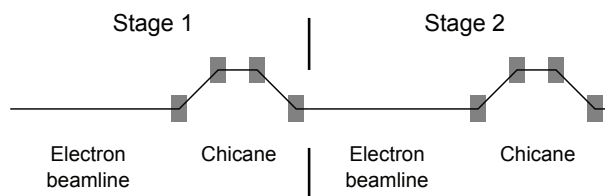


Figure 1: Schematic layout of a two-stage longitudinal space-charge amplifier (LSCA) configuration [1].

beamline, the electrons in the higher-density regions expand longitudinally introducing an energy change. The longitudinal dispersion  $R_{56}$  of the chicanes converts these energy changes into a density modulation. Starting from shot noise, a strong density modulation can be achieved in two to four stages.

LSC amplification was studied experimentally at the Next Linear Collider Test Accelerator (NLCTA) at SLAC, where the impact of compression changes on spontaneous undulator radiation was measured [6]. At the Source Development Laboratory (SDL) at the National Synchrotron Light Source (NSLS) at Brookhaven National Laboratory (BNL), a modulated current profile was generated at the photoinjector with a modulated laser pulse. Microbunching gain was observed at wavelengths suitable for THz generation [7]. In Ref. [8], detailed investigations of the MBI using direct measurements of electron bunches with an RF deflector are presented.

In this contribution, we give an overview of LSCA studies performed at the FEL user facility FLASH [9] in which the amplification process was initiated by modulating the electron bunch by means of an external laser pulse. The amplified energy modulation is applied to suppress the lasing process. First results of these experiments have already been presented in Refs. [10, 11].

## EXPERIMENTAL SETUP

The measurements presented in this contribution were performed at the FEL user facility FLASH at DESY, Hamburg [9]. The schematic layout of the facility is shown in Fig. 2. The superconducting linear accelerator (linac) driving the FEL delivers high-brightness electron bunches with energies up to 1.25 GeV. At a repetition rate of 10 Hz, bunch trains consisting of up to 800 bunches at a 1-MHz repetition rate can be produced. The facility has been upgraded by a second undulator beamline FLASH2, which is currently under commissioning [12].

For these measurements, the hardware of the sFLASH seeding experiment has been used. It is installed in the FLASH1 electron beamline between the collimation section (dogleg) and the undulator system, compare Fig. 3. The electron bunches arriving from the collimation section of FLASH1 are modulated in an electromagnetic undulator (5 periods of  $\lambda_u = 20$  cm,  $K_{\max} = 10.8$ ) by the 800-nm laser pulses arriving from the seeding laser system. After the modulator, chicane  $C_1$  with variable  $R_{56}$  is installed. For studies of LSC effects, we use a combination of a transverse-

\* Work supported by Federal Ministry of Education and Research of Germany under contract No. 05K10PE1, 05K10PE3, 05K13GU4, 05K13PE3, and the German Research Foundation program graduate school 1355.

<sup>†</sup> christoph.lechner@desy.de

## MULTI-BEAMLINE OPERATION TEST AT SACLA

Toru Hara<sup>\*</sup>, Takahiro Inagaki, Kazuaki Togawa, Ryota Kinjo, Hideki Takebe<sup>#</sup>, Chikara Kondo, Yuji Otake, Hitoshi Tanaka  
 RIKEN SPring-8 Center, Sayo-cho, Hyogo 679-5198, Japan  
 Kenji Fukami  
 JASRI, Sayo-cho, Hyogo 679-5149, Japan

### Abstract

After the installation of the second undulator beamline (BL2), multi-beamline operation has been started at SACLA since January 2015. 30 Hz electron bunches are alternately deflected to two beamlines using a kicker magnet and a DC twin-septum magnet. Since all undulator beamlines are placed downstream of the linear accelerator at SACLA, the beam energies are changed from bunch to bunch to obtain broad tunability of the laser wavelengths between the beamlines. In the multi-beamline operation, stable lasing is successfully achieved at the two beamlines with pulse energies around 100-150  $\mu\text{J}$ . The peak current is currently limited to about 1 kA due to the CSR effects at a doglegged beam transport to BL2. The status and operational issues related to the multi-beamline operation of SACLA are reported.

### INTRODUCTION

In order to meet the growing demand for XFEL user operation, a new undulator beamline (BL2) was installed in September 2014 at SACLA. Following this installation, a DC switching magnet was replaced by a kicker magnet and a DC twin-septum magnet in January 2015 to start pulse by pulse multi-beamline operation [1].

The undulator hall of SACLA can accommodate five undulator beamlines and they are all placed in parallel to each other [2]. In conventional facility designs, the beamlines of low photon energies branch off from the middle of a linear accelerator, where the electron beam energy is still low (Fig. 1 (a)) [3, 4]. At SACLA, however, all beamlines are placed downstream of the accelerator to make the facility compact (Fig. 1 (b)). Instead, the electron beam energy is controlled from bunch to bunch to obtain a wide spectral range between beamlines [5].

Figure 2 is a schematic of the SACLA facility. BL3 is the first undulator beamline installed in the midst of the five beamlines, so the electron beam travels straight from the end of the accelerator. The second beamline, BL2, is placed next to BL3. The undulators of BL2 and BL3 have the same parameters with a magnet period of 18 mm. In the beam transport to BL2, the electron beam is deflected twice by  $3^\circ$  in a dogleg.

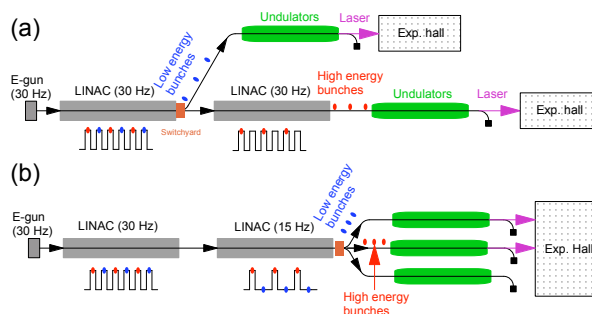


Figure 1: Multi-beamline schemes of XFEL facilities, (a) conventional layout and (b) SACLA.

In addition to the XFEL beamlines, there is a beam transport line to the SPring-8 storage ring, which is called XSBT (XFEL to Synchrotron Beam Transport). Since SACLA is planned to be used as a low-emittance injector in the upgrade project of SPring-8, XSBT will be used for the electron beam injection to the upgraded low-emittance ring in future [6].

### BEAMLINE SWITCHYARD

A beamline switchyard is composed of a kicker magnet and a DC twin-septum magnet installed at the end of the linear accelerator. The switchyard deflects the electron beam in three directions ( $+3^\circ$ ,  $0^\circ$  and  $-3^\circ$ ), and each direction corresponds to BL2, BL3 and XSBT respectively. To ensure the electron beam orbit stability, the deflection angle of the kicker is kept small as  $\pm 0.53^\circ$ . Then the DC twin-septum, locating 5.2 m downstream of the kicker (Fig. 3), deflects the beam by  $\pm 2.47^\circ$ . The stability requirement for the kicker is  $1 \times 10^{-5}$  (peak-to-peak) equivalent to an angular orbit error of 0.1  $\mu\text{rad}$ .

The kicker has a length of 0.4 m and its yoke is made with laminated silicon steel plates of 0.35 mm thickness. A ceramic vacuum duct is used at the kicker magnetic gap to eliminate the effects of eddy currents.

The DC twin-septum is composed of two identical septum magnets symmetrically-placed from side to side. Each septum magnet deflects the electron beam in opposite direction and the electron bunches for BL3 pass through between the two septums [1].

A pulsed power supply of the kicker magnet is a non-resonant type. It generates a bipolar trapezoidal waveform of current at up to 60 Hz, which is the maximum repetition of the electron beam at SACLA. The polarity, amplitude and repetition of the pulses can be arbitrarily changed according to the direction of deflection, beam energy and repetition of the electron bunches.

\*toru@spring8.or.jp

<sup>#</sup>Present address: Okinawa Institute of Science and Technology (OIST)

# FIRST SIMULTANEOUS OPERATION OF TWO SASE BEAMLINES IN FLASH

M. Scholz\*, B. Faatz, S. Schreiber, J. Zemella, DESY, Hamburg, Germany

## Abstract

FLASH2, the second undulator beamline of the FLASH FEL user facility at DESY (Hamburg, Germany) is under commissioning. Its first lasing was achieved in August 2014. FLASH is the first soft X-ray FEL operating two undulator beamlines simultaneously. Both undulator beamlines are driven by a common superconducting linear accelerator with a beam energy of up to 1.25 GeV. Fast kickers and a septum are installed to distribute one part of the electron bunch train to FLASH1 and the other part to FLASH2 with full repetition rate. The commissioning of FLASH2 takes place primarily in parallel to FLASH1 user operation. Various beam optics measurements have been carried out in order to ensure the required electron beam quality for efficient SASE generation. This paper reports the status of the FLASH2 commissioning.

## INTRODUCTION

FLASH [1–3], the free-electron laser (FEL) at DESY, Hamburg, Germany, delivers high brilliance XUV and soft X-ray FEL radiation for photon experiments. The superconducting accelerator technology used in the FLASH linac allows RF pulse lengths up to 800  $\mu\text{s}$ . That makes it possible to accelerate electron bunch bursts with several hundred bunches. The bursts come with a repetition rate of 10 Hz and the maximum repetition rate of the single bunches within the bursts is 1 MHz. The bursts can be divided into parts, which can then be assigned to different undulator beamlines.

During a shutdown in 2013, FLASH was upgraded with a second undulator beamline [4, 5]. Fast kickers and a DC Lambertson-Septum are installed downstream the FLASH linac allowing to distribute the electron beam either to FLASH1 or to the extraction arc leading to FLASH2. Figure 1 shows the first extraction components. The schematic layout of the FLASH facility is shown in Fig. 2.

Due to fixed gap undulators, the photon wavelength delivered by FLASH1 determines the electron beam energy. FLASH2 is equipped with a variable gap undulator thus the photon energy can also be changed, within limits, by varying the undulator gap size. First lasing in the new undulator beamline was achieved on August 20, 2014 [6] and several different machine setups have been tested since then. The commissioning of FLASH2 takes place mostly in parallel to FLASH1 user operation. In this paper, we describe the parallel operation of the two undulator beamlines as well as the commissioning status of FLASH2.

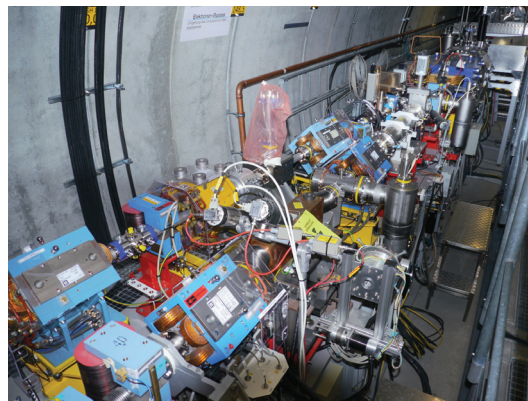


Figure 1: The first elements of the extraction arc leading the electrons to the new beamline FLASH2 are depicted on the left hand side. The beamline on the right hand side is FLASH1.

## RF CONTROL FOR SIMULTANEOUS OPERATION

The RF-pulse is shared between the electron bunch trains for FLASH1 and FLASH2. For a 800  $\mu\text{s}$  long FR-pulse, the total maximum number of bunches, with a bunch repetition rate of 1 MHz, is 800. The bunch pattern (number of bunches and intratrain repetition rate) and bunch charge can be different for FLASH1 and FLASH2. This is realized by using two independent injector lasers in parallel.

Between the two bunch trains there is a gap of about 50  $\mu\text{s}$ , which is required to rise the current of the FLASH2 extraction kickers and to establish a current flat-top that ensures the same kick for all bunches in the burst. The kicked bunches are deflected by a septum magnet to the FLASH2 beamline. Other bunches travel straight through the septum to FLASH1.

The gap between the bunch trains can also be used to change the RF pulse amplitudes and phases (both within limits) in the accelerating modules in order to adjust the beam energy and the compression for both beamlines separately. Figure 3 shows the RF steps of two coupled modules (ACC4 and ACC5) during parallel operation of FLASH1 and FLASH2. The picture shown is taken after a FLASH2 dispersion measurement during which the beam energy in FLASH2 was changed by  $\pm 3$  MeV. This was achieved by changing the FLASH2 RF amplitude in the modules accordingly. FLASH1 delivered FEL beam for a user experiment during this measurement thus its RF settings must stay unchanged. In addition to the different amplitudes, the phases of the modules were set to 1.5 degree off-crest for FLASH1 while the FLASH2 bunches were accelerated on-crest.

\* matthias.scholz@desy.de

# DISTRIBUTED SEEDING FOR NARROW-LINEWIDTH HARD X-RAY FREE-ELECTRON LASERS\*

D.C. Nguyen<sup>#</sup>, P.M. Anisimov, C.E. Buechler, J.W. Lewellen, Q.R. Marksteiner  
LANL, Mail Stop H851, Los Alamos, New Mexico, USA

## Abstract

We describe a new FEL line-narrowing technique called distributed seeding (DS), using Si(111) Bragg crystal monochromators to enhance the spectral brightness of the MaRIE hard X-ray free-electron laser. DS differs from self-seeding in three important aspects. First, DS relies on spectral filtering of the radiation at multiple locations along the undulator, with a monochromator located every few power gain lengths. Second, DS performs filtering early in the exponential gain region before SASE spikes start to appear in the radiation longitudinal profile. Third, DS provides the option to select a wavelength longer than the peak of the SASE gain curve, which leads to improved spectral contrast of the seeded FEL over the SASE background. Time-dependent Genesis simulations show the power-vs-z growth curves for DS exhibit behaviors of a seeded FEL amplifier, such as exponential growth region immediately after the filters of the seeding approaches considered, the two-stage DS spectra produce the highest contrast of seeded FEL over the SASE background and that the three-stage DS provides the narrowest linewidth with a relative spectral FWHM of  $8 \times 10^{-5}$ .

## INTRODUCTION

X-ray free-electron lasers (XFELs) routinely operate in the SASE mode, whereby the radiation power grows exponentially with distance in a long undulator as a single electron bunch amplifies its own undulator radiation all the way to saturation. The radiation slips ahead of the electrons by the slippage distance  $N_u \lambda_0$ , where  $N_u$  is the number of undulator periods and  $\lambda_0$  is the resonance wavelength, forming randomly distributed wave-packets within a single radiation pulse. In the exponential gain regime, these wave-packets develop into high-intensity longitudinal spikes, each of which is coherent within a coherence length given by

$$l_c = \frac{\lambda_0}{6\sqrt{\pi\rho}} \sqrt{\frac{z}{L_G}},$$

where  $\lambda_0$  is the resonance wavelength,  $z$  is the distance traversed by the electrons in the undulator,  $L_G$  is the 1D power gain length, and  $\rho$  is the Pierce parameter. At saturation ( $z \sim 20 L_G$ ), the coherence length is

$$l_c^{sat} \approx \frac{\lambda_0}{2\sqrt{\pi\rho}}.$$

For an XFEL with sub-Angstrom output wavelength,  $\rho$  is on the order of  $5 \times 10^{-4}$ , and thus the coherence length at saturation is on the order of 20 nm. The mean separation between these spikes is  $\Delta z_{spike} \leq 2\pi l_c$ , or about 100 nm, much shorter than the overall radiation pulse length (~tens of  $\mu\text{m}$ ). The frequency spectrum of a SASE XFEL consists of hundreds of narrow spectral lines, each being the Fourier transform of the radiation overall temporal duration, within an envelope that is the Fourier transform of the individual temporal spikes. The overall SASE spectrum has a relative bandwidth FWHM of

$$\frac{\Delta\lambda}{\lambda_0} = \frac{4\ln 2}{\sqrt{\pi}} \rho,$$

or about 0.1% for the typical  $\rho$  of an XFEL. The large bandwidth and poor temporal coherence of the SASE XFEL preclude its use in applications that require a high degree of longitudinal coherence such as three-dimensional coherent X-ray diffractive imaging.

SASE self-seeding has been studied and successfully employed to reduce the XFEL bandwidth to a fraction of an electron volt [1-5]. This technique relies on monochromatizing the SASE radiation from the first part of the undulator and then re-injecting the monochromatic seed into the second part of the undulator for amplification. Hard X-ray self-seeding can be performed either with a Bragg crystal monochromator as suggested by Saldin *et al.* [1], or a diamond wake crystal as suggested by Geloni *et al.* [2]. Self-seeding at both hard and soft X-ray energies has been demonstrated at the Linac Coherent Light Source [3, 4], where the seeded FEL spectra typically exhibit a narrow spectral line on top of a broadband SASE background. Geloni *et al.* also proposed using cascade self-seeding [5] to improve the contrast of self-seeded FEL over SASE.

We present a new concept of distributed seeding (DS) using multiple silicon Bragg crystal monochromators. DS differs from SASE self-seeding in three important aspects. First, DS relies on spectral filtering of the radiation at more than one location along the undulator. For this study, we consider both the two-filter and three-filter DS with a spectral filter located every five power gain lengths. Second, DS performs filtering early in the exponential gain region before SASE spikes start to appear in the radiation longitudinal profile to ensure the

\*Work supported by the US DOE / NNSA under contract DE-AC52-06NA25396.  
#dcnguyen@lanl.gov

# TUNABLE HIGH-POWER TERAHERTZ FREE ELECTRON LASER AMPLIFIER\*

G. Zhao<sup>#</sup>, S. Huang, W. Qin, L. Zeng, K. Liu

Institute of Heavy Ion Physics, School of Physics, Peking University, Beijing 100871, China

C. H. Chen, Y. C. Chiu, Y. C. Huang

Institute of Photonics Technologies, Department of Electrical Engineering,

National Tsinghua University, Hsinchu 30013, Taiwan

## Abstract

In this paper we present an ongoing project under the collaboration between Peking University (PKU) in Beijing and National Tsinghua University (NTHU) in Taiwan to develop tunable wavelength THz with high peak and average power from a THz free-electron laser (FEL) amplifier driven by a superconducting accelerator system at PKU and a tunable THz seed which is provided by a THz parametric amplifier (TPA). Simulation results show that narrow-band, wavelength-tunable THz radiation with 0.05-0.8 MW peak power and Watt-level average power can be expected.

## INTRODUCTION

THz have attracted much interest in many undisclosed phenomena. Especially in non-invasive diagnosis, security scanning, physics study and manufacturing. THz radiation sources are developing very fast. Free-electron laser (FEL) is an important technology to generate high-power THz radiation [1]. SASE THz FEL is difficult to realize because it requires high electron bunch charge, so most of the THz FEL devices are operating in the FEL oscillator [2,3]. We would like to develop another method—seeded amplifier. We try to use THz seed and superconducting accelerator to generate THz radiation with high peak power and average power simultaneously. THz FEL amplifier was first proposed by C.Sung et al in 2006. They used a TW CO<sub>2</sub> laser through different frequency generation (DFG) in GaAs crystal to generate THz seed [4,5]. We will choose a more compact design to generate THz seed by optical technology—THz parametric amplifier (TPA), which can produce wavelength tunable from 1 to 6 THz and narrow-band spectrum THz. In this paper, we present FEL simulation of THz FEL amplifier and preliminary study on TPA THz seed.

## SYSTEM LAYOUT

Our THz FEL amplifier system comprises two major components, the FEL amplifier and the THz seed. Figure 1 shows the configuration of the THz parametric amplifier. A pulse laser at 1064 nm and a wavelength tunable external-cavity diode laser (ECDL) pump a lithium niobate (LN) or KTiOPO<sub>4</sub> (KTP) crystal, then

generate a tunable narrow-band THz seed. Figure 2 shows the superconducting accelerator system at PKU, including the DC-SRF photoinjector which has been put into operation since 2014 and can provide 3MeV electron beam with bunch charge up to 60 pC, a SRF linac with two 1.3GHz Tesla-type cavities and a planer undulator. This superconducting system is expected to deliver high repetition rate electron beam with the energy of 8-25 MeV. It is under installation and will be operated in this autumn.

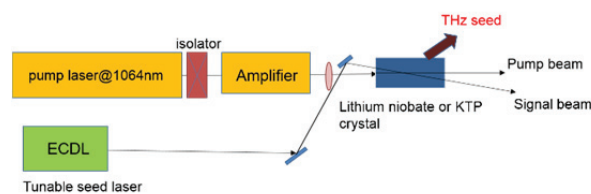


Figure 1: Configuration of the TPA THz seed system.

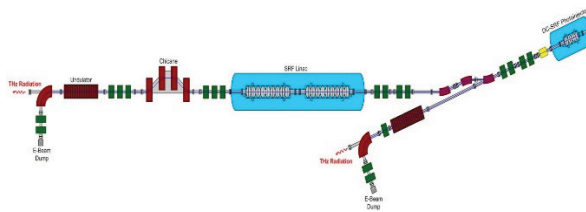


Figure 2: Superconducting accelerator system at PKU.

## THz PARAMETRIC AMPLIFIER

In recent years, tunable THz-wave sources with high temporal and spatial coherence using the resonant frequency of ferroelectric crystal lattices at room temperature are popular. TPA can generate tunable coherent radiation [6]. This optical technology is based on tunable light scattering from the long wavelength side of the A<sub>1</sub>-symmetry mode in LN which has a high gain coefficient from 0.5 THz to 3 THz [7]. Molecular of crystal absorb photons of pump laser and transit to a virtual energy level. Near-infrared (NIR) photons and THz photons from the vibrational mode of molecular will be generated through Stimulated Raman Scattering (SRS) process. The frequency of THz photon equals to the difference between the frequency of pump laser and seed laser. The output NIR, which has the same frequency with the seed laser, usually used to derive the THz information. The output THz is distributed in a certain angle which

\* Institute of Heavy Ion Physics, School of Physics, Peking University, Beijing 100871, China  
# zhaogang@pku.edu.cn

# THE MICROBUNCHING INSTABILITY AND LCLS-II LATTICE DESIGN

M. Venturini\*

Lawrence Berkeley National Lab, Berkeley, CA 94720 USA

## Abstract

The microbunching instability is a pervasive occurrence when high-brightness electron beams are accelerated and transported through dispersive sections, like bunch-compression chicanes or distributions beamlines. If left uncontrolled, the instability can degrade the beam brightness and compromise the FEL performance. This paper contains a discussion of how consideration of the microbunching instability is informing the LCLS-II design and determining the specifications for the laser heater and transport lines. We review some of the expected and not so-expected phenomena that we have encountered while carrying out high-resolution macroparticle simulations of the instability and the analytical models developed to interpret the numerical results.

## INTRODUCTION

LCLS-II is a 4<sup>th</sup>-generation high-rep rate FEL light source soon to enter the construction phase at SLAC [1, 2]. The 4 GeV super-conducting Linac will occupy the first third of the existing SLAC Linac tunnel; a long ( $\sim 2$  km) transport line will bypass the remaining sections of the normal-conducting machine and deliver the beam to the existing undulator hall, with a fast kicker distributing the beam between the hard (HXR) and soft (SXR) x-ray FEL undulators. The baseline design (100 pC bunches with  $I_f \simeq 800$  A or higher peak current at the FELs and  $I_{gun} \simeq 3$  A at the gun) calls for two-stage magnetic-compression at 250 and 1600 MeV beam energy in addition to significant velocity-bunching or 'ballistic' compression in the injector before the beam becomes ultra-relativistic. Use of a third magnetic chicane placed immediately before the spreader at full 4 GeV beam energy is under consideration but will not be discussed here. For a summary of relevant machine parameters, see Table 1.

As in all 4<sup>th</sup>-generation light sources the microbunching instability is expected to be significant. The instability can be seeded by shot noise or other noise sources at the injector photo-cathode and develops through a combination of collective effects (primarily space-charge) and transport/compression along dispersive sections. The main adverse effect is the generation of uncorrelated or micro-correlated energy-spread growth. The instability can result into loss of radiated power and/or degradation of the radiation spectral properties, with tolerance to the instability depending on the mode of FEL operation (SASE, self-seeding, external seeding).

There are two aspects relevant to the instability that are specific to LCLS-II: the presence of long transport lines

between the Linac and the undulators and reliance on velocity bunching for compression. Both have potentially aggravating effects. While in low rep-rate LCLS-class injectors, which are usually operated without velocity bunching, plasma oscillations at low energy tend to have a generally smoothing effect on perturbations to the charge density [3], the effect can be reduced or reversed in the presence of velocity bunching compression [4, 5]. This is most relevant for the instability seeded by non-uniformity in the photo-gun laser profile. Here we will not address this issue, focusing instead on consideration of microbunching seeded by shot noise, for which it is appropriate to model the development of the instability starting from the exit of the injector. In our study we use a combination of analytical and numerical methods to characterize the main drivers of the instability and related phenomena, and identify strategies for machine-design optimization. Topics of interest discussed here include the anomalous heating induced by the laser heater, the development of the instability through the magnetic compressors, and its further amplification through the transport lines downstream of the Linac. Our macroparticle simulations, carried out with the code IMPACT [6], are based on idealized models of the beam distribution (*e.g.* temporal flat-top, 6D water-bag) having the nominal characteristics (emittance, peak current) of the baseline beam at the exit of the injector and always employ the same number of macroparticles as the number of electrons to minimize spurious effects. Results from start-to-end simulations starting from the photo-cathode and including modelling of the radiation output are reported elsewhere [7, 8].

Table 1: LCLS-II Baseline Settings

Charge/bunch	100 pC
Peak current at exit of injector, $I_{inj}$	14 A
Peak current at FEL, $I_f$	800 A
Transverse normalized rms emittance, $\epsilon_n$	0.3 $\mu\text{m}$
Beam energy at exit of injector, $E_{inj}$	100 MeV
Beam energy at BC1, $E_{bc1}$	250 MeV
Beam energy at BC2, $E_{bc2}$	1.6 GeV
Beam energy at FEL, $E_f$	4 GeV
BC1 $R_{56}$ , $R_{56}^{bc1}$	-55 mm
BC2 $R_{56}$ , $R_{56}^{bc2}$	-38 mm
BC1 compression factor, $C_{bc1}$	$\sim 6$
BC2 compression factor, $C_{bc2}$	$\sim 10$

\* mventurini@lbl.gov

# THZ PHOTO-INJECTOR FEM BASED ON SPONTANEOUS COHERENT EMISSION FROM A BUNCH OF NEGATIVE-MASS ELECTRONS\*

I.V. Bandurkin, A.V. Savilov<sup>#</sup>, Institute of Applied Physics, Nizhny Novgorod, Russia

## Abstract

It is proposed to utilize the effect of negative mass for stabilization of the effective axial size of very dense and short electron bunches produced by photo-injector guns by using combined undulator and strong uniform magnetic fields. It has been shown that in the "abnormal" regime, in which an increase in the electron energy leads to a decrease in the axial velocity of the electron, due to the negative-mass effect the Coulomb repulsion of electrons leads to their attraction and formation of a fairly stable and compact bunch "nucleus". The use of the negative-mass regime may provide realization of a source of the terahertz radiation, which is based on a long-pulse coherent spontaneous undulator emission from a short dense moderately-relativistic (5.5 MeV) photo-injector electron bunch with a high (up to 20%) efficiency and a narrow frequency spectrum.

## INTRODUCTION

Laser-driven photo-injectors allow formation of fairly compact and accessible sources of dense electron bunches with a moderate energy of 3-6 MeV, sub-picosecond and picosecond pulse durations, and charges of up to 1 nC and greater. These bunches can be further accelerated up to the GeV energy level for the use in short-wavelength FELs or directly exploited for radiation in the THz frequency range. In the latter case, they can be used, in particular, for realization of comparatively simple and compact sources operating in the regime of spontaneous coherent undulator radiation of electrons [1-4]. This type of radiation is realized, when the effective axial length of bunches in the radiation section is shorter than the operating wavelengths. In this situation, the wave packets emitted by each of the electrons add up basically in phase; this provides high level of radiation power.

Evidently, the length of the operating region is strictly limited by the Coulomb particle repulsion leading to an increase in bunch sizes and, first of all, in the axial size of the bunch. In this letter, we propose a method of weakening the axial repulsion significantly and, simultaneously, of confining particles in the transverse direction by means of using the radiation of electrons in combined undulator and strong uniform guiding magnetic fields. The corresponding effect is similar to the Negative Mass Instability which is well-known in cyclic accelerators [5,6] and Cyclotron Resonance Masers [7-9]. In the combined field, the negative-mass effect can occur when the electron cyclotron frequency corresponding to the guiding magnetic field exceeds the bounce frequency

of electron oscillations in the periodic undulator field. In such "abnormal" regime, an increase in the energy of the particle leads to a decrease in its axial velocity [10-13] and axial Coulomb repulsion of the electrons leads to their effective mutual attraction which slows down bunch degradation. The use of this regime can result in a substantial increase in the effective length of the coherent spontaneous emission, and, therefore, an increase in the power and narrowing of the spectrum of the output radiation pulse.

In this letter, we study a possibility to realize a powerful and very efficient source of long-pulse coherent radiation of the terahertz frequency range on the basis of the Israeli THz Source [3] as an example of the proposed approach. This THz source is based on the using coherent spontaneous undulator emission from a short dense photo-injector electron bunch with moderate energy (5.5 MeV). The stabilization of the axial size of the bunch (which is required to provide the coherent character of the radiation) is due to the negative-mass regime of the motion of the bunch through a long operating undulator. An undulator with a strong uniform magnetic field providing the negative-mass effect is proposed and designed for this experiment [14].

## NEGATIVE-MASS EFFECT

For demonstration of the negative-mass effect, let us first recall the known properties of the electron motion in a helical undulator with period  $d_u$  and a homogeneous axial magnetic field  $B_0$  (Fig. 1a) within the approximation of negligible transverse inhomogeneity of the undulator field as well as the perturbations caused by the Coulomb and radiated fields [10-12]. The normalized oscillatory (transverse) electron momentum obeys the equation:

$$p_{\perp} = K / \Delta,$$

where  $K$  is the undulator parameter in the absence of the guiding field,  $B_0 = 0$ , and  $\Delta = 1 - \Omega_c / \Omega_u$  is the mismatch between the relativistic electron cyclotron frequency  $\Omega_c = eB_0 / mc\gamma$  and the undulator (bounce) frequency  $\Omega_u = h_u V_z$ . The dependence of the transverse electron velocity on the cyclotron frequency has a resonance character (Fig. 1b);  $V_{\perp}(\Omega_c)$  is an increasing function at low axial magnetic fields ( $\Omega_c < \Omega_u$ ) and a decreasing function at high magnetic fields ( $\Omega_c > \Omega_u$ ).

The Coulomb interaction leads to an increase in the energies of the particles placed in the bunch front and to decrease in the energies of the electrons being in the tail. The type (positive/negative mass) of the Coulomb interaction is determined by the dependence of the axial

\*Work partially supported by the Russian Scientific Foundation (Project 14-19-01723).

#savilov@appl.sci-nnov.ru

# FURTHER STUDIES OF UNDULATOR TAPERING IN X-RAY FELs

Alan Mak\*, Francesca Curbis, Sverker Werin, MAX IV Laboratory, Lund University, Sweden

## Abstract

We further the studies of the model-based optimization of tapered free-electron lasers presented in a recent publication [Phys. Rev. ST Accel. Beams **18**, 040702 (2015)]. Departing from the ideal case, wherein the taper profile is a smooth and continuous function, we consider the more realistic case, with individual undulator segments separated by break sections. Using the simulation code GENESIS, we apply our taper optimization method to a case, which closely resembles the FLASH2 facility in Hamburg, Germany. By comparing steady-state and time-dependent simulations, we examine how time-dependent properties alter the optimal taper scenario. From the simulation results, we also deduce that the “traditional” empirical method, whereby the intermediate radiation power is maximized after closing every undulator gap, does not necessarily produce the highest final power at the exit of the undulator line.

## INTRODUCTION

Present-day imaging experiments at x-ray free-electron laser (FEL) facilities call for an increased number of photons within a shorter pulse duration [1, 2]. To meet the stringent demand on the radiation power, the technique of undulator tapering has been revisited in recent years, and much theoretical effort has been dedicated to the optimization of this technique [3–6].

In a recent publication [6], we propose a modification to the Kroll-Morton-Rosenbluth (KMR) model [7], which serves as a method of optimizing the taper profile. The method features a variable phase of the resonant particle, and opens up possibilities for further enhancement of radiation power beyond the constant-phase model.

In the ideal case, the taper profile  $K(z)$  is a smooth and continuous function. However, most existing taperable x-ray FELs, such as FLASH2 [8] and SACLA [9], consist of individual undulator segments separated by break sections. With these limitations, a reduction of radiation power from the ideal case is inevitable.

The break sections are needed for beam focusing, trajectory correction and diagnostics. However, vacuum diffraction of the optical beam in the break sections leads to a decrease in the on-axis field strength, which also causes particle detrapping [3].

Also, as each undulator segment is uniform within itself, the segment length sets a limit on the rate at which  $K$  can decrease, and hence a limit on the bucket deceleration rate. Furthermore, if the segment length is larger than the synchrotron period, the electron beam can absorb energy momentarily from the optical beam [6].

In this article, we study a case with 2.5-m undulator segments separated by break sections. Using the simulation code GENESIS [10], we adapt our taper optimization method to these limitations, and obtain the highest possible power. We then compare the simulation results obtained in the steady-state mode and the time-dependent mode, quantifying the effects of time-dependent properties.

The case chosen for our simulation studies is intended to match the design parameters of the FLASH2 facility, which achieved its first lasing [11] in August 2014.

## CASE DEFINITION

For the simulation studies in this article, we choose a case with main parameters as shown in Table 1. These parameter values are within the designed range for the FLASH2 facility [8].

Table 1: Main Parameters for the Simulated Case

Parameter	Symbol	Value
Electron beam energy	$E$	1.25 GeV
Peak current	$I$	2.5 kA
Bunch charge	$Q$	630 pC
Bunch length	$\sigma_t$	30 $\mu$ m
Energy spread	$\sigma_E$	0.5 MeV
Normalized emittance	$\varepsilon_{x,y}$	1.4 $\mu$ m rad
Average beta function	$\langle \beta_{x,y} \rangle$	6 m
Radiation wavelength	$\lambda$	6 nm
Undulator period	$\lambda_w$	31.4 mm
Undulator segment length	$L_{\text{seg}}$	2.5 m

The undulator segments considered in this case are planar. The lattice for the transverse focusing of the electron beam is in a FODO configuration. The period of the FODO cell is 6.6 m, in which two quadrupole magnets are 3.3 m apart from one another.

The FLASH2 facility has 12 undulator segments [8]. But in our simulation studies, we first consider a total of 30 segments, for the purpose of understanding the FEL dynamics over a long distance. After that, we consider the more realistic 12-segment case, by discarding all the subsequent segments in the simulations.

## TAPER OPTIMIZATION METHOD

Our taper optimization method is detailed in a recent publication [6]. The method is based on the KMR model [7] and a modification thereto. It considers a resonant particle with phase-space coordinates  $(\psi_R, \gamma_R)$ . With a constant phase  $\psi_R(z) = \psi_R(0)$ , it is known as the ordinary KMR

\* alan.mak@maxlab.lu.se

# THRESHOLD OF A MIRROR-LESS PHOTONIC FREE-ELECTRON LASER OSCILLATOR PUMPED BY ONE OR MORE ELECTRON BEAMS

A. Strooisma, P.J.M. van der Slot\*, K.J. Boller

Mesa<sup>+</sup> Institute for Nanotechnology, University of Twente, Enschede, The Netherlands

## Abstract

Transmitting electrons through a photonic crystal can result in stimulated emission and the generation of coherent Cerenkov radiation. Here we consider a photonic-crystal slab consisting of a two-dimensional, periodic array of bars inside a rectangular waveguide. By appropriately tapering the bars at both ends of the slab, we numerically show that an electromagnetic wave can be transmitted through the photonic-crystal slab with close to zero reflection. Furthermore, the photonic-crystal slab allows transmission of electrons in the form of one or more beams. We design the tapered photonic-crystal slab to have a backward wave interaction at low electron-beam energy of around 15 kV, that results in distributed feedback of the radiation on the electrons without any external mirrors being present. Here we discuss the dynamics of the laser oscillator near threshold and numerically show that the threshold current can be distributed over multiple electron beams, resulting in a lower current per beam.

## INTRODUCTION

Electron beams have been used to generate incoherent and coherent radiation over a large spectral range. Among the huge range of sources are microwave devices [1, 2], gyrotrons [1, 3], synchrotrons [4] and free-electron lasers (FELs) [5–8]. These sources can be divided in two classes, the so-called fast-wave (e.g., gyrotrons, synchrotrons and FELs) and slow-wave or Cerenkov devices (e.g., traveling wave tubes, Smith-Purcell and Cerenkov free-electron lasers). Here we focus on the slow-wave devices that use an interaction structure to slow down the phase velocity of the wave to make the electron move synchronous with the wave. This phase matching results in bunching of the electrons on the scale of the radiation wavelength and is responsible for the generation of coherent radiation [1, 2, 9]. The slow-wave devices are very efficient and powerful sources of radiation at microwave frequencies, however, when scaled to higher frequencies the output power drops. The reason for this is that the characteristic size of the interaction structure reduces when the operating frequency increases. The maximum current that can be transported through the interaction structure is also reduced and, hence, the output power. However, in a photonic free-electron laser (pFEL) a photonic crystal is used as interaction structure to slow down the wave. Electrons streaming through a photonic crystal can move synchronous with a co-propagating wave and emit coherent Cerenkov radiations [9, 10]. A photonic crystal typically has many parallel channels through which

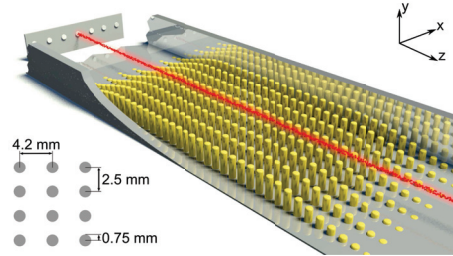


Figure 1: Schematic view of the photonic free-electron laser with a single electron beam. The red dots represent the electrons. The inset shows the orientation of the coordinate system.

the electrons can propagate. For example, the photonic crystal shown in Fig. 1 allows up to seven beams to propagate in parallel through the photonic structure. Therefore, when the photonic crystal shrinks in size to support higher operating frequencies, one can increase the transverse extent of the crystal to create more parallel channels for the electrons and keep the total current streaming through the crystal constant. As the current per individual electron beam will decrease, it is of interest to investigate the behavior of a photonic free-electron laser near threshold when pumped by one or multiple electron beams.

The remainder of this paper is organized as follows. We first present the photonic crystal considered in this paper and then we use a particle-in-cell code (CST particle studio 2014) to investigate the performance near threshold of the backward-wave pFEL oscillator when pumped by a single electron beam in the center of the photonic crystal. This is followed by investigating the performance when the same oscillator is pumped by several electron beams and the paper concludes with a discussion and outlook.

## TAPERED PHOTONIC CRYSTAL

The photonic free-electron laser considered here is shown schematically in Fig. 1. The photonic crystal consists of 8 rows of 40 posts placed in a rectangular waveguide, where the height of the  $n$ th post in a row is given by:

$$h_n = \begin{cases} h_0 \cos^2 \left( \frac{\pi}{2} \left( \frac{n}{11} - 1 \right) \right) & \text{if } 1 \leq n \leq 10 \\ h_0 & \text{if } 10 < n \leq 30 \\ h_0 \cos^2 \left( \frac{\pi}{2} \frac{n-30}{11} \right) & \text{if } 30 < n \leq 40 \end{cases}, \quad (1)$$

where  $h_0 = 4$  mm is the full post height. The other dimensions of the photonic crystal are a post radius of 0.75 mm, a distance between post centers of 2.5 mm along the  $z$  axis and 4.2 mm along the  $x$  axis. The waveguide has a cross-section of 33.6 by 8.0 mm. The taper at both ends of the crystal is

\* p.j.m.vanderslot@utwente.nl

# THREE-DIMENSIONAL, TIME-DEPENDENT SIMULATION OF FREE-ELECTRON LASERS

H.P. Freund

Department of Electrical and Computer Engineering, Colorado State University, Fort Collins, USA

P.J.M. van der Slot<sup>#</sup>

Mesa<sup>+</sup> Institute for Nanotechnology, University of Twente, Enschede, the Netherlands,

Department of Electrical and Computer Engineering, Colorado State University, Fort Collins, USA

## Abstract

Simulation codes modeling the interaction of electrons with an optical field inside an undulator are an essential tool for understanding and designing free-electron lasers (FELs). A new code under development, named MINERVA, uses a modal expansion for the optical field. A Gaussian expansion is used for free-space propagation, and an expansion in waveguide modes for fully guided propagation, or a combination of the two for partial guiding at THz frequencies. MINERVA uses the full Newton-Lorentz force equation to track the particles through the optical and magnetic fields. We describe the main features of MINERVA, and show comparisons between simulations and experiments conducted using the LCLS.

## INTRODUCTION

Simulation codes modeling the interaction of electrons with an optical field inside an undulator are an essential tool for understanding and designing free-electron lasers (FELs). As there exists a large variety of FELs ranging from long-wavelength oscillators using partial wave guiding to single-pass soft and hard x-ray FELs that are either seeded or starting from noise (*i.e.*, Self-Amplified Spontaneous Emission or SASE), a simulation code should be capable of modeling this huge variety of FEL configurations. A new code under development, named MINERVA, is capable of modeling such a large variety of FELs. The code uses a modal expansion for the optical field including a Gaussian expansion for free-space propagation, or an expansion in waveguide modes for fully-guided propagation, or a combination of the two for partial guiding, which is typically used at THz frequencies. MINERVA uses the full Newton-Lorentz force equations to track the particles through the optical and magnetic fields. Here we describe the main features of MINERVA and compare simulations with experiments conducted using the LCLS at SLAC.

A variety of different free-electron laser (FEL) simulation codes have been developed over the past several decades such as GINGER [1], MEDUSA [2], TDA3D [3], and GENESIS [4], among others. These codes typically undergo continuous development over their usable lifetimes. As a result, the codes become increasingly complex as new capabilities are added or

older capabilities are deleted, and this tends to compromise their performance. It also renders it increasingly more difficult to make further modifications that might be needed. Because of this, we decided to develop a new code using a “clean-slate” approach having the properties and characteristics that we desired.

## SIMULATION PROPERTIES

The formulation used in MINERVA describes the particles and fields in three spatial dimensions and includes time dependence as well. Electron trajectories are integrated using the complete Newton-Lorentz force equations. No wiggler-averaged-orbit approximation is made. The magnetostatic fields can be specified by analytical functions for a variety of analytic undulator models (such a planar or helical representations), quadrupoles, and dipoles. These magnetic field elements can be placed in arbitrary sequences to specify a variety of different transport lines. As such, MINERVA can set up field configurations for single or multiple wiggler segments with quadrupoles either placed between the undulators or superimposed upon the undulators to create a FODO lattice. Dipole chicanes can also be placed between the undulators to model various optical klystron and/or high-gain harmonic generation (HG) configurations. A variety of undulator models is available, including: (1) either flat- or parabolic-pole-face planar undulators, (2) helical undulators, and (3) a representation of an APPLE-II undulator that can treat arbitrary elliptic polarizations. The fields can also be imported from a field map.

The electromagnetic field is described by a modal expansion. For free-space propagation, MINERVA uses Gaussian optical modes, while waveguide modes are used when the wavelength is comparable to the dimensions of the drift tube. As a result, MINERVA can treat both long and short wavelength FELs. A combination of the Gaussian and waveguide modes is also possible when there is partial guiding at, for example THz frequencies.

The electromagnetic field representations are also used in integrating the electron trajectories, so that harmonic motions and interactions are included in a self-consistent way. Further, the same integration engine is used within the undulator(s) as in the gaps, quadrupoles, and dipoles, so that the phase of the optical field relative to the electrons is determined self-consistently when propagating the particles and fields in the gaps between the undulators.

<sup>#</sup>p.j.m.vanderslot@utwente.nl

# A MIRROR-LESS, MULTI-BEAM PHOTONIC FREE-ELECTRON LASER OSCILLATOR PUMPED FAR BEYOND THRESHOLD

A. Strooisma, P.J.M. van der Slot\*, K.J. Boller

Mesa<sup>+</sup> Institute for Nanotechnology, University of Twente, Enschede, The Netherlands

## Abstract

In a photonic free-electron laser one or multiple electron beams are streaming through a photonic crystal to generate coherent Cerenkov radiation. Here we consider a photonic-crystal slab consisting of a two-dimensional, periodic array of bars inside a rectangular waveguide, with both ends tapered to provide complete transmission of an electromagnetic wave. By appropriately designing the photonic-crystal slab, a backward wave interaction at low electron beam energy of around 15 kV can be obtained. The backward wave interaction provides distributed feedback without any external mirrors being present. We numerically study the dynamics of the laser oscillator when pumped far beyond threshold with one or multiple electron beams. We show that using multiple beams with the same total current provide better suppression of higher-order modes and can produce more output power, compared to the laser pumped by a single beam of the same total current.

## INTRODUCTION

The coherent emission of traditional laser oscillators is typically limited to a discrete set of emission frequencies, which is determined by the transition between bound-electron states having discrete energy levels, by the discrete set of longitudinal modes of the resonator or by a combination of both [1]. Free-electron lasers (FELs) partly overcome this by generating coherent radiation using unbound, also called free, electrons, which have a continuous energy distribution and can therefore emit at any desired frequency [2, 3]. However, whenever an oscillator configuration is used, the emission of an FEL will again be in the longitudinal modes of the resonator. Note that the free electrons need higher kinetic energy to emit shorter wavelengths, e.g., energies of a few MeV are required to generate THz radiation, while several to tens of GeV are required to emit soft- and hard x-ray radiation.

It is therefore desirable to have a coherent radiation source based on free electrons that would be compact, continuously tunable and preferably require much lower energy electrons (compared to undulator-based FELs) to generate a specific frequency. At the same time this source should provide a feedback mechanism that does not require an external resonator. The photonic free-electron laser (pFEL) [4] is a such a light source that fulfills these requirements and has other advantages as well.

In a pFEL gain is provided by electrons streaming through a photonic crystal embedded in a waveguide as shown in Fig. 1. The photonic crystal slab considered here consists

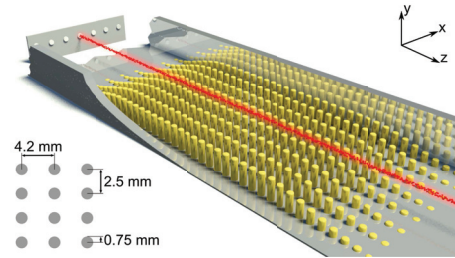


Figure 1: Schematic view of the photonic free-electron laser with a single electron beam. The red dots represent the electrons. The inset shows the orientation of the coordinate system.

of a periodic array of metal posts placed inside a metallic waveguide that provides the vacuum required to transport the electrons. Note that this photonic crystal possesses many natural channels for the electrons to propagate through (e.g., up to seven in Fig. 1). This allows the total current to be divided over many electron beams, lowering the current density in each individual beam. This results in higher quality electron beams and easier beam transport [5] than would be possible with a single electron beam. On the other hand, when keeping the current density in the individual beams constant, increasing the number of electron beams provides a simple way of scaling the output power of the source.

When an electron beam streams through the photonic crystal, spontaneous Cherenkov radiation is emitted [6], albeit with different properties [7] compared to the emission in bulk materials. The spontaneous emission will contain Bloch eigenmodes of the photonic crystal slab that are velocity matched with the electrons for a low-order spatial harmonic. If the Bloch eigenmode has a longitudinal electric field component, then the mutual interaction between radiation field and electrons results in bunching of the electrons and hence the build-up of a coherent radiation field at the velocity-matched frequency.

The remaining part of this paper is organized as follows. We first investigate the properties of the tapered photonic crystal slab considered in this paper which includes the dispersion of the lowest order Bloch eigenmode. Then we investigate the performance of the mirrorless pFEL oscillator when pumped by a single electron beam in the center of the photonic crystal slab. This is followed by investigating the performance when the same oscillator is pumped by several electron beams and the paper concludes with a discussion and outlook.

\* p.j.m.vanderslot@utwente.nl

# QUANTUM NATURE OF ELECTRONS IN CLASSICAL X-RAY FELS\*

Petr M. Anisimov<sup>#</sup>, LANL, Los Alamos, NM 87545, USA

## Abstract

An x-ray free electron laser (FEL) is considered by many to be a completely classical device. Yet, some have investigated operating regimes where the underlying physics transitions from a classical to a quantum description. Focusing on the collective behaviour of electrons, they have introduced symmetrized bunching operators and have found an additional energy spread due to recoil, mediated through a quantum FEL parameter.

This work focuses on the quantum nature of a single electron, which is best described, not by a point particle, but by a wave packet. Owing to free space dispersion, one can define the smallest-sized wave packet at an FEL entrance that remains as such throughout an FEL. By utilizing this packet size, we have developed a 1D FEL theory that includes how quantum effects affect bunching.

The smallest-sized wave packet is related to the quantum FEL parameter and offers new insights into the classical-to-quantum transition. It can be generalized to include 3D effects and offers a convenient way to classify FELs. Our theory indicates that gain reduction due to quantum averaging is much stronger than previously believed and will significantly affect harmonic lasing in x-ray FELs (XFELs).

## INTRODUCTION

Interest in XFELs has grown in response to the expanding scientific demand in coherent x-ray light sources. XFELs, such as the LCLS at SLAC (USA) [1] and SACLA at Spring-8 (Japan) [2], deliver ultra-bright X-ray pulses having femtosecond duration. Their peak brilliance is about eight orders of magnitude higher than that from most other X-ray sources. The combination of high pulse energy and femtosecond pulse duration of coherent XFEL pulses has created new fields of research in ultrafast chemistry, structural biology and coherent diffractive imaging [3].

The FEL was invented by John Madey [4] who used a quantum mechanical description to arrive at a classical result for the low-gain lasing regime. Thus, the FEL is considered by many to be a completely classical device [5-7]. However, there has been a significant effort to formulate a quantum mechanical description for FELs [8-12] even though XFELs built to date are well described by the classical theory (as their bandwidth is much larger than the recoil frequency) [13].

The quantum regime for FEL operation discussed in Ref. [13] was further investigated in Refs. [14-19]. It was shown that the classical-to-quantum transition is controlled by a “quantum FEL parameter”, defined as the

ratio between the FEL bandwidth and the photon recoil energy [20]. The quantum regime of operation requires the quantum FEL parameter to be small, a regime that cannot be reached by existing XFELs [1, 2].

Future XFELs are now being designed in response to demand for ever shorter radiation wavelengths and narrower bandwidths. However, cost limitations for future facilities drives their design to utilize accelerators with as low a beam energy as possible. These opposing design criteria exacerbate quantum mechanical effects requiring careful consideration of their impact on lasing performance.

Here we focus on the quantum nature of a single electron and determine how it affects classical XFEL performance. Starting with the classical 1D theory and an analysis of the free space dispersion of an electron wave packet, we construct a hybrid 1D FEL theory that accounts for quantum uncertainty of the electron position inside an XFEL. This theory facilitates a unified description of XFELs and indicates that the planned MaRIE XFEL at Los Alamos National Lab [21] will be affected.

## CLASSICAL 1D THEORY

XFELs are lasers that use relativistic electrons moving freely through a periodic magnetic structure in order to generate radiation. The magnetic structure, an undulator, is characterized by wiggle period  $\lambda_u$  and strength parameter  $K = eB_0/k_u mc$ , where  $B_0$  is a peak magnetic field and  $k_u = 2\pi/\lambda_u$ . In a planar undulator, electrons with energy  $\gamma_0$  in  $mc^2$  units generate x-ray radiation at a wavelength  $\lambda = \frac{\lambda_u}{2\gamma_0^2}(1 + K^2/2)$ .

The fundamentals of FEL instability are captured by the 1D theory with universal scaling in terms of the FEL parameter  $\rho = \frac{1}{2\gamma_0} \sqrt[3]{\frac{I}{I_A} \frac{\lambda_u^2 K^2 J J_1}{8\pi A}}$  for an electron beam with the peak current  $I$  and the transverse area  $A$ . Here  $I_A = 17$  kA is the Alfvén current and  $J J_n = J_{[n/2]}(nY) + J_{[n/2]+1}(nY)$  with  $Y = -K^2/(4+2K^2)$  is the energy exchange parameter. The independent variable is the distance along the undulator,  $z = \bar{v}_z t / L_{g0}$ , measured in the units of the 1D gain length  $L_{g0} = \lambda_u / 4\pi\rho$ ; and the  $\alpha^{\text{th}}$  electron is described by its ponderomotive phase with respect to the radiation,  $\theta_\alpha = (k + k_u)\bar{v}_z t - kct$ , and the relative energy detuning,  $\eta_\alpha = (\gamma - \gamma_0)/\rho\gamma_0$ . The complete set of coupled first-order differential equations has the following form:

\*Work supported by the U.S. Department of Energy through the LANL/LDRD Program. LA-UR-15-26403  
#petr@lanl.gov

# HIGH FIDELITY START-TO-END NUMERICAL PARTICLE SIMULATIONS AND PERFORMANCE STUDIES FOR LCLS-II

G. Marcus, Y. Ding, P. Emma, Z. Huang, T. O. Raubenheimer, L. Wang  
SLAC, Menlo Park, CA 94025, USA

J. Qiang, M. Venturini, LBNL, Berkeley, CA 94720, USA

## Abstract

High fidelity numerical particle simulations that leverage a number of accelerator and FEL codes have been used to analyze the LCLS-II FEL performance. Together, the physics models that are included in these codes have been crucial in identifying, understanding, and mitigating a number of potential hazards that can adversely affect the FEL performance, some of which are discussed in papers submitted to this conference [1, 2]. Here, we present a broad overview of the LCLS-II FEL performance, based on these start-to-end simulations, for both the soft X-ray and hard X-ray undulators including both SASE and self-seeded operational modes.

## INTRODUCTION

The LCLS-II is an advanced x-ray FEL light source that consists of two independently tunable undulators capable of producing radiation covering a large spectral range that can be fed by both a CW superconducting RF (SCRF) linac or by the existing copper linac [3]. Each undulator beamline will be dedicated to the production of either hard (HXR) or soft (SXR) x-ray photons and will incorporate self-seeding [4, 5] infrastructure to produce narrow-bandwidth and longitudinally coherent FEL pulses. Additional details regarding the baseline design can be found elsewhere [3, 6, 7].

It has been found that the relatively low electron beam energy of 4 GeV (compared to the nominal operation of LCLS) along with an extended transport distance from the end of the linac to the entrance of the undulators leaves the electron beam susceptible to a space-charge driven microbunching instability (MBI) [8–10]. This MBI manifests as large slice current and energy modulations that can potentially degrade the FEL performance. In addition, the space-charge MBI is the leading candidate responsible for the production of a self-seeded spectral ‘pedestal’ which is seen in both experiment [11] and in simulation [12] and is the topic of current theoretical study [2, 13].

This paper reports the results of high fidelity numerical particle simulations using the suite of codes IMPACT [14–16] and GENESIS [17]. These simulations include the effects of three-dimensional space charge, coherent and incoherent synchrotron radiation, RF cavity wakefields and resistive wall wakefields in the generation, acceleration and transport of the electron beam from the cathode to the undulator for three charge distributions: 20 pC, 100 pC, and 300 pC. To model the initial shot noise of the electron beam, the real number of electrons were tracked from the cathode.

The various charge distributions were then used to define the electron beams in GENESIS, where resistive wall wake-field effects are also included in the FEL simulations. SASE has been studied across the tuning ranges for each of the individual charge distributions for both the HXR and SXR undulators and include fully time-dependent taper optimizations. Preliminary results for self-seeding with the 100 pC electron beam will also be discussed.

## ELECTRON BEAM PROPERTIES

A detailed start-to-end simulation study of the accelerator beam delivery system is reported elsewhere [1, 18]. Below, we present the electron beam longitudinal phase space (LPS) and critical slice parameters for each of the charge distributions discussed above at the entrance to the SXR undulator. The LPS of the electron beams at the entrance to the HXR undulator show less effects of MBI for reasons discussed in [18]. This sets the stage for detailed FEL simulations in the following section.

### 20 pC

Figure 1 shows the LPS along with various slice properties of the 20 pC electron beam that has been tracked to the SXR undulator. The core of the distribution is roughly 8  $\mu\text{m}$  long,

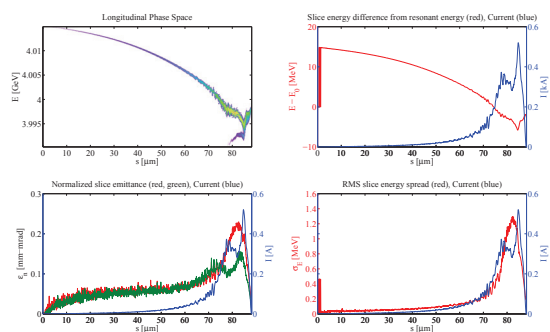


Figure 1: Slice properties of the 20 pC electron beam that has been tracked to the SXR undulator. Top left: longitudinal phase space; top right: slice energy deviation from the resonant energy (red) and current (blue); bottom left: normalized slice emittance (x-red, y-green) and current (blue); bottom right: rms slice energy spread (red) and current (blue).

is slightly chirped with the head of the beam having a lower energy, and has a  $I \sim 300$  A current. The normalized slice emittance is less than  $\epsilon_n \sim 0.2 \mu\text{m}$  in both transverse planes, so while the current is rather low, the beam is sufficiently bright such that it can produce greater than 20  $\mu\text{J}$  of energy

# HIGH-GAIN FEL IN THE SPACE-CHARGE DOMINATED RAMAN LIMIT

I. Gadjev, C. Emma, A. Nause, J. Rosenzweig, UCLA, Los Angeles, USA

## Abstract

While FEL technology has reached the EUV and X-ray regime at existing machines such as LCLS and SACLA, the scale of these projects is often impractical for research and industrial applications. Sub-millimeter period undulators can reduce the size of a high-gain EUV FEL, but will impose stringent conditions on the electron beam. In particular, a high-gain EUV FEL based on undulators with a sub-millimeter period [1] will require electron beam currents upwards of 1 kA at energies below 100 MeV. Coupled with the small gap of such undulators and their low undulator strengths,  $K < 0.1$ , these beam parameters bring longitudinal space-charge effects to the foreground of the FEL process. When the wavelength of plasma oscillations in the electron beam becomes comparable to the gain-length, the 1D theoretical FEL model transitions from the Compton to the Raman limit [2]. In this work, we investigate the behavior of the FEL's gain-length and efficiency in these two limits. The starting point for the analysis was the one-dimensional FEL theory including space-charge forces. The derived results were compared to numerical results of Genesis 1.3 simulations. This theoretical model predicts that in the Raman limit, the gain-length scales as the beam current to the  $-1/4^{\text{th}}$  power while the efficiency grows as the square root of the beam current.

## INTRODUCTION

The attractiveness of sub-millimeter undulators is the ability to produce EUV and X-ray FELs in a compact space. A 100 MeV electron beam is easily obtainable in 10 meters with current acceleration technology and produces EUV light in an undulator of 800  $\mu\text{m}$  period. A high-gain FEL requires beam currents in the kA scale in order to achieve saturation. The small aperture of such micro-undulators drives the transverse size of the beam to the 10  $\mu\text{m}$  scale while their small undulator strength,  $K_{und} \approx 0.01$ , reduces the coupling of the beam and radiation. All these factors contribute to bring longitudinal space-charge effects to the foreground of compact FELs based on micro-undulators.

The typical FEL operation regime is the Compton regime, in which space charge is negligible. Marcus et al. [3] have shown that longitudinal space-charge increases the gain-length and provided a Ming Xie type of fit to the gain. However, if the longitudinal space-charge is strong enough, it can no longer be treated as only a correction to the Compton regime. Gover and Sprangle [2] treat the limit in which space-charge is dominant as a separate FEL regime. The transition into the Raman regime can be quantified as the set of undulator and beam parameters such that:  $2k_p L_G > \pi$ .

We will show that in the Raman limit, the gain-length and efficiency of the FEL change their scaling with the beam current from the typical scaling in the Compton regime. The gain-length tapers off to a  $I_0^{-1/4}$  scaling at very high beam currents, while the efficiency is boosted to a  $I_0^{1/2}$  scaling. The Raman limit presents a new mode of operation of the FEL. We investigate the behavior of gain and efficiency in the Raman limit. The analysis is carried out solely through the one-dimensional FEL theory in order to isolate the effects of longitudinal space-charge. To study FEL efficiency we begin by providing insight into the conditions for saturation. The 1D FEL theory yields analytic solutions for the gain, whose validity extends to the Compton and Raman limits. The efficiency is deduced by finding the saturation power that results for a given gain and saturation distance. The analytic expressions are then compared to simulations. A simple numerical approach was treated by a linear finite-difference numerical integration of the one-dimensional FEL equations with and without the space-charge terms. As a third consistency check, genesis 1.3 simulations were implemented. Since genesis 1.3 includes three-dimensional effects, the beam parameters for the simulated beams were chosen so as to minimize the effect of 3D space-charge, diffraction, and emittance.

## 1-D FEL THEORY

Longitudinal space charge is quantified by the relativistic plasma wave-number, and its effects on the FEL performance can be studied in the 1-D limit. The relativistic plasma wave-number is defined as:

$$k_p = \frac{\sqrt{2I_0}}{\sqrt{I_A \gamma^3 \sigma_x^2}}$$

The Alfein current is,  $I_A = 4\pi\epsilon_0 m_e c^3 / e$ . The beam current, energy, and transverse size are  $I_0$ ,  $\gamma$ ,  $\sigma_x$ , respectively. The transition into the Raman regime can be quantified as the set of undulator and beam parameters such that:

$$2k_p L_G > \pi$$

The gain-length is defined through the solutions of the third-order ODE for the electric field. Assuming the field has the form,  $\vec{E}(z) \sim \exp(\alpha z)$ , then the root with a positive real part defines the gain-length as:

$$\alpha^3 + i4k_u \alpha^2 + (k_p^2 - 4k_u^2 \eta^2) \alpha - i8k_u^3 \rho^3 = 0$$

$$\rightarrow L_G = \frac{1}{2\Re[\alpha_+]}$$

# COHERENT THOMSON SCATTERING RADIATION GENERATED BY USING PEHG

S. Chen, K. Ohmi, D. Zhou, KEK, 1-1 Oho, Tsukuba 305-0801, Japan

## Abstract

Electron beam is density modulated by the phase-merging effect to obtain ultra-short longitudinal structures in the phase space. Coherent radiations are then generated by the coherent Thomson scattering between the phase-merged beam and a long wavelength laser pulse.

## INTRODUCTION

It is able to generate intense short wavelength radiation by the Thomson scattering between relativistic electron beam and an incident high-field laser beam. In the case of back-scattering, the radiation wavelength is expressed by [1]

$$\lambda_r = \frac{\lambda_L}{4\gamma^2} \left( 1 + \frac{a_L^2}{2} + \gamma^2 \theta^2 \right) \quad (1)$$

where the dimensionless vector potential  $a_L$  of the incident laser can be expressed as

$$a_L = \frac{eE_L}{m_e c \omega_L} = 0.85 \times 10^{-9} \lambda_L [\mu\text{m}] I_0^{1/2} [\text{W}/\text{cm}^2] \quad (2)$$

Equation 1 has the similar form with the radiation wavelength of undulator radiation except for a Doppler-shift factor of  $4\gamma^2$  rather than  $2\gamma^2$ . Usually the wavelength of incident laser is much shorter than undulator period length. Therefore, to obtain radiation with same wavelength, it requires much lower electron beam energy than that of the undulator radiation. However, the radiation of Thomson scattering is usually incoherent.

If the electron bunch has longitudinal structure shorter than the radiation wavelength, coherent Thomson scattering radiation can be generated. Several methods to obtain such a longitudinal structure have been discussed previously [2–4]. In this paper, we propose to use the phase-merging effect method realized by transverse gradient undulator (TGU), which is referred as PEHG in FEL [5–7], to modulate the electron bunch and generate short longitudinal phase space structures. Then a long wavelength laser in THz region [8] is used as laser undulator to generate coherent Thomson scattering radiation with such a beam.

## LASER-BEAM INTERACTION IN UNDULATOR

The Hamiltonian of laser-beam interaction in a planar undulator is expressed as follows

$$H = (1 + \delta) - \sqrt{(1 + \delta)^2 - \left( \mathbf{p} - \frac{\mathbf{a}}{\gamma} \right)^2 - \frac{1}{\gamma^2}}, \quad (3)$$

where  $a_x = \hat{a}_u \cos k_u s + \hat{a}_L \cos k_L z$ .

The equations of electron motion are expressed by

$$\begin{aligned} x' &= \left( p_x - \frac{a_x}{\gamma} \right) \frac{1}{p_s}, \\ p_x' &= \frac{1}{\gamma p_s} \left( p_x - \frac{a_x}{\gamma} \right) \frac{da_x}{dx} \\ z' &= - \frac{\left( p_x - \frac{a_x}{\gamma} \right)^2 + p_y^2 + \frac{1}{\gamma^2}}{p_s (p_s + 1 + \delta)}, \\ \delta' &= \frac{1}{\gamma p_s} \left( p_x - \frac{a_x}{\gamma} \right) \frac{da_x}{dz} \\ p_s &= \sqrt{(1 + \delta)^2 - \left( \mathbf{p} - \frac{\mathbf{a}}{\gamma} \right)^2 - \frac{1}{\gamma^2}} \end{aligned} \quad (4)$$

Equation 4 can be solved numerically by, for example, Runge-Kutta integration. The radiation emitted by an electron can be calculated by the Heaviside-Feynman expression

$$\mathbf{E}_i(\mathbf{x}_o, t) = \frac{e}{4\pi\epsilon_0} \left[ \frac{\mathbf{R}_i}{R_i^3} + \frac{\mathbf{R}_i}{c} \frac{d}{dt} \frac{\mathbf{R}_i}{R_i^2} + \frac{1}{c^2} \frac{d^2}{dt^2} \frac{\mathbf{R}_i}{R_i} \right] \quad (5)$$

Here "i" denotes the  $i$ -th electron and  $\mathbf{R}_i$  is the vector between observation point  $\mathbf{x}_o$  and the electron position  $\mathbf{x}_i$ . Then the total radiation field can be calculated using the superposition principle. A numerical simulation code using this method has been developed by K. Ohmi [2] and will be used in this work.

## DENSITY MODULATION BY PEHG

### Basic Principle of PEHG

In traditional HGHG [9, 10], the harmonic components contained in the density modulated bunch are measured by the bunching factor

$$b_n = \langle e^{-in\theta_j} \rangle = e^{-\frac{1}{2}n^2\sigma_\gamma^2 \left( \frac{d\theta}{d\gamma} \right)^2} J_n(n\Delta\gamma \frac{d\theta}{d\gamma}). \quad (6)$$

As is seen in Eq. 6, the bunching factor reduces exponentially with the harmonic number increases due to the non-zero energy spread  $\sigma_\gamma$ . The performance of density modulation of traditional HGHG is restricted so that it is hard to obtain sufficiently short longitudinal structures in the phase space.

PEHG [5, 7] was proposed to improve the harmonic number of traditional HGHG by replacing the modulator undulator with a TGU with transverse field gradient  $\alpha$ . Meanwhile, a dog-leg section with a dispersion strength  $\eta$  is put

## RECENT PROGRESS IN UPGRADE OF THE HIGH INTENSITY THz-FEL AT OSAKA UNIVERSITY

G. Isoyama#, M. Fujimoto, S. Funakoshi, K. Furukawa, A. Irizawa, R. Kato, K. Kawase, A. Tokuchi, R. Tsutsumi, M. Yaguchi, ISIR, Osaka University, Ibaraki, Osaka 567-0047, Japan

### Abstract

The THz-FEL based on the 40 MeV, L-band electron linac is working in the wavelength region from 25 to 150  $\mu\text{m}$  or in the frequency region from 2 to 12 THz. For basic study on FEL physics and its applications, the linac and the FEL are upgraded to have higher stability and intensity in operation of the FEL. The high voltage power supply of the inverter type is remodelled and the solid state switch is developed in place of the thyatron for the klystron modulator, so that fractional variations of the klystron voltage are reduced from  $2 \times 10^{-4}$  to  $8 \times 10^{-6}$  (rms). As a result, fractional variations of the FEL macropulse energy are reduced to 2.4 % (rms). A new grid pulser for the thermionic electron gun of the linac is developed, which generates a series of pulses with the duration of 5 ns at intervals of 36.8 ns. Using the grid pulser, charge in an electron bunch is increased four times higher though the bunch intervals quadruple, so that the micropulse energy increases more than ten times higher than that in the conventional operation mode. The maximum micropulse energy in the new operation mode exceeds 0.1 mJ/micropulse at wavelengths around 70  $\mu\text{m}$  (4.3 THz). Application experiments have begun using the high intensity and stable FEL beam.

### INTRODUCTION

We have been conducting a free-electron laser based on the L-band electron linac at the Research Laboratory for Quantum Beam Science of the Institute of Scientific and Industrial Research (ISIR), Osaka University. The first lasing was achieved in 1994 at wavelengths from 32 to 40  $\mu\text{m}$ . We then began remodelling the FEL to expand the wavelength region towards the longer wavelength side and obtained lasing at 150  $\mu\text{m}$  or 2 THz in 1998 [1], which was the longest wavelength at that time obtained with FELs based on RF linacs. However, the intensity of the FEL was not high enough to reach the power saturation level and its stability was low because the linac was constructed in 1970s and not for FEL. We had an opportunity to upgrade the linac for higher stability and reproducibility in operation in 2003. In doing so, we have added a new operation mode for FEL, in which the RF pulse duration is increased from 4  $\mu\text{s}$  for the standard operation mode to 8  $\mu\text{s}$ , and the number of amplifications is increased not twice but three times higher because the first 2  $\mu\text{s}$  part of the electron pulse is lost in the FEL beam line owing to an energy variation there generated by the filling time of the RF power and the onset of the beam loading in the acceleration tube of the linac. As a result,

the FEL is operated in the high intensity reaching power saturation and operational stability is significantly improved [2].

We have been upgrading the THz-FEL further. In this paper, we will report results of the recent progress of the FEL in stability and power.

### STABILIZATION

The stability of the FEL output power is crucial for basic study on FEL and its applications. It depends strongly on stability of the linac and hence all the possible measures at that time were taken in the previous remodelling of the linac. Nevertheless, the macropulse energy of FEL fluctuated by some tens of a percent. Crucial parameters for the linac stability are the RF power and its phase provided to the 1.3 GHz RF structures, including the pre-buncher, the buncher, and the 3 m long acceleration tube. These parameters strongly depend on the voltage generated with the klystron modulator and applied to the klystron. The stability of the klystron voltage  $V_k$  is primarily determined by a high voltage power supply of the klystron modulator. The large energy

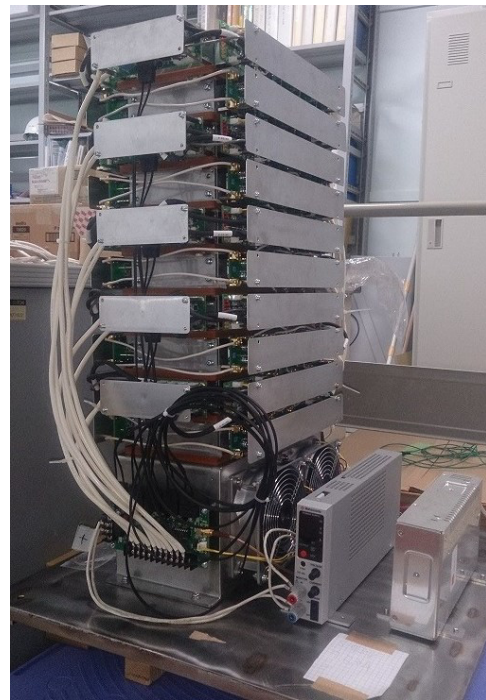


Figure 1: Solid state switch 2nd model for the klystron modulator. The maximum holding voltage is 25 kV and the peak current is 6 kA for 8  $\mu\text{s}$  pulses at a repetition frequency of 60 Hz.

# PERFORMANCE AND TOLERANCE STUDIES OF THE X-RAY PRODUCTION FOR THE X-BAND FEL COLLABORATION

J. Pfingstner\*, E. Adli, University of Oslo, Oslo, Norway

## Abstract

The X-band FEL collaboration is currently designing an X-ray free-electron laser based on X-band acceleration technology. This paper reports on the recent progress on the design of the undulator part of this machine including simulations of the X-ray production process. The basic parameters have been chosen and a beam transport system has been designed, considering strong and weak focusing of quadrupole and undulator magnets. Simulations of the X-ray production process have been carried out with realistic input beam distributions from particle tracking studies of the linac design team. The expectable X-ray properties for SASE and seeded FEL operation have been investigated and also undulator taper options have been studied.

## INTRODUCTION

The X-band collaboration is a group of 12 institutes and universities with the common interest of using X-band acceleration technology for FEL applications. The higher acceleration gradients achievable with X-band structures allow making linacs shorter and more power efficient as S-band and C-band linac used nowadays. The recent advances in the X-band technology [1] have encouraged the X-band collaboration to design a soft and a hard XFEL based on the X-band technology [2]. An important part of this effort is the design of the undulator section and the simulation of the X-rays production process, which is the subject of this paper. Topics that will be covered are the basic parameter choice, the beam transport lattice, and the simulations of the most important X-ray parameters for different modes of operation.

## UNDULATORS AND ELECTRON BEAM

The parameter of the electron beam and the undulator section are chosen by taking into account the experience of existing facilities, e.g. SwissFEL [3] and LCLS [4]. The undulator section consists of 13 permanent magnet undulators [5] of each 3.96 m in length. The undulator magnets have a period length  $\lambda_u$  of 15 mm and a maximal undulator parameter  $K$  of 1.3, which allows reaching an X-rays wavelength of 1 Å with a beam energy of 6 GeV. The modules are separated by gaps of 0.72 m to provide space for quadrupole magnets, beam position monitors, beam loss monitors and phase shifters. The quadrupole magnets are used to control the beam size (FODO lattice) as will be discussed below.

With the described undulator parameters, a beam energy of about 6 GeV is necessary to reach the specified X-ray wavelength of 1 Å. The beam current has to be  $>3$  kA to

enable the production of X-ray with on a GW level, and to achieve a reasonably short saturation length. Preferably the beam current should be uniform along the bunch, which implies a bunch charge of 200 pC assuming a bunch length of about 15  $\mu\text{m}$ . To keep the electrons and the X-rays in a resonance condition, there are limits on the transverse emittance  $\epsilon$  and the energy spread  $\sigma_E$  of the electron beam [6], which are for the chosen parameters  $<0.3$   $\mu\text{m}$  and  $<2 \times 10^{-4}$ , respectively.

An electron beam B0 with the stated properties has been created artificially and will act in the performed simulations as a reference. Complementary, two beams, B1 and B5, have been provided by the linac team, which have been created with particle tracking using PLACET [7]. In contrast to B0, the bunch charge of B1 and B5 is 250 pC. The two beams correspond to different bunch compressor setups. As can be seen in Fig. 1, neither B1 nor B5 reach the specified beam current yet, since the optimisation of the linac and the bunch compressors is an on-going effort.

## BEAM TRANSPORT SYSTEM

The electron beam size is controlled in the undulator section due to the focusing of the quadrupole magnets, which are located in the gap between the undulator magnets. The magnet strengths are adjusted to form a FODO lattice. The size of the  $\beta$ -function is a trade off between high current density (small  $\beta$ -function), and small longitudinal velocity change of the electrons due to their betatron motion (large  $\beta$ -function). An expression for the optimal average  $\beta$ -function  $\beta_{opt}$  has been derived in [8] and is for our parameters 15 m.

If only the strong focusing of the quadrupole magnets is considered, the lattice design can be performed with simple

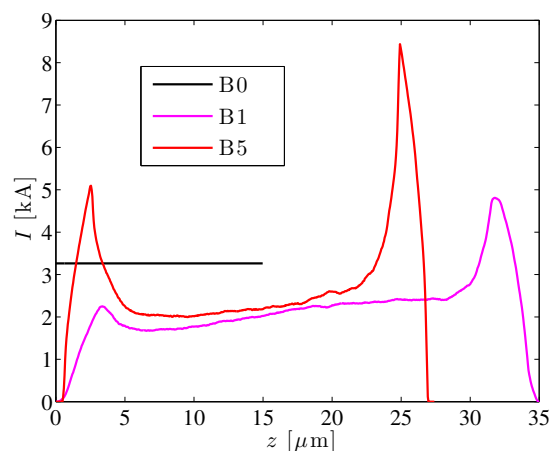


Figure 1: Current profile along the different considered bunches. B0 is an artificially created reference bunch.

\* juergen.pfingstner@cern.ch

# PLANS FOR AN EEHG-BASED SHORT-PULSE FACILITY AT THE DELTA STORAGE RING\*

S. Hilbrich<sup>†</sup>, F.H. Bahnsen, M. Bolsinger, M. Jebramcik, S. Khan, C. Mai, A. Meyer auf der Heide, R. Molo, H. Rast, G. Shayeganrad, P. Ungelenk,

Center for Synchrotron Radiation (DELTA), TU Dortmund University, 44227 Dortmund, Germany

## Abstract

The 1.5-GeV synchrotron light source DELTA, operated by the TU Dortmund University, includes a short-pulse facility based on the coherent harmonic generation (CHG) technique, which allows for the generation of radiation pulses with wavelengths down to 53 nm and durations of 50 fs. In order to reach even shorter wavelengths, the present setup will be modified to employ the echo-enabled harmonic generation (EEHG) and femtoslicing techniques.

## INTRODUCTION

At DELTA, a 1.5-GeV synchrotron light source operated by the TU Dortmund University (see Fig. 1), ultrashort coherent synchrotron radiation pulses are provided by a short-pulse facility [1] based on coherent harmonic generation (CHG) [2]. The goal is to generate radiation at wavelengths down to 53 nm with a pulse duration of 50 fs. In order to access even shorter wavelengths, the present facility will be modified [3] to employ the echo-enabled harmonic generation (EEHG) technique [4] and the femtoslicing scheme [5] as additional radiation sources.

### Coherent Harmonic Generation

As part of the CHG technique [2], the electron energy is modulated sinusoidally by a co-propagating laser pulse in an undulator (modulator). The laser pulse is typically 1000 times shorter than the electron bunch in the storage ring. Downstream of the modulator, the electrons pass a magnetic chicane resulting in a microbunching which gives rise to co-

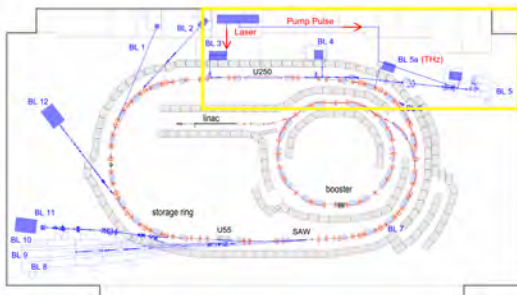


Figure 1: Sketch of the synchrotron light source DELTA. The yellow frame marks the CHG facility in the northern part of the storage ring. Synchrotron radiation is provided by dipole magnets, the undulators U55, U250 and the superconducting asymmetric wiggler (SAW).

\* Work supported by DFG, BMBF, FZ Jülich and by the Federal State NRW.

<sup>†</sup> svenja.hilbrich@tu-dortmund.de

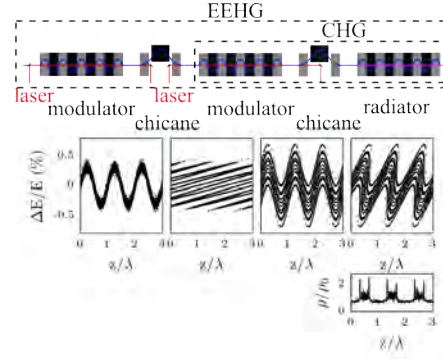


Figure 2: Top: Schematic view of the EEHG and CHG setup. Center: The electron distribution in longitudinal phase space (relative energy deviation  $\Delta E/E$  versus longitudinal coordinate  $z$  in units of the laser wavelength  $\lambda$ ) before and after the first and second chicane. Bottom: Electron density distribution after the second chicane in the case of EEHG.

herent radiation at the laser wavelength or harmonics thereof in a second undulator (radiator). The bunching factor characterizes the correlation between the longitudinal positions of the electrons with respect to the laser wavelength  $\lambda$  and is defined as [6]

$$b_n = \frac{1}{N} \left| \sum_{k=1}^N e^{-2\pi i z_k n / \lambda} \right|, \quad (1)$$

where  $n$  is the harmonic number,  $N$  is the number of electrons and  $z$  is the longitudinal position of an electron. The power of the CHG radiation scales as  $P_n(\lambda) \sim N^2 b_n^2(\lambda)$  with  $b_n(\lambda) \sim e^{-n^2}$  [7, 8]. This short-pulse technique can only be employed if the intensity of the short coherent pulse is higher than that of the long incoherent background ( $\sim N$ ). This is the case for harmonics up to  $n \approx 5$ .

### Echo-Enabled Harmonic Generation

The EEHG scheme [4], which was originally proposed for FEL seeding, requires one more modulator and chicane compared to the CHG setup. In the first modulator, the electron energy is modulated sinusoidally with the periodicity of the laser wavelength. In the first chicane, the electron distribution is strongly sheared in the longitudinal phase space (see Fig. 2). In the second modulator, the electron energy is modulated again with a second laser pulse and in the following chicane, a density modulation with high harmonic content is generated. For EEHG, the bunching factor scales as  $b_n(\lambda) \sim n^{-1/3}$ , if the energy modulation amplitude and chicane strength are optimized for each harmonic [9].

## THE X-BAND FEL COLLABORATION

J. Pfingstner\*, E. Adli, University of Oslo, Oslo, Norway  
 A. Aksoy, Ö. Yavaş, Ankara University, Ankara, Turkey  
 M. J. Boland, T. K. Charles, R. Dowd, G. S. LeBlanc, Y.-R. E. Tan, K. P. Wootton, D. Zhu,  
 Synchrotron Light Source Australia, Clayton, Australia  
 N. Catalan-Lasheras, A. Grudiev, A. Latina, D. Schulte, S. Stapnes, I. Syrathev, W. Wunsch,  
 CERN, Geneva, Switzerland  
 G. D'Auria, S. Di Mitri, C. Serpico, Elettra-Sincrotrone, Trieste, Italy  
 C. J. Bocchetta, A. I. Wawrzyniak, Solaris, Jagiellonian University, Krakow, Poland  
 G. Burt, Lancaster University, Lancaster, UK  
 A. Charitonidis, E. N. Gazis, National Technical University of Athens, Greece  
 Z. Nergiz, Nigde University, Nigde, Turkey  
 W. Fang, Q. Gu, Shanghai Institute of Applied Physics, Shanghai, China  
 D. Angal-Kalinin, J. Clarke, STFC, Daresbury Laboratory, Cockcroft Institute, Daresbury, UK  
 T. Ekelöf, M. Jacewicz, R. Ruber, V. Ziemann, Uppsala University, Uppsala, Sweden  
 X. J. A. Janssen, VDL ETG T&R B.V., Eindhoven, Netherlands

### Abstract

The X-band FEL collaboration is currently designing an X-ray free-electron laser based on X-band acceleration technology. Due to the higher accelerating gradients achievable with X-band technology, a X-band normal conducting linac can be shorter and therefore potentially cost efficient than what is achievable with lower frequency structures. This cost reduction of future FEL facilities addresses the growing demand of the user community for coherent X-rays. The X-band FEL collaboration consists of 12 institutes and universities that jointly work on the preparation of design reports for the specific FEL projects. In this paper, we report on the on-going activities, the basic parameter choice, and the integrated simulation results. We also outline the interest of the X-band FEL collaboration to use the electron linac CALIFES at CERN to test FEL concepts and technologies relevant for the X-band FEL collaboration.

### INTRODUCTION

A major factor in the cost of the construction of a linac driven FEL facility is the accelerator technology adopted. For normal conducting facilities, a substantial part of the costs is determined by the linac operating frequency, which strongly influences space requirements and power consumption. Most of the operational facilities use S-band linacs, operating at 3 GHz, or newly designed C-band linacs, operating at 6 GHz. The use of higher frequencies can allow an increase of the operating gradient and the efficiency, with an overall reduction of the machine length and the cost. These advantages could be further enhanced if the operating frequency can be extended to the X-band region (i.e. 12 GHz), where the operating gradients can be almost doubled compared to those of C-band structures. During the last decades, research and development of X-band accelerator technolo-

gies has seen a tremendous progress within the context of the next generation of electron-positron Linear Colliders, where very high gradients are necessary to achieve the multi-TeV beam energies within reasonable length. The possibility to operate X-band accelerating structures at gradients higher than 100 MV/m, has been recently demonstrated in the context of the CERN CLIC (Compact Linear Collider) Collaboration, with a very low RF Breakdown Rate ( $BDR/m < 3 \times 10^{-7}$ ) [1]. This has suggested that the X-band technology may represent a useful solution to get very compact and cost effective multi-GeV linacs, opening the way for new less expensive FEL facilities. This option seems to be even more attractive if we consider that most of the future X-ray FELs will be designed to operate with very short and low-charge electron bunches, minimising unwanted wake field effects. Starting from the FEL output specifications provided by users (i.e. wavelength range, energy per pulse, pulse duration, pulse structure, etc.), the objective of the X-band FEL collaboration is to analyse three possible scenarios: a soft X-ray FEL, a hard X-ray FEL and the extension of an existing facility. Other efforts involve identifying, designing and testing, a common X-band RF unit for the three sources, on a dedicated test stand. This effort will demonstrate the maturity of the technology, validating the hardware and the use of X-band in this area of strategic scientific interest.

### COLLABORATION AND SPECIFIC INTERESTS

The X-band FEL collaboration consists of 12 institutes and universities (see affiliation of authors), which share the common interest of using X-band technology for FELs. Some of the envisioned projects within this collaboration are summarised in the following.

\* juergen.pfingstner@cern.ch

# BEAM COMMISSIONING AND INITIAL MEASUREMENTS ON THE MAX IV 3 GeV LINAC

S. Thorin, J. Andersson, F. Curbis, , M. Eriksson, L. Isaksson, O. Karlberg,  
D. Kumbaro, F. Lindau, E. Mansten, D. Olsson, S. Werin, MAX IV Laboratory, Lund, Sweden

## Abstract

The linear accelerator at MAX IV was constructed for injection and top-up to the two storage rings and as a high brightness driver for the Short Pulse Facility. It is also prepared to be used as an injector for a possible future Free Electron Laser.

Installations were completed and beam commissioning started in the early fall of 2014.

In this paper we present the progress during the first phase of commissioning along with results from initial measurements of optics, emittance, beam energy and charge.

## BACKGROUND

The MAX IV facility [1] is the successor of the MAX-lab accelerators at Lund University and includes two storage rings, a full energy linac and a Short Pulse Facility (SPF). The rings will be operated at 1.5 and 3 GeV. The SPF will be a single pass spontaneous linac lightsource, producing sub-ps spontaneous X-ray pulses. The injector will be flexible enough to drive both injection and top-up for the storage rings, and produce high brightness pulses for the SPF. The long term strategic plan for the facility include an X-ray FEL, and the linac was developed to be fully prepared to handle the high demands for an FEL driver.

The first phase of linac commissioning was completed in the beginning of May 2015, and after a few months shut-down for final installations and system tests of the 3 GeV MAX IV storage ring, the linac was recommissioned and started the process of injections for storage ring commissioning.

## MAX IV LINAC GENERAL DESIGN

For injection and top up to the storage rings a thermionic gun with a pulse train chopper system is used [2]. In high brightness mode we use a 1.6 cell photo cathode gun capable of producing an emittance of 0.4 mm mrad at a charge of 100 pC [3]. The gun will be operated together with a kHz Ti:sapphire laser at 263 nm. The same laser will be used for timing and synchronisation of the whole accelerator and the SPF.

The acceleration is done in 39 warm S-band linac sections together with 18 RF units, each consisting of a 35 MW klystron and a solid state modulator. The klystrons are operated at the lower power of 25 MW which reduces the operational cost and gives a total redundancy in energy of 0.6 GeV.

The beam is kicked out for injection into the storage rings at 1.5 and 3 GeV. Bunch compression is done in double achromats [4] at 260 MeV and at full energy, 3 GeV, after

extraction to the storage ring. A schematic view of the layout can be seen in Figure 1.

## STATUS OF BEAM COMMISSIONING

Commissioning of the MAX IV linac started in August 2014 using the thermionic RF gun. While high power conditioning was still ongoing in the main linac, the injection system including thermionic gun, chopper and first linac structure was started up and characterised. In November 2014 the high brightness photo cathode gun produced electrons at MAX IV for the first time. During December we reached both transfer lines to the storage rings (Figure 3) and entered the second bunch compressor where we could measure the electron energy. Full energy, 3 GeV, was reached in February 2015. Beam from the high brightness gun was delivered through the SPF section to the main beam dump in the following month. A first hint of light at MAX IV was detected from an old MAX-lab undulator that is now temporarily installed the SPF [5] (Figure 2).

In the beginning of August 2015, after a few months machine shut-down, the linac was recommissioned with the purpose to start injecting in to the 3 GeV storage ring. The beam reached the first screen in the storage ring on the August 11 (Figure 4).

## CHARGE MEASUREMENTS

Beam charge is measured with Current Transformers at several points through the machine and with Faraday Cups at each beam dump (Figure 5). The charge specification for storage ring injection with the thermionic gun is 1 nC within a 100 ns bunch train for each linac shot. This was achieved at the beam dump in the centre of the 3 GeV transferline, but for radiation safety reasons not more than 750 pC is accelerated during normal operation and ring commissioning.

The nominal charge specification for the SPF is 100 pC, which has been achieved and delivered though the undulator section. A charge range from 20 to 200 pC has been accelerated though the whole linac and into the second bunch compressor.

## EMITTANCE SCANS

Emittance and twiss parameters are measured before and after both bunch compressors using quad scans. The quad scan station before BC1 is the first point to measure emittance from the electron guns.

## Thermionic Gun

For the thermionic gun the measured horizontal normalized emittance is around 30 mm mrad, which is higher than

# STATUS OF THE ALICE IR-FEL: FROM ERL DEMONSTRATOR TO USER FACILITY

N.R. Thompson<sup>1</sup>, J.A. Clarke<sup>1</sup>, T. Craig<sup>2</sup>, D.J. Dunning<sup>1</sup>, O.V. Kolosov<sup>3</sup>, A. Moss<sup>1</sup>, Y.M. Saveliev<sup>1</sup>,  
M.R.F. Siggel-King<sup>1,2</sup>, M. Surman<sup>1</sup>, P.D. Tovee<sup>3</sup>, P. Weightman<sup>2</sup>

<sup>1</sup>Accelerator Science and Technology Centre (ASTeC), STFC Daresbury Laboratory, UK

<sup>2</sup>Department of Physics, The University of Liverpool, L69 3BX, UK

<sup>3</sup>Department of Physics, Lancaster University, LA1 4YB, UK

## Abstract

The ALICE (Accelerators and Lasers In Combined Experiments) accelerator at STFC Daresbury Laboratory in the UK was conceived in 2003. It was constructed as a short-term Energy Recovery Linac (ERL) demonstrator to develop the underpinning technology and expertise required for a proposed 600MeV ERL-based FEL facility. In this paper we present an update on the performance and status of ALICE which now operates as a funded IR-FEL user facility. We discuss the technological challenges of evolving a short-term demonstrator into a stable, reliable user facility and present a summary of the current scientific programme.

## BRIEF HISTORY OF ALICE

In 2000 a proposal was developed at Daresbury Laboratory for 4GLS, a combined XUV/VUV/IR FEL facility driven by a 600MeV ERL [1]. This was to be a complementary photon source to the hard and soft X-ray sources of the ESRF and Diamond Light Source respectively. In 2003 funding was obtained to build a lower energy prototype, ERLP, to enable development of the underpinning technologies and expertise: assembling and operating TESLA cavities and cryomodules; operation of an ERL and associated RF, synchronisation and optics; photoinjector technologies; FEL techniques and operation; longitudinal beam dynamics and simulation; and diagnostic techniques and instrumentation. ERLP was sited in reused experimental areas, leading to some layout restrictions. The project benefitted greatly from collaboration with Jefferson Laboratory. In particular, the 350kV DC photocathode gun was based on the JLab design and a number of quadrupole magnets and chicane assemblies were provided on loan. The FEL wiggler had previously been used on the JLab IR-Demo FEL [2] and was re-engineered for variable gap operation. The FEL mirror cavities were loaned by LURE where they had previously been used on the CLIO FEL. The intention was to run ERLP for two years as an accelerator test facility before decommissioning.

Procurement and construction began through 2004/5. First beam from the gun was in August 2006 followed by a period of commissioning using a dedicated gun diagnostic beamline. 2007 was a challenging year: the gun suffered from strong field emission, rapidly deteriorating QE, mechanical failure inside the cathode ball, conditioning resistor failure and vacuum leaks. Nevertheless, by the end of 2007 100pC was achieved at 350keV with QE>3%. Unfortunately,

the linac suffered field emission which limited the gradient to 27 MeV rather than the design value of 35 MeV.

In 2008 the 4GLS project was cancelled and ERLP was re-named ALICE. By October, after repairs to the booster linac cryomodule at ACCEL and the installation of a smaller ceramic in the gun (generously loaned by Stanford University) the milestone of energy recovery was achieved.

As suggested by the new name, the purpose of the facility shifted in 2009 towards laser-related experiments and user exploitation. Coherently enhanced broadband THz was extracted from the final dipole of the bunch compression chicane, Compton back-scattering off a TW laser in a head-on geometry was successfully demonstrated [3] and electro-optic sampling was implemented as an electron bunch length diagnostic.

By 2010 the FEL undulator was installed and lasing was achieved in October that year. Details of the commissioning process up to first lasing, including a summary of the beam optics design, can be found elsewhere [4].

Larger scale user programmes commenced in 2011 after commissioning of the THz and FEL beamlines. The THz beam was transported to a tissue culture laboratory for biological experiments to determine safe limits of exposure of human cells to THz and the effect of THz on the differentiation of stem cells [5]. A Scanning Near-Field Optical Microscope (SNOM) was installed and integrated with the IR beamline—further details are given later in this paper.

In 2012, while the user programmes progressed, time was also spent studying the transverse and longitudinal beam dynamics [6] and the effect of chicane  $R_{51}$  and  $R_{52}$  on the THz emission.

ALICE is now funded via a three-year EPSRC grant [7] to provide three months of user IR-FEL/THz beamtime per year. A number of technology upgrades and operational improvements have been implemented to transition ALICE from a test facility to a stable, reliable user facility. These are described in subsequent sections. The layout of ALICE is shown in Figure 1.

## RECENT UPGRADES

**Digital Low-Level RF (DLLRF)** Work had been started at Daresbury in 2009 to develop DLLRF systems to replace the existing analog systems. The motivations were: to have the ability to modify loop parameters during operations; to allow complicated control algorithms such as adaptive feed forward to overcome beam loading; to en-

## HPC SIMULATION SUITE FOR FUTURE FELS

R.J. Allan<sup>1</sup>, L.T. Campbell<sup>2,3</sup>, A.J.T. Colin<sup>4</sup>, D. Dunning<sup>3</sup>, B.W.J. McNeil<sup>2</sup>,  
B. Muratori<sup>3</sup>, J.D.A. Smith<sup>5</sup>, N.R. Thompson<sup>3</sup>, P. Traczykowski<sup>2</sup>, P. Williams<sup>3</sup>

<sup>1</sup>The Hartree Centre, STFC Daresbury Laboratory, Warrington, UK

<sup>2</sup>SUPA, Department of Physics, University of Strathclyde, Glasgow, UK

<sup>3</sup>ASTeC, STFC Daresbury Laboratory and Cockcroft Institute, Warrington, UK

<sup>4</sup>SUPA, Department of Physics and Astronomy, University of Glasgow, Glasgow, UK

<sup>5</sup>Tech-X UK Ltd, Sci-Tech Daresbury, Warrington, UK

### Abstract

A new HPC simulation suite, intended to aid in both the investigation of novel FEL physics and the design of new FEL facilities, is described. The integrated start-to-end suite, currently under development, incorporates both plasma (VSim) and linac (ELEGANT, ASTRA, VSim) accelerator codes, and will include the 3D unaveraged FEL code Puffin to explore novel FEL methods.

### INTRODUCTION

Free Electron Lasers are now operating successfully in SASE mode at X-ray wavelengths [1, 2] with others planned or under development [3]. Like the first conventional lasers developed in the early 1960s, X-ray FELs are in their infancy and have the potential for further significant development, particularly with respect to their temporal coherence, pulse durations, potential to deliver synchronised, multi-colour output, and the possibility of being driven by new electron beam sources. Research is now focussing on these future possibilities. Experimental facilities such as [4] and [5] are designed with the dedicated purpose of testing out new techniques for such improved output. At the same time, plasma accelerators have emerged as a promising potential driver of future FELs, with the potential to reduce the size and cost of the facilities.

FEL simulation codes are fundamental tools in the investigation of FEL theory, novel methods and the design of facilities. The most commonly used codes perform approximations including the Slowly Varying Envelope Approximation (SVEA) on the radiation field [6], averaging the electron motion over an undulator period, and discretisation of the electron beam and radiation field into 'slices' (of minimum width equal to the radiation wavelength) over which periodic boundary conditions are applied [7].

As a consequence of these approximations, the averaged SVEA codes are unable to model processes occurring at a sub-resonant wavelength scale (equivalently radiation outside a narrow bandwidth centred on the resonant frequency) [8], or significant changes in the electron beam phase space such as current redistribution during the FEL interaction [9, 10]. While these effects are not important for the basic operation of the FEL, some advanced methods currently proposed to improve the temporal output in the next generation of FELs rely on just such processes [11, 12].

SVEA codes are also unable to model the Coherent Spontaneous Emission (CSE) arising from current gradients in the electron pulse; this can act as a strong seed for the FEL interaction [13]. For these reasons it is necessary to use unaveraged, non-SVEA codes to model FELs driven by Laser Plasma Accelerators (LPAs), which typically produce short, broadband electron beams.

The FEL simulation code PUFFIN (Parallel Unaveraged Fel INtegrator) was developed [14] to be free of the averaging and SVEA approximations which limit other commonly used codes. The primary aim of PUFFIN was to provide a flexible research resource that can be adapted to test new ideas and methods for future FEL development. It was therefore not focused on FEL facility design and leaves it lacking in some features desirable to those designing real experiments. It also lacks simulation paths to and from other accelerator codes, and a good visual on-site interface for outputs.

In the following, we describe a start-to-end (s2e) simulation suite currently under development. It is anticipated that it will aid in the design of the UK CLARA FEL test facility [5] and in interpreting the results of experiments to be performed there. As part of the project, Puffin will undergo development, both to optimize algorithms for new HPC architectures and to implement useful physical features required for proper facility simulation. The suite will include a common visual interface throughout the simulator which will use ASTRA [15], elegant [16, 17] and VSim [18] for the accelerator simulators in conjunction with Puffin for

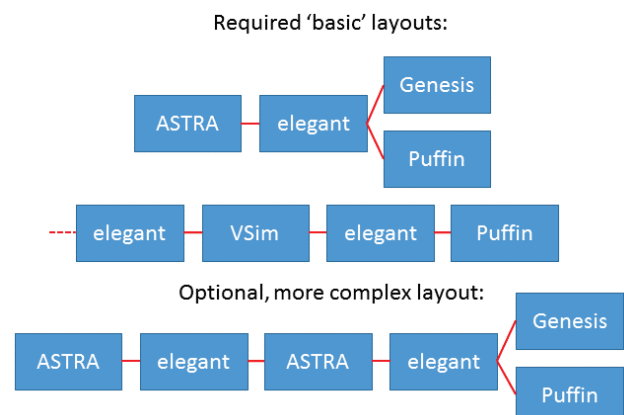


Figure 1: Various simulation layouts afforded by the suite.

# TIME LOCKING OPTIONS FOR THE SOFT X-RAY BEAMLINE OF SwissFEL

E. Prat and S. Reiche

Paul Scherrer Institut, Villigen, Switzerland

## Abstract

SwissFEL is an FEL facility presently under construction at the Paul Scherrer Institute that will serve two beamlines: Aramis, a hard X-ray beamline which is under construction and will provide FEL radiation in 2017 with a wavelength between 0.1 and 0.7 nm; and Athos, a soft X-ray beamline which is in its design phase and is expected to offer FEL light in 2021 for radiation wavelengths between 0.7 and 7 nm. A passive synchronization of the FEL signal to a laser source is fundamental for key experiments at Athos, such as time-resolved resonant inelastic X-ray scattering (RIXS) experiments. In this paper we explore different options to achieve this time synchronization by means of energy modulating the electron beam with an external laser.

## INTRODUCTION

The SwissFEL facility, presently under construction at the Paul Scherrer Institute, will provide SASE and self-seeded FEL radiation at hard (1–7 Å) and soft (7–70 Å) X-ray FEL beamlines [1]. SwissFEL will operate with electron beam charges varying between 10 and 200 pC and beam energies from 2.1 to 5.8 GeV. The hard X-ray beamline, Aramis, is expected to have the first user experiments in 2017, while the soft X-ray beamline Athos will lase by 2021.

Pivotal experiments for Athos, such as time-resolved resonant inelastic X-ray scattering (RIXS) experiments [2], require a very precise knowledge of the arrival time of the FEL pulse. More generally, pump-probe experiments need an accurate synchronization between the pump and the probe (FEL pulse). This can be achieved with a passive synchronization between the FEL pulse and a conventional laser. One possibility would be to use a laser-based seeding scheme, either direct seeding with a strong HHG source [3] or by employing more complicated layouts like the High-Gain Harmonic Generation (HGHG) [4] and the Echo-Enabled Harmonic Generation [5] schemes. However, laser-based seeding has at present limitations at a radiation wavelength of around 5 nm [6], and going beyond seems very difficult due to shot noise degradation issues [7] from the spontaneous undulator radiation. An alternative approach to passively lock the FEL pulse with an external laser is by energy modulating the electrons that will produce FEL radiation via interaction with a laser pulse in a wiggler magnet. Unlike the methods mentioned above, which induces a coherent signal at the resonant wavelength, the following methods slice the bunch by allowing the bunch to drive the SASE FEL amplification only where it had an overlap with the laser signal.

One possibility to do that is with the ESASE (Enhanced-SASE) mechanism [8], in which a dispersive section (nor-

mally a magnetic chicane) is used to convert the energy modulation of the electrons into a density modulation prior to the FEL generation in the undulator beamline. The higher current will drive the FEL amplification faster than the unmodulated beam.

Another option [9] is that the electrons are injected after the modulator directly into the radiator without the need of any dispersive section. The modulation generates an effective energy chirp in the beam that can be exactly compensated with a linear tapering of the undulator field [10]. By tapering one can force that only a very short slice of the bunch produces FEL radiation, while the rest of the electrons will not lase since the tapering will bring them out of the resonance condition. This scheme requires a more powerful laser system than in the ESASE configuration.

The ideal configuration is with an one-period modulator and a few-cycle laser pulse – in such a case a perfectly synchronized FEL pulse is generated. If the modulator has more periods, several short FEL pulses will be generated, which will not be perfectly locked since the modulation and therefore the FEL signal are lengthened. The advantage of this latter option is that the required laser power will be reduced.

In this contribution we will explore the ESASE and the “energy chirp” schemes to achieve the time synchronization of the FEL pulse. Figure 1 shows a schematic layout for these two options.

## SIMULATION SETUP

The numerical simulations are done for a radiation wavelength of 1 nm, considering the layout for the soft X-ray beam line Athos with 4 m long undulator modules and 75 cm intra-undulator break sections, which hold the focusing quadrupole and the measurements of the beam positions. The FEL process in the radiator section is simulated with

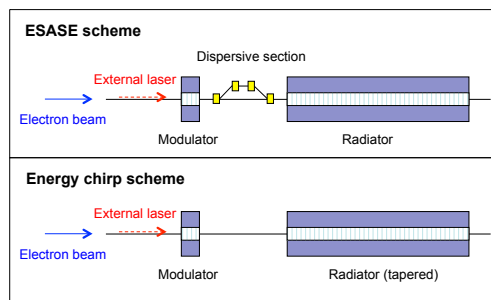


Figure 1: Conceptual layout for slicing the electron beam by an external signal. Either a current modulation or a strong energy chirp (upper and lower plot, respectively) is used to select the part of the bunch which lases.

## RECENT STUDY IN iSASE

K. Fang, C. Pellegrini, J. Wu, SLAC National Accelerator Laboratory, Menlo Park, CA 94025, USA

S. Hsu, University of California, San Diego, CA, 92093, USA

C. Emma, C. Pellegrini, University of California, Los Angeles, CA 90095, USA

### Abstract

The Improved Self-Amplified Spontaneous Radiation (iSASE) scheme has the potential to reduce SASE FEL bandwidth. This is achieved by repeatedly delaying the electrons with respect to the radiation pulse using phase shifters in the undulator break sections. It has been shown that the strength, locations and sequences of phase shifters are important to the iSASE performance. The particle swarm optimization algorithm is used to explore the phase shifters configuration space globally.

### INTRODUCTION

Improved Self Amplified Spontaneous Emission (iSASE) [1, 2] is capable of improving spectrum by increasing cooperation length. Electrons are delayed with respect to the optical field by phase shifters in the FEL lattice. And connection is built up between electrons that are separated by several coherent spikes width away. With proper interference between new grown field and optical field, bandwidth can be reduced.

There has been effort to investigate the mechanism of study the proper phase delay configuration. There is study proposes to arrange phase shifter strength in a geometric or reverse geometric sequence. In this kind of configuration, the largest phase delay creates a small period frequency comb modulation in the power spectrum. When the second largest phase delay, which is half of the largest delay, has a good phase match, it eliminates some of the side band peaks and amplifies the central peak. Using this scheme, the central peak can be effectively selected. There are also other schemes uses prime number phase delay [3] and random phase delay [4] to improve the FEL bandwidth.

Some optimization method, such as simulated annealing method [5], has been used to optimize iSASE. The method is able to explore the solution space locally around a reverse geometric sequence configuration, but not yet conclusive. This study focuses on the global optimization of iSASE phase delay configuration.

### iSASE

FEL bandwidth is improved by repeatedly delaying the electron bunch with respect to the optical field. After each phase delay, the interference effect between the shifted light field and the new grown field from energy and density modulated electron beam appears as a modulation to the FEL power spectrum [6],

$$P(\nu; z) = P_0(\nu; z)T(\nu, \phi, a), \quad (1)$$

$$T(\nu, \phi, a) \propto 1 + |a|^2 + 2|a| \cos(\nu\phi + \varphi). \quad (2)$$

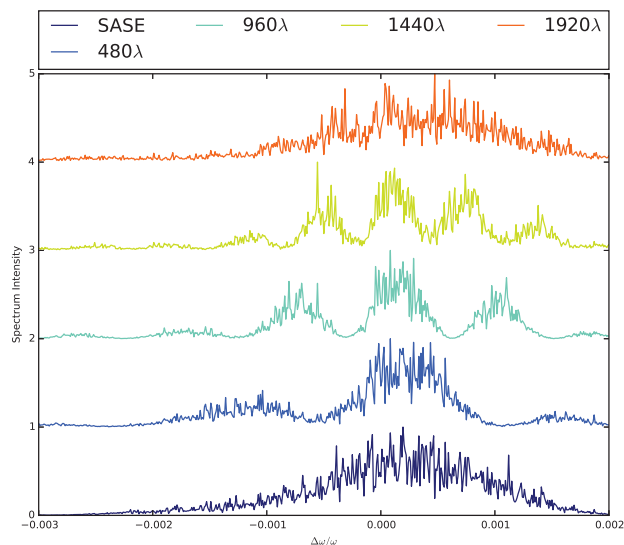


Figure 1: Modulation can be seen in the FEL power spectrum after the first phase shifter. The modulation period decreases with larger phase delay. Yet there is a limit ( $960\lambda$ ) where the modulation pattern no longer exists. This is because the dispersive effect in the phase shifter strong enough to wash out the density modulation in the electron bunch. Only the optical field carries the pure SASE spectrum through the phase shifter.

Here  $\phi$  is the integer phase delay. The modulation period is inversely proportional to  $\phi$ .  $\varphi$ , the fractional phase delay, controls the center of the modulation function.  $a$  is the relative amplitude between the shifted optical field and the new grown field. The dispersive effect in the phase shifter can cause damping to electron bunching and even distort the electron bunch density modulation. The interference effect is degraded by the dispersive effect. Therefore it sets a upper limit to the tolerable phase delay value (Fig. 1). A narrow filtering function can be generated using multiple modulation functions with different modulation periods.

### PARTICLE SWARM OPTIMIZATION

Particle swarm optimization algorithm mimics the behavior of bird flocking. The candidate solutions, which are called particles, have position and velocity. At the beginning, particles are randomly distributed in the solution space with random velocity. As particles sweep through the solution space, particles find solutions with different cost values. During the process, particles are also attracted by the good solutions, with lower cost values, that have been experienced by the particles. And these good solutions may

# FUNDAMENTAL LIMITATIONS OF THE SASE FEL PHOTON BEAM POINTING STABILITY

E.A. Schneidmiller, M.V. Yurkov, DESY, Hamburg, Germany

## Abstract

The radiation from Self Amplified Spontaneous Emission Free Electron Laser (SASE FEL) [1, 2] has always limited value of the degree of transverse coherence. Two effects define the spatial coherence of the radiation: the mode competition effect, and the effect of poor longitudinal coherence. For the diffraction limited case we deal mainly with the effect of the poor longitudinal coherence leading to significant degradation of the spatial coherence in the post-saturation regime. When transverse size of the electron beam significantly exceeds diffraction limit, the mode competition effect does not provide the selection of the ground mode, and spatial coherence degrades due to contribution of the higher azimuthal modes. Another consequence of this effect are fluctuations of the spot size and pointing stability of the photon beam. These fluctuations are fundamental and originate from the shot noise in the electron beam. The effect of pointing instability becomes more pronouncing for shorter wavelengths. Our study is devoted to the analysis of this effect and description of possible means for improving the degree of transverse coherence and the pointing stability.

## INTRODUCTION

Previous studies have shown that coherence properties of the radiation from SASE FEL strongly evolve during the amplification process [3–7]. At the initial stage of amplification the spatial coherence is poor, and the radiation consists of a large number of transverse modes [7–15]. Longitudinal coherence is poor as well [16–18]. In the exponential stage of amplification the transverse modes with higher gain dominate over modes with lower gain when the undulator length progresses. This feature is also known as the mode competition process. Longitudinal coherence also improves in the high gain linear regime [18–20]. The mode selection process stops at the onset of the nonlinear regime, and the maximum values of the degree of the transverse coherence and of the coherence time are reached at this point. The undulator length required to reach saturation is in the range from about nine (hard x-ray SASE FELs) to eleven (visible range SASE FELs) field gain lengths [3]. The situation with the transverse coherence is favorable when the relative separation of the field gain between fundamental and higher modes exceeds 25-30%. In this case the maximum degree of transverse coherence can exceed the value of 90% [3, 7]. Further development of the amplification process in the nonlinear stage leads to visible degradation of the coherence properties.

Relative separation of the gain of the FEL radiation modes depends on the value of the diffraction parameter. Increase of the value of the diffraction parameter results in a smaller

relative separation of the gain of the modes. In this case we deal with the mode degeneration effect [9, 12]. Since the number of gain lengths to saturation is limited, the contribution of the higher spatial modes to the total power grows with the value of the diffraction parameter, and the transverse coherence degrades. Large values of the diffraction parameter are typical for SASE FELs operating in the hard x-ray wavelength range [21–25].

In this paper we perform analysis of the radiation modes, and find their ranking in terms of the field gain. The main competitor of the ground TEM<sub>00</sub> is the first azimuthal TEM<sub>10</sub> mode. When contribution of TEM<sub>10</sub> mode to the total power exceeds a few per cent level, a fundamental effect of bad pointing stability becomes to be pronouncing. The power of the effect grows with the electron beam size in the undulator. We present detailed analysis of this effect for Free Electron Laser FLASH [26, 27] which currently takes place due to the weak focusing in the undulator resulting in large values of the diffraction parameter and conditions of the "cold" electron beam [28]. Our analysis shows that operation with a stronger focusing of the electron beam and a lower peak current would allow one to improve both, the degree of transverse coherence and the pointing stability of the photon beam at FLASH.

The figure of merit for operation of optimized SASE FEL is the ratio of the geometrical emittance to the radiation wavelength,  $\hat{\epsilon} = 2\pi\epsilon/\lambda$  [3–5]. Parameter space of optimized SASE FELs is typical for the hard x-ray regime. We show that SASE FELs operating at short wavelengths and low electron beam energy with the value of  $\hat{\epsilon} > 1$  suffer from the mode degeneration effect resulting in significant degradation of the spatial coherence and pointing stability of the photon beam. The effect of the photon beam pointing jitter is a fundamental one, and can not be eliminated by eliminating of the jitters of machine parameters.

## ANALYSIS OF THE RADIATION MODES

We consider an axisymmetric model of the electron beam. It is assumed that the transverse distribution function of the electron beam is Gaussian, so the rms transverse size of matched beam is  $\sigma = \sqrt{\epsilon\beta}$ , where  $\epsilon$  is the rms beam emittance and  $\beta$  is the beta-function. In the framework of the three-dimensional theory, the operation of a short-wavelength FEL amplifier is described by the following parameters: the diffraction parameter  $B$ , the energy spread parameter  $\hat{\Lambda}_T^2$ , the betatron motion parameter  $\hat{k}_\beta$  and detuning parameter  $\hat{C}$  [11, 12]:

$$\begin{aligned} B &= 2\Gamma\sigma^2\omega/c, & \hat{C} &= C/\Gamma, \\ \hat{k}_\beta &= 1/(\beta\Gamma), & \hat{\Lambda}_T^2 &= (\sigma_E/E)^2/\rho^2, \end{aligned} \quad (1)$$

# MEASUREMENT OF SPATIAL DISPLACEMENT OF X-RAYS IN CRYSTALS FOR SELF-SEEDING APPLICATIONS

A. Rodriguez-Fernandez\*, B. F. Pedrini, S. Reiche, Paul Scherrer Institut, 5232 Villigen PSI, Switzerland

K. D. Finkelstein, CHESS, Cornell University, Ithaca, New York, USA

## Abstract

SASE Free-electron laser (FEL) radiation arises from shot noise in the electron bunch, which is amplified along the undulator section and results in X-ray pulses consisting of many longitudinal modes [1]. The output bandwidth of FELs can be decreased by seeding the FEL process with longitudinally coherent radiation. In the hard x-ray region, there are no suitable external seeding sources. Self-seeding represents a viable alternative. The X-ray beam is separated from the electrons using a magnetic chicane, and then monochromatized. The monochromatized X-rays serve as a narrowband seed, after recombination with the electron bunch, along the downstream undulators. This scheme generates longitudinally coherent FEL pulses.

Geloni et al. [2] have proposed monochromatization based on Forward Bragg Diffraction (FBD), which introduces a delay of the narrowband X-rays pulse of the order of femtoseconds that can be matched to the delay of the electron bunch due to the chicane. The FBD process produces a small transverse displacement of the X-ray beam, which may result in the loss of efficiency of the seeding process [3]. Preliminary results from an experiment performed at Cornell High Energy Synchrotron Source (CHESS) seem to confirm the predicted transverse displacement, which is therefore to be taken into account in the design of self-seeding infrastructure for optimizing the FEL performance.

## INTRODUCTION

X-ray free-electron lasers (FELs) relying on the self-amplified spontaneous emission (SASE) exhibit peak brightnesses many orders of magnitude larger than that from insertion devices at third-generation synchrotron sources [4,5]. The SASE radiation spectrum consists of many longitudinal modes, as a result of shot noise initiation of the amplification process in the electron beam [1,6]. For high-gain FELs, the normalized frequency bandwidth is  $\Delta\omega/\omega \sim \rho$ , where  $\rho$  is the FEL Pierce parameter [7]. At the future Swiss Free Electron Laser facility  $\rho = 4 \cdot 10^{-4}$ .

The bandwidth can be reduced by seeding the FEL with longitudinally coherent radiation coming from an external source. In the hard X-ray regime, where no external sources are available, a self-seeding scheme has been proposed by Geloni et al. [2]. This method exploits the time-domain features of the radiation transmitted in forward direction by a thin crystal in Bragg or Laue

diffraction geometry, called the “wake monochromator”. Unfortunately, the Forward Bragg Diffraction (FBD) process produces a small transverse displacement of the narrow-bandwidth, time-delayed X-ray seeding pulse, which results, if not compensated, in the loss of efficiency of the seeding process [3,8]. Until now the transverse displacement has not been studied experimentally. For a proper design of the seeding infrastructure, a quantitative understanding is mandatory, especially at the shorter wavelengths of 1 Å and below that will be offered at the Swiss Free Electron Laser (SwissFEL) facility.

With this contribution, we intend to present first results from an experimental study of the transverse displacement due to FBD. Our first experiment was performed at beamline C1 of the CHESS facility. These first results help to guide new experiments at FEL facilities. The present investigations will serve to validate or ameliorate our simulation tool. This will then be applied to calculate the propagation of the X-ray signal through the designed self-seeding unit of SwissFEL with the simulation software for FELs, GENESIS [9].

## THEORY OF TIME DEPENDENT X-RAY DYNAMICAL DIFFRACTION

Shvyd’ko et al. [3] present a series of analytic expressions resulting from a spatiotemporal system of wave equations which represent the shape and power of the monochromatic wave generated by an incident broad spectrum beam. In a previous work Lindberg et al. [8] presented how, from the coupled wave system of Bragg diffraction one can obtain solutions for both reflected and transmitted wave fields. They showed the relation between the resulting temporal profile and crystal properties, which include the x-ray extinction length  $\Lambda$ , the incident angle  $\theta$  for specific reflection, and in the case of the forward diffracted contribution, thickness  $d$  of the crystal. If the system of waves is solved for an incoming pulse beam it is possible to observe ‘echos’. The transverse displacement  $\Delta x_0$  is given by

$$\Delta x_0 = c \tau \cos(\theta), \tag{1}$$

where  $c$  is the speed of light and  $\tau$  denotes the time difference between the undiffracted beam and the ‘echo’ leaving the rear surface.

### Spatiotemporal Dynamical Diffraction

Lindberg and co-workers in Ref [8] derive an expression for the reflected and forward diffracted

\*angel.rodriguez@psi.ch

# A MODIFIED SELF-SEEDED X-RAY FEL SCHEME TOWARDS SHORTER WAVELENGTHS

L. Zeng<sup>#</sup>, S. Huang, W. Qin, K. Liu, J. Chen

Institute of Heavy Ion Physics, School of Physics, Peking University, Beijing 100871, China

Y. Ding, G. Marcus, Z. Huang

SLAC National Accelerator Laboratory, Menlo Park, CA 94025, USA

## Abstract

We present a modified self-seeded free-electron laser (FEL) scheme of harmonic generation to extend soft x-ray FEL towards shorter wavelength. Different from classical HGHG scheme whose seed laser is a conventional laser with a longer wavelength, this scheme uses a regular self-seeding monochromator to generate a seed laser, followed by a HGHG configuration to produce shorter-wavelength radiations. We perform start-to-end simulations to demonstrate the second and third harmonic FELs from a soft x-ray self-seeding case at the fundamental wavelength of 1.52 nm. The FEL performance will be discussed.

## \*INTRODUCTION

There are two main schemes for single pass short wavelength FELs: SASE [1,2] and HGHG [3,4]. Until recently, most of the modern high-gain FELs in short wavelength (e.g., x-ray) region have been operated in SASE mode (Emma et al., 2010 [5]; Ishikawa et al., 2012 [6]), which is characterized by excellent transverse coherence. However, SASE has poor temporal coherence and large shot-to-shot fluctuations in both the time and frequency domain because it starts from shot noise.

HGHG scheme can generate fully coherent and high gain harmonic radiation of seed laser. However, single stage harmonic number  $n$  is limited since the energy spread is increased  $n$  times during the energy modulation which makes the induced energy spread exceed the  $\rho$  of radiator. So far, the highest harmonic obtained with single HGHG is the 13th harmonic at 20nm using a 1.2 GeV beam at FERMI FEL [7]. In order to reach higher harmonics, so as to obtain ultrashort wavelength and fully coherent FEL, several schemes have been suggested in recent years. Among them, the cascaded HGHG scheme with the help of “fresh bunch” technique was first proposed in 2001 [8]. Recently, 4.3 nm radiation (60th harmonic of a 260 nm UV laser) has been achieved with a two stage HGHG configuration at FERMI [9]. Another harmonic bunching technique, EEHG [10], has been proof-of-principle demonstrated at SLAC [11] and the third harmonic has been observed at SDUV-FEL, then further amplified to saturation (Zhao et al., 2012 [12]). Currently, coherent radiation at 160 nm (15th harmonic of a 2400 nm seed laser) has been produced at SLAC [13].

So far, the cascaded HGHG and EEHG have difficulty in generating hard X-ray FEL. For classic HGHG scheme, it cannot reach hard x-ray region due to lack of external seeds with short enough wavelengths [14]. Besides, the optical properties of HGHG FEL are determined by the quality of seed laser, so a high quality seed laser is required. On the other hand, self-seeding [15] starts from SASE, and a monochromator is used before saturation to generate a purified seed. This seed is then well aligned and interact with the electron beam, which is delayed by a bypass chicane, until saturation to produce near Fourier-transform-limited X-ray pulses. This self-seeding scheme works for both soft and hard x-ray FELs and has been demonstrated recently [14]. For x-ray FEL with the photon energy below 2 keV, a grating-based monochromator can be used [14]; while for x-ray FEL with the photon energy above 4.5 keV, diamond-based monochromator is more popular [16]. The self-seeded FEL in the energy region between 2 to 4.5 keV is more difficult due to lack of monochromator materials. In this paper, we study a new scheme combining the self-seeding and HGHG scheme to produce fully coherent x-rays which could fill the above energy gap not easily achieved by regular seeding schemes.

## HGHG BASED ON SELF-SEEDING

The proposed scheme, HGHG based on self-seeding, is shown in Fig. 1, which consists of two stages: SASE stage and HGHG stage. In this preliminary work, we are trying to generate 0.76 nm and 0.51 nm x-ray FELs which are the second and third harmonic of the 1.52 nm radiation from SASE undulator, respectively.

The first stage follows the regular self-seeding setup, including a SASE undulator, a monochromator, and a bypass chicane. A 4.3 GeV electron beam is sent to the 19.8-m-long undulator ( $U_S$ ) which is resonant at 1.52 nm and operates in the linear amplification region, so the output radiation has the usual SASE properties. The monochromator filters out a narrow bandwidth signal from the SASE radiation, which is used as the seed laser for the downstream HGHG.

The second stage FEL uses the seed laser and electron beam from the former stage to generate harmonic radiation. Here we should notice that, different from external seed laser whose peak power is at hundred megawatt level (e.g., 100 MW in FERMI FEL-1 [7]) in classic HGHG scheme, our seed power is limited to be lower than several hundred kilowatts in order to avoid damage to the monochromator optics [14]. As a result, we

<sup>#</sup>zengling@pku.edu.cn

# STUDIES OF UNDULATOR TAPERING FOR THE CLARA FEL

I.P.S. Martin, Diamond Light Source, Oxfordshire, UK

R. Bartolini, Diamond Light Source, Oxfordshire, UK

and John Adams Institute, University of Oxford, UK

D. Dunning, N. Thompson, ASTeC, STFC Daresbury Laboratory, UK

## Abstract

Undulator tapering is a well-known method for enhancing the performance of free-electron lasers [1]. It works by keeping the resonant wavelength constant, despite variation in the electron beam energy. Both the energy-extraction efficiency and the spectral brightness of the FEL can be improved using this technique. In this paper we present recent studies of undulator tapering for the CLARA FEL in both SASE and seeded modes. The methods used to optimise the taper profile are described, and the properties of the final FEL pulses are compared.

## INTRODUCTION

Undulator tapering is a well-known and widely used technique for improving the performance of free-electron lasers [1]. It works by keeping the resonant wavelength matched to the bunching in the electron beam, despite the changing energy of the electrons as they travel along the length of the undulator. It was originally proposed as a way to improve the energy extraction efficiency of an FEL [2–5], but has since found many other applications. For example, when tapering is combined with self-seeding, it provides a route to coherent, high-power, hard x-ray FELs [5, 6]. Alternatively, it can be used in combination with an external laser modulator to generate short, fully coherent radiation pulses by restricting high FEL-gain to the energy-chirped sections of the electron bunch [7–9]. Similarly, energy-chirps arising from velocity bunching or longitudinal space charge can be compensated using an undulator taper [10, 11]. A reverse undulator taper can also be used to *suppress* FEL power, whilst still allowing a high degree of bunching to develop within the electron bunch. This can then be used for a variety of applications, such as generating circularly polarised light in a helical undulator after-burner [12].

In view of this diverse range of applications for undulator tapering, the topic is currently one of interest for study at the CLARA FEL currently under construction [13, 14]. CLARA aims to provide a test facility at which a wide range of current and future FEL schemes can be tested experimentally, and so the suitability of the proposed layout for effective tapering needs to be established at an early stage.

In this paper we present preliminary studies of undulator tapering using the CLARA FEL. We study two cases, namely seeded and SASE operation at 266 nm, and for each case investigate the performance of undulator tapering at improving the final FEL pulse quality.

## TAPER OPTIMISATION METHODS

The basic principle of undulator tapering is simple, that is, the resonant wavelength should be kept constant by matching the undulator strength parameter  $a_u$  to the changing electron energy. In practice however, establishing the optimum taper profile is not straight-forward. Here, we compare two contrasting techniques.

The first method relates to the 1D Kroll-Morton-Rosenbluth (KMR) formalism [1, 3]. In this, a Hamiltonian method is used to define a fixed synchronous phase  $\Psi_r$  that relates the rate of energy-extraction to the particle energy, the field amplitude and  $a_u$ . The  $\Psi_r$  parameter also defines the ponderomotive bucket area, and so the selection of  $\Psi_r$  becomes a trade-off between capturing the greatest number of particles (small  $\Psi_r$ ) and maximising the rate at which energy is extracted from the electron beam (large  $\Psi_r$ ). A modification of this method was recently proposed in [15], in which  $\Psi_r$  is allowed to vary along the radiator. The problem then changes from finding the optimal fixed-value of  $\Psi_r$  to one of optimising  $d\Psi_r/dz$ . In this study, we investigate a linear increase of the form:

$$\Psi_r(z) = \frac{\pi}{2L_d} z \quad (1)$$

where  $L_d$  is the so-called *detrapping length* (bucket area shrinks to zero at  $z = L_d$ , see [15] for details). With this parameter defined, the problem reduces to one of iteratively solving the equation:

$$a_u(z + \Delta z) = a_u(z) - \frac{\sqrt{2}e}{m_e c^2} \frac{\lambda_r}{\lambda_u} f_B(z) E_0(z) \sin \Psi_r(z) \Delta z \quad (2)$$

where  $f_B$  is the Bessel factor for a planar undulator and the radiation field amplitude  $E_0$  is found at each step from time independent GENESIS calculations [16]. Solving Eqn. 2 gives a continuous taper profile; this has been converted to a stepped taper for later analysis using full, time dependent simulations.

The second method investigated is direct optimisation of the taper profiles using time-dependent GENESIS simulations. Whilst 3D, time-dependent simulations are slow, they automatically include various limiting effects such as radiation refraction and diffraction, radial dependence of the radiation field and the growth of sidebands that are missing from the 1D, steady-state method outlined above [17].

In principle, arbitrary taper profiles can be optimised in this way. However, to simplify the problem we investigate

# MEASUREMENT UNCERTAINTIES IN GAS-BASED MONITORS FOR HIGH REPETITION RATE X-RAY FEL OPERATIONS\*

Y. Feng<sup>#</sup>, J. Krzywinski, M. Campell, D. W. Schafer, E. Ortiz, M. Rowen, T. O. Raubenheimer, SLAC, Menlo Park, CA 94025, USA

## Abstract

Thermodynamic simulations using a finite difference method were carried out to investigate the measurement uncertainties in gas-based X-ray FEL diagnostic monitors under high repetition rate operations such as planned for the future LCLS-II soft and hard X-ray FEL's. For monitors using relatively high gas pressures for obtaining sufficient signals, the absorbed thermal power becomes non-negligible as repetition rate increases while keeping pulse energy constant. The fluctuations in the absorbed power were shown to induce significant measurements uncertainties, especially in the single-pulse mode. The magnitude of this thermal effect depends nonlinearly on the absorbed power and can be minimized by using a more efficient detection scheme in which the gas pressure can be set sufficiently low.

## INTRODUCTION

The Linac Coherent Light Source (LCLS) currently operating at SLAC National Accelerator Laboratory will soon start to construct, under the LCLS-II project, a new 4 GeV continuous-wave (CW) superconducting radio frequency (SCRF) linear accelerator, in addition to the existing normal conducting RF Cu linac (CuRF). There will be two new variable-gap undulators to be placed in the existing LCLS undulator tunnel: a new soft X-ray undulator and a hard X-ray undulator that would replace the existing LCLS fixed-gap undulator. Both new undulators, when fed by the SCRF linac, could run at a very high repetition rate up to  $\sim 1$  MHz, nearly 4 orders of magnitude higher than the LCLS 120 Hz operation. Both undulators will operate in the Self Amplified Spontaneous Emission [1] (SASE) mode with the option to be self-seeded over certain energy ranges. Due to the intrinsic stochastic nature of the SASE lasing process and other extrinsic random mechanisms in the linac, many important parameters of the FEL beam fluctuate randomly from pulse to pulse [2]. For example, the pulse intensity can vary by as much as a 10% in the SASE mode to nearly 100% in the seeded mode [3]. Many diagnostic devices are needed to help the accelerator operators to optimize the lasing performance, and to enable the users to normalize the experimental data [4-8].

The various diagnostic devices are typically located in the Front-End Enclosure (FEE) just downstream of the undulator but upstream of any experimental endstations. They are often required to be highly transmissive and minimally intrusive as to introduce only negligible

wavefront distortion or transverse coherence degradation. Because of the close proximity of FEE to the effective source location, which is somewhere between the FEL saturation point and the end of undulators (EOU), the power density of the beam at the device locations is quite high, and the diagnostic devices must be based on using a gas medium or a thin solid film to avoid damages while assuring the transmission requirement. For soft X-ray FEL beams in particular, gas-based concepts are the only viable solutions because of the high absorption cross-section at these energies even for the very low  $Z$  materials. For pulse energy measurement, LCLS-II is planning to install two Gas Detector Monitors [9] (GMD's), one of the original design for very soft X-rays and another the latest version specifically optimized for covering higher X-ray energies, on the soft X-ray transport line in the FEE for the SCRF high repetition rate FEL beam. Both GMD's should be capable of providing pulse-to-pulse measurements at greater than 1 MHz repetition rate, but would require very low operating pressures on the order of only  $10^{-5}$  hPa because of the highly efficient direct detection of the ions/electrons from photoionization by the impinging FEL beam.

On the LCLS-II hard X-ray transport line in the FEE, the existing LCLS  $N_2$  gas energy detectors [10] (GED's) shown in Figure 1 will be re-purposed with upgrades for providing pulse-to-pulse measurements of both the high repetition rate FEL when driven by the SCRF linac as well as the 120 Hz high pulse energy FEL when driven by the CuRF linac. The GED concept is based on the detection of the near ultraviolet (UV) optical radiation from the  $N_2$  molecules excited by the secondary electrons, which are produced by the primary photoelectron via collisions with the  $N_2$  molecules. This indirect radiation process in a GED, in contrast to what happens in a GMD, is far less efficient, and thus requires the use of a much higher operation pressure of order 0.01 to 1 hPa, an increase of 3 to 5 orders of magnitude.

Gas-based systems such as the gas attenuator used for LCLS and also being planned for LCLS-II, however, have been shown to exhibit density depression or the so-called "filamentation" effect [11], when the energy absorbed in the gas medium is sufficiently high so that it can no longer be considered as being merely a small perturbation. The effective attenuation not only depends on the pressure, but also on many other physical attributes of the attenuator system itself, including gas type and its thermal properties, the length and radius of the gas tube, the transverse profile of the FEL beam [12]. If the input pulse energy fluctuates as in any SASE based FEL pulses, the attenuation received by any given pulse also varies substantially but in a delayed and hysteric manner and is

\*Work supported by DOE under Contract #. DE-AC02-76SF00515.  
#yfeng@slac.stanford.edu

# FACILITY UPGRADES FOR THE HIGH HARMONIC ECHO PROGRAM AT SLAC'S NLCTA

B. Garcia\*, M.P. Dunning, C. Hast, E. Hemsing, T.O. Raubenheimer  
SLAC, Menlo Park, California, USA  
D. Xiang, Shanghai Jiao Tong University, Shanghai

## Abstract

The Echo program currently underway at SLAC's Next Linear Collider Test Accelerator (NLCTA) aims to use Echo-Enabled Harmonic Generation (EEHG) to produce considerable bunching in the electron beam at high harmonics of a 2400 nm seed laser. The production of such high harmonics in the EUV wavelength range necessitates an efficient radiator and associated light diagnostics to accurately characterize and tune the echo effect. We have installed and commissioned the Visible to Infrared SASE Amplifier (VISA) undulator, a strong focusing two meter long planar undulator of Halbach array design with 1.8 cm period length. To characterize the output radiation, we have designed, built, and calibrated a grazing incidence EUV spectrometer which operates between 12–120 nm with resolution sufficient to resolve individual harmonics. An absolute wavelength calibration is achieved by using both EEHG and High Gain Harmonic Generation (HGHG) signals from the undulator.

## INTRODUCTION

The NLCTA at SLAC is a low-energy X-band test accelerator which delivers a beam at up to 165 MeV with normalized projected emittance of <2 mm-mrad, and bunch charge of up to 200 pC. The current layout of the main NLCTA beamline is shown in Figure 1 (for a discussion of the previous state of the facility and upgrades, see [1]), and we briefly review it here. The beam is generated from a UV photocathode illuminated by a 266 nm, 1 ps long laser pulse and accelerated through a 1.6 cell BNL/SLAC/UCLA S-band gun. After, it is boosted to 60 MeV by an X-band accelerating structure (X1), and continues to the Echo portion of the beamline where it is accelerated again to 120 MeV (X2). An orbital bump is generated by small chicane (C0) to allow insertion of the first seed laser, which modulates the beam in the first undulator (U1), followed by the first dispersive chicane (C1), second modulator (U2), and final dispersive chicane (C2). An additional boost is provided by the third X-band structure (X3) to bring the beam energy to ~160 MeV, where the beam then enters the two meter VISA undulator (U3) to radiate. Finally, photons can be diverted into either the Extreme Ultraviolet (EUV) or Vacuum Ultraviolet (VUV) spectrometer and associated diagnostics, and electron beam energy is finally measured with a dipole energy spectrometer.

The NLCTA is currently involved in investigating advanced beam phase space manipulation techniques, particularly Echo-Enabled Harmonic Generation (EEHG) [2]. This

technique involves using a two-modulator, two-chicane setup in order to generate density modulations in the electron beam at a high harmonic of the initial seed laser. The first laser modulator imprints an energy modulation on the beam, which is then macroscopically sheared by a strong first chicane. This creates a fine energy banding structure in the electron beam, effectively decreasing the slice energy spread of the individual beamlets. The beam is then modulated in a second undulator, and this modulation converted into density modulation by standing the energy modulation upright (similar to the manipulation in the more common High-Gain Harmonic Generation scheme [3]). Thus, a density modulation recovers at a wavenumber given by  $k = nk_1 + mk_2$ , where  $n, m$  are integers, and  $k_1, k_2$  are the wavenumbers of the first and second laser (which may be identical). This allows, for example, the single stage seeding of a x-ray free-electron laser via conventional lasers with harmonic numbers of perhaps up to 100 [4]. It is worth noting that such single stage seeding is difficult with alternate schemes, as the required energy modulation to reach high harmonics quickly exceeds the FEL bandwidth  $\rho$ , while in EEHG the required modulation remains comparatively small even for high harmonics.

At SLAC, this technique has been demonstrated in a series of proof of principle experiments, first to generate the 3rd and 4th harmonic of a 1600 nm seed [5]. This was then extended to the 15th harmonic of a 2400 nm seed, reaching down into the VUV at 160 nm [6]. One ultimate goal for the harmonic extension of the EEHG technique is to demonstrate the ~75th harmonic of a seed laser. At this harmonic, one can seed a x-ray FEL with a 266 nm laser and reach solidly into the x-ray regime, obtaining fully coherent light. Therefore, there has been a push to reach to these high harmonics at NLCTA, which has required the installation of a new radiating undulator along with an associated EUV photon spectrometer to characterize the harmonic generation.

## THE VISA UNDULATOR

The previous radiation of the 15th harmonic of a 2400 nm seed laser was obtained using a 120 MeV beam and an X-band microwave undulator with tuneable K value and effective undulator period of 1.39 cm [7]. In order to more effectively radiate low wavelengths, we both increased the beam energy and installed a new, longer undulator.

To boost the beam energy, we added one additional X-band accelerating structure (X3) of 1 meter length following C2. This structure in the current configuration provides an additional 45 MeV of beam energy, bringing the total

\* bryantg@stanford.edu

# DESIGN OF THE MID-INFRARED FEL OSCILLATOR IN CHINA

Li Heting, Jia Qika, Zhang Shancai<sup>#</sup>, Wang Lin

NSRL, University of Science and Technology of China, Hefei, 230029, China

## Abstract

In 2014, Xiamen University and other three research organizations received the approval to realize an infrared free electron laser (IR-FEL) for fundamental of energy chemistry. The IR-FEL covers the spectral range of 2.5-200  $\mu\text{m}$  and will be built in NSRL. Two FEL oscillators driven by one Linac will be used to generate mid- infrared and far-infrared lasers. In this article we describe the design studies for the mid-infrared FEL oscillator.

## INTRODUCTION

Under the financial support of Natural Science Foundation of China, the project of infrared laser for fundamental of energy chemistry is building up an infrared light source in Hefei. The National Synchrotron Radiation Laboratory (NSRL) of USTC is responsible for the design, construction and commissioning of IRFEL apparatus. It will be a dedicated experimental facility aiming at energy chemistry research, whose core device is a free electron laser (FEL) generating 2.5-200  $\mu\text{m}$  laser for photo excitation, photo dissociation and photo detection experimental stations. Similar as the IR-FEL at the Fritz-Haber-Institute in Berlin [1,2], two oscillators driven by one Linac will be used to generate mid- infrared (2.5-50  $\mu\text{m}$ ) and far-infrared (40-200  $\mu\text{m}$ ) lasers.

The MIR-FEL is planned to laser earlier and in this paper, we will focus on the design of the MIR-FEL oscillator. To meet the user requirements, the undulator, optical cavity and electron beam for the MIR-FEL are designed and described. Then simulations using Optical-Propagate Code (OPC) [3] have been done and the results will be shown. We finally summarize in the last section.

## DESIGN GOAL

As mentioned above, there will be three experimental stations in the first stage. The users of these stations have brought out their requirements on the IR-FEL performance, as given in Table.1. In addition, some users have extra requirements, for example, the photo excitation and dissociation stations require that the peak and average power of IR-FEL should be as high as possible. in the next section.

It is worth pointing out that the broad wavelength range and high radiation intensity brings us much difficulties in the design of electron Linac and optical cavities. For example, the short-wavelength FEL requires short electron bunch to achieve high peak current while the long-wavelength FEL requires long electron bunch to suppress the slippage effect, and the short-wavelength FEL requires a short Rayleigh length of the optical cavity

to get a considerable big spot size and an appropriate outcoupling on the mirror while the case of the short-wavelength FEL is opposite. Therefore, the design is to find a balance for the object wavelength range.

Table 1: Design Goal of the IR-FEL

Parameters	Specification
Covering spectrum	2.5 ~ 200 $\mu\text{m}$
MIR FEL oscillators	2.5 ~ 50 $\mu\text{m}$
FIR FEL oscillators	40 ~ 200 $\mu\text{m}$
Macro-pulse length(FW)	5~ 10 $\mu\text{s}$
Repetition of macro-pulse	20 Hz
Macro-pulse energy	~100 mJ
Micro-pulse length (RMS)	5 ~ 10 ps
Micro-pulse energy	1 ~ 50 $\mu\text{J}$
Bandwidth	0.3 ~ 3 %
Continuous tunability	200 ~ 300 %

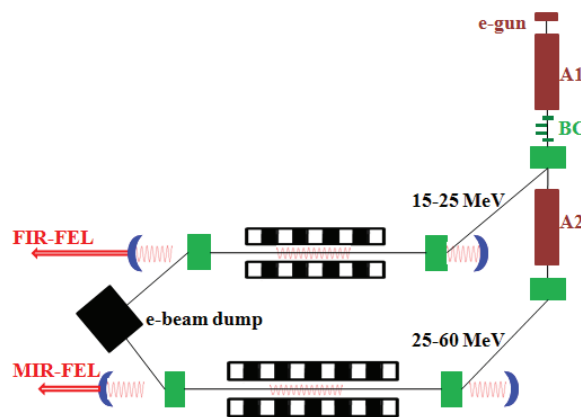


Figure 1: Schematic of the projected IR-FEL.

## MIR-FEL DESIGN

### Layout

As shown in Fig. 1, the IR-FEL is composed of two FEL oscillators driven by one electron Linac. Two accelerating tubes are used to accelerate the electron beam. Between the first and the second accelerating tube, a four-dipole magnetic chicane is designed as an optional operation condition. Its purpose is to reduce the micro-pulse length and increase the peak current of the electron bunch for the short-wavelength FEL, and for the long-wavelength FEL, it also can increase the micro-pulse length to suppress the slippage effect.

It is very important that we choose the thermionic electron gun as the electron source [4]. Using special gate control system, the electron bunch chain will be extracted from the gun, with micro-pulse length of 1 ns, optional

<sup>#</sup>shancai @ustc.edu.cn

# SINGLE PICOSECOND THz PULSE EXTRACTION FROM THE FEL MACROPULSE USING A LASER ACTIVATING SEMICONDUCTOR REFLECTIVE SWITCH

K. Kawase<sup>#</sup>, R. Kato, A. Irizawa, M. Fujimoto, K. Furukawa, K. Kubo, G. Isoyama,  
Osaka University, Osaka, Japan

## Abstract

The THz-FEL at the Institute of Scientific and Industrial Research (ISIR), Osaka University can generate high-intensity THz pulses or FEL macropulses, which comprise approximately 100 micropulses at 37 ns intervals in the 27 MHz mode or 400 micropulses at 9.2 ns intervals in the 108 MHz mode. The maximum macropulse energy in the 27 MHz mode reaches 26 mJ at a frequency of 4.5 THz and the micropulse energy is estimated to be 0.2 mJ. To open new areas of studies with high intensity THz radiation for user experiments, we are developing a single pulse extraction system from the pulse train using a laser activating semiconductor reflective switch. We have succeeded in extracting a single THz pulse, duration of which is estimated to be less than 20 ps, from the FEL macropulse using a gallium arsenide wafer for the switch.

## INTRODUCTION

THz radiation sources recently have been demanded from various scientific and industrial fields [1]. Although there is some THz source, the FEL-based THz radiation source has a great advantage comparing with the other types of source. The remarkable aspects of the THz-FEL are its peak intensity and narrowness of the bandwidth.

The THz-FEL at the ISIR is an oscillator type FEL driven by an rf-linac. Thus, the generated FEL forms a pulse train (macropulse). The macropulse consists of a number of THz micropulses. The micropulse duration is typically similar to the electron bunch duration, thus that duration is about 20 ps in ours. In our case, we have two types of the linac operation for the FEL experiment. The first type of the operation is the dc-beam extraction from the electron-gun and pulsing by the rf-cavity with the frequency of 108 MHz. In this case, the FEL macropulse consists of approximately 400 micropulses with the separation of 9.2 ns. The second type is the pulsed-beam extraction from the gun using the grid-pulsed electric circuits with the repetition frequency of 27 MHz. In this case, the FEL macropulse consists of approximately 100 pulses with the separation of 37 ns. In the latter case, we achieved the macropulse energy of 26 mJ at the radiation frequency of 4.5 THz. The maximum micropulse energy is estimated to be over 200  $\mu$ J [2, 3].

There are requirements to extract a single micropulse for the investigations of the nonlinear response of materials in order to avoid thermal effects due to the irradiation of the pulse train. To meet these requirements, we are developing the single pulse extraction using a laser

activating semiconductor reflective switch, which is also referred as a plasma mirror [4 - 9].

Generally non-doped semiconductors are insulators and thus they have a high transmittance for the radiation in the THz range. Because the THz-FEL radiation is linearly polarized, we can quench the reflecting radiation from the surface of a semiconductor wafer by setting the incident angle to Brewster's angle. Using an intense infrared laser pulse with the photon energy above the band gap energy and irradiating it on the semiconductor wafer, electron-hole plasma is generated on the surface and it becomes a high reflector for the THz radiation. After the diffusion and recombination of the excited electrons, it returns the insulator with a high transmittance. Therefore, we can apply this mechanism into the reflective switching technique to extract a single THz-pulse. The schematic diagram of this mechanism is shown in Fig. 1.

In this paper, we report the overview and present status of the single THz pulse extraction in our FEL facility.

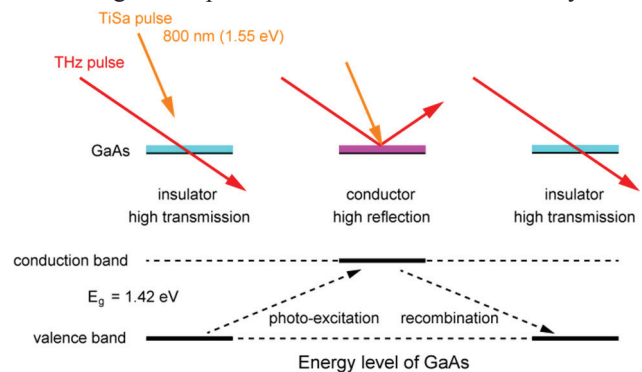


Figure 1: Schematic diagram of the laser activating semiconductor reflective switching for the THz pulse.

## EXPERIMENTAL SETUP

The experiment is done using the L-band linac and THz-FEL system at the ISIR, Osaka University [3]. A schematic diagram of the L-band linac and FEL system is shown in Fig. 2. The generated THz-FEL pulses are transported through the vacuum duct to the outside of the radiation shielding area. To activate the semiconductor reflective switch, we use a mode-locked Ti:Sapphire laser system (Spit Fire, Spectra-Physics). The pulse repetition rate of the laser system is 960 Hz and the pulse energy is about 1 mJ. The pulse duration is typically 100 fs and the wavelength is centered at 800 nm. The pulse timing is synchronized to the rf of the linac system. The laser system is placed just beside the user area for the THz-FEL as shown in Fig. 2.

# TIME DEPENDENT STUDY FOR AN X-RAY FEL OSCILLATOR AT LCLS-II

J. Zemella<sup>1,2</sup>, W. M. Fawley<sup>1</sup>, R. R. Lindberg<sup>3</sup>, and T. J. Maxwell<sup>1</sup>

<sup>1</sup>DESY, Hamburg, Germany

<sup>2</sup>SLAC, Menlo Park CA, USA

<sup>3</sup>ANL, Argonne IL, USA

## Abstract

The LCLS-II with its high repetition rate and high quality beam will be capable of driving an X-ray free electron laser oscillator at higher harmonics in the hard X-ray regime (0.1 nm). The oscillator consists of a low loss X-ray crystal cavity using diamond Bragg crystals with meV bandwidth. The expected average spectral flux has been estimated to be at least two orders of magnitude greater than present synchrotron-based sources with highly stable, coherent pulses of duration 1 ps or less for applications in Mössbauer spectroscopy and inelastic x-ray scattering. A more detailed study of the start up of a fifth-harmonic X-ray FEL oscillator at LCLS-II will be presented with full, time-dependent simulations.

## INTRODUCTION

The planned LCLS-II cryogenic linac based on TESLA technology [1, 2] at SLAC will be operated in ‘cw-mode’ with a repetition rate of 0.929 MHz. This enables one to develop new concepts for generating hard X-rays including low-gain FEL schemes such as X-ray free electron laser oscillators (XFELO) based on a high reflectivity crystal cavity with narrow bandwidth in the order of 10 meV [3]. The advantages of an XFELO are the full coherence and spectral purity of the X-ray pulse compared to state of the art sources like SASE (self amplified spontaneous emission) FELs (LCLS-I [4], SACLA [5]) based on a stochastic process leading to fluctuating pulse properties. Self seeding technique is able to improve longitudinal coherence in hard X-ray [6] but not reaching full, stable longitudinal coherence and typically include a broad SASE background that may complicate, e.g., precision inelastic X-ray scattering (IXS) experiments.

The design beam energy of the LCLS-II cryogenic linac is 4 GeV. To generate Ångstrom wavelengths one can instead amplify a higher harmonic of the FEL pulse [7]. We consider in this paper the fifth harmonic at 14.4 keV using the Bragg reflection of Diamond (hkl)=(733) where (hkl) are the Miller indices.

We present progress on the feasibility study started last year where initial performance estimates were presented in [8]. This paper is focused on verifying the startup process of the XFELO and saturation pulse properties using the time-dependent simulation code Ginger [9] in oscillator mode, extended to simulate higher harmonics.

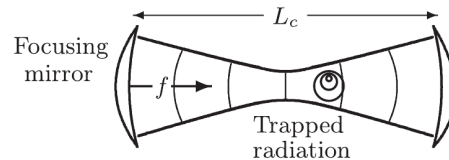


Figure 1: Used cavity design used in Ginger simulations.

## LAYOUT

The cavity model used in simulations is depicted in Fig. 1. Two focusing elements define the waist  $\omega_0$  inside the undulator which can be expressed by the Rayleigh length  $Z_R$  and the wavelength  $\lambda$

$$Z_R = \frac{\pi\omega_0^2}{\lambda}, \quad (1)$$

$$f = \frac{L_c}{4} + \frac{Z_R^2}{L_c}, \quad (2)$$

with cavity length  $L_c$  and focal strength  $f$  of the mirrors. Spectral filtering from the Bragg reflectors is done by applying the wavelength-dependent complex reflectivity of the two Bragg crystals, one thick (high-reflectivity) and one thin (extraction mirror) crystal. The path length change induced by Bragg reflection leading to cavity length detuning is compensated here by multiplying the complex reflectivity with the proper group delay phase factor as described in [10]. The assumed crystal reflectivity of both Bragg C\*(733) crystals is shown in Fig. 2. For the present study the modified cavity design shown in Fig. 1 is a modification of the tunable, four crystal, zig-zag cavity scheme previously discussed. However, for gain studies only matched mode size, Rayleigh length, and electron beam beta function in the undulator must be matched which can be achieved by the cavity described. Of course this may change with a more precise description of the 3D angular divergence which is not addressed here.

## SIMULATIONS

For simulating an XFELO for LCLS-II a 167 fs long Gaussian current profile with 120 A peak current and 200 keV Gaussian energy spread is assumed. Further parameters are gathered in Table 1.

Some optimization steps were performed for optimizing FEL gain. The first step is to find the right energy detuning, shown in the scan of Fig. 3 to maximize gain in steady state.

# NUMERICAL STUDIES OF THE INFLUENCE OF THE ELECTRON BUNCH ARRIVAL TIME JITTER ON THE GAIN PROCESS OF AN XFEL-OSCILLATOR FOR THE EUROPEAN XFEL

C. Maag, J. Zemella, DESY, Hamburg, Germany  
J. Rossbach, University of Hamburg, Germany

## Abstract

The superconducting linac of the European XFEL Laboratory in Hamburg will produce electron bunch trains with a time structure that allow in principle the operation of an XFEL (X-ray FEL-Oscillator). The electron bunches of the European XFEL have an expected length between 2 and 180 fs (FWHM) with an expected arrival time jitter of about 30 fs (RMS). A jitter of the electron bunch arrival time leads to a detuning between the electron and photon pulse. Since an XFEL-Oscillator relies on a spatial overlap of electron and photon pulse, the influence of a lack of longitudinal overlap is studied. The simulations are performed for different bunch lengths and levels of arrival time jitter. The results of a simulation are presented where angular, transversal and arrival time jitter are taken into account simultaneously, assuming parameters expected for the European XFEL Linac.

## INTRODUCTION

The recently proposed concept of an XFEL described in [1, 2] potentially offers performance complementary to a SASE (self-amplified spontaneous emission) based FEL. The proposed XFEL uses a crystal cavity to provide narrow band feedback of the SASE radiation and has the potential to produce hard x-rays with energies between 5 and 20 keV. While the extracted peak power of such an XFEL (about 50 MW) is predicted to be lower by about 3 orders of magnitude compared to SASE-FELs, the bandwidth will be in the order of  $\Delta\nu/\nu \approx 10^{-5} - 10^{-7}$  which is 2 - 4 orders of magnitude more narrow than the bandwidth of a SASE-FEL ( $\Delta\nu/\nu \approx 10^{-3}$ ). The pulses of an XFEL will have a significantly larger longitudinal coherence up to full longitudinal coherence along the photon pulse [3]. Building an XFEL requires components which have to perform on the edge of today's technical feasibility, including the production and acceleration of high-brightness electron beams, the optimization of radiation generation in the undulator and the electron and x-ray beam guidance so as to overlap the electron bunch with the x-ray pulse to obtain optimal FEL gain. In this paper the influence of a lack of overlap is studied, whereby the focus rests on the arrival time jitter between electron bunch and x-ray pulse. The currently lowest arrival time jitter of 30 fs was achieved with a synchronization system reported in [4] using 60 fs (RMS) long electron bunches. At the European XFEL a synchronization system similar to that is planned to be implemented [5] and it is assumed that the arrival time jitter will decrease for bunches shorter than 60 fs. At the European XFEL electron

bunches with a length between 180 fs and 2 fs are planned to be generated. Due to the fact that the arrival time jitter of the electron bunches at the European XFEL will be of the order of the bunch length some impact on the XFEL operation can be expected. To quantify the impact of the arrival time jitter on the XFEL operation simulations using the code GENESIS 1.3 [6] have been performed. The simulations have been performed for bunch lengths of 178 fs and 18.8 fs (FWHM) with three levels of arrival time jitter each. Since not only the arrival time is subjected to jitter exemplarily a simulation has been performed that incorporates bunch position and angular jitter as well. The jitter levels used in this exemplary simulation are the levels expected for European XFEL Linac.

Table 1: Input Parameters of the Simulations

Parameter	unit	Setup 1	Setup 2
Electron energy	GeV	14.5	14.5
Bunch charge	nC	1	0.1
Bunch length (FWHM)	fs	178	18.8
Peak current	kA	4.9	5
Normalized emittance	$\mu\text{m}$	1	0.3
Slice energy spread	MeV	1.5	2.04
Beta function at waist	m	7.5	7.5
Radiation wavelength	$\text{\AA}$	1.027	1.027
Undulator length	m	15	15
Undulator period	m	0.03	0.03
Cavity length	m	66.62	66.62
Outcoupled radiation	%	4	4
Cavity losses	%	4	4

## SIMULATIONS

The simulations were performed with the single pass FEL code GENESIS 1.3 together with an oscillator extension code [7] which calculates the propagation of the output radiation field in the cavity of one GENESIS run and use it as the seed radiation for a subsequent GENESIS run. The calculation of the field propagation inside the cavity comprises the free space propagation, the spectral filtering due to the Bragg reflection, the transformation due to the focusing elements and the outcoupling of a fraction of the radiation at one of the crystal mirrors. The spectral band-pass filter that is applied to the radiation to simulate the Bragg reflection (4 4 4) at a Diamond crystal has a width of  $\Delta\lambda/\lambda \approx 1.66 \cdot 10^{-6}$  (FWHM) which corresponds to a Fourier-limited pulse duration of about 180 fs (FWHM).

## NEW ELLIPSOIDAL LASER AT THE UPGRADED PITZ FACILITY

J. Good<sup>#</sup>, G. Asova<sup>†</sup>, M. Bakr<sup>‡</sup>, P. Boonpornprasert, M. Gross, C. Hernandez-Garcia<sup>§</sup>, H. Huck, I. Isaev, D. Kalantaryan, M. Khojoyan<sup>θ</sup>, G. Kourkafas, M. Kraslinikov, D. Malyshev<sup>§</sup>, D. Melkumyan, A. Oppelt, M. Otevrel, Y. Renier, T. Rublack, F. Stephan, G. Vashchenko, Q. Zhao<sup>¶</sup>,  
 Deutsches Elektronen-Synchrotron, Zeuthen, Germany  
 I. Hartl, S. Schreiber, Deutsches Elektronen-Synchrotron, Hamburg, Germany  
 A. Andrianov, E. Gacheva, E. Khazanov, S. Mironov, A. Poteomkin, V. Zelenogorsky,  
 Institute of Applied Physics, IAP, Nizhny Novgorod, Russia  
 E. Syresin, JINR, Dubna, Moscow Region, Russia  
 O. Lishilin, G. Pathak, Hamburg University, Hamburg, Germany

### Abstract

High brightness photoinjectors for superconducting linac-based FELs are developed, optimized and characterized at the Photo Injector Test facility at DESY in Zeuthen (PITZ). Last year the facility was significantly upgraded with a new prototype photocathode laser system capable of producing homogeneous ellipsoidal pulses. Previous simulations have shown that the corresponding pulses allow the production of high brightness electron bunches with minimized emittance. Furthermore, a new normal conducting RF gun cavity was installed with a modified two-window waveguide RF feed layout for stability and reliability tests, as required for the European XFEL. Other relevant additions to the facility include beamline modifications for improved electron beam transport through the PITZ accelerator, refinement of both the cooling and RF systems for improved parameter stability, and preparations for the installation of a plasma cell. This paper describes the facility upgrades and reports on the operational experience with the new components.

### ELLIPSOIDAL LASER SYSTEM

Previously reported [1] low emittance beams were obtained using a flat-top temporal laser profile with 60 MV/m in the RF gun, and more recently new measurements have been taken with a Gaussian temporal laser profile and 53 MV/m [2]. Also recently it was found that the transverse halo of the laser must be taken into account [3]. In earlier simulations it was found that uniform ellipsoidal charge distributions with sharp charge transition boundaries would produce even higher beam quality. Furthermore, it was shown that such electron bunches are also less sensitive to machine parameter jitter [4] and therefore increase the reliability and stability - crucial parameters for single-pass FELs such as FLASH and the European XFEL.

<sup>#</sup> james.david.good@desy.de

<sup>†</sup> on leave from BAS INRNE, 1784 Sofia, Bulgaria

<sup>‡</sup> on leave from Assiut University, 71515 Assiut, Egypt

<sup>§</sup> on leave from JLab, Newport News, VA 23606, USA

<sup>¶</sup> on leave from IMP/CAS, 730000 Lanzhou, China

<sup>§</sup> now at Helmholtz-Zentrum Berlin, Berlin, Germany

<sup>θ</sup> now at Synchrotron SOLEIL, Paris, France

Naturally, a homogenous ellipsoidal photocathode laser pulse can be used to produce such charge distributions. Consequently, such a laser system has been developed for PITZ by the Institute of Applied Physics in Nizhny Novgorod, under the framework of a joint German-Russian research activity [5].

The system produces quasi-ellipsoidal laser pulses in the infrared through spectral amplitude-phase masking.

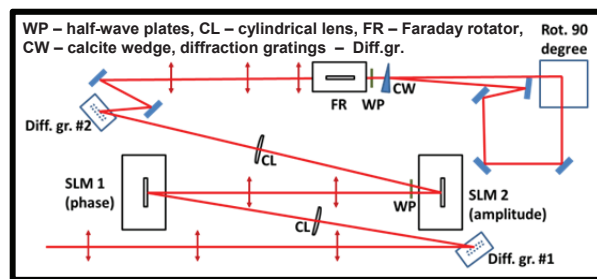


Figure 1: Schematic overview of the 3D shaper.

The shaper consists of two diffraction gratings, two Spatial Light Modulators, and various optical elements (Fig. 1). A chirped infrared laser pulse is transformed into the spectral domain with a diffraction grating and imaged onto Spatial Light Modulators (SLMs) whereupon masks such as in Fig. 2 are applied. The beam is then recombined via another grating, rotated 90° about its propagation axis, and passed back through the shaper again. This shapes the perpendicular transverse axis and produces a quasi-ellipsoidal distribution. Finally, the beam is converted from infrared to the ultraviolet via non-linear 4<sup>th</sup> harmonic frequency conversion.

Simulations have been done to produce the mask in Fig. 2a) which is expected to roughly produce the quasi-ellipsoidal distribution in Fig. 2b).

Simulations have shown that these improved laser pulses have the potential to further reduce the emittance of the generated electron bunches at PITZ [4].

# OPERATION OF A SLIT EMITTANCE METER IN THE MAX IV GUN TEST STAND

J. Andersson\*, F. Curbis, M. Isinger, F. Lindau, S. Werin  
MAX IV Laboratory, Lund University, Lund, Sweden

## Abstract

The MAX IV facility in Lund, Sweden is currently under commissioning. There are two guns in the current MAX IV injector, one thermionic gun for storage ring injection and one photocathode gun for the Short Pulse Facility. There is a possibility of extending the facility to include a Free Electron Laser. To investigate how the beam from the injector can be improved and how to match it to the future requirements for a FEL, the emittance meter from SPARC has been recommissioned at the MAX IV gun test stand. In this paper we report on the progress of this work and results from the first measurements.

## INTRODUCTION

The MAX IV facility [1] is under construction in Lund, Sweden and includes two storage rings for production of synchrotron radiation and a short pulse facility (SPF) [2]. Both storage rings and the SPF are injected from a full energy LINAC and the injector for the LINAC has two different guns, a thermionic gun and a photocathode gun. The thermionic gun is used for ring injection but due to the requirements of short bunches and the long tail of low energy electrons, the thermionic gun is unsuitable for injection to the SPF. A 1.6 cell photocathode gun will be used instead, based on the BNL/SLAC type for FERMI@Elettra [3], operating at a frequency of 2.9985 GHz.

The performance of the photocathode gun needs to be improved, especially with regards to the emittance. Better experimental understanding of the different components of the injector is needed to find parameters to deliver an electron beams that meets the requirements. One of the diagnostic possibilities is to measure the emittance and beam envelope evolution along the injector. Earlier experiments using a pepperpot [4] has been carried out, but that setup was limited to one longitudinal position. The SPARC [5] emittance meter was placed in the vicinity to the MAX IV gun test stand after earlier experiments, and it was investigated to see if the slit- and mechanical parameters of the emittance meter was compatible with the expected beam performance from the MAX IV test gun.

## MEASUREMENT PARAMETERS

The beam properties from the gun were simulated using ASTRA [6]. The result from simulations is a beam with kinetic energy of 3-5 MeV, charge of 50 - 500 pC and an emittance in the range of 0.3 to 5 mm mrad depending on operating parameters. In the first stage it is planned that

the measurements are made using a single slit measurement device. Using the formulas from the appendix in [7] it is possible to estimate the dimensions of the mask and drift length to be able to resolve a beam with these properties.

The dimensions of the slit are a thickness of at least 0.5 mm tungsten to scatter the unwanted parts of the beam and a slit width of 50  $\mu\text{m}$  to create emittance dominated beamlets. A slit separation of 200  $\mu\text{m}$  was decided upon and to properly be able to resolve the divergence of the beam a drift space of 0.2 - 0.4 meters was used. The first tests were done using the same slit separation for all positions along the beam.

## MEASUREMENT SYSTEM

The parameters for the emittance measurement device for the MAX IV gun test stand [8] are compatible with the SPARC emittance meter parameters. It was decided to re-commission the SPARC emittance meter and install it into the MAX IV gun test stand to use it to investigate the beam performance. Motors, motor control and cameras was changed, but no mechanical changes were made to the system and it is in principle as described in reference [5]. The different motor axis were configured and calibrated, and after calibration the position accuracy was checked to make sure that the different axis positions could be repeated.

Gun test overview

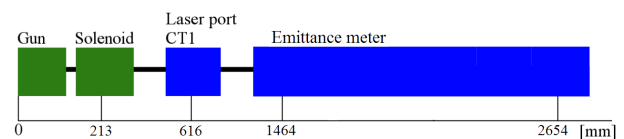


Figure 1: Schematic over the MAX IV test gun stand with emittance meter installed, the minima and maxima positions of the slit is marked.

A schematic of the test stand after the installation of the emittance meter can be seen in Figure 1 and Figure 2 shows a picture of the actual complete system. With the emittance meter installed at its current position in the beamline it is possible to measure with slit positions from 1.46 m up to 2.65 m.

The gun used in the test stand is of the same design as the gun currently used in the injector for the SPF at MAX IV. Measurements using the bead pull technique has verified that the field in this gun matches the field in the installed gun well. For the test setup a solenoid magnet produced by Scanditronix is used which is able to produce a maximum

\* joel.andersson@maxlab.lu.se

# INITIAL COMMISSIONING RESULTS OF THE MAX IV INJECTOR

J. Andersson\*, F. Curbis, M. Eriksson, D. Kumbaro, F. Lindau, E. Mansten, D. Olsson, S. Thorin, S. Werin MAX IV Laboratory, Lund University, Lund, Sweden

## Abstract

The MAX IV facility in Lund, Sweden is currently under commissioning. In the MAX IV injector there are two guns, one thermionic gun for storage ring injection and one photocathode gun for the Short Pulse Facility. The commissioning of the injector and the LINAC has been ongoing for the last year and ring commissioning is due to start shortly. In this paper we will present the results from beam performance experiments for the injector at the current stage of commissioning.

## INTRODUCTION

The MAX IV facility [1] is under commissioning in Lund, Sweden. The facility has two storage rings for production of synchrotron radiation, one with 1.5 GeV and one with 3 GeV electrons. There is also a short pulse facility (SPF) [2] for the production of short pulses. The storage rings and the SPF are injected from a full energy LINAC. The injector for the LINAC has two electron guns, one thermionic gun [3] and one photocathode gun where the thermionic gun is used for ring injection. Due to the requirements of short bunches the thermionic gun is unsuitable for injection to the SPF and instead a 1.6 cell photocathode gun is used.

The commissioning of the injector and the LINAC started during the fall of 2014 and beam was commissioned until the recent shutdown period in May of 2015. During the commissioning all subsystems in the injector have been tested and brought online.

## THE MAX IV INJECTOR

The injector system can be seen pictured in Figure 1. There are two parts of the injector, one leg where the thermionic gun is installed that injects into the main beam line through a 120 degree bend in an energy filter, and one straight leg for the photocathode gun.

### Thermionic Gun Leg

The thermionic gun produces a beam from a BaO cathode using thermal heating. The beam is focused on an aperture using a solenoid, and between the solenoid and the aperture a chopper system [4] is shaping the beam into a suitable temporal structure for ring injection. For the initial ring commissioning scheme this will be three 3 GHz bunches within 10 ns (100 MHz) repetition time. The pulse length for each LINAC shot is 100 ns, where the pulse length is controlled using a stripline that is excited with a high-voltage pulse. The beam is refocused using a second solenoid, and then the beam proceeds into the first quad of the energy filter. The energy filter consist of four quadrupole magnets

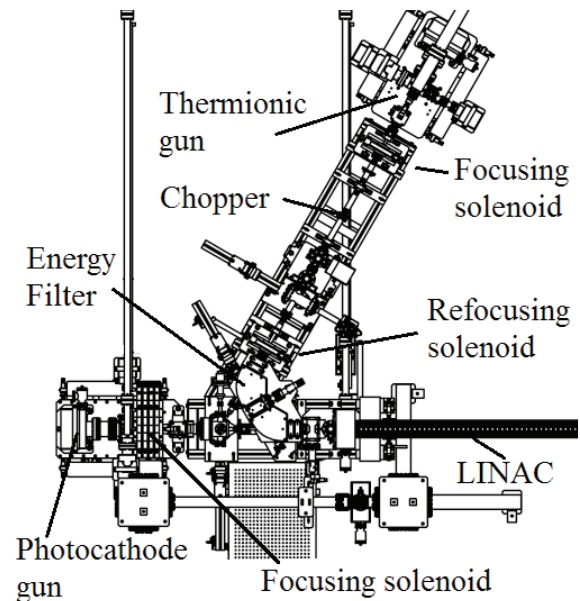


Figure 1: Blueprint of MAX IV pre-injector.

for focusing in the horizontal and vertical planes, two are located before the bending magnets and two located after. Between the two bending magnets there is a quadrupole magnet used to control the dispersion. There is also a scraper in the center of the energy filter, making it possible to adjust how much of the low energy tail of the beam that is accepted into the LINAC. The energy filter has a mechanical energy acceptance of about 200 keV and the beam is after the energy filter sent into the first structure of the LINAC. There exists multiple current transformers along the thermionic leg to measure the charge after the gun, before the energy filter and after the energyfilter.

### Photocathode Gun Leg

The photocathode gun is operating at 2.9985 GHz and is based on the BNL/SLAC type for FERMI@Elettra [5]. The gun is powered by a 4  $\mu$ s RF pulse via a SLED system. A laser with a wavelength of 263 nm is used to extract electrons from a copper cathode. The laser system is a KM Labs Dragon with cryogenic cooled Ti:Sapphire crystals. The laser has an oscillator at 76.9 MHz and its pulses are amplified, first in a regenerative amplifier and secondly in a multipass amplifier. Two kHz pump lasers are used to pump the amplifiers in the laser system. The pulse from the multipass amplifier is frequency tripled to a wavelength of 263 nm. The laser pulse is transported in an evacuated transport system from the laser room into the LINAC tunnel and is then focused on an iris where the beam size can be adjusted. The iris is imaged onto the cathode and the laser

\* joel.andersson@maxlab.lu.se

## CONSTRUCTION OF THE EU-XFEL LASER HEATER\*

M. Hamberg\*, V. Ziemann, Uppsala University, Uppsala, Sweden

### Abstract

Installation of the laser heater for the EU-XFEL is completed and first commissioning runs are imminent. We discuss the installation of the key elements and provide an outlook of the commissioning phase.

### INTRODUCTION

The low momentum spread of the cold electron bunches emitted from the photo-cathode of the EU-XFEL makes the accelerator sensitive to micro bunching instabilities. A laser heater is implemented to overcome this. In this proven concept a laser beam is overlapping the electron bunches as they are travelling through an undulator in a chicane. The net result after leaving the chicane is a decreased phase-space density i.e. warmer electron bunches [1-2].

The EU-XFEL laser heater is a Swedish in-kind contribution. Setup and tests were described earlier [3-4]. This paper focus on the installation of the key elements such as laser laboratory setup, laser transport vacuum system, laser routing and stabilisation system, optical stations and ultra-high vacuum (UHV) chambers before ending with an outlook.

### IR LASER SOURCE SETUP

Directly after the IR laser source located on level 5 in the injection building all optical parts such as: Mirror mounts, beam-expansion telescope, retro-reflector stage (for time delay adjustment), safety shutter, active mirror mount and flip mirror for realignment are now installed. The system is also prepared for easily implementing motorized filter wheel and  $\lambda/2$  rotation stage if the commissioning shows that this is a favorable position.

Furthermore a PLC system box is constructed, programmed, tested and ready to work in this location. The last mirror in this location is actively adjusted with the routing and stabilization system described below.

### LASER TRANSPORT VACUUM SYSTEM

Leaving the optical table on level 5 the laser directly enters a 40 m long DN63 vacuum pipe system used to preserve the laser beam from atmospheric disturbances. The system was assembled during November to May. The strategy of the system is to use ion pumps to reduce disturbances from vibrations.

Initially the system was closed and turbo stations left to work one week before the ion pumps were switched on and the turbo stations removed. After two weeks monitoring at the three ion pumps in the system the pressure was below  $10^{-6}$  mbar and the trend a steady decrease.

In early June, test of the motorised routing system inside of the vacuum was undertaken. We investigated the

behaviour of the pressure when the stepper motors work inside of the vacuum. It was clear that the pressure up to that time had decreased to about  $2 \times 10^{-7}$  mbar. When the motors started and therefore also start outgassing in the process, the pressure rose to below  $4 \times 10^{-6}$  mbar (well in the safe region). After turning off the motors, the pressure quickly dropped down to  $6 \times 10^{-7}$  mbar. A view of part of the system is shown in Figure 1 whereas the pressure rise is illustrated in Figure 2.

In the last passage of the IR laser transport vacuum system at level 7 the laser enters goes from the wall out over the optical station 0 and towards the remaining laser heater setup (see overview in Figure 3).



Figure 1: Vacuum chamber located close to the electron gun in the injector hall (red mount). The laser is redirected from the vertical shaft downstream the tunnel wall.

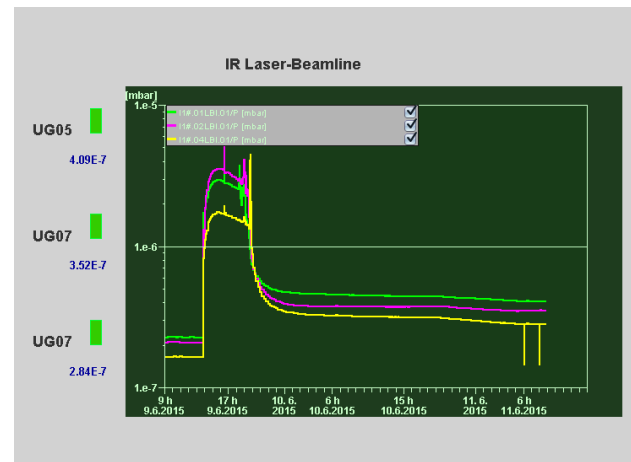


Figure 2: Pressure rise in laser transport vacuum system due to motors outgassing.

# SIMULATION AND DESIGN OF LOW EMITTANCE RF ELECTRON GUN

C. Saisard\*, S. Rimjaem, Plasma and Beam Physics (PBP) Research Facility,  
 Department of Physics and Materials Science, Faculty of Science,  
 Chiang Mai University, Chiang Mai 50200, Thailand

## Abstract

Generation of high-brightness electron beam is one of the most critical issues in development of advanced electron accelerators and light sources. At the Plasma and Beam Physics (PBP) Research Facility, Chiang Mai University, a low emittance RF electron gun is under the development. This RF-gun is planned to be used as an electron source for a future IR/THz FEL facility. An extra resonant cavity is added to the modified design of the existing PBP-CMU RF-gun in order to reduce the transverse sliced emittance. This cell is coupled to the main full-cell via a side-coupling cavity. The electromagnetic field distributions inside the cavities are simulated by using the CST Microwave Studio 2012<sup>®</sup>. Then, beam dynamic simulations utilizing the program PARMELA are performed. Both RF and beam dynamic simulation results are reported and discussed in this contribution.

## INTRODUCTION

The high brightness electron beam is essential in development of the next generation electron accelerators and light sources. The brightness of electron beams depends on the beam peak current and 6-dimensional emittance. This characteristic requires the high quality beams emitting from the electron injector. An electron gun of the linac-based THz radiation source at the Plasma and Beam Physics (PBP) Research Facility, Chiang Mai University, is driven by a 7 MW-klystron at the resonant frequency of 2856 MHz. It consists of 1.6 cell S-band standing-wave structure and a tungsten dispenser thermionic cathode with Os/Ru coating. The present RF-gun design was optimized to produce electron beams with longitudinal distribution suitable for using an alpha magnet as a magnetic bunch compressor. Together with a downstream linac section and related beam transport components, electron beams with the bunch length in order of femtosecond can be obtained [1]. In order to improve the transverse properties of electron beams, new modified design of the RF-gun is conducted [2]. The previous study results suggest that by adding TM<sub>010</sub> pillbox cavity next to the main full-cell is able to reduce the sliced emittance and line up the sliced phase spaces [3].

In this work, an extra resonant cavity is added to the PBP-CMU RF electron gun to modify the dynamics of electrons. This extra cell is connected to the end of the full-cell and the RF power is coupled from the full cell to the extra cell via the side coupling cavity. The electromagnetic fields inside the resonant cavities are simulated by using the program CST Microwave Studio (MWS) 2012<sup>®</sup> [4]. The dynamics of elec-

trons under the influence of the electromagnetic fields are studied by using a particle tracking program PARMELA [5]. RF parameters of the cavities and beam dynamics study results of electron beams are the main points, which are presented and discussed here.

## SIMULATION OF ELECTROMAGNETIC FIELDS

The PBP-CMU RF gun consists of two main cavities, which operates in  $\pi/2$  mode for acceleration at the resonant frequency of 2856 MHz. The existing RF-gun has asymmetric shape due to side-coupling cavity opening holes and an RF waveguide input port, which lead to asymmetric beam distribution. By rotating the direction of the side-coupling cavity to vertical direction, the asymmetric feature of electron beams reduced [2]. In this research, an extra cell is added downstream the full cell and it is coupled via a side coupling cavity in vertical direction as shown in Fig. 1 and Fig. 2. The mode of acceleration is kept to be at  $\pi/2$  mode and at this mode the resonant frequency of the whole gun is around 2857.3 MHz. The RF parameters for each cell are listed in Table 1.

The electromagnetic field distributions in each mode is solved by using the *Eigenmode Solver* feature in CST MWS. Only boundary conditions at the end of the RF input port and at the end of the extra cell are Dirichelet, otherwise the Neumann boundary conditions is used. The hexahedral mesh is chosen and the total number of mesh cells is 265,650. The amplitude of axial electric field ratio between each cell, which implies to energy gain, can be adjusted by moving tuning rod inside the side coupling cavity. The axial electric field distribution along the beam propagating direction is shown in Fig. 3. The peak field ratio between the cells shown, in Table 2, are adjusted for optimizing electron bunch compression using the alpha magnet, which will be discussed later in other report.

Table 1: RF Parameters of Each Cell at  $\pi/2$ -mode

RF parameters	half cell	full cell	extra cell
Resonant frequency (MHz)	2866.3	2876.0	2870.0
Shunt impedance (M $\Omega$ )	3.45	7.99	5.75
Power (W)	290.8	358.2	318.6
Stored energy (mJ)	0.225	0.378	0.257
R-upon-Q	248	419.34	392.5
Accelerating Voltage (MV)	2.11	2.65	2.63

\* chaipattana\_s@cmu.ac.th

# SIMULTANEOUS OPERATION OF THREE LASER SYSTEMS AT THE FLASH PHOTOINJECTOR

S. Schreiber\*, J. Roensch-Schulenburg, B. Steffen, C. Gruen, K. Klose, DESY, Hamburg, Germany

## Abstract

The free-electron laser facility FLASH at DESY (Hamburg, Germany) operates two undulator beamlines simultaneously. Both undulator beamlines are driven by a common linear superconducting accelerator with a beam energy of up to 1.25 GeV. The superconducting technology allows the acceleration of trains of several hundred microsecond spaced bunches with a repetition rate of 10 Hz. A fast kickers-septum system is installed to distribute one part of the electron bunch train to FLASH1 and the other part to FLASH2 keeping the full 10 Hz repetition rate for both beamlines. In order to deliver different beam properties to each beamline, the FLASH photoinjector uses two independent laser systems to generate different bunch pattern and bunch charges. One laser serves the FLASH1 beamline, the other the FLASH2 beamline. A third laser with adjustable laser pulse duration is used to generate ultra-short bunches for single spike lasing.

## INTRODUCTION

FLASH [1–3], the free-electron laser (FEL) user facility at DESY (Hamburg) simultaneously operates two undulator beamlines [4–6]. It delivers high brilliance XUV and soft X-ray SASE radiation to photon experiments. FLASH is a user facility since 2005.

FLASH is a linear accelerator with a photoinjector followed by a superconducting linear accelerator. The maximum electron beam energy is 1.25 GeV, allowing SASE lasing down to 4 nm. The FLASH1 undulator beamline is in operation since 2004, the new FLASH2 beamline since 2014.

More details on the FLASH facility and its present status as well as on simultaneous operation of two beamlines can be found in these proceedings [3, 6].

A unique feature of FLASH is its superconducting accelerating technology. It allows to accelerate several thousand electron bunches per second. The bunches come in bursts with a repetition rate of 10 Hz. The maximal burst duration is 0.8 ms, the smallest distance between single bunches is 1  $\mu$ s allowing a maximum number of 800 bunches per burst or 8000 bunches per second. FLASH has two undulator beamlines: FLASH1 and FLASH2. The burst of electron bunches is shared between them, keeping the 10 Hz repetition rate of the accelerator for each beamline.

An important and unique feature of FLASH is, that beam parameters and bunch pattern can vary for the two undulator beamlines: experiments with different wavelengths, pulse durations, and pulse pattern are possible at the same time.

The flexibility is realized with three main features. Firstly, variable gap undulators allow to adjust the wavelength for FLASH2 experiments, while the beam energy is determined by the wavelength required for FLASH1 lasing with its fixed gap undulators. Secondly, different photoinjector laser systems operated in parallel allow different charges, different pulse pattern, and to create a variable gap between the subbursts for FLASH1 and FLASH2. Thirdly, the low-level RF control of the accelerating structures are able to adjust phases and amplitudes – to a certain extent – independently for both beamlines, thus making different compression schemes possible. For details on FLASH2 photon beam parameters, the reader is referred to [4].

FLASH has three photoinjector lasers. Two lasers provide bursts of laser pulses with high single pulse energy but fixed single pulse duration. A third system has the feature of short and variable pulse duration optimized for high compression for ultra-short single spike SASE photon pulses.

The most promising method to achieve such short pulses is to compress the electron bunch to the femtosecond level. In the most extreme case the lasing part of the bunch is as short as one longitudinal optical mode. These so-called single-spike SASE pulses [7, 8] are bandwidth limited, longitudinally coherent.

In order to mitigate space charge forces, a low bunch charge of 20 pC is applied. It is generated at the gun by a short laser pulse of less than 1 ps (rms), thus substantially reducing the bunch compression factor required for bunch durations of a few femtoseconds only.

## THE ELECTRON SOURCE

The electron source of FLASH is a photoinjector based on a normal conducting L-band 1.5 cell RF-gun. The gun is operated with an RF power of 5 MW at 1.3 GHz, corresponding to a maximal accelerating field at the cathode of 52 MV/m. The RF pulse duration is up to 850  $\mu$ s, sufficient for generation of the required bunch trains of 800  $\mu$ s duration. The repetition rate is 10 Hz. The beam momentum at the gun exit is 5.6 MeV/c.

As discussed in the introduction, the RF pulse length of the gun is adapted to the high duty cycle of the superconducting accelerator.

FLASH can accelerate many thousands of electron bunches per second. In order to keep the average power of the laser system reasonably small, a photocathode with a high quantum efficiency is used.

Cesium telluride has been proven to be a reliable and stable cathode material with a quantum efficiency above 5 % for a wavelength around 260 nm. The lifetime is more than 400 days of continuous operation [9]. The bunch charge

\* siegfried.schreiber@desy.de

# LIFETIME OF Cs<sub>2</sub>Te CATHODES OPERATED AT THE FLASH FACILITY

S. Schreiber<sup>#</sup>, S. Lederer, DESY, Hamburg, Germany

## Abstract

The injector of the free-electron laser facility FLASH at DESY (Hamburg, Germany) uses Cs<sub>2</sub>Te photocathodes. We report on the lifetime, quantum efficiency (QE), and darkcurrent of photocathodes operated at FLASH during the last year. Cathode 618.3 has been operated for a record of 439 days with a stable QE in the order of 3%. The fresh cathode 73.3 shows an enhancement of emitted electrons for a few microseconds of a 1 MHz pulse train.

## INTRODUCTION

FLASH [1–3], the free-electron laser (FEL) user facility at DESY (Hamburg) delivers high brilliance XUV and soft X-ray SASE radiation to photon experiments. FLASH is a user facility since 2005.

The maximum electron beam energy is 1.25 GeV, allowing SASE lasing down to 4 nm. The FLASH1 undulator beamline is in operation since 2004, a new FLASH2 beamline since 2014. More details on the FLASH facility and its present status as well as on simultaneous operation of two beamlines can be found in these proceedings [3, 4].

A unique feature of FLASH is its superconducting accelerating technology. It allows to accelerate several thousand electron bunches per second. The bunches come in bursts with a repetition rate of 10 Hz. The maximal burst duration is 0.8 ms, the smallest distance between single bunches is 1 μs allowing a maximum number of 800 bunches per burst or 8000 bunches per second.

## THE ELECTRON SOURCE

The electron source of FLASH is a photoinjector based on a normal conducting L-band 1.5 cell RF-gun. The gun is operated with an RF power of 5 MW at 1.3 GHz, corresponding to a maximal accelerating field at the cathode of 52 MV/m. The RF pulse duration is up to 850 μs, sufficient for generation of the required bunch trains of 800 μs duration. The repetition rate is 10 Hz. The beam momentum at the gun exit is 5.6 MeV/c.

As discussed in the introduction, FLASH can accelerate many thousands of electron bunches per second. In order to keep the average power of the laser system reasonably small, a photocathode with a high quantum efficiency is used.

Cesium telluride (Cs<sub>2</sub>Te) has been proven to be a reliable and stable cathode material with a good quantum efficiency (QE) for a wavelength around 260 nm [5, 6]. The bunch charge required for FLASH SASE operation is between 20 pC and a bit more than 1 nC. For a QE of 5%, a single laser pulse of 100 nJ at 262 nm produces a charge of 1 nC (linear regime). For a burst of 800 pulses with 1 MHz and 10 bursts per second, this corresponds to a burst power

<sup>#</sup>siegfried.schreiber@desy.de

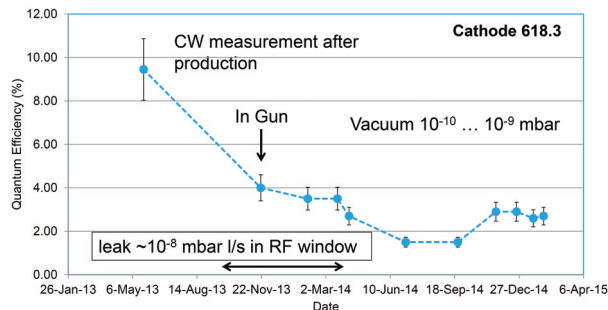


Figure 1: Quantum efficiency of cathode 618.3 during operation at FLASH.

of 100 mW and an overall average power of 0.8 mW. With a laser pulse duration of 6.5 ps (rms), the peak power is 80 kW. These are all reasonable low numbers to avoid damage or ablations of the cathode thin film or of laser beamline components. For details on the FLASH injector laser systems, the reader is referred to [7] and references therein.

## QUANTUM EFFICIENCY

For practical reasons, we define the quantum efficiency (QE) as the ratio of the numbers of photons impinging the photocathode and the number of electrons emitted – while the RF-gun is operated at its nominal working point. The extracted charge is measured with a calibrated toroid at the RF-gun exit, the laser energy with a calibrated joulemeter [8] in front of the vacuum window. The transmission of the quartz window and the reflectivity of the in-vacuum mirror is taken into account. Finally the QE is obtained by a linear fit of the charge as a function of laser energy – before space charge effects saturate the emission. For an example of such a fit, the reader is referred for instance to [9, 10].

The nominal working point of the RF-gun is at an accelerating field of 52 MV/m (on-crest) and a launch phase of 38° from the zero-crossing point. This phase has been chosen years ago and has been kept as a reference since then. The launch phase for maximum energy gain and minimum energy spread is 45° and is used for SASE operation.

## Longterm Operation of a Cs<sub>2</sub>Te Cathode

Figure 1 shows the quantum efficiency of cathode 618.3 during operation at FLASH for a period of 439 days. The cathode has been produced with the usual recipe. A thin film of Cs<sub>2</sub>Te with a diameter of 5 mm is deposited on a polished molybdenum plug. Figure 2 shows a photo of the cathode. For details on the production of cathodes see [10, 11].

The QE is always measured at the center of the cathode with RF-gun operation parameters as discussed above. Figure 1 also shows the QE measured just after production with a Hg-lamp at the preparation chamber. During operation in

## PAL-XFEL CAVITY BPM PROTOTYPE BEAM TEST AT ITF

Sojeong Lee, Young Jung Park, Changbum Kim, Seung Hwan Kim, D.C. Shin  
Heung-Sik Kang, Jang Hui Han, In Soo Ko  
PAL, Pohang, Kyungbuk, Korea

### Abstract

To achieve sub-micrometer resolution, The Pohang Accelerator Laboratory X-ray Free electron Laser (PAL-XFEL) undulator section will use X-band Cavity beam position monitor (BPM) systems. Prototype cavity BPM pick-up was designed and fabricated to test performance of cavity BPM system. Fabricated prototype cavity BPM pick-up was installed at the beam line of Injector Test Facility (ITF) at PAL for beam test. Under 200 pC beam charge condition, the signal properties of cavity BPM pick-up were measured. Also, the dynamic range of cavity BPM was measured by using the corrector magnet. In this paper, the design and beam test results of prototype cavity BPM pick-up will be introduced.

### INTRODUCTION

The Pohang Accelerator Laboratory X-ray Free Electron Laser (PAL-XFEL) facility will use 10 GeV linac and undulator beamlines to provide X-ray FEL radiation to users. By using the self-amplified spontaneous emission (SASE) schematic, PAL-XFEL will provide X-rays in ranges of 0.1 to 0.06 nm for hard X-ray line and 3.0 nm to 1.0 nm for soft X-ray line [1]. To generate X-ray FEL radiation, the PAL-XFEL undulator section requires high resolution beam position monitoring systems with  $<1 \mu\text{m}$  resolution. At first phase, the PAL-XFEL will be operated at a repetition rate of 60 Hz with 0.2 nC electron beam charge [2]. To achieve this high resolution requirement under single electron beam with low charge condition, the PAL-XFEL undulator section will use the cavity Beam Position Monitors (cavity BPMs) for beam trajectory monitoring. Total 49 units of cavity BPM system will be installed in between each undulators with other diagnostics tools. Before fabrication of the PAL-XFEL cavity BPM pick-ups, the prototypes of cavity BPM were fabricated to test the performance of cavity BPM pick-ups.

### PAL-XFEL CAVITY BPM PICK-UP DESIGN

The operation frequency of PAL-XFEL cavity BPM system was set as X-band frequency. Due to the limitation of installation space, the compact cavity BPM pick-up was required. To achieve high resolution and compact pick-up size, the X-band operation frequency, 11.424 GHz, was chosen for PAL-XFEL cavity BPM system. Also, for easy installation and maintenance, the PAL-XFEL cavity BPM pick-ups adopt the SMA feed through as output signal port. Under these two conditions, the PAL-XFEL cavity BPM pick-up was designed.

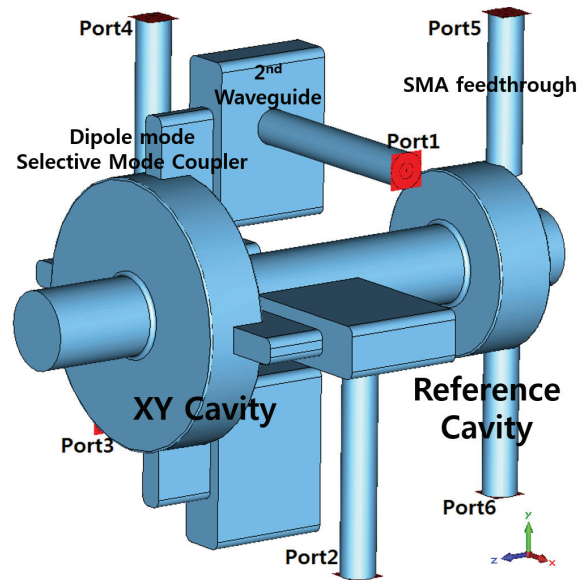


Figure 1: Modeling of PAL-XFEL cavity BPM pick-up vacuum part.

The PAL-XFEL cavity BPM pick-up consists of two cavities, reference cavity and XY cavity. The reference cavity uses  $\text{TM}_{010}$  mode, monopole mode, of pill box cavity. The amplitude of  $\text{TM}_{010}$  mode is proportional to the electron beam charge. By using this property of monopole mode, the reference cavity can measure the bunch charge, and this reference cavity signal is used to normalize the amplitude of XY cavity signal. On the other hand, the XY cavity uses  $\text{TM}_{110}$  mode, dipole mode, of pill box cavity. The amplitude  $\text{TM}_{110}$  mode is proportional to the bunch charge and offset of electron beam. Thus, the XY cavity can measure beam position by using excited dipole mode of XY cavity and reference cavity signal.

Figure 1 shows the inner structure modeling result of PAL-XFEL cavity BPM pick-up. Reference cavity is designed as simple structure, for easy fabrication. In case of XY cavity, the dipole mode selective coupler for suppressing the monopole mode signal of XY cavity. This dipole mode selective coupler structure was proposed and adopted for LCLS cavity BPM pick-ups [3,4]. Each SMA feed through is installed on the second waveguide of XY cavity. This second waveguide was adopted to minimize the brazing effect on the pill box part of XY cavity.

Table 1 shows the RF parameters of PAL-XFEL cavity BPM pick-up. The RF parameters of each cavity were calculated by using CST Microwave Studio module [5]. Both cavities were designed as high Q value and over coupled structure. Also, R/Q value of each cavity, one of factor de-

## SPARK EL - SINGLE PASS BPM

M. Znidarcic, Instrumentation Technologies, Solkan, Slovenia

### Abstract

Monitoring and subsequent optimization of the electron linacs and beam transfers requires specific instrumentation for beam position data acquisition and processing. Spark EL is the newly developed prototype intended for position monitoring in single or multi bunch operation linacs and transfer lines. The motivation, processing principles and first results are presented.

### INTRODUCTION

In this paper we introduce a compact platform that aims to host a wide range of applications. First instrument built on this platform is Libera Spark EL (see Fig. 1 and Fig. 2). The instrument is designed for processing of electron beam in linear accelerators and beam transfers.



Figure 1: Housing prototype.



Figure 2: Libera Spark EL back panel.

### A NEW PLATFORM

Looking at the beam instrumentation used to monitor and stabilize an accelerator, every device suits a specific role, but it is possible to identify some key components that are always present:

- RF front-end and analogue signal processing chains
- Internal communication buses
- Power supply unit
- Cooling system

In this new development, we take advantage of the latest advances in SoC technology to introduce a compact platform (see Fig. 3) that combines a high level of hardware integration with our knowledge regarding reconfigurable analogue signal processing.

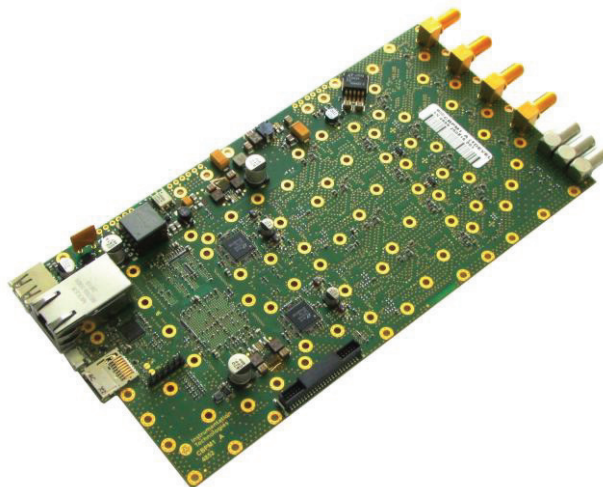


Figure 3: Libera Spark EL.

### HW and SW Integration

Hardware and software are designed taking in account the balance between generality and optimization. It will be always possible to add specific features to customize it, opening at the same time the way for developing different applications, as shown in Fig. 4.

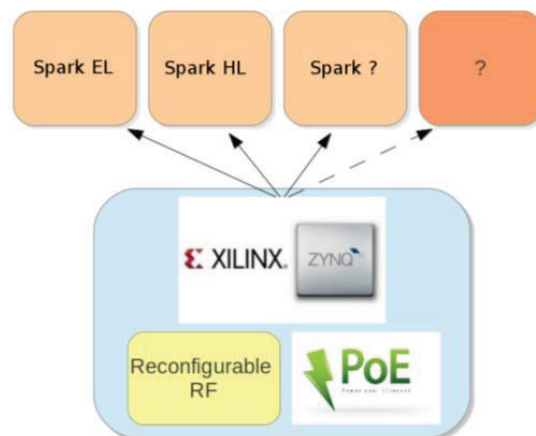


Figure 4: Platform concept based on SoC.

The core part is the SoC Xilinx Zynq 7020 [1] which combines the high-speed processing of the FPGA together with the flexibility of a CPU, all within the same chip. The inner communication between the two entities and the chance to share the same memory removes at the same time two of the biggest bottle-necks that still characterize separate-chip solutions:

- No communication protocols needed
- No data copy between FPGA and CPU.

The specifics of the analogue front-end cover the user requirements. Integrations with specific band-pass filters, phase-locked-loop (PLL) and variable attenuators are

# MTCA.4 PHASE DETECTOR FOR FEMTOSECOND-PRECISION LASER SYNCHRONIZATION

E. Janas<sup>1,2,\*</sup>, K. Czuba<sup>2</sup>, M. Felber<sup>1</sup>, M. Heuer<sup>1</sup>, U. Mavrič<sup>1</sup>, H. Schlarb<sup>1</sup>  
<sup>1</sup> DESY, Hamburg, Germany

<sup>2</sup> ISE, Warsaw University of Technology, Poland

## Abstract

For time-resolved experiments at FELs such as the European XFEL an accurate synchronization of the machine is essential. The required femtosecond-level synchronization we plan to achieve with an optical synchronization system, in which an inherent part is the master laser oscillator (MLO) locked to the electrical reference. At DESY we develop a custom rear transition module in MTCA.4 standard, which will allow for different techniques of phase detection between the optical and the electrical signal, as well as locking to an optical reference using a cross-correlator. In this paper we present the current status of the development, including two basic solutions for the detection to an RF. One of the methods incorporates an external drift free detector based on the so-called MZI setup. The other one employs the currently used down-converter scheme with subsequent improvements. The module can serve for locking a variety of lasers with different repetition rates.

## INTRODUCTION TO OPTICAL SYNCHRONIZATION SYSTEM AT THE EUROPEAN XFEL

The optical synchronization system planned for the European XFEL has a range of uses. It is employed in these locations of the facility, where the most demanding synchronization precision is necessary. First of all, it serves as a reference for a number of lasers in the machine, including pump-probe laser for time resolved experiments. The lasers can be directly locked to the optical synchronization system using laser-to-laser locking stations (L2L) described in [1]. Another applications are precise bunch arrival-time monitors or a support for the 1.3 GHz coaxial cable based timing distribution, suffering from the drifts arising with a distance from the signal source in the cables because of their thermal expansion. The electrical synchronization system, mainly supplying the LLRF stations along the FEL, comprises of so-called interferometer links which task is to extend the possible synchronization distances [2]. Nevertheless, to achieve the required stabilities of the timing signal at different locations along over 3km long accelerator, the system has to be resynchronized to the optical reference. At DESY, we have developed a module called REFM-OPT, which promises to achieve sub-10fs synchronization precision between electrical and optical signal over longer time periods [3]. The REFM-OPT utilizes the laser-to-RF phase detector (L2RF)

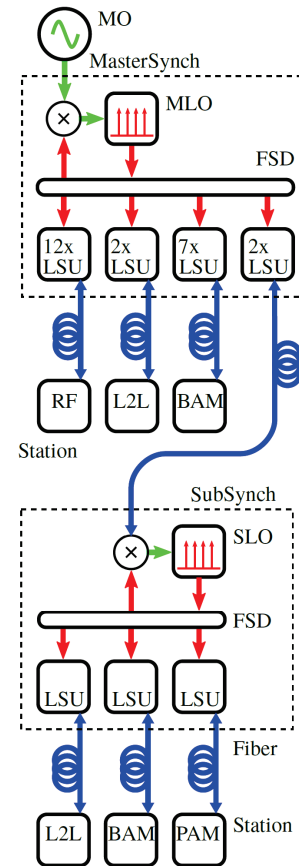


Figure 1: Optical synchronization scheme of the European XFEL. Description of system components: Master Oscillator (MO), Master Laser Oscillator (MLO), Slave Laser Oscillator (SLO), Free-Space Distribution (FSD), Link Stabilization Unit (LSU), Laser-to-Laser synchronization (L2L), Laser-to-RF synchronization (RF), Bunch Arrival-time Monitor (BAM) - beam diagnostics directly using the laser pulse train, Photon Arrival-time Monitor (PAM). Figure source: courtesy of Cezary Sydlo

of an extraordinary performance presented in [4], where we obtained 3.6 fs peak-to-peak phase drift over 24 h.

An overview of the optical synchronization system is shown in Figure 1. It incorporates the current solution used at DESY's mother facility FLASH (about ten times smaller than the European XFEL), with subsequent improvements and extensions. The signal source is a master laser oscillator (MLO), which is a commercial mode-locked laser with pulse duration of 200 fs at a repetition rate of 216.67 MHz. The MLO in turn is locked to the master oscillator (MO), the

\* Ewa.Janas@desy.de

# PROTOTYPE OF THE IMPROVED ELECTRO-OPTICAL UNIT FOR THE BUNCH ARRIVAL TIME MONITORS AT FLASH AND EUROPEAN XFEL

H. Dinter\*, M.K. Czwalińska, C. Gerth, K. Przygoda, R. Rybaniec, H. Schlarb, C. Sydlo  
DESY, Hamburg, Germany

## Abstract

At today's free-electron lasers, high-resolution electron bunch arrival time measurements have become increasingly more important in fast feedback systems providing accurate timing stability for time-resolved pump-probe experiments and seeding schemes. At FLASH and the upcoming European XFEL a reliable and precise arrival time detection down to the femtosecond level has to cover a broad range of bunch charges, which may even change from 1 nC down to 20 pC within a bunch train. This is fulfilled by arrival time monitors which employ an electro-optical detection scheme by means of synchronised ultra-short laser pulses. At both facilities, the new bunch arrival time monitor has to cope with the special operation mode where the MHz repetition rate bunch train is separated into several segments for different SASE beam lines. Each of the segments will exhibit individual timing jitter characteristics since they are generated from different injector lasers and can be accelerated with individual energy gain settings. In this paper, we describe the recent improvements of the electro-optical unit developed for the bunch arrival time monitors to be installed in both facilities.

## INTRODUCTION

The signal creation, detection and analysis in the electron bunch arrival time monitor is split into several subsystems, each fulfilling a particular task at their respective position in the signal processing chain. These include:

- The **RF unit** comprising four broadband pickups mounted in the beam tube in order to capture the electric field induced by the passing electron bunches [1]. The signals of opposite pickups are combined for a reduced position dependence of the measurement, re-

sulting in two independent RF channels for the arrival time detection: Left + Right and Top + Bottom [2].

- The **electro-optical (EO) unit** converting the RF signal into an amplitude modulation of time-stabilised, ultra-short laser pulses provided by the optical synchronisation system [3,4] in order to achieve a high temporal sensitivity.
- **Electronics** for signal readout and control of the individual subsystems [5]. This part also performs communication with high-level control systems.

The general layout of the signal processing chain is illustrated in Fig. 1.

## ELECTRO-OPTICAL UNIT

In this paper, we focus on the recent developments for the electro-optical part of the detection system. A schematic of the optical signal chain is shown in Fig. 2. Synchronised laser pulses enter the optical circulator at the top left and exit it on the right. A subsequent fast bidirectional fibre-optical switch acts as a selector which optical delay line is to be used for the current electron bunch subtrain.

After passing the delay stage and travelling back through the optical switch, the laser pulses are directed to the downward facing port of the circulator. An optical amplifier increases the signal level before it is split into three branches: one clock channel used as a trigger input for the sampling electronics and two channels leading to electro-optical modulators (EOM) corresponding to the two RF signal channels.

One of the signal paths leading to the EOMs provides the possibility of introducing an additional time delay through a separate optical delay stage. This can be used for adjusting the relative timing between the two channels, which might be necessary due to different RF cable lengths.

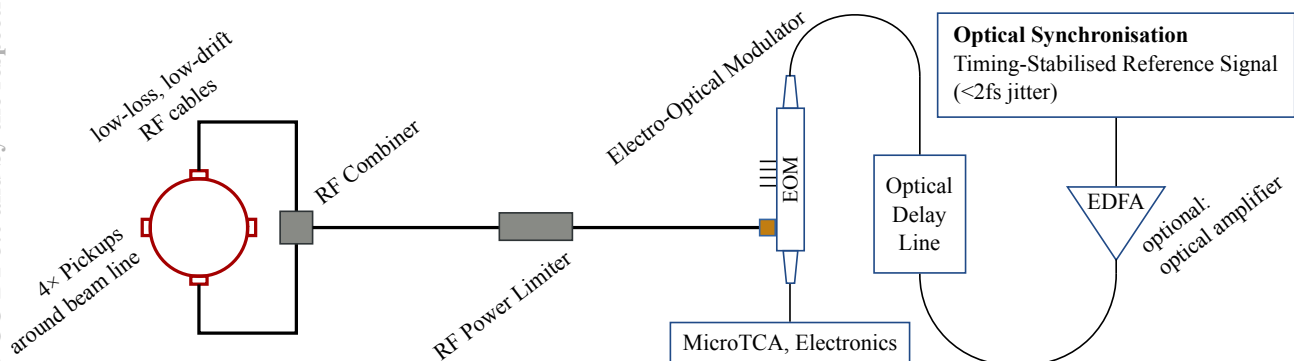


Figure 1: Basic layout of the cabling scheme (only one detection channel is shown).

\* hannes.dinter@desy.de

# EXTENSION OF EXISTING PULSE ANALYSIS METHODS TO HIGH-REPETITION RATE OPERATION: STUDIES OF THE “TIME-STRETCH STRATEGY”

E. Roussel, C. Evain, M. Le Parquier, C. Szwaj, S. Bielawski,  
PhLAM/CERLA, Villeneuve d’Ascq, France

L. Manceron, J.-B. Brubach, M.-A. Tordeux, J.-P. Ricaud, L. Cassinari, M. Labat,  
M.-E Couprie, P. Roy, Synchrotron SOLEIL, Gif-Sur-Yvette, France

## Abstract

We examine how the “photonic time-stretch strategy” can be used to upgrade existing FEL Electro-Optic Sampling (EOS) setups to high repetition rates. Tests made at SOLEIL showed a capability of 88 MHz acquisition rate of single-shot EOS signals. The time-resolution limits is found to be identical to the limits of classical spectral encoding. Technically, time-stretch EOS systems can be build from existing spectral encoding systems, by adding an output optical device.

## BRIEF REVIEW OF THE SPECTRAL ENCODING AND TIME-STRETCH METHODS

### *Spectrally Encoded Electro-optic Sampling (Time to Wavelength Conversion)*

A powerful technique to analyze electron bunch shapes (or short THz pulses produced, e.g., by CSR) consists to convert the temporal information into the spectral domain of a laser pulse [1–6] (spectral encoding). The principle is displayed in Fig. 1. The spectral information is analyzed by a single-shot optical spectrum analyzer, which is composed of a grating and a CCD or CMOS camera. Although very efficient and widely used for electron bunch diagnostics, this strategy present a limitation in term of acquisition rate, because of the speed limitation of currently available cameras (typically hundreds of kilo frame/s). Hence it will be challenging to use further this technique in high-repetition rate FELs (as well as LINACs, storage rings, etc.).

### *Time Stretch Strategy (Time-to-time Conversion)*

The photonic time-stretch technique has been developed in a different context than accelerator physics [7]. The idea consists in converting the ultrafast signal under investigation into a “slowed-down” replica. This is two-step process (Fig. 2). First the pulse is encoded into the spectral domain (as for the classical spectral encoding method). The second step consists in using dispersion in a long fiber, so that the optical spectrum is converted back into the time domain. Using a sufficient length of fiber, the output replica can be easily stretched up to the nanosecond domain, and thus can be recorded using a photodetector and an oscilloscope. This technique can typically reach tens to hundreds of MHz acquisition rates.

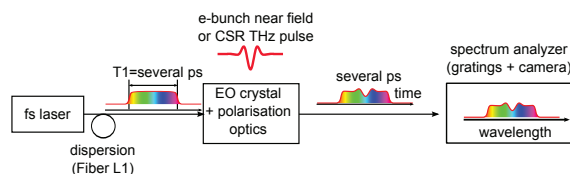


Figure 1: Classical electro-optic detection with spectral encoding. The pulse information is encoded into the spectral domain and recorded using a single-shot spectral analyzer. The main acquisition rate limitations stems from the camera used in the spectrum analyzer.

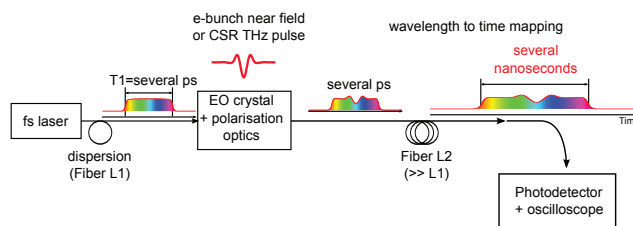


Figure 2: Principle of electro-optic sampling with time-stretch: a “slowed-down” replica of the bunch shape (or THz pulse) is produced. The output signal is recorded using a single pixel detector and an oscilloscope.

## EXPERIMENTAL TESTS OF THE TIME-STRETCH EOS STRATEGY AT SOLEIL

We have explored the possibility to use this method to record electric fields produced by electron bunches at SOLEIL. Instead of probing the near-field electric field of an electron bunch, we attempted to detect the CSR THz pulses emitted by the electron bunch. As for the SLS EOS system [3], we used a GaP crystal and a 1040 nm mode-locked Yb fiber laser. The complete time-stretch setup is detailed in Ref. [8].

A typical series of single pulse is represented in Fig. 3. The stretch factor between the THz pulses and the oscilloscope pulses is  $M = 190$  (i.e., 1 ps correspond to 190 ps at the oscilloscope input). The acquisition rate was fixed by the laser repetition rate (88 MHz). This speed enabled to study the CSR pulses emitted at the AILES beamline in

# REAL-WORLD CONSIDERATIONS FOR CROSSED-POLARIZED UNDULATOR RADIATION CONVERSION\*

W.M. Fawley<sup>†</sup>, E. Allaria, and E. Ferrari, Sincrotrone Trieste S.C.p.A., Trieste, Italy

## Abstract

Cross-polarized (X-POL) configurations are a means to produce circularly-polarized radiation output from purely planar-polarized undulators. Recent polarization results from both the FERMI FEL-1 [1] at XUV wavelengths and Shanghai DUV-FEL [2] at visible wavelengths have confirmed that such configurations do work for single pass FELs. However, analysis of both FERMI and SINAP results indicate that the quantitative degree of planar to circular conversion can be significantly affected by several experimental details. Full conversion requires not only equal intensity of the two cross-polarized beams but also perfect overlap in space and time of their far-field amplitude and phase patterns. From simple theoretical analysis we examine a number of possible factors that can degrade the net linear to circular conversion efficiency. In addition to the previous suggestions by Ferrari *et al.* of problems with unbalanced powers and transverse phase variation arising from different effective emission  $z$  locations for the two cross-polarized radiation pulses, we also consider separate degradation effects of imperfect downstream overlap of the two linearly-polarized beams arising from different emission tilt angles and mode sizes. We also discuss optimizing the conversion efficiency by aperturing the radiation pulses downstream of the undulators.

## INTRODUCTION

In addition to such attractive properties such as wavelength tunability, ultrashort and ultrabright output radiation, and multiple pulse production, free-electron lasers (FELs) with the proper undulator configurations can also produce variable polarization pulses. Because in many facilities linearly-polarized undulators have been favored due to their lower cost and often lower error content in comparison with variable-polarization designs such as the APPLE [3] and DELTA designs [4], the cross-polarized (X-POL) configuration has been suggested [5] as a relatively straight-forward means to produce output radiation with a high degree of circular polarization from purely linearly-polarized undulators. The X-POL arrangement has been studied for FEL amplifiers both theoretically [6, 7] and experimentally in the optical wavelength regime with circular-polarization degree 80% or greater [2].

Recently, experiments in October 2013 [1, 8] and more recently in February 2015 at the seeded FERMI FEL-1 facility [9] have shown the X-POL idea works reasonably well

at wavelengths down to 26 nm. However, the 2013 results showed a global, maximum circular degree of polarization  $P_{CIR} \leq 0.5$ , suggesting that a careful tuning of the overall FEL system can be crucial for proper X-POL optimization. Indeed, the more recent X-POL results of February 2015 that included a careful optimization of the FEL using an online polarization diagnostic have shown significant improvement with a maximum  $P_{CIR} \geq 0.8$ . For the 2013 results, Ferrari *et al.* [8] suggested that an angular variation in far-field transverse eikonal phase between the horizontal- and vertically-polarized radiation due to different longitudinal source points in the undulator underlaid much of poor X-POL conversion. However, there are other possible degradation effects such as power imbalance of the two polarized fields and also imperfect spatial overlap arising from different emission tilt angles and mode sizes.

In the remainder of this paper we discuss these degradation issues and also the experimental procedures by which we believed we strongly improved the X-POL conversion efficiency as shown by the 2015 results.

## THEORETICAL ANALYSIS

Inasmuch we are interested in the degree of circular polarization at a measurement point produced by spatial and temporal overlap of linearly-polarized sources the radiation properties are best described by the linear polarization basis for the Stokes parameters (see, *e.g.*, Eq. 7.27 of Jackson [10]):

$$\begin{aligned} S_0 &\equiv a_H^2 + a_V^2 & S_2 &\equiv 2a_H a_V \cos \phi_{HV} \\ S_1 &\equiv a_H^2 - a_V^2 & S_3 &\equiv 2a_H a_V \sin \phi_{HV} \end{aligned} \quad (1)$$

where  $a_H$  and  $a_V$  are the *local* field amplitudes of the two polarized beams, and  $\phi_{HV} \equiv \varphi_H - \varphi_V$  is the difference of their eikonal phases.  $S_1$  is the local, linearly-polarized signal lying in the horizontal/vertical plane while  $S_2$  gives the strength of the signal component that is linearly-polarized in the skew planes at  $45^\circ/135^\circ$ . Finally,  $S_3$  measures the strength of the component with perfect circular polarization. The local value of the linear degree of polarization (the quantity that is actually measured in the FERMI studies discussed in the next section)  $P_{LIN} = \sqrt{S_1^2 + S_2^2}/S_0$ . The area integral of  $S_0$  is proportional to the total power  $P_{TOT}$  of the two polarized beams while that of  $S_1$  directly scales as  $P_H - P_V$ . The area integrals of  $S_2$  and  $S_3$  depend upon the details of their spatial overlap and relative phase at the measurement point. For the remainder of this discussion, we presume that the two sources are time-steady, monochromatic, exactly orthogonal, and define the horizontal and vertical planes.

Because the polarization measurements (see §III) are made in a "global" sense (here global refers to the total area

\* This work was funded by the FERMI project of Elettra- Sincrotrone Trieste, supported in part by the Italian Ministry of University and Research under grants FIRB-RBAP045JF2 and FIRB-RBAP06AWK3

<sup>†</sup> william.fawley@elettra.eu

# TECHNICAL OVERVIEW OF BUNCH COMPRESSOR SYSTEM FOR PAL XFEL

H.G. Lee, D.H. Na, S.B. Lee, B.G. Oh, Y.J. Suh, H.S. Suh, Y.G. Jung, D.E. Kim, K.H. Park,  
H.S. Kang, K.W. Kim  
Pohang Accelerator Laboratory, POSTECH, KOREA

## Abstract

Pohang Accelerator Laboratory(PAL) is developing a SASE X-ray Free Electron Laser based on 10 GeV linear accelerator. Bunch compressor (BC) systems are developed to be used for the linear accelerator tunnel. It consists of three(BC1, BC2, BC3\_H) hard X-ray line and one(BC3\_S) soft X-ray line. BC systems are composed of four dipole magnets, three quadrupole magnet, BPM and collimator. The support system is based on an asymmetric four-dipole magnet chicane in which asymmetry and variable  $R_{56}$  can be optimized. This flexibility is achieved by allowing the middle two dipole magnets to move transversely. In this paper, we describe the design of the stages used for precise movement of the bunch compressor magnets and associated diagnostics components.

## INTRODUCTION

A bunch compressor support system has been fabricated and tested for the PAL XFEL. The machine of the PAL XFEL consists of four main sections: the linear accelerator, the hard x-ray undulator hall, the soft x-ray undulator hall and the experimental area. The accelerator, schematically shown in Figure 1, comprises the gun, the laser heater, four accelerating sections groups (L1–L4), four bunch compressors (BC1, BC2, BC3\_H and BC3\_S) and the spreader. The physics design of the magnetic bunch compressor is based on an asymmetric four-dipole chicane configuration [1]. The BC purpose is to reduce the electron bunch length, thus increasing the peak current, taking advantage of the beam correlated energy spread. Due to the accelerating process, there is an inherent longitudinal energy spread in the electron bunch. Passing through four bending magnets chicane, the path length is energy dependent and the electron bunch is compressed. At each bend, the electron bunch head delays with respect to the tail. Mounting high homogeneity magnetic field dipoles and having diagnostic devices centre on the beam at each chicane position are the main advantages of the movable chicane.

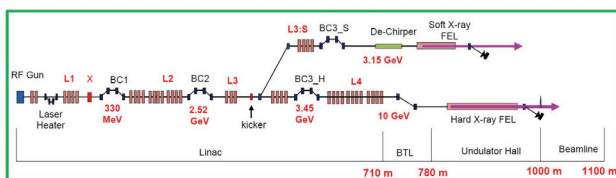


Figure 1: The schematic layout of the 3-BC lattice.

## BUNCH COMPRESSOR OVERVIEW

The BC support system, shown in Figure 2 and Table 1, consist of four dipole magnets (DM), two tweak quadrupole magnets and a skew quadrupole magnet, two corrector magnets, BPM, collimator, screen and CSR monitor. The position of such diagnostic devices remains fixed with respect to the central dipoles.

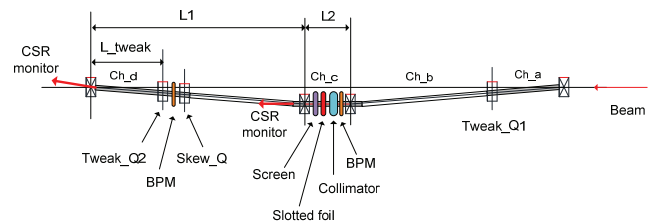


Figure 2: Layout of the BC support system.

Table 1: Major Parameters of the BC Support System

	BC1	BC2	BC3_H	BC3_S
Dipole angle , deg	4.9	3.0	1.7	1.7
Dipole length , m	0.2	0.7	0.7	0.7
L1 , m	4.4845	7.1905	7.597	6.397
L2 , m	1.2	1.8	1.8	1.8
L tweak , m	1.146	1.3483	2.349	1.349
Aperture diameter of Tweak Quad , mm	44 (Q11)	44 (Q11)	44 (Q11)	44 (Q11)

The support systems of BC are composed of two fixed support and a moving support. The two central dipoles are mounted on a moving support that can have up to 627.0 mm motion orthogonal to the beam axis. A servo motor provides movement to the central stage and a linear encoder controls its exact position. The position accuracy of dipoles is within 50  $\mu$ m.

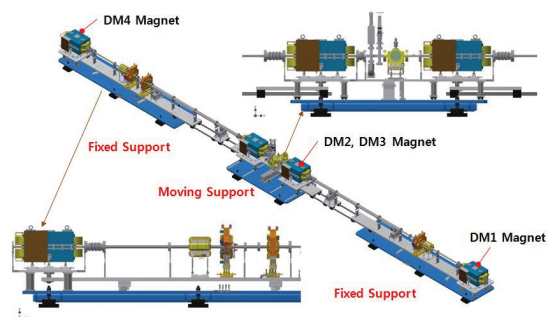


Figure 3: 3D modelling of BC support system.

The chicane is symmetric (DM1–DM2 distance is equal to DM3–DM4 distance). Tweak Q1 (Q2) is placed between DM1 (DM3) and DM2 (DM4). The quadrupole

## DESIGN CHALLENGE AND STRATEGY FOR THE LCLS-II HIGH REPETITION RATE X-RAY FEL PHOTON STOPPERS\*

J. Krzywinski, J. T. Delor, P. A. Montanez, E. Ortiz, M. Rowen, T. O. Raubenheimer, Y. Feng<sup>#</sup>,  
SLAC, Menlo Park, CA 94025, USA

### Abstract

The unique combination of the extremely high single-pulse peak fluence and the enormous average power density of the high repetition rate X-ray FEL's such as the future LCLS-II presents tremendous technical challenges to design, implementation, and operation of the photon stoppers. We have carried out finite-element-analysis studies of potential working designs including water-cooled normal-incidence CVD diamond and water-cooled grazing-incidence B<sub>4</sub>C constructions to verify the validity of these concepts, in terms of remaining below the safe limits of melting or mechanical failure from fatigue. The CVD diamond design is new, novel, and compact, but bears the risk of not having been experimentally tested; whereas the B<sub>4</sub>C approach is less practical due to a very small incidence angle required for sufficiently reducing the power density to not to melt. It was also shown that analytical methods for calculating the temperature distribution are reasonably accurate and can provide, for simple design geometries, immediate design guidance without often time-consuming numerical simulations.

### INTRODUCTION

The X-ray beam properties of the LCLS-II high repetition rate Free-Electron Laser (FEL) present both conceptual and implementation challenges to developing insertable devices that will stop such a beam securely and reliably. Existing stopper designs currently deployed on LCLS-I operating at a repetition rate of only 120 Hz will not work for LCLS-II which produces similar single pulse energies but with a maximum repetition rate up to 1 MHz; an nearly four orders of magnitude increase. The unique combination of the extremely high peak fluence and the enormous average power density for even an unfocused beam, unprecedented at existing third generation synchrotron sources or the current fourth generation low repetition rate X-ray FEL's, requires new solutions.

In this report we explore some of the possible solutions that can push the limits of the allowable average and peak power beyond what were considered up until now. As a starting point we set the requirement that the stopper should be able to stop/absorb a beam with an average power of up to 200 W and maximum credible single-pulse energy from 2 to 10 mJ [1]. The specific beam parameters considered were: 100 kHz, 2 mJ and 20 - 50 fs long pulses over the X-ray energy range of 0.2 to 5 keV, producing an average power of 200 W. The authors have not identified a solution for stopping a beam at a kW level

average power at the writing of this paper.

The combination of an enormous average incident power density (W/cm<sup>2</sup>) and an extremely high peak fluence (J/cm<sup>2</sup> per pulse) suggests that the ideal material for stopping such X-ray beams should have both high thermal conductivity and low-Z number; a low-Z material is needed to avoid instantaneous damage. While there are several materials that can be considered, the most compelling candidate is the chemical-vapor-deposition (CVD) diamond that possesses exceptional high thermal conductivity. However we also recognize that there is a potential risk that diamond has not been tested with respect to the instantaneous damage limit (usually specified in the unit of eV/atom), especially under high repetition conditions when other factors such as the cyclical thermal fatigue, phase transitions, and chemical stability are to be considered. A further challenge is the operation at or near the carbon K-edge where the X-ray absorption length decreases dramatically, thus creating very high instantaneous radiation dosage. This instantaneous damage problem can be possibly mitigated by coating the CVD diamond by a thin layer of also low-Z material B<sub>4</sub>C, which is better damage-resistant but has a poor thermal conductivity. The results of this study are described in section 2.

We have also investigated the possibility of using B<sub>4</sub>C-based stoppers at a grazing incidence to alleviate potential issues because of its low thermal conductivity. It has been proven that the LCLS B<sub>4</sub>C-based stoppers can effectively handle the FEL peak fluence, but the relatively poor thermal conductivity of B<sub>4</sub>C (~ 30 W/m·K at room temperature) raises a serious question of whether such a material can be used as stoppers for high power density beams. We have thus explored solutions using grazing incidence conditions where the power is spread over a sufficiently large area. Grazing incidence copper-based stoppers have been successfully used at synchrotron sources to stop many kilowatts X-ray beams, and grazing incidence B<sub>4</sub>C-based stoppers are also being planned for at the European XFEL facility. We sought to answer the question of how the maximum allowable average power density depends on the angle of incidence. The results of this study are given in section 3. The conclusions of these studies together with some comparisons are presented in section 4.

### CVD DIAMOND BASED STOPPERS

CVD diamond has an excellent thermal conductivity, almost two orders of magnitude higher than that of B<sub>4</sub>C at room temperatures and above. Therefore, one could expect it to work at normal incidence. Two cases were

\*Work supported by DOE under Contract #. DE-AC02-76SF00515.  
<sup>#</sup>yfeng@slac.stanford.edu

# THE HIGHLY ADJUSTABLE MAGNET UNDULATOR

M. Hamberg, Uppsala University, Uppsala, Sweden

## Abstract

The highly adjustable magnet undulator is a concept aiming for flexibility and extensive tunability of undulator settings in the linear as well as the helical regime. I report about suggested layout, magnetic simulations.

## INTRODUCTION

Insertion devices such as undulators play an important role in accelerator physics in synchrotron storage rings as well as free electron lasers. Typical use is for creating photon radiation used for various investigations in medicine, biology, crystallography, chemistry, physics and other scientific areas. It can also be used for charged particle beam manipulation together with or without external radiation sources in order to manipulate the particle beam in various ways such in HGHG, EEHG and ORS setups.

The undulators used today are typically limited by their flexibility. This includes having a fixed undulator period, limited tapering options, inability to be quasiperiodically tuned and more. To overcome these limitations I present an idea of a highly adjustable magnet (HAM) undulator.

## UNDULATOR CONCEPT

In the HAM-undulator, magnets are mounted in stacked rotating discs. Each disc comprises a magnet-couple, or magnetic structure pair, where their separations towards each other and the beamline can be adjusted independently. A center cross section view of three discs (in a real undulator many more discs will be implemented), and a front view are depicted in Fig. 1. The electron beam will travel through the center hole of the setup in which a vacuum pipe is implemented.

The system is modular and based on that each disc is identically constructed and then stacked in front of each other and secured in undulator end-plates on each side of the disc stack providing rigid reference surfaces. The full disc setup structure comprising the undulator end-plates and the disc stack can be secured on to a girder.

Since the magnet couples are built into a rotating disc the rotation around the beam axis can be adjusted arbitrary compared to the other discs. Furthermore, depending on the rotation angle between each disc, the helical angle can be changed. Additionally tapering of the magnetic field can be achieved in longitudinal and transversal direction. Tapering effects can also be achieved for helical cases.

The permanent magnet structures are connected to the rotation disc via adjustment means, so that the position of one magnet can be adjusted relative the other permanent magnet structure in the magnet pair. The adjustment means could be arranged to both adjust position of the magnet and to tilt the magnet relative a thought normal to

the electron beam. This allow for transverse tapering of the undulator. Longitudinal tapering is achieved by for each disc decrease (or increase) the permanent magnet structure pair separation slightly throughout the undulator.

Each magnet structures in the structure pair could be made up as a simple transverse triple combination of directed permanent magnets to amplify the magnetic flux at the beam position. To alleviate the effect from magnet forces a thin layer of magnet material in longitudinal direction may be added on each magnet structure.

The undulator setup can be controlled by a standard PLC system. Due to the inherent construction no shimming is necessary.

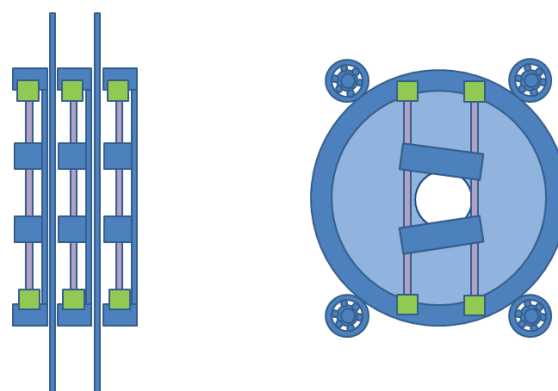


Figure 1: Left: Centre cross section view of three discs (in a real undulator many more discs will be implemented). Right: Front view of one disc with the magnet structure pair on each side of the centre hole.

## EXAMPLE OF USAGE AND BENIFITS

Due to the flexibility of the construction one undulator can be used for many purposes.

- Linearly polarized light can be produced when the magnet couples are aligned with interchanging magnetic field of each disc (up down up etc.).
- Linearly polarized light of longer wavelengths can be produced by pairing rotating discs, as schematically illustrated in Fig. 2 (figure seen from side view with electron beam in centre).
- Circularly polarized light can be produced when the discs are rotated such that an additional rotation angle of up to 90 degrees is implemented for each passed dic, as schematically illustrated in Fig. 3, where figure is depicted from front with electron beam in center. In the figure the rotation angle is called alpha and four magnet structure pairs are implemented.
- Combinations of disc rotations can be implemented aiming for producing light with e.g. two

# BEAM DYNAMICS SIMULATION FOR THE UPGRADED PITZ PHOTO INJECTOR APPLYING VARIOUS PHOTOCATHODE LASER PULSES

Mahmoud Bakr<sup>#</sup>, G. Vashchenko, M. Khojayan<sup>\*</sup>, M. Krasilnikov, F. Stephan  
DESY Zeuthen 17538, Germany

## Abstract

Production of electron bunches with extremely small transverse emittance is the focus of the PITZ (Photo Injector Test facility at DESY in Zeuthen) scientific program. PITZ is one of the leading laboratories on generation and optimization of high brightness electron bunches with different charges for free electron laser (FEL) machines such as FLASH and the European XFEL. In 2011 using a photocathode laser with a flattop temporal profile, PITZ has revealed record low transverse properties emittance values at different bunch charges. However, further improvement of beam quality with smaller emittance is foreseen using a cathode laser system, capable of producing 3D ellipsoidal bunches. Numerical simulations were performed to study and compare the beam dynamics of electron beams produced with 3D ellipsoidal and flattop laser profiles. Different bunch charges from 20 pC up to 4 nC are considered in the simulation, in order to find an optimum PITZ machine setup which yields the lowest transverse emittance. In the present paper, the simulation setup, conditions, and results of the comparison are presented and discussed.

## INTRODUCTION

The handiness of a high brightness electron source is one of the key issues for successful operation of linac-based free electron lasers like, FLASH [1] and the European XFEL [2]. The self-amplified spontaneous emission (SASE) of the FELs process requires an extremely high space charge density of the radiating electron bunches implying high peak current, low energy spread and small transverse emittance of the electron beam. Such high quality beams are mandatory for efficient SASE generation in a single pass through long undulators with narrow gaps [3]. However, the above-mentioned properties are hard to be improved in a linac and thus the emittance has to be minimized already in the photocathode injector.

The Photo Injector Test facility at DESY, Zeuthen site (PITZ), aims to produce electron bunches with extremely small transverse emittance. A flattop temporal profile of the cylindrical pulses has been used at PITZ to reduce the transverse emittance of space charge dominated beams compared to the Gaussian pulse shape previously used [4]. The lower beam emittances reported from PITZ were obtained with a flattop temporal laser profile from Cs<sub>2</sub>Te cathodes. The photocathode laser pulse shaping is considered as a powerful tool to optimize the photo injector per-

formance. Thus, a further improvement is foreseen from the cathode laser pulse shaping. The overall brightness of a photo injector can be further improved by using an ideal electron bunch profile, which, according to simulations, is 3D ellipsoidal (hereinafter ellipsoidal) in space and time [5]. Because of the fact that the space charge force fields inside the bunch are linear, the ellipsoidal beam distribution is an ideal beam distribution for high brightness charged beam applications with the best transverse and longitudinal bunch compression. Such electron bunches not only have lower emittance, but are also less sensitive to jitter of machine parameters, thus allowing more stable and reliable operation, which is a key requirement for SASE-FELs facilities like FLASH and the European XFEL.

Simulations have been performed at PITZ to study the feasibility of using an ellipsoidal laser shape instead of flattop and Gaussian laser profiles [6]. The results have revealed a better injector performance when using the ellipsoidal laser profile. Further improvement was expected when shifting the second accelerating cavity (CDS booster) and the first emittance measurement screen (EMSY1) by ~40 cm upstream. Moreover, simulations for the imperfections of the ellipsoidal laser shape for 1 nC showed that the transverse emittance value is still smaller than the optimized emittance value for the flattop laser shape [7]. Recently, a new photocathode laser system capable of producing ellipsoidal pulses has been installed at PITZ [8]. It is foreseen to operate the new system in parallel to the nominal one that generates cylindrical pulses with various temporal profiles. First electrons were already generated by the new laser system; however, emittance measurements are not yet performed.

A schematic layout of the current PITZ setup is shown in Fig. 1. The PITZ photocathode RF gun delivers electron bunches up to several nC with a maximum mean momentum of up to 7 MeV/c generated from a Cs<sub>2</sub>Te cathode. The gun is surrounded by two solenoids: main and bucking. The main solenoid is used for the transverse beam focusing, while the bucking solenoid is meant to compensate the remaining longitudinal magnetic field at the cathode. The final maximum momentum after the booster is up to 25 MeV/c. The transverse emittance of the electron beam is measured by the emittance measurement system, (EMSY1 located at 5.27 m downstream the cathode), using a single slit scan technique [9]. Additionally, there are many diagnostics devices available for the full characterization of electron beams. A detailed description of the PITZ setup can be found elsewhere [10].

The aim of this contribution is to check the feasibility of using the ellipsoidal laser beams in comparison to the flattop shaped pulses by means of the lowest transverse

<sup>#</sup> On leave from: Physics Department, Assiut University, Assiut 71516, Egypt, [mahmoud.bakr@desy.de](mailto:mahmoud.bakr@desy.de).

<sup>\*</sup>Now working in LOLA lab France

# BENCHMARK OF ELEGANT AND IMPACT \*

L. Wang<sup>#</sup>, P. Emma and T. Raubenheimer SLAC, Stanford, CA 94309, USA  
 J. Qiang, LBNL, Berkeley, CA 94720, USA

## Abstract

The beam dynamics codes ELEGANT and IMPACT have many users. We use these two codes for the design of LCLSII. Both codes use a 1D model for the coherent synchrotron radiation (CSR) in bend magnets. In addition, IMPACT has a 3D space-charge model, while ELEGANT uses a 1D model. To compare the two codes, especially the space-charge effects, we systematically benchmark the two codes with different physics aspects: wakefields, CSR and space-charge forces.

## INTRODUCTION

The new LCLS-II high-repetition rate FEL project at SLAC [1] will use a new superconducting linac composed of TESLA-like RF cavities in continuous wave (CW) operation, in order to accelerate a 1-MHz electron beam to 4 GeV. Fig. 1 shows the optics of the hard x-ray beam of LCLS-II linac. The new superconducting linac is driven by a new high-rate injector [2], will replace the existing SLAC copper linac in sectors 1-7 (101.6 m/sector), while the remaining Cu RF structures in sectors 7-10 will be removed and replaced with a simple beam pipe and focusing lattice (the “linac extension”). The existing 2-km PEP-II bypass line (large  $\beta$  section in Fig. 1) will be modified to transport electrons from the linac extension in sector 10 through more than 2.5 km and into either of two undulators in the existing LCLS undulator hall. The overall design of the linac can be found in [3].

We use both ELEGANT and IMPACT codes for the LCLS-II design. The main difference in term of physics included is the space charge: ELEGANT uses 1D longitudinal space charge (LSC) model while IMPACT has 3D model. The long pass beamline at LCLS-II makes the space charge effect stronger compared to LCLS and the beam energy of LCLSII is low. Therefore strong micro-bunching instability is expected. Recently, it is found that the transverse space charge is also important and can add addition energy modulation to the beam [4]. Therefore it is important to check the impact of 3D space charge model compared to the 1D LSC model.

In this benchmark we use LCLS-II Hard X-ray linac as shown in Fig 1. The initial beam energy is 100 MeV and has an ideal Gaussian distribution in longitudinal direction with *rms* beam size of 1.0 mm and energy spread of 1 keV. The uncorrelated energy spread is increased downstream by using a 6 keV laser heater. The bunch charge is 100 pC. The particles are tracked through LCLS-II linac to the beginning of the undulator. We did step-by-step comparisons: first step for pure optics, all

collective effects are turned off. Then the wakefields, CSR and space charge are added one-by-one.

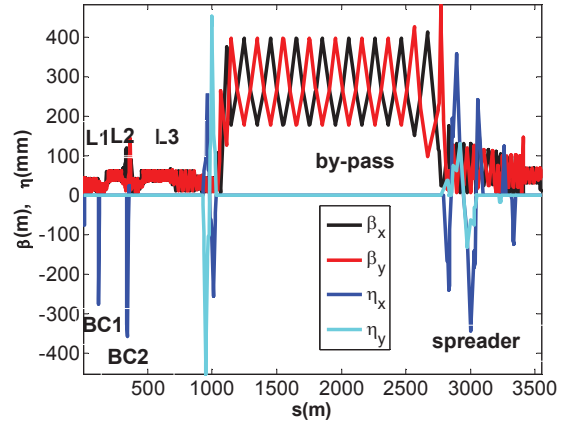


Figure 1: Optics (HXR) of the LCLS-II linac.

## PURE OPTICS

To compare different collective effects, it is important to study a case when all collective effects are turned off. This means the wake fields (geometric wake of rf linac and resistive wall wake of the beam pipe), CSR and space charge are not included. The main parameters of the linac set-up are: the rf phase at L1, linearizer and L2 are  $-12.7^\circ$ ,  $-150^\circ$  and  $-15.5^\circ$ , respectively.

Figure 2 shows the phase space and the current profile before the undulator. There is an excellent agreement between both codes as expected. The peak current is about 1 kA with single spike. If the simulation starts with real injector beam, the final beam usually is flat at core of the beam with double horns at head and tail of the bunch. The beam energies are 250 MeV and 1.647 GeV at BC1 and BC2, respectively. Note that the BC2 beam energy in nominal design is 1.6 GeV. We use slight different beam energy here.

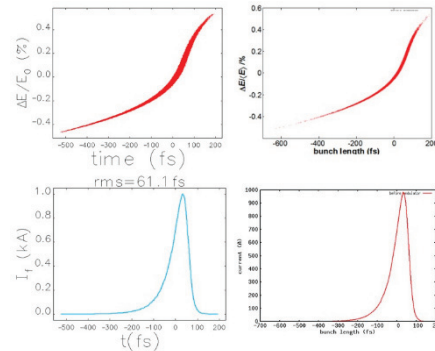


Figure 2: Longitudinal phase space (top) and current profile (bottom) at the beginning of undulator without collective effects from ELEGANT (left) and IMPACT (right).

\*Work supported by Department of Energy Contract No. DE-AC02-76SF00515  
<sup>#</sup>wanglf@SLAC.stanford.edu

## EFFECT OF HOT IONS AT LCLS-II\*

L. Wang<sup>#</sup>, T. O. Raubenheimer, SLAC, Stanford, CA 94309, USA

## Abstract

The ions in a linac with high repetition rate, such as ERL, draw more attention recently. LCLS-II has a long linac with 1 MHz repetition rate. The ions, in general, are not deeply trapped due to the long bunch spacing. The effect of ion thermal energy becomes important in this regime. The beam dynamics with ions are studied both theoretically and numerically. There is a linear growth in amplitude, instead of exponential growth as traditional fast ion instability. This linear growth set a maximum bunch-train length to limit the beam amplitude to fractional beam sigma. We also extend our works to different regimes where the motions of ions from stable to partially stable.

## INTRODUCTION

The new LCLS-II high-repetition rate FEL project at SLAC [1] will use a new superconducting linac composed of TESLA-like RF cavities in continuous wave (CW) operation, in order to accelerate a 1-MHz electron beam to 4 GeV. Figure 1 shows the optics (top) of the hard x-ray beam and the beam size (100 pC) of LCLS-II linac (bottom). The new superconducting linac is driven by a new high-rate injector [2], will replace the existing SLAC copper linac in sectors 1-7 (101.6 m/sector), while the remaining Cu RF structures in sectors 7-10 will be removed and replaced with a simple beam pipe and focusing lattice (the “linac extension”). The existing 2 km PEP-II bypass line (large  $\beta$  section in Fig. 1) will be modified to transport electrons from the linac extension in sector 10 through more than 2.5 km and into either of two undulators in the existing LCLS undulator hall. The overall design of the linac can be found in [3].

There is a low temperature ( $\sim 2\text{K}$ ) for the superconducting linac (L1, L2, L3 in Fig. 1), while the rest linac has room temperature ( $\sim 300\text{K}$ ) with a thermal energy about  $0.04\text{eV}$ . In most storage ring light source, the beam potential is much large than  $1\text{eV}$ , for instance  $100\text{eV}$  for SPEAR3 beam. Therefore, the thermal energy of the ion can be safely neglected. In LCLS-II, the beam is small and the bunch spacing is long where the thermal energy is comparable and even larger than the beam potential. In this case, the thermal energy should be included. The effective ion size with the thermal energy effect can be estimated as

$$\sigma_i^2 \approx \frac{\sigma_e^2}{2} + \frac{v_0^2}{2\omega^2} = \alpha^2 \sigma_e^2, \quad (1)$$

where  $\sigma_e$  is the electron beam size,  $v_0$  is the ion speed at the thermal energy. When the thermal energy is negli-

gible, the ion size is about  $1/\sqrt{2}$  times of the electron beam size.

This paper is organized as the following: section II presents the detail simulations and section III introduces our theoretical model to explain the feature of the simulations.

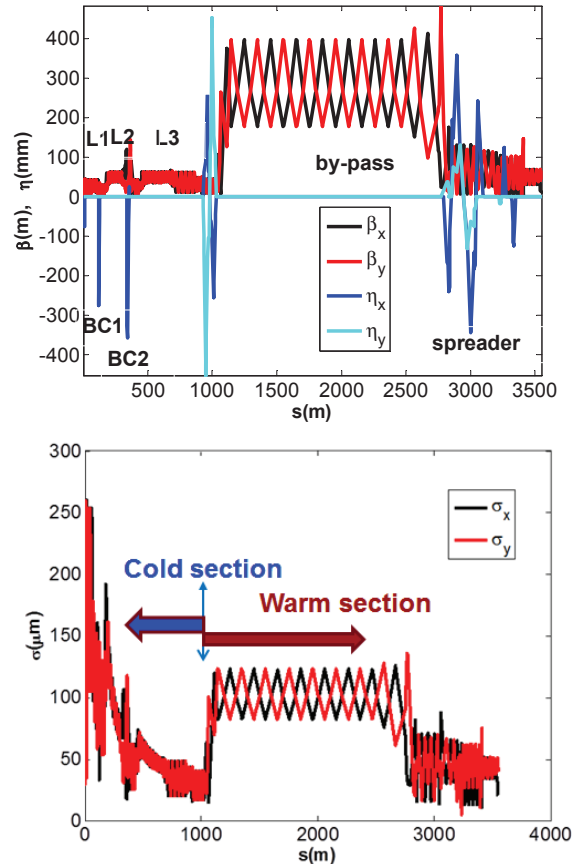


Figure 1: Optics (HXR) (top) and beam size (100 pC, bottom) of the LCLS-II linac.

## SIMULATION

Simulations have a number of advantages: the non-linearity of the ion-cloud force is automatically included; the effects of beam optics and bunch-train with arbitrary beam filling pattern can be easily handled; a realistic vacuum model with multi-gas species is straightforward in simulation. A Particle in Cell (PIC) code based on a wake-strong model is used here [4].

The temperature is set to 10 K and 300K in the superconducting linac and warm section, respectively. In simulation we use multiple gases vacuum model [H2 (90%), H2O (1%), CO2 (1%), CO (7%) and CH4 (1%)]. We will use this vacuum component through this paper. The total vacuum pressure of 1 nTorr and 10 nTorr are assumed for the cold and warm section, respectively. The real vacuum should be better.

\*Work supported by Department of Energy Contract No. DE-AC02-76SF00515

<sup>#</sup>wanglf@SLAC.stanford.edu

# ELECTRON BEAM PHASE SPACE TOMOGRAPHIE AT THE EUROPEAN XFEL INJECTOR

M. Scholz\*, B. Beutner, DESY, Hamburg, Germany

## Abstract

Transverse emittances as well as the energy spread and the peak current of the electron bunches are important parameters for high-gain free electron lasers such as the European XFEL. Investigations of the 6D phase space characterization would give important indications to optimize the beam quality for SASE operation. The injector of the European XFEL includes, inter alia, a laser heater, a transverse deflecting cavity (TDS), a spectrometer, a diagnostic section with four screens as well as several quadrupole magnets. In this paper, we will discuss the possibilities to characterize the 6D phase space of the electron beam in the injector of the European XFEL.

## INTRODUCTION

Crucial electron beam parameters like the minimum slice and projected emittances as well as the minimum energy spread are defined by the injector system. SASE FELs like the European XFEL [1] depend strongly on the emittance and the energy spread, thus it is significant to investigate and optimize these parameters. A reconstruction of the two transverse phase spaces, preferably time resolved, and of the longitudinal phase space will be of use to accomplish this task.

A separate beam dump at the end of the European XFEL injector and a concrete shielding wall between the injector and the subsequent machine components allow to start the injector commissioning while the linac is still under construction.

In this paper we study the possibilities to use the XFEL injector components for measurements that are required to reconstruct the transverse and longitudinal phase spaces of the electron beam.

## EUROPEAN XFEL INJECTOR

A schematic layout of the European XFEL injector is presented in the upper part of Fig. 1. Two superconducting accelerating modules are installed in the linac, a 1.3 GHz module and a third harmonic module to linearize the longitudinal phase space of the particle distributions. The beam energy downstream these modules is 130 MeV.

A subsequent diagnostic section including a transverse deflecting cavity as well as four screens [2] and a spectrometer allow to study the electron beam quality. The TDS installed in the XFEL injector is a 16 cell traveling wave S-band RF waveguide structure operating with a frequency of 2.997 GHz [3]. The streak is applied in the vertical plane. A following periodic FODO section is designed such that the

betatron phase advances between the TDS and the screens are optimized for emittance and bunch length measurements. Figure 1 shows the default beta functions in the XFEL injector from the electron gun to the injector dump.

Four fast kickers can deflect single bunches out of a long bunch train such that one bunch can be observed on each screen. That makes it possible to measure electron beam optics and emittances online during SASE operation. The screens can also be moved into the electron beam so that the measurements can take place without kickers.

The default beam optics in the injector was not designed to measure the slice emittances with quadrupole scans as required for the reconstruction of the transverse phase spaces. Several special beam optics that fulfill the requirements and that can be realized with the available beam optics elements had to be developed.

## TOMOGRAPHY

The tomography technique [4] allows to reconstruct an inner structure using cross sections of the volume taken from different viewing angles. The reconstruction of an electron beam's transverse phase space can be obtained with several projections of the particle distribution while the beam rotates in the respective phase space [5]. The latter can be achieved with a scan of the betatron phase  $\phi_x$  respectively  $\phi_y$  using quadrupole magnets between an optics reference point and a screen where the measurements take place. The optics reference point is the position where the Twiss functions and the emittance will be reconstructed. The range of the phase scan  $\Delta\phi_{i, \text{ref} \rightarrow \text{screen}}$  has to be about 180 deg [6]. The number of required projections depends on the reconstruction algorithm. More projections will lead to a better reconstruction result. We decided to apply the maximum entropy (MENT) algorithm [7] that requires a comparatively small number of measurement steps. However, a fixed electron beam optics and a measurement with the four screens in the diagnostic section is not sufficient. The four steps that can be achieved with these screens are not enough for the tomographic reconstruction. For this reason, a phase scan with quadrupoles, in steps of 10 degree phase advance, will be used. The beam will be observed on the last screen upstream the spectrometer magnet.

All beam optics calculations were carried out using the optimization and tracking code elegant [8].

## Horizontal Phase Space

The injector TDS enables horizontal slice emittance measurements. This makes it possible to reconstruct the horizontal phase space of single bunch slices. The use of the TDS entails additional constraints on beam optics. The vertical

\* matthias.scholz@desy.de

# THz BASED PHASE-SPACE MANIPULATION IN A GUIDED IFEL\*

E. Curry<sup>†</sup>, S. Fabbri, P. Musumeci, UCLA, Los Angeles, CA 90049, USA  
A. Gover, Tel-Aviv University, Tel-Aviv 69978, Israel

## Abstract

We propose a guided IFEL interaction driven by a broadband THz source to compress a relativistic electron bunch and synchronize it with an external laser pulse. A high field single-cycle THz pulse is group velocity-matched to the electron bunch inside a waveguide, allowing for a sustained interaction in a magnetic undulator. The THz pulse is generated via optical rectification from the external laser source, with a measured peak field of up to 4.6 MV/m. We present measurements of the THz waveform before and after a parallel plate waveguide with varying aperture size and estimate the group velocity. We also present results from a preliminary 1-D multi-frequency simulation code we are developing to model the guided broadband IFEL interaction. Given a 6 MeV, 100 fs electron bunch with an initial  $10^{-3}$  energy spread, as can be readily produced at the UCLA PEGASUS laboratory, the simulations predict a phase space rotation of the bunch distribution that will reduce the initial timing jitter and compress the electron bunch by nearly an order of magnitude.

## INTRODUCTION

As the development of THz sources pushes towards higher power, the pursuit of THz applications in accelerator physics has become an active field of research. In addition to the unique advantages of THz radiation for imaging and spectroscopy [1], the THz frequency range offers a middle ground in beam manipulation between the high-acceleration-gradient of laser wavelengths and the broad phase-acceptance window of RF. The transverse kick imparted to an electron bunch in an X-band RF deflector, like the one used for temporal diagnostics at LCLS [2], could be accomplished by a THz field that is over fifty times smaller. The higher frequency of THz relative to RF may also allow for improvement of the breakdown limitations in an accelerating structure [3]. Where laser coupling in a typical FEL results in microbunching of the electron beam, an FEL interaction with THz radiation could capture and compress the entire bunch within a single ponderomotive bucket.

At the UCLA PEGASUS laboratory, we intend to demonstrate the compression of a 1 pC electron bunch using ponderomotive coupling with a THz pulse. A single Ti:Sapph laser source will be used to generate THz through optical rectification while simultaneously driving a 1.6 cell S-band photogun. The ponderomotive force produced by the THz and undulator fields gives the electron bunch an energy chirp, resulting in longitudinal compression after a drift section.

\* Work supported by DOE grant DE-FG02-92ER40693 and NSF grant PHY-1415583.

<sup>†</sup> ecurry@physics.ucla.edu

The THz pulse is synchronized with the external laser pulse. When the phase of the ponderomotive bucket is centered on the average arrival time of the electron bunches, the induced energy chirp works to accelerate late bunches and decelerate early bunches towards the optimal timing, compensating for the inherent time-of-arrival jitter that accrues over the course of the initial electron bunch acceleration.

## ZERO-SLIPPAGE IFEL

The resonance condition of a standard inverse free electron laser (IFEL) assumes slippage between the electron bunch and the laser waveform to maintain a phase synchronism condition as they propagate in free-space. For the single-cycle THz pulse produced by optical rectification, an interaction can be sustained by satisfying a "zero-slippage" condition, or grazing dispersion curve condition, in which the THz group velocity is matched to the average longitudinal speed of the electron bunch [4][5], in addition to satisfying the phase synchronism condition. This velocity-matching occurs when the dispersion curves for the waveguide and electron beam, shown in Fig. 1, have the same slopes. The control of THz pulse group velocity can be accomplished by a waveguide. This technique has the added benefit of preserving the on-axis field intensity over the length of the guide rather than operating in the diffraction limited regime.

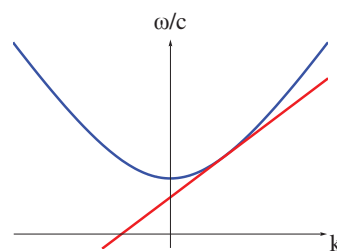


Figure 1: The dispersion curves for a waveguide (blue) and electron beam (red). The "zero-slippage" condition occurs when their slopes, corresponding to radiation group velocity and average longitudinal bunch velocity, are equal.

The THz frequency range is an ideal candidate for this guided IFEL technique. Although higher frequencies can offer a larger acceleration gradient, the size of the guiding structures becomes prohibitively difficult for co-propagation of electrons and laser. The length scales necessary for a THz guiding structure are large enough to permit alignment of the electron beam and accommodate the oscillating trajectory of the electrons in an IFEL without clipping. For reasonably low charge, wakefield effects in the guiding structure are negligible.

## ENERGY JITTER MINIMIZATION AT LCLS\*

Lanfa Wang<sup>#</sup>, Timothy Maxwell, Franz-Josef Decker, Andrew Benwell, Axel Brachmann, Anatoly Krasnykh, Zhiron Huang, James Turner, William Colocho, Tang Tao  
SLAC, Stanford, CA 94309, USA

### Abstract

The energy jitter of the electron beam affects FELs in self-seeded modes if the jitter is large compared to the FEL parameter, effectively reducing the average brightness when shots are seeded off-energy. We work in multiple ways to reduce jitter, including hardware improvement and optimizing linac set-up. Experiments demonstrated better than 20% and 40% relative energy jitter reduction for 13.6 and 4 GeV linac operation, respectively. This paper discusses the global optimization of linac set-up using Multi-Objective Genetic Algorithm (MOGA). The solutions always suggest that we can largely reduce the energy jitter from a weak compression at BC1 and a stronger compression at BC2. Meanwhile low beam energy at BC2 also reduces the energy jitter, which is confirmed by the experiment.

### INTRODUCTION

The impact of energy jitter on self-seeded FELs is understood by considering the flux transmitted through an X-ray monochromator. Assuming SASE with Gaussian bandwidth  $\sigma_{\text{SASE}}$  incident on a monochromator, the ratio  $F$  of off-energy transmitted X-ray flux to on-energy flux due to *rms* electron relative energy jitter  $\sigma_e$  is given by

$$F(\sigma_e) = \frac{\sigma_{\text{SASE}}}{\sqrt{\sigma_{\text{SASE}}^2 + 4\sigma_e^2}}. \quad (1)$$

For self-seeding, this implies the average available seed power degrades unless  $\sigma_e \ll \sigma_{\text{SASE}} / 2$ . Should sufficient undulator length be available to reach post-saturation, slightly weaker seed intensities can in principle be stabilized to near-nominal in post-mono amplification. In this way, self-seeding can be slightly more robust against energy jitter vs. direct SASE filtering alone.

Figure 1 illustrates this energy dependence during the 2014 development of soft X-ray self-seeding (SXRSS) at the LCLS [1] at 540 eV. The fraction of X-ray power within twice the self-seeded bandwidth plotted as a function of  $\delta e$  shows the 0.12% rms energy jitter yields a 50% reduction of the average narrow-band X-ray intensity (0.1 vs. 0.2 mJ). Therefore, improving linac energy stability has the potential double the average spectral brightness achievable by SXRSS.

Over the years the beam stability and jitter have been investigated [2-7] to study and identify jitter sources and improve stability of the LCLS. Over recent years, a group

of experts worked together to improve the energy jitter, including improving klystron station stability and other hardware, automated data logging, developing online linear models, etc. Experiments demonstrated better than 25% and 40% relative energy jitter reduction for 13.6 and 4 GeV linac operation, respectively, over the past year.

Here we present our global optimization of the linac to reduce the machine energy jitter. The simulation model and the optimized solutions for hard x-ray and soft x-ray beams are discussed in the following sections. Hardware upgrades will be briefly discussed towards the end.

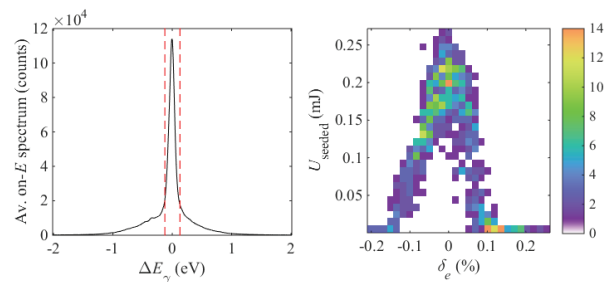


Figure 1: Average on-energy SXRSS spectra and range of fractional integration range (left). 2D histogram of partial pulse intensities  $U_{\text{seeded}}$  as a function of  $\delta_e$  (right).

### JITTER SOURCE AND SIMULATION MODEL

The primary source of the jitter is from the linac rf. The variation of pulse-to-pulse energy and timing jitter accumulates along the linac, each station adding in quadrature, and therefore has a large impact on beam jitter. Timing jitter at an rf station induces energy jitter as

$$\delta E(\varphi_0) = -e\omega_{rf}\hat{V}\sin(\varphi_0)\delta t. \quad (2)$$

Additionally, amplitude fluctuations of rf klystrons along the linac generate an additional term to beam energy jitter as

$$\delta E(\varphi_0) = -e\hat{V}\sin(\varphi_0)\delta\varphi + e\cos(\varphi_0)\delta\hat{V}. \quad (3)$$

The first and secondary term on the left of the equation comes from the phase jitter and voltage jitter, respectively. For off-crest acceleration prior to bunch compression, the dominant contribution of the beam energy jitter is the beam timing/phase jitter at the rf stations as shown in Eq. 2. This timing jitter works similar as the rf phase jitter. Its effective rf phase jitter is

$$\delta\varphi_{rf,eff} = \omega_{rf}\delta t \quad (4)$$

\*Work supported by Department of Energy Contract No. DE-AC02-76SF00515  
#wanglf@SLAC.stanford.edu

## FAST PARTICLE TRACKING CODE\*

L. Wang<sup>#</sup>, SLAC, Stanford, CA 94309, USA*Abstract*

This paper presents a fast particle tracking (FPT) code for linac beam dynamics. It includes wake fields, coherent synchrotron radiation (CSR) and longitudinal space charge. We systematically benchmark the FPT with ELEGANT with different physics aspects: pure optics, wakefields, CSR and space-charge forces.

**MODEL**

The FPT code is originally developed to study the collective effects, including wakefields and CSR. There are two models for CSR: 1D CSR in free space [1] and 2D CSR with resistive wall beam pipe. In the 2D case, the CSR is calculated by another Finite Element Method (FEM) code based on the paraxial equation [2] and input it to FPT. Currently, the transverse collective effect is off. We are able to simply turn on/off different collective effects. These features make the code much fast compared other detail codes, meanwhile it includes the main physics we are interested.

The longitudinal spacing charge (LSC) has been recently added. It includes analytical methods for both round Gaussian and uniform beam model and numerical LSC module. The LSC impedances of a round Gaussian and uniform beam are

$$\frac{z_{||}^{gau,free}(k)}{L} = i \frac{1}{4\pi\epsilon_0} \frac{k}{\gamma^2\beta c} e^{-\frac{k^2\sigma_z^2}{2\gamma^2}} Ei\left(-\frac{k^2\sigma_z^2}{2\gamma^2}\right), \quad (1)$$

$$\frac{z_{||}^{rd,free}(k)}{L} = i \frac{1}{\kappa\pi a^2\epsilon_0\beta c} \left[1 - \frac{\kappa a}{\gamma} K_1\left(\frac{\kappa a}{\gamma}\right)\right]. \quad (2)$$

where  $E_i$  is the exponential integral function and  $K_1$  is the modified Bessel function of the second kind. Note that the LSC impedance of the Gaussian beam can be approximated as the one of uniform beam with  $\sigma = a/\sqrt{2}$  and  $\sigma = a/\sqrt{3}$  at short and long wavelength regime, respectively. But there is no simple approximation at the frequencies near  $\frac{\kappa a}{\gamma} \sim 1$  as shown in Fig. 1. The LSC impedance for arbitrary transverse beam shape with arbitrary beam pipe can be calculated numerically with FEM method [3].

In the following sections we benchmark FPT with ELEGANT with different physics aspects: pure optics, wakefields, CSR and space-charge forces. The collective effects are added step-by-step. In the benchmark we use LCLS-II linac. The initial beam has ideal Gaussian distribution in longitudinal direction with *rms* beam size of 1.0 mm and energy spread of 1.0 keV. The initial beam

energy is 100 MeV. The particles are tracked through the linac and we compare the beam after the second bunch compressor (BC2).

**WITHOUT COLLECTIVE EFFECTS**

To compare different collective effects, it is important to study a case when all collective effects are turned off. This means the wake field, CSR and space charge are not included. The main parameters of the linac set-up are: the rf phase at L1, linearizer and L2 are  $-12.7$ ,  $-150$  and  $-15.5$  degree, respectively. Figure 2 shows the phase space and current profile after BC2. There is an excellent agreement. The beam energies are 250 MeV and 1.60 GeV at BC1 and BC2, respectively. If we increase the energy at BC2 to 1.647 GeV (we use this energy for the rest of comparisons), the peak current reduced to 1.0 kA due to the reduction of relative energy chirper as shown in Fig. 3. There are excellent agreements for both beam energies when the collective effects are turned off.

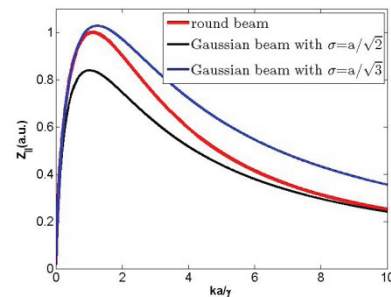


Figure 1: Comparison of the longitudinal space charge impedance of a round uniform and Gaussian beam.

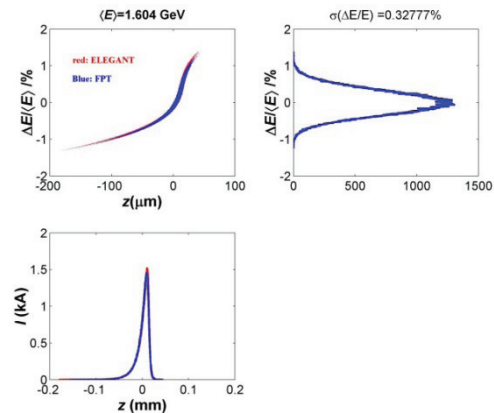


Figure 2: Longitudinal phase space at the end of BC2 without collective effects, beam energy at BC2 is 1.6 GeV. ELEGANT (red); FPT (blue).

\*Work supported by Department of Energy Contract No. DE-AC02-76SF00515

<sup>#</sup>wanglf@SLAC.stanford.edu

# CATHODE ION BOMBARDMENT IN LCLS AND LCLS-II RF GUN\*

L. Wang<sup>#</sup>, A. Brachmann, F. Decker, Z. Li, T.O. Raubenheimer,  
J. Schmerge, F. Zhou, SLAC, Stanford, CA 94309, USA

## Abstract

This paper studies the ions bombardment on the cathode in the LCLS and LCLS-II gun. LCLS operates at a low repetition rate of 120 Hz while LCLS-II will operate at 1 MHz rate. Therefore, it is important to estimate the ion bombardment.

A PIC code is used to track arbitrary particles (ions and electron here) in arbitrary 2D/3D electromagnetic field and solenoid field to estimate the possibility of ion bombardment. The LCLS gun has 1.6 cells while the LCLS-II gun is a quarter wave resonator (LBNL APEX gun) so the frequencies of the two guns are quite different. These characteristics make the ion dynamics quite different. In this paper we estimate the bombardment for various ion species.

## LCLS GUN

The surface analysis of the first LCLS cathode provides evidence for complex hydrocarbon contamination [1]. The trajectory simulation of ions in LCLS gun shows strong possibility of ion back bombardment [2-3]. Here we do the trajectory simulation with one purpose-written code which can accurately model the ion generation (position and timing) and RF pulse. Both RF field and emittance compensation solenoid field are included. Electrons emitted from the cathode enter the rf cavity and move towards the solenoid region while ions are generated along the electrons' path. The electrons move quickly out of the cavity but the ions move much slower. Ions are tracked until they hit the cathode, hit the cavity surface or exit the cavity.

The on-axis electric field and the solenoid field for the LCLS gun are shown in Fig. 1. The cathode is located at the  $z=0$ . The electric field has a peak value at the cathode surface and the center of the full cell with the minimum field located at  $z=3.34$  cm at the iris. Fig. 2 shows the electric fields of the rf gun. When an electron emitted from the cathode surface enters the second cavity, the rf electric field changes direction and the electron continues to accelerate through the second cell. The focusing solenoid is located 20 cm downstream of the cathode with zero field at the cathode. In all simulations, 2D field maps are used for both gun rf and solenoid fields.

The LCLS gun is pulsed at 120 Hz with an rf pulse that has a flat top order of  $1 \mu\text{s}$  duration and decay time approximately  $0.5 \mu\text{s}$  [4]. Electrons are generated at the peak rf pulse and therefore ions are also generated at the peak rf pulse. Since ions move slowly, they see the remaining rf pulse and their dynamics are strongly affected by the decaying pulse. Most ions run away from

the cavity regime or hit the cathode before the next rf pulse.

Table 1 lists the main parameters for the LCLS gun and solenoid. For comparison, the parameters for the LCLS-II gun are also listed. The LCLS gun operates pulsed at 2856 MHz, while the LCLS-II gun is continuous-wave (CW) at a much lower frequency of 187 MHz. The LCLS gun has two cells while the LCLS-II gun is comprised of a single cell. Multiple cells make the ion dynamics much more complicated.

In this study we consider only the ions generated by beam gas ionization. Ions are uniformly generated along the electron beam path ( $z$ -direction) in the simulation. In reality, the beam ionization cross-section varies with beam energy with a large cross-section for low beam energy ranging from  $100\text{eV}$  to  $1\text{MeV}$ . Ions born at different locations will see different initial rf field as shown in Fig. 3.

Table 1: Main Simulation Parameters

Description	LCLS	LCLS-II
rf frequency (MHz)	2856	187
Peak field (MV/m)	140	22
rf phase (degree)	-60	-8
rf Pulse length ( $\mu\text{s}$ )	$\sim 3$	CW
Repetition rate (kHz)	0.12	1000
Solenoid field (T)	0.24	0.04
Beam energy(MeV)	5.9	0.8

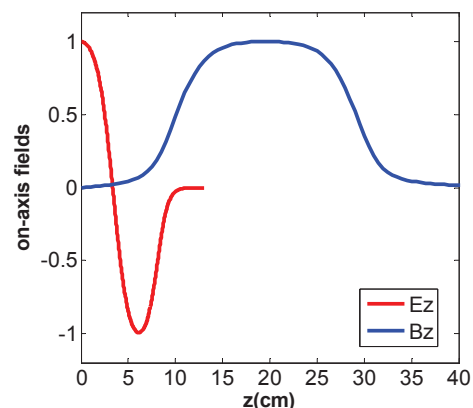


Figure 1: The normalized on-axis gun rf electric field and solenoid field.

\*Work supported by Department of Energy Contract No. DE-AC02-76SF00515

<sup>#</sup>wanglf@SLAC.stanford.edu

# RESULTS FROM THE NOCIBUR EXPERIMENT AT BROOKHAVEN NATIONAL LABORATORY'S ACCELERATOR TEST FACILITY\*

N. Sudar, P. Musumeci, J. Duris, I. Gadjev, Department of Physics and Astronomy, UCLA, Los Angeles, CA 90045, USA

M. Polyanskiy, I. Pogorelsky, C. Swinson, M. Fedurin, K. Kusche, M. Babzien, BNL ATF, Upton, NY 11973, USA

## Abstract

Conversion efficiencies of electrical to optical power in a Free Electron Laser are typically limited by their Pierce parameter,  $\rho \sim 0.1\%$ . Introducing strong undulator tapering can increase this efficiency greatly, with simulations showing possible conversion efficiencies of  $\sim 40\%$ . Recent experiments performed with the Rubicon Inverse Free Electron Laser have demonstrated acceleration gradients of  $\sim 100$  MeV/m and high particle trapping efficiency by coupling a pre-bunched electron beam to a high power CO2 laser pulse in a strongly tapered helical undulator [1,2]. By reversing the undulator period tapering and re-optimizing the field strength along the Rubicon undulator, we obtain an Inverse Free Electron Laser decelerator, which we have aptly renamed Nocibur. This tapering profile is chosen so that the change in beam energy defined by the ponderomotive decelerating gradient matches the change in resonant energy defined by the undulator parameters, allowing the conversion of a large fraction of the electron beam power into coherent narrow-band radiation [3]. We discuss this mechanism as well as results from a recent experiment performed with the Nocibur undulator at Brookhaven National Laboratory's Accelerator Test Facility.

## INTRODUCTION

The UCLA Particle Beam Physics Laboratory, in collaboration with Brookhaven National Laboratory's Accelerator Test Facility (ATF), has recently utilized the Inverse Free Electron Laser (IFEL) mechanism to use optical energy from a high power CO2 laser to accelerate a 52 MeV electron beam to 92 MeV in  $\sim 0.5$  m [1]. These experiments utilized the strongly tapered helical Rubicon undulator to demonstrate highly efficient conversion between optical and electrical energy. This process in reverse, electro-optical conversion, represents a potentially attractive source for high peak power and high average power radiation source.

The Nocibur experiment at ATF utilizes a strongly tapered helical undulator to couple a pre-bunched electron beam to a high power CO2 laser, using the Inverse Free Electron Laser mechanism to now decelerate the electrons (Fig. 1). By designing the undulator tapering such that the FEL resonance condition is maintained as the beam decelerates, energy lost by the beam is converted into coherent radiation by way of stimulated emission [3]. By

decelerating large fractions of the beam to  $\sim 50\%$  the initial beam energy, electro-optical conversion efficiencies of up to  $\sim 40\%$  are attainable.

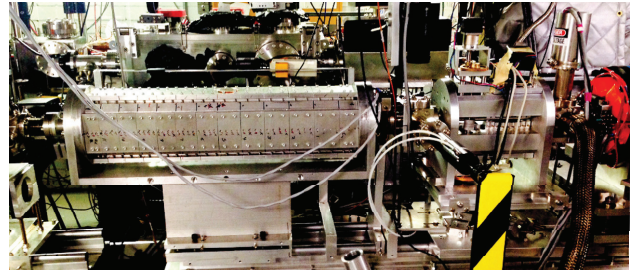


Figure 1: Nocibur undulator and pre-buncher installed in ATF beamline.

## DESIGN OF UNDULATOR TAPERING

The undulator tapering is designed to match the ponderomotive gradient set by the undulator and laser parameters to the FEL resonance condition, chosen such that the resonant phase remains constant throughout the deceleration (Fig. 2). In the case of this experiment we choose the resonant phase to be  $\Psi_r = -\pi/4$ .

Description	Definition
Undulator wavelength	$k_w = 2\pi / \lambda_w$
Laser wavelength	$k = 2\pi / \lambda$
Normalized laser vector potential	$K_l = \frac{e E_0}{m_0 c^2 k}$
Normalized undulator vector potential	$K = \frac{e B}{m_0 c k_w}$
Decelerating Gradient	$\frac{d\gamma}{dz} = \frac{e}{mc^2} E \cdot \beta \rightarrow \frac{d\gamma^2}{dz} = 2 k K_l K \sin(\psi_r)$
Resonance Condition ( $\frac{d\psi}{dz} = 0$ )	$\gamma^2 = \frac{\lambda_w}{2\lambda} (1 + K^2)$
Undulator Tapering Differential Equation	$\frac{dK}{dz} = \frac{2 k K K_l \sin(\psi_r) - \frac{d\lambda_w}{dz} \frac{1+K^2}{2\lambda}}{\lambda_w K/\lambda}$

Figure 2: Derivation of differential equation determining K tapering.

The Nocibur undulator was previously used in the Rubicon IFEL acceleration experiments. To create the necessary decelerating gradient the Rubicon undulator period tapering was reversed and the field strength was re-tuned to match the K tapering solution to the differential equation (Fig. 3). The undulator was modeled in Radia, tuned and measured with a hall probe and the second integral was zeroed using pulse wire measurements (Fig. 3).

\*Work supported by U.S. Dept. of Energy grant DE-FG02-92ER40693.

# LASER WAKEFIELD ACCELERATION USING A LASER PRODUCED ALUMINIUM PLASMA\*

Jaehoon Kim<sup>#</sup>, Younghoon Hwangbo, Seok-Gy Jeon, KERI, Ansan, Korea  
Woo Je Ryu, Kyung Nam Kim, Seong Hee Park, Nikolay Vinokurov, KAERI, Daejeon, Korea

## Abstract

In laser wakefield accelerator, usually a gas target is used to generate plasma medium. With this gas target, the pressure of the system cannot be kept as low as possible for electron beam application such as seeding the storage ring. To reduce this vacuum problem in LWFA, a plasma generated from solid Al target was used as plasma medium. A fundamental beam from the Q-switched ns pump laser in the Ti:sapphire power amplifier was used to generate a plasma from solid Al target. The plasma density was controlled by changing the distance between the main laser pulse for electron acceleration and the solid target. The plasma density was measured by the interferometer. The measured density indicates that the average charge of the ion in pre-plasma was 4.4. The main pulse ionized the Al plasma up to Al XII which means that the ionization injection could be used as an injection scheme. A 28 TW fs laser was used to accelerate the electron. A quasi-monochromatic electron was generated. The peak energy was 70 MeV and energy spread was 15 %. The divergence of the beam was 12 mrad in horizontal direction and 6 mrad in vertical direction.

## INTRODUCTION

An interaction between ultrahigh intensity fs laser and plasma can be used as an electron accelerator which is called as a laser wakefield accelerator (LWFA) [1]. Due to the development of the chirped pulse amplification (CPA) technology, a compact table top ultrahigh intensity fs laser is available [2,3]. The feasibility of LWFA to accelerate the electron is already demonstrated. The main difference between the LWFA and conventional electron accelerator is the acceleration media. In LWFA, a plasma is used as acceleration medium, and such medium can support much higher acceleration field. A compact high energy electron accelerator is possible due to this strong acceleration field in LWFA. Besides the small system size, LWFA can generate a very short femtosecond time scale electron bunches because the acceleration region is very narrow [4]. The measured electron bunch length was less than 50 fs which was measured by using the coherent radiation transition[5,6]. A femtosecond x-ray can be generated using these femtosecond electron bunches which is very useful for the measurement of the dynamics of materials in femtosecond time scale [7-9].

In LWFA, typically a gas target is used to generate a plasma medium for the acceleration. But in vacuum

sensitive applications such as an injector for a storage ring, the gas nozzle is not feasible because the gas injected into the vacuum chamber increases the pressure of the whole system. A plasma generated from a solid target can be used such an application because the number of particle injected into the vacuum chamber is much less than gas target. With solid target, the method to control the plasma density is needed because the plasma generated from a solid target by a laser expands very fast [10].

In this work, the feasibility of the laser produced plasma from solid target as an acceleration medium for a laser wakefield acceleration was studied. A density of the plasma was controlled by the distance between the main laser and the target and it was measured by using a Nomarski interferometer. The experimental results show that a laser produced plasma can be a good candidate of the acceleration medium for LWFA in vacuum sensitive applications.

## EXPERIMENT

To remove vacuum problem in LWFA with gas target, a plasma generated from a solid target was used as an acceleration medium for the LWFA. The experimental setup is shown in Fig. 1. The residual fundamental laser beam after the second harmonic generation from the pump laser of the main amplifier in the Ti:sapphire laser was used to generate a pre-plasma. By this method, the other laser is not needed to generate the pre-plasma. The laser was focused in line at a pure Al target by using a cylindrical lens and a biprism. The biprism was used to generate a uniform line intensity. If the intensity of the pre-pulse is too high, the plasma density at the interaction is too low because of the fast plasma expansion [10]. The size of the solid target is 2 mm wide and 25 mm long. After each laser shot, the target was moved 1 mm in x direction to supply a fresh surface. The laser line width at the target was controlled by the distance between the target and the cylindrical lens. In this experiments, the line width was 0.7 mm.

A ultrahigh intensity Ti:sapphire laser was used to accelerate electrons. The pulse duration of the laser was 25 fs and the peak power was 28 TW. The laser was focused at the pre-plasma by an off-axis parabolic mirror. The focal length of the OAP was 326 mm. The measured laser spot size was 5.4  $\mu\text{m}$ . The time delay between the pre- and main pulse was fixed due to the optical pass length and was 140 ns.

The density of the pre- and main plasma was measured by using a Nomarski interferometer. A parts of the main pulse is used as a probe pulse after converted to the second harmonic pulse. A fast Fourier transform was used

<sup>#</sup>jkim@keri.re.kr

# TERAHERTZ SOURCE UTILIZING RESONANT COHERENT DIFFRACTION RADIATION AT KEK ERL TEST ACCELERATOR\*

Y. Honda<sup>†</sup>, A. Aryshev, M. Shevelev, M. Shimada, KEK, Tsukuba, Ibaraki, Japan

## Abstract

A test accelerator of energy recovery linac scheme, cERL, has been under commissioning at KEK. One of the feature of ERL is that it can realize a high repetition rate and continuous operation of a short bunched beam. It is a suitable place to test a light source based on resonant coherent radiation, such as an resonant coherent diffraction radiation (CDR) system. An optical cavity is formed on the beam orbit to build-up CDR. If the fundamental frequency of the cavity coincides with the beam repetition rate, the stored radiation can stimulate the radiation in the following bunches. We show a simple estimation of the radiation power based on a model of coupling between beam and cavity eigen modes. An ideal case example for cERL beam parameter is shown.

## INTRODUCTION

One of the feature of ERL type of accelerator is that it can produce a short bunched beam at high repetition rate. It enables us to use it as a THz radiation source based on coherent radiation. CDR (Coherent Diffraction Radiation) is a coherent radiation produced by beam passing near a conductive target. Since it does not destroy a beam, the radiator can be installed in a loop of high averaged current ERL machine. As an advanced layout of CDR, it can be arranged to be a resonator scheme [1]. By coherently adding the radiation in a multi-bunched beam, it can extract radiation power much effectively. A test accelerator, cERL, which has been constructed recently in KEK, should be an ideal place to test the resonant CDR scheme.

Figure 1 shows the schematic of the resonant CDR system. An optical resonator of fundamental frequency that matches with beam repetition is placed on the beam axis. The cavity mirrors has a hole in the center so that beam can pass through. Electromagnetic wave excited in the resonator by a beam can be understood as CDR or higher-order modes of the resonator. Since the transverse profile of the mode is a donuts shape, it can be stored in a resonator formed by mirrors with hole.

Since electromagnetic wave in the resonator positively stimulates the radiation of the following bunches, the radiation power grows in square relation to bunch number. In order to extract the radiation, one of the cavity mirrors is designed to have transmission. Then it can be reflected to a transverse port using a parabolic mirror.

Here, we show the calculation of interaction of beam and resonator, and estimate radiation power assuming cERL beam parameter in an ideal case [2].

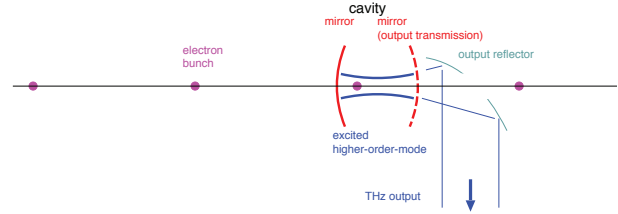


Figure 1: Schematic of resonant CDR.

## HIGHER-ORDER GAUSS BEAM

The excited modes are odd order transverse modes of the resonator. Here we calculate the lowest one,  $TM_{10}$  mode.

Transverse field of  $TM_{10}$  mode is written as follows.

$$E_{10}^x = \frac{A}{w(z)} \frac{x}{w(z)} \exp\left(-\frac{x^2 + y^2}{w^2(z)}\right) \cdot \exp[i(\omega t - kz + \phi(z))] \quad (1)$$

$$w(z) = w_0 \sqrt{1 + \frac{z^2}{z_0^2}} \quad (2)$$

$$z_0 = \frac{\pi w_0^2}{\lambda} \quad (3)$$

$$\phi(z) = 2 \tan^{-1}\left(\frac{z}{z_0}\right) \quad (4)$$

$\nu$  is the optical frequency of radiation,  $c$  is the speed of light,  $k = 2\pi/\lambda$ ,  $\omega = 2\pi\nu$ ,  $\omega/k = c$ .  $A$  is a scale factor for normalization.  $w(z)$  is the size at location  $z$ ,  $w_0$  is the size at the waist.  $\phi(z)$  is known as Gouy phase which depends on the order of transverse mode, the factor 2 means the first order mode.  $z_0$  is Rayleigh length.

Electromagnetic wave is a transverse wave in the case of an uniform plane wave. But, in cases of waves with spatial structure such as higher-order transverse modes, there exists a longitudinal field. The following relation can be shown from Helmholtz equation.

$$ikE^z = \frac{\partial E^x}{\partial x} \quad (5)$$

From Eq. 1, longitudinal field of  $TM_{10}$  mode is obtained as follows.

$$E_{10}^z = -\frac{i}{k} \frac{A}{w^2(z)} \left(1 - \frac{2x^2}{w^2(z)}\right) \exp\left(-\frac{x^2 + y^2}{w^2(z)}\right) \cdot \exp[i(\omega t - kz + \phi(z))] \quad (6)$$

When beam of speed  $c$  passes on the center axis, it feels the longitudinal field of

$$E_{10}^z(x = y = 0) = -\frac{A}{kw^2(z)} \exp[i2\phi(z)] \quad (7)$$

ISBN 978-3-95450-134-2

\* Work supported by KAKENHI

<sup>†</sup> yosuke@post.kek.jp

# LEBRA FREE-ELECTRON LASER ELICITS ELECTRICAL SPIKES FROM THE RETINA AND OPTIC NERVE OF THE SLUG *LIMAX VALENTIANUS*

F. Shishikura<sup>#</sup>, K. Hayakawa, Y. Hayakawa, M. Inagaki, K. Nakao, K. Nogami, T. Sakai, T. Tanaka  
 Laboratory for Electron Beam Research and Application, Nihon University, Chiba, Japan  
 Y. Komatsuzaki

Departments of Physics, College of Science and Technology, Nihon University Chiba, Japan

## Abstract

Since 2001, the Laboratory for Electron Beam Research and Application (LEBRA) has been providing tunable free-electron lasers (FELs) encompassing the near-infrared (IR) region and part of the mid-IR region (0.9–6.5  $\mu\text{m}$ ), and generating visible wavelengths up to 400 nm by means of nonlinear optical crystals. We used LEBRA-FEL to irradiate the retina of slugs (*Limax valentianus*), and determined which FEL wavelengths generate electrical spikes from a retina-optic nerve preparation. In the dark-adapted state, blue FEL light (peak wavelength: 470 nm) efficiently elicited electrical spikes from the retina. The results are consistent with a previous study where a xenon arc lamp with interference filters was used to produce monochromatic visible light. The retina produced detectable electrical spikes when repeatedly irradiated with pulsed FEL below 5 Hz. We extended the wavelengths to the near-IR regions (0.8–2.5  $\mu\text{m}$ ); however, we detected no electrical response.

## INTRODUCTION

Free electron lasers (FELs), such as the one developed by the Laboratory for Electron Beam Research and Application (LEBRA), produce high-energy, tunable pulsed radiation (wavelength range: 0.4–6.5  $\mu\text{m}$ ), which is ideal as a radiation source for investigating photochemical reactions in living organisms. Previously, we verified that visible FELs can control the germination of lettuce seeds, a well-known photochemical reaction in plants that is promoted by red light (660 nm) and inhibited by far-red light (740 nm) [1].

In this work, we investigated the efficiency of FEL for photic stimulation in an electrophysiological study. The eye (or retina) and optic nerve of the slug *Limax valentianus* is particularly useful for this purpose because the retina and optic nerve can be readily dissected free from the amputated eyestalk of the adult animal. The dissected retina-optic nerve preparation can be used for more than 12 h in a plastic chamber filled with snail Ringer solution [2]. Furthermore, the retina is big enough to be illuminated easily by the LEBRA-FEL micro-irradiation system, which contains a quartz fiber, and the optic nerve is large enough for signals to be recorded using a conventional capillary suction electrode. In the dark-adapted state, FEL irradiation experiments show that the peak wavelength of the spectral sensitivity curve is 470 nm.

<sup>#</sup>shishikura@lebra.nihon-u.ac.jp

## MATERIALS AND METHODS

### Animals

*L. valentianus* slugs, which are terrestrial and nocturnal, were collected locally and maintained for at least seven generations. These animals were kept under dark, wet conditions in plastic boxes placed in an incubator (SLC25A, Mitsubishi-Engineering Co., Japan) at 19.0 °C.

### Dissection

Adult specimens (2.1–2.4 g) were used. Each animal was anesthetized with an injection of 500  $\mu\text{L}$  of snail Ringer's solution [2] containing 50 mM  $\text{MgCl}_2$ . The snail Ringer's solution was a modification of Ramsey's Ringer solution [3]. The retina (about 0.25 mm diameter) and optic nerve (about 40  $\mu\text{m}$  diameter) were isolated by micro-dissection in snail Ringer's solution. The optic nerve was removed free from surrounding tissue, and cut apart from the base of the retina. The retina-optic nerve preparations of both eyes were fixed with small tungsten wire pins (3 mm long, 0.1 mm diameter) on a sloping transparent sheet of silicon in fresh Ringer's solution in a small plastic chamber. The preparations in Ringer's solution were used in experiments for 1 day.

### FEL Stimulation

In an earlier experiment [2], a xenon arc lamp (500 W) with a series of interference filters was used for producing monochromatic light. Here, we used the LEBRA-FEL as a radiation source, the beam specifications of which are detailed elsewhere [4,5]. LEBRA-FEL can generate sharp peak emissions of high-energy, high-coherency, tunable pulsed radiation from 0.4–6.5  $\mu\text{m}$ , and narrow spectral bandwidths. LEBRA can generate 4 or 5 wavelengths for the irradiation experiments over a day.

The setup of the LEBRA-FEL micro-irradiation systems has been described in our previous study [1]. A quartz fiber (0.6 mm diameter; Edmund Optics, Tokyo, Japan) was installed on a holder (H-7; Narishige Group, Tokyo, Japan) of a micro-manipulator (MMO-220A, Narishige Group), and delivered visible light wavelengths and near-infrared (IR) wavelengths up to 3  $\mu\text{m}$ . A dissection microscope and recording apparatus were placed in a Faraday cage, as shown in Fig. 1.

We used a light-emitting diode (LED) at a constant wavelength of 460 nm (20  $\mu\text{W s}^{-1}$  at 4.7 V) as a test light that was placed in the FEL delivery path and removed when the FEL was switched on. The intensities of the

## COTR RESISTANT PROFILE MONITOR\*

H. Loos<sup>†</sup>, SLAC National Accelerator Laboratory, Menlo Park, CA 94025, U.S.A.

### Abstract

Electron beam accelerators used as drivers for short wavelength FELs need ultra-high brightness beams with small emittances and highly compressed bunch lengths. The acceleration and beam transport process of such beams leads to micro-bunching instabilities which cause the emergence of coherent optical transition radiation (COTR). The effect of COTR on profile monitors based on OTR or fluorescent screens can be quite detrimental to their intended use to measure beam sizes and profiles. This presentation will review past observations of the beam diagnostics issues due to COTR and discuss various mitigation schemes for profile monitors as well as present experience with such implementations.

### INTRODUCTION

Free electron laser facilities for the generation of soft and hard x-rays [1–5] utilize high brightness linear accelerators which have to produce electron beams of exceptional quality to achieve lasing in a feasible length of undulator. The beams of multi-GeV energy need to have sub-micrometer transverse emittance,  $10^{-4}$  energy spread and 10s of fs or even shorter bunch durations for a total charge of the order of few 100 pC. Such parameters necessitate the measurement of transverse beam sizes and profiles from the injector area all the way to the undulators to establish beam emittance measurements throughout the accelerator so that machine tuning and optimization to maintain the high brightness beam into the undulators becomes possible. Furthermore, the 2-dimensional transverse beam distribution is needed to diagnose transverse coupling and to measure the time-resolved beam size or energy spread in conjunction with a transverse deflecting structure [6]. The most convenient method to obtain images of the transverse beam distribution is to use a profile monitor, i.e. a screen of some material intercepting the electron beam and emitting visible light imaged onto a CCD camera. The small, typically only several 10s of  $\mu\text{m}$  beam sizes make the use of scintillating crystals or thin foils generating optical transition radiation (OTR) [7] advantageous. The latter method was envisioned as the main transverse beam diagnostic for many XFEL accelerators because of the instantaneous response of OTR, and the absence of charge density dependent saturation effects or image resolution diluting depth effects as for thick scintillating crystals [8].

The ultra-high brightness of the XFEL accelerators—needed to enable coherent radiation at x-ray wavelengths—however poses a challenging problem for transverse beam diagnostics as became apparent for the first time during the

commissioning of the LCLS injector [9]. It became obvious then that imaging beam distributions using OTR screens can lead to completely unreliable results due to coherent effects from the longitudinal structure in the bunch distribution, i.e. the emission of coherent optical transition radiation (COTR).

The following sections first provide a brief summary of the COTR issue, then a review of various mitigation schemes to provide images of the beam distribution that are not affected by COTR artifacts, and concluding with results from tests of the PSI design profile monitor at SwissFEL and LCLS.

### COTR OBSERVATIONS

Coherent optical transition radiation is the process by which the light emission of a charged particle intercepting the boundary between two different media is not just the sum of the intensity of the light from individual particles as desired for OTR based beam diagnostics, but where longitudinal structure in the bunch at visible wavelengths leads to a coherent superposition of the emitted light fields, and hence an increase of the light intensity which can be a factor up to the number of particles if the bunch length itself is shorter than visible wavelengths.

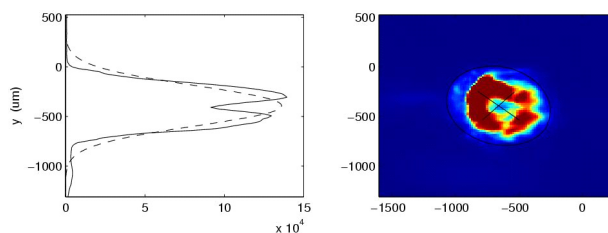


Figure 1: An image of the COTR radiation in the LCLS injector after BC1 observed with extreme bunch compression. From [9].

The initial observation of COTR [10] occurred in a deliberate way from an electron beam temporally modulated by the SASE process at visible wavelengths, which lead to the coherent enhancement of the incoherent OTR intensity by several orders of magnitude within the narrow SASE bandwidth. The first observation of broadband visible COTR at LCLS [9, 11] as shown in Fig. 1 was unexpected, but soon explained as a result of micro-bunching induced by the longitudinal space charge instability [12]. Subsequently the COTR effect has also been documented at most other high-brightness accelerators, both equipped with photo or thermionic cathode guns [13–16], with the latter requiring several bunch compression stages. Summaries of these observations can be found in [14, 17].

There are several implications of the COTR effect on the beam profile measurement. The light intensity can be greatly increased from a small factor for uncompressed

\* Work supported by US DOE contract DE-AC02-76SF00515.

<sup>†</sup> loos@slac.stanford.edu

# DIFFRACTION RADIATION MONITOR

Y. Taira<sup>#</sup>, AIST, Tsukuba, Japan

## Abstract

Diffraction radiation is one of non-destructive electron beam diagnostic techniques. A circular aperture, rectangular slit, and edge are used as a diffraction radiation targets. A transverse size, divergence, bunch charge, position, and bunch length can be measured by analysing a spatial distribution of DR. In the case of that the electron beam energy is low and the bunch length of the electron beam is in the range of few ps to sub-ps, coherently enhanced diffraction radiation with the wavelength of sub-mm to mm range is used. A spatial distribution of coherently enhanced diffraction radiation generated from an edge and slit was measured with a terahertz camera.

## INTRODUCTION

Diffraction radiation (DR) is generated when a charged particle moves in the vicinity of a boundary between two media with different dielectric constants. The charged particle does not directly interact with the material. An electric field with an effective electric field radius of  $\gamma\lambda/2\pi$  ( $\gamma$  is the Lorentz factor of the charged particle,  $\lambda$  is the observed wavelength of DR) interact with the material. In the condition that the distance between the charged particle and the boundary,  $d$ , is larger than the effective electric field radius, no radiation generates. The boundary gets close to the charged particle, DR is generated.

DR is mainly used for the non-destructive electron beam diagnostics. Visible wavelength of DR is usually used for the beam diagnostic of a high energy electron beam. Beam size measurement as small as 14  $\mu\text{m}$  was achieved at KEK-ATF by a rectangular slit [1]. Simultaneous measurement of the beam size, divergence, and position of the electron beam was proposed and experimentally investigated at the FLASH, DESY [2].

On the other hand, long wavelength of DR is used for low energy electron beam diagnostics. If the Lorentz factor and wavelength of DR are 100 and 500 nm, the effective electric field radius is calculated to be 8.0  $\mu\text{m}$ . This value is much smaller than the typical beam size. Thus, long wavelength of DR such as a far-infrared or terahertz radiation have to be measured. When  $\gamma = 80$  and  $\lambda = 0.2$  mm, the effective electric field radius is calculated to be 2.5 mm. This value is much larger than the typical beam size and a fabrication of the mechanical slit is also easy.

Long wavelength radiation of DR is generated via coherent radiation. Coherent radiation is generated when the electron bunch length is much smaller than the wavelength of DR generated from the electron. Frequency spectrum of coherent radiation is strongly depended on

the electron bunch length. Thus the beam diagnostic using the coherent diffraction radiation (CDR) is applied to the bunch length measurement at the low energy electron beam facilities [3-6].

In the previous research [7], feasibility study of beam position measurement using CDR generated from the slit was reported. It was found that an asymmetry distribution of CDR was sensitive to the beam position with respect to the slit center.

In this proceedings, spatial distribution and relative intensity of CDR generated from an edge and slit is reported to make clear the basic properties of CDR.

## EXPERIMENT SETUP

Spatial distribution measurement of CDR was conducted at an S-band compact electron linac at AIST. The electron beam was generated from a photocathode RF gun and accelerated up to 40 MeV by two accelerating tubes. Number of bunch in the macro pulse was 23 and repetition rate of the macro pulse was 25 Hz. The electron beam was then compressed in the longitudinal direction at an achromatic arc section. The compressed electron beam passed through a slit target for generating CDR. The electron beam size was controlled by three quadrupole magnets installed in the upper stream of the slit target. The bunch charge was 0.1 ~ 0.3 nC/bunch.

Schematic illustration of the spatial distribution measurement of CDR is shown in Fig. 1. The slit target was tilted at 45 degree. Thus the backward CDR was emitted toward the perpendicular direction against the electron beam trajectory. Backward CDR was collimated by a 100 mm focal length lens and leaves the vacuum duct through a z-cut crystal quartz window with the thickness of 9 mm. The radiation was then reflected by two silver mirrors, and passes through a wire grid linear polarizer (Specac, GS57203), a lens with the focal length of 50 mm, infrared blocking filter (NEC, IRV-TF030), and a terahertz camera.

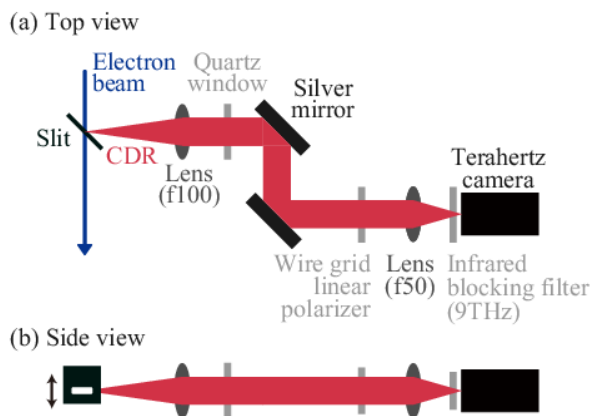


Figure 1: Schematic illustration of the spatial distribution measurement of CDR using a terahertz camera.

<sup>#</sup>yoshitaka-taira@aist.go.jp

## FIRST RESULTS OF THE SRF GUN TEST FOR CeC PoP EXPERIMENT\*

I. Pinayev<sup>#</sup>, Z. Altinbas, S. Belomestnykh, K. Brown, J.C. Brutus, A. Curcio, A. Di Lieto, C. Folz, D. Gassner, M. Harvey, J. Jamilkowski, Y. Jing, D. Kayran, R. Kellerman, R. Lambiase, V.N. Litvinenko, G. Mahler, M. Mapes, W. Meng, T. Miller, M. Minty, G. Narayan, P. Orfin, T. Rao, J. Reich, B. Sheehy, J. Skaritka, L. Smart, K. Smith, L. Snyderstrup, V. Soria, R. Than, C. Theisen, J. Tuozollo, E. Wang, G. Wang, B. Xiao, T. Xin, W. Xu, A. Zaltsman, BNL, Upton, NY 11973, USA

### Abstract

We have started the first tests of the equipment for the coherent electron cooling proof-of-principle experiment. After tests of the 500 MHz normal conducting cavities we proceeded with the low power beam tests of a CW SRF gun. The results of the tests with record beam parameters are presented.

### INTRODUCTION

The coherent electron cooling experiment (CeC PoP) [1, 2] is expected to demonstrate cooling of a single hadron bunch in RHIC. A superconducting RF gun operating at 112 MHz frequencies generates the electron beam. 500-MHz normal conducting cavities provide energy chirp for ballistic compression of the beam. 704-MHz superconducting cavity will accelerate beam to the final energy. The electron beam merges with the hadron beam and after cooling process is steered to a dump. The FEL-like structure enhances the electron-hadron interaction. The electron beam parameters are shown in the Table 1.

Table 1: Parameters of the Electron Beam

Parameter	Value
Energy	22 MeV
Bunch charge	1-5 nC
Normalized emittance	< 5 mm mrad
Energy spread	< 10 <sup>-3</sup>

### GUN DESIGN

The CeC PoP gun has quarter-wave structure and operates at 113 MHz. Its design is shown in Fig. 1. The gun cavity is placed inside cryostat with thermal and magnetic shields. The cathode stalk is inserted into cone and is kept at room temperature. Such design allows having at room temperature a CsK<sub>2</sub>Sb cathode, which is inserted inside of the stalk. The stalk itself serves as a cavity field pick-up.

The hollow fundamental power coupler (FPC) is inserted from the flat side of the cavity and let the generated beam go outside. The RF power is provided by a 2-kW solid-state amplifier. The FPC is surrounded by a gun solenoid, which is the first focusing element.

The cavity is coarsely tuned with two manual tuners

while the fine frequency change is performed with help of the FPC, which is placed on a translation stage.

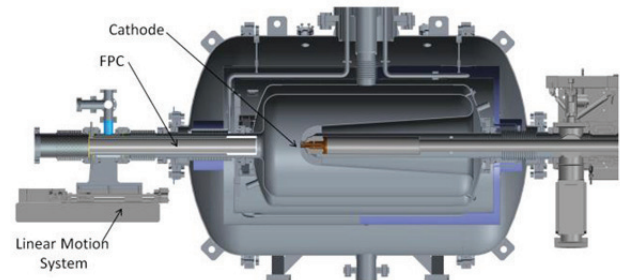


Figure 1: Layout of the superconducting gun.

The fundamental power coupler is followed by a laser cross which serve for launching of the drive laser beam onto the cathode and allows to serve the cathode as well.

### TEST SET-UP

The tests performed were done with partially installed equipment and the components are shown in Fig. 2. The main systems components are:

- cathode manipulation system with “garage”, which serves for storage and insertion of the photocathodes.
- the gun itself.
- six solenoids for beam focusing.
- two copper 500 MHz cavities for energy chirp.
- beam diagnostics.
- drive laser.

A brief description of each system is below.

#### Drive Laser

The drive laser is Picolo AOT-1 built by Innolas. It generates up to 6 μJ pulse at 532 nm wavelength. The pulse duration is 0.7 ps and maximal repetition rate is 5 kHz. The initial r.m.s. spot size on the cathode is 1.5 mm. This laser is used for the test only and will be replaced with a new one capable to generate 78 kHz pulses with 1 kW peak power and tunable pulse length.

#### Diagnostics

The beam diagnostics include integrated current transformer (ICT) with sensitivity of 0.8 nV s/nC. During test the ICT output was connected to the LeCroy digital oscilloscope. The ICT is installed immediately after the laser cross allowing observing beam leaving the gun.

\*Work supported by Department of Energy

<sup>#</sup>pinayev@nsl.gov

# SwissFEL STATUS REPORT

R. Ganter on behalf of the SwissFEL team, PSI, Villigen, Switzerland

## Abstract

SwissFEL is a 5.8-GeV linac which sends electron bunches at 100 Hz into a 60-m long in-vacuum undulator line to produce hard X-rays between 0.1 nm and 0.7 nm (Aramis line). The SwissFEL machine design is based on a low emittance beam with tight tolerances on RF phase stability. The first lasing of SwissFEL is planned for early 2017 and two end-stations should then be brought into operation in the same year. The delivery of the SwissFEL building to PSI is planned for fall this year, but some rooms are already completed and currently in use for component assembly. The production of the C-band RF accelerating structures has now reached the nominal rate of 5 structures/month. Two different RF solid-state modulator prototypes have demonstrated voltage pulse stability lower than 20 ppm but reliability tests are still ongoing. The undulator assembly and measurement sequences have started and 13 undulators are planned to be ready in the tunnel by October 2016. Large series of components like magnets, vacuum systems and mechanical supports are already in house and undergoing assembly. Photonics components for beamlines and for two end stations are ordered and planned to be ready for 2017. The next important milestone is the commissioning of the injector, the first 120 meters, in Spring 2016.

## INTRODUCTION

The overall layout of SwissFEL is shown in Fig. 1. In order to tune the FEL wavelength of Aramis between 1 and 7 Angström, the electron beam energy can be varied between 2.1 and 5.8 GeV. This is achieved with Linac 3 which either accelerates or decelerates the beam. This enables the energy at the extraction point towards Athos (end of Linac 2) to stay always constant and equal to 3 GeV. Genesis simulations, assuming a slice emittance of 0.2  $\mu\text{m}$ , lead to a pulse energy as high as 1.4 mJ at 1  $\text{\AA}$  in

the case of long pulses with 200-pC charge (Fig. 2). At the end of the undulator line, electrons are deviated vertically down towards a 240-ton shielded beam dump [1]. The SwissFEL injector will produce two bunches separated by 28 ns at a repetition rate of 100 Hz. The second bunch is deflected after Linac 2 in the transfer line (Fig. 1) towards the soft X-ray Athos line.

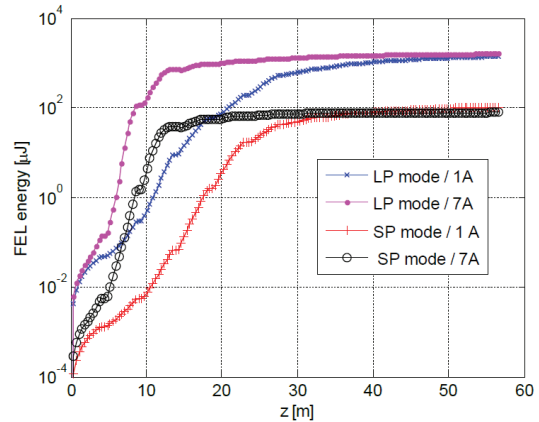


Figure 2: Genesis simulation of FEL pulse energy growth for two bunch charges, 200-pC long pulses (LP) and 10-pC short pulses (SP), and for two wavelengths: 1 and 7 Angström (graph from [2]).

## STATUS OF BUILDING AND INFRASTRUCTURE

SwissFEL is a two-storey building from cathode source ( $z = 0$  m) to the end of last linac ( $z \sim 460$  m). All the RF power plants as well as the rest of the infrastructure are situated on the top floor. As a consequence, all the cabling and cooling lines come down from the ceiling as can be seen in the pictures of Fig. 3.

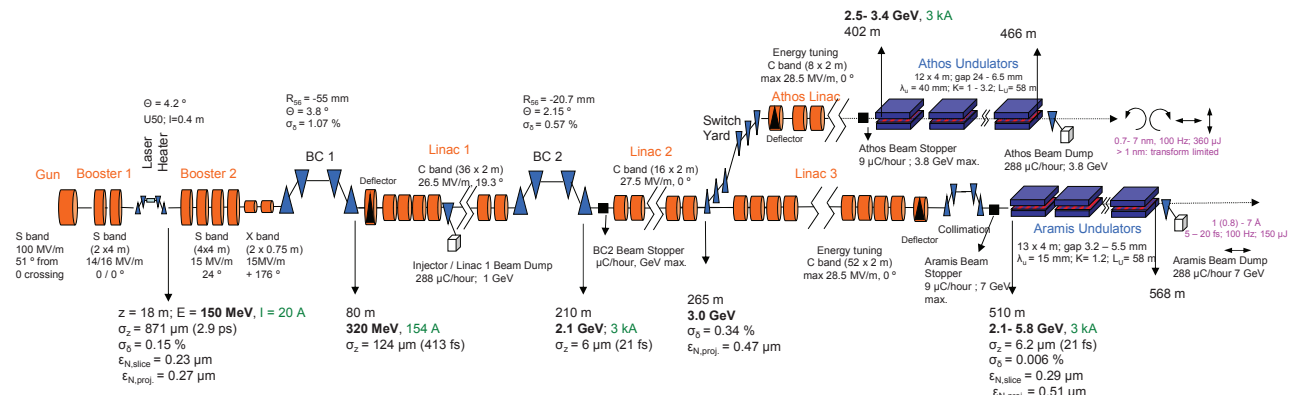


Figure 1: SwissFEL layout with the hard X-ray FEL line Aramis and the future Athos line to be built after 2018 (some parameters are merely indicative and only valid for a specific mode of operation).

## A TWO-COLOR STORAGE RING FEL\*

J. Yan<sup>†</sup>, Y.K. Wu, H. Hao, S. Mikhailov, V. Popov

DFELL/TUNL and Department of Physics, Duke University, Durham, NC, USA

J.Y. Li, NSRL, University of Science and Technology of China, Anhui, China

N.A. Vinokurov, Budker Institute of Nuclear Physics, Novosibirsk, Russia

S. Huang, Institute of Heavy Ion Physics, Peking University, Beijing, China

J. Wu, SLAC National Accelerator Laboratory, Menlo Park, CA, USA

### Abstract

Using different undulator configurations on the Duke storage ring, we have successfully achieved lasing with a novel two-color storage ring FEL. Using a pair of dual-band FEL mirrors, simultaneous lasing was realized in IR (around 720 nm) and in UV (around 360 nm). With this two-color FEL, we have demonstrated independent wavelength tuning of either IR or UV lasing. With careful tuning, we have also realized harmonic lasing with the UV lasing tuned to the second harmonic of the IR lasing. The tuning of harmonic two-color lasing has also been demonstrated with the locked wavelengths. Furthermore, we have demonstrated good control of the FEL power sharing between the two colors. The two-color FEL has created new opportunities to drive a two-color Compton  $\gamma$ -ray beam at the High Intensity  $\gamma$ -ray Source at Duke.

### INTRODUCTION

Multi-color lasers have found many important applications in scientific research. One example is wavelength-division multiplexing, which utilizes multiple optical signals at different wavelengths multiplexed into a shared fiber for enhancing the efficiency of communication systems. Multi-color lasers with good colinearity are particularly important in research, since the laser beams of different colors can be co-propagated over a long distance, collimated and focused simultaneously. For example, two optical pulses with different wavelengths but controllable time delay can be used in pump-probe spectroscopy to measure the fast dynamics of the system under investigation. Some other applications of multi-color lasers include photomixing processes for terahertz radiation generation and differential absorption lidar. The typical approach to realize simultaneous multi-color lasing is using a dispersive or diffractive wavelength filter such as a prism or grating, either intracavity or in an external feedback cavity. Such a technology has been implemented in conventional lasers with different gain media such as dye [1, 2], solid-state [3, 4], semiconductor [5, 6] and fiber [7]. However, the wavelength tunability of these lasers is typically limited by the bandwidth of the gain medium.

Since the theoretical prediction and the first experimental demonstration by Madey in the 1970s [8, 9], free-electron lasers (FELs) have seen great development over the past

few decades, and have become increasingly attractive light sources in a number of research areas. A common low-gain FEL configuration uses an optical cavity to trap and amplify electron beam radiation in a device termed an oscillator FEL [10]. An oscillator FEL can be driven either by an electron storage ring or a linac. Oscillator FELs mainly operate in the spectral region from IR to vacuum UV. The natural advantages of an FEL such as its broadband gain medium (an electron beam) and the single optical cavity configuration make the oscillator FEL an excellent device for the multi-color lasing with good wavelength tunability and colinearity. Since early 1990s, multi-color, especially two-color FEL operations have been developed and realized with several linac based FELs. The first two-color linac FEL operation was demonstrated on CLIO [11], an oscillator FEL operating in the mid-infrared regime, where two FEL wavelengths were produced by the same electron beam and two undulators with different undulator strengths inside a single optical cavity. Two other linac based oscillator FELs reported successful two-color operations later [12, 13]. Another FEL configuration, the high-gain single-pass FEL, is mainly driven by linacs and does not use an optical cavity. In these FELs, the amplification of the FEL beam is realized in a single pass via the interaction between the electron beam and its radiation in a long undulator array [14, 15] or with an external laser [16, 17]. Single-pass FELs are now high-performance coherent light sources in the extreme UV and x-ray regimes. Recently two-color operations have also been experimentally demonstrated with several single-pass FELs [18–22] in the short-wavelength spectral regions.

Unlike in a linac, an electron beam in a storage ring is recycled so that it participates in the FEL interaction repeatedly over a large number of passes. Therefore, the physics challenges for the two-color operation of a storage-ring FEL include the control and management of two competing lasing processes and maintenance of simultaneous lasing at two wavelengths in multiple passes. The first experimental demonstration of two-color FEL operation at the Duke FEL facility, in which simultaneous generation of two FEL wavelengths (IR and UV) with a harmonic relationship was realized, was reported in Ref [23]. In this article, we report an experimental study of two-color lasing using a different undulator configuration. The experimental results show good performance of this two-color operation in terms of wavelength tunability, power tunability and power stability. In addition, this two-color FEL can serve as a photon

\* Work supported in part by the US DOE grant no. DE-FG02-97ER41033.

<sup>†</sup> junyan@fel.duke.edu, 1-919-660-2667.

## WAVEGUIDE THz FEL OSCILLATORS\*

Sergey Miginsky<sup>#</sup>, Nikolay Vinokurov, KAERI, Daejeon, Korea; Budker INP, Novosibirsk, Russia  
Sangyoon Bae, Boris Gudkov, Kyu Ha Jang, Young Uk Jeong, Hyun Woo Kim, Kitae Lee, Jungho  
Mun, Seong Hee Park, Gyu Il Shim, KAERI, Daejeon, Korea

### Abstract

In today's world there is a significant demand for FEL-based THz radiation sources. They have a wide tuning range, a narrow band of radiation, and comparably high peak and average emission power. There are a significant number of these machines in the world, operating or in the development.

The main difference between a long-wave FEL, of THz or a millimeter band, and a conventional one is a too big transverse size of the fundamental mode of an open optical resonator. It claims a large gap in an undulator that dramatically decreases its strength. Both factors sorely decrease the amplification and the efficiency, and often make lasing impossible.

The main way to solve this problem is to use a waveguide optical resonator. It decreases and controls the transverse size of the fundamental mode. However, the waveguide causes a number of problems: power absorption in its walls; higher modes generation by inhomogeneities, as it is not ideal; electron beam injection into a FEL is more sophisticated; also outcoupling is more complicated; finally, the resonator detuning control claims some special solutions. The waveguide dispersion relation differs from one in the free space. It shifts up the wavelength of the FEL, changes the optimal detuning, and creates a parasitic mode near the critical wavelength of the waveguide. These problems and possible solutions to them are considered.

### INTRODUCTION

Outstanding parameters of THz FELs, like a wide tuning range, a narrow band of radiation, and comparably high peak and average emission power cause a significant number of these machines in the world. Several examples one can find in [1–7]. These machines differ significantly from each other and are intended for different purposes. One can easily found that FELs provide incomparably higher power than oscillators of other types in THz region [8].

However, there are several significant problems in development of THz FELs. Most one is that the fundamental mode of an open optical resonator has too big size in this case. It causes a decrease of the gain directly by weakening interaction between a wave and electrons and indirectly by an increase in an undulator gap that causes a sharp decline in strength of the latter.

\*Work was supported by the World Class Institute (WCI) program of the National Research Foundation of Korea (NRF) funded by the Ministry of Education, Science and Technology of Korea (MEST) (NRF Grant Number: WCI 2011-001).

<sup>#</sup>Miginsky@gmail.com

Thereby, extremely high peak current is necessary to obtain lasing. An effective method to improve the situation is the use of a waveguide optical resonator instead of open one. In this case the size of its mode can be significantly reduced together with an undulator gap. Wherein, a number of other problems arise. Energy absorption in the waveguide walls reduces the loop gain. Higher modes generation on waveguide inhomogeneities produces a similar effect. Beam injection into this resonator can be a complicated problem. Light outcoupling can be also not so easy. The wave group velocity in a waveguide depends on the wavelength, so the resonator should be retuned for each wavelength to keep the detuning. It is another sophisticated problem. Conducting of a beam through a narrow waveguide is not easy problem too. All these problems should be solved for a waveguide FEL.

### WAVEGUIDE RESONATORS

Several types of waveguides shown in Fig. 1 can be used in FELs. Electric field in all the cases is horizontal. Each of them has some advantages and drawbacks.

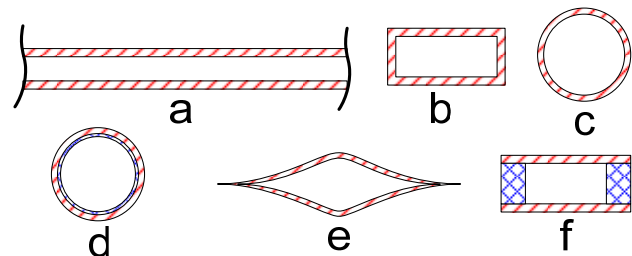


Figure 1: Types of waveguides: a – parallel-plate, b – rectangular, c – circular, d – with dielectric coating, e – special shape, f – rectangular with dielectric walls.

A parallel-plate waveguide concentrates wave power along the vertical coordinate only, while along the horizontal one it is similar to empty space. Thus, in the vertical plane the electric field distribution is cosine-like with zeroes at the walls, and in the horizontal one it is the well-known Gaussian free-space mode. It can be placed in a planar undulator only. One can conclude that the most effect of this waveguide is the decrease of the undulator gap. Power loss in this waveguide typically is not so big and can be easily evaluated using the following formula

$$\alpha \cong \frac{\pi}{2l} \frac{1}{1 + \frac{i\zeta}{kl}}, \quad (1)$$

# SATURATION DYNAMICS, FINE SPECTRUM, AND CHIRP CONTROL IN A CW FEL OSCILLATOR

H. S. Marks<sup>#</sup>, A. Gover, H. Kleinman, Tel Aviv University, Israel  
 D. Borodin, A. Damti, M. Einat, A. Friedman, M. Kanter, Y. Lasser, Y. Lurie, Y. Vashdi,  
 A. Yahalom, Ariel University, Israel

## Abstract

Here we report in brief the results of an experimental study of the saturation dynamics and the optimal conditions for maximal radiation power extraction in a Free Electron Laser (FEL) oscillator. The Israeli Electrostatic Accelerator Free Electron Laser (EA-FEL) is capable of providing lasing pulses at frequencies between 95-110 GHz (depending on the electron beam energy). A critical parameter affecting the performance of the laser is the reflectivity and transmission of the out-coupling element of the resonator.

By attaching a variable reflectivity out-coupling element (based on a series of wire-grid polarisers) to the resonator of our EA-FEL we demonstrate the ability to optimise performance depending upon the desired output. For maximum lasing time the out-coupling from the resonator must be minimized, although sufficient for some radiation to leave. For maximum peak-power the reflectivity must be set differently depending upon the energy of the electron-beam (in MeV), which relates to the frequency emitted, and to the magnitude of the electron-beam current (in A). Mode competition ceases and a single longitudinal resonator mode is established more quickly the higher the reflectivity (important for short pulses).

The variable out-coupling allows us to operate optimally over a large range of frequencies and beam currents which would be impossible with an element with fixed reflectivity.

## INTRODUCTION

Most FELs are based on RF-Linac acceleration technology that provides a periodic train of picosecond range e-beam pulses. FEL oscillators constructed based on such accelerators operate in principle as analogues of conventional mode-locked lasers [1]. In such oscillators, the laser radiation pulses are a superposition of numerous longitudinal modes of the resonator. By contrast, FEL oscillators based on electrostatic acceleration, which are the focus of the current article, can operate in a quasi-CW mode, namely their pulse duration is much longer than the time for several photon round-trips in the resonator. Such FEL oscillators operate analogously to conventional CW lasers of homogeneously broadened gain medium.

Consequently, they can operate at a single longitudinal radiation mode, and the physics of their steady state saturation and output coupling power optimization can be analysed in terms of conventional laser theory. Though

there are many FEL oscillators operating in the world [2], there are few operating electrostatic accelerator FELs in which the laser oscillator physics and specifically the problem of power out-coupling optimization can be studied experimentally. The Israeli Electrostatic Accelerator FEL (EA-FEL) is one of them. Another is the UCSB FEL [3]. Both can operate in a quasi-CW mode. The Dutch FOM-FEL operated along similar principles and at higher power but has since been dismantled [4]. An EA-FEL has also been built in Korea [5]. The Israeli Tandem EA-FEL has at its heart a fixed linearly polarised Halbach Wiggler [6].

## POWER OUT-COUPLING OPTIMISATION

The subject of optimal power outcoupling for attaining maximum lasing power output is treated by most standard texts on lasers [7-10]. This same subject of optimal power outcoupling in EA-FEL has not been studied extensively so far. The Israeli FEL group experimented with optimisation of power outcoupling of an FEM operating at microwave frequencies [11]. The matter was also treated by us theoretically in relation to our Tandem EA-FEL, which is the subject of this paper [12].

Table 1: General System Parameters of the EA-FEL

Beam Current	0.5-3 A
$B_w$ (Wiggler Field Amplitude)	0.193 T
$\lambda_w$	44.4 mm
$A_e$ (Effective area of mode)	$40.1 \times 10^{-6} m^2$
$L_w$ – Wiggler Length	989 mm
Beam Kinetic Energy	1.4 MeV

Within the limitations of our measurement range, single mode operation is generally observed. The time for single mode operation depends upon the roundtrip reflectivity. We arrive at this conclusion from looking at the lasing spectra, which we obtain from heterodyne mixing of the attenuated laser signal. We use an oscilloscope with a sampling rate of 5 GHz (Agilent – DSO-X3104A), with an analog bandwidth of 1 GHz. In producing the output the mixer doesn't discriminate between lasing frequencies above or below the local oscillator; so the 1 GHz bandwidth of the oscilloscope shows scanning over a range of over 2 GHz ( $\pm 1$  GHz from the local oscillator). So any demonstration of single mode operation is limited to 2 GHz. Though, the gain bandwidth of lasing is also limited, lasing further from the

# RF GUN DARK CURRENT SUPPRESSION WITH A TRANSVERSE DEFLECTING CAVITY AT LCLS\*

James R. Lewandowski, R. Clive Field, Alan Fisher, Heinz-Dieter Nuhn, James Welch SLAC National Accelerator Laboratory, Menlo Park, California 94025, U.S.A

### Abstract

A significant source of radiation signals in the LCLS Undulator has been identified as being generated by dark current emitted from the LCLS RF Photocathode Gun. Radiation damage to permanent magnets over time can lead to degraded performance and significant cost for replacement. A method of using an existing transverse deflector cavity with a modified RF pulse has been tested and shows promise for eliminating the radiation dose from RF gun dark current that is generated in time before and after the production beam pulse.

### DARK CURRENT IN ACCELERATOR STRUCTURES

Dark current in high gradient accelerator structures results from electrons being emitted from the surfaces of the accelerator cavity walls. With the proper phase of the electric field these particles can be captured and accelerated along with the main production beam. Even though these stray particles are accelerated within the acceptance envelope of main beam they may have slightly different energy and orbit. In FEL machines such as LCLS this dark current can be transported through the entire linac and then lost in the Undulator magnets depositing their energy into magnet material causing degradation of the magnetic field over time [1]. An existing S-Band Transverse RF deflector which is used for beam diagnostic bunch length measurements is located in the LCLS injector and is the tool used for our dark current suppression tests.

### TRANSVERSE DEFLECTOR CAVITIES

RF deflector structures as in Figure 1, were developed in the early days of SLAC for use in high energy physics experiments as fast kickers to send beam to multiple experiments, separate particles with different momentum [2] or they can be used to streak the beam for measuring bunch length as in LCLS or any other beam measurement experiment. In our application as a dark current suppression device we take advantage of the fast fill time characteristics of the traveling wave deflector structure. The fill time of the S-Band deflector used in the LCLS injector is around 55ns.

This fast fill time allows us to create an rf pulse with two lobes which has a zero field between the lobes.

We can time the arrival of the beam such that it sits between the lobes and is minimally perturbed while

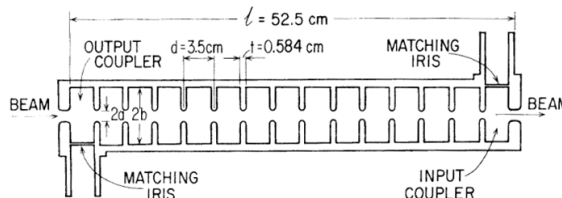


Figure 1: S-Band LOLA deflector sketch[2].

any dark current will see the maximum deflection with proper phasing of the cavity. The perturbed dark current can then be intercepted by existing collimators and purged out of the system. This scheme has been tested during several machine development days and is ready to be tested with user operation.

### DARK CURRENT RADIATION SIGNAL

The LCLS undulator is instrumented with lead shielded optically stimulated luminescent dosimeters, or OSL dosimeters, electronic RADFETs, and Lucite detectors with photomultiplier tubes [1]. The initial dark current signals were observed on the PMT signals when the rf gun cathode laser was shuttered. With no production electron beam being produced there were still radiation signals present in the undulator which encompassed the rf pulse length of the gun. When power to the rf gun was taken away the signal disappeared. Even with collimation some particles which are on energy and orbit were getting through the entire linac system and depositing their energy in the undulator. A typical configuration for 9.5keV x-ray energy can yield a dose measured in the RADFET monitors of 4R/day as shown in Figure 2.

Typical Undulator Dose @ 9.5KeV  
 ≈ 4R/Day

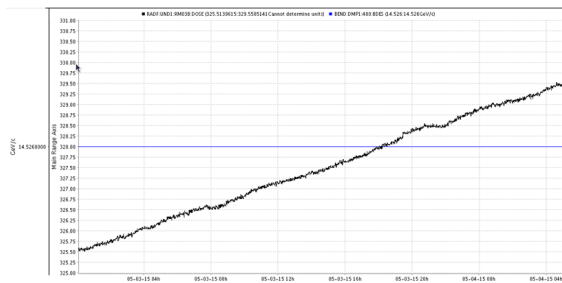


Figure 2: 24 hour RADFET 24 hour dose for 9.5KeV X-rays.

A reduction of the dose accumulated from the stray dark current electrons would be beneficial to the lifetime of the undulator magnets. The method of using the transverse deflector cavity has shown to be an effective solution in this endeavour.

\*Work supported by U.S. Department of Energy, Office of Basic Energy Sciences, under Contract DE-AC02-76SF00515  
 #jiml@slac.stanford.edu

# SIMULATING SINGLE CRYSTAL COPPER PHOTOCATHODE EMITTANCE\*

T. Vecchione<sup>#</sup>, SLAC National Accelerator Laboratory, Menlo Park, CA 94025, U.S.A.

## Abstract

The performance of free-electron lasers depends on the quality of the electron beam used. In some cases this performance can be improved by optimizing the choice of photocathode with respect to emittance. With this in mind, electronic structure calculations have been included in photoemission simulations and used to predict the emittance from single crystal copper photocathodes. The results from different low-index surfaces are reported. Within the model assumptions the Cu(100) surface was identified as having minimal emittance, particularly when illuminated by 266 nm light and extracted in a 60 MV/m gradient. These findings may guide future experimental work, leading to improved machine performance.

## INTRODUCTION

In photocathode-based free-electron lasers (FEL) much of the overall emittance comes from the photocathode itself. Surprisingly, the choice of which photocathode to use is often a result of historical precedent rather than systematic study. In these cases it is important to optimize the choice of photocathode with respect to emittance. Reductions in emittance can increase both the brightness and the energy of the x-rays produced and can save money by allowing undulators to be installed that are shorter in length.

Xie published a model that is useful for illustrating the dependence of FEL performance on emittance [1]. In this model the undulator saturation power,  $P_{sat}$ , is given as a function of the beam power,  $P_{beam}$

$$P_{sat}[\epsilon_x] = 1.6\rho[\epsilon_x] \left( \frac{L_{1d}[\epsilon_x]}{L_g[\epsilon_x]} \right)^2 P_{beam} \quad (1)$$

and the saturation length,  $L_{sat}$ , is given as a function of the input noise power,  $P_n$ .

$$L_{sat}[\epsilon_x] = L_g[\epsilon_x] Ln \left[ \frac{P_{sat}[\epsilon_x]}{\alpha P_n} \right] \quad (2)$$

Both the saturation power and the saturation length depend on the FEL parameter,  $\rho$ , which in turn depends implicitly on emittance,  $\epsilon_x$ , through the beam size,  $\sigma_x$ . The FEL parameter for a planar undulator is given by

$$\rho[\epsilon_x] = \left( \left( \frac{I}{I_A} \right) \left( \frac{\lambda_u}{2\pi\sigma_x[\epsilon_x]} \right)^2 \left( \frac{1}{2\gamma} \right)^3 \times \left( \frac{K}{\sqrt{2}} \left( J_0 \left[ \frac{K^2}{4+2K^2} \right] - J_1 \left[ \frac{K^2}{4+2K^2} \right] \right) \right)^2 \right)^{1/3} \quad (3)$$

For the sake of brevity, all other important definitions can be found in either [1] or in a comprehensive review of FEL theory by Huang and Kim [2].

Figure 1 uses Eq. (1), (2) and (3) to plot the projected percent increase in radiated power and the percent decrease in saturation length as functions of a percent decrease in emittance for the LCLS-I.

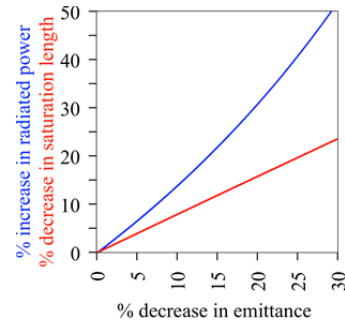


Figure 1: A significant improvement in FEL performance is predicted from lower emittance. For the LCLS-I at 8 keV and an initial emittance of 1  $\mu\text{m}$  a 20% decrease in emittance gives either a 31% increase in radiated power or a 16% decrease in saturation length.

It is reasonable to assume that a change in emittance at the photocathode will lead to a similar change in emittance at the undulator.

The biggest challenge in evaluating photocathodes for use in FELs is in accurately predicting their emittance. Analytical expressions for metal photocathodes have been derived by Dowell and Schmerge [3], Eq. (4), and by Vecchione [4], Eq. (5). Equation (5) maintains the full Fermi-Dirac distribution in the final result. One consequence of this is that the emittance at non-zero temperatures is non-zero even when the photon energy,  $\hbar\omega$ , equals the effective work function,  $\phi_{eff}$ . In the zero temperature limit Eq. (5) reduces to Eq. (4).

$$\epsilon_n = \sigma_x \sqrt{\frac{\hbar\omega - \phi_{eff}}{3mc^2}} \quad (4)$$

$$\epsilon_n = \sigma_x \sqrt{\frac{kT}{mc^2}} \sqrt{\frac{Li_3 \left[ -Exp \left[ \frac{e}{kT} (\hbar\omega - \phi_{eff}) \right] \right]}{Li_2 \left[ -Exp \left[ \frac{e}{kT} (\hbar\omega - \phi_{eff}) \right] \right]}} \quad (5)$$

$$Li_n[z] = \frac{(-1)^{n-1}}{(n-2)!} \int_0^1 \frac{1}{t} Log[t]^{n-2} Log[1-zt] dt$$

\*Work supported by US DOE contract DE-AC02-76SF00515.

<sup>#</sup>tvecchio@slac.stanford.edu

# RECENT UNDERSTANDING AND IMPROVEMENTS OF THE LCLS INJECTOR\*

F. Zhou,<sup>†</sup> D. Bohler, Y. Ding, S. Gilevich, Z. Huang, H. Loos, and D. Ratner  
SLAC, Stanford, CA 94309, USA

## Abstract

Ultraviolet drive laser and copper photocathode are the key systems for reliably delivering  $<0.4 \mu\text{m}$  of emittance and high brightness free electron laser (FEL) at the linac coherent light source (LCLS). Characterizing, optimizing and controlling laser distributions in both spatial and temporal directions are important for ultra-low emittance generation. Spatial truncated Gaussian laser profile has been demonstrated to produce better emittance than a spatial uniform beam. Sensitivity of the spatial laser distribution for the emittance is measured and analysed. Stacking two 2-ps Gaussian laser beams significantly improves emittance and eventually FEL performance at the LCLS in comparison to a single 2-ps Gaussian laser pulse. In addition, recent observations at the LCLS show that the micro-bunching effect depends strongly on the cathode spot locations. The dependence of the micro-bunching and FEL performance on the cathode spot location is mapped and discussed.

## INTRODUCTION

The cost and performance of the x-ray free electron laser (FEL) [1-2] depends critically on the emittance of the electron beam from the injector source. Producing and maintaining the desired ultra-small emittance ( $<0.4 \mu\text{m}$  for 180-250 pC) is one of the major challenges for operations of Linac Coherent Light Source (LCLS). Major injector source emittance includes cathode thermal emittance, space charge, and RF-contributed emittance [3-4]. According to the LCLS operational experience, the photocathode drive laser distributions sensitively affect injector emittance thereby hard x-ray FEL performance. The LCLS drive laser system is a frequency tripled, chirped-pulse amplification system based on Ti:sapphire. The system consists of mode-locked oscillator, followed by a pulse stretcher oscillator, a regenerative amplifier, two multi-pass amplifiers, pulse compressor, and finally a frequency tripler to convert the IR laser to 253 nm. The 253 nm laser beam is finally delivered to the copper photocathode through a long in-vacuum transport from the laser room on the ground to the 10-m deep SLAC linac tunnel.

The performance of the complex LCLS laser systems is sensitive to the external environment such as humidity, temperature and dusts and aging equipment. For 24/7 operating laser systems, minor environment change may cause optical misalignments, even optics damage, resulting in changes of spatial and temporal laser

distributions on the cathode. Measuring, optimizing and controlling the desired spatial and temporal laser profiles on the cathode are of particular importance for maintaining the desired ultra-low emittance and maximizing x-ray FEL performance. As the drive laser systems, the LCLS copper photocathode is also of importance for the emittance and the micro-bunch instability ( $\mu\text{BI}$ ). Recently we observed at the LCLS that the  $\mu\text{BI}$  is different at different cathode spots, causing different hard x-ray FEL performance (e.g., pulse intensity and bandwidth). Impacts of drive laser distributions and photocathode on the emittance,  $\mu\text{BI}$  and FEL performance are measured and analysed. This paper is organized as follows. Section II will introduce the measures of the spatial laser distribution and laser impacts on emittance. Emittance dependence on the temporal laser distribution is presented in Section III. In section IV, the dependence of the  $\mu\text{BI}$  and x-ray FEL performances on the laser location across the photocathode is mapped and discussed. The results are finally summarized.

## MEASURING, OPTIMIZING AND CONTROLLING SPATIAL LASER DISTRIBUTION FOR ULTRA-LOW EMITTANCE

Many previous studies showed the drive laser must be uniform in transverse dimensions on the photocathode to produce the best emittance beam. However, recently simulations and experimental observations at the LCLS [5] show that the truncated-Gaussian spatial laser beam produces a better emittance beam than uniform laser does. Figure 1 (top) shows the different spatial lineout-intensity distributions including uniform-like (a), truncated-Gaussian (b), and Gaussian-like (c). The projected and time-sliced emittances of three distributions are simulated, as shown in Fig. 1 (bottom), using ImpactT code [6] for 150 pC. The emittance with the truncated-Gaussian distribution improves  $\sim 30\%$  in comparison to the uniform-like laser or Gaussian-like beam.

Maintaining and controlling the spatial truncated-Gaussian laser beam on the photocathode, however, is not trivial for 24/7 operational laser systems. For example, it is difficult to maintain both shoulders a1 and a2 shown in Fig. 1(b) of the truncated-Gaussian distribution to be balanced through the complex laser systems and 10's meters-long laser transport. Extensive simulations show that the unbalanced shoulders increase the emittance. Therefore, having quantitative measures is crucial for characterizing, optimizing and controlling the spatial laser beam shapes and degree of asymmetry of both shoulders for ultra-small emittance beam. The following sub-

\* The work is supported by DOE under grant No. DE-AC02-76SF00515.

<sup>†</sup> zhoufeng@slac.stanford.edu

# ENERGY SPREAD CONSTRAINTS ON FIELD SUPPRESSION IN A REVERSE TAPERED UNDULATOR\*

J. MacArthur, A. Marinelli, A. Lutman, H.-D. Nuhn, Z. Huang  
SLAC National Accelerator Laboratory, Menlo Park, CA, USA

## Abstract

A 3.2 m variable polarization Delta undulator [1] has been installed at the end of the LCLS undulator line. The Delta undulator acts as an afterburner in this configuration, using bunching from upstream planar undulators to produce radiation with arbitrary polarization. To optimize the degree of polarization from this device, a reverse taper has been proposed [2] to suppress background radiation produced in upstream undulators while still microbunching the beam. Here we extend previous work on free electron lasers with a slowly varying undulator parameter [3] to show there is a strong energy spread dependence to the maximum allowable detune from resonance. At LCLS, this energy spread limitation keeps the reverse taper slope in the slowly varying regime and limits the achievable degree of circular polarization.

## INTRODUCTION

Circularly polarized x-rays can be used to probe ultrafast demagnetization processes [4], image nanoscale spin order [5], and probe the chirality of biomolecules [6]. However, no x-ray Free Electron Lasers (FELs) offer direct production of circular x-rays. A helical undulator called the Delta undulator is being commissioned at the Linac Coherent Light Source (LCLS) to address this shortcoming [7].

The Delta undulator is not long enough to operate alone and reach appreciable power levels. The electron beam must therefore be prepared in advance of the Delta undulator to maximize the power produced in the circular polarization mode. A reverse tapered planar undulator line preceding the Delta undulator was proposed [2] to maximize the microbunching in a beam entering the Delta undulator while suppressing the background linear field. In this paper we present a constraint on the effectiveness of the reverse taper technique in FELs with a relatively large energy spread.

In the following sections, the 1D FEL equations are explored in the slowly varying detune regime. For an undulator of period  $\lambda_u$ , Pierce parameter  $\rho$ , and  $z$ -dependent resonant energy  $\gamma_r(z)$ , the detune from the initial energy  $\gamma_0$  is

$$\delta = \frac{\gamma_0 - \gamma_r(z)}{\gamma_0}. \quad (1)$$

The detune is slowly varying when its change over a gain length  $L_G \approx \lambda_u/4\pi\rho$  is significantly less than the gain bandwidth, which is typically several  $\rho$  [3]. Thus the slowly

varying technique is valid when

$$\frac{\lambda_u}{4\pi\rho} \left| \frac{d\delta}{dz} \right| < \rho. \quad (2)$$

At LCLS, successful 720 eV reverse taper configurations operate with a maximum reverse taper detune of  $\delta = -0.005$  applied over six undulator modules, or 20 m. These conditions mandate a Pierce parameter satisfying

$$\rho > \sqrt{\frac{\lambda_u}{4\pi} \left| \frac{d\delta}{dz} \right|} = 7.7 \times 10^{-4}. \quad (3)$$

Typical 720 eV reverse taper runs operate at a peak current of 5 kA with a 30  $\mu\text{m}$  transverse beam size, resulting in a Pierce parameter of  $2.2 \times 10^{-3}$ . It is therefore instructive to apply the slowly varying solution of the FEL equations to soft x-ray experiments at LCLS.

In the following section we review important aspects of FELs with slowly varying parameters. In subsequent sections we apply this formalism to a reverse tapered undulator to calculate an energy spread limit on the effectiveness of a reverse tapered undulator line. Finally, 3D simulations are compared with results from the 1D theoretical framework.

## WKB REVIEW

The Vlasov and Maxwell equations can be expressed in matrix form [3],

$$\frac{d}{d\bar{z}} \begin{pmatrix} a_v \\ f_v \end{pmatrix} = iM \begin{pmatrix} a_v \\ f_v \end{pmatrix}, \quad (4)$$

$$M = \begin{pmatrix} -\bar{v} & -i \int_{-\infty}^{\infty} d\bar{\eta} \\ -i \frac{d\bar{v}}{d\bar{\eta}} & -(\bar{\eta} - \bar{\delta}) \end{pmatrix}. \quad (5)$$

The dimensionless FEL variables used here are

$$\bar{z} = 2\rho k_u z \quad (6)$$

$$\bar{\eta} = \frac{\gamma(z) - \gamma_c(z)}{\gamma_0\rho} \quad (7)$$

$$\bar{\delta} = \frac{\gamma_c(z) - \gamma_r(z)}{\gamma_0\rho} \quad (8)$$

$$\bar{v} = \frac{\Delta v}{2\rho} \quad (9)$$

$$a_v = -\frac{eK[\text{JJ}]}{4\gamma_0^2 m c^2 k_u \rho} e^{-i\Delta v k_u z} E_v \quad (10)$$

$$f_v = \frac{2k_u \rho^2}{k_0} F_v, \quad (11)$$

where  $\rho$  and  $k_u$  are the Pierce parameter and undulator wavenumber. The Lorentz factor  $\gamma_0$  defines the mean beam

\* Work supported by U.S. DOE Office of Basic Energy Sciences under Contract No. DE-AC02-76SF00515.

# LASER HEATER TRANSVERSE SHAPING TO IMPROVE MICROBUNCHING SUPPRESSION FOR X-RAY FELS

S. Li\*, A. Fry, S. Gilevich, Z. Huang, A. Marinelli, D. Ratner, J. Robinson  
SLAC, Menlo Park, CA 94025, USA

## Abstract

In X-ray free electron lasers (FELs), a small amount of initial density or energy modulation in the electron beam can be amplified through the acceleration and bunch compression process. The undesired microbunching on the electron bunch will increase slice energy spread and degrade the FEL performance. The Linac Coherent Light Source (LCLS) laser heater (LH) system was installed to increase the uncorrelated energy spread in the electron beam in order to suppress the microbunching instability. The distribution of the induced energy spread depends strongly on the transverse profile of the heater laser and has a large effect on microbunching suppression. In this paper, we present theoretical calculations for the LH induced energy spread and discuss strategies to shape the laser profile in order to obtain better suppression of microbunching. We present analysis and potential methods to achieve Gaussian and Gaussian-like energy spread on the electron beam.

## INTRODUCTION

At the Linear Coherent Light Source (LCLS), the laser heater (LH) system was installed in the injector area to suppress the microbunching instability by increasing the uncorrelated energy spread [1, 2]. The interaction between the heater laser and the electron beam takes place in a short undulator and gives rise to an energy modulation on the electron beam. The distribution of the laser-heater-induced energy spread affects the suppression of the microbunching instability. The energy modulation amplitude each electron experiences varies depending on the location of the electron relative to the laser transverse profile. Therefore one can control the energy spread distribution by transversely shaping the heater laser profile, and hence improve the suppression of microbunching instability.

In this paper we present theoretical calculations to relate the laser transverse profile with laser-heater-induced energy spread distribution. We discuss two methods of generating Gaussian-like energy spread using a fundamental Gaussian mode and a Laguerre-Gaussian (LG) mode, and compare their microbunching suppression effect and power efficiency. Lastly, we investigate the possibility of implementing a Gaussian speckle distribution, an approach independent of the transverse electron distribution.

## LASER HEATER SUPPRESSION THEORY

The energy modulation induced by laser-electron interaction is obtained in [1],

$$\begin{aligned} \delta_L(r) &= \sqrt{\frac{P_L}{P_0}} \frac{KL_u}{\gamma_0 \sigma_r} \left[ J_0 \left[ \frac{K^2}{4 + 2K^2} \right] - J_1 \left[ \frac{K^2}{4 + 2K^2} \right] \right] f(r) \\ &\equiv Af(r), \end{aligned} \quad (1)$$

where  $P_L$  is the peak laser power,  $P_0 = I_A mc^2 / e \approx 8.7 \text{GW}$ ,  $K$  is the undulator strength parameter,  $\gamma_0$  is the relativistic factor of electron beam energy,  $L_u$  is undulator period,  $\sigma_r$  is the rms spot size of the laser,  $J_{0,1}$  are the Bessel functions,  $r$  is the radial position of the electron, and  $f(r)$  describes any arbitrary transverse profile of the laser beam. On the right hand side of the equation, we group the constants in front of the laser profile  $f(r)$  into one constant  $A$ .

If we assume a Gaussian electron distribution and integrate the energy-modulated electron beam in transverse and longitudinal coordinates, we get the expression for the modified energy distribution,

$$\begin{aligned} V(\delta) &= \frac{1}{\pi \sigma_x^2 \sqrt{2\pi} \sigma_{\delta 0}} \int r dr d\xi \frac{e^{-\frac{r^2}{2\sigma_x^2} - \frac{\xi^2}{2\sigma_{\delta 0}^2}}}{\sqrt{\delta_L(r)^2 - (\delta - \xi)^2}} \\ &\approx \int \frac{1}{\pi \sigma_x^2} r dr e^{-\frac{r^2}{2\sigma_x^2}} \frac{1}{\sqrt{\delta_L(r)^2 - \delta^2}}, \end{aligned} \quad (2)$$

where  $\sigma_x$  is the rms size of the electron beam, and  $\sigma_{\delta 0}$  is the initial energy spread in the electron beam.  $\sigma_{\delta 0}$  is typically 1 to 3 keV, and is relatively small compared to the induced energy spread which will be shown below to be around a few tens of keV. Thus we ignore its contribution in the last line of Eq. (2) and throughout the rest of this paper.

The microbunching gain is defined as the ratio of the final bunching factor to the initial bunching factor  $\left| \frac{b_f}{b_0} \right|$ , which can be approximated as [1]

$$G \approx \frac{I_0}{\gamma I_A} \left| k_f R_{56} \int_0^L ds \frac{4\pi Z(k_0; s)}{Z_0} \right| S_L \left( k_f R_{56} A, \frac{\sigma_r}{\sigma_x} \right), \quad (3)$$

where  $I_0$  is the peak current,  $I_A$  is the Alfvén current,  $k_f = Ck_0$  is the compressed modulation wave number through compression  $C$ ,  $Z(k; s)$  is the longitudinal space charge impedance defined below (Eq. (4)), and  $S_L$  is the gain suppression factor defined as the Fourier transform of  $V(\delta)$ . The impedance function is

$$Z(k, s) = \frac{iZ_0}{\pi k r_b^2} \left[ 1 - \frac{k r_b}{\gamma} K_1 \left( \frac{k r_b}{\gamma} \right) \right], \quad (4)$$

\* siqili@slac.stanford.edu

# FOUR-DIMENSIONAL MODELS OF FREE ELECTRON LASER AMPLIFIERS AND OSCILLATORS

J. Blau\*, K. Cohn, W. B. Colson

Physics Department, Naval Postgraduate School, Monterey, CA 93943, USA

## Abstract

New four-dimensional models of free electron lasers (FELs) are described, for both amplifier and oscillator configurations. Model validation and benchmarking results are shown, including comparisons to theoretical formulas and experiments.

## INTRODUCTION

Over the past 25 years at the Naval Postgraduate School, we have developed a suite of computer programs to model free electron lasers [1, 2]. We have separate programs for different types of FELs (i.e., single-pass amplifiers or multi-pass oscillators) under various conditions (i.e., short or long pulses), with graphics optimized to understand the results for each type of FEL.

Our programs can be classified according to the number of dimensions in the model. The one-dimensional (1D) and two-dimensional (2D) programs run very rapidly on laptop and desktop computers. The 1D programs are helpful in visually understanding basic principles such as electron bunching, optical gain and saturation, and in many cases give good descriptions of FEL performance. The 2D programs are useful when longitudinal effects such as pulse slippage and desynchronism are dominant. The three-dimensional (3D) and four-dimensional (4D) programs typically run on multi-core or cluster computers, and are useful when transverse effects such as optical mode distortion are significant. Each of the programs produces extensive graphical output to enhance physical understanding and reveal trends.

This paper describes the new 4D models that we have developed over the past several years, taking advantage of advances in computer technology that enable these programs to run efficiently on readily available hardware such as Linux clusters. We also present results showing how we have validated and benchmarked the new models.

## DESCRIPTION OF THE MODELS

### Dimensionless Parameters

All of our models use dimensionless parameters that simplify the equations, provide intuitive insight, and generalize the results [3]. Longitudinal coordinates are normalized to the undulator length  $L$ , and transverse coordinates are normalized to a characteristic optical mode radius  $\sqrt{L\lambda}/\pi$ , where  $\lambda$  is the optical wavelength. The dimensionless time is defined by  $\tau = ct/L$  where  $c$  is the speed of light.

Phase space coordinates follow the microscopic bunching of the electrons on the scale of an optical wavelength. The

electron phase is defined as  $\zeta = (k + k_0)z - \omega t$  where  $k = 2\pi/\lambda$  is the optical wavenumber,  $k_0 = 2\pi/\lambda_0$  is the undulator wavenumber,  $\lambda_0$  is the undulator period,  $\omega = kc$  is the optical frequency, and  $z$  is the electron's position along the undulator axis at time  $t$ . The dimensionless phase velocity then becomes  $v = d\zeta/d\tau = L[(k + k_0)\beta_z - k]$  where  $\beta_z = v_z/c$ .

The dimensionless undulator parameter is given by  $K = eB\lambda_0/2\pi mc^2$ , where  $B$  is the rms field strength,  $e$  is the electron charge and  $m$  is the electron mass (in cgs units). For most FELs,  $K \sim 1$ .

The dimensionless optical field amplitude is defined as  $|a| = 4\pi NeKLE/\gamma^2 mc^2$ , where  $N$  is the number of undulator periods,  $E$  is the electric field amplitude, and  $\gamma$  is the Lorentz factor. When  $|a| \ll \pi$  the optical fields are weak and there is very little electron bunching. When  $|a| \sim \pi$ , there can be significant electron bunching, producing growth of the optical fields. When  $|a| \gg \pi$ , strong optical fields can cause many of the electrons to become trapped in closed phase space orbits, leading to the onset of saturation.

The optical fields are driven by the dimensionless current density,  $j = 8N(e\pi KL)^2 \rho/\gamma^3 mc^2$ , where  $\rho$  is the particle density. When  $j \lesssim 1$ , the weak-field gain is low, but when  $j \gg 1$ , the FEL can have high gain. A typical FEL oscillator has  $j \sim 100$  and moderate weak-field gain. An FEL amplifier, with a much longer undulator, can have  $j \sim 10^5$  and very high gain over a single pass.

### Model Assumptions and Methods

The first 4D model that we developed in the early 1990s assumed the electron beam is well inside the optical mode [4]. In that case, all of the electrons in each longitudinal slice of the pulse interact with the same optical field, so the microscopic bunching is uniform across each slice. This assumption significantly reduces the computational and memory requirements for the simulation; for instance, instead of large 3D arrays for the electron phase  $\zeta$  and phase velocity  $v$ , only 1D arrays are required.

Our new 4D models are more general, including the full evolution in  $(x, y, z, t)$  of the electrons and optical pulses. The programs are parallelized, with each process following an optical wavefront  $a(x, y)$  and sample electrons for a single longitudinal slice of the optical pulse  $a(z)$  along the undulator axis. In each slice, the optical wavefront is represented by the field amplitude and phase over a rectangular grid, and approximately 30,000 sample electrons are assigned transverse phase space coordinates  $(x, \theta_x, y, \theta_y)$  in addition to their longitudinal phase space coordinates  $(\zeta, v)$ . To reduce shot noise effects, a quiet start algorithm [5] is used to assign the initial phase space coordinates, taking

\* blau@nps.edu

# DEVELOPMENT OF PHONON DYNAMICS MEASUREMENT SYSTEM BY MIR-FEL AND PICO-SECOND LASER

T. Murata<sup>#</sup>, H. Zen, T. Katsurayama, T. Nogi, S. Suphakul, K. Torgasin, T. Kii, K. Masuda, H. Ohgaki, Institute of Advanced Energy, Kyoto University, Kyoto 611-0011, Japan

K. Yoshida, Kumamoto institute for Photo-Electro Organics, Kumamoto 862-0901, Japan and Department of Applied Chemistry and Biochemistry, Kumamoto University, Kumamoto 860-8555, Japan

K. Hachiya, Graduate School of Energy Science, Kyoto University, Kyoto 606-8501, Japan

## Abstract

Coherent control of a lattice vibration in bulk solid (mode-selective phonon excitation: MSPE) is one of the attractive methods in the solid state physics because it becomes a powerful tool for the study of ultrafast lattice dynamics (e.g. electron-phonon interaction and phonon-phonon interaction). Not only for that, MSPE can control electronic, magnetic, and structural phases of materials. In 2013, we have directly demonstrated MSPE of a bulk material with MIR-FEL (KU-FEL) by anti-Stokes Raman scattering spectroscopy. For the next step, we are starting a phonon dynamics measurement to investigate the difference of physical property between thermally excited phonon (phonon of equilibrium state) and optically excited phonon (phonon of non-equilibrium state) by time-resolved method in combination with a pico-second laser and MIR-FEL. By using pico-second laser, we can also expect to perform the anti-Stokes hyper-Raman scattering spectroscopy to extend MSPE method to the phonon mode which has Raman inactive (or some of the infrared inactive modes). As the first step, we have commissioned the time-resolved phonon measurement system and started the measurement on 6H-SiC. Consequently, we succeeded in a development of a phonon dynamics measurement system and the temporal resolution of the developed system was around 10 ps.

## INTRODUCTION

The electron-phonon interaction influences physical properties of solid-state materials. Thus, the clarification of the interaction is required for understanding basic physical properties of solid-state materials and developing high-performance devices [1,2]. To clarify the interaction, it is important to understand the relation between the electronic state and the excitation of a particular lattice vibration (phonon).

Mode-selective phonon excitation (MSPE) is one of the useful methods for clarification of the relation between electronic state and the excitation of a particular phonon mode. Especially, a mid-infrared pulse laser is strong tool for MSPE. By irradiating a mid-infrared pulse laser tuned absorption wavelength of a specific phonon, the direct excitation of a specific phonon mode is available [3,4]. We have developed a technique which can

directly observe excitation condition of particular phonon mode by using anti-Stokes Raman scattering spectroscopy (Fig. 1) [3]. By using the technique, the MSPE by MIR-FEL has been directly demonstrated with the sample material of 6H-SiC (Fig. 2) [3]. Then, we have started development of phonon dynamics measurement system by MIR-FEL and pico-second laser to investigate the differences of phonon property between selective excitation and thermal (non-selective) excitation.

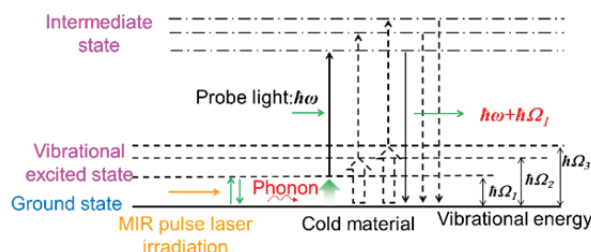


Figure 1: Schematic of the principle of anti-Stokes Raman scattering by MIR laser irradiation with cold material [3].

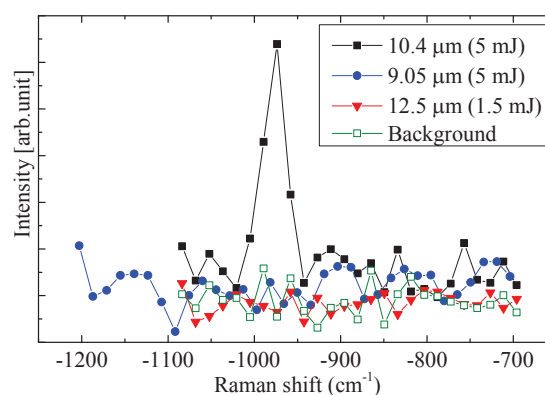


Figure 2: Anti-Stokes Raman scattering spectra with MIR-FEL and nano-second laser at 14 K [3].

## PHONON DYNAMICS MEASUREMENT SYSTEM

Figure 3 shows the schematic diagram of developed phonon dynamics measurement system. In this system, the second harmonic of pico-second Nd:YVO<sub>4</sub> laser (probe light) [5] and MIR-FEL (pump light) are simultaneously irradiated. The wavelength and pulse

<sup>#</sup> murata.tomoya.46s@st.kyoto-u.ac.jp

# LCLS-II: STATUS OF THE CW X-RAY FEL UPGRADE TO THE SLAC LCLS FACILITY\*

T.O. Raubenheimer<sup>#</sup> on behalf of the LCLS-II Collaboration,  
SLAC, Menlo Park, CA 94025, USA

## Abstract

The LCLS-II will be a CW X-ray FEL upgrade to the existing LCLS X-ray FEL at the SLAC National Accelerator Laboratory (SLAC). This paper will describe the overall layout and performance goals of the upgrade project.

## INTRODUCTION

The LCLS-II is an X-ray Free-Electron Laser (FEL) which will upgrade the LCLS FEL at SLAC. The LCLS-II is designed to deliver photons between 200 eV and 5 keV at repetition rates as high as 1 MHz (929 kHz) using a superconducting RF linac (SCRF) linac while still providing pulses at short wavelengths and high X-ray pulse energy over the photon range of 1 to 25 keV using the existing 120 Hz copper RF (CuRF) LCLS linac. The project consists of a new 4 GeV SCRF linac, extensive beam transport systems, and two new variable gap undulators.

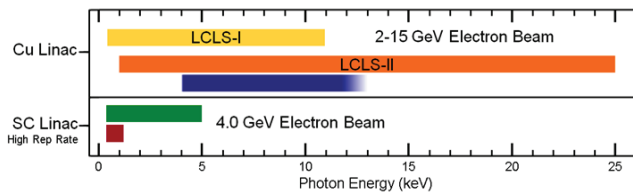


Figure 1: Schematic illustrating the performance of the LCLS and the LCLS-II upgrade where ■ represents SASE at 120 Hz, ■ represents Self-Seeding at 120 Hz, ■ represents SASE at high rate, and ■ represents Self-Seeding at high rate.

The LCLS-II will extend the high peak brightness capability and flexibility of LCLS while also having the ability to provide MHz rate beams from a CW SCRF linac; the parameters are shown in Table 1. The operating regimes are illustrated in Figure 1 and listed below:

1. Soft X-ray photons from SASE and self-seeding between 0.2 and 1.3 keV at MHz rates, with an average X-ray power in excess of 20 Watts;
2. Hard X-ray photons from SASE between 1.0 and 5.0 keV at MHz rates with an average X-ray power in excess of 20 Watts and with the possibility of a future upgrade to self-seeding operation at energies between 1 and 4 keV;

3. Hard X-ray photons with SASE between 1 and 25 keV and self-seeding between 4 keV and 13 keV at 120 Hz, with mJ-class pulses and performance comparable to or exceeding that of LCLS.

The upgrade is expected to significantly extend the XFEL science capability at SLAC; elements of the science program that will be enabled by the LCLS-II is documented in Ref. [1].

The LCLS-II project is being constructed by a collaboration of US laboratories consisting of Argonne National Lab. (ANL), Cornell University (CU), Fermilab (FNAL), Jefferson Lab. (JLab), Lawrence Berkeley National Lab. (LBNL), and SLAC. In addition, the project has substantial assistance from the EuXFEL project as well as the other international laboratories focused on SCRF development and XFEL's.

The SCRF linac will be installed in the first third (1 km) of the SLAC linac tunnel and a bypass line will bring the high rate beam around the middle third of the existing linac and the existing LCLS CuRF linac as illustrated in Figure 2. Beams from both the CuRF and the SCRF linac will be transported to the existing LCLS Undulator Hall where, to cover the full photon-energy range, the existing LCLS fixed gap undulator will be removed and the facility will install two variable-strength (gap-tunable) undulators, one dedicated to the production of Soft X-rays (SXR Undulator) from 0.2 to 1.3 keV and one dedicated to production of Hard X-rays (HXR Undulator) from 1.0 to 25.0 keV. The facility will also allow the possibility of generating near transform-limited pulses using self-seeding as well as downstream monochromators.

As illustrated in Figure 2, the facility is constructed to either deliver high-rate beam from the SCRF linac to both the SXR and HXR undulators, or to deliver the high-rate beam to the SXR undulator and deliver beam from the existing copper CuRF linac at 120 Hz to the HXR undulator.

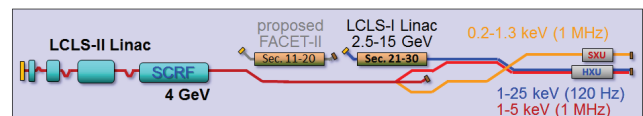


Figure 2: Schematic layout of the LCLS-II project.

\* Work supported by DOE Contract: DE-AC02-76-SF00515

<sup>#</sup> torr@stanford.edu

## FREE ELECTRON LASERS IN 2015

K. Cohn<sup>#</sup>, J. Blau, W. B. Colson, J. Ng, M. Price

Physics Department, Naval Postgraduate School, Monterey, CA 93943, USA

### Abstract

Thirty-nine years after the first operation of the free electron laser (FEL) at Stanford University, there continue to be many important experiments, proposed experiments, and user facilities around the world. Properties of FELs operating in the terahertz (THz) infrared (IR), visible, ultraviolet (UV), and X-ray wavelength regimes are tabulated and discussed.

### LIST OF FELS IN 2015

The following tables list existing (Table 1) and proposed (Tables 2, 3) relativistic free electron lasers (FELs) in 2015. The 1<sup>st</sup> column lists a location or institution, and the FEL's name in parentheses. References are listed in Tables 4 and 5; another useful reference is: [http://sbfel3.ucsb.edu/www/vl\\_fel.html](http://sbfel3.ucsb.edu/www/vl_fel.html).

The 2<sup>nd</sup> column of each table lists the operating wavelength  $\lambda$ , or wavelength range. The longer wavelength FELs are listed at the top and the shorter wavelength FELs at the bottom of each table. The seven orders of magnitude of operating wavelengths indicate the flexible design characteristics of the FEL mechanism.

In the 3<sup>rd</sup> column,  $t_b$  is the electron bunch duration (FWHM) at the beginning of the undulator, and ranges from almost continuous-wave to short sub-picosecond time scales. The expected optical pulse length in an FEL oscillator can be several times shorter or longer than the electron bunch depending on the optical cavity Q, the FEL desynchronization and gain. The optical pulse can be many times shorter in a high-gain FEL amplifier, or one based on self-amplified spontaneous emission (SASE). Also, if the FEL is in an electron storage-ring, the optical pulse is typically much shorter than the electron bunch. Most FEL oscillators produce an optical spectrum that is Fourier transform limited by the optical pulse length.

The electron beam kinetic energy  $E$  and peak current  $I$  are listed in the 4<sup>th</sup> and 5<sup>th</sup> columns, respectively. The next three columns list the number of undulator periods  $N$ , the undulator wavelength  $\lambda_0$ , and the rms undulator parameter  $K = eB\lambda_0/2\pi mc^2$  (cgs units), where  $e$  is the electron charge magnitude,  $B$  is the rms undulator field strength,  $m$  is the electron mass, and  $c$  is the speed of light. For an FEL klystron undulator, there are multiple undulator sections as listed in the  $N$ -column; for example 2x7. Some undulators used for harmonic generation have multiple sections with varying  $N$ ,  $\lambda_0$ , and  $K$  values as shown. Some FELs operate at a range of wavelengths by varying the undulator gap as indicated in the table by a range of values for  $K$ . The FEL resonance condition,  $\lambda = \lambda_0(1+K^2)/2\gamma^2$ , relates the fundamental wavelength  $\lambda$  to

$K$ ,  $\lambda_0$ , and the electron beam energy  $E = (\gamma-1)mc^2$ , where  $\gamma$  is the relativistic Lorentz factor. Some FELs achieve shorter wavelengths by using coherent harmonic generation (CHG), high-gain harmonic generation (HG), or echo-enabled harmonic generation (EEHG).

The last column lists the accelerator types and FEL types, using the abbreviations listed after Table 3.

The FEL optical power is determined by the fraction of the electron beam energy extracted and the pulse repetition frequency. For a conventional FEL oscillator in steady state, the extraction can be estimated as  $1/(2N)$ ; for a high-gain FEL amplifier, the extraction at saturation can be substantially greater. In a storage-ring FEL, the extraction at saturation is substantially less than this estimate and depends on ring properties.

In an FEL oscillator, the optical mode that best couples to the electron beam in an undulator of length  $L = N\lambda_0$  has a Rayleigh length  $z_0 \approx L/12^{1/2}$  and has a fundamental mode waist radius  $w_0 \approx (z_0\lambda/\pi)^{1/2}$ . An FEL typically has more than 90% of its power in the fundamental mode.

At the 2015 FEL Conference, there were three new lasings reported: the mid-IR FEL oscillator at Kyoto University was operated with a photocathode, the 3<sup>rd</sup> stage of the Novosibirsk THz FEL operated at 9  $\mu\text{m}$ , and the XUV FEL at DESY (FLASH) demonstrated cascaded SASE operation. Progress continues on many other existing and proposed FELs around the world; several large X-ray FEL facilities are scheduled to come online over the next couple of years.

### ACKNOWLEDGMENTS

The authors are grateful for support from the HEL-JTO.

<sup>#</sup>krcohn@nps.edu

# PHOTON ENERGIES BEYOND THE SELENIUM K-EDGE AT LCLS\*

F.-J. Decker, W. Colocho, Y. Ding, R.H. Iverson, H. Loos, J.C. Sheppard, H.V. Smith,  
J. L. Turner, SLAC, Menlo Park, CA 94025, USA

## Abstract

The Linac Coherent Light Source (LCLS) was designed for photon energies of 830 eV to 8.3 keV [1]. This range was widened and up to 11.2 keV photons have been already delivered to users. The selenium K-edge at 12.6578 keV is very interesting since selenium can replace sulphur in biological structures and then that structure can be precisely measured. To reach 12.7 keV, the electron energy would need to be raised by about 6% which initially did not seem possible. The trick was to change the final compression scheme from a highly correlated energy spread and moderate R56 in the compression chicane to moderate energy spread and large R56. The same bunch length can be achieved and RF energy is freed up, so the overall beam energy can be raised. Photons up to an energy of 12.82 keV (1.3% above the K-edge) with a pulse intensity of 0.93 mJ were achieved. The photon energy spread with this setup is wider at around 40-50 eV FWHM, since less correlated energy spread is left after the compression.

## INTRODUCTION

To achieve FEL lasing above the selenium K-edge, it was necessary to increase to electron beam energy to 16.9 GeV which is above the energy reach of the standard LCLS linac configuration. A crucial component of the energy increase was accomplished through raising the beam energy in the second bunch compressor (BC2) by accelerating closer to the crest of the RF in second Linac section (L2). The reduced energy spread from nearer to crest operation required an increase in the R56 of the BC2 chicane to achieve to nominal bunch compression required for FEL performance.

This paper starts with a brief historical perspective. A discussion of the BC2 chicane issues follows along with a note on the changes to L2 and expectations from LiTrack simulations. The paper concludes with a discussion of the FEL performance at the selenium K-edge energy.

## HISTORY

In May of 2013 an experiment started with the third harmonic to reach 11.2 keV. The low flux caused a try to use the fundamental at higher than “normal” photon energy. This yielded 50 times more photons. A final test followed quickly by pushing the limits; 11.92 keV was reached. The corresponding wavelength was still 4% longer than an Ångström (or 12.4 keV) and even further away from an interesting energy at 12.6578 keV, the

selenium K-edge. The corresponding electron energy difference of 6% (five RF stations) seemed too much to overcome easily. Adding a modulator and RF klystron and splitting the four accelerating sections of an existing station into 2+2 would give only 41% more energy, so about 12 additional modulator plus klystrons would be required. In the search for ways to raise the energy and since we had already performed a beam test, we missed the now obvious way to do it (using the available energy better).

This changed in July of 2014 when one of our Variable Voltage Substations (VVS) burnt up. We lost the energy contribution of 16 klystrons and were limited to about 7.0 keV, right where the then current experiment wanted to run. One of us felt the pressure that someone might ask him the next morning: “Why didn’t you think of ...?”, and came up with the brilliant idea, that we can trade the correlated energy spread (chirp) in L2 versus the R56 in the BC2 (Bunch Compressor 2) chicane. He also recognised the major limit since the bend magnets have to be raised for the R56 and then again for the higher energy, giving a quadratic behaviour and the power goes then with the fourth order of the required change.

## BC2 BEND MAGNETS

The bend magnets for the BC2 bunch compressor have to carry the main burden for the highest energy running. The maximum field strength was raised to 10 kG-m or 250 A current (from 200 A), which is 50% more in the maximum power and about three times than typical running conditions.

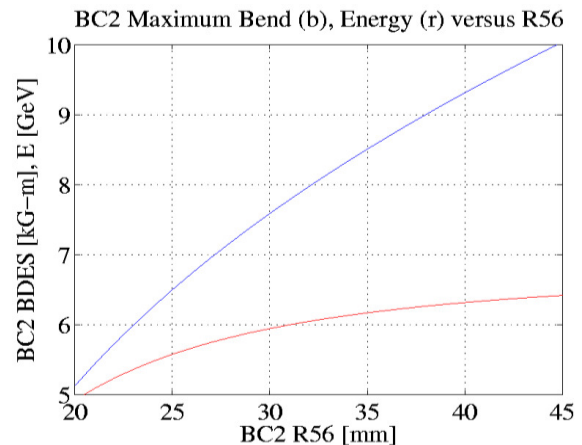


Figure 1: BC2 maximum bend strength and L2 energy versus R56 of the BC2 chicane.

\*Work supported by U.S. Department of Energy, Contract DE-AC02-76SF00515.

## TWO BUNCHES WITH NS-SEPARATION WITH LCLS\*

F.-J. Decker, S. Gilevich, Z. Huang, H. Loos, A. Marinelli, C.A. Stan, J.L. Turner, Z. van Hoover, S. Vetter, SLAC, Menlo Park, CA 94025, USA

### Abstract

The Linac Coherent Light Source (LCLS) delivers typically one electron bunch. Two-bunch operation is also possible, and is used to generate XFEL (x-ray free electron laser) pulse pairs for pump / probe experiments. Pulse pairs from two electron bunches with up to 100 fs separation have been already produced using a split and delay in the laser which produces them on the gun cathode [1]. Here we present a method to produce two bunches with longer separations by the combining two laser systems. This method allows any time separation within the limits imposed by RF and safety systems. We achieved separations up to 35 ns (limited by a beam safety system), different beam energies, and also vertical separations of several beam diameters. The vertical separation enabled a successful user experiment, and although it led to large fluctuations in the X-ray pulse energy it also provided an efficient pulse intensity scan.

### INTRODUCTION

An early two-bunch test in 2010 [2] with 8.4 ns bunch separation revealed the possibilities and constrains of multi-bunch operation. This two-bunch mode was initially envisioned to increase the hit rate in LCLS experiments as jets carrying samples could move sufficiently between bunches to expose a new part of the jet. Unfortunately, XFEL pulses also induce pressure waves and explosions, which damage the jets over distances longer than the jet translation between bunches, even for delays of a few

hundred ns [3]. Two-bunch operation with ns delays is nevertheless ideal for the investigation of these shock waves and explosions. The setup used in 2010 was upgraded and adjusted, as described in the next sections, for a user experiment [4] on XFEL explosions.

### LASERS

Two mostly identical laser systems are used for the gun cathode at LCLS, and in standard operation a mirror selects one of the beams (Fig. 1). We added a 50/50 splitter (combiner) that can be interchanged with the mirror to either select one of the beams or combine them. The timing of each laser and the intensity of the combined beam could be controlled remotely. For the experiments reported here, we did not have remote and separate intensity control for the two lasers to adjust continuously the charge of the electron bunches, but we could set the ratio of the final FEL intensities to either 1:10 or 2.5:5 by moving the timing of the heater laser to coincide with the arrival of either the second or the first laser pulse. Only one bunch could be heated, since the timing delay stage is after the combination. This setup was sufficient for the experiments, and several improvements remain possible for the laser system concerning two-bunch operation, such as individual intensity control, laser heater for both bunches, and pointing control. Figure 2 shows the control layout used to run either one of the lasers for single bunches, or to combine them for two bunches.

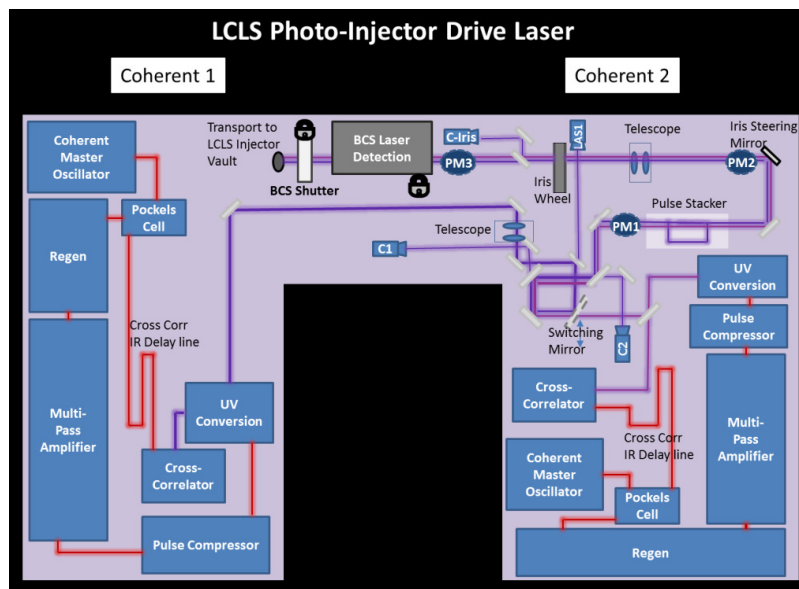


Figure 1: The laser system setup consists of two Coherent lasers, which can be selected with the switching mirror.

\*Work supported by U.S. Department of Energy, Contract DE-AC02-76SF00515.

# EFFECT OF MICROBUNCHING ON SEEDING SCHEMES FOR LCLS-II

G. Penn, J. Qiang, LBNL, Berkeley, CA 94720, USA  
 P. Emma, E. Hemsing, Z. Huang, G. Marcus,  
 T.O. Raubenheimer, L. Wang, SLAC, Menlo Park, CA 94025, USA

## Abstract

External seeding and self-seeding schemes are particularly sensitive to distortions and fluctuations in the electron beam profile. Wakefields and the microbunching instability are important sources of such imperfections. Even at modest levels, their influence can degrade the spectrum and decrease the output brightness. These effects are evaluated for seeded FELs at the soft X-ray beam line of LCLS-II. FEL simulations are performed in GENESIS based on various realistic electron distributions obtained using the IMPACT tracking code. The sensitivity depends on both the seeding scheme and the output wavelength.

## INTRODUCTION

At LCLS-II [1], the bandwidth is expected to be improved over SASE [2] through the use of self-seeding [3,4] schemes which filter out all but a narrow spectral bandwidth of the radiation somewhere in the middle of the undulators used for FEL amplification. Seeding using external lasers is another means by which a narrow spectrum can be produced, and includes other benefits such as more control over the x-ray pulse. Here we consider the self-seeding and echo-enabled harmonic generation (EEHG) schemes. Self-seeding is already being used at LCLS [5], while EEHG has been demonstrated at NLCTA [6] up to the 15th harmonic (160 nm).

Any attempt to generate coherent x-ray radiation from an electron beam is subject to phase variations caused by longitudinal variations in the electron bunch, through physical effects such as wake fields and the microbunching instability [7]. Laser heaters (LH) are currently used in LCLS to control the microbunching instability, and will be used in LCLS-II as well. In this paper, we consider two settings of the laser heater power, which produce microbunching at substantially different amplitude. The laser heater is set to that a slice energy spread of either 6 keV or 12 keV is produced at the end of the laser heater section, before bunch compression. We then characterize the sensitivity of each FEL scheme to microbunching by comparing the spectrum under these two settings.

The impact of wake fields is considered as well in these studies. When external lasers are used, they are modelled in an idealized fashion because the effect of laser errors is fairly well understood and broadly similar for different seeding schemes, except that EEHG has tighter tolerances on the laser power. It may be possible for carefully optimized lasers to improve performance even further, but because microbunching varies on a shot-by-shot basis there are limited possibilities to counteract this particular effect.

## ELECTRON BEAM AND UNDULATOR PARAMETERS

The simulations shown below use particles obtained from start-to-end (S2E) simulations of the injector and linac accelerating the beam to 4 GeV, using the code IMPACT [8]. Previous studies [1,9] used beams derived from ASTRA [10] and ELEGANT [11] which included wake fields and coherent synchrotron radiation (CSR) but only included space charge forces at very low energies. The IMPACT simulations which generated the beams used here track a very large number of particles for higher fidelity, have a full 3D space charge model, and a better algorithm for CSR [12]. The nominal parameters for the electron beam and the main undulator sections for producing radiation are given in Table 1. The longitudinal phase space of the beams are shown in Fig. 1. Note the substantial decrease in levels of microbunching at the higher laser heater settings.

The final undulators have a period of 39 mm and cover a tuning range from 250 eV to 1.3 keV. We study x-ray radiation pulses at 540 eV and 1.2 keV. When external lasers are used, they operate at a wavelength of approximately 260 nm.

Table 1: Example Beam and Undulator Parameters for Soft X-ray Production at LCLS-II

Parameter	Symbol	Value
<b>Electron Beam:</b>		
Bunch charge	$Q$	300 pC
Electron energy	$E$	4 GeV
Peak current	$I$	1 kA
Emittance	$\epsilon_N$	0.43 $\mu\text{m}$
Energy spread	$\sigma_E$	0.5 MeV
Beta function	$\beta$	15 m
<b>Final undulators:</b>		
Undulator period	$\lambda_u$	39 mm
Undulator segment length	$L_{\text{seg}}$	3.4 m
Break length	$L_b$	1.2 m
Min. magnetic gap	$g_{\text{min}}$	7.2 mm
Max. undulator parameter	$K_{\text{max}}$	5.48

## LAYOUTS FOR DIFFERENT FEL SCHEMES

The layouts for the two main schemes are shown in Fig. 2. FEL simulations were performed using GENESIS [13]. These and other schemes have previously been considered in the LCLS-II Conceptual Design Report [14] for idealized

# INFLUENCE OF SEED LASER WAVEFRONT IMPERFECTIONS ON HGHG SEEDING PERFORMANCE

T. Plath\*, C. Lechner, Universität Hamburg, Germany  
 S. Ackermann, J. Bödewadt, DESY, Hamburg, Germany

## Abstract

To enhance the spectral and temporal properties of a free-electron laser, the FEL process can be seeded by an external light field. The quality of this light field strongly influences the final characteristics of the seeded FEL pulse. To push the limits of a seeding scheme and reach the smallest possible wavelengths it is therefore crucial to have a thorough understanding of relations between laser parameters and seeding performance. In this contribution, we numerically study the influence of laser wavefront imperfections on high-gain harmonic generation seeding at the seeding experiment at FLASH.

## INTRODUCTION

To overcome statistical fluctuations of the radiation generated by a free-electron laser (FEL) that starts up from noise, the FEL process can be seeded by an external coherent source. In case of seeding schemes like high-gain harmonic generation (HGhg), a laser is used to imprint a sinusoidal energy modulation on the electron bunch. The quality of this modulation and the resulting bunching is strongly determined by the imperfections of the seed laser.

Since it is not practical to place a wavefront sensor at the region of interaction within the modulator undulator in order to measure laser wavefronts directly, often only the transverse intensity profile on screens can be used to diagnose the light field. From these measurements one can measure the transverse laser spot size as well as calculate the beam quality factor  $M^2$ .

Typically, simulations of seeding schemes are conducted with a perfect wavefront of the seed light field. Such a laser beam has a beam quality factor of  $M^2 = 1$ . As the beam quality factor degrades, additional modes arise in the transverse profile and the intensity distribution as well as the phase of the laser degrades in quality. Figure 1 shows exemplary the intensity profile of a laser beam with  $M^2 = 1.0$ ,  $M^2 = 2.0$  and  $M^2 = 3.0$ .

Using numerical methods we have investigated the influence of wavefront imperfections with a beam quality factor of up to  $M^2 = 5.8$ .

## NUMERICAL METHODS

All FEL simulations presented in this contribution have been conducted with GENESIS 1.3 [1]. The simulations have been conducted for the experimental seeding setup at FLASH1 [2]. The relevant parameters are given in Table 1.

The transfer matrix option of GENESIS 1.3 has been used in order to both match the beam into the radiator and introduce the right amount of dispersive strength to bunch the

Table 1: Simulation Parameters for FEL Simulations at the Seeding Experiment at FLASH

Lattice modulator		
Undulator period	$\lambda_u$	20 cm
Periods per undulator	$N_u$	6
Undulator parameter	$K_{rms}$	1.9
Lattice radiator		
Number of undulators		4
Undulator period	$\lambda_u$	31.4 mm
Periods per undulator	$N_u$	60 (4th one: 120)
Undulator parameter	$K_{rms}$	1.8
Laser pulse		
Wavelength	$\lambda_L$	267 nm
Peak power	$P_L$	300 MW
FWHM duration	$\Delta\tau$	50 fs
Electron beam		
Peak current	$I_{max}$	1500 A
Energy	$E$	675 MeV
Energy spread	$\sigma_E$	200 keV
Normalized emittance	$\epsilon_{n,x}, \epsilon_{n,y}$	1.5 mm mrad

electron beam. Thus, this simulation does not include any collective effects.

To properly model the seed laser imperfections, a field file that gives the complex electric field on each point of a three-dimensional grid has been used. This field was generated with the numeric algorithm described in [3]. It is based on the description of partially coherent beams using Hermite-Gaussian modes and allows the Monte Carlo driven generation of a modal composition for a given value of  $M^2$ .

In order to keep the axial symmetry of the seed field, only TEM<sub>*m**n*</sub> modes with even *m*, *n* have been considered. Since there are many possible combinations generating the same beam quality factors, the one with the minimum number of modes has been chosen. The total beam size has been kept constant along all profiles of a simulation run leading to the TEM<sub>00</sub> mode getting smaller and less intense with higher  $M^2$  as can be seen in Figure 2.

## SIMULATION RESULTS

For a sufficient modulation to be built up even for the higher values of  $M^2$ , we chose a seed laser peak power of 300 MW, a full-width half maximum seed duration of  $\Delta\tau = 50$  fs and a FWHM spot size of the laser beam of 800  $\mu\text{m}$ .

# FIRST LASING OF AN HGHG SEEDED FEL AT FLASH

Kirsten Hacker, Shaukat Khan, Robert Molo  
DELTA, TU Dortmund, Germany

Sven Ackermann, Ralph Wolfgang Assmann, Jörn Bödewadt, Nagitha Ekanayake,  
Bart Faatz, Ingmar Hartl, Rosen Ivanov, Tim Laarmann, Jost Müller, Holger Schlarb  
DESY, Hamburg, Germany

Philipp Amstutz, Armin Azima, Markus Drescher, Leslie Lamberto Lazzarino,  
Christoph Lechner, Theophilos Maltezopoulos, Tim Plath, Jörg Rossbach  
University of Hamburg, Germany

## Abstract

The free-electron laser facility FLASH at DESY operates in SASE mode with MHz bunch trains of high-intensity extreme ultraviolet and soft X-ray FEL pulses. A seeded beamline which is designed to be operated parasitically to the main SASE beamline has been used to test different external FEL seeding methods. First lasing at the 7th harmonic of a 266 nm seed laser using high-gain harmonic generation has been demonstrated.

## INTRODUCTION

The seeding section at the Free-electron Laser in Hamburg (FLASH) facility was named sFLASH and designed to be operated in parallel with the FLASH1 and FLASH2 SASE sections [1] (Fig. 1). These three beamlines have been operated simultaneously in SASE mode with a peak current of 1.3 kA and wavelengths of 13.7 nm in FLASH1, 20 nm in FLASH2, and 38.1 nm in

sFLASH. Operation of the sFLASH section in seeded-mode can potentially be done parasitically with <kA peak currents and improved quadrupole alignment.

Seeding takes place when the electron bunch interacts with a laser pulse within an undulator magnet known as a modulator. The resulting sinusoidal energy modulation is transformed into a density modulation via longitudinal dispersion (Fig. 2). For a seeded FEL using the High-Gain Harmonic Generation (HG) scheme, microbunch trains with the periodicity of the seed laser wavelength will radiate at a harmonic of the microbunch repetition rate when they are sent through an FEL radiator tuned to that harmonic; shorter microbunches will have higher harmonic content [2,3].

For the first time at FLASH, lasing at the 7th harmonic of a 266 nm seed using high-gain harmonic generation has been demonstrated. The 266 nm seed pulses were generated from 800-nm Ti:sapphire light by using a frequency tripler made up of BBO crystals and crystalline quartz waveplates [4]. The mean pulse energy was  $(12 \pm 12) \mu\text{J}$ , the maximum pulse energy was  $75 \mu\text{J}$ , and the estimated gain length was  $\sim 0.9 \text{ m}$ . The bandwidth was  $0.2 \text{ nm}$  (FWHM) with  $\Delta\lambda/\lambda = 5.2 \times 10^{-3}$ . Future efforts will be concentrated on improving the stability of the seeded beam, parasitic operation, and progress towards Echo-Enabled Harmonic Generation (EEHG) [5,6] seeding.

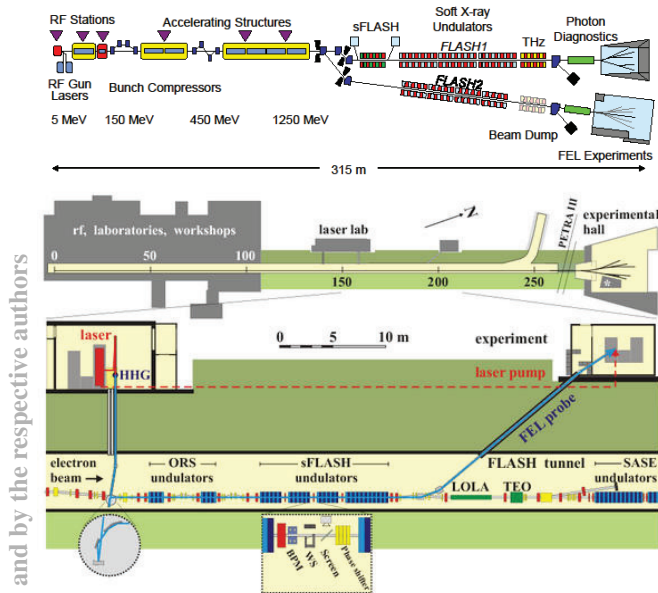


Figure 1: Layout of the FLASH facility and the sFLASH seeding section. The sFLASH section is designed to be operated in parallel with SASE generation in FLASH1 and FLASH2. It is followed by the RF deflector LOLA which makes longitudinal phase space distribution measurements. The seed laser is split so that part can be sent to the FEL user station for pump-probe experiments.

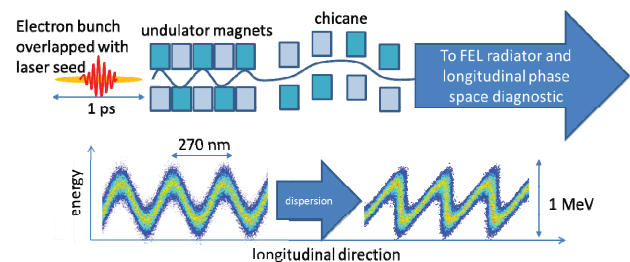


Figure 2: The HGHG experiment uses electron bunches with a peak current between 0.5 and 1 kA together with a 266 nm seed pulse, a 5 period undulator, and a chicane with  $\sim 100 \mu\text{m}$  of longitudinal dispersion.

## MILESTONES

The HGHG seeding experiment was conceptualized in 2011 [5,7] and a dedicated seed injection setup was partially commissioned in 2012 [8], but filamentation of

# MEASUREMENTS AND SIMULATIONS OF SEEDED MICROBUNCHES WITH COLLECTIVE EFFECTS

K. Hacker\*, R. Molo, S. Khan, DELTA, TU Dortmund, Germany  
 S. Ackermann, J. Boedewadt, M. Dohlus, N. Ekanayake, T. Laarmann, H. Schlarb,  
 DESY, Hamburg, Germany  
 L. L. Lazzarino, C. Lechner, Th. Maltezopoulos, T. Plath, J. Rossbach,  
 Universitaet Hamburg, Germany

## Abstract

Measurements of the longitudinal phase-space distribution of electron bunches seeded with an external laser were done in order to study the impact of collective effects on seeded microbunches in free-electron lasers. When the collective effects of Coulomb forces in a drift space and coherent synchrotron radiation in a chicane are considered, velocity bunching of a seeded microbunch appears to be a viable alternative to compression with a magnetic chicane under high-gain harmonic generation seeding conditions. Measurements of these effects on seeded electron microbunches were performed with an RF deflecting structure and a dipole magnet which streak out the electron bunch for single-shot images of the longitudinal phase-space distribution. Particle tracking simulations in 3D predicted the compression dynamics of the seeded microbunches with collective effects.

## INTRODUCTION

Seeding takes place when the electron bunch interacts with a laser pulse within an undulator magnet known as a modulator. The resulting sinusoidal energy modulation is transformed into a density modulation via longitudinal dispersion. For a seeded FEL using the High-Gain Harmonic Generation (HG) scheme, microbunch trains with the periodicity of the seed laser wavelength will radiate at a harmonic of the microbunch repetition rate when they are sent through an FEL radiator tuned to that harmonic; shorter microbunches will have higher harmonic content [1,2].

The longitudinal dispersion used to compress microbunches is typically provided through the energy-dependent path in a series of bending magnets which compose a magnetic chicane, but this will result in coherent synchrotron radiation (CSR) emitted by the tail of the bunch early in a bend catching up with the head of the bunch, producing an inhomogeneous energy loss along the bunch which is proportional to the peak current, bend radius, and bend length [3,4]. While typically of concern on the macrobunch scale due to nonlinear chirps which broaden the FEL spectrum, CSR is also of concern when it changes the energy, energy spread, or bunch length on the microbunch scale. Since the harmonic content of a seeded beam is given by the Fourier transform of the longitudinal current distribution, a change in the microbunch length has a direct impact on the high harmonic content. Here, we present simulations

\*kirsten.hacker@desy.de

and measurements of the effect of CSR on the longitudinal phase-space distributions of seeded electron microbunches compressed in a chicane and we contrast it with the effect of Coulomb forces on seeded electron microbunches which are primarily compressed through velocity bunching in a drift space with quadrupole focusing optics.

In [5], the concept that Coulomb forces and velocity bunching could be used to reduce the energy spread for soft X-ray HG applications was investigated due to the requirement that the HG seeded beam in a proposed seeding design would need to drift for 20 meters before entering the radiator. Here, a condensed presentation is given of measurements and 3D simulations [6] performed with conditions at the Free-electron Laser in Hamburg (FLASH). The investigation of these microbunch collective effects was done with an RF deflector and dipole spectrometer which streak out a 700 MeV electron bunch for single-shot measurements of the particle distribution in longitudinal phase-space (Fig. 1). Quantitative agreement with simulations was observed within the error bars of the measurements and original physical interpretations are used to explain new effects discovered in the measurement method.

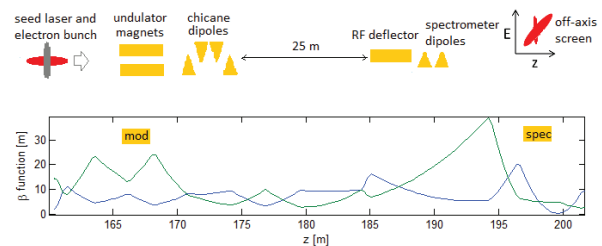


Figure 1: Layout of experimental setup. A seed laser is used to modulate the energy of the electron beam. The energy modulation is converted into density modulation through dispersion in a chicane, a drift, or in the dipoles of the spectrometer. The longitudinal phase space distribution is measured on an off-axis screen after the RF deflector and spectrometer.

## MEASUREMENTS

Longitudinal phase space distribution measurements done at the Free-electron Laser in Hamburg (FLASH) are compared to particle tracking simulations for different compression settings of the chicane at the entrance to a 25-m long stretch of beamline with a beta-function which varies from 3 to 23 m and an average beam radius of

# DEVELOPMENT ACTIVITIES RELATED TO RF CABLES FOR GOOD PHASE STABILITY

Jinyul Hu<sup>#</sup>, Heung-Soo Lee, Heung-Sik Kang, PAL, POSTECH, Pohang, South Korea

## Abstract

XFEL systems require extreme RF stabilities in amplitude and phase. RF cables as parts of the systems also require very high stabilities. RF cable measurements are performed to choose good cables. A simple measurement method and test results are presented. To enhance the phase stability of RF cables a prototype jacket surrounding a RF cable is constructed and the test result is described. Finally, a modification for phase measurement of RF cables is presented.

## INTRODUCTION

XFEL(X-ray Free Electron Laser) systems can generate X-rays much brighter than those from current storage rings constructed around the world. In this strength, several XFEL construction projects are in progress. Among them are PAL-XFEL at PAL, South Korea, European XFEL at DESY, Germany[1], SwissFEL at PSI, Switzerland[2], and LCLS2 at SLAC, USA[3]. There are already two XFEL systems in operation, which are LCLS at SLAC[3] and SACLA in Japan[4]. But to achieve the X-rays planned, FEL machines must be very stable in several aspects including RF stabilities.

The required pulse-to-pulse RF stabilities for PAL-XFEL are 0.02% in rms amplitude and 0.03° in rms phase. Additionally, the drift of RF fields caused by the environmental temperature change must also be minimized to obtain stable X-rays. To consider the drift of RF illustratively, let us use Fig. 1.

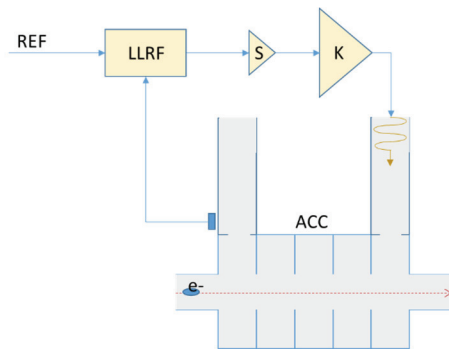


Figure 1 : RF station sketch.

Figure 1 shows a simplified RF station of a XFEL or a linac. The LLRF receives the reference CW(REF) through a coaxial cable, and it emits RF pulses into the SSA(S) through a coaxial cable. The SSA(S) amplifies the small RF pulses in mW level into kW level, which are sent through a coaxial cable to drive the klystron(K). The klystron(K) amplifies the RF pulses into about 80MW

<sup>#</sup>hju@postech.ac.kr

level and sends them to the accelerating column(ACC) through waveguides. Then the electron beams going through the column are accelerated synchronously with RF fields.

If all the components of Fig. 1 are not sensitive to the temperature variation and other causes, there will be no drift in RF fields, and there will be no needs to optimize the components and control by feedback. But in real situation, all the components are sensitive to temperature change more or less. So, each component should be optimized in temperature, or put in temperature controlled rack to minimize the drift. Though local feedback and global feedback corrects the drifts by temperature change, it should be preceded optimizing components to minimize the drifts by temperature change. The cables and waveguides applied must also be optimized with temperature change.

In this article, we present our activities to minimize the RF drifts within RF cables by temperature change for XFEL.

## CABLE SELECTION ACTIVITES

Cable manufacturers do not always provide RF drift data by temperature variation. Some papers treating this topic[5] do not consider S-band used for PAL-XFEL. So, the drift measurement for our PAL-XFEL machine was carried out to select adequate RF cables.

### Setup for RF Drift Measurement

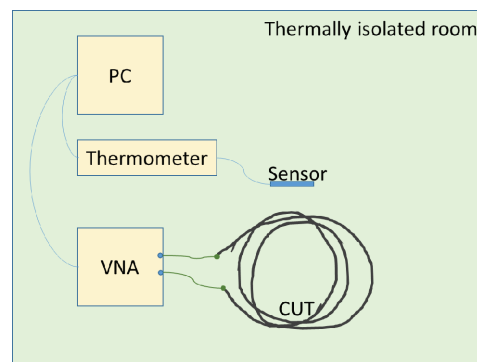


Figure 2 : RF drift measurement setup.

Figure 2 shows the simple setup invented for the drift measurement of cables. Within the thermally isolated room(usual room which is enclosed by ordinary wall), RF Vector Network Analyser(VNA) in connection with the cable under test(CUT), and the precision thermometer are used. PC for data acquisition is adopted. The above devices act as small heaters. With this setup, RF drift data along temperature are collected by the PC.

The drift data gathered include VNA drift also. The VNA drift must be removed from the data. To do the

# PRODUCTION STATUS OF ACCELERATOR COMPONENTS

N. Shigeoka<sup>#</sup>, M. Kimura, S. Miura, K. Okihira  
Mitsubishi Heavy Industries, Ltd., Mihara, Hiroshima, Japan

## Abstract

Mitsubishi Heavy Industries, LTD. (MHI) has been delivered various kinds of accelerator components to multiple FEL facilities. Recently we completed production of S-band accelerating structures for PAL-XFEL. Currently we are manufacturing C-band waveguide network for SwissFEL. Production status and results of above-mentioned products are reported in this paper.

## INTRODUCTION

MHI has started manufacturing of accelerator components such as accelerating structures in 1960s. For example, in a field of normal conducting accelerator, in recent years, MHI had handled mass production of C-band choke-mode accelerating structures and SLED for Riken SACLA, production of DTL, SDTL (Separated DTL), ACS (Annular Coupled Structure) for JAEA/KEK J-PARC [1]. In latest years, MHI manufactured over 120 S-band accelerating structures for PAL-XFEL project [2-4] and shipment has completed in March 2015. In addition, MHI has accepted order of C-band waveguide network prototype (CWNP) for SwissFEL project [5] in June 2014 and has been already delivered to PSI in December 2014 [6]. MHI also has been accepted order of 26 C-band waveguide network series (CWNS) and the production of them is in progress now.

## S-BAND ACCELERATING STRUCTURES FOR PAL-XFEL

Mass-production of the S-band 3 m long accelerating structure [7-8] started in June 2012 and finished at March 2015. Totally 120 structures has been delivered to PAL. Appearance of the structure is shown in Fig. 1 and main parameters are shown in Table 1.

Results of LLRF measurement after tuning are shown in Fig. 2. It shows excellent performance of production.

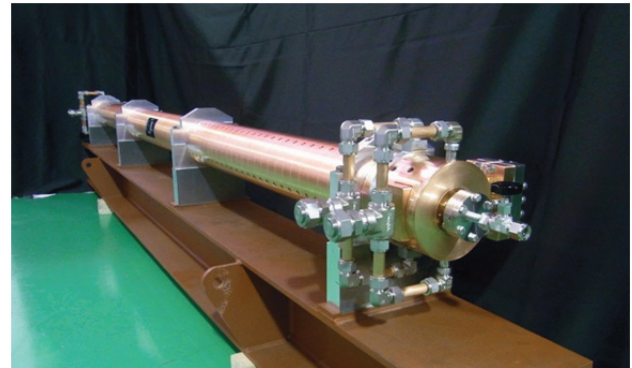


Figure 1: Appearance of the S-band accelerating structure for PAL-XFEL.

Table 1: Main Parameters of the S-band Accelerating Structure for PAL-XFEL

Item	Value
Operating frequency	2856 MHz
Accelerating type	C. G.
Phase shift per cavity	$2\pi/3$
Unloaded Q	13,000
Attenuation constant	0.56
Input / Output VSWR	< 1.05
Phase error	< +/- 2.5 degree
Number of cells	82 + 2 coupler cells
Filling time	0.84 $\mu$ s
Length	3 m
Coupler type	Quasi-symmetrical

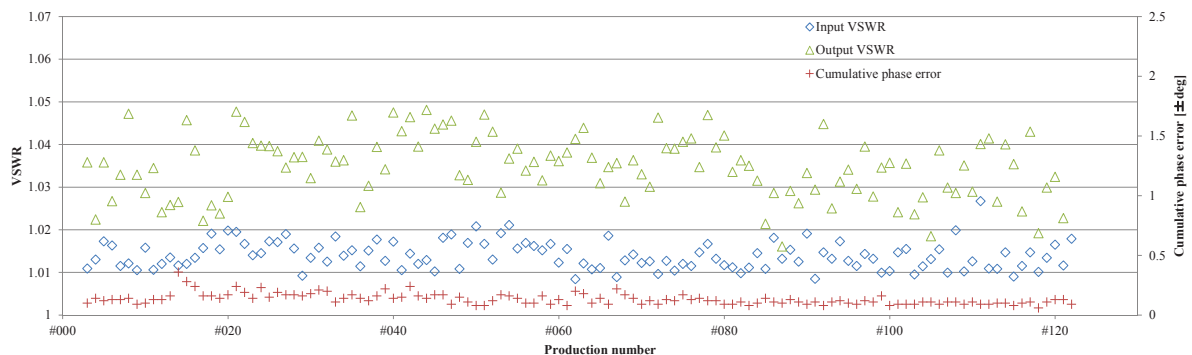


Figure 2: Input / Output VSWR and cumulative phase error of 120 S-band structure for PAL-XFEL after tuning.

<sup>#</sup>nobuyuki\_shigeoka@mhi.co.jp

ISBN 978-3-95450-134-2

658

FEL Technology and HW: Gun, RF, Laser, Cathodes

# COMMISSIONING AND FIRST PERFORMANCE OF THE LINAC-BASED INJECTOR APPLIED IN THE HUST THz-FEL

T.N. Hu, Q.S. Chen, Y.Q. Xiong, B. Qin, P. Tan, L. Cao, J. Li, W. Chen

State Key Laboratory of Advanced Electromagnetic Engineering and Technology, HUST,  
Wuhan 430074, China

Y.J. Pei\*, Z.X. Tang, Z.Y. Zhao, J. Liu

National Synchrotron Radiation Laboratory, USTC, Hefei 230029, China

## Abstract

The construction of a compact high-power THz source based on the free electron laser (FEL), which is constructed in HUST, is undergoing. Before the end of 2014, we have installed most of the key components, completed conditioning of the LINAC-based FEL injector, and performed first beam experiment. During last 5 months, we have established a high efficient beam diagnostic system with a reliable online monitor platform and precise data processing methods. At present, longitudinal properties such as the micro-pulse width and the energy spread are kept to a reasonable level, while transverse emittance compensation by adjusting focusing parameters is still undergoing. In this paper, we will give the summary on the commissioning schedule, detailed commissioning plan, the development of the commissioning and first performance of the LINAC, etc.

## INTRODUCTION

### Brief Descriptions of the FEL-based LINAC

The THz-FEL facility is mainly composed of a novel EC-ITC RF gun (which consists of a DC electron gun and two independent standing-wave cavities), constant gradient travelling wave structure with a collinear absorbing load and an input coupler which makes the electric field be symmetry, and its focusing coil, beam diagnostics system, microwave power system, vacuum system, control system and so on [1]. The layout and main parameters of the LINAC are given by Fig. 1 and Table 1 respectively, and beam diagnostic equipments are sketched by Fig. 1 either.

By applying the EC-ITC RF gun as the pre-LINAC, and adopting the elements already exist these methods, the length of the whole beam line can be compressed into 2 m, which contributed to a more compact layout for the whole facility.

### Beam Diagnostic System

For the sake of compactness, the beam diagnostic system should use the elements which already exist in the facility as far as possible [2]. As Fig. 1 shows, the online beam testing system contains two Toroids, one Flag with a fluorescent screen and a OTR screen, energy analysis system, two fluorescent targets, and three CCD (Charge-

Table 1: Main Specifications

Parameter	Unit	Value
Energy	MeV	4-15
Current	A	0.571 (Macro pulse)
Width	us	1-5 (Macro pulse)
	ps	1-10 (Micro pulse)
Energy spread	%	0.2-0.5
Nor. emittance	mm mrad	<15
RF frequency	MHz	2856
Input power	MW	20

Coupled Device) cameras.

In order to measure the beam length, we will adopt a method which is by means of a relation of electron energy and its phase in the Linac. When beam located at the "0" phase, the energy spread will change less. If the beam phase located in  $\varphi$  which is different from the "0", their energy spread will change and larger than initial energy spread. This change depend on beam length, so measuring these energy, energy spread and their phase, we can get pulse width [3].

Obviously, we will use quadrupole scanning technique perform normalized emittance measurement [4]. Since the beam matrix at Target2 can be written as  $\Sigma_1$ . And the beam matrix at the entrance of the Quadrupole chosen to be scanned is  $\Sigma_0$ . So that the two beam matrixes can be connected by the transmission matrix of the Quadrupole  $M$ ,  $\Sigma_1 = M \Sigma_0 M'$ , If we change the current of the Quadrupole three times, three different beam spot sizes  $\sigma_{11}(1)$ ,  $\sigma_{11}(2)$ ,  $\sigma_{11}(3)$  will be obtained on Target2 by CCD3, then we can obtain the following equation set,

$$\begin{pmatrix} \sigma_{11}(1) \\ \sigma_{11}(2) \\ \sigma_{11}(3) \end{pmatrix} = \begin{pmatrix} m_{11}^2(1) & 2m_{11}(1)m_{12}(1) & m_{12}^2(1) \\ m_{11}^2(2) & 2m_{11}(2)m_{12}(2) & m_{12}^2(2) \\ m_{11}^2(3) & 2m_{11}(3)m_{12}(3) & m_{12}^2(3) \end{pmatrix} \begin{pmatrix} \sigma_{11}(0) \\ \sigma_{12}(0) \\ \sigma_{22}(0) \end{pmatrix} \quad (1)$$

By solving above equation set, parameters used to calculate the normalized emittance can be determined, and the following formula should be used,

\* Authors to whom correspondence should be addressed.

Electronic addresses: yjpei@ustc.edu.cn

# STUDY ON BEAM MODULATION TECHNIQUE USING A MASKED CHICANE AT FAST (FERMILAB ACCELERATOR SCIENCE AND TECHNOLOGY) FACILITY\*

Y. M. Shin, Department of Physics, Northern Illinois University, Dekalb, IL 60115, USA, and  
FNAL, Batavia, IL 60510, USA

A. Green, Department of Physics, Northern Illinois University, Dekalb, IL 60115, USA  
D. R. Broemmelsiek, D. J Crawford, A. Lumpkin, FNAL, Batavia, IL 60510, USA

## Abstract

Longitudinal density modulations on electron beams can improve machine performance of beam-driven accelerators and FELs with resonance beam-wave coupling. The sub-ps beam modulation has been studied with a masked chicane by the analytic model and simulations with the beam parameters of the Fermilab Accelerator Science and Technology (FAST) facility. With the chicane design parameters (bending angle of  $18^\circ$ , bending radius of 0.95 m and  $R_{56} \sim -0.19$  m) and a nominal beam of 3-ps bunch length, the analytic model showed that a slit-mask with slit period 900  $\mu\text{m}$  and aperture width 300  $\mu\text{m}$  generates about 100- $\mu\text{m}$  modulation periodicity with 2.4% correlated energy spread. With the designed slit mask and a 3-ps bunch, particle-in-cell simulations (CST-PS), including nonlinear energy distributions, space charge force, and coherent synchrotron radiation (CSR) effect, also result in  $\sim 100$   $\mu\text{m}$  of longitudinal modulation. The beam modulation has been extensively examined with three different beam conditions, 2.25 ps (0.25 nC), 3.25 ps (1 nC), and 4.75 ps (3.2 nC), by extended 3D tracking simulations (Elegant). The modulated bunch generation is tested by a slit-mask installed at the chicane of the ASTA 20-MeV injector beamline and the preliminary test result is presented in the paper.

## INTRODUCTION

The masked chicane technique [1–3] has been investigated with the 50 MeV linac in the Fermilab Accelerator Science and Technology (FAST) facility, which is currently being constructed and commissioned in Fermilab [4]. A tungsten slit-mask is currently installed in a magnetic chicane, consisting of four bending dipole magnets, downstream of the 50 MeV photoinjector and the bunch performance and sub-ps micro-bunch generation capability are examined with analytic calculations and PIC simulations.

For the theoretical evaluation on bunching performance, the linear bunching theory is derived to check bunch-to-bunch distance and microbunch length with FAST nominal beam parameters (RMS bunch length  $\sigma_{z,i}$  is 3 ps and energy ratio  $\tau$  is around 0.1) are analyzed by the linear bunching theory, which was tested by beamline

simulations using Elegant code and CST-PS. Space charge forces and CSRs are included in the simulations with nonlinear charge distribution over macro-particles. For Elegant simulations, bunch charge distribution and the beam spectra are mainly investigated with three different bunch charges, 0.25 nC, 1 nC, and 3.2 nC, under two RF-chirp conditions of minimum and maximum energy spreads. The corresponding bunch length for the maximally chirped beam is 2.25, 3.25, and 4.75 ps and the correlated energy spread is 3.1, 4.5, and 6.2 % respectively for bunch charge of 0.25 nC, 1 nC, and 3.2 nC.

## ANALYTIC DESIGN

The magnetic chicane is designed with four dipoles and a slit mask with slit spacing,  $W$ , and aperture width,  $a$ , is inserted in the middle of the bunch compressor (dispersion region). A positive linear energy-phase correlation is imposed by accelerating the beam off the crest of the RF wave in the linear accelerator before the beam is injected into the masked chicane. In this way, the chicane disperses and re-aligns the particles with respect to their energies in phase space. The input beam is then compressed and the phase space ellipse is effectively rotated toward the vertical. In the middle of the chicane, the beam is partially blocked by the transmission mask and holes are introduced in the energy-phase ellipse. The beam is deliberately over-bunched in the second half of the chicane and the beam ellipse is slightly rotated past the vertical. Accompanied with a steeper phase-space slope, the linear energy-phase correlation is preserved by over-bunching. The projection of the beam ellipse on the time axis therefore generates density modulations at a period smaller than the grid spacing.

The microscopic structure of a bunch can be controlled with a masked chicane under compression by adjusting the grid period and/or by varying the chicane magnetic field. In principle, if a grid period (or slit-spacing) is smaller than a hundred microns, a modulation wavelength of the bunched beam is possibly cut down to a few tens of microns. The beamline for the mask is originally designed with the four dipoles having bending angle of  $18^\circ$ , bending radius  $R = 0.95$  m, and dipole separation  $D = 0.68$  m. The 125  $\mu\text{m}$  thick tungsten mask with a slit-array is designed with period of  $W = 900$   $\mu\text{m}$  and aperture width of  $a = 300$   $\mu\text{m}$  ( $\sim 33$  % transparency).

\*Work supported by the DOE contract No.DEAC02-07CH11359 to the Fermi Research Alliance LLC.

# FEMTOSECOND TIMING DISTRIBUTION AT THE EUROPEAN XFEL

C. Sydlo, F. Zummack, J. Mueller, M. Felber, M.K. Czwalińska, C. Gerth, H. Schlarb,  
 DESY, Hamburg, Germany  
 S. Jablonski, Warsaw University of Technology, Warsaw, Poland

## Abstract

Accurate timing synchronization on the femtosecond timescale is an essential installation for time-resolved experiments at free-electron lasers (FELs) such as FLASH and the upcoming European XFEL. To date the required precision levels can only be achieved by a laser-based synchronization system. Such a system has been successfully deployed at FLASH and is based on the distribution of femtosecond laser pulses over actively stabilized optical fibers. For time-resolved experiments and for special diagnostics it is crucial to synchronize various laser systems to the electron beam with a long-term stability of better than 10 fs.

The upcoming European XFEL has raised the demands due to its large number of stabilized optical fibers and a length of 3400 m. Specifically, the increased lengths for the stabilized fibers had necessitated major advancement in precision to achieve the requirement of less than 10 fs precision. This extensive rework of the active fiber stabilization has led to a system exceeding the current existing requirements and is even prepared for increasing demands in the future. This paper reports on the laser-based synchronization system focusing on the active fiber stabilization for the European XFEL, discusses major complications, their solutions and the most recent performance results.

## INTRODUCTION

For the European XFEL a very strong emphasis is put on accurate timing and on the optical timing distribution. Already in the very first expansion stage 27 stations will receive optical synchronization with the option to extend this number to 44 stations. Additionally, the length of the accelerator increases by an order of magnitude compared to FLASH, which has a length of 300 m. This has necessitated a thorough planning and redesign of the existing optical synchronization system at FLASH. In the following an overview is given.

The master-oscillator (MO) distributes a stabilized 1.3 GHz reference to which the master laser-oscillator (MLO), with a repetition rate of 216.7 MHz (a sixth of the MO frequency), is locked. The stabilized pulse train from the MLO is split into multiple channels and guided to the individual link stabilization units (LSUs) through the free-space distribution (FSD). Each LSU actively stabilizes the effective length of its assigned optical link fiber, which can conveniently be guided through the entire FEL to stations obliged to femtosecond timing stability. One notable feature in this optical synchronization system is the slave laser-oscillator (SLO) at the end of the FEL. A sub-synchronization will be located in the experimental hall at the end of the beamlines

to facilitate all the synchronization needs for the pump-probe lasers on-site. Additionally, it will stabilize all stations between 2.1 km and the end of the experimental hall. Hence, two more links with a length of 3.6 km are provided for SLO to MLO locking. On the one hand, this serves as a redundancy improving reliability and robustness. On the other hand, these two long links can be cross-correlated in-situ for diagnostics providing numbers for the actual synchronization accuracy.

## CONCEPT

The optical synchronization system for the European XFEL will adopt to the greatest possible extent the proven and reliable system from FLASH. The long term experience with the optical synchronization system at FLASH has led to numerous enhancements and deeper understanding of the issues involved in such a complex and sensitive precision arrangement. Consequently, for the European XFEL an inimitable possibility arises to incorporate all the gathered knowledge from the bottom up into a new benchmark setting synchronization system.

The distribution of a highly stable optical pulse train to different stations along the complete European XFEL is divided into multiple steps which need individual attention.

The key system of the optical reference distribution is the master laser oscillator (MLO) which is stabilized by a phase-locked loop against the master oscillator (MO), which again is frequency stabilized by a Global Positioning System receiver to ensure best possible long term performance. The locking of the optical pulse train of the MLO against the RF signal of the MO requires a photodiode to convert the optical signal to an electrical for phase comparison. The phase difference is fed back by a feedback loop into the MLO. However, a conventional photodiode set-up is subjected to the AM-to-PM effect [1–3], where amplitude variations convert into phase variations. Despite the very high optical power stability of the deployed MLO minimising the degradation of phase variation due to the aforementioned effect, a more sophisticated method will be introduced for MLO locking. This method is inherently free of the AM-to-PM effect and has already proven high performance [4].

The stabilized optical pulse train is split free space by polarizing beam splitters into multiple channels to feed all link stabilization units (LSU). To accommodate the large number of LSUs - up to 24 LSUs are used on one optical table - they need to be placed efficiently. The optical free space path for each individual channel reaches a certain length. The lengths are kept identical to maintain identical beam parameters for each LSU. However, a distance of about 2 m has to be covered in free space on the optical table.

ISBN 978-3-95450-134-2

# ELECTRON BEAM DIAGNOSTICS FOR FEL STUDIES AT CLARA

S. Spampinati<sup>#</sup>, University of Liverpool & The Cockcroft Institute, Cheshire, UK  
D. Newton, University of Liverpool, Liverpool, UK

## Abstract

CLARA (Compact Linear Accelerator for Research and Applications) is a proposed 250 MeV, 100–400 nm FEL test facility at Daresbury Laboratory [1]. The purpose of CLARA is to test and validate new FEL schemes in areas such as ultra-short pulse generation, temporal coherence and pulse-tailoring. Some of the schemes that can be tested at CLARA depend on a manipulation of the electron beam properties with characteristic scales shorter than the electron beam. In this article we describe the electron beam diagnostics required to carry on these experiments and simulations of FEL pulse and electron beam measurements.

## INTRUCTION

Some of the most advanced schemes proposed to improve FEL performance depend on a manipulation of the electron beam properties with characteristic scales of several coherence lengths and shorter than the electron beam [2–4]. We are interested to test, among other schemes, mode locking FEL and femto-slicing for the production of trains of short pulses [4–7]. The implementation of these schemes at CLARA requires a 30 - 50  $\mu\text{m}$  modulation of the beam energy acquired via the interaction with an infrared laser beam in a short undulator (modulator). The performance of these FEL schemes depends on this energy modulation. So monitoring the longitudinal phase space of the electron beam is important to perform and to realize these experiments. A deflecting cavity [8] installed in the last part of the FEL line will allow the longitudinal beam distribution to be observed on a screen placed after the dipole leading to the beam dump. The FEL line of CLARA, as shown in Fig. 1a, is composed of two modulators separated by a dispersive section, seventeen radiators and an afterburner. The afterburner is composed by a series of short undulators and delay chicanes. A possible layout of the diagnostic system placed at the end of the CLARA undulator from the afterburner is shown in Fig. 1b.

In this design, the electron beam is deflected vertically by the deflecting cavity. This deflection maps the electron beam longitudinal coordinate to the vertical coordinate on an intercepting screen after the spectrometer dipole magnet; the dipole converts the particle's energy to the screen horizontal coordinate. Consequently, the electron beam longitudinal phase space is imaged on the screen, and the energy modulation taking place in the modulator can be studied and optimized. Another interesting application of this diagnostic beam line could be the study of the FEL process taking place in the different operation modes of CLARA.

<sup>#</sup>simone.spampinati@cockcroft.ac.uk

ISBN 978-3-95450-134-2

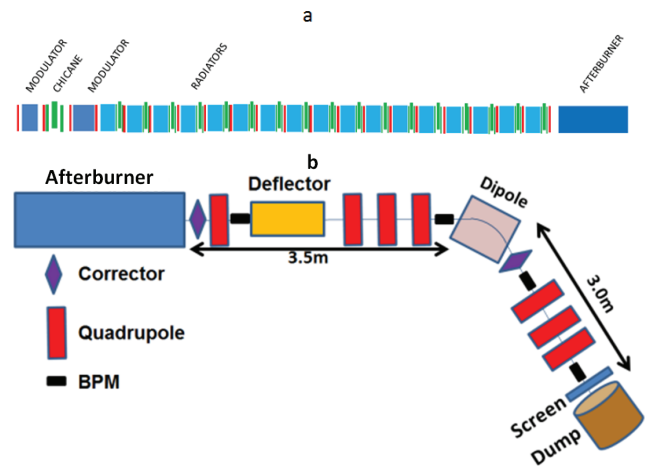


Figure 1: Top: FEL line of CLARA. Bottom: Layout of the phase space diagnostics composed by of a transverse deflector and an energy spectrometer.

## OPTICS OPTIMIZATION AND RESOLUTIONS

The vertical beam size at the screen, after deflection, is [9]:

$$\sigma_y = \sqrt{\sigma_{y,0}^2 + (S\sigma_z)^2} \quad (1)$$

where  $\sigma_{y,0}$  the vertical beam size at the screen location without deflection is,  $\sigma_z$  is the longitudinal beam size and  $S$  is the calibration factor representing the strength of the beam deflection [9]:

$$S = \frac{e_0 V k}{pc} \sqrt{\beta_{y,S} \beta_{y,D}} |\sin \Delta\Psi| \quad (2)$$

here  $k = \frac{2\pi}{\lambda}$  with  $\lambda = 10.01\text{cm}$  for an S-band cavity

(frequency of 2.998 GHz).  $V_0$  is the deflecting voltage,  $\beta_{y,D}$  and  $\beta_{y,S}$  are vertical betatron functions at the deflector and the screen, respectively.  $\Delta\Psi$  is the vertical betatron phase advance between the deflector and the screen. The size of the image of the beam detected on the screen will be increased by the system resolution (screen and CCD pixel size) and:

$$\sigma_y = \sqrt{\sigma_{y,0}^2 + \sigma_{screen}^2 + (S\sigma_z)^2} \quad (3)$$

where  $\sigma_{Screen}$  is the screen and CCD resolution.

# THE PROTOTYPE OF NEW VARIABLE PERIOD UNDULATOR FOR NOVOSIBIRSK FREE ELECTRON LASER

I.V. Davidyuk , O.A. Shevchenko, V.G. Tcheskidov, N.A. Vinokurov, BINP, Novosibirsk, Russia

## Abstract

To improve the parameters of the second stage Novosibirsk free electron laser one plans to replace the existing electromagnetic undulator by permanent-magnet variable-period undulator (VPU). The VPUs have several advantages compared to conventional undulators, which include wider radiation wavelength tuning range and an option to increase the number of poles for shorter periods with constant undulator length. Both these advantages will be realized in the new undulator under development in Budker INP.

The idea of the permanent-magnet VPU was proposed just several years ago and it has not been properly tested yet. There are some technical problems, which have to be solved before this idea can be implemented in practice. To check the solution of these problems we designed and manufactured a small undulator prototype, which has just several periods. In this paper, the results of mechanical and magnetic measurements of this undulator prototype are presented and compared with simulations.

## INTRODUCTION

The VPU for the NovoFEL under development at Budker INP has a remarkable feature which is the possibility to change the number of periods. The new undulator will replace the electromagnetic one used in the second stage FEL. The old undulator has the period  $\lambda_u$  120 mm and the field amplitude  $B_0$  varying from zero to 0.13 T. It is installed on the bypass of the second horizontal track [1]. The tuning range of the existing FEL is 35 to 80 microns. Application of the VPU will allow shifting the short wavelength boundary to 15 microns [2].

The available free length for the undulator is four meters. Electron energy at the second stage FEL is 22 MeV. One can find most important parameters of the VPU in Table 1.

Table 1: Basic Undulator Parameters

Parameter	Limits
Undulator period $\lambda_u$ (mm)	48 - 96
Radiation wavelength ( $\mu\text{m}$ )	15 - 70
Number of periods	40 - 80
Filed amplitude on the undulator axis (kGs)	0.94 - 1.9
Deflection parameter	0.42 - 1.79

## UNDULATOR GEOMETRY

To ensure low diffraction losses at maximum radiation wavelength, the diameter of the circle inscribed into the aperture of undulator was chosen to be 50 mm. As field amplitude  $B$  exponentially decreases with growth of  $g/\lambda_u$ , where  $g$  is the undulator gap, one can obtain the limitation

that  $\lambda_u$  should not be too small compared to  $g$ , so we chose minimum  $\lambda_u$  to be 48 mm. [2]

Each undulator block consists of one permanent magnet and two iron plates. The permanent magnets are made of NdFeB. In simulations we used a permanent magnet with a remanence of 1.3T. We optimized the dimensions of the magnets and iron plates to obtain a maximum field amplitude with a minimum period.

The transverse cross-sections of the iron plate and permanent magnet with final dimensions are presented in Fig. 1. The longitudinal sizes (thicknesses) are 20 mm for the magnets and 2 mm for the iron plates.

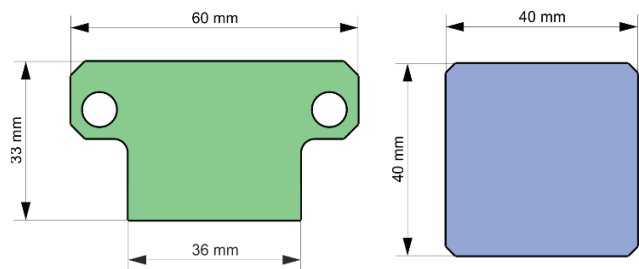


Figure 1: Transverse cross-sections of the iron plate and permanent magnet.

The opposite plates of two blocks adjacent in the longitudinal direction form one pole. Each couple of the right and left blocks at the top is combined in one unit, which can move as a whole, as can be seen from the Fig. 2. Each couple of the right and left blocks at the bottom also forms a similar movable unit.

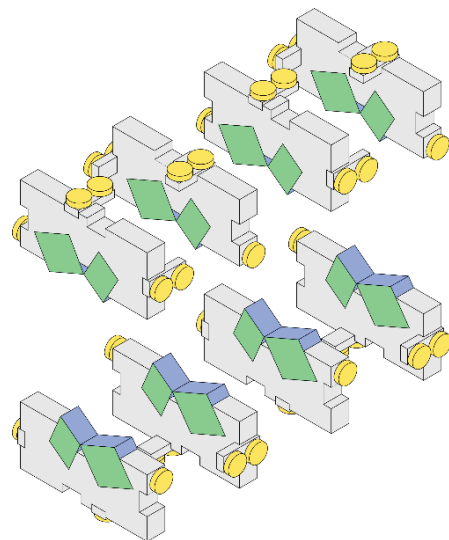


Figure 2: Undulator units disposition.

The top and bottom units are not connected. Blocks in one unit are tilted relative to each other, therefore the free aperture is a rhomb. This configuration provides field

ISBN 978-3-95450-134-2

## STUDIES OF LCLS FEL DIVERGENCE\*

J.L. Turner, P. Baxevanis, F.-J. Decker, Y. Ding, Z. Huang, J. Krzywinski, H. Loos, G. Marcus, N. Norvell, SLAC, Menlo Park, CA 94025, U.S.A.

### Abstract

Simulations show various impacts on x-ray divergence. With the motivation to maximize intensity at the focus, these LCLS beam studies were designed to study parameter space and beam qualities impacting divergence, and therefore aperture related clipping and diffraction. With multiple simultaneous users, beam constraints increase, requiring an improving knowledge of the mechanism of impact of changing parameters. These studies have that goal in order to improve beam control.

### MOTIVATION

Intensity lost at the focus is a strong function of capture by the mirror systems given the impact of diffraction, see Figure 1.

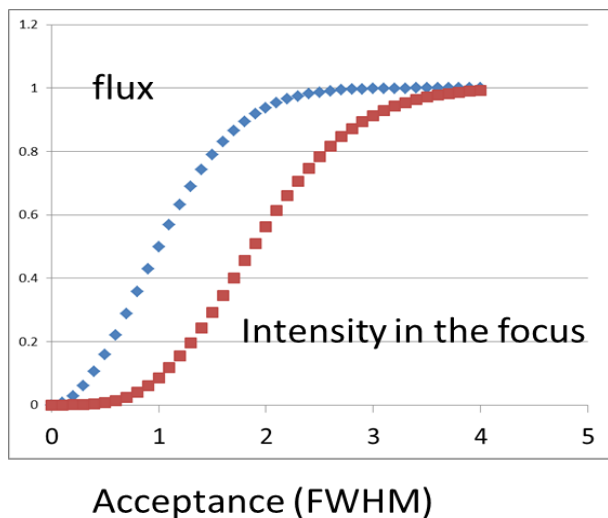


Figure 1: Vertical axis is relative intensity, horizontal axis acceptance of mirror systems cutting in both planes. Blue line is the intensity cut off by mirrors. Red line is the intensity at a downstream focus. Diffraction effects are taken into account.

### STUDY APPROACH

We have made many measurements in the Front End Enclosure (FEE) where the distance is relatively close, 87 meters from the end of the undulator. Since increasing the FEL intensity via longitudinal collimation [1] (see Y. Ding’s WEP024), we run into the dilemma of either saturating our diagnostic (YAGs) or attenuating the fundamental to the point where third harmonic will begin to impact the measurement. So we extend our measurements to a diagnostic near the Far Hall (FEH) 335 meters from the end of the undulator (Figure 2).

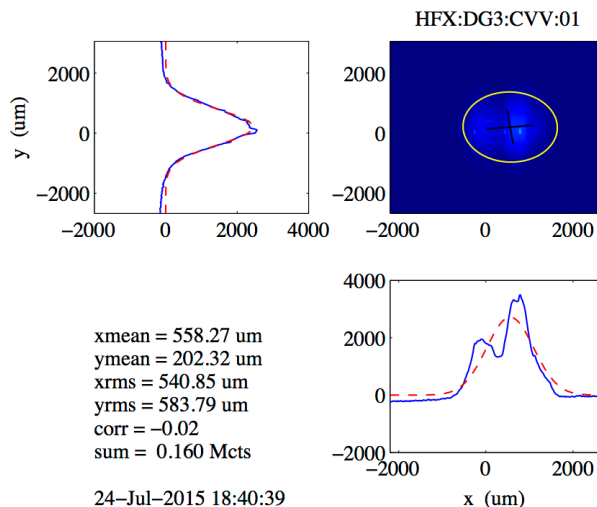


Figure 2: Beam size measured at the Far Hall 335 meters from the end of the undulator. Energy is 8.2 keV. Note the horizontal distortion is due to mirror figure error and diffraction effects [2].

### Divergence Model

We applied Z. Huang and K. J. Kim approximation [3], derived in the linear regime, to calculate the photon source size (eq. 2) and the divergence (eq. 3). 1D gain length  $L_{1D}$ , in the equation 1, was generated using the Ming Xie parameterization [4]

$$\sigma_D = \sqrt{\lambda L_{1D} / 4\pi} \quad (1)$$

$$\sigma_{ph} \approx \sqrt{\sigma_D \sigma_{el}} \quad (2)$$

$$\sigma_{\theta} = \lambda / 4\pi \sigma_{ph} \quad (3)$$

Figure 3 shows confidence in the Z. Huang and K.J. Kim model (HK model) by corroboration with start to end simulation, which were performed using the GENESIS code [5]. The simulation produces a curved wave front at the end of the undulator, which is then back propagated to the source point, and forward propagated to imager points (see Figure 5).

Figure 4 shows that simulation at 300eV indicates the HK model, derived in the linear regime, should also be good in the non-linear regime.

\*Work supported by U.S. Department of Energy, Office of Basic Energy Sciences, under Contract DE-AC02-76SF00515.

# CONTROL OF GAP DEPENDENT PHASE ERRORS ON THE UNDULATOR SEGMENTS FOR THE EUROPEAN XFEL

Yuhui Li, Joachim Pflueger

European XFEL, Notkestr 85, 22607 Hamburg, Germany

## Abstract

Strong magnetic forces in long undulators always result in some girder deformation. This problem gets more serious in long gap tuneable undulators. In addition the deformation varies with changing forces at different gaps resulting in gap dependent phase errors. For the undulators for the European XFEL this problem has been studied thoroughly and quantitatively. A compensation method is presented which uses a combination of suitable shims and pole height tuning. It is exemplified by tuning one of the undulator segments for the European XFEL back to specs.

## INTRODUCTION

The European X-ray free electron laser (EXFEL) facility is currently under construction [1]. It uses a superconducting accelerator with a maximum energy of up to 17.5 GeV and the concept of Self-Amplified-Spontaneous-Emission (SASE) [2,3]. Three gap tuneable undulator systems called SASE1, SASE2 and SASE3 are used. SASE1 and SASE2 are hard X-ray FELs using 35 undulator segments each with a period length of 40mm, called U40s. Their total length is 205m. By a suitable choice of beam energy and undulator gap the wavelength can be tuned from 0.05 to 0.4nm. SASE3 is a soft X-ray FEL using 21 undulator segments with a period length of 68mm, called U68s and a total length of 121m. Its wavelength can be tuned from 0.4 to 5.2nm. All undulator segments of the EXFEL are 5m long and use identical mechanical drive and support systems, which are designed to comply with worst case requirements. Table 1 gives a summary of specifications for the Undulator Systems for the EXFEL.

Table 1: Specifications of the Undulator Segments for the EXFEL

	SASE1/2	SASE3
<b>Undulator Type</b>	U40	U68
<b>Period Length [mm]</b>	40	68
<b>Segment Length [m]</b>	5	5
<b>Operational Gap Range [mm]</b>	10-20	10-25
<b>K-Parameter Range</b>	1.65 - 3.9	4 - 9
<b>Max. Phase Error [Degree]</b>	≤ 8	≤ 8
<b>Radiation Wavelength [nm]</b>	0.05-0.4	0.4 – 5.2

A strong magnetic force is acting between the girders of an undulator, which is proportional to the square of magnetic field and therefore strongly gap dependent as

well. For example in an U68 operated at lowest gap of 10mm the maximum magnetic force amounts to about 17 tons. This leads to unavoidable mechanic deformation of the girders, resulting in a modulation of the parallel gap profile. Although it can be minimized by a suitable mechanic design, it cannot be avoided completely. Moreover, for given girder cross section, deformation increases with the 3rd power of its length. Therefore the mechanical design of the girders for the 5m long undulator segments for the EXFEL needed to be a compromise between acceptable girder deformation and technical effort i.e. amount of material and cross section.

In this paper the effects of girder deformation on EXFEL U40 undulator segments are studied and their gap dependence and impact on magnetic and optical properties are investigated. A method using a combination of shims and pole height tuning is described, which can be used to effectively reduce optical phase errors resulting from girder deformation. It is exemplified on an U40 undulator segment for the EXFEL.

## PHASE ERRORS INDUCED BY GAP DEFORMATION

On all EXFEL undulators gap dependent parabolic deformation is observed to some extent. Pole Height Tuning (PHT) is used as the standard tool for field error correction, which allows to shift each pole vertically by about  $\pm 300\mu\text{m}$  [4]. It is a perfect tool for static corrections of any deformation at one gap. In order to limit overall deformation and its effect on phase jitter a “Tuning Gap” was selected, which is about halfway inside the operational gap range. 14mm and 16mm were selected for U40s and U68s, respectively. At the tuning gap any deformation of the poles is completely eliminated using PHT. The resulting deformation profile of the poles is sketched in Fig.1 a-c): At lowest gap, Fig. 1a), there is only moderate concave gap deformation. At the tuning gap, Fig. 1b), there is none. Above the tuning gaps the gap deformation gets convex. Two points should be emphasized: 1.) Girder deformation is small and the typical pole height adjustments to compensate deformation are in the range  $\pm 50\text{-}60\mu\text{m}$  or less. 2.) The focus is on pole deformation. The deformation of the aluminum support girders cannot be changed. They are perfectly flat only under force free conditions at large gaps and gradually deform from flat to concave towards small gaps. This situation is sketched in Fig. 1a-c) as well.

The result of girder deformation is that the  $K$  - parameter slightly varies parabolically along the undulator axis by typically a few tenth of a percent as shown in Fig.1. As a result the phase error varies [5]:

# EMITTANCE MEASUREMENTS AT THE PAL-XFEL INJECTOR TEST FACILITY

J. H. Lee, J. H. Han, J. H. Hong, H. Yang, C. H. Kim, S. J. Park, S. J. Lee, I. S. Ko  
Pohang Accelerator Laboratory, Pohang, 37673, Korea

## Abstract

The PAL-XFEL Injector Test Facility (ITF) at PAL has been operating for experimental optimization of electron beam parameters and for beam test of various accelerator components. It consists of a photocathode RF gun, two S-band accelerating structures, a laser heater system, and beam diagnostics such as ICTs, BPMs, screens, beam energy spectrometers and an RF deflector. Projected and slice emittance measurements were carried out by using single quadrupole scan. In this paper, we present the emittance measurements.

## INTRODUCTION

PAL-XFEL is under construction. The building is ready and the accelerator components are being installed. PAL-XFEL will generate 0.1 nm FEL radiation using 10 GeV electron beam at the hard X-ray beamline and 1 nm FEL using 3 GeV beam at the soft X-ray beamline. The design parameter of the injector is 0.4 mm mrad slice emittance at 200 pC [1]. Injector Test Facility (ITF) have been operated to study the injector beam dynamics and to test the accelerator components.

## EXPERIMENTAL SETUP

The ITF accelerator consists of an S-band 1.6 cell photocathode RF gun, two S-band accelerating columns, solenoids and beam diagnostics including quadrupoles, ICTs, BPMs, YAG/OTR screens, beam energy spectrometers and an RF deflector. A schematic layout is shown in Fig. 1. A quadrupole and a YAG screen for single quad scan are located at 13.22 m and 15.86 m from the cathode, respectively. We measure the electron beam energy using the beam energy spectrometers and the YAG screens. An RF deflector is located before at the quadrupole for studying longitudinal properties of a bunch. In the RF deflector, the transverse kick varies sinusoidally in time so each part of the electron bunch receives a time-dependent kick[2, 3].

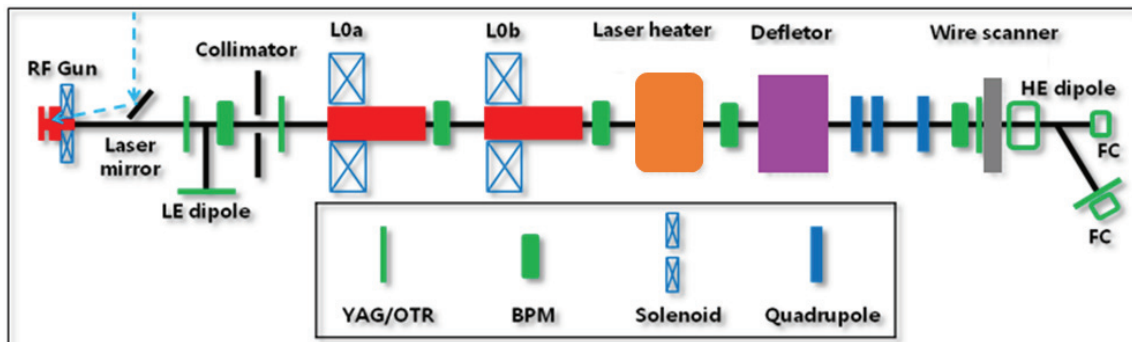


Figure 1: Schematic layout of Injector Test Facility at Pohang Accelerator Laboratory.

## Single Quad Scan

Single quadrupole scan was used for emittance measurements in this paper. The transformation matrix in beam dynamics is described as

$$\begin{pmatrix} x \\ x' \end{pmatrix} = M \begin{pmatrix} x_0 \\ x'_0 \end{pmatrix} = \begin{pmatrix} C & S \\ C' & S' \end{pmatrix} \begin{pmatrix} x_0 \\ x'_0 \end{pmatrix} \quad (1)$$

and

$$\begin{pmatrix} \beta \\ \alpha \\ \gamma \end{pmatrix} = \begin{pmatrix} C^2 & -2CS & S^2 \\ -CC' & CS' + C'S & -SS' \\ C'^2 & -2C'S' & S'^2 \end{pmatrix} \begin{pmatrix} \beta_0 \\ \alpha_0 \\ \gamma_0 \end{pmatrix} \quad (2)$$

Where,  $M$  is the beam transport matrix,  $\alpha, \beta, \gamma$  is the twiss parameters. The transport matrix composed of drift space and quadrupole is represented as

$$M = M_d M_F, \quad M_d = \begin{pmatrix} 1 & L \\ 0 & 1 \end{pmatrix}, \quad M_F = \begin{pmatrix} 1 & 0 \\ -kl & 1 \end{pmatrix} = \begin{pmatrix} C & S \\ C' & S' \end{pmatrix}$$

$M_d$  and  $M_F$  are drift space and quadrupole transformation matrices, respectively with thin lens approximation ( $|kl| \ll 1$ ) [4].  $k$  is the quadrupole strength,  $l$  is the effective length of the quadrupole, and  $L$  is distance between the quadrupole and screen. The beam emittance is related with the area of ellipse in phase space. Utilizing the definition of the ellipse equation in phase space and beam matrix,

$$\sigma_{11} = C^2 \sigma_{0,11} + 2SC \sigma_{0,12} + S^2 \sigma_{0,22} \quad (3)$$

$$\sigma_{11} \sigma_{22} - \sigma_{12}^2 = \epsilon^2 \quad (4)$$

Where,

$$\sigma = \begin{pmatrix} \sigma_{11} & \sigma_{12} \\ \sigma_{21} & \sigma_{22} \end{pmatrix} = \epsilon^2 \begin{pmatrix} \beta & -\alpha \\ -\alpha & \gamma \end{pmatrix}, \quad \sigma_{12} = \sigma_{21}.$$

Using the above equations, we can get a relation as a function of quadrupole strength  $k$  [5]. Therefore, the beam emittance is calculated by measuring the beam size at different quadrupole strengths on YAG screen. The specifications of the quadrupole used for single quad scan is described in Table 1.

# LONGITUDINAL ELECTRON BUNCH SHAPING EXPERIMENTS AT THE PAL-ITF \*

Seong-Yeol Kim, Ji-Min Seok, Kook-Jine Moon, Moses Chung<sup>†</sup>, UNIST, Ulsan, 689-798, Korea  
 Heung-Sik Kang, Chul Hoon Kim, Juho Hong, Jang-Hui Han, PAL, Pohang, 790-834, Korea  
 J. Thangaraj, Fermilab, Batavia, IL 60510, USA

## Abstract

Longitudinal shaping of electron beam has received much attention recently, due to its potential applications to THz generation, dielectric wakefield acceleration, improvement of FEL performance, and controlled space-charge modulation. Using a set of alpha-BBO crystals, shaping of laser pulse and electron bunch on the order of ps is tested at the Injector Test Facility (ITF) of Pohang Accelerator Laboratory (PAL). Initial experimental results will be presented with analytical theory and numerical simulations

## INTRODUCTION

Bunch- and current-shaping of low energy electron beams are essential beam manipulation techniques for compact light sources, narrowband radiation generation, two-color FEL's, seeding techniques, advanced accelerators, mitigation of collective effects, and diagnostics [1]. To have a precise control of the longitudinal profile of the electron beam, a method to shape the photocathode drive laser is often used.

Several techniques to shape the longitudinal laser pulses of picosecond durations were introduced in recent years, such as line-delay technique, echelon lenses, acousto-optic programmable dispersive filter, or DAZZLER, to mention a few examples. In particular, the direct UV pulse shaping using alpha-BBO crystals is known to be a relatively cheap, compact, and power-efficient technique [2, 3].

In this work, we present initial experimental results on the shaping of laser pulses and electron bunches on the order of ps obtained at the Injector Test Facility (ITF) of Pohang Accelerator Laboratory (PAL) using a set of alpha-BBO crystals. We note that, for the PAL-XFEL, a flat-top longitudinal profile is considered in addition to the nominal Gaussian profile, for the improvement of projected emittances [4]. Using three sets of alpha-BBO crystals, for example, we indeed expect to have a flat-top beam distribution to a good approximation.

## BASIC THEORY

The temporal separation between two polarizations, i.e., the ordinary wave (perpendicular to the optical axis) and the extraordinary wave (parallel to the optical axis) is given by [2]

$$\Delta t = L \left| \frac{1}{v_{ge}} - \frac{1}{v_{go}} \right| = \frac{L}{c} |n_{ge} - n_{go}| = \frac{L}{c} \Delta n_g, \quad (1)$$

\* This work was supported by the 2015 Research Fund (1.150124.01) of UNIST(Ulsan National Institute of Science and Technology)

<sup>†</sup> mchung@unist.ac.kr

where  $L$  is the length of the crystal,  $v_{go} = c/n_{go}$  and  $v_{ge} = c/n_{ge}$  are the group velocities of the o-wave and e-wave respectively. Here,  $c$  is the speed of light in vacuum, and  $n_{go}$  and  $n_{ge}$  are group indices of refraction of the o-wave and e-wave respectively.

We use commercially available alpha-BBO's for this experiment. The high temperature phase Barium Borate (alpha-BBO,  $\alpha$ -BBO) is a negative uniaxial crystal with a strong birefringence (large  $\Delta n_g$ ) over the broad transparent range from 189 nm to 3500 nm. Two alpha-BBO crystals of lengths 7.5 mm and 15 mm are used. Since the spot size of the UV laser (253 nm) used for this experiment is rather big, the clear aperture (diameter) of the alpha-BBO crystals are chosen to be 15 mm. An anti-reflection coating is applied on the surfaces of the alpha-BBO crystals, which also protects the surfaces from ambient moisture. The alpha-BBO crystals are kept inside the clean room to avoid moisture absorption, and they are mounted on the precision rotation stages.

The indices of refraction are given by the Sellmeier equations ( $\lambda$  in  $\mu\text{m}$ ) as (see also Fig. 1)

$$n_o^2 = 2.7471 + 0.01878/(\lambda^2 - 0.01822) - 0.01354\lambda^2, \quad (2)$$

$$n_e^2 = 2.37153 + 0.01224/(\lambda^2 - 0.01667) - 0.01516\lambda^2. \quad (3)$$

The group index of refraction ( $n_g$ ) is calculated from the index of refraction ( $n$ ) as (see also Fig. 2)

$$n_g(\lambda) = n(\lambda) - \left( \frac{dn(\lambda)}{d\lambda} \right) \lambda. \quad (4)$$

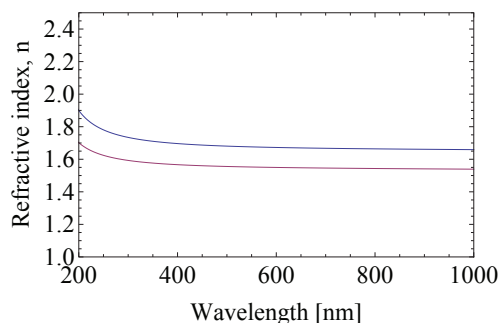


Figure 1: Indices of refraction for o-wave (blue) and e-wave (red) calculated by Sellmeier's formula.

For  $L = 7.5$  mm, we expect  $\Delta t = 6.55$  ps, and for  $L = 15$  mm,  $\Delta t = 13.1$  ps. The laser intensity of multiple Gaussian beams can be approximate as

$$I(t) = \sum_{i=1}^n \frac{1}{n} \exp\left(-\frac{(t-t_i)^2}{2\sigma_i^2}\right). \quad (5)$$

# NUMERICAL AND EXPERIMENTAL STUDIES ON ELECTRON BEAM PROPERTIES FROM ASYMMETRIC RF-GUN\*

S. Rimjaem<sup>#</sup>, N. Chaisueb, N. Kangrang, E. Kongmon, K. Kosaentor, J. Saisut, C. Thongbai, W. Thongpakdi, P. Wichaisirimongkol

Plasma and Beam Physics Research Facility, Department of Physics and Materials Science, Faculty of Science, Chiang Mai University, Chiang Mai 50200, Thailand

## Abstract

The electron linear accelerator at the Plasma and Beam Physics (PBP) Research Facility, Chiang Mai University (CMU), Thailand, is used to produce femtosecond electron bunches for generation of THz radiation. The main components of the PBP-CMU linac are a thermionic RF electron gun, an alpha magnet, an S-band travelling-wave linac structure, quadrupole lens, steering magnets, and various diagnostic components. The RF-gun consists of a 1.6 cell S-band standing-wave structure and a side-coupling cavity. The 2856 MHz RF wave is transmitted from the klystron to the gun through a rectangular waveguide input-port. Both the RF input-port and the side-coupling cavity cause an asymmetric electromagnetic field distributions inside the gun. This leads to asymmetric transverse shape with larger emittance value. Beam dynamic simulations were performed to investigate the effect of the asymmetric fields on the electron properties by using the code PARMELA. Simulation results suggest that the beam with a maximum kinetic energy of 2.51 MeV, a bunch charge of 0.21 nC and horizontal and vertical emittance values of 20.43 and 19.55 mm-mrad can be achieved. The experiments to investigate the performance of the RF-gun were performed. The results show that at optimal condition the gun can produce the beam of about 2  $\mu$ s (FWHM) pulse width with a maximum kinetic energy of  $\sim$ 2.8 MeV and a macropulse charge of  $850.1 \pm 34.7$  nC.

## INTRODUCTION

A linac-based THz radiation source at the Plasma and Beam Physics (PBP), Chiang Mai University, consists of an S-band thermionic RF electron gun, an alpha magnet, a travelling-wave linac structure, quadrupole focusing magnets, beam steering magnets, transition radiation stations and several diagnostic components. An electron source is a 1.6-cell S-band standing-wave RF-gun. A thermionic cathode is installed at the center of the rear wall of the first half-cell. A WR-284 rectangular RF waveguide is connected to the RF-gun at the radial wall of the full-cell. The RF wave from the full-cell is coupled to the half-cell through a side-coupling cavity. Opening holes between the main cavities and the RF input-port as well as the side-coupling cavity cause asymmetric electromagnetic field distributions inside the gun. In order

to study the effect of this feature on the electron beam properties, 3D RF and beam dynamics simulations of the first PBP-CMU RF-gun were performed. The study results show that electron beams produced from asymmetric RF-gun have asymmetric transverse shape and larger transverse emittance than the beams produced from the symmetric one [1]. This RF-gun was dismantled from the PBP-CMU linac system. Then, the new RF-gun was installed in July 2011. It has both common and different features with the previous one. Numerical and experimental studies were conducted to investigate the characteristics and the performance of the new RF-gun.

## PRESENT PBP-CMU RF-GUN

The current RF electron gun in the PBP-CMU linac system was constructed at the High-energy Optics and Electronics (HOPE) Laboratory, National Tsing Hua University and the National Synchrotron Radiation Research Center (NSRRC), Taiwan, R.O.C [2]. The design of this gun is similar to the first PBP-CMU RF-gun with some different features, which are a nose-cone thermionic cathode, an adjustable tuning plug, a smaller opening hole of the RF input-port on the full-cell radial wall. Moreover, cooling channels are located inside the wall of the gun cavities for better gun temperature control. The 3D drawing and the inner cut-view of the present PBP-CMU RF-gun are shown in Fig. 1.

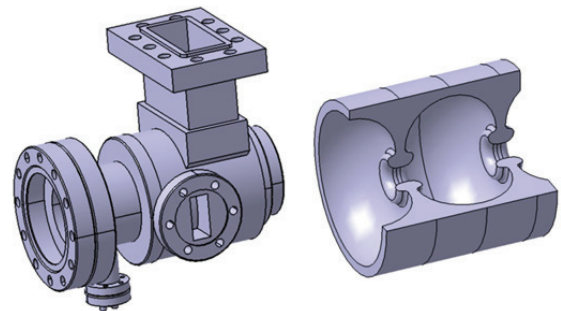


Figure 1: 3D drawing and inner cut-view of the present RF-gun at the PBP-CMU linac facility.

This RF-gun was transported from NSRRC to Chiang Mai University and has been installed as the electron source of the PBP-CMU linac after the cavity re-tuning process. According to the study results in [3], the flat-cathode is used instead of the nose-cone one to decrease the transverse emittance of electron beams at the RF-gun exit. The gun was operated with the forward RF peak power of 3.65 MW and 3  $\mu$ s (FWHM) pulse width. The

\*Work supported by the CMU Junior Research Fellowship Program.

<sup>#</sup>Corresponding author: sakhorn.rimjaem@cmu.ac.th

## STUDY ON UNDULATOR RADIATION FROM FEMTOSECOND ELECTRON BUNCHES

N. Chaisueb<sup>†</sup>, S. Rimjaem, Plasma and Beam Physics (PBP) Research Facility, Department of Physics and Materials Science, Faculty of Science, Chiang Mai University, Chiang Mai 50200, Thailand

### Abstract

Linac-based terahertz (THz) source at the Plasma and Beam Physics (PBP) Research Facility, Chiang Mai University (CMU), Thailand, consists of a thermionic RF electron gun, an alpha magnet for magnetic bunch compressor, a travelling wave S-band accelerating structure for post acceleration, and various beam diagnostic instruments. The PBP-CMU linac system can produce relativistic femtosecond electron bunches, which are used to generate coherent THz radiation via transition radiation technique. To increase the radiation intensity, an electromagnetic undulator will be added in the beam transport line. The designed electromagnetic undulator has 35 periods with a period length of 64 mm and a pole gap of 15 mm. This study investigates the dependence of the electron beam energy and longitudinal bunch length on the coherent undulator radiation. The numerical simulation and procedure to generate the undulator radiation in the THz regime by using femtosecond electron bunches produced at the PBP research facility is reported and discussed in this contribution. Numerical calculation result shows that the energy of the undulator radiation, which is produced from electron bunches with an energy of 5 - 20 MeV, a peak current of 33 - 55 A, and an effective bunch length of 180 - 300 fs can reach 14  $\mu$ J.

### INTRODUCTION

In the last decade, electromagnetic radiation in the THz regime has become interesting spectrum in many applications. The THz radiation can pass through non-metallic materials, but it is reflected by metal and is absorbed by liquid. Due to this unique characteristic, the THz radiation is used in several researches involved THz spectroscopy and non-destructive distinguish analysis of different density materials, e.g. THz imaging, which can be used in many applications. For examples, it is used to detect metallic and non-metallic weapons, explosive materials, and drugs through concealing obstacles such as clothing or packaging. Therefore, it is useful for airport security, homeland security and defense [1]. Moreover, it is possibly used to observe the correctness of the integrated circuits, such as semiconductor devices and electronic cards, which are enclosed in non-metallic package [2]. A tooth cavity in enamel and the cancerous region compared to the healthy region of human tissue can also be detected by THz imaging [3]. This leads to widely studies in development of THz light sources, detectors, and several experimental techniques.

<sup>†</sup>natthawut\_chai@cmu.ac.th

At Chiang Mai University, relativistic electron bunches produced from the PBP-CMU linac system was firstly used to generate THz radiation by transition radiation technique in March 2006 [4]. The electron beam is produced from the RF-gun with the maximum kinetic energy of about 2 - 2.5 MeV and a bunch length of around 100 - 200 ps [5]. The beam with long bunch length was then compressed and accelerated by using the alpha magnet and the travelling wave s-band linac structure, respectively. Then, it arrives at the experimental station with the bunch length of 180 - 300 fs and the total energy of 10 - 15 MeV. Transition radiation is emitted when electrons passing through a boundary between two different dielectric media. At the PBP facility, a thin Al-foil was placed in the electron's path at the experimental station. Then, the radiation is emitted from the interface between vacuum and the Al-foil resulting from an electric field discontinuity at the transition area of the materials with different dielectric constants. The radiation was, then, measured by using a Michelson interferometer and a pyroelectric detector. The spectrum of the THz transition radiation generated from electron beam with an electron energy of 10 MeV and a bunch length of 200 fs overs the wave number of about 80  $\text{cm}^{-1}$  with the radiation energy of around 9 - 22  $\mu$ J per macropulse [4]. The produced THz radiation was used to create THz images via a transmission mode of imaging technique for several materials, such as cut-pattern in Al-foils, raw and cooked rice grains, water drop, and a fresh leaf [4].

The power of the THz radiation generated from the present setup of the PBP-CMU linac via transition radiation is merely in milliwatt scale resulting in low-resolution THz images. Therefore, a plan to increase the power or the intensity of the THz radiation by using a coherent undulator radiation method is conducted. This is in order to be able to apply the THz radiation in various researches for distinguishing material components with high resolution.

### UNDULATOR MAGNET

In the future setup of the accelerator system, an electromagnetic undulator will be inserted as the new experimental station in the beam line as shown in Fig. 1. Typical undulator magnets compose of a periodic structure of dipole magnets. A static magnetic field is alternating along the length of the undulator with a certain period length. Electrons in a short bunch moving through the undulator magnetic field are oscillating in the transverse direction and emitting the radiation coherently. Therefore, the undulator radiation of femtosecond

# SIMULATION OF CASCADED LONGITUDINAL-SPACE-CHARGE AMPLIFIER AT THE FERMILAB ACCELERATOR SCIENCE & TECHNOLOGY (FAST) FACILITY\*

A. Halavanau<sup>1</sup>, and P. Piot<sup>1,2</sup>

<sup>1</sup> Department of Physics and Northern Illinois Center for Accelerator & Detector Development, Northern Illinois University, DeKalb, IL 60115, USA

<sup>2</sup> Accelerator Physics Center, Fermi National Accelerator Laboratory, Batavia, IL 60510, USA

## Abstract

Cascaded longitudinal space-charge amplifier (LSCA) have been proposed as a mechanism to generate density modulation over a broad spectral range. The scheme was recently demonstrated in the optical regime and confirmed the production of broadband optical radiation. In this paper we investigate, via numerical simulations, the performances of a cascaded LSCA beamline at the Fermilab Accelerator Science & Technology (FAST) facility to produce broadband ultraviolet radiation. Our studies are carried using a three-dimensional space charge algorithm coupled with *ELEGANT* and including a tree-based grid-less space-charge algorithm.

## INTRODUCTION

It has been long recognized that collective effects such as coherent synchrotron radiation, wakefield and longitudinal space charge can lead to a microbunching instabilities when combined with bunch compressors (BC) commonly employed in electron linacs. Over the recent years, longitudinal space charge (LSC) has gained considerable interest as a simple mechanism to form attosecond structures on the bunch current distribution for the subsequent generation of intense broadband radiation pulses [1, 2].

The corresponding beamline configuration is relatively simple: it consists of focusing sections (e.g. FODO cells) which ensure the beam size is kept small and where energy modulations due to the space charge impedance accumulate, interspaced with BC sections. The BCs convert the incoming energy modulation into a density modulation. Several of these (FODO+BC) modules are cascaded so to result in a large final density modulation.

Motivated by the recent experimental demonstration of LSCA in the optical regime [2] along with the possible use of high-peak current beams produced in laser-plasma wakefield accelerators [3], we investigate the possible combination of a cascaded LSCA scheme to produce broadband ultraviolet radiation at the Fermilab Accelerator Science & Technology (FAST) facility which couples a high-brightness photoinjector with a superconducting accelerator [4].

## SIMULATION METHODS & SETUP

The simulation method employed for our numerical studies has been described elsewhere [5, 6]. In brief we simulate the beam dynamics simulation, including space charge effect, is modeled with the Barnes-Hut algorithm [7] within *ELEGANT* [8]. The space-charge kicks are applied at discrete user-defined locations using the *ELEGANT*'s script command. In its current implementation, the calculations are rather slow (due to files being written out and read in at each space-charge kick location) but the algorithm is being implemented within the *ELEGANT* main distribution and will eventually be part of future *ELEGANT* releases.

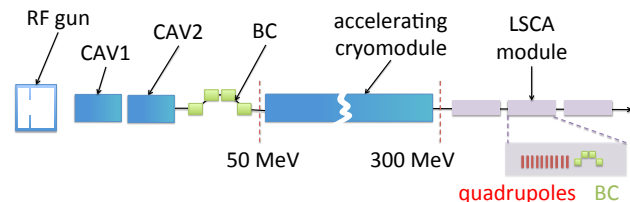


Figure 1: Overview of FAST Facility and the Proposed LSCA. The legend is as follows: "CAVx": accelerating cavities, "BC": magnetic chicane bunch compressor, the red and green rectangles are respectively quadrupole and dipole magnets.

The simulation setup is based on the configuration available at the FAST facility (formerly known as ASTA) [4]; see Fig. 1. In short, the beam is produced from a photocathode located in a  $1+\frac{1}{2}$  radiofrequency (RF) gun and accelerated to  $\sim 50$  MeV by two superconducting TESLA cavities. Downstream of the cavities the beam can be manipulated (e.g. longitudinally compressed) and diagnosed before its injection in a ILC-type accelerating cryomodule composed of eight TESLA cavities. Downstream of the cryomodule, the beam, with energy up to  $\sim 300$  MeV, can be injected into the IOTA ring or transported to experiments arranged along a  $\sim 70$  m transport line. Conversely the 70-m beamline, with proper optics, could support the investigation of cascaded LSCAs to produce broadband ultraviolet radiation as discussed in this paper; see also Fig. 1.

Numerical optimization of the electron-beam formation and acceleration to  $\sim 50$  MeV was carried out with *ASTRA* [9] for various charges. The results combined with a mild bunch compression in the 50-MeV bunch compressor chicane, could produce bunches with peak current of

\* This work was supported by the US Department of Energy under contract DE-SC0011831 with Northern Illinois University. Fermilab is operated by Fermi Research Alliance, LLC under Contract No. DE-AC02-07CH11359 with the US DOE.

# MINMIZATION OF THE EMITTANCE GROWTH INDUCED BY COHERENT SYNCHROTRON RADIATION IN ARC COMPRESSOR\*

Xiyang Huang<sup>#</sup>, Xiaohao Cui, Yi Jiao, Gang Xu

Key Laboratory of Particle Acceleration Physics and Technology,  
Institute of High Energy Physics, Chinese Academy of Sciences, Beijing, China

## Abstract

Coherent synchrotron radiation (CSR) is a critical issue when electron bunches with short bunch length and high peak current transporting through a bending system in high-brightness light sources and linear colliders. For example, a high peak current of electron beam can be achieved by using magnetic bunch compressor, however, CSR induced transverse emittance growth will limit the performance of bunch compressor. In this paper, based on our ‘two-dimensional point-kick analysis’, an arc compressor with high compression factor is studied. Through analytical and numerical research, an easy optics design technique is introduced that could minimize the emittance dilution within this compressor. It is demonstrated that the strong compression of bunch length and the transverse emittance preservation can be achieved at the same time.

## INTRODUCTION

In ERL designs, recirculation arcs are often used to compress the bunch length. In order to achieve compression, an ultra-relativistic electron beam with energy chirp passes through the bending system. Since the trajectory is curved, electrons emit coherent synchrotron radiation (CSR) and may induce energy modulation along the bunch and dilutes transverse emittance, leading to degradation of the beam quality [1-3]. To suppress the undesirable emittance growth, several design strategies have been proposed [4-8]. However, most of these designs reach a high compression factor by adopting a low bunch charge. In this paper, the point-kick analysis [8] is reviewed and be applied to an arc compressor consists of double bend achromats (DBAs) to achieve emittance preservation with high bunch charge.

## POINT-KICK ANALYSIS OF CSR EFFECT

In the ‘‘steady-state’’ approximation for a Gaussian line-charge distribution beam, the CSR-induced rms relative energy spread depends linearly on both  $L_b$  and  $\rho^{2/3}$  [9-11].

$$\Delta E_{rms} = 0.2459 \frac{eQ\mu_0 c_0^2 L_b}{4\pi\rho^{2/3}\sigma_z^{4/3}}, \quad (1)$$

where  $e$ ,  $Q$ ,  $\rho$ ,  $\sigma_z$ ,  $L_b$ ,  $\mu_0$ ,  $c_0$  represent the charge of a single particle, the bunch charge, the bending radius of the orbit, the rms bunch length, the bending path, the

permeability of vacuum, and the speed of light, respectively.

Therefore the CSR effect in a dipole was linearized by assuming  $\delta_{(csr)} = kL_b/\rho^{2/3}$ , where  $k$  depends only on the bunch charge  $Q$  and the bunch length  $\sigma_z$ , and is in unit of  $m^{1/3}$ . In addition, it was shown that the CSR-induced coordinate deviations after a passage through a dipole can be equivalently formulated with a point-kick at the centre of the dipole (see Fig. 1), which is of the form [8]

$$X_k = \begin{pmatrix} \rho^{4/3} k [\theta \cos(\theta/2) - 2 \sin(\theta/2)] \\ \sin(\theta/2) (2\delta + \rho^{1/3} k \theta) \end{pmatrix}, \quad (2)$$

where  $\delta = \delta_0 + \delta_{csr}$ , is the particle energy deviation at the entrance of the dipole, with  $\delta_0$  being the initial particle energy deviation and  $\delta_{csr}$  being that caused by CSR in the upstream path.

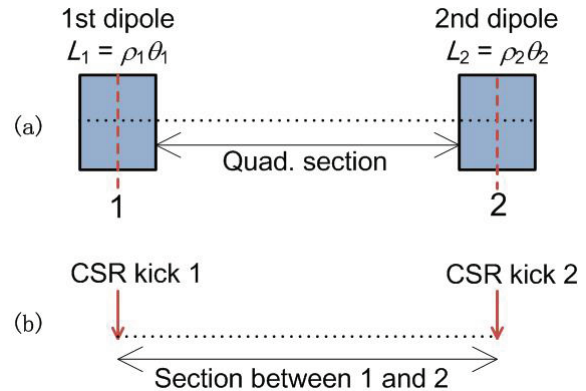


Figure 1: Schematic layout of a two-dipole achromat and physical model for the analysis of the CSR effect with two point kicks. The point 1 and 2 indicate the centres of the first and the second dipole, respectively.

## EMITTANCE PRESERVATION OF A CHIRPED BEAM AFTER A DBA

In this section, we will present the derivation of the CSR-minimization condition for a DBA with symmetric layout. As sketched in Fig. 1, the bending angles of the first and the second dipole are denoted by  $\theta$ , the bending radii of these dipoles are the same, denoted by  $\rho$ . According to the point-kick analysis, CSR kicks occur at the centres of the two dipoles (denoted by 1, 2, in Fig. 1), and between the adjacent kicks only one 2-by-2 transfer matrix of the horizontal betatron motion is considered. For simplicity, it is assumed that the initial particle coordinates relative to the reference trajectory are  $X_0 =$

\*work supported by National Natural Science Foundation of China (11475202, 11405187).

<sup>#</sup>huangxy@ihep.ac.cn

# START-TO-END SIMULATION OF THE LCLS-II BEAM DELIVERY SYSTEM WITH REAL NUMBER OF ELECTRONS\*

J. Qiang<sup>#</sup>, M. Venturini, C. Mitchell, C. Papadopoulos, LBNL, Berkeley, CA94720, USA  
 Y. Ding, P. Emma, Z. Huang, G. Marcus, Y. Nosochkov, T. O. Raubenheimer, L. Wang, M. Woodley, SLAC, Menlo Park, CA 94025, USA

## Abstract

The LCLS-II as a next generation high repetition rate FEL based X-ray light source will enable significant scientific discoveries. In this paper, we report on progress in the design of the accelerator beam delivery system through start-to-end simulations. We will present simulation results for three charges, 20 pC, 100 pC and 300 pC that are transported through both the hard X-ray beam line and the soft X-ray beam line for FEL radiation.

## INTRODUCTION

Next generation high brightness FEL X-ray light sources provide great opportunity for scientific discovery in many fields. The LCLS-II as an upgrade to the current LCLS FEL at SLAC will deliver photons of energy between 200 eV and 5 keV at a repetition rate as high as 1 MHz and is being actively designed under a multi-laboratory collaboration [1]. Figure 1 shows a schematic layout of the LCLS-II beam delivery system [2]. It consists of a high repetition rate photo-injector to generate and accelerate the electron beam to 100 MeV, a laser heater (LH) to suppress microbunching instability, a section of superconducting linac L1 to accelerate the beam to 250 MeV, a bunch compressor BC1, a second section of superconducting linac L2 to accelerate the beam to 1.6 GeV, a bunch compressor BC2, and a third section of superconducting linac L3 to accelerate the beam to 4 GeV, a long bypass transport line, and a magnetic kicker to spread the electron beam to a soft X-ray transport beam line and to a hard X-ray transport beam line. The superconducting linacs in all three sections are made of 1.3 GHz 9 cell superconducting cavities except the two cryomodules of 3.9 GHz third harmonic cavities right before the BC1 to linearize longitudinal phase space.

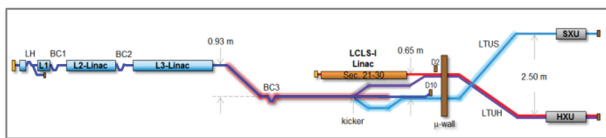


Figure 1: A schematic layout of the LCLS-II.

## COMPUTATIONAL SETUP

All simulations presented in this study were done using a 3D parallel beam dynamics simulation framework IMPACT [3-5]. It includes a time-dependent 3D space-

\*Work supported by the Director of the Office of Science of the US Department of Energy under Contract no. DEAC02-05CH11231 and Contract no. DE-AC02-76SF00515.

<sup>#</sup>jqiang@lbl.gov

charge code module IMPACT-T to simulate photo-electron beam generation and acceleration through the photo RF gun, buncher and boosting cavities, and a position-dependent 3D space-charge code module to simulate electron beam transport through the superconducting linac system. Besides the 3D space-charge effects, the simulation also includes coherent synchrotron radiation (CSR) effects through a bending magnet, incoherent synchrotron radiation inside the bending magnet, RF cavity structure wakefield, and resistive wall wakefield. All simulations were done using the real number of electrons for three bunch charges, 20 pC, 100 pC, and 300 pC, to capture the initial shot noise of the beam, which can have important impact on the final beam quality and FEL performance due to the microbunching instability [6-8]. The total computational time takes from a few hours to about 14 hours on thousands of processors at the NERSC supercomputer center [9].

## SIMULATION RESULTS

The simulation starts with an initial particle distribution behind the cathode. The choice of the initial electron beam parameters and the RF gun, the solenoid, the buncher cavity, and the boosting cavities parameters was based on a multi-variable multi-objective optimization [10]. Figure 2 shows the longitudinal phase space distribution and the current profile at the exit of the injector.

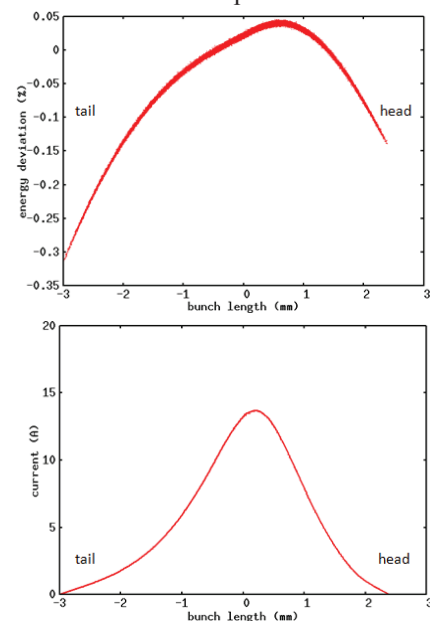


Figure 2: Longitudinal phase space (top) and current profile (bottom) at the exit of the injector.

# DISPERSION OF CORRELATED ENERGY SPREAD ELECTRON BEAMS IN THE FREE ELECTRON LASER

L.T. Campbell<sup>1,2</sup> and A.R. Maier<sup>3</sup>

<sup>1</sup>SUPA, Department of Physics, University of Strathclyde, Glasgow, UK

<sup>2</sup>ASTeC, STFC Daresbury Laboratory and Cockcroft Institute, Warrington, UK

<sup>3</sup>Center for Free-Electron Laser Science and Department of Physics, University of Hamburg, Luruper Chaussee 149, 22761 Hamburg, Germany

## Abstract

The effect of a correlated linear energy chirp in the electron beam in the FEL, and how to compensate for its effects by using an appropriate linear taper of the undulator magnetic field have previously been investigated considering relatively small chirps. In the following, it is shown that larger linear energy chirps, such as those found in beams produced by laser-plasma accelerators, exhibit dispersive effects in the undulator, and require a non-linear taper on the undulator field to properly optimise.

## INTRODUCTION

In the FEL, it is well known that an energy spread correlated with the temporal bunch coordinate, or an energy chirp, in the electron beam can be compensated for by using an appropriate taper of the undulator magnetic field [1]. For the case of a linear energy chirp, it was previously derived that a linear taper is necessary, with gradient proportional to the gradient of the chirp, and this result was derived considering small variations in energy due to the chirp.

However, with the increased interest in novel accelerator concepts as FEL drivers, *e.g.* use of plasma accelerators [2–4] or the synthesis of broadband beams from linacs as in [5], the case of larger chirps has become more relevant. In this regime, dispersive effects can no longer be ignored, and the beam current and energy spread are a function of propagation distance through the undulator. Consequently, the gain length of the FEL is then itself a function of distance. In addition, dispersion due to the chirp will cause the gradient of the chirp to vary upon propagation, meaning that the taper necessary to compensate the chirp is also a function of undulator propagation length, and will not be linear.

FEL codes which employ ‘slices’ with periodic boundaries to model the electron beam [6–9] cannot model this dispersion properly, as the electrons cannot travel between slices, and so cannot model any current redistribution through the undulator. In addition, the Slowly Varying Envelope Approximation (SVEA) [10] means that they cannot model a broadband range of frequencies produced by large energy differences due to the chirp and/or a large taper. So-called ‘unaveraged’ FEL codes [11–15] are free of these limitations.

In the following, a general case of a large chirp which can be fully compensated with a taper is identified, which re-

duces to the previous, well known case only when dispersive effects are neglected. This simple case allows an analytic prediction for the variation in the gain length at a fixed frequency, which is compared to results from the unaveraged FEL code Puffin [11].

## REVISITING THEORY IN SCALED NOTATION

Using the scaled notation of [11], the propagation distance through the undulator is scaled to the 1D gain length, and the temporal coordinate in the stationary radiation frame is scaled to the 1D cooperation length, so that, respectively,

$$\bar{z} = \frac{z}{L_g} \quad (1)$$

$$\bar{z}_2 = \frac{ct - z}{L_c}. \quad (2)$$

The scaled axial velocity of the  $j^{\text{th}}$  electron is defined as

$$p_{2j} = \frac{d\bar{z}_{2j}}{d\bar{z}} = \frac{\beta_{zr}}{1 - \beta_{zr}} \frac{1 - \beta_{zj}}{\beta_{zj}}, \quad (3)$$

where  $\beta_{zj} = v_{zj}/c$  is the  $z$  velocity in the undulator normalised to the speed of light. The subscript  $r$  denotes some reference velocity, which is usually sensible to take as the mean velocity of the beam, but which in general may be any velocity, as the model presented in [11] allows a broadband description of both the radiation field and the electron energies. The ‘ $r$ ’ denotes the resonant condition for this reference velocity, so that the reference resonant frequency is denoted by

$$k_r = \frac{\beta_{zr}}{1 - \beta_{zr}} k_w, \quad (4)$$

and the electrons with  $p_{2j} = 1$  are resonant with the reference frequency.

Tapering is achieved by varying  $\alpha(\bar{z}) = \bar{a}_w(\bar{z})/\bar{a}_{w0}$ , which is the relative change in the magnetic undulator field from its initial value, as defined in [16].

The gradient of an electron beam chirp may then be defined as

$$\frac{dp_{2j}}{d\bar{z}_2} \approx -\frac{2}{\gamma_r} \frac{d\gamma}{d\bar{z}_2}, \quad (5)$$

assuming small deviations in energy, a small chirp so that

$$\frac{dp_{2j}}{d\bar{z}_2} \ll 1, \quad (6)$$

# FEMTOSECOND X-RAY PULSE GENERATION WITH AN ENERGY CHIRPED ELECTRON BEAM

C. Emma, C. Pellegrini, UCLA, Los Angeles, CA 90095 USA

Y. Ding, G. Marcus, A. Lutman, Z. Huang, A. Marinelli, SLAC, Menlo Park, CA 94025, USA

## Abstract

We study the generation of short (sub 10 fs) pulses in the X-ray spectral region using an energy chirped electron beam in a Self Amplified Spontaneous Emission Free Electron Laser (SASE FEL) and a self-seeding monochromator [1-4]. The monochromator filters a small bandwidth, short duration pulse from the frequency chirped SASE spectrum. This pulse is used to seed a small fraction of the long chirped beam, hence a short pulse with narrow bandwidth is amplified in the following undulators. We present start-to-end simulation results for LCLS operating in the soft X-ray self-seeded mode with an energy chirp of 1% over 30 fs and a bunch charge of 150 pC. We show the possibility to generate 5 fs pulses with a bandwidth 0.3 eV. We also assess the possibility of further shortening the pulse by utilizing one more chicane after the self-seeding stage and shifting the radiation pulse to a “fresh” part of the electron beam. Experimental study on this short pulse seeding mode has been planned at the LCLS.

## INTRODUCTION

Ultrashort x-ray pulses of femtosecond to sub-femtosecond duration are important for time-resolved ultrafast studies in chemistry, biology, and material science. Operating in the self-amplified spontaneous radiation (SASE) mode [1], different schemes have been proposed in the past years to shorten the x-ray pulses. One such method, using a configuration similar to the selfseeding setup, was first proposed by Schroeder et al. [2]. In this mode, the electron beam has a time-energy correlation and a monochromator selects a narrow-bandwidth seed to interact with a small fraction of the chirped bunch. The central wavelength is determined by the monochromator hence the output central wavelength would be stable against beam energy jitter. In this paper we study the generation of femtosecond level pulses in start-to-end simulations for the LCLS beam.

A time-energy chirped beam can be generated in an over-compression mode in the second chicane compressor at LCLS. In this mode, the bunch head has higher beam energy than the tail. This chirped beam generates wide-bandwidth SASE radiation before the Soft X-ray Self Seeding (SXRSS) chicane. We choose the appropriate number of undulator sections to reach a radiation power on the 10MW level before the SXRSS monochromator. After the monochromator grating, we achieve a narrow-bandwidth seed determined by the monochromator resolving power. For a resolving power  $R$  the rms bandwidth is  $\sigma_m = 1/(2.355 \cdot R)$ . After the monochromator the pulse duration is given by [4]:

$$\sigma_{t,m}^2 = \frac{\sigma_\omega^2 + \sigma_m^2}{u^2} + \frac{1}{4\sigma_m^2} \quad (1)$$

where  $\sigma_\omega$  is the SASE bandwidth,  $\sigma_m$  is the monochromator bandwidth and  $u = \Delta\omega/\Delta t$  is the energy chirp on the beam. After the amplification process the pulse duration shortens and is dominated by the SASE bandwidth and the energy chirp  $\sigma_{t,f} \approx \sigma_\omega/u$ . The pulse length expected as a function of the electron beam chirp is shown in Fig. 1. Slip-page of the radiation spike along the chirped beam requires reverse tapering of the undulator field in order to preserve the resonance condition and amplify a short pulse [5, 6]. In the amplifying section after the SXR monochromator only a small fraction of the chirped bunch is on resonance with the seed and will undergo microbunching at the radiation wavelength. To increase the gain and further shorten the pulse duration we consider using a second chicane as an additional delay to shift the radiation pulse to a “fresh” part of the beam downstream of the SXR monochromator. This ensures that the radiation will be continually amplified by a fresh bunch. The delay can be optimized to achieve shorter pulses and superradiant effects may also further shorten the pulse duration.

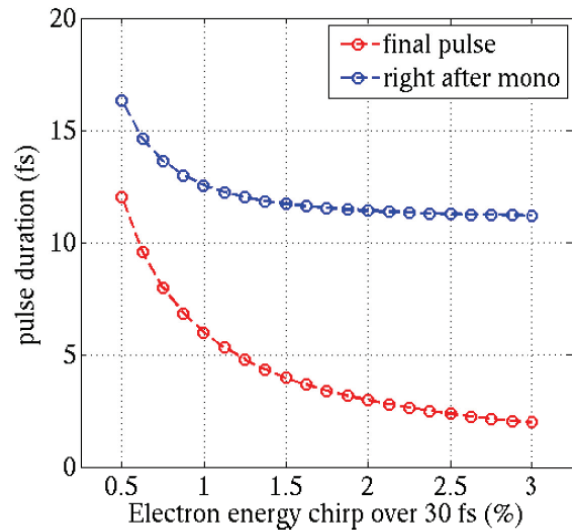


Figure 1: Theoretical expected pulse duration given by Eq. 1 right after the mono and at the end of the undulator. Prediction is in excellent agreement with simulation results for a beam with a 1 % chirp over 30 fs.

# TAPERING STUDIES FOR TW LEVEL X-RAY FELS WITH A SUPERCONDUCTING UNDULATOR AND BUILT-IN FOCUSING\*

C. Emma, C. Pellegrini, UCLA, Los Angeles, CA 90095 USA  
K. Fang, J. Wu, SLAC, Menlo Park, CA 94025, USA

## Abstract

Tapering optimization schemes for TeraWatt (TW) level X-ray Free Electron Lasers (FELs) are critically sensitive to the length of individual undulator and break sections. Break sections can be considerably shortened if the focusing quadrupole field is superimposed on the undulator field, increasing the filling factor and the overall extraction efficiency of the tapered FEL. Furthermore, distributed focusing reduces the FODO length and allows one to use smaller beta functions, reducing particle de-trapping due to betatron motion from the radial tails of the electron beam. We present numerical calculations of the tapering optimization for such an undulator using the three dimensional time dependent code GENESIS. Time dependent simulations show that 8 keV photons can be produced with over 3 TW peak power in a 100m long undulator. We also analyze in detail the time dependent effects leading to power saturation in the taper region. The impact of the synchrotron sideband growth on particle detrapping and taper saturation is discussed. We show that the optimal taper profile obtained from time independent simulation does not yield the maximum extraction efficiency when multi-frequency effects are included. A discussion of how to incorporate these effects in a revised model is presented.

## INTRODUCTION

In this work we analyze the tapering optimization of a high efficiency [1] TW-level X-ray FEL using time independent and time dependent GENESIS simulations. We show that the solution obtained for the optimal taper profile in time independent simulations does not yield the maximum extraction efficiency when fully time dependent physics is included in the dynamics of the the electron beam and radiation field system. We study the optimization for a superconducting, 2 cm period, helical undulator with built in focusing. This undulator design is optimized for maximum efficiency, reduction of intra module undulator length, strong transverse focusing, short gain length and minimum total undulator length.

## UNDULATOR DESIGN

We apply the tapering optimization method [2] to an undulator designed specifically to achieve TW power X-ray pulses in the shortest possible undulator length. Our ideal undulator is superconducting, with a short 2 cm period and a peak on axis field  $B_0$  of 1.6 T. For a double helix bifilar magnet with equal and opposite currents this field is given

Table 1: GENESIS Simulation Parameters

Parameter Name	Parameter Value
Beam Energy	12.975 GeV
Peak Current	4000 A
Normalized Emittances	0.3/0.3 $\mu\text{m rad}$
Average beta function	5 m
RMS Energy Spread	$10^{-4}$
Bunch Length	6 fs
Seed radiation power	5-25 MW
Radiation Wavelength	1.5 $\text{\AA}$
Rayleigh Length	10 m
Undulator Period	2 cm
Undulator Parameter	3
Quadrupole Focusing Strength	26.4 T/m
Undulator Section Length	1 m
Undulator Break Length	20 cm
FEL parameter	$1.66 \times 10^{-3}$
3-D Gain Length	65 cm

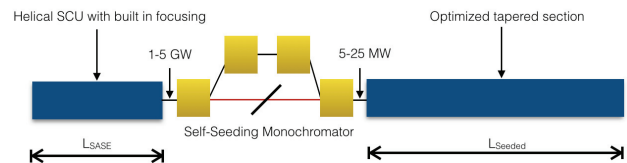


Figure 1: Schematic of the undulator for hard X-ray multi TW peak power output, designed to achieve high extraction efficiency in the shortest possible distance.

by [3]:

$$B_0 = \frac{4k_u I}{10^5} [k_u a K_0(k_u a) + K_1(k_u a)], \quad (1)$$

where  $I$  is the current in the coils,  $k_u = 2\pi/\lambda_u$  is the undulator wavenumber,  $a$  is the helix radius and  $K_0$  and  $K_1$  are modified Bessel functions. For a helical bore radius  $a = 7.5$  mm the total current required through the coils is  $I = 484$  A which, considering coils of  $\sim \text{mm}^2$  surface area, gives a current density below the critical value for superconducting NbTi or Nb<sub>3</sub>Sn wires. From the point of view of operation a superconducting undulator has advantages such as resistance to radiation damage and reduced sensitivity to wakefields, for a more detailed description see Ref. [4]. The undulator is helically polarized as this increases the effect of refractive guiding in the post-saturation regime and improves the FEL performance [5].

\* Work supported by: DOE Grant Number DE-SC0009983

## ADVANCES ON THE LUNEX5 AND COXINEL PROJECTS

M. E. Couprie, C. Benabderrahmane, P. Berteaud, C. Bourassin-Bouchet, F. Bouvet, J. Bozek, F. Briquez, L. Cassinari, L. Chapuis, J. Daillant, J. Da Silva, D. Denetière, Y. Dietrich, M. Diop, J. P. Duval, M. El Ajjouri, T. El Ajjouri, C. Herbeaux, N. Hubert, M. Khojoyan, M. Labat, N. Leclercq, A. Lestrade, A. Loulergue, P. Marchand, O. Marcouillé, J. L. Marlats, F. Marteau, C. Miron, P. Morin, A. Nadji, R. Nagaoka, F. Polack, F. Ribeiro, J. P. Ricaud, G. Sharma, P. Rommeluère, P. Roy, K. Tavakoli, M. Thomasset, M. Tilmont, M. A. Tordeux, M. Valléau, J. Vétéran, W. Yang, D. Zerbib, Synchrotron SOLEIL, France  
 S. Bielawski, C. Evain, M. Le Parquier, C. Szwaj, PhLAM/ CERLA, Lille, France  
 E. Roussel, FERMI@ELETTRA, Sincrotrone Trieste, Basovizza, Italy  
 G. Lambert, V. Malka, A. Rousse, C. Thauray, Lab. d'Optique Appliquée, Palaiseau, France  
 G. Devanz, C. Madec, A. Mosnier, CEA/DSM/IRFU/SACM, Saclay, France  
 D. Garzella, CEA/DSM/IRAMIS/ LIDyL, Saclay, France  
 N. Delerue, M. El Khaldi, W. Kaabi, F. Wicek, Laboratoire de l'Accélérateur Linéaire, Orsay, France  
 X. Davoine, CEA/DAM/DIF, Bruyère-Le-Châtel, France  
 A. Dubois, J. Lüning, LCPMR, Paris-VI, France

### Abstract

LUNEX5 (free electron Laser Using a New accelerator for the Exploitation of X-ray radiation of 5th generation) aims at investigating compact and advanced Free Electron Laser (FEL). It comprises one one hand a 400 MeV superconducting linac for studies of advanced FEL schemes, high repetition rate operation (10 kHz), multi-FEL lines, and one the other hand a Laser Wake Field Accelerator (LWFA) for its qualification by a FEL application, an undulator line enabling advanced seeding and pilot user applications in the 40-4 nm spectral range. Following the CDR completion, different R&D programs were launched, as for instance on FEL pulse duration measurement, high repetition rate electro-optical sampling. The COXINEL ERC Advanced Grant aims at demonstrating LWFA based FEL amplification, thanks to a proper electron beam manipulation, with a test experiment under preparation. As a specific hardware is also under development such as a cryo-ready 3 m long undulator of 15 mm period is under development.

### INTRODUCTION

Since the laser discovery [1] and the first FEL [2] in the infra-red in Stanford on MARK III, followed by the ACO FEL in Orsay [3] in the visible and UV, and then in the VUV using harmonic generation [4] in the VUV, free electron lasers count nowadays as unique light sources in terms of their properties. Since the early FEL times, performance characterisation and quest for improvement was one of the major concerns. For example, in the case of the Super-ACO storage ring based FEL in France [5,6], the FEL dynamics was actively studied [7-10] and led to the first use of a UV FEL, even in combination with synchrotron radiation for pump-probe two-color experiments [11-16]. Oscillators and coherent harmonic generation also enable adjustable polarisation thanks to the use

of elliptically polarised undulators [17-18]. So far, FEL oscillators have been limited to the VUV [19] because of the issues related to the mirror performance and degradation at short wavelengths [20-21]. Short-wavelength FELs then evolved towards high-gain single-pass-based systems [22] in the SASE [23] and seeded [24] configurations. Presently, VUV-X tuneable coherent sub-ps pulses FEL light sources around the world provide record peak powers (typically GW), peak and average brilliance at short wavelengths. FEL user facilities (FLASH1, FLASH2 [25-26], FERMI@ELETTRA in the seeded configuration [27], LCLS [28] and SACLA [29] in the hard X-ray) enable to explore unknown phenomena in various scientific domains. Different directions are now explored for performance improvement.

In France, activity has been performed in the frame of international collaborations on seeding, enabling to reduce the intensity fluctuations, jitter, the saturation length, in particular with a seed being generated from high-order harmonics generated in gas [30-32]. There is also interest for two-color operation, with first studies on CLIO [33] and in the pulse splitting configuration [34]. Characterisation of FEL properties is also of concern, both transversally [35] and longitudinally [36].

### LUNEX5 PROJECT

The LUNEX5 [37-41] demonstrator project (shown in Fig. 1) aims at exploring several directions for the production of short, intense, and coherent pulses between 40 and 4 nm on the first, third and fifth harmonics. It relies first on a 400-MeV superconducting linac (SC) with two to three modified XFEL-type cryomodules at 1.3 GHz for high repetition rate CW and thus multiple user operation. The electron bunch is compressed due to a dogleg with sextupoles, enabling phase space linearization and cancellation of the second order dispersion [41].

# INCLUSION OF ADVANCED FIELDS AND BOUNDARY CONDITIONS IN THE ANALYTIC THEORY FOR HIGH GAIN FELs

P. Niknejadi and J.M.J. Madey

University of Hawai'i at Manoa, Honolulu, HI 96822, USA

## Abstract

The efforts in realizing x-ray free electron lasers (FELs) and enhancing their performance has stimulated remarkable theoretical developments and experimental advances in the field. Yet, the successful operation of x-ray FELs based on the self-amplified spontaneous emission (SASE) principle which has made them a powerful new tool, has beckoned our attention for better understanding a comprehensive physical basis of the theory that has the potential to improve the temporal structure and spectral optimization of these sources. We have previously explained the advantages of including the coherent radiation reaction force as a part of the solution to the boundary value problem for FELs that radiate into "free space" (SASE FELs) and discussed how the advanced field of the absorber can interact with the radiating particles at the time of emission. Here we present the outline of our theoretical approach which follows from eigenmode analysis of optical guiding in FELs. We will also discuss in some detail the experimental setup that could verify and/or further our understanding of the the underlying physics of these devices.

## INTRODUCTION

When formulated in the language of covariant action-at-a-distance, the solution to the boundary value problem corresponding to an oscillating particle within a spherical absorbing shell of arbitrary density is dominated by the interference of the retarded and advanced forces originating in the accelerated and absorbing particles [1]. This leads to a force on the accelerated particle exactly equal to that needed to match the power carried by radiation to the particles in the absorbing shell. Therefore a time-symmetric definition of electrodynamics provides non-diverging solution and origin for the radiation reaction field and satisfies Maxwell's energy integral [2]. In fact, it has also been shown that the action-at-a-distance formulation is not essential and the assumption of time-symmetry suffices for the conservation of energy [3]. The reliance of theory of SASE FELs on classical electrodynamics and their operational dependency on coherent radiation at femtosecond scale provides an excellent opportunity for the test and further study of the time-symmetric approach to electrodynamics.

## DISCUSSION OF THE THEORY AND CONCEPT

Description of FEL interactions by Kimel and Elias [4] includes a viable model of the coherent radiation reaction in covariant form valid for radiation into free-space. In time-symmetric electrodynamics this can be introduced by taking

in to account both the advanced and retarded field of the source and absorbing (non-emitting) particles. Applying that principle to the beam traveling in a SASE FEL, we start by considering both the advanced and retarded field/potential of both the absorber and the electrons (the emitter). It is important to note that in the absence of reflector/refractor/target in front of the electron beam traveling in  $z$ , the absorbers are the cosmological particles; and when including the effect of an absorber that far, the field and forces being considered approach the retarded field of experience). Now we must include half the retarded (outgoing) field of the emitters and the half the advanced (incoming) field of the target. The interaction of the advanced field of the target with the radiating electrons ensures energy conservation on the one hand, and on the other hand imposes the fields and forces initiated from the target on the source.

## Non-reflecting Boundary Condition

The target mentioned above introduces a non-reflecting boundary condition to the system of the equations that must be solved. Here we refrain from calling the target an absorber to avoid confusion, since the role of the target is not absorbing the emitted photons but to be the origin of the advanced fields acting on the beam. For such signals carried on electromagnetic waves (advanced or retarded) the invariant interval  $(cdt)^2 - dr^2$  between the emission of a wave and it's absorption at the non-reflecting boundary is always identically zero. So by that measure, which is the covariant statement of the distance in space-time separating transmitter and receivers, the emission and absorption of the retarded and advanced waves are all simultaneous. This has been illustrated in Figure 1. Note that the advanced wave of the non-reflecting boundary (mirror) co-propagates with the fields of the undulator acting on the electrons. (The characteristics of the mirror (partially reflecting) and why it was chosen for our experiment will be explained in the next section.)

## Advanced Field and Evolution of Coherent Bunching in SASE

The SASE FEL starts from a randomly phased electron beam. After a few undulator periods the randomly phased electron beam gets bunched. The coherent radiation emitted by tightly bunched electron beams plays a critical role in the analysis and operation of free electron lasers. For conducting or reflecting (resonator mirror) FELs, a normal mode analysis of operation already includes the relevant boundary conditions. However, in order to arrive at a comprehensive first-principles field-based analysis of the intense radiation emitted into free-space by devices that work based on the

# HIGH-POWER ULTRASHORT TERAHERTZ PULSES GENERATED BY A MULTI-FOIL RADIATOR WITH LASER-ACCELERATED ELECTRON PULSES

Jeongsang Jo<sup>1</sup>, Young Uk Jeong<sup>1</sup>, Seong Hee Park<sup>1</sup>, Kitae Lee<sup>1</sup>, Kyu-Ha Jang<sup>1</sup>, Wooje Ryu<sup>1</sup>, Hana Kim<sup>1</sup>, Kyung Nam Kim<sup>1</sup>, Boris Gudkov<sup>1,2</sup>, Sergey Miginsky<sup>1,2</sup>, Nikolay A. Vinokurov<sup>1,2</sup>  
<sup>1</sup> Korea Atomic Energy Research Institute, 1045 Daedeok-Daero, Yuseong-gu, Daejeon, 305-353, Republic of Korea  
<sup>2</sup> Budker Institute of Nuclear Physics, Siberian Branch of Russian Academy of sciences, 11 Lavrentyev Prospect, Novosibirsk 630090, Russia

## Abstract

Terahertz (THz) wave is an attractive source for a variety of research including imaging, spectroscopy, security, etc. We proposed a new scheme of high-power and ultrashort THz generation by using the coherent transition radiation from a cone-shaped multi-foil radiator [1] and a rectangle-shaped multi-foil radiator. To perform the proof-of-principle of the multi-foil THz radiator, we used 80~100 MeV electron bunches from laser-plasma acceleration. While a cone-shaped multi-foil radiator has a circular polarization with a conic wave, we made a rectangle-shaped multi-foil radiator that has a linear polarization in a plane-like wave, which can be used more widely for various applications. We can easily control the power of multi-foil radiator by adjusting the number of foils. We compare the THz power ratio between 2 sheet and multi sheets using cooled bolometer. We will measure the pulse duration and bandwidth of the THz wave from the multi-foil radiators in a single-shot by using electro-optic sampling and cross-correlation method [2].

## INTRODUCTION AND BACKGROUND

Since THz wave has different property to existing the electromagnetic wave, it is expected to be critical source in medical industry, security and various researches. But, the THz power from photo conductive antenna, Electro-optics and transition radiation is not sufficient to commercialize the item using the THz wave so far. It is dilemma in the THz industrial region. The new multifoil radiator may achieve gigawatt-level peak power using short electron bunch (70~100MeV, 25fs) [1].

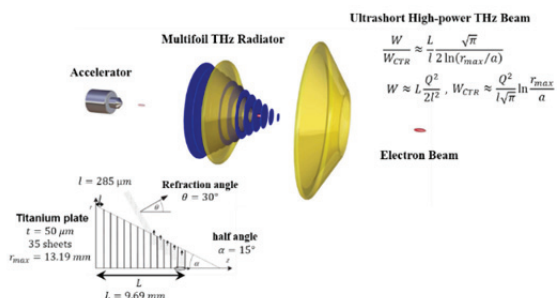


Figure 1: Radial polarization type multifoil radiator.

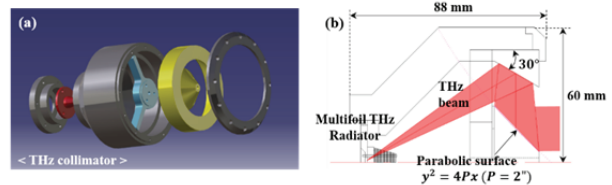


Figure 2. (a) 3D scheme of THz collimator with radiator, (b) The cross-sectional view of THz collimator.

Figure 1 is a THz generation process scheme of the radial polarization type multifoil radiator. 50 μm thickness Circular flat 35 sheets Ti plates with successively decreasing radii are stacked as a truncated cone. The gaps between Ti plates are filled with air and are equal. When short electron bunch propagate through Ti plates along z-axis, transition radiation is generated and is transferred to the edge of radiator along gap of Ti plate as waveguide. At edge of plate, all the transition radiation form one of the wavefront in phase. Then, the coherence wave pulse propagate outward with donut beam shape and it's collimated by special type collimator mirror in Fig. 2.

Figure 3 is linear polarization type radiator, it's consist of a half of the radial polarization type radiator with 5 μm thickness, 70 sheets Ti plates and collimation mirror. In the case that transition radiation by short electron bunch propagate upwards, it is radiated outward without collimation. Other case that transition radiation propagate downwards, it is collimated by parabolic reflector. This reflected and collimated beam is propagated along Ti plate. Finally, it is radiated outward with linear polarization as same process radial type radiator.

Figure 4 shows real image of the radial polarization type multifoil radiator and the linear polarization type multifoil radiator.

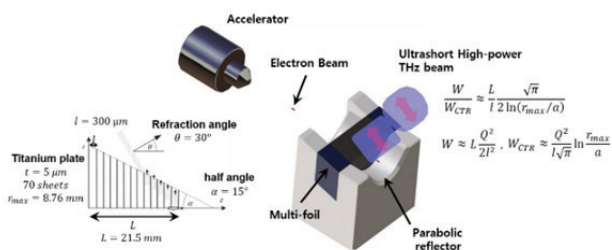


Figure 3: Linear polarization type multifoil radiator.

# MICROBUNCHING-INSTABILITY-INDUCED SIDEBANDS IN A SEEDED FREE-ELECTRON LASER

Z. Zhang<sup>1,2</sup>, Y. Ding<sup>1</sup>, W. M. Fawley<sup>1</sup>, Z. Huang<sup>1\*</sup>, J. Krzywinski<sup>1</sup>,  
A. Lutman<sup>1</sup>, G. Marcus<sup>1</sup>, A. Marinelli<sup>1</sup>, and D. Ratner<sup>1</sup>

<sup>1</sup> SLAC, Menlo Park, CA 94025, USA

<sup>2</sup> Tsinghua University, Beijing 100084, China

## Abstract

The measured spectrum of the soft X-ray self-seeding at the LCLS has a pedestal-like distribution around the seeded frequency, which limits the spectral purity and seeding applications without a post-undulator monochromator. In this paper, we study the origins of the pedestals and focus on the contributions of microbunching instability prior to the FEL undulator. We show that both energy and density modulations can induce sidebands in a seeded FEL. Theory and simulations are used to analyze the sideband content relative to the seeding signal. The results place a tight constraint on the longitudinal phase space uniformity for a seeded FEL.

## INTRODUCTION

Many efforts have been devoted to improve the longitudinal coherence and spectral purity of the X-ray free-electron lasers (FELs) since the unequivocal success of existing facilities which are based on the self-amplified spontaneous emission (SASE) [1, 2]. While the relative bandwidth of SASE FELs are limited to at least  $10^{-3}$  or larger, one can decrease the output bandwidth and increase the longitudinal coherence by initiating the FEL process with a coherent seed [3–6], or by imprinting the electron beam with a coherent density modulation (bunching) at the wavelength of interest [7–10]. Under ideal circumstances (high-quality seed of sufficient power and uniform electron beam, etc.), one can obtain completely coherent, high-power X-ray pulses that approach Fourier limit.

However, imperfections of the electron beam or of the seed will reduce the quality of the seeded FEL output [11–14]. In the measurement of self-seeded soft X-ray radiation spectrum at the Linac Coherent Light Source (LCLS) [6], there is often a pedestal-like distribution around the seeded frequency. In the absence of a post-undulator monochromator, this contamination limits the spectral purity and may degrade certain user applications. Further studies have ruled out the possibility that the pedestal-like distributions in the spectra come from the spectrometer noise or the monochromator optics. Microbunching instability growth of the electron beam prior to the undulator, mostly induced by the longitudinal space charge during the long-distance acceleration and drift sections [15, 16] and directly observed at the LCLS recently [17], is identified as the main source for these spectral pedestals. In this paper, we show that both energy and density modulations can induce sidebands in a seeded FEL.

Theory and simulations are used to analyze the sideband content relative to the seeding signal. The results place a tight constraint on the longitudinal phase space uniformity for a seeded FEL.

## THEORETICAL ANALYSIS

To understand the basic physics of the pedestals, we consider a two-frequency system: the seed and the sideband. The FEL is seeded by a monochromatic radiation whose frequency is at or near the natural FEL resonant frequency  $\omega_1$  and the electron beam initially has a longitudinal long-wavelength modulation at frequency  $\omega_s$ . We describe the longitudinal phase space of the electron beam with the electron ponderomotive phase  $\theta \equiv (k_1 + k_u)z - \omega_1 t$  and normalized energy deviation from resonance  $\eta \equiv (\gamma - \gamma_0)/\gamma_0$ , where  $k_1 (= \omega_1/c)$  and  $k_u$  are the wave numbers of the radiation and undulator. We will find the following dimensionless variables to be useful in the analysis:

$$\hat{z} \equiv 2k_u \rho z, \quad (1)$$

$$\hat{\eta} \equiv \frac{\eta}{\rho}, \quad (2)$$

$$a_\nu \equiv \frac{eK[JJ]}{8\gamma_0^2 m c^2 k_u \rho^2} E_\nu, \quad (3)$$

where the normalized frequency  $\nu = 1 + \Delta\nu \equiv \omega/\omega_1$  and  $\nu = 1$  is the resonant frequency.  $K$  is the normalized field of the undulator and  $[JJ]$  is the Bessel function factor. With these dimensionless variables, the pendulum equations of the two-frequency system can be written as

$$\frac{d\theta}{d\hat{z}} = \hat{\eta}, \quad (4)$$

$$\frac{d\hat{\eta}}{d\hat{z}} = a_1 e^{i\theta} + a_s e^{i\nu\theta} + c.c., \quad (5)$$

$$\frac{da_1}{d\hat{z}} = -b_1, \quad (6)$$

$$\frac{da_s}{d\hat{z}} + i\Delta\nu a_s = -b_s, \quad (7)$$

with the bunching parameters at the seed and the sideband frequency

$$b_1 \equiv \langle e^{-i\theta} \rangle, \quad (8)$$

$$b_s \equiv \langle e^{-i\nu\theta} \rangle. \quad (9)$$

The subscript "1" denotes the variables of the seed and "s" the sideband, respectively. We also introduce the collective

\* zrh@slac.stanford.edu

# CONCEPTUAL THEORY OF SPONTANEOUS AND TAPER-ENHANCED SUPERRADIANCE AND STIMULATED SUPERRADIANCE\*

A. Gover, University of Tel-Aviv, Tel-Aviv, Israel

R. Ianconescu, University of Tel-Aviv, Tel-Aviv and Shenkar College, Ramat Gan, Israel

A. Friedman, Ariel University, Ariel, Israel

C. Emma, P. Musumeci, UCLA, Los Angeles, USA

## Abstract

In the current work we outline the fundamental physical concepts of Spontaneous Superradiance (SR), Stimulated Superradiance (ST-SR), Taper-Enhanced Superradiance (TES) and Taper-Enhanced Stimulated Superradiance Amplification (TESSA), and compare their Fourier and Phasor formulations in a model of radiation mode expansion. Detailed further analysis can provide better design concepts of high power FELs and improved tapering strategy for enhancing the power of seeded short wavelength FELs. We further discuss the extensions of the model required for full description of these radiation processes, including diffraction and spectral widening effects.

## INTRODUCTION

In the context of radiation emission from an electron beam Dicke's superradiance (SR) [1] is the enhanced radiation emission from a pre-bunched beam. Stimulated Superradiance (ST-SR) is the further enhanced emission of the bunched beam in the presence of a phase-matched radiation wave. These processes were analyzed for Undulator radiation in the framework of radiation field mode-excitation theory [2]. In the nonlinear saturation regime the synchronism of the bunched beam and an injected radiation wave may be sustained by wiggler tapering [3]. Same processes are instrumental also in enhancing the radiative emission in the tapered wiggler section of seeded FEL [4]. Here we outline the fundamental physical concepts of Spontaneous Superradiance (SR), Stimulated Superradiance (ST-SR), Taper-Enhanced Superradiance (TES) and Taper-Enhanced Stimulated Superradiance Amplification (TESSA), and compare their Fourier and Phasor formulations in a model of radiation mode expansion. Detailed further analysis can provide better design concepts of high power FELs and improved tapering strategy for enhancing the power of seeded short wavelength FELs. We further discuss the extensions of the model required for full description of these radiation processes, including diffraction [5] and spectral widening effects.

## SUPERRADIANT AND STIMULATED SUPERRADIANCE OF SPONTANEOUS EMISSION

As a starting point we review the theory of superradiant (SR) and stimulated superradiant (ST-SR) emission from

\* This research was supported in part by a grant from the United States-Israel Binational Science Foundation(BSF), Jerusalem, ISRAEL

free electrons in a general radiative emission process. In this section we use a spectral formulation, namely, all fields are given in the frequency domain as Fourier transforms of the real time dependent fields:

$$\check{A}(\underline{r}, \omega) = \int_{-\infty}^{\infty} A(\underline{r}, t) e^{i\omega t} dt \quad (1)$$

We use the radiation modes expansion formulation of [2], where the radiation field is expanded in terms of an orthogonal set of eigenmodes in a waveguide structure or in free space (eg. Hermite-Gaussian modes):

$$\{\check{E}_q(\underline{r}), \check{H}_q(\underline{r})\} = \{\check{E}_q(\underline{r}_\perp), \check{H}_q(\underline{r}_\perp)\} e^{ik_q z} \quad (2)$$

$$\check{E}(\underline{r}, \omega) = \sum_{\pm q} C_q(z, \omega) \check{E}_q(\underline{r}) \quad (3)$$

$$\check{H}(\underline{r}, \omega) = \sum_{\pm q} C_q(z, \omega) \check{H}_q(\underline{r}) \quad (4)$$

The excitation equations of the mode amplitudes is:

$$\frac{d\check{C}_q(z, \omega)}{dz} = \frac{-1}{4P_q} \int d^2 \underline{r}_\perp \check{J}_\perp(\underline{r}, \omega) \cdot \check{E}_q^*(\underline{r}), \quad (5)$$

which is formally integrated and given in terms of the initial mode excitation amplitude and the currents

$$\check{C}_q(z, \omega) - \check{C}_q(0, \omega) = -\frac{1}{4P_q} \int dV \check{J}_\perp(\underline{r}, \omega) \cdot \check{E}_q^*(\underline{r}), \quad (6)$$

where

$$P_q = \frac{1}{2} Re \iint \check{E}_q \times \check{H}_q d^2 r_\perp = \frac{|\check{E}_q(\underline{r}_\perp = 0)|^2}{2Z_q} A_{em}, \quad (7)$$

That defines the mode effective area  $A_{em}$  in terms of the field of the mode on axis  $\check{E}_q(\underline{r}_\perp) = 0$ .

For a particulate current (an electron beam):

$$J(\underline{r}, t) = \sum_{j=1}^N -ev_j(t) \delta(\underline{r} - \underline{r}_j(t)) \quad (8)$$

The field amplitude increment appears as a coherent sum of contributions (energy wavepackets) from all the electrons in the beam: The contributions can be split into a spontaneous part (independent of the presence of radiation field) and stimulated (field dependent) parts:

$$\check{C}_q^{out}(\omega) - \check{C}_q^{in}(\omega) = -\frac{1}{4P_q} \sum_{j=1}^N \Delta \check{W}_{qj} \quad (9)$$

# SMITH-PURCELL RADIATION FROM MICROBUNCHED BEAMS MODULATED AFTER PASSING THE UNDULATORS IN FELS\*

D.Yu. Sergeeva<sup>1,#</sup>, A.P. Potylitsyn<sup>1,2</sup>, A.A. Tishchenko<sup>1</sup>, M.N. Strikhanov<sup>1</sup>,  
<sup>1</sup>National Research Nuclear University MEPhI, Moscow, Russia  
<sup>2</sup>National Research Tomsk Polytechnic University, Tomsk, Russia

## Abstract

We suggest using the Smith-Purcell effect from microbunched beams modulated after passing the undulators in FELs as an extra source of monochromatic radiation. We investigate theoretically characteristics of Smith-Purcell radiation in THz and X-ray frequency regions for two types of distribution of the particles in the beam. The expression for spectral-angular distribution of such radiation is obtained and analyzed, both for fully and partially modulated beams. The intensity of Smith-Purcell radiation is shown to be able to increase both due to the periodicity of the beam and the periodicity of the target. The numerical results prove that such radiation source can be an effective instrument for different FEL users, supplementary for the main FEL source.

## INTRODUCTION

Smith-Purcell radiation (SPR) is a promising scheme for creating the intense source of radiation. SPR is convenient for beam diagnostics because of large emission angles. The intensity of SPR is proportional to the squared number of strips in the periodic target (grating). Besides the intensity of radiation can be increased if it is generated by the beam having periodic inner structure. Such microbunched beams can be obtained in FEL, in the process of the beam modulation in undulator. Therefore, the beam after passing the undulator in FEL can generate intensive radiation from the grating before passing to a dump (see scheme in Fig. 1). Changing an emission angle it is possible to produce quasimonochromatic radiation with different wavelengths in a broad range in comparison with the modulation period.

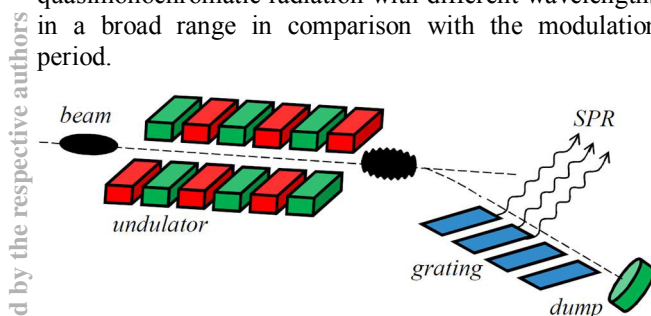


Figure 1: Scheme of using the microbunched beam modulated after passing the undulator for generating intensive Smith-Purcell radiation.

We theoretically investigate SPR generated by the microbunched beam of relativistic electrons. The beam is assumed to have periodic internal structure with the period  $\lambda_0$ . The number of the particles with the charge  $e$  is  $N$ , the number of microbunches is  $N_b$ . The beam moves at a constant distance  $h$  above the grating surface with the constant velocity  $\mathbf{v} = (v, 0, 0)$ . The period of the grating is  $d$ , the single strip width is  $a$ ,  $N_{st}$  is the number of the strips in the grating. The qualitative scheme is shown in Fig. 2.

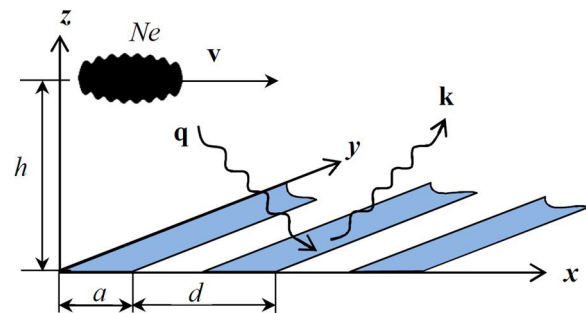


Figure 2: Qualitative scheme of generating the Smith-Purcell radiation.

## MODULATED BEAM

The distribution of the particles in the modulated beam can be described by two ways. We will mark the values obtained for these distributions by  $f$  and  $g$  as the superscripts.

The first one is convenient to describe the beam which has a lot of microbunches with rather short delay between them. In this case the inner structure of each microbunch is negligible. Such kind of beams is produced, for example, in FELs like FLASH, Germany. The longitudinal profile of beam modulated in the undulator in this case can be described by the function

$$f_{long}(x) = \frac{2}{\sqrt{\pi}\sigma_x} \frac{\exp[-x^2/\sigma_x^2] (\mu + \sin^2(\pi x/\lambda_0))}{1 + 2\mu - \exp[-\pi^2\sigma_x^2/\lambda_0^2]}, \quad (1)$$

with  $\sigma_x$  being the character size of the bunch in  $x$  direction;  $\mu$  defining the “depth” of the modulation: if  $\mu = 0$  then the beam is fully modulated, if  $\mu \rightarrow \infty$  then the beam has the Gaussian form;  $\lambda_0$  being the period of the modulation. The function in Eq. (1) is shown in Fig.3.

\*Work supported by the Leverhulme Trust International Network, grant IN-2015-012 and by the Ministry of Science and Education of the Russian Federation, grant № 3.1110.2014/K.

#dysergeyeva@mephi.ru

# COMMISSIONING OF THE DELTA POLARIZING UNDULATOR AT LCLS\*

H.-D. Nuhn<sup>#</sup>, S.D. Anderson, R.N. Coffee, Y. Ding, Z. Huang, M. Ilchen, Y. Levashov, A.A. Lutman, J. MacArthur, A. Marinelli, S.P. Moeller, F. Peters, Z. Wolf, SLAC National Accelerator Laboratory (SLAC), USA  
 A.B. Temnykh, Cornell University (CLASSE), USA  
 G. Hartmann, J. Viehhaus, Deutsches Elektronen-Synchrotron (DESY), Germany  
 J. Buck, European XFEL GmbH (XFEL.EU), Germany  
 A.O. Lindahl, University of Gothenburg Department of Physics, Sweden

## Abstract

The Linac Coherent Light Source (LCLS) generates linearly polarized, intense, high brightness x-ray pulses from planar fixed-gap undulators. While the fixed-gap design supports a very successful and tightly controlled alignment concept, it provides only limited taper capability (up to 1% through canted pole and horizontal position adjustability) and lacks polarization control. The latter is of great importance for soft x-ray experiments. A new 3.2-m-long compact undulator (based on the Cornell University Delta design [1]) has been developed and installed in place of the last LCLS undulator segment (U33) in October 2014. This undulator provides full control of the polarization degree and  $K$  value. Used on its own, it produces fully polarized radiation in the selected state (linear, circular or elliptical) but at low intensity. To increase the output power by orders of magnitude, the electron beam is micro-bunched by several (~10) of the upstream LCLS undulator segments operated in the linear FEL regime. As unavoidable by-product, this micro-bunching process produces moderate amounts of horizontally linear polarized radiation which mixes with the radiation produced by the Delta undulator. This unwanted radiation component has been greatly reduced by the reverse taper configuration, as suggested by E. Schneidmiller and M. Yurkov [2]. Full elimination of the linear polarized component was achieved through spatial separation combined with transverse collimation. The paper describes these and other methods tested during commissioning. It also presents results of polarization measurements showing high degrees of circular polarization in the soft x-ray wavelength range (500 eV-1500 eV).

## INTRODUCTION

The design and measurement plans for the first 3.2-m-long Delta undulator for the LCLS were described in an FEL2013 paper [3]. Since then, these plans have been implemented close to the original schedule; the parameters listed in Table 1 of the FEL2013 paper all apply. Installation occurred in October 2014. (Figure 1)

\* Work was supported by U.S. Department of Energy, Office of Basic Energy Sciences, under Contract DE-AC02-76SF00515. A.B. Temnykh is supported U.S. National Science Foundation awards DMR-0807731 and DMR-DMR-0936384

<sup>#</sup> nuhn@slac.stanford.edu

Beam based commissioning took place from October 2014 to May 2015. During this period operational techniques were developed that allowed to operate the Delta undulator at performance levels significantly exceeding expectations. Beam based commissioning was followed by the first user experiments in June 2015. The following will discuss quadrant tuning, magnet field mapping, and beam based commissioning. Tuning and magnetic field mapping made use of experience obtained in the course of construction and testing of the 0.3-m model at Cornell and the 1-m long prototype at SLAC.



Figure 1: 3.2-m long LCLS Delta undulator installed at the end of the LCLS undulator line.

## MAGNET BLOCKS

Each of the four rows of the Delta undulator contains 391 magnet blocks, four per period, arranged as Halbach array [4]. The first and last three blocks in each row are mounted at larger distances to the beam axis to accomplish end-field matching. Each magnet block is glued to an Al holder (Figure 2), which has been designed to also secure the magnet, mechanically, in case of glue

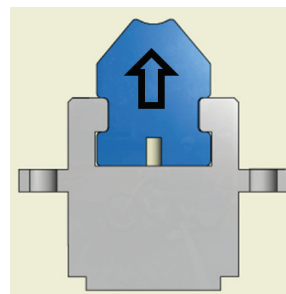


Figure 2: Ni coated PM blocks epoxied to Al holders. (Design by T. Montagne, SLAC)

# PHOTON DIAGNOSTICS AND PHOTON BEAMLINES INSTALLATIONS AT THE EUROPEAN XFEL

Jan Grünert, Andreas Koch, Naresh Kujala, Wolfgang Freund, Marc Planas, Florian Dietrich, Jens Buck, Jia Liu, Harald Sinn, Martin Dommach, Serguei Molodtsov, European XFEL GmbH, Albert-Einstein-Ring 19, 22761 Hamburg, Germany

## Abstract

The European X-ray Free-Electron-Laser (XFEL.EU) is a new 4th generation light facility which will deliver radiation with femtosecond and sub-Ångström resolution at MHz repetition rates, and is currently under construction in the Hamburg metropolitan area in Germany. Special diagnostics [1,2] for spontaneous radiation analysis is required to tune towards the lasing condition. Once lasing is achieved, diagnostic imagers [3], online monitors [4], and the photon beam transport system [5] need to cope with extreme radiation intensities. In 2015 the installation of machine equipment in the photon area of the facility is in full swing. This contribution presents the progress on final assemblies of photon diagnostics, the installation status of these devices as well as of the beam transport system, and recent design developments for diagnostic spectrometers and temporal diagnostics.

## CONTENTS

This paper starts with a brief overview of the photon part of the European XFEL facility, outlines the photon diagnostics devices, details on the current status of the assembly of final devices. It continues with the status of the installations of photon diagnostics and beam transport system in the tunnels. Some recent design developments for advanced diagnostics are presented and finally, a schedule outlook is given.

## INTRODUCTION

### General Facility Layout

The general layout of the photon part of the European XFEL facility is shown in Fig.1 and is described in more detail elsewhere, e.g. in [5]. There are three undulators, of which the two called SASE1 and SASE2 provide hard X-ray FEL radiation up to 24keV in the fundamental, while SASE3 caters the soft X-ray domain below 3keV (SASE means self-amplified spontaneous emission). The photon diagnostics and beam transport system is located in all photon tunnels indicated in orange, called XTD1 through XTD10. The tunnels lead to the experimental hall XHEXP1, where in the startup phase there will be six experimental endstations. As an example for the beam transport and diagnostics layout, Fig. 2 shows the elements in the SASE1 beamline inside the tunnels XTD2 and XTD9 as well as shaft building XS3.

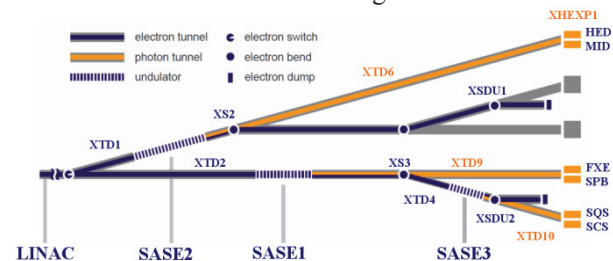


Figure 1: General facility layout, photon part

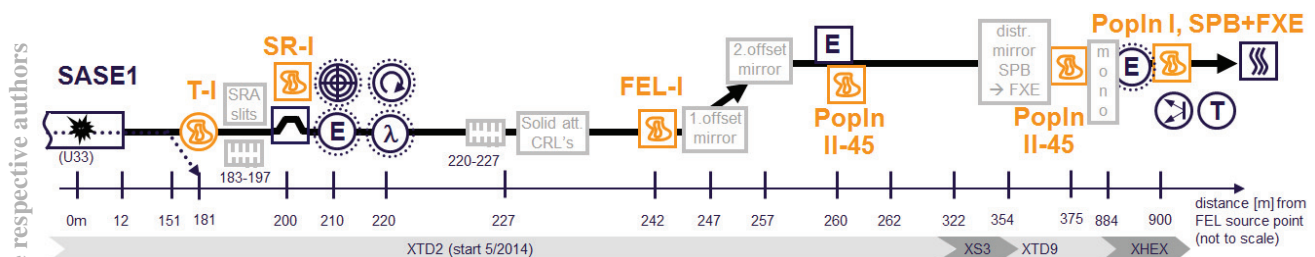


Figure 2: SASE1 beamline as an example for beam transport and diagnostics layout. Elements in the SASE1 beamline inside the tunnels XTD2 and XTD9 as well as shaft building XS3 are shown. Beam transport and optics elements are in grey, diagnostic imagers in orange, other diagnostics in black. From source to experimental hall, there are the transmissive imager (T-I), the synchrotron radiation absorber (SRA), the K-Monochromator with its spontaneous radiation imager (SR-I), the gas based online systems X-ray Gas Monitor (XGM) and PhotoElectron Spectrometer (PES) surrounded by differential pumping systems, the solid attenuators and Compound Refractive Lenses (CRLs), the FEL imager (FEL-I), the two offset mirrors, the MCP-based detector (denoted “E” here), a pop-in monitor type II-45°, the distribution mirror to switch between SPB and FXE endstation, another pop-in monitor type II-45°, a crystal monochromator, another XGM with its differential pumping, plus advanced diagnostics for timing and wavefront in the experimental endstation. Not shown is the HiREX spectrometer which was now added to the layout just upstream of the distribution mirror.

# STATUS REPORT OF PAL-XFEL UNDULATOR PROGRAM

D.E. Kim\*, Y.G. Jung, W.W. Lee, H.S. Kang, I.S. Ko, M.H. Cho,  
 H.G. Lee, S.B. Lee, B.G. Oh, H.S. Suh, K.H. Park, PAL, POSTECH, Pohang, Korea  
 Suren Karabekyan, Joachim Pflueger, EU-XFEL, Hamburg, Germany

## Abstract

PAL-XFEL is a SASE based FEL using S-band linear accelerator, photo cathode RF Gun, and hybrid undulator system for final lasing. The undulator system is based on EU-XFEL undulator design with necessary modifications. The changes include new magnetic geometry reflecting changed magnetic requirements, and EPICs based control system. The undulator system is in measurement and tuning stage targeting to finish installation within 2015. In this report, the development, tuning, measurement efforts for PAL-XFEL undulator system will be reported.

Table 1: Major Parameters of the PAL-XFEL Undulator System

Parameter	Unit	Value	Value
Undulator Line		HXU	SXU
Beam energy	GeV	10.0	3.15
Min gap	mm	8.30	8.30
Period	mm	26.0	35.0
Length	m	≈5.0	≈5.0
$B_{eff}$	T	0.812	1.016
K		1.973	3.321
Phase jitter	deg	< 7.0	< 7.0
Number		$18+\alpha$	$6+\alpha$

## INTRODUCTION

The Pohang Accelerator Laboratory (PAL) has been developing SASE based light sources since 2011. The target wavelength is 0.1 nm for hard X-ray SASE radiation, with 10 GeV class S-band linear accelerator. For soft X-ray SASE, 3.0 nm FEL radiation using 3.15 GeV electron beam is assumed. To achieve this target, a few key components like low emittance (0.5  $\mu$ m) photo cathode RF gun, and EU-XFEL style out vacuum undulator system are being developed [1]. For undulator system, there will be 18 undulators for hard X-ray line and 6 planar undulators with additional two EPU's (Elliptically Polarized Undulator) are expected for soft X-ray line. The EPU's will be used for polarization control at the last stages of lasing. The major parameters of the X-ray FEL and undulator line is slightly changed recently and the updated parameters are shown in Table 1. A minor changes were the magnetic gap and period. The gap was changed from old 7.2mm to 8.3 mm resulting period change from 24.4 mm to 26.0 mm maintaining 0.1 nm SASE lasing at 10 GeV electron beam energy. The number of required units for soft X-ray SASE line is estimated to be 6 units of 5 m long planar undulators with 2 additional EPU's. The major parameters of the undulator system is summarized in Table 1. And schematic layout of hard X-ray, and soft X-ray undulator lines are shown in Fig .1.

## UNDULATOR SYSTEM

For the PAL-XFEL undulators, the EU-XFEL design and technology [2-4] was adopted and further developed. The EU-XFEL design is a well proven using standardization and optimization for mass serial production [3,4] and was successfully used for the production of 91 undulators for the EU-XFEL. The schematics and major subsystems are shown in Figure 2.

Following EU-XFEL, pole height tuning is used. The poles can be shifted by about  $\pm 150 \mu$ m in vertical direction and tilted by  $\pm 2$  mrad using tuning studs and locking screws. This is a big advancement as compared to using conventional magnetic and/or non-magnetic shims. In contrast to shims, Pole Height Tuning is bi-polar and continuous. Magnetic shims are unipolar and only weaken poles. In addition they are only available in discrete steps. By using Pole Height Tuning an undulator can be readily assembled at a supplier. Provided that suitable a magnetic measurement facility is available the tuning is readily done in house.

At PAL a full scale prototype undulator was built. It is based on the EU-XFEL concept with some modification reflecting different magnetic periods and pole gaps. In addition, precision tilt meters were attached to the girders to monitor parallel motion. Unfortunately this prototype is based on the old magnetic periods of 24.4 mm and old magnetic gap of 7.2 mm. But it is, however, a good test bed to check the mechanical integrity and to develop the entire pole tuning schemes. The completed undulator was mechanically tested by installing precision external gap sensor by comparing the rotary encoder values and the actual gaps

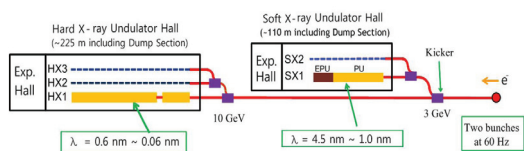


Figure 1: FEL undulator line plan of PAL-XFEL.

## POLE HEIGHT TUNING

For deeper analysis field measurements need to be analyzed. First, for each pole a local-K is defined for each pole using the following definition [5]. This is a half period field

\* dekim@postech.ac.kr